



TECHNICAL REPORT 0-6906-R1
TXDOT PROJECT NUMBER 0-6906

Evaluation of Chemical Solutions to Concrete Durability Problems

Dr. Bruno Fong-Martinez
Jeremy Wheelless
Dr. Thanos Drimalas
Dr. Kevin J. Folliard

Submitted August 2020; Published June 2021

<http://library.ctr.utexas.edu/ctr-publications/0-6906-R1.pdf>



Technical Report Documentation Page

1. Report No. FHWA/TX-20/0-6906-R1		2. Government Accession No.	3. Recipient's Catalog No.	
4. Title and Subtitle Evaluation of Chemical Solutions to Concrete Durability Problems			5. Report Date Submitted August 2020; Published June 2021	
7. Author(s) Bruno Fong-Martinez, Jeremy Wheelless, Thano Drimalas, Kevin Folliard			6. Performing Organization Code	
9. Performing Organization Name and Address Center for Transportation Research The University of Texas at Austin 3925 W. Braker Lane, 4 th Floor Austin, TX 78759			8. Performing Organization Report No. 0-6906-R1	
12. Sponsoring Agency Name and Address Texas Department of Transportation Research and Technology Implementation Division P.O. Box 5080 Austin, TX 78763-5080			10. Work Unit No. (TRAIS)	
			11. Contract or Grant No. 0-6906	
			13. Type of Report and Period Covered Technical Report January 2016–August 2020	
			14. Sponsoring Agency Code	
15. Supplementary Notes Project performed in cooperation with the Texas Department of Transportation.				
16. Abstract The reinforced concrete infrastructure in Texas has been plagued by various durability-related issues over the years, including deterioration from alkali-silica reaction (ASR), delayed ettringite formation (DEF), and corrosion of reinforcing steel. For many of these durability problems, fly ash has been the remedy of choice; however, with changes in fly ash quality and quantity spurred by new emissions standards and changes in fuel sources, concern has arisen that fly ash may not be as available or effective in the future. Thus, there exists a need to evaluate other solutions to reinforced concrete durability problems besides the traditional use of fly ash. This need formed the basis for the research described in this report. A range of materials were tested, including corrosion inhibitors (calcium nitrite, calcium nitrate, others), ASR and/or DEF inhibitors (lithium nitrate), integral water repellants, nanoparticles (silica and dispersible C-S-H), and gypsum as an additive to improve sulfate resistance of Class C fly ash. These materials were tested under a comprehensive laboratory testing program, with tests including heat of hydration, strength, electrical resistivity, corrosion potential, chloride diffusivity, sorptivity, and expansion (due to ASR, DEF, or sulfate attack). Corresponding field specimens were stored at three different outdoor sites in Texas and evaluated for ASR and/or DEF, as well as for corrosion potential (marine site). Lastly, the research team performed a forensic evaluation of a bridge deck in Amarillo, focusing on possible causes of cracking and remedies for future decks. Several products evaluated in this project showed some potential for improved durability and increased service lives for concrete infrastructure. Although there was no single product that was able to improve all durability aspects (like Class F fly ash), there may be opportunities for some of the products to be used in targeted applications to address specific durability requirements				
17. Key Words Chemical admixtures, Concrete durability, Alkali-silica reaction, ASR, Delayed ettringite formation			18. Distribution Statement No restrictions. This document is available to the public through the National Technical Information Service, Springfield, Virginia 22161; www.ntis.gov.	
19. Security Classif. (of report) Unclassified	20. Security Classif. (of this page) Unclassified	21. No. of pages TBD	22. Price	



**THE UNIVERSITY OF TEXAS AT AUSTIN
CENTER FOR TRANSPORTATION RESEARCH**

Evaluation of Chemical Solutions to Concrete Durability Problems

Dr. Bruno Fong-Martinez
Jeremy Wheelless
Dr. Thanos Drimalas
Dr. Kevin J. Folliard

CTR Technical Report: 0-6906-R1
Report Date: Submitted August 2020; Published June 2021
Project: 0-6906
Project Title: Chemical Solutions to Durability Problems
Sponsoring Agency: Texas Department of Transportation
Performing Agency: Center for Transportation Research at The University of Texas at Austin

Project performed in cooperation with the Texas Department of Transportation and the Federal Highway Administration.

Disclaimers

Author's Disclaimer: The contents of this report reflect the views of the authors, who are responsible for the facts and the accuracy of the data presented herein. The contents do not necessarily reflect the official view or policies of the Federal Highway Administration or the Texas Department of Transportation (TxDOT). This report does not constitute a standard, specification, or regulation.

Patent Disclaimer: There was no invention or discovery conceived or first actually reduced to practice in the course of or under this contract, including any art, method, process, machine manufacture, design or composition of matter, or any new useful improvement thereof, or any variety of plant, which is or may be patentable under the patent laws of the United States of America or any foreign country.

Engineering Disclaimer

NOT INTENDED FOR CONSTRUCTION, BIDDING, OR PERMIT PURPOSES.

Research Supervisor: Kevin Folliard

Acknowledgments

The authors express appreciation to the TxDOT Project Director, members of the PMC Committee and to the TxDOT Amarillo district office who helped with the field site investigations.

Table of Contents

Chapter 1. Introduction and Scope.....	1
1.1. Introduction.....	1
1.2. Scope of Project.....	1
1.3. Outline of Report.....	2
Chapter 2. Effect of Lithium Admixture on ASR and DEF.....	3
2.1. Background.....	3
2.1.1. Alkali-Silica Reaction.....	3
2.1.2. Delayed Ettringite Formation.....	8
2.1.3. Lightweight Aggregate.....	10
2.2. Experimental Investigation.....	12
2.2.1. Materials.....	12
2.2.2. Time Release Method.....	14
2.2.3. Mixture Proportions.....	20
2.2.4. Test Matrix.....	23
2.2.5. Specimens.....	26
2.3. Experimental Results and Discussion.....	34
2.3.1. Discussion on Exposure Blocks.....	34
2.3.2. Discussion on Time Release Method.....	37
2.3.3. Lab Specimens—Cylinders.....	38
2.3.4. Lab Specimens—Concrete Prisms.....	41
2.3.5. Lab Specimens—Mortar Bars.....	47
2.3.6. Field Specimens—Exposure Blocks.....	58
2.4. Further Research.....	73
2.4.1. Field Samples.....	73
2.4.2. Lab Samples.....	74
2.4.3. Time Release Method.....	74
2.4.4. Lithium.....	75
2.4.5. LWFA Effect on ASR.....	75
2.5. Conclusions.....	75
2.6. References.....	76
Chapter 3. Performance of Corrosion Inhibitors in Lab and Field Testing.....	80
3.1. Introduction.....	80
3.2. Background.....	80

3.2.1. Corrosion Primer.....	80
3.2.2. Corrosion Prevention Methods	84
3.2.3. Corrosion Inhibitors	84
3.2.4. Alternative Theories on Corrosion Mechanisms	88
3.2.5. Causes of Long-Term Corrosion	88
3.3. Experimental Investigation	91
3.3.1. Materials	91
3.3.2. Mixture Proportions	93
3.3.3. Test Matrix.....	94
3.3.4. Specimens	94
3.3.5. Testing Procedures.....	103
3.4. Experimental Results and Discussion.....	118
3.4.1. Lab Specimens—Cylinders and Disks.....	118
3.4.2. Lab Specimens—Corrosion Beams	125
3.4.3. Field Specimens—Marine Exposure Blocks	130
3.5. Further Research	143
3.6. Conclusions.....	144
3.7. References.....	146
Chapter 4. Effect of Permeability Reducing Admixtures on Concrete Durability	149
4.1. Introduction.....	149
4.2. Background	149
4.2.1. Admixture Products	149
4.2.2. Testing Procedures.....	152
4.2.3. Exposure Sites.....	152
4.3. Experimental Investigation	156
4.3.1. Materials	156
4.3.2. Mixture Proportions	159
4.3.3. Test Matrix and Testing Procedures	159
4.4. Experimental Results and Discussion.....	162
4.4.1. Isothermal Calorimetry	162
4.4.2. Compressive Strength	163
4.4.3. Resistivity	165
4.4.4. Absorption.....	167
4.4.5. Chloride Diffusion Coefficient	170

4.4.6. NCHRP 244 Series II.....	172
4.4.7. Sodium Sulfate.....	175
4.4.8. Calcium Sulfate.....	181
4.4.9. Alkali-Silica Reaction.....	183
4.4.10. Marine Exposure Blocks.....	186
4.5. Further Research	188
4.6. Conclusions.....	188
4.7. References.....	189
Chapter 5. Effect of Nano-Admixtures on Concrete Durability.....	190
5.1. Introduction.....	190
5.2. Background.....	190
5.2.1. Mechanisms	190
5.2.2. Challenges.....	192
5.2.3. Current Research.....	194
5.2.4. Research Objectives.....	195
5.2.5. Nano-CSH.....	196
5.2.6. Testing Procedures.....	197
5.3. Experimental Investigation	198
5.3.1. Materials	198
5.3.2. Mixture Proportions	199
5.3.3. Test Matrix.....	200
5.3.4. Samples and Testing Procedures	200
5.4. Experimental Results and Discussion.....	201
5.4.1. Isothermal Calorimetry	201
5.4.2. Compressive Strength.....	204
5.4.3. Resistivity	205
5.4.4. Chloride Diffusion Coefficient	206
5.4.5. Alkali-Silica Reaction.....	208
5.5. Further Research	212
5.6. Conclusions.....	212
5.7. References.....	213
Chapter 6. Use of Gypsum for Sulfate Resistance of Mortars and Concrete	215
6.1. Background.....	215
6.2. Naming Convention.....	218

6.3. Materials	218
6.3.1. Fly Ash.....	219
6.3.2. Cements.....	220
6.3.3. Particle Characterization.....	221
6.3.4. Material Characterization.....	222
6.4. Testing Methods.....	223
6.4.1. ASTM C 1012 Testing.....	223
6.4.2. Limewater Submergence Testing	226
6.4.3. Isothermal Calorimetry	226
6.4.4. X-Ray Diffraction and Rietveld Refinement	227
6.5. Results and Discussion	227
6.5.1. Exposure Conditions.....	228
6.5.2. Limewater Submergence Testing	228
6.5.3. Isothermal Calorimetry and Maximum Heat	237
6.5.4. Qualitative and Quantitative X-Ray Diffraction.....	256
6.5.5. ASTM C 1012 Testing.....	280
6.5.6. Comparative Analysis of All Testing	295
6.6. Conclusions.....	309
6.7. References.....	310
Chapter 7. Amarillo Bridge Deck Investigation Report	314
7.1. Introduction.....	314
7.1.1. Background.....	314
7.2. Field Visit.....	320
7.2.1. General Information.....	320
7.2.2. Preliminary Determinations	327
7.3. Proposed Experimental Investigation	328
7.3.1. Materials	328
7.3.2. Mixture Proportions	329
7.3.3. Test Matrix.....	329
7.3.4. Samples and Testing Procedures	329
7.3.5. Forensic Investigation.....	330
7.4. Actual Experimental Investigation	330
7.4.1. Preliminary Concrete Test Results.....	330
7.4.2. Admixture Interaction on Paste Samples.....	332

7.4.3. Alkali-Silica Reaction Testing.....	336
7.5. Further Research	337
7.6. Conclusions.....	338
7.7. References.....	339
Chapter 8. Conclusion.....	340
8.1. Conclusions.....	340
8.2. Recommendations for Future Research.....	341

List of Tables

Table 2.1 Cement chemical composition (%) by mass.....	12
Table 2.2 Aggregate properties.....	13
Table 2.3 ASTM C1260 Aggregate Gradation.....	21
Table 2.4 Concrete test matrix.....	23
Table 2.5 DEF mortar bar test matrix.....	25
Table 3.1 Deficiency categories.....	81
Table 3.2 Chloride threshold values with calcium nitrite admixture (30% concentration) (ConcreteWorks, 2017).....	87
Table 3.3: Cement chemical composition (% by mass).....	91
Table 3.4 Aggregate properties.....	91
Table 3.5 Test matrix.....	94
Table 3.6 Testing procedures.....	104
Table 3.7: Correlation between bulk electrical resistivity and RCPT (RCON2, Giatec Scientific).....	105
Table 3.8: Notes on interpretation of half-cell measurements with copper-copper sulfate reference electrode (ASTM C876, Appendix X1.1).....	112
Table 3.9 Chloride loading zone.....	115
Table 3.10 Visual rating methodology adapted from Fahim (2018).....	116
Table 3.11 Mean absolute error (MAE) for chloride analysis on lab samples.....	122
Table 3.12 Notes on interpretation of half-cell measurements with copper-copper sulfate reference electrode (ASTM C876, Appendix X1.1).....	125
Table 3.13 Chloride loading zone.....	127
Table 3.14 Corrosion beam testing summary.....	129
Table 3.15 Mean absolute error (MAE) for chloride analysis on marine exposure blocks.....	134
Table 3.16 Exposure block chloride parameters based on ASTM C1556 model.....	142
Table 3.17 Service life models—time to corrosion initiation (years) [chloride threshold, CT, % mass of concrete].....	142
Table 3.18 Testing summary and product rating.....	146
Table 4.1 Chemical composition of cementitious materials (% by mass).....	156
Table 4.2 Aggregate properties.....	157
Table 4.3 Admixture product details.....	158
Table 4.4 Test matrix.....	159
Table 4.5 Test Procedures Matrix.....	161
Table 4.6 Mean absolute error (MAE) from chloride analysis.....	172

Table 4.7 Exposure conditions for sodium sulfate samples.....	175
Table 4.8 Exposure conditions for calcium sulfate samples.....	181
Table 5.1 Chemical composition of cementitious materials (% by mass).....	198
Table 5.2 Aggregate properties.....	199
Table 5.3 Cementitious mixture proportions	200
Table 5.4 Testing procedures.....	201
Table 5.5 Mean absolute error (MAE) from chloride analysis.....	207
Table 6.1 XRF and QXRD analysis results for fly ashes	219
Table 6.2 XRF, QXRD, and Bogue calculations for cements used in this study	220
Table 6.3 Average particle size and particle size distribution for ash used herein.....	222
Table 6.4 Mortar mixture proportions for ASTM C1012 testing of cement C1.....	224
Table 6.5 Mortar mixture proportions for ASTM C1012 testing of cement C2.....	225
Table 6.6 Mixture proportions for LST and Isothermal Calorimetry	226
Table 6.7 Defined exposure conditions per ACI Table 19.3.1.1	228
Table 6.8 LST expansion results for cement C1 with 35% replacement of ashes F1-F3.....	229
Table 6.9 LST expansion results for cement C1 with 20% replacement of ashes F1-F3.....	231
Table 6.10 LST expansion results for cement C2 with 35% replacement of ashes F1-F3.....	233
Table 6.11 LST expansion results for cement C2 with 20% replacement of ashes F1-F3.....	235
Table 6.12 Maximum heats and corresponding gypsum contents for mix C1-F1(35).....	239
Table 6.13 Comparison of heat of hydration performance to Lerch’s guidelines	255
Table 6.14 Summary of AFt and AFm formation of two ages of mortar mixtures containing no gypsum for all mixtures with cement C1 and fly ash replacement amounts of 35%.....	257
Table 6.15 Summary of AFt and AFm formation of two ages of mortar mixtures containing no gypsum for all mixtures with cement C1 and fly ash replacement amounts of 20%.....	259
Table 6.16 Summary of AFt and AFm formation of two ages of mortar mixtures containing no gypsum for all mixtures with cement C2 and fly ash replacement amounts of 35%.....	260
Table 6.17 Summary of AFt and AFm formation of two ages of mortar mixtures containing no gypsum for all mixtures with cement C2 and fly ash replacement amounts of 20%.....	261
Table 6.18 Summary of QXRD results for mixtures C1-F1(35), C1-F2(35), and C1- F3(35).....	263
Table 6.19 Summary of QXRD results for mixtures C1-F1(20), C1-F2(20), and C1- F3(20).....	267

Table 6.20 Summary of QXRD results for mixtures C2-F1(35), C2-F2(35), and C2-F3(35)	271
Table 6.21 Summary of QXRD results for mixtures C2-F1(20), C2-F2(20), and C2-F3(20)	275
Table 6.22 Summary of expansion limits imposed by ASTM C 1157 and C 595	281
Table 6.23 Summary of ASTM C1012 mortar bar expansion results for mixture C1-F1(35)	281
Table 6.24 Summary of ASTM C1012 mortar bar expansion results for mixture C1-F2(35)	282
Table 6.25 Summary of ASTM C1012 mortar bar expansion results for mixture C1-F3(35)	283
Table 6.26 Summary of ASTM C1012 mortar bar expansion results for mixture C1-F1(20)	284
Table 6.27 Summary of ASTM C1012 mortar bar expansion results for mixture C1-F2(20)	285
Table 6.28 Summary of ASTM C1012 mortar bar expansion results for mixture C1-F3(20)	286
Table 6.29 Summary of ASTM C1012 mortar bar expansion results for mixture C2-F1(35)	287
Table 6.30 Summary of ASTM C1012 mortar bar expansion results for mixture C2-F2(35)	288
Table 6.31 Summary of ASTM C1012 mortar bar expansion results for mixture C2-F3(35)	289
Table 6.32 Summary of ASTM C1012 mortar bar expansion results for mixture C2-F1(20)	290
Table 6.33 Summary of ASTM C1012 mortar bar expansion results for mixture C2-F2(20)	291
Table 6.34 Summary of ASTM C1012 mortar bar expansion results for mixture C2-F3(20)	292
Table 6.35 Complete summary of ASTM C 1012 mortar bar expansion results for all 56 mixtures tested in this research study	293
Table 6.36 Summary of passing results of ASTM C 1012 testing that meet Lerch's recommendations for a properly retarded cement	309
Table 7.1 Cast-in-place concrete mixture proportions (per cubic yard)	317
Table 7.2 Amarillo weather conditions for 11/23/16.....	320

List of Figures

Figure 2.1 LWFA AC as a function of admixture concentration	16
Figure 2.2 LWFA ponding (left) and drying LWFA with cool air (right).....	17
Figure 2.3 LWFA ponding conditions	20
Figure 2.4 Central Texas Exposure Site in Austin.....	26
Figure 2.5 Texas Marine Exposure Site in Port Aransas	27
Figure 2.6 ASR exposure blocks and measurement points	30
Figure 2.7 Preheating process in environmental chamber with thermocouple system highlighted (left) and mixing of Cooked block (right).....	30
Figure 2.8 ASR exposure block form in new condition (left) and locations of exposure sites in Texas (right).....	31
Figure 2.9 Temperature profile for select blocks [$T(^{\circ}\text{F}) = T(^{\circ}\text{C}) \cdot 1.8 + 32$]	31
Figure 2.10 Exposure block temperature profile during first 48 hours [$T(^{\circ}\text{F}) = T(^{\circ}\text{C}) \cdot 1.8 +$ 32].....	32
Figure 2.11 DEF heat curing procedure for mortar bars based on Kelham (1996) method [$T(^{\circ}\text{F}) = T(^{\circ}\text{C}) \cdot 1.8 + 32$].....	34
Figure 2.12 Exposure blocks bulldozed as part of Hurricane Harvey cleanup process in Port Aransas	36
Figure 2.13 Exposure block bolts being bent (left) and bolt repaired by bending back (right).....	36
Figure 2.14 ASTM C128 cone test performed on LWFA	38
Figure 2.15 28-day compressive strength for Uncooked (left) and Cooked (right) mixtures with reactive aggregate FA1 as a function of lithium dosage	39
Figure 2.16 28-day compressive strength for Uncooked (left) and Cooked (right) mixtures with reactive aggregate FA2 as a function of lithium dosage	40
Figure 2.17 28-day compressive strength for LWFA Uncooked (left) and Cooked (right) mixtures with reactive aggregate FA1 as a function of lithium dosage	40
Figure 2.18 28-day compressive strength for LWFA Uncooked (left) and Cooked (right) mixtures with reactive aggregate FA2 as a function of lithium dosage	41
Figure 2.19 ASTM C1293 expansion over time for reactive aggregate FA1 with varying lithium dosages.....	42
Figure 2.20 ASTM C1293 expansion over time for reactive aggregate FA2 with varying lithium dosages.....	43
Figure 2.21 ASTM C1293 expansion over time for reactive aggregate FA1 with varying lithium dosages without control	43
Figure 2.22 ASTM C1293 expansion over time for reactive aggregate FA2 with varying lithium dosages without control	44

Figure 2.23 ASTM C1293 expansion over time for LWFA FA1 mixtures with varying lithium introductory methods	45
Figure 2.24 ASTM C1293 expansion over time for LWFA FA2 mixtures with varying lithium introductory methods	46
Figure 2.25 Difference in ASTM C1293 expansion over time between LWFA control (solid) and standard control (dashed) for FA1 aggregate.....	46
Figure 2.26 Difference in ASTM C1293 expansion over time between LWFA control (solid) and standard control (dashed) for FA2 aggregate.....	47
Figure 2.27 Expansion over time for Standard DEF mortar bar immersed in water (DEF only) with reactive aggregate FA1 with varying lithium dosages.....	48
Figure 2.28 Expansion over time for Standard DEF mortar bar immersed in water (DEF only) with reactive aggregate FA2 with varying lithium dosages.....	49
Figure 2.29 Expansion over time for LWFA DEF mortar bars immersed in water (DEF only) with reactive aggregate FA2 and with varying lithium introductory methods	49
Figure 2.30 Expansion over time for control mortar bars immersed in water (DEF only) with various forms of reactive aggregates.....	50
Figure 2.31 Expansion over time for Standard DEF mortar bar above water (ASR and DEF) with reactive aggregate FA1 with varying lithium dosages	51
Figure 2.32 Expansion over time for Standard DEF mortar bars above water (ASR and DEF) with reactive aggregate FA2 with varying lithium dosages	52
Figure 2.33 Expansion over time for Standard DEF mortar bar above water (ASR and DEF) with reactive aggregate FA1 with varying lithium dosages without control	52
Figure 2.34 Expansion over time for LWFA DEF mortar bars above water (ASR and DEF) with reactive aggregate FA2 and with varying lithium introductory methods.....	53
Figure 2.35 Expansion over time for control mortar bars above water (ASR and DEF) with various forms of reactive aggregates.....	53
Figure 2.36 Closeup of Figure 2.52	54
Figure 2.37 Comparison of expansion over time for isolated DEF vs. combined ASR + DEF mortar bars with varying aggregates.....	56
Figure 2.38 Comparison of expansion over time for isolated DEF vs. combined ASR + DEF mortar bars with LWFA FA2 aggregate	57
Figure 2.39 Comparison of expansion over time for DEF + ASR mortar bars and 1293 ASR concrete prisms with varying aggregates standing over water	57
Figure 2.40 Comparison of expansion over time for DEF + ASR mortar bars and 1293 ASR concrete prisms for LWFA mixtures standing over water	58
Figure 2.41: Reference data of exposure block expansion over time for three aggregates with varying reactivity (NR – nonreactive; MR – moderately reactive; HR – highly reactive). Blocks are in Uncooked (ASR) and Cooked (ASR + DEF) condition. (Drimalas and Folliard, 2020)	60

Figure 2.42 Exposure block expansion over time for FA1 aggregate mixtures in Cooked and Uncooked condition with varying lithium dosages	61
Figure 2.43 Exposure block expansion over time for FA1 aggregate in Cooked and Uncooked condition without lithium.....	61
Figure 2.44 Exposure block expansion over time for FA1 aggregate control mixtures in Uncooked condition. Includes reference data from older control specimen cast for previous projects.	62
Figure 2.45 Expansion data for Uncooked exposure blocks made with reactive aggregate FA2. Mixture Type III is control (no lithium) for FA2. All other mixtures were made with a Type I cement and contain various admixtures.....	64
Figure 2.46 Exposure block expansion over time for FA1 aggregate in Cooked condition (ASR + DEF) with varying lithium dosages	66
Figure 2.47 Exposure block expansion over time for FA2 aggregate in Cooked condition (ASR + DEF) with varying lithium dosages	66
Figure 2.48 Exposure block expansion over time for FA1 aggregate in Cooked condition (ASR + DEF) with varying lithium dosages without control.....	67
Figure 2.49 Exposure block expansion over time for FA2 aggregate in Cooked condition (ASR + DEF) with varying lithium dosages without control.....	67
Figure 2.50 Exposure block expansion over time for FA1 aggregate in Uncooked condition with varying lithium dosages	68
Figure 2.51 Exposure block expansion over time for FA2 aggregate in Uncooked condition with varying lithium dosages	68
Figure 2.52 Exposure block expansion over time for FA2 aggregate in Cooked condition with and without lithium in Texas Marine Exposure Site.....	69
Figure 2.53 Exposure block expansion over time for FA2 aggregate in Uncooked condition with and without lithium in Texas Marine Exposure Site.....	70
Figure 2.54 Exposure block expansion over time for LWFA FA1 in Cooked condition with varying lithium introductory methods.....	71
Figure 2.55 Exposure block expansion over time for LWFA FA2 in Cooked condition with varying lithium introductory methods.....	72
Figure 2.56 Exposure block expansion over time for LWFA FA1 in Uncooked condition with varying lithium introductory methods.....	72
Figure 2.57 Exposure block expansion over time for LWFA FA2 in Uncooked condition with varying lithium introductory methods.....	73
Figure 3.1 Marine Exposure Site in Port Aransas.....	95
Figure 3.2 Galvanized chain corroding & rubber tire (left), visible abrasion on block corners (middle), and galvanized chain failing (right)	98
Figure 3.3 Galvanic corrosion (left), loss of cross section (middle), and chain/bolt abrasion (right)	98
Figure 3.4 Wave lifted block off chain (left) and rope failure (right).....	99

Figure 3.5 Reinforced marine exposure block cross section schematic. Not to scale. (1 in. = 25.4 mm)	99
Figure 3.6 Marine exposure block materials.....	100
Figure 3.7 Marine exposure block casting (left) and curing (right).....	100
Figure 3.8 Lowering blocks (left), hanging blocks (middle), measuring blocks (right).....	101
Figure 3.9 ASTM G109 schematic (left), and corrosion concrete beam with visible salt deposits (right).....	102
Figure 3.10: Evident cracking on side and bottom of beam specimen (left), and confirmation of unintended corrosion at bottom layer of rebar due to salt solution leaking (right)	102
Figure 3.11 Sample schematic per ASTM C1556 (left), and test specimen being profiled (right).....	103
Figure 3.12 Sample plot of chloride profile for a given exposure time	107
Equation 3.4: Fitting Equation Based on Fick's Second Law of Diffusion (ASTM C1556).....	108
Figure 3.13 Half-cell potential measurement diagram ASTM C876 (left), Measurement on field specimen (right)	111
Figure 3.14 Saw-cutting corrosion beams (left), and rust staining visible after saw-cutting (right).....	113
Figure 3.15 Bottom portion of beam after saw-cutting (left), and profile grinding at rebar cover depth (right).....	114
Figure 3.16 Varying chloride loadings across surface (left), and chloride mapping system – rectangle indicates ponding area (right)	115
Figure 3.17 Visible crack in corrosion beam ponding area (left), and removal of top reinforcement bar from corrosion beam (right).....	117
Figure 3.18 Rebar visual rating example—after removal from corrosion beam (left sample) and after cleaning procedure (right sample)	117
Figure 3.19 Compressive strength at 28 days	118
Figure 3.20 Resistivity values after two years of storage	120
Figure 3.21 Revised resistivity values	120
Figure 3.22 Apparent chloride diffusion coefficients of lab samples	123
Figure 3.23 ASTM C1556 sum of squared errors for diffusion coefficients of lab samples.....	123
Figure 3.24 Selected chloride profiles for lab samples.....	124
Figure 3.25 Selected chloride content models for lab samples.....	124
Figure 3.26 G109 final half-cell potential measurements.....	126
Figure 3.27 Chloride mapping of select G109 samples	128
Figure 3.28 Examples of corrosion beam testing including rebar visual examination and rating, chloride content, and half-cell measurements.....	130

Figure 3.29 Marine exposure block half-cell measurements, initial values	131
Figure 3.30 Marine exposure block half-cell measurements, 16 months exposure.....	132
Figure 3.31 Marine exposure block half-cell measurements, 25 months exposure.....	132
Figure 3.32 Marine exposure block half-cell measurements, 37 months exposure.....	133
Figure 3.33 Apparent chloride diffusion coefficient of field samples	135
Figure 3.34 ASTM C1556 sum of squared errors for diffusion coefficients of field samples	136
Figure 3.35 Field sample chloride model—Product P (3 years exposure)	136
Figure 3.36 Field sample chloride model—Product D (3 years exposure).....	137
Figure 3.37 Exposure block visual examination: biological growth (left and middle) and rust staining (right)	138
Figure 4.1 Water beading on sample with topical sealer product IWR-C (bottom) when compared to sample without sealer (top)	151
Figure 4.2 Central Texas Exposure Site in Austin.....	153
Figure 4.3 Outdoors trough at Central Texas Exposure Site. Contains submerged and standing prisms exposed to soil doped with sodium sulfate.	154
Figure 4.4 Site 1 in Van Horn (sodium sulfate environment).....	154
Figure 4.5 Site 2 in Van Horn (calcium sulfate environment)—samples are placed in creek (right) below bridge (left)	155
Figure 4.6 Site 2 samples are stored inside a lobster cage below bridge (left) and samples are lifted to road level via bucket (right).....	155
Figure 4.7 Samples being rinsed (left) and measured (right).....	156
Figure 4.8 Rate of heat evolution from isothermal calorimetry on pastes with various admixtures	162
Figure 4.9 Cumulative heat from isothermal calorimetry on pastes with various admixtures	163
Figure 4.10 Concrete compressive strength at 28 days for OPC mixtures at 0.45 w/c (left) and 0.70 w/c (right)	164
Figure 4.11 Concrete compressive strength at 28 days for FA mixtures at 0.45 w/c	164
Figure 4.12 Resistivity at 28 days for OPC mixtures with various admixtures at 0.45 w/c (left) and 0.70 w/c (right)	166
Figure 4.13 Resistivity values at various ages for FA mixtures	166
Figure 4.14 ASTM C1585 absorption samples.....	168
Figure 4.15 Initial (left) and secondary (right) absorption rate per ASTM C1585 for FA mixtures with 0.45 w/.....	168
Figure 4.16 Initial absorption rate per ASTM C1585 for OPC mixtures with 0.45 w/c (left) and 0.70 w/c (right)	169

Figure 4.17 Secondary absorption rate per ASTM C1585 for OPC mixtures with 0.45 w/c (left) and 0.70 w/c (right)	169
Figure 4.18 Apparent chloride diffusion coefficient for various mixtures	171
Figure 4.19 Sum of squared errors for diffusion coefficient calculations per ASTM C1556	171
Figure 4.20 Concrete cube samples for NCHRP 244 Series II testing in drying condition	173
Figure 4.21 Mass gain summary per NCHRP 244 Series II for OPC mixtures with 0.45 w/c (left) and 0.70 w/c (right)	173
Figure 4.22 Mass change with time based on NCHRP 244 Series II conditioning for OPC mixtures with 0.45 w/c	174
Figure 4.23 Mass change with time based on NCHRP 244 Series II conditioning for OPC mixtures with 0.70 w/c	174
Figure 4.24 Sodium sulfate solution samples exhibiting minimal (left) and significant (right) loss of cohesion	176
Figure 4.25 Concrete prism expansion over time for mixtures exposed to standard sodium sulfate solution testing.....	177
Figure 4.26 Concrete prism expansion over time for mixtures exposed to cyclical sodium sulfate solution testing.....	178
Figure 4.27 Failed samples submerged in sodium sulfate trough.....	179
Figure 4.28 Concrete prism expansion over time for mixtures submerged in outdoors sodium sulfate trough	179
Figure 4.29 Samples standing in sodium sulfate trough	180
Figure 4.30 Concrete prism expansion over time for mixtures standing in outdoors sodium sulfate trough	181
Figure 4.31 Concrete prism expansion over time for mixtures submerged in calcium sulfate solution	182
Figure 4.32 Concrete prism expansion over time for mixtures submerged in outdoors calcium sulfate trough	183
Figure 4.33 Standard ASTM C1293 concrete prism expansion for various admixtures	184
Figure 4.34 Modified ASTM C1293 concrete prism expansion for various admixtures	185
Figure 4.35 ASR exposure block expansion over time for various product.....	186
Figure 4.36 Marine exposure block half-cell measurements, initial values	187
Figure 4.37 Marine exposure block half-cell measurements, 5 months exposure.....	187
Figure 5.1 Mortar bar 14-day expansion due to ASR per ASTM C1567 for various fly ash types and contents (Drimalas, 2019).....	196
Figure 5.2 Rate of heat evolution from isothermal calorimetry on SCM mortars with various admixtures	202

Figure 5.3 Cumulative heat from isothermal calorimetry on SCM mortars with various admixtures	202
Figure 5.4 Rate of heat evolution from isothermal calorimetry on SCM mortars with various dosages of nano-CSH admixture	203
Figure 5.5 Concrete compressive strength at 3 days for OPC (left) and SCM (right) mixtures	204
Figure 5.6 Concrete compressive strength at 28 days for OPC (left) and SCM (right) mixtures	205
Figure 5.7 Resistivity values at various ages	206
Figure 5.8 Apparent chloride diffusion coefficient for OPC (left) and SCM (right) mixtures	207
Figure 5.9 Sum of squared errors for diffusion coefficient calculations per ASTM C1556	208
Figure 5.10 ASTM C1567 mortar bar expansion for SCM mixtures	209
Figure 5.11 ASTM C1567 mortar bar expansion for delayed SCM mixtures with nano-CSH and without	210
Figure 5.12 ASTM C1293 concrete prism expansion for OPC mixtures	211
Figure 5.13 ASTM C1293 concrete prism expansion for SCM mixture	211
Figure 6.1 CaO – SiO ₂ – Al ₂ O ₃ ternary phase diagram [5] with mullite, anorthite, and ghelenite regions annotated by author	217
Figure 6.2 Fly ash glass distribution on CaO-SiO ₂ -Al ₂ O ₃ ternary phase diagram [15].....	221
Figure 6.3. Crystalline and amorphous oxide contents of fly ashes [15].....	223
Figure 6.3 LST expansion results for cement C1 with 35% replacement of ashes F1-F3.....	230
Figure 6.4 LST expansion results for cement C1 with 20% replacement of ashes F1-F3.....	232
Figure 6.5 LST expansion results for cement C2 with 35% replacement of ashes F1-F3.....	234
Figure 6.6 LST expansion results for cement C2 with 20% replacement of ashes F1-F3.....	236
Figure 6.7 LST expansion results for cement C2 with 20% replacement of ashes F1-F3.....	236
Figure 6.8 Heat evolution as a function of time [2]; additional annotations (in red) by the author of this report	238
Figure 6.9. Cumulative heat results from isothermal calorimetry of mix C1-F1(35).....	239
Figure 6.10. Heat of hydration and maximum heat curves for mixture C1-F1(35).....	240
Figure 6.11. Heat of hydration and maximum heat curves for mixture C1-F2(35).....	241
Figure 6.12. Heat of hydration and maximum heat curves for mixture C1-F3(35).....	242
Figure 6.13. Heat of hydration and maximum heat curves for mixture C1-F1(20).....	243
Figure 6.14 Heat of hydration and maximum heat curves for mixture C1-F2(20).....	244
Figure 6.15. Heat of hydration and maximum heat curves for mixture C1-F3(20).....	245
Figure 6.16 Heat of hydration and maximum heat curves for mixture C2-F1(35).....	246

Figure 6.17. Heat of hydration and maximum heat curves for mixture C2-F2(35).....	247
Figure 6.18 Heat of hydration and maximum heat curves for mixture C2-F3(35).....	248
Figure 6.19. Heat of hydration and maximum heat curves for mixture C2-F1(20).....	249
Figure 6.20 Heat of hydration and maximum heat curves for mixture C2-F2(20).....	250
Figure 6.21 Heat of hydration and maximum heat curves for mixture C2-F3(20).....	251
Figure 6.22. Typical heat of hydration curve.....	253
Figure 6.23. Heat of hydration curve meeting Lerch’s guidelines	254
Figure 6.24. Typical behavior observed in the maximum heat curves	256
Figure 6.25 Comparison of AFt and AFm formation of two ages of mortar mixtures containing no gypsum for all mixtures with cement C1 and fly ash replacement amounts of 35%	258
Figure 6.26. Comparison of AFt and AFm formation of two ages of mortar mixtures containing no gypsum for all mixtures with cement C1 and fly ash replacement amounts of 20%	259
Figure 6.27 Comparison of AFt and AFm formation of two ages of mortar mixtures containing no gypsum for all mixtures with cement C2 and fly ash replacement amounts of 35%	260
Figure 6.28. Comparison of AFt and AFm formation of two ages of mortar mixtures containing no gypsum for all mixtures with cement C2 and fly ash replacement amounts of 20%	261
Figure 6.29. Qualitative and Quantitative XRD analysis for mixture C1-F1(35)	264
Figure 6.30. Qualitative and Quantitative XRD analysis for mixture C1-F2(35)	265
Figure 6.31 Qualitative and Quantitative XRD analysis for mixture C1-F3(35)	266
Figure 6.32. Qualitative and Quantitative XRD analysis for mixture C1-F1(20)	268
Figure 6.33. Qualitative and Quantitative XRD analysis for mixture C1-F2(20)	269
Figure 6.34 Qualitative and Quantitative XRD analysis for mixture C1-F3(20)	270
Figure 6.35. Qualitative and Quantitative XRD analysis for mixture C2-F1(35)	272
Figure 6.36. Qualitative and Quantitative XRD analysis for mixture C2-F2(35)	273
Figure 6.37 Qualitative and Quantitative XRD analysis for mixture C2-F3(35)	274
Figure 6.38. Qualitative and Quantitative XRD analysis for mixture C2-F1(20)	276
Figure 6.39 Qualitative and Quantitative XRD analysis for mixture C2-F2(20)	277
Figure 6.40. Qualitative and Quantitative XRD analysis for mixture C2-F3(20)	278
Figure 6.41 Annotated typical characteristics corresponding to numbered list of observations.....	279
Figure 6.42. ASTM C1012 mortar bar expansion results for mixture C1-F1(35).....	282
Figure 6.43. ASTM C1012 mortar bar expansion results for mixture C1-F2(35).....	283
Figure 6.44. ASTM C1012 mortar bar expansion results for mixture C1-F3(35).....	284

Figure 6.45 ASTM C1012 mortar bar expansion results for mixture C1-F1(20).....	285
Figure 6.46. ASTM C1012 mortar bar expansion results for mixture C1-F2(20).....	286
Figure 6.47. ASTM C1012 mortar bar expansion results for mixture C1-F3(20).....	286
Figure 6.48. ASTM C1012 mortar bar expansion results for mixture C2-F1(35).....	287
Figure 6.49. ASTM C1012 mortar bar expansion results for mixture C2-F2(35).....	288
Figure 6.50. ASTM C1012 mortar bar expansion results for mixture C2-F3(35).....	289
Figure 6.51. ASTM C1012 mortar bar expansion results for mixture C2-F1(20).....	290
Figure 6.52. ASTM C1012 mortar bar expansion results for mixture C2-F2(20).....	291
Figure 6.53. ASTM C1012 mortar bar expansion results for mixture C2-F3(20).....	292
Figure 6.54 Comparison of expansion data from LST, QXRD analysis, and maximum heat curves for mixture C1-F1(35).....	296
Figure 6.55. Comparison of expansion data from LST, QXRD analysis, and maximum heat curves for mixture C1-F2(35).....	297
Figure 6.56. Comparison of expansion data from LST, QXRD analysis, and maximum heat curves for mixture C1-F3(35).....	298
Figure 6.57 Comparison of expansion data from LST, QXRD analysis, and maximum heat curves for mixture C1-F1(20).....	299
Figure 6.58 Comparison of expansion data from LST, QXRD analysis, and maximum heat curves for mixture C1-F2(20).....	300
Figure 6.59. Comparison of expansion data from LST, QXRD analysis, and maximum heat curves for mixture C1-F3(20).....	301
Figure 6.60. Comparison of expansion data from LST, QXRD analysis, and maximum heat curves for mixture C2-F1(35).....	302
Figure 6.61 Comparison of expansion data from LST, QXRD analysis, and maximum heat curves for mixture C2-F2(35).....	303
Figure 6.62 Comparison of expansion data from LST, QXRD analysis, and maximum heat curves for mixture C2-F3(35).....	304
Figure 6.63 Comparison of expansion data from LST, QXRD analysis, and maximum heat curves for mixture C2-F1(20).....	305
Figure 6.64 Comparison of expansion data from LST, QXRD analysis, and maximum heat curves for mixture C2-F2(20).....	306
Figure 6.65 Comparison of expansion data from LST, QXRD analysis, and maximum heat curves for mixture C2-F3(20).....	307
Figure 7.1 Metal deck specifications	314
Figure 7.2 Precast concrete panel specifications	315
Figure 7.3 Batch ticket.....	316
Figure 7.4 Bridge deck layout.....	319

Figure 7.5 Amarillo weather data for 11/23/16 from WeatherUnderground website.....	320
Figure 7.6 Loop 335 at BNSF RR inspection	321
Figure 7.7 Crack documentation and coring procedure	321
Figure 7.8 Typical cracks observed on Loop 335 bridge deck	322
Figure 7.9 Crack map—Loop 335 site.....	323
Figure 7.10 Coring area	324
Figure 7.11 Rebar struck while coring.....	325
Figure 7.12 Intersection of two precast panels below cast-in-place slab (left), and cracking visible throughout core and around aggregate (right)	325
Figure 7.13 Core from section with extensive cracking (left), and core from section with no cracking (right).....	326
Figure 7.14 Rebar placed at a depth of 3.5 in. from the top of slab (left), and rebar imprint at the bottom of core (right)	326
Figure 7.15 Reinforcement placement.....	327
Figure 7.16 Time of set testing [1,000 psi = 6.9 MPa]	331
Figure 7.17 Semi-adiabatic calorimetry (Q-Drum) on concrete cylinders [$T(^{\circ}\text{F}) = T(^{\circ}\text{C}) \cdot 1.8$ + 32]	332
Figure 7.18 Rate of heat evolution from isothermal calorimetry on sieved mortar.....	332
Figure 7.19 Rate of heat evolution from isothermal calorimetry on ternary blend paste samples without admixtures	334
Figure 7.20 Rate of heat evolution from isothermal calorimetry on ternary blend paste samples with admixtures	334
Figure 7.21 Rate of heat evolution from isothermal calorimetry on OPC paste samples with admixtures.....	335
Figure 7.22 Rate of heat evolution from isothermal calorimetry on paste samples with reference cement	335
Figure 7.23 Rate of heat evolution from isothermal calorimetry on paste samples with Amarillo cement.....	336
Figure 7.24 Mortar bar expansion with time per ASTM C1567 for Amarillo Coarse Aggregate with varying SCM contents	337
Figure 7.25 Mortar bar expansion with time per ASTM C1567 for Amarillo Fine Aggregate with varying SCM contents	337

List of Acronyms

AC	absorption capacity
ASR	alkali-silica reaction
C-S-H	calcium silicate hydrates
DEF	delayed ettringite formation
HRWR	high-range water-reducing
IWR	integral water repellent
LIME	Laboratory for Infrastructure Materials Engineering
LST	limewater submergence testing
LWFA	lightweight fine aggregate
MAE	mean absolute error
MWC	mixture water conditioner
NS	nano-silica
OPC	ordinary portland cement
QXRD	quantitative x-ray diffraction
RCPT	rapid chloride permeability test
SCM	supplementary cementing material
SD	surface dry
SF	silica fume
SG	specific gravity
SRA	shrinkage reducing admixture
TxDOT	Texas Department of Transportation
UTMSI	University of Texas at Austin Marine Science Institute
VMA	viscosity modifying admixture
w/c	water–cement ratio
XRD	x-ray diffraction
XRF	x-ray fluorescence

Chapter 1. Introduction and Scope

1.1. Introduction

The reinforced concrete infrastructure in Texas has been plagued by various durability-related issues over the years, including deterioration from alkali-silica reaction (ASR), delayed ettringite formation (DEF), corrosion of reinforcing steel, and excessive shrinkage cracking. For many of these problems, fly ash has been the remedy of choice; however, with changes in fly ash quality and quantity spurred by new emissions standards and changes in fuel sources, there is a concern that fly ash may not be as available or effective in the future. As such, there exists a need to evaluate other solutions to reinforced concrete durability besides the traditional use of fly ash (or other traditional supplementary cementing materials [SCMs]).

This report summarizes the findings from TxDOT Project 0-6906, *Chemical Solutions to Durability Studies*. This project, funded by the Texas Department of Transportation (TxDOT), was aimed at evaluating alternative, chemical solutions to durability problems, such as the use of corrosion inhibitors, ASR and/or DEF inhibitors, integral water repellants, and gypsum as an additive to improve sulfate resistance of Class C fly ash. This project started in January 2016 and was completed in August 2020. This report summarizes the overall results from this comprehensive research project, which includes both laboratory and outdoor exposure site evaluations.

1.2. Scope of Project

As part of this project, the research team reviewed and synthesized published literature related to chemical solutions to concrete durability problems. Based on this review, a wide range of materials were selected and procured for the project, including corrosion inhibitors (calcium nitrite, calcium nitrate, others), ASR and/or DEF inhibitors (lithium nitrate), integral water repellants, nanoparticles (silica and dispersible calcium silicate hydrates [C-S-H]), and gypsum as an additive to improve sulfate resistance of Class C fly ash. These materials were tested under a comprehensive laboratory testing program, with tests including heat of hydration, strength, electrical resistivity, corrosion potential, chloride diffusivity, sorptivity, and expansion (due to ASR, DEF, or sulfate attack). Corresponding field specimens were stored at three different outdoor sites in Texas and evaluated for ASR and/or DEF, as well as for corrosion potential (marine site). Lastly, the research team performed a forensic evaluation of a bridge deck in Amarillo, focusing on possible causes of cracking and remedies for future decks.

1.3. Outline of Report

This report is based on the MS thesis of Jeremy Wheelless (2018) and PhD dissertation of Bruno Fong-Martinez (2020). The project findings are organized into the following chapters:

- **Chapter 2** focuses on the use of lithium nitrate to mitigate expansions due to ASR and/or DEF in laboratory and field samples. The study also explored an alternate method of admixture introduction by incorporation within saturated lightweight fine aggregate (LWFA).
- **Chapter 3** investigates the use of corrosion inhibitors in reducing corrosion potential in reinforced concrete samples in the lab and at a marine exposure site in Port Aransas, TX.
- **Chapter 4** presents the results from a comprehensive evaluation of admixtures that are reported to reduce permeability. Various laboratory tests were used to methodically evaluate permeability parameters (sorptivity, chloride diffusion, electrical resistivity), while field samples were also cast to assess their ability to reduce deterioration.
- **Chapter 5** focuses on the use of products based on nanotechnology. These nano-based admixtures or nanomaterials are evaluated in a suite of laboratory transport and durability tests.
- **Chapter 6** focuses on the use of gypsum to improve the sulfate resistance of mortar and concrete containing Class C fly ash.
- **Chapter 7** presents a case study evaluating bridge deck cracking in Amarillo, TX. Some potential causes for the observed cracking are identified and suggestions for reducing future deck cracking are presented.
- **Chapter 8** summarizes the main conclusions from this project and identifies potential areas for future research.

Chapter 2. Effect of Lithium Admixture on ASR and DEF

This chapter will present the work performed pertaining to mitigating expansion due to ASR and/or DEF. As part of the study, one lithium nitrate admixture product was used at varying dosages with two reactive aggregates to determine its ability to reduce expansion due to ASR and/or DEF. Additionally, a novel admixture introductory method was employed with the goal of optimizing admixture effectiveness. Performance was assessed through the evaluation of lab (concrete prisms and mortar bars) and field (exposure blocks) specimens. The ability to compare results between large field samples and standard lab samples is particularly critical when dealing with ASR, as discrepancies have been observed with testing methods. Current testing results show an overall improvement in performance across lithium dosages and introductory methods. However, even at a sample age of four years, exposure block results are considered preliminary and differences between dosages and introductory methods may not become conclusive until later ages.

2.1. Background

This section includes pertinent background information related to ASR and DEF mechanisms, details regarding the use of lightweight aggregate for the time release procedure, and an overview of field samples and the outdoors exposure site.

2.1.1. Alkali-Silica Reaction

ASR is a major concrete durability problem that affects infrastructure worldwide. While ASR has been extensively studied since being identified in the 1940s by Stanton (1940), its precise mechanisms are not yet fully understood. The current literature includes relevant theories that have allowed the industry to recognize ASR as a significant concern and to an extent have provided appropriate guidance on how to prevent it. Like with other durability issues, the concrete industry has heavily relied on the use of SCMs to mitigate ASR deterioration. However, the risk of ASR will likely become more prevalent in the future as the use of fly ash diminishes. Facing future challenges, the industry is in dire need of new developments that will assist in the prevention, detection, and rehabilitation of structures affected by ASR. The background information on ASR presented is based on a review by Rajabipour et al. (2015).

2.1.1.1. Mechanism

ASR involves a deleterious internal process within concrete initiated by the reaction between hydroxyl ions in the pore solution and reactive forms of silica found in certain

aggregates. Hydroxyl ions attack unstable silica structures, forming an alkali-silica gel composed primarily of sodium, potassium, silica, and minor amounts of calcium. The ASR gel is susceptible to swelling in the presence of moisture, and internal pressures caused by the gel expanding can eventually surpass the concrete's tensile strength and cause cracking. Listed below are the four conditions that must be present for ASR to occur. Each condition will be further discussed below.

- Presence of reactive silica
- Presence of hydroxyl ions
- Presence of soluble calcium
- Presence of moisture

2.1.1.1.1. Reactive Silica

Silica (SiO_2) is one of the most abundant components on earth and is a key mineral present in aggregates worldwide. Certain aggregates contain amorphous forms of silica, which given their metastable state have a higher tendency to react.

Aggregates can be classified by reactivity as non-reactive, moderately reactive, highly reactive, or very highly reactive. The classifications are set in ASTM C1778 and are based on performance values as tested by ASTM C1260 or ASTM C1293.

Numerous variables regarding aggregate reactivity are still undetermined such as the effects of aggregate particle size, location and amount of reactive silica, and the presence of other mineral components.

Evidence of a pessimum effect has been observed with certain aggregates (Hobbs, 1988). In these cases, a certain level of silica content is optimal, and expansion can be suppressed by increasing or decreasing the aggregate content. Particle size can cause a similar pessimum effect (French, 1995).

Reactive silica may be present at the aggregate surface or deeper within the particle. This indicates that ASR gel may form not only at the aggregate-paste interface, but also within aggregates.

Aggregates vary widely and trends observed in a specific aggregate may not be present in others.

2.1.1.1.2. Hydroxyl Ions

A high concentration of alkalis (K^+ , Na^+ , Ca^+) exists in the concrete pore solution. These alkalis are counteracted to obtain charge balance by the presence of hydroxyl ions (OH^-). The presence of alkalis effectively determines the pH of the concrete, and the solubility of reactive silica increases at high pH values. Thus, enough alkalis are required for hydroxyl ions to attack the reactive silica.

Alkalis are mainly introduced into concrete through cement as it contains traces of potassium (K_2O) and sodium (Na_2O) oxides. The oxides can be quantified through x-ray fluorescence (XRF) as a percentage of cement mass. While there are two alkali components (sodium and potassium), for convenience these values are combined into an equivalent alkali value (Na_2O_{eq}) by converting the potassium oxide content into an equivalent sodium oxide content per Equation 2.1.

$$Na_2O_{eq} = Na_2O + 0.685 \cdot K_2O \quad \text{Eq. 2.1}$$

While the alkali loading is expressed in terms of sodium oxides, it should be noted that most cements have a higher potassium oxide content. Additionally, lab testing often boosts alkalis to promote the ASR reaction and sodium hydroxide (NaOH) is the preferred alkali employed. It is unclear whether the industry's choice of selecting one alkali over the other affects the overall ASR testing mechanism.

Alkalis may also be introduced through SCMs, aggregates, and external sources such as deicing salts or saltwater. However, alkali contents are typically only calculated as a function of cement content and may neglect alkali contribution from these additional sources, particularly due to uncertainties in the amount of alkalis released from sources other than portland cement.

2.1.1.1.3. Soluble Calcium

- The presence of soluble calcium is critical for the continuation of the ASR reaction. As the alkalis become involved in the formation of ASR gel, the pH of the pore solution will decrease accordingly. Soluble calcium can then replace the 'tied up' alkalis in the ASR gel through a cation exchange. This process, known as alkali recycling, effectively liberates alkalis and allows for further reactions to continue until all reactive silica or soluble calcium are exhausted.
- It is also theorized that the presence of calcium changes the potential for reaction and expansion of the ASR gel. Experimental tests have found that a steady supply of calcium is needed for significant expansion to occur. In the absence of calcium,

silica can dissolve without causing expansion. However, the exact mechanisms involved have not been determined yet.

- Soluble calcium is readily available in most concretes as calcium hydroxide, $\text{Ca}(\text{OH})_2$, which is widely present in cement paste. The dissolution of calcium hydroxide involves calcium undergoing a cation exchange with alkalis in the ASR gel and hydroxyl being released into the pore solution, increasing pH. According to Hansen (1944), the process can be observed as cement paste visibly darkens with consumption of calcium hydroxide.
- Through alkali recycling, expansions have been reported to continue in concrete dams for decades (Thomas, 2001).

2.1.1.1.4. Moisture

- ASR gel is hygroscopic and will swell based on moisture availability.
- Various theories exist detailing the ASR gel swelling mechanisms.
- A minimum internal relative humidity of 80% has been reported to be required for expansive ASR (Stark, 1991).

2.1.1.2. Mitigation Methods

ASR mitigation methods can target the previously mentioned conditions and prevent the reaction by removing or reducing harmful factors. However, given the complexity of the reaction, employing a combination of methods may provide the best performance. Various mitigation methods are presented below. The focus of this study is the use of lithium admixtures as a mitigation method.

2.1.1.2.1. Reactive Silica

- If possible, the use of non-reactive aggregates is recommended. However, this is often not feasible as aggregate sources are limited and shipping aggregate is not economical.
- If a producer has ample experience with aggregates, such as chert, that exhibit a pessimum effect, an overloading of reactive aggregate could be used to curb expansion. However, this would require careful consideration and prudent technical guidance.

2.1.1.2.2. Hydroxyl Ions and Calcium Solubility

- Alkali content can be limited to maintain hydroxyl ions in check. A sliding scale of equivalent alkali loadings is used in AASHTO R80 and ASTM C1778, with lower alkali loading thresholds specified for aggregates with higher levels of reactivity. The alkali loading thresholds used in the recommended practices (AASHTO and ASTM) only account for alkali contribution from cement; therefore, other considerations must be made for potential alkali contributions from SCMs, aggregates, admixtures, and the environment.
- The use of SCMs promotes pozzolanic activity, which reduces alkalinity, consumes calcium hydroxide, binds alkalis, and reduces permeability. All of these factors reduce the potential for ASR expansion.

2.1.1.2.3. Moisture

- Limiting concrete's exposure to moisture can deter ASR. Indoor, dry concrete is generally considered protected from damage. Outdoor concrete conditions may be improved by providing drainage, sealers or waterproofing membranes, and cladding. An internal relative humidity below 80% is generally deemed sufficient to limit ASR-induced expansion (Pedneault, 1996).

2.1.1.2.4. Lithium

- The use of lithium was first reported to mitigate ASR by McCoy and Caldwell (1951). Various forms of lithium have been tested and the current preferred form is lithium nitrate (LiNO_3) as it does not raise pH like other lithium compounds do.
- Lithium admixtures are notoriously costly since lithium is a scarce material in high demand from various industries.
- The use of lithium has been empirically proven to mitigate expansion due to ASR. However, its mechanisms are not precisely understood. The following theories are listed by Rajabipour et al. (2015) as possible lithium effects:
 - o Reduce dissolution of silica
 - o Prevent the formation of alkali-silica gel
 - o Reduce repulsive forces between the colloidal gel particles of ASR, thus reducing swelling

- o Incorporation of lithium into the alkali-silica gel, altering its properties and expansion
- Tremblay et al. (2010) proposed that the most likely mitigation theory involved the increased chemical stability and reduced dissolution of reactive silica in the presence of lithium.
- A dosage based on a molar ratio of lithium to alkalis $[Li]/[Na + K]$ of 0.74 is based on McCoy and Caldwell's work. This dosage will be referred to as the 100% dosage in this study. However, it is now understood that there is no single dosage rate that is applicable across all cases, as different aggregates have been shown to require different lithium dosages to mitigate ASR expansion (Tremblay et al., 2004). There is also no established correlation between aggregate reactivity and required dosage.
- Drimalas et al. (2012) found that 75% of the standard dosage rate was able to mitigate expansions of the same aggregate used in the present study up to an age of 3,500 days.
- Tremblay et al. (2007) observed that, as early as 7 to 28 days, the molar ratio of $[Li]/[Na + K]$ in the pore solution decreased to approximately half of the initial ratio, indicating that lithium ions are preferentially incorporated in hydration products over alkalis.
- The external application of lithium has been explored as a repair option but has seen limited success given the low penetration depth (Thomas et al., 2007).
- Hargis et al. (2013) explored the concept of aggregate passivation by soaking reactive fine aggregates in lithium hydroxide (LiOH) solution. The goal was to create a lithium silicate passivation layer by reacting aggregate with LiOH. Expansion in accelerated mortar testing (ASTM C1260) was effectively reduced through this method, and it was suggested that silica dissolution becomes hindered by the presence of the passivation layer on the aggregate surface.

2.1.2. Delayed Ettringite Formation

DEF is an internal form of sulfate attack causing expansion within the cement paste. The mechanism presents itself in concrete that has been subject to high temperatures at an early age and involves the reformation of ettringite in hardened concrete at later stages. A critical concrete temperature of 70 °C (158 °F) has been identified as a general threshold for DEF. Structures susceptible to temperatures in this range include precast members that are steam-cured as well as mass concrete elements that can self-produce considerable amounts of heat as hydration occurs.

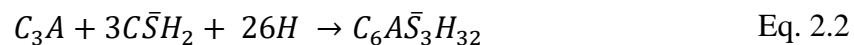
2.1.2.1. Mechanism

The production of ettringite is a normal occurrence in the early hydration process created by the reaction of calcium aluminates with gypsum (Equation 2.2). Its presence is innocuous at early stages when the paste is in a plastic state. Moreover, ettringite can further react with calcium aluminates to create monosulfate (Equation 2.3), and both components can exist in the cement paste without creating distress. Even the growth of large ettringite crystals due to Ostwald ripening can be accommodated in voids and cracks present throughout the matrix. DEF, however, involves the formation of ettringite at later stages within small pores in hardened concrete (Equation 2.4), which induces stress as expansive ettringite crystals are reformed.

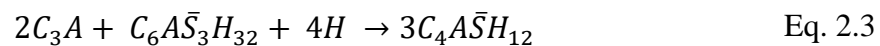
During the early hydration process, increased temperatures can cause the incongruent dissolution of ettringite, releasing alumina and sulfate. Simultaneously, the formation of C-S-H is accelerated by the elevated temperatures and leads to the entrapment of alumina and sulfate within the C-S-H layers. While the alumina is firmly bound within the C-S-H layers, the sulfate is loosely attached and is described as being adsorbed (Taylor et al., 2001). At later ages and at ambient temperatures, sulfates are slowly released back into the pore solution and can reform as a delayed version of ettringite in the hardened concrete. The delayed reformation of ettringite in the presence of moisture leads to severe expansion, which will be present throughout the cement paste. The expansion of the paste is assumed to produce cracks both in the paste itself and at the aggregate interface. The new development of cracks provides space for the further recrystallization of ettringite and portlandite without significantly contributing to expansion. The growth of ettringite crystals at the paste-aggregate interface effectively creates sulfate rings around aggregate particles.

The presence of DEF is often seen in conjunction with ASR. Generally, ASR is considered to take place before DEF and act as a catalyst for it (Diamond and Ong, 1994). It is believed that the pH reduction associated with active ASR stabilizes ettringite and promotes DEF.

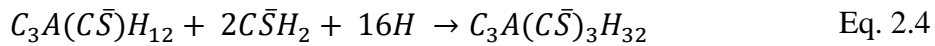
Calcium Aluminates + Gypsum → Ettringite (AFt)



Calcium Aluminates + Ettringite → Monosulfate (AFm)



Monosulfate + C-S-H Released Sulfate → Ettringite (AFt) [*Expansive*]



2.1.2.2. Mitigation Methods

Since the occurrence of DEF can be connected to a critical temperature, mitigation methods focus on maintaining concrete temperatures below the threshold. From a materials perspective, the use of adequate SCMs can lower the heat of hydration, modify microstructure, and effectively prevent DEF. In a precast plant, proper quality control practices should prevent from temperatures increasing to dangerous levels, and in a mass concrete field setting, the use of cooling pipes within the concrete may be employed.

Ekolu et al. (2007) observed the dual effectiveness of lithium nitrate in mitigating expansions due to isolated DEF cases and cases of both ASR and DEF. Further work by Ekolu et al. (2017) provided updated evidence of lithium's continuous effectiveness after monitoring samples for six years. According to observations, it was suggested that in the presence of lithium, sulfate and alumina do not become entrapped within the C-S-H layers during heat-curing. Instead, lithium is preferentially absorbed by C-S-H. However, it is noted that this effect alone could not account for the reduction in expansion as the dissolved sulfate and alumina at elevated temperatures would be free to reform into ettringite once ambient temperature and moisture conditions were restored. Thus, it is theorized that some of the lithium ions remaining in the pore solution may form a modified ettringite product that is less or non-expansive. This could involve the replacement of Ca ions in delayed ettringite with lithium ions, similar to the cation exchange mechanism proposed for the mitigation of ASR with the use of lithium.

2.1.3. Lightweight Aggregate

Lightweight aggregate is a manufactured product created by heating specific raw materials capable of bloating during the heating process (Chandra and Berntsoon, 2002). As the aggregate expands and bloats, air bubbles form and the porosity of the aggregate increases, allowing it to have a decreased density and increased absorption capacity (AC). The use of lightweight aggregates can reduce concrete density and consequently structure dead loads. Additionally, the increased AC is used to introduce internal curing water into concrete. The use of internal curing provides enhanced hydration and can reduce potential for shrinkage (Bentz and Weiss, 2010). As a reference, the standard fine aggregate used in this study has a specific gravity (SG) of 2.6 and AC below 1%, while the expanded shale LWFA used has property values of 1.9 and 20%, respectively. Given that moisture absorption in LWFA

is a time-dependent process, the term “saturated surface dry” (SSD) would be incorrect to use. Therefore, in accordance with the related literature (Holm et al., 2004), the term “surface dry” (SD) will be used instead in the case of LWFA.

2.1.3.1. Effects of Lightweight Aggregate on ASR

LWFA is known to inherently have high contents of alumina and silica. These properties have promoted the study of finely ground LWFA as a pozzolanic material (Dahl et al., 2007). Furthermore, the use of LWFA has shown the ability to decrease ASR expansion (Bremner et al., 2007). This beneficial effect is independent from the use of lithium and is theorized to be a result of pozzolanic activity and dilution of the pore solution (Li et al., 2018).

Li et al. (2018) found that the use of LWFA decreased alkalinity in the pore solution while increasing the alumina concentration. The reduction in alkalinity is not believed to be a result of dilution in the pore solution from the release of internal curing water. Instead, it is theorized that ions (Na^+ , K^+ , OH^-) from the pore solution can diffuse into the relatively neutral solution inside the LWFA pores. Conversely, alumina from the LWFA is believed to leach into the pore solution as the two components react. Additionally, reaction products, likely C-A-S-H type, were observed within LWFA pores and are considered to be evidence of pozzolanic activity between the LWFA, pore solution, and surrounding cement. The creation of these products involves alkalis and hence further reduces the alkali availability for ASR at an early age.

The presence of soluble alumina has been known to mitigate ASR expansion. A review by Rajabipour et al. (2015) provides the following summary of theories for the role of alumina in mitigating ASR:

- Reduced rate of silica dissolution from aggregates by adsorption of alumina on the surface of reactive silica and/or by the formation of a diffuse zeolite barrier
- Reduced pore solution pH by the formation of C-A-S-H, which improves alkali binding capacity over C-S-H
- Reaction with and consumption of portlandite to form calcium aluminate phases
- Reduced swelling of ASR gel
- Denser pore structure and reduced permeability

2.2. Experimental Investigation

The ASR/DEF testing series consisted of evaluating the effect of lithium admixture dosage, aggregate type, and exposure conditions on expansion due to ASR, DEF, or a combination of both. Two sources of fine aggregates were used, each with a different level of reactivity, to examine the admixture effectiveness based on aggregate reactivity. For each mixture, large field specimens were cast in conjunction with standard laboratory samples to establish correlation.

Lab samples consisted of concrete prisms of 75 mm (3.0 in.) square cross-section and 285 mm (11.25 in.) in length, mortar bars of 25 mm (1.0 in.) square cross-section and 285 mm (11.25 in.) in length, and concrete cylinders of 100 mm (4.0 in.) diameter by 200 mm (8.0 in.) in length. Field samples, or exposure blocks, consisted of large concrete cubes with 38.1 cm (15.0 in.) sides.

DEF was intentionally promoted in test samples by using a mixture design with high cement content and an ASTM C150 Type III cement (with increased fineness), along with preheating of batch materials and heat curing of the blocks. For field samples, the label of Uncooked and Cooked was used. Uncooked samples were made with reactive aggregates and were thus prone to ASR, while Cooked blocks underwent heat treatment in addition to containing reactive aggregates, making them susceptible to both ASR and DEF. Lab samples were stored in various conditions in order to isolate cases of ASR only, DEF only, or ASR and DEF.

2.2.1. Materials

2.2.1.1. Cementitious

A Type III cement was used for all mixtures in the ASR/DEF series. Chemical composition of the cement was analyzed by XRF and results are summarized in Table 2.1. The XRF analysis was performed by TxDOT at the Cedar Park Campus. Based on Blaine testing performed, the Type III cement was found to have a fineness value of 575 m²/kg.

Table 2.1 Cement chemical composition (%) by mass

	SiO ₂	Al ₂ O ₃	Fe ₂ O ₃	CaO	SO ₃	MgO	K ₂ O	Na ₂ O	Na ₂ O _e
ASTM Type III	19.68	5.65	2.23	64.57	4.25	1.17	0.96	0.15	0.78

2.2.1.2. Aggregates

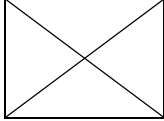
Two reactive fine aggregates were used for testing. While both aggregates are classified as “very highly reactive” in accordance with ASTM C1778, based on their ASTM C1293 expansion values, one aggregate is significantly more reactive than the other. The more

aggressive reactive fine aggregate was obtained from a source in El Paso, TX and is labeled as FA1. The lesser reactive aggregate was obtained from Robstown, TX and is labeled as FA2.

One source of non-reactive limestone coarse aggregate from San Antonio, TX was used and is labeled as CA. The non-reactive coarse aggregate was not sieved and fractioned as stated in ASTM C1293 Section 7.2.3 since no behavior difference was expected based on aggregate size. Additionally, it should be noted that the coarse aggregate used was from the bottom of an aggregate pile and contained noticeable amounts of dust on its surface. This factor is theorized to have contributed to the low slumps obtained when mixing.

LWFA from Streetman, TX in the form of expanded shale was used for the Time Release series and is labeled as LWFA. A 24-hour prewetting procedure was used for saturating the aggregate. The LWFA desorption value used was referenced from previous research by Castro et al. (2011). Table 2.2 summarizes aggregate properties. Desorption values are typically not relevant to normal weight aggregates and thus were not included.

Table 2.2 Aggregate properties

Aggregate	Absorption Capacity	SG - SSD	Desorption
FA1	0.7%	2.59	
FA2	0.7%	2.62	
CA	3.1%	2.47	
LWFA	20.0%	1.89*	

*SD condition based on 24-hour prewetting

2.2.1.3. Admixtures

A polycarboxylate-based high-range water-reducing admixture (HRWR) with an SG of 1.08 was used in dosages ranging from 3 to 9 fl. oz. per 100 lbs. of cement (oz./cwt). Uncooked (ASR only) mixtures required smaller dosages (3–4.5 oz./cwt) than Cooked (ASR and DEF) mixtures (6 oz./cwt). However, for the LWFA mixtures, dosages for both cases increased to 6 oz./cwt for Uncooked mixtures and 9 oz./cwt for Cooked mixtures.

A 50% sodium hydroxide (NaOH) solution was used to boost the concrete alkali loading up to the required 1.25% $\text{Na}_2\text{O}_{\text{eq}}$ level by mass of cement, as stated by ASTM C1293. For every pound of 50% NaOH solution used, batch water was reduced by 0.5 pounds to maintain the target water–cement ratio (w/c).

A lithium nitrate (LiNO_3) admixture with a concentration of 30% and SG of 1.2 was utilized at various dosages. Water reduction instructions from the manufacturer indicate that for every pound of admixture included, 0.7 pounds of water must be removed from the batch water to maintain the target w/c. Admixture dosage, as described by the manufacturer

and shown in Equation 2.6, is based on the alkali content of the cement and the amount of the cement in the mixture. There is no consideration made for aggregate reactivity in determining the dosage. A sample calculation is included below for what will be referred to as the 100% dosage (4.87 gal/yd³).

$$Dosage \left(\frac{lb}{yd^3} \right) = \frac{Cement \left(\frac{lb}{yd^3} \right) * Alkali Content(\%) * Dosage Multiplier}{100} \quad \text{Eq. 2.6}$$

$$Cement Content per ASTM C1293 = 708.0 \frac{lb}{yd^3}$$

$$Cement Alkali Content by Mass per ASTM C1293 = 1.25\%$$

$$Dosage Multiplier = 0.55$$

$$Sample Calculation: \frac{708.0 * 1.25 * 0.55}{100} = 4.87 \frac{gal}{yd^3} = 48.7 \frac{lb}{yd^3}$$

2.2.2. Time Release Method

The novel approach for introducing lithium admixture into concrete consisted of using saturated LWFA. While saturated LWFA has been widely used for purposes of internal curing (Holm et al., 2004), its use as an alternative method of admixture introduction is far more limited. Bentz (2005) proposed the concept and named it FLAIR (Fine Lightweight Aggregates as Internal Reservoirs). His work focused on introducing shrinkage reducing admixtures (SRA) via FLAIR and showed potential. The concept is particularly appealing when considering admixtures such as lithium that are known to become tied up within the early hydration products. Thus, the purpose of saturating the LWFA with lithium is to theoretically ‘protect’ lithium from becoming entrapped within early hydration products. Once early hydration is finalized, ideally the lithium would be released from within the LWFA pores in a ‘time release’ manner similar to the internal curing process. This could allow lithium to maintain its initial molar ratio at later stages and thus increase its effectiveness in the long term. While the concept itself is simple and guidelines are available in the literature regarding internal curing (Bentz et al., 2005), the use of a chemical admixture in lieu of water drastically alters the situation. In practice, the use of admixture saturated LWFA is as exciting as it is problematic. Given the lack of previous established research and guidelines on the subject, numerous assumptions were made throughout the testing process. Indeed, much further research is needed to validate this novel concept. A detailed description of the assumptions and limitations used by the researchers is included in this section.

2.2.2.1. Absorption

Special considerations were made to account for the fact that LWFA will inherently absorb a chemical admixture differently from water. Assuming that standard aggregate properties are known (AC, SG-SD, and desorption value), it is important to investigate how these properties will change when admixtures are absorbed instead of water. Spragg et al. (2011) examined how concrete absorbed various solutions containing deicing salts. They observed that the deicing solutions were absorbed at a reduced rate and mentioned that the reduction was related to the square root of the ratio of surface tension and viscosity. Preliminary testing performed for this study appeared to indicate that AC was indeed reduced when ponding the aggregate in lithium admixture as compared to water ponding. Correspondingly, when the aggregate was ponded in a diluted solution of the admixture, the AC increased. The commercial lithium admixture used has a 30% concentration by mass of solution. For the dilution tests, the admixture was further diluted to 20%, 15%, and 10% concentrations with the addition of deionized water. The aggregate was then ponded in solutions of varying concentration for 24 hours prior to AC testing as per ASTM C128. A detailed description of testing procedures is included further in this section. The preliminary results indicate that AC could indeed be affected by specific properties of the absorbed solution. AC values obtained are shown in Figure 2.1, where water ponding is considered as 0% concentration and the standard admixture is considered as 30% concentration. From Figure 2.1, it is observed that the data can be highly variable, even for repeat tests at the same concentrations (data points at 0% and 30% concentration). Moreover, it is possible that the standardized test used to obtain AC values may not be valid or applicable for admixture absorption.

Additionally, some consideration should be given to the composition of the actual solution being absorbed by the aggregate. Considering that the admixture itself is a solution composed of 70% water and 30% lithium nitrate by mass, it may be the case that the aggregate preferentially absorbs a diluted version of the solution. That is, the aggregate could be more readily absorbing the water portion within its pores while the lithium nitrate portion remains on the aggregate surface. For the purposes of the research it was assumed that the aggregate absorbed the admixture in the same proportions as its original composition. Assuming this, however, also has implications regarding the SG properties of the aggregate. If the aggregate contains a denser liquid than water within its pores, then its SG-SD will theoretically be higher than when absorbing water. Nevertheless, test values for SG-SD of aggregate saturated with lithium show minimal difference from that of water saturation. This could potentially be due to a seemingly lower AC with the use of admixtures. That is, while the liquid being absorbed is denser, there is less of it being absorbed, and, thus, the opposing factors result in a negligible effect on SG-SD.

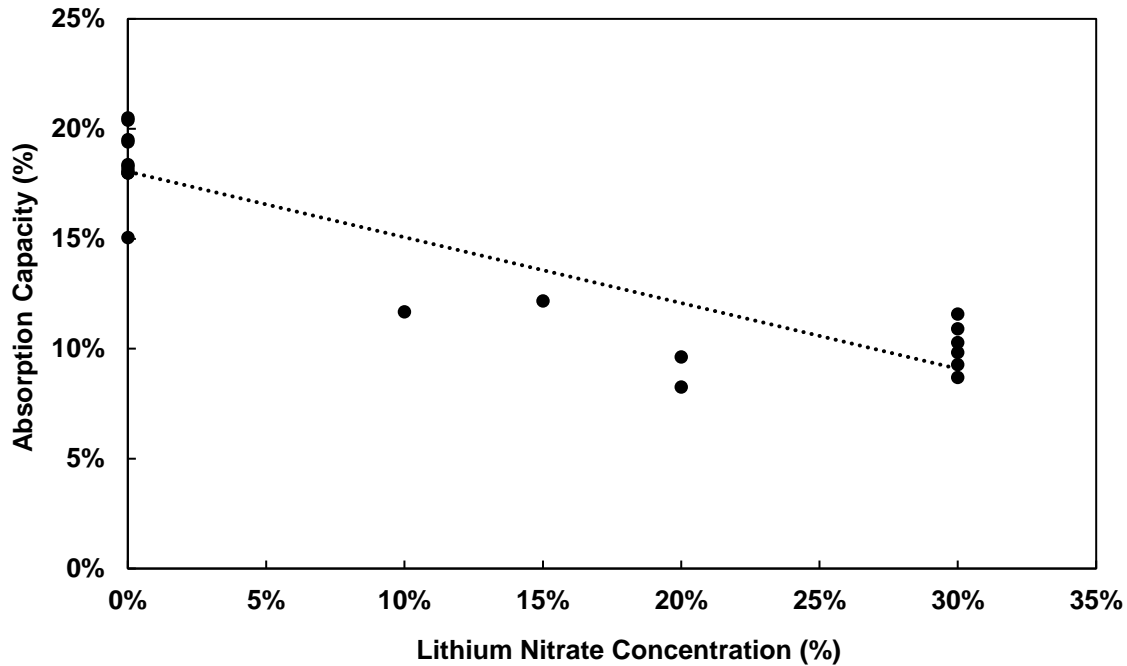


Figure 2.1 LWFA AC as a function of admixture concentration

2.2.2.2. Absorption Capacity Test (ASTM C128) Adapted to LWFA

The following paragraph details the procedure, based on ASTM C128, used to determine LWFA AC when saturating with lithium admixture. As previously mentioned, this test was repeated for different levels of admixture concentration by increasing the water content of the ponding solution. For all cases, the aggregate was oven-dried, allowed to cool down, and then submerged in solution for 24 hours. Aggregate was ponded in enough solution so that a visible layer of solution was standing above the aggregate (Figure 2.2). Following the ponding period, the aggregate was decanted by placing it on top of a #200 sieve and allowed to drain on its own for a few minutes.

The aggregate was then manually dried on top of the #200 sieve by using a heat gun set on cool mode to blow room temperature air while aggregate was continuously stirred by hand (Figure 2.2). This drying method allowed for the excess water to easily drain through the sieve. While a small portion of fines also passed through the sieve and were lost, it was assumed that these fines do not significantly contribute to AC properties of the aggregate. Research by Castro et al. (2011) found that larger aggregate particles tend to have larger pores that are easier to fill and are, therefore, more influential in determining absorption. At several intervals during the drying process, the cone test, as described by ASTM C128, was performed on the aggregate to determine if the SD condition had been reached. The manual drying process typically took two to three hours to reach the SD state. Given the

variability and labor-intensive nature of having to manually stir and blow dry for hours for each sample, a more automated method is highly recommended for future testing.

Once the aggregate reached the SD condition, it was weighed and placed in an oven overnight at 105 °C (221 °F). The dry aggregate was weighed the following day. The loss of mass was assumed to be solely attributed to the evaporation of water from the admixture solution. That is, the mass lost from oven drying represented 70% of the mass of admixture absorbed by the SD aggregate. Thus, a 30% solid mass of lithium nitrate was assumed to be left in the sample. Upon visual inspection the oven dried material exhibited traces of solid remains on its surface. For the cases using a diluted solution with lower concentration levels, the water loss represented (100 – Concentration)% of the mass of admixture absorbed. AC was then calculated based on Equation 2.5, in which the *Admixture Absorbed* term is used as previously described and the *Oven Dry Sample* parameter must only account for the dry mass of the aggregate, i.e., the mass of assumed solid lithium remaining in the pores must be subtracted.

$$AC(\%) = \frac{\text{Admixture Absorbed (mass)}}{\text{Oven Dry Sample (mass)}} \quad \text{Eq. 2.5}$$

Considering the many factors involved and the overall uncertainty in calculating a definitive AC when saturating with admixtures, it was decided that mixture proportions would be based on aggregate properties obtained when testing with only water. While this decision disregards the previously described admixture AC testing, it allows for a consistent set of values to be used throughout. Therefore, the AC, desorption, and SG at SD values used in mixture proportioning lithium saturated LWFA were obtained from standardized tests performed with water only.



Figure 2.2 LWFA ponding (left) and drying LWFA with cool air (right)

2.2.2.3. Batching and Mixing Procedure

The procedure used to saturate LWFA with lithium admixture for concrete mixing is described in this section. Firstly, the amount of lithium that must be introduced into the system via LWFA was determined. Only one dosage was employed so mixtures contained either 0% or 100% of the standard dosage. This quantity, however, must be increased to account for the desorption property of the aggregate. That is, while the aggregate may absorb a certain amount of liquid, only a portion of that amount is able to be released based on relative humidity conditions. Thus, the total admixture mass was introduced through a certain amount of LWFA based on its AC and desorption value. Typical mixtures required around 169 kg/m^3 (285 lb./yd^3) of oven-dry LWFA in order to accommodate a 100% lithium dosage of approximately 34 kg/m^3 (57 lb./yd^3). The relatively high amount of LWFA required is a result of the considerable amount of admixture recommended by the dosage equation (Equation 2.6). Subsequently, the required mass of LWFA was converted into an equivalent volume based on its SG-SD value. For concrete mixtures, this equivalent LWFA volume was then removed from the non-reactive coarse aggregate proportions. Approximately 25% of the non-reactive coarse aggregate volume was replaced by LWFA.

During the batching procedure, the necessary amount of oven-dry LWFA was placed in a bucket and ponded with enough admixture for there to be a visible layer of standing solution at the top. The admixture used for ponding was used in its original condition without dilution. For there to be a visible layer of liquid solution standing above the aggregate, roughly an amount of solution equivalent to 45% of the aggregate's oven-dry mass was required. While this process would be highly impractical and uneconomical at large scales, it was done to ensure that enough solution was available for maximum absorption. If only an amount of solution equal to the LWFA AC had been added (~20%), it is likely that absorption would not have been uniform. The LWFA was ponded for 24 hours prior to mixing.

Following the ponding procedure, a small opening at the bottom of the bucket was used for decanting the excess solution while carefully avoiding the loss of aggregate. The bucket was decanted by gravity for ten minutes. The remaining material was subsequently weighed. At this point, the material mass was assumed to include admixture-saturated aggregate as well as excess admixture on the aggregate surface. The theoretical mass of the admixture-saturated aggregate was used to back calculate the amount of excess admixture on the aggregate surface. The mix water content was then reduced to account for the excess moisture on the aggregate surface. The water reductions, however, accounted for only 70% of the excess solution on the aggregate surface since the remaining portion was considered as lithium nitrate. This process potentially introduces a slightly higher dosage of lithium than intended due to the excess admixture on aggregate surfaces. For the purposes of this research this additional amount of admixture was neglected due to its nominal amount.

Following these steps, the LWFA was then mixed as a standard aggregate in accordance with ASTM C192. It should be noted that further water reductions were not made to account for the lithium inside of the aggregate pores. It was assumed that, like with internal curing, the lithium within the aggregate pores does not contribute to the batch water or affect the ultimate w/c (Castro et al., 2011).

2.2.2.4. Ponding Conditions and Controls

The principal objective in introducing lithium via saturated LWFA is to evaluate and compare its effectiveness to the standard introductory method, i.e., introducing it in the batch water. To fully capture this behavior two different controls must be used for reference: one to evaluate the effect of LWFA on ASR and/or DEF independent of lithium and another evaluate the effect of lithium introduction method on ASR and/or DEF. The presence of the two controls allows for the accurate examination of the effect of lithium in the presence of LWFA and, more importantly, the influence of lithium introduction method. The four ponding conditions utilized to study these effects are illustrated in Figure 2.3. A comparison between Control 2 and Time Release/Solution Ponding mixtures can appropriately examine the advantages of one introductory method over the other. It should be noted that only the first three conditions were utilized in concrete mixtures, as the fourth condition was later added to subsequent mortar mixtures based on observations from the concrete mixtures.

After casting the LWFA concrete mixtures, it became evident that ponding aggregate in an excess of admixture per the time release method would be utterly impractical in a large scale. Therefore, an additional ponding scenario was employed in the subsequently cast DEF LWFA mortar mixtures. The new ponding condition recognized that the lithium admixture at a 100% dosage is costly enough and utilizing the admixture itself as a ponding solution would be prohibitively expensive. Thus, the fourth ponding condition would instead attempt to optimize the effectiveness of a 100% dosage by saturating the aggregate in a combined solution of admixture and water. The various ponding conditions are illustrated in Figure 2.3. The ellipses drawn within the aggregate particles represent the intended contents of the LWFA pores: internal curing water for Conditions 1 and 2 (blue), lithium admixture for Condition 3 (green), and a combination of water and lithium admixture for Condition 4 (mixed).

2.2.2.4.1. LWFA Ponding Conditions

- Control 1: LWFA saturated with water as in internal curing. No lithium added. 0% dosage.

- Control 2: LWFA saturated with water as in internal curing. 100% lithium dosage added in batch water.
- Time Release: LWFA saturated with 100% lithium dosage.
- Solution Ponding: LWFA saturated with a combined solution of water and lithium. 100% lithium dosage. *Condition only used in mortar bar mixtures.

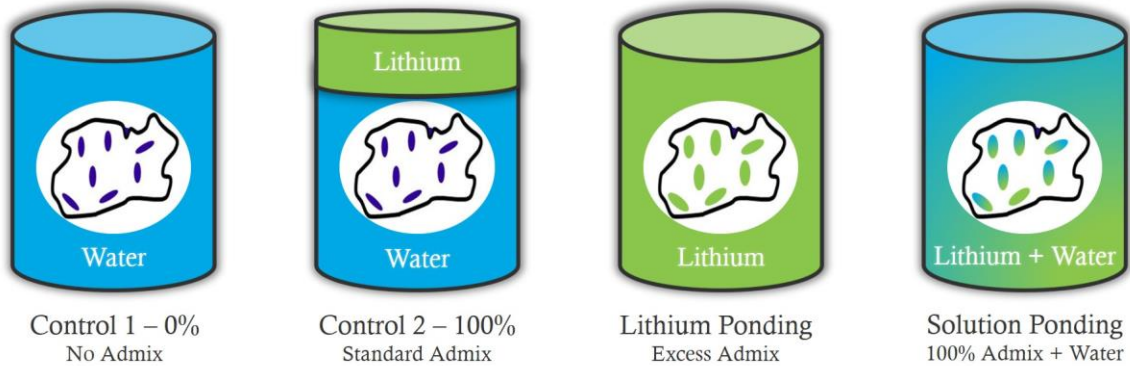


Figure 2.3 LWFA ponding conditions

2.2.3. Mixture Proportions

2.2.3.1. Primary Concrete Matrix

Mixture proportions complied with ASTM C1293 requirements. The standard concrete mixtures (Mixtures 1–10 on Table 2.4) included 420 kg/m³ (708 lb./yd³) of cement, 176 kg/m³ (297 lb./yd³) of water (w/c = 0.42), 1062 kg/m³ (1790 lb./yd³) of non-reactive coarse aggregate, and 625 kg/m³ (1053 lb./yd³) of reactive aggregate FA1 or 628 kg/m³ (1059 lb./yd³) of reactive aggregate FA2. Aggregate proportions are based on an oven-dry condition.

High dosages, up to 200% of the standard dosage, of lithium admixture were used throughout the project. Previous research (Eklolu et al., 2007) theorized that high dosages may be required to mitigate expansion due to both ASR and DEF. Alkali content was boosted per ASTM C1293 specifications using a 50% NaOH solution. The boosting procedure provides an equivalent alkali loading of 5.3 kg/m³ (8.9 lb./yd³), which far exceeds recommended limits used to prevent ASR (~1.8 kg/m³) [~3.0 lb./yd³]. Water reductions were made based on the addition of lithium and NaOH solution.

Typical batch volumes were around 0.03 m³ (2.75 ft³) and included 3 prisms, 3 cylinders, and 1 exposure block. Slumps tended to be low (50–100 mm) [2–4 in.] even after the addition of superplasticizers. Factors that could have contributed to this include the high

cement content, use of Type III cement, dusty coarse aggregate, and the preheating process for the Cooked mixtures.

2.2.3.2. LWFA Concrete Matrix

Mixture proportions for LWFA concrete mixtures (Mixtures 11–16 on Table 2.4) differed slightly as a portion of the non-reactive coarse aggregate was replaced by the LWFA. The level of replacement was based on the quantity of LWFA needed to introduce a 100% lithium dosage via the ‘time release’ method. LWFA mixtures had around 25% of the coarse aggregate volume replaced by an equivalent volume of LWFA. Control 1 and Control 2 mixtures were ponded in an amount of water equal to the batch water plus the internal curing water for 24 hours prior to mixing. Internal curing water is not considered to affect the effective w/c ratio and therefore no further water reductions were made. The specific batching and mixing procedures are detailed in Section 2.2.2.3.

2.2.3.3. Primary Mortar Matrix

Mixture proportioning for DEF mortar bars was based on ASTM C1260, with mixtures cast with both reactive aggregates, FA1 and FA2. The mortar was not doped with a sodium hydroxide solution as in ASTM C1293 and lithium dosage was solely based on alkali contribution from the cement. Water reductions were made according to the dosage of lithium admixture used. The mortar was proportioned to be 1 part cement to 2.25 parts fine aggregate by mass. The fine aggregate was brought to an oven-dry condition and was subsequently sieved, washed, and graded based on the requirements stated by ASTM C1260. Typical batches were made for 12 mortar bars (135 in³). Sample proportions for a 4-mortar bar mixture are included in Table 2.3.

Table 2.3 ASTM C1260 Aggregate Gradation

Gradation for DEF Testing for 4 mortar bars			
Fine Aggregate	Retained on Sieve #	Mass (%)	Quantity (g)
	#8	10%	132.0
	#16	25%	330.0
	#30	25%	330.0
	#50	25%	330.0
	#100	15%	198.0
	Total Fine Aggregate →		
Cement →			586.7
Water →			275.5

2.2.3.4. LWFA Mortar Matrix

In the concrete LWFA mixtures the non-reactive coarse aggregate was replaced at a fixed volume by the LWFA, leaving the amount of reactive fine aggregate intentionally unchanged. In mortar, however, either the cement or the reactive aggregate must be replaced by the LWFA, and any change in these proportions will affect the alkali/silica ratio, which could alter reactivity potential. The least intrusive scenario determined was to replace a portion of the reactive fine aggregate with the LWFA. The replacement level was minimized by only requiring enough LWFA for the assigned lithium dosage to be introduced into the mixture. While this effectively decreased the amount of reactive aggregate per unit volume of mortar, the same ratio of silica/alkali was maintained throughout mixtures. LWFA mortar mixtures had around an 18% volume of reactive fine aggregate replaced by an equivalent volume of LWFA.

Mortar bars for the LWFA DEF series were cast using only the less reactive aggregate, FA2. The LWFA used to replace some of the mortar sand was ponded in a series of four different solutions, as previously described in Section 2.2.2.4 (Figure 2.3). The same mixture proportions were used for the LWFA DEF mortar bars as was done for the Primary Mortar Matrix (Section 2.2.3.3), apart from a partial replacement of reactive sand with LWFA. The reactive sand was replaced at an equivalent rate by reducing equal proportions of each specified aggregate gradation. Water reductions were made according to the dosage of lithium admixture used. For the Control 1 and 2 ponding conditions, the dry LWFA was ponded in an amount of water equal to the batch water plus the internal curing water for 24 hours prior to mixing. Conversely, Condition 3 involved ponding in an excess of pure lithium admixture. Careful consideration went into detailing Condition 4 as a diluted form of the admixture was intended to be absorbed by the aggregate. Since it was preferred to maintain a substantial admixture concentration in the diluted solution, the amount of water was minimized. From previous experience, it was found that the dry LWFA required ~45% of its own mass as solution for liquid to be visible on top and to promote uniform absorption. Therefore, a similar approach was utilized for Condition 4. The following example provides rough quantities detailing Condition 4: 700 g of oven-dry LWFA were ponded in 300 g of solution, which was comprised of 140 g of lithium admixture and 160 g of water. If the AC of the aggregate is estimated to be 20%, it was assumed that 140 g of the diluted solution would be absorbed by the 700 g of aggregate and that the remaining 160 g of diluted solution would be part of the batch water.

Given the variability in how the LWFA was ponded, calorimetry and strength testing were performed on the DEF LWFA mixtures to ensure a comparable w/c was maintained. The data show a comparable level of heat of hydration and strengths at various ages that suggests a comparable w/c was achieved through the various ponding scenarios.

2.2.4. Test Matrix

2.2.4.1. Concrete

The primary testing matrix is composed of 16 concrete mixtures with varying aggregates, lithium admixture dosages, Cooked/Uncooked conditions, and exposure locations. The test matrix, listed on Table 2.4, was used for casting concrete exposure blocks, prisms, and cylinders.

Each of the 16 mixtures was cast in a Cooked and Uncooked condition. For example, Mixture 4 includes two exposure blocks, 4C (Cooked) and 4U (Uncooked). The test matrix can be further detailed as follows:

- The first eight mixtures (Mixtures 1–8) contain the two different reactive fine aggregates with various dosages of lithium (0%, 75%, 100%, and 150%). The corresponding exposure blocks for these mixtures are located at the Central Texas Exposure Site.
- Mixtures 9 and 10 are repeat mixtures of Mixtures 5 and 7, respectively. These mixtures, however, have their corresponding exposure blocks located at the Texas Marine Exposure Site.
- Mixtures 11–16 refer to the concrete mixtures containing saturated LWFA, including the testing of two reactive aggregates at 0% and 100% lithium. The exposure blocks for these mixtures are located at the Central Texas Exposure Site.

Table 2.4 Concrete test matrix

Mixture #	Mixture ID	Aggregate	Lithium	Cooked/Uncooked	Location	Date Mixed
1	1C	FA1	0%	Cooked	UT Exp	3/7/2016
	1U			Uncooked		
2	2C	FA1	75%	Cooked	UT Exp	3/15/2016
	2U			Uncooked		
3	3C	FA1	100%	Cooked	UT Exp	3/15/2016
	3U			Uncooked		
4	4C	FA1	150%	Cooked	UT Exp	3/30/2016
	4U			Uncooked		
5	5C	FA2	0%	Cooked	UT Exp	4/29/2016
	5U			Uncooked		
6	6C	FA2	75%	Cooked	UT Exp	5/24/2016

Mixture #	Mixture ID	Aggregate	Lithium	Cooked/Uncooked	Location	Date Mixed
	6U			Uncooked	UT Exp	5/24/2016
7	7C	FA2	100%	Cooked	UT Exp	5/24/2016
	7U			Uncooked	UT Exp	5/24/2016
8	8C	FA2	150%	Cooked	UT Exp	5/31/2016
	8U			Uncooked	UT Exp	5/31/2016
9	9C	FA2	0%	Cooked	Port A	5/12/2016
	9U			Uncooked	Port A	5/10/2016
10	10C	FA2	100%	Cooked	Port A	5/10/2016
	10U			Uncooked	Port A	5/10/2016
11	11C	SAT – FA1	0%	Cooked	UT Exp	7/21/2016
	11U			Uncooked	UT Exp	6/6/2016
12	12C	SAT – FA1 Standard Admix	100%	Cooked	UT Exp	7/26/2016
	12U			Uncooked	UT Exp	6/9/2016
13	13C	SAT – FA1 Time Release	100%	Cooked	UT Exp	7/18/2016
	13U			Uncooked	UT Exp	6/16/2016
14	14C	SAT – FA2	0%	Cooked	UT Exp	7/21/2016
	14U			Uncooked	UT Exp	6/6/2016
15	15C	SAT – FA2 Standard Admix	100%	Cooked	UT Exp	7/26/2016
	15U			Uncooked	UT Exp	6/9/2016
16	16C	SAT – FA2 Time Release	100%	Cooked	UT Exp	7/18/2016
	16U			Uncooked	UT Exp	7/19/2016

2.2.4.2. Mortar

The DEF mortar bar test matrix includes 12 unique mixtures, as listed on Table 2.5. The first eight mixtures include the two reactive aggregates with various dosages of lithium admixture (0%, 100%, 150%, and 200%). The last four mixtures evaluate only the less reactive aggregate, FA2, with the use of LWFA and lithium at 0% and 100% dosages. Each of the 12 mortar mixtures was stored in three different storage conditions as follows:

- Immersed in limewater at 23 °C (to leach alkalis, prevent ASR, but trigger DEF)
- Immersed in limewater + lithium (50/50 by volume) at 23 °C (lithium added in soak solution to minimize lithium leaching)

- Stored above water at 38 °C as in ASTM C1293 (to promote both ASR and DEF, based on previous work)

Table 2.5 DEF mortar bar test matrix

Mixture ID	Aggregate	Lithium	Condition	Date Mixed
J1-2	FA1	0%	Oven Limewater Li+Limewater	6/5/2017
J2	FA1	100%	Oven Limewater Li+Limewater	6/6/2017
J3	FA1	150%	Oven Limewater Li+Limewater	6/8/2017
J4	FA1	200%	Oven Limewater Li+Limewater	6/21/2017
W1-2	FA2	0%	Oven Limewater Li+Limewater	6/5/2017
W2	FA2	100%	Oven Limewater Li+Limewater	6/6/2017
W3	FA2	150%	Oven Limewater Li+Limewater	6/8/2017
W4	FA2	200%	Oven Limewater Li+Limewater	6/21/2017
WL1	SAT - FA2	0%	Oven Limewater Li + Limewater	6/12/2017
WL2	SAT - FA2 Standard Admix	100%	Oven Limewater Li + Limewater	6/12/2017
WL3	SAT - FA2 Time Release	100%	Oven Limewater Li + Limewater	6/14/2017
WL4	SAT - FA2 Solution Ponding	100%	Oven Limewater Li + Limewater	6/14/2017

2.2.5. Specimens

2.2.5.1. Field Specimens – Exposure Blocks

2.2.5.1.1. Overview and Exposure Site

Casting large exposure blocks has been a proud tradition and staple of the University of Texas at Austin Laboratory for Infrastructure Materials Engineering (LIME) for many years. The main idea behind the exposure blocks/field samples is to create a more representative sample that realistically mimics the behavior of an actual field structure. Placing the blocks in an outdoor environment exposes them to realistic conditions, cycling through the seasons, and provides a more accurate scenario than the typical accelerated lab setup. Additionally, the large sample size reduces the leaching of alkalis, which is a key concern in ASR lab testing. The exposure blocks are used to measure concrete expansion over time and are visually assessed.

LIME researchers have established exposure sites throughout the state of Texas. Each of the site locations was strategically chosen to study the effect of environmental and climatic conditions on concrete durability. The main site, known as the Central Texas Exposure Site and shown in Figure 2.4, is at LIME's location in Austin, TX and is used as a reference point. Additional specimens were also placed at the Texas Marine Exposure Site, shown in Figure 2.5, located at the University of Texas at Austin Marine Science Institute (UTMSI) in Port Aransas.



Figure 2.4 Central Texas Exposure Site in Austin



Figure 2.5 Texas Marine Exposure Site in Port Aransas

2.2.5.1.2. Description

Exposure blocks (38.1 cm [15.0 in.] cubes) were cast for each of the 16 mixtures listed on Table 2.4. Each mixture involved the casting of two specimens, one in the Cooked condition and another in the Uncooked condition (described later in this section), for a total of 32 blocks. Exposure blocks were used to measure expansion of concrete over time as well as to provide a visual condition assessment. Stainless steel bolts were embedded into the concrete with a portion of the bolt protruding from the block. The exposed end of the bolt was previously ‘tapped’ to create an indentation for the measuring device. The distance between two given bolts was monitored over time to measure expansion. Each block contained 16 bolts: four in the front and back faces, two in the left and right faces, and four on the top face. These points allow for 10 expansion measurements across different directions. Figures 2.6 and 2.8 show general details about the blocks.

To create the ASR and ASR + DEF cases, the exposure blocks were differentiated as Cooked (DEF + ASR) and Uncooked (ASR only). The destabilization of ettringite responsible for DEF occurs when concrete is exposed to a presumed critical temperature of 70° C for approximately 12 hours in its early age. Therefore, to create these conditions within the Cooked exposure blocks the following measures were taken:

- Cement and aggregate were preheated to 60 °C (140 °F) for 24 hours before mixing.
- Batch water was preheated to 38 °C (100 °F) for 24 hours before mixing.

- Following casting, exposure blocks were placed in an environmental chamber set to 60 °C (140 °F).
- To generate and retain heat, insulated forms were used, and layers of heavy blankets were placed on the blocks while they were in the 60 °C (140 °F) environmental chamber.
- Burlap and blankets were kept wet throughout to provide moisture during curing.
- Thermocouples were embedded within the block, one at the bottom and another at mid-height, to monitor internal concrete temperature.
- Exposure blocks were kept inside the environmental chamber at 60 °C (140 °F) for first 24 hours.
- Following the first 24 hours, the environmental chamber was turned off and its door was left slightly ajar. Block was kept inside to let it cool down slowly and avoid risk of thermal shock.
- At 48 hours, the block was removed from the environmental chamber and demolded.

Figure 2.7 illustrates the preheating process. Figures 2.9 and 2.10 include the block temperature profiles acquired from thermocouples embedded within the concrete. The plotted values represent the average readings between the thermocouples inserted at mid-height and bottom of the form. Given the heavy layers of insulation, no significant difference between thermocouple placement was noticed. Most thermocouples were removed upon demolding at 48 hours; however, in some cases they were left longer to monitor the effect of demolding. For example, Mixtures 2C, 3C, and 5C were demolded at later stages, allowing them to further cool down gradually, and did not exhibit the sudden temperature drop seen in Mixtures 8C and 9C in Figure 2.9. Additionally, the temperature profile for one Uncooked block (14U) was measured as a reference and is also shown in plots. Figure 2.10 focuses on the temperature profile during the first 48 hours, where it can be observed that the Cooked blocks surpassed the DEF critical temperature of 70 °C (158 °F) for several hours. Notes and observations from the plots are included below as a summary.

Notes:

- Most thermocouples were disconnected and stopped logging temperatures after approximately 48 hours. However, a few exceptions were made.

- Mixtures 8C and 9C show a subsequent temperature drop caused by demolding at 48 hours. That is, blocks were demolded, but thermocouples were left recording to examine temperature behavior beyond demolding.
- Due to scheduling issues, Mixtures 2C and 3C were demolded at 72 hours. Mixture 5C was demolded at 96 hours. The effect of this can be observed in the slow temperature decrease as opposed to the sharper drop when demolded at 48 hours as seen in Mixtures 8C and 9C.
- Data for an Uncooked mixture (14U) is shown for comparison. In contrast, the Uncooked blocks are batched from materials stored at room temperature and are demolded after 24 hours.

Observations:

- All Cooked mixtures plotted were able to reach and maintain the critical temperature of 70 °C (158 °F) for a minimum of 12 hours.
- A slight reduction in the temperature gradient is seen starting at 24 hours. This is the time at which the oven is turned off. An even greater temperature drop was observed after demolding the Cooked blocks at 48 hours.
- Temperature data were not recorded for Mixtures 1C, 10C, 11C, 12C, 13C, 14C, 15C, and 16C. Thermocouples were not available for Mixture 1C. For the remaining mixtures (10C–16C), enough data had been collected to confirm that the blocks were reaching the critical temperature for the desired time. Therefore, temperatures were not further recorded.

After demolding, exposure blocks were wrapped in wet burlap and covered in plastic to allow for proper curing. Specimens remained indoors at 23 °C (73 °F) and were cured until they reached an age of 7 days. Following this, initial measurements were made, and blocks were placed outdoors at the Central Texas Exposure Site. Blocks belonging to Mixtures 9 and 10 were placed at the Texas Marine Exposure Site in Port Aransas at an age of 83 days. Subsequent measurements were made periodically. To minimize the effect of expansion due to temperature differentials, blocks are preferably measured at a temperature 23 °C (73 °F) and with cloud cover.

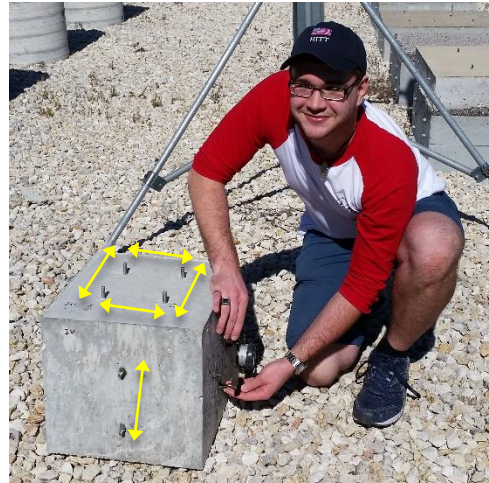
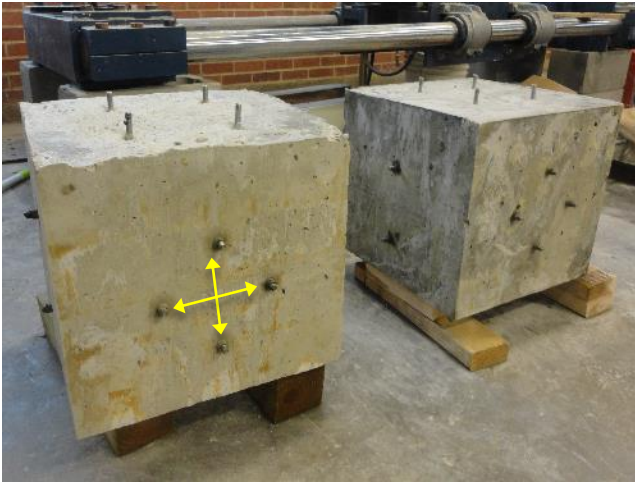


Figure 2.6 ASR exposure blocks and measurement points



Figure 2.7 Preheating process in environmental chamber with thermocouple system highlighted (left) and mixing of Cooked block (right)

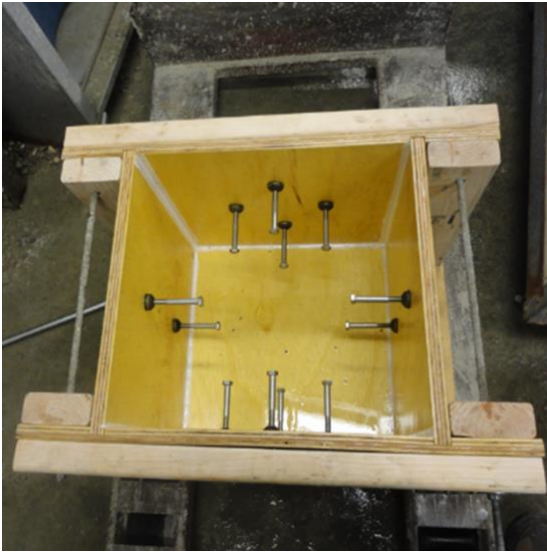


Figure 2.8 ASR exposure block form in new condition (left) and locations of exposure sites in Texas (right)

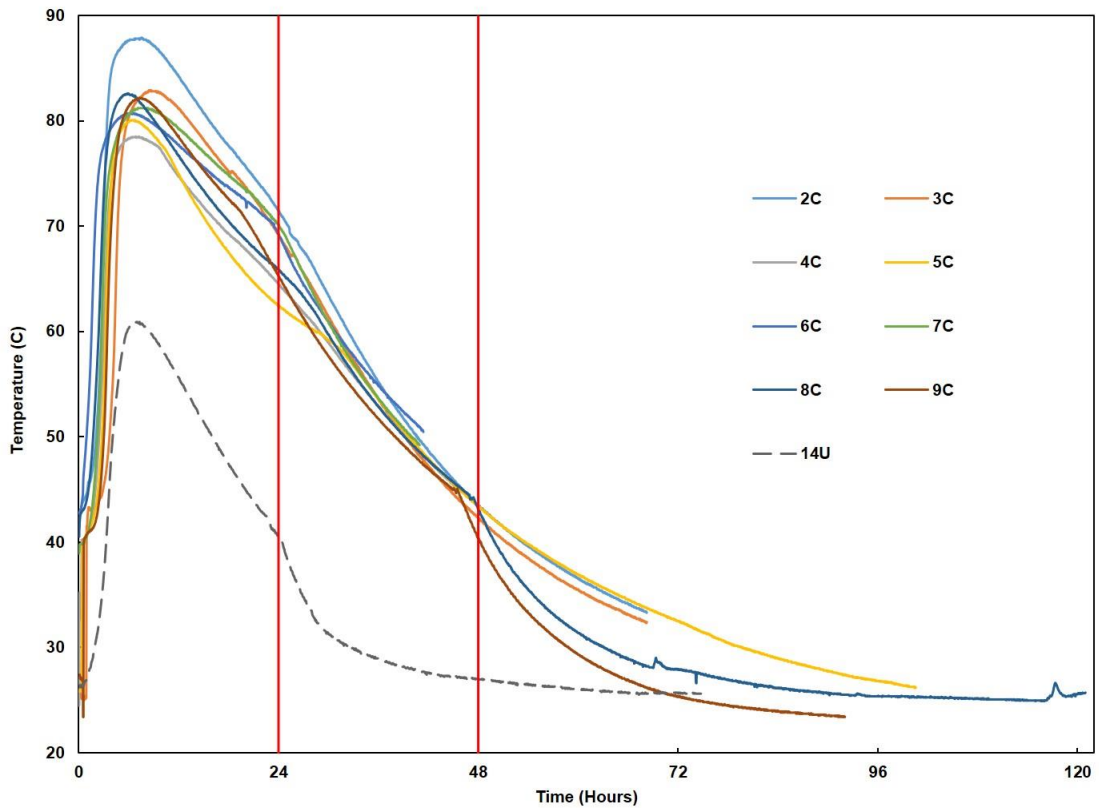


Figure 2.9 Temperature profile for select blocks [$T(^{\circ}F) = T(^{\circ}C) \cdot 1.8 + 32$]

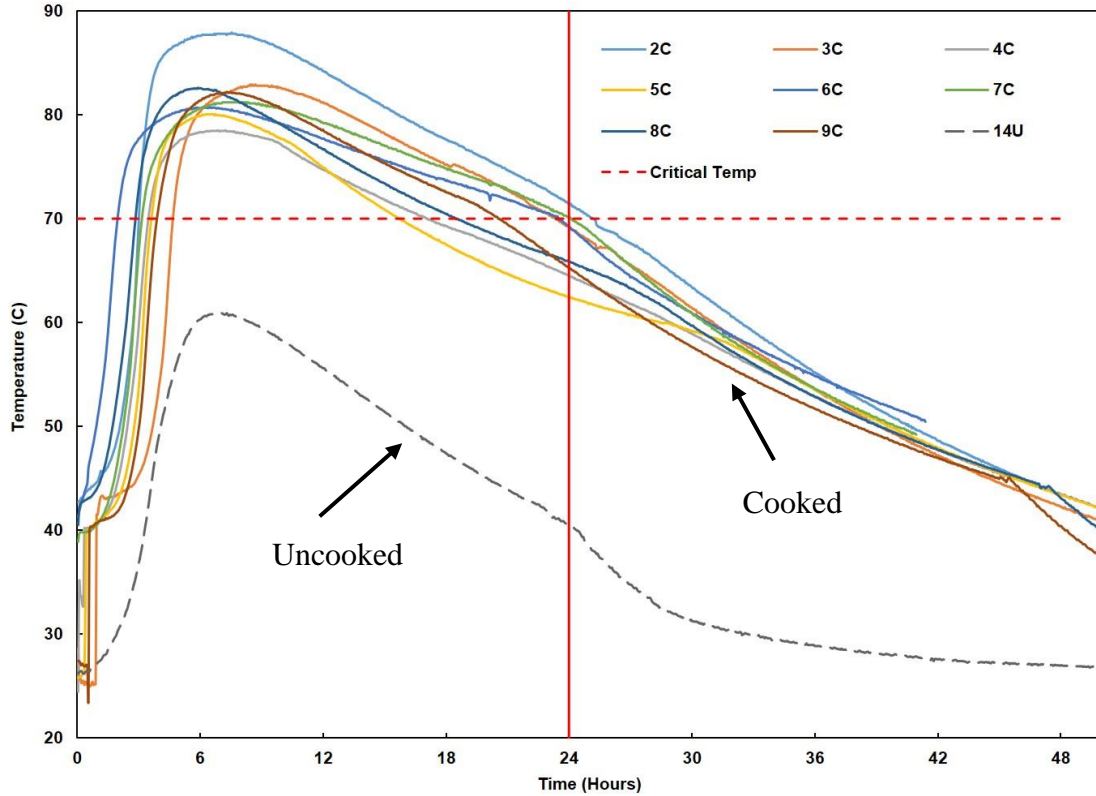


Figure 2.10 Exposure block temperature profile during first 48 hours [$T(^{\circ}F) = T(^{\circ}C) \cdot 1.8 + 32$]

2.2.5.2. Lab Specimens – Concrete Cylinders

In conjunction with every exposure block, a set of 3 concrete cylinders of 100 mm (4.0 in.) diameter by 200 mm (8.0 in.) in length was cast for quality control purposes in accordance with ASTM C31. Cylinders were demolded after 24 hours, placed in a fog room, and tested in compression at 28 days in accordance with ASTM C39. While compressive strength is not a key factor in this study, it was used as a general indicator for concrete quality and consistency. Given that the same w/c and mixture proportions were used across all mixtures, similar strengths were expected. Additionally, compressive strength was used to examine the influence of lithium dosage on the effective w/c and the effect of LWFA internal curing on strength.

2.2.5.3. Lab Specimens – Concrete Prisms

One set of 3 concrete prisms of 75 mm (3.0 in.) square cross-section and 285 mm (11.25 in.) in length was cast with each of the Uncooked mixtures to be tested for expansion per ASTM C1293. It should be noted that the concrete prism samples were cast only for the Uncooked (ASR only) mixtures. Given the small sample size, concrete prisms were not

expected to develop sufficient heat to reach the critical DEF temperature even if placed in the 60 °C (140 °F) environmental chamber. Heat-cured mortar bars were cast as the equivalent lab sample for the Cooked mixtures.

Prisms were demolded at 24 hours and initial measurements were made. Prisms were subsequently stored at 38 °C (100 °F) and measured periodically in accordance with ASTM C1293. The objective for the concrete prism test was to examine the effect of lithium dosage on mitigating expansion due to solely ASR and determining a correlation with its corresponding field sample. Results from previous exposure blocks have indicated discrepancies between lab and field samples, typically with lab samples passing within the test time frame but with field samples failing at later stages.

2.2.5.4. Lab Specimens – DEF Mortar Bars

In terms of developing DEF, a benefit of casting large samples such as the exposure blocks is their ability to create and maintain a large amount of heat during the early hydration stages. For the Cooked mixtures, while the oven itself was only set to 60 °C (140 °F), the heat of hydration created by the large sample allowed it to reach internal concrete temperatures above 80 °C (176 °F). In comparison, a small lab sample such as a concrete prism placed in the same oven would not be able to generate enough heat to reach the critical temperature needed to decompose ettringite and trigger DEF. For this reason, a separate testing procedure was implemented to create the lab sample equivalent of the Cooked (ASR and DEF) exposure blocks.

While there is no established, standardized test method for DEF testing, a commonly used heat treatment procedure developed by Kelham (1996), shown in Figure 2.11, was selected for this project. After undergoing the specified heat treatment, mortar bar samples were stored in three varying storage conditions and periodically measured for expansion. To isolate DEF, specimens were immersed in limewater. This condition is intended to have a similar effect to ASR as the pH is reduced by the leaching of alkalis, favoring the release of sulfate from the C-S-H layers and triggering DEF.

In accordance with the Kelham test method, mortar bars of 25 mm (1.0 in.) square cross-section and 285 mm (11.25 in.) in length were cast using steel molds and were immediately placed in a sealed container resting above water. The container was then placed in a programmable environmental chamber and was subject to the following temperature profile:

- Maintain 23 °C (73 °F) for 4 hours.
- Ramp up temperature at a rate of 18 °C/hour (32.5 °F/hour) for 4 hours to reach the peak temperature of 95 °C (203 °F).

- Maintain peak temperature of 95 °C (203 °F) for 12 hours.
- Ramp down temperature at a rate of 18 °C/hour (32.5 °F/hour) for 4 hours to reach 23 °C (73 °F) upon completion of cycle.
- After 24 hours specimens were removed from the oven and demolded.

The following are notes and observation learned after the first test run:

- PVC pipes were first used to hold the steel molds above water inside the containers. However, the curing temperatures were so high that they caused the PVC pipe to soften and buckle under the weight. Subsequent mixtures utilized steel pipes to hold molds above water.
- Upon removal from the oven, significant drying was observed on the top surface of mortar bars. In subsequent mixtures, the plastic container was sealed with tape to prevent evaporation.

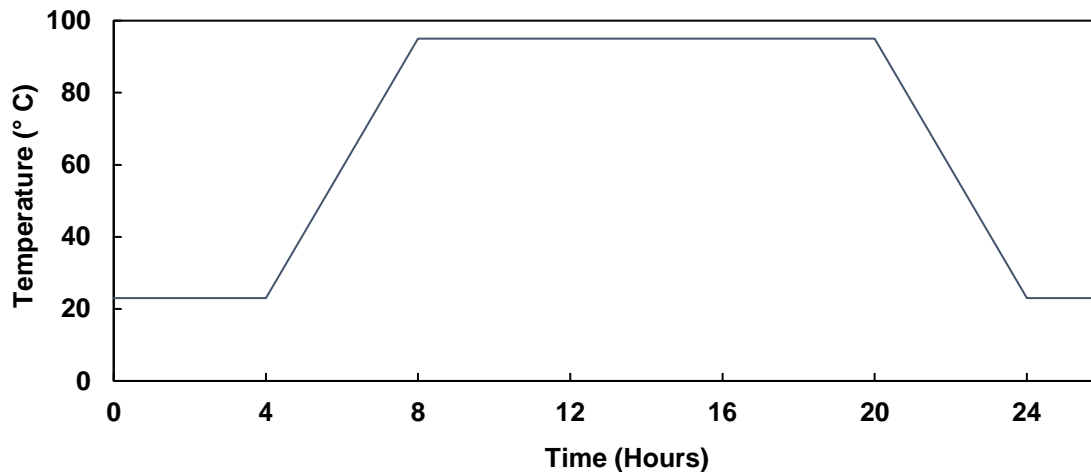


Figure 2.11 DEF heat curing procedure for mortar bars based on Kelham (1996) method [$T(^{\circ}F) = T(^{\circ}C) \cdot 1.8 + 32$]

2.3. Experimental Results and Discussion

2.3.1. Discussion on Exposure Blocks

2.3.1.1. Correlation to Lab Samples

Given logistical challenges with casting and monitoring outdoor exposure blocks, laboratory testing remains the mainstay of recommended practices. This approach,

however, relies on accelerated tests, which are known to take too long or be too short, to be too harsh or not harsh enough, and to give false positive and false negative results. Therefore, exposure blocks are created to determine a correlation between field samples, which more accurately predict actual field performance, and lab samples being run at unrealistic conditions to accelerate results.

Leaching of alkalis is a significant concern in ASR lab samples as it effectively plateaus the reaction, whereas in a field setting the reaction can continue for years. The standard ASTM C1293 concrete prism test is known to plateau and develop an S-shaped expansion curve even for very highly reactive aggregates. The exposure blocks cast for this study minimize the potential for leaching, allowing for the continuation of the reaction and providing a more realistic scenario.

2.3.1.2. Texas Marine Exposure Site

Placing test samples in an uncontrolled, outdoor environment has inherent complexities. One such complexity encountered in this project was a natural disaster, making ‘real world’ conditions a little too real. The arrival of Hurricane Harvey along the Texas coast in the Fall of 2017 devastated the town of Port Aransas and caused serious damage to the UTMSI facilities. As part of the cleanup and reconstruction process, exposure blocks were bulldozed off to the side, as seen in Figure 2.12. The movement of blocks resulted in several measurement bolts being bent or damaged (Figure 2.13). As concrete expansion is calculated by measuring the distance between bolts, in some cases it was not possible to determine if the change in distance was due to expansion or due to secondary damage. The blocks were eventually placed back in their original spot and attempts to repair measurement points were made. However, some points were beyond repair and it remains unclear if the disturbance exacerbated damage in already-cracked blocks.



Figure 2.12 Exposure blocks bulldozed as part of Hurricane Harvey cleanup process in Port Aransas



Figure 2.13 Exposure block bolts being bent (left) and bolt repaired by bending back (right)

2.3.1.3. Sample Complications

The main complication regarding exposure blocks was related to the position of the stainless-steel bolts protruding from the block. The screws were tapped at one end to create an indentation, which was used to insert the comparator and measure the distance between two bolts. However, the variability in formwork and tapping location resulted in a few points being farther away than the comparator could measure. Additionally, expansion in control specimens was so severe that within a short time the comparator was unable to measure expansion in several instances. When these situations occurred, a small metal disk

was epoxied to the end of faulty bolts. The disk contains a prefabricated indentation that was placed and oriented in such a way as to decrease the distance between two bolts. An alternative method used for fixing this issue was to carefully bend the screw inwards to decrease the distance between the two bolts. While these measures were able to resolve the issue, it is recommended to consider new methods to monitor expansion of future specimens. In the case of samples experiencing severe expansion, the loss of measurement points led to an artificial reduction in average expansion as previously high expansion values could no longer be included in the calculations. Moreover, even though measurement points were eventually repositioned, the expansion that occurred before the issue was noticed was technically unaccounted.

2.3.2. Discussion on Time Release Method

The absorption of chemical solutions by aggregates was found to profoundly vary when compared to water absorption. Moreover, the process of introducing admixtures via saturated LWFA introduced several complexities to the study. In general, the following questions were determined to be critical to fully capture the mechanism and behavior of the Time Release method:

- How does LWFA absorb chemical admixtures differently than water?
- How can LWFA admixture absorption and desorption be accurately measured?
- Does the concentration of the solution absorbed by LWFA maintain its initial concentration ratio?
- How can the time of admixture release be determined?
- How can ponding and mixing procedures be standardized when absorbing admixtures?
- How can performance in admixture-absorbed mixtures be compared fairly with control mixtures?

2.3.2.1. Cone Test (ASTM C128)

The standard test to measure fine aggregate AC, ASTM C128, uses the cone test as one of its key steps. The cone test is based on the concept of fine aggregate particles sticking together as a result of surface tension arising from excess moisture on the aggregate surfaces. When the aggregate contains a moisture content higher than SD, the excess moisture on the aggregate surface will cause it to remain in a uniform cone shape after it has been tamped and the mold has been removed, similar to how sandcastles are held

together. This indicates the sample requires further drying. Once the aggregate reaches the SD condition, it will theoretically not be able to hold its shape and will consequently exhibit a ‘slight slump.’ An example of this is shown in Figure 2.14. However, given the variability in drying techniques, cone test intervals, and interpretation of the term ‘slight slump,’ test results should be interpreted carefully. Moreover, in the case of LWFA, the conditions are even more complex given the fact that the aggregate is being saturated with a more viscous and sticky liquid than water. In fact, it may be possible that the stickiness of the lithium-saturated aggregate invalidates the use of the cone test for measuring AC. Alternative options for determining SD condition should be considered for further research.



Figure 2.14 ASTM C128 cone test performed on LWFA

2.3.3. Lab Specimens—Cylinders

2.3.3.1. Compressive Strength

Cylinders were cast primarily as a quality control measure to ensure consistency across mixtures. As expected, the addition of lithium admixture did not affect concrete compressive strength. Manufacturer guidelines for water reduction were followed to guarantee that the target w/c was maintained with increasing admixture dosage.

In general, the preheating process carried out for the Cooked mixtures resulted in slightly higher strengths. It should be noted that the cylinders did not undergo the same heat curing as the exposure blocks did. Cylinders were made from the same preheated materials but were left curing at room temperature, were demolded at one day, and were subsequently placed in a fog room at room temperature. Since the cylinders were only tested at 28 days it is not possible to conclude if the strength increase was an early age development.

Mixtures containing LWFA exhibited slightly higher strengths than the standard aggregate mixtures. This could be due to pozzolanic activity or improved hydration through internal curing. If internal curing mechanisms are at play, it is worth noting that these can improve hydration even when comparing samples that are all maintained in a fog room. Furthermore, the increase in strength is notable since LWFA mixtures had a portion of coarse aggregate replaced by the inherently weaker LWFA. Strength results are shown in Figures 2.15–2.18.

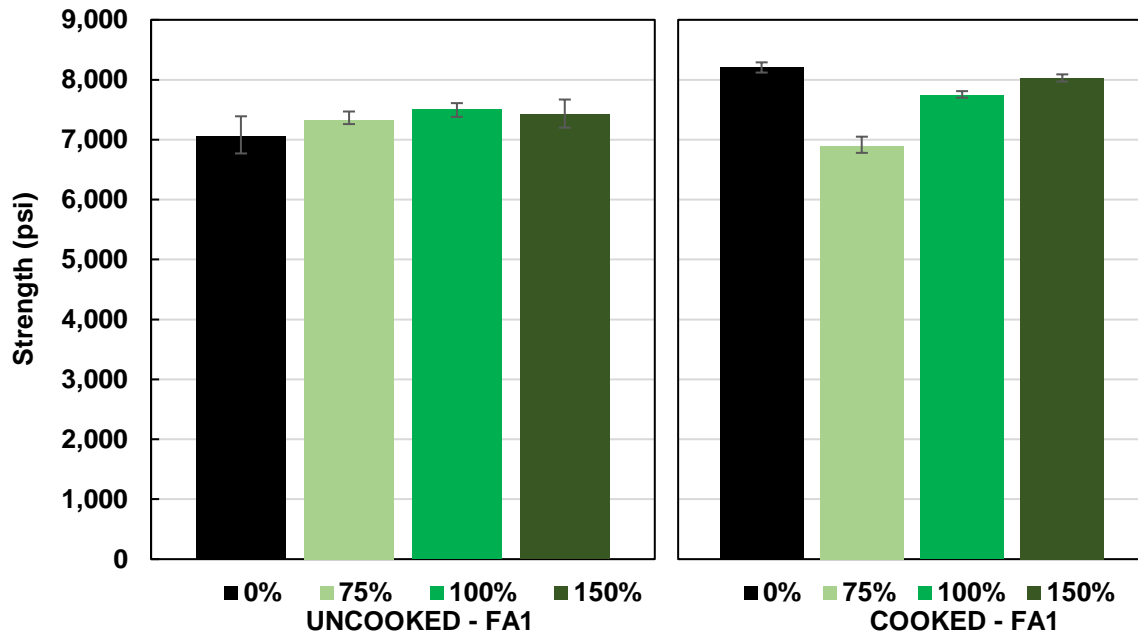


Figure 2.15 28-day compressive strength for Uncooked (left) and Cooked (right) mixtures with reactive aggregate FA1 as a function of lithium dosage

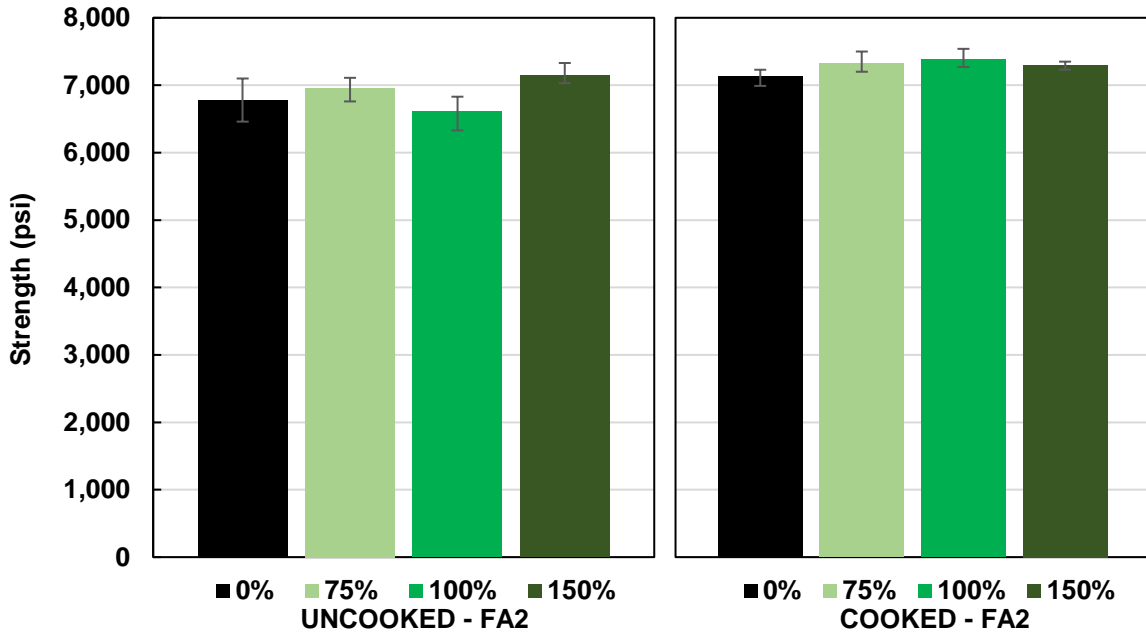


Figure 2.16 28-day compressive strength for Uncooked (left) and Cooked (right) mixtures with reactive aggregate FA2 as a function of lithium dosage

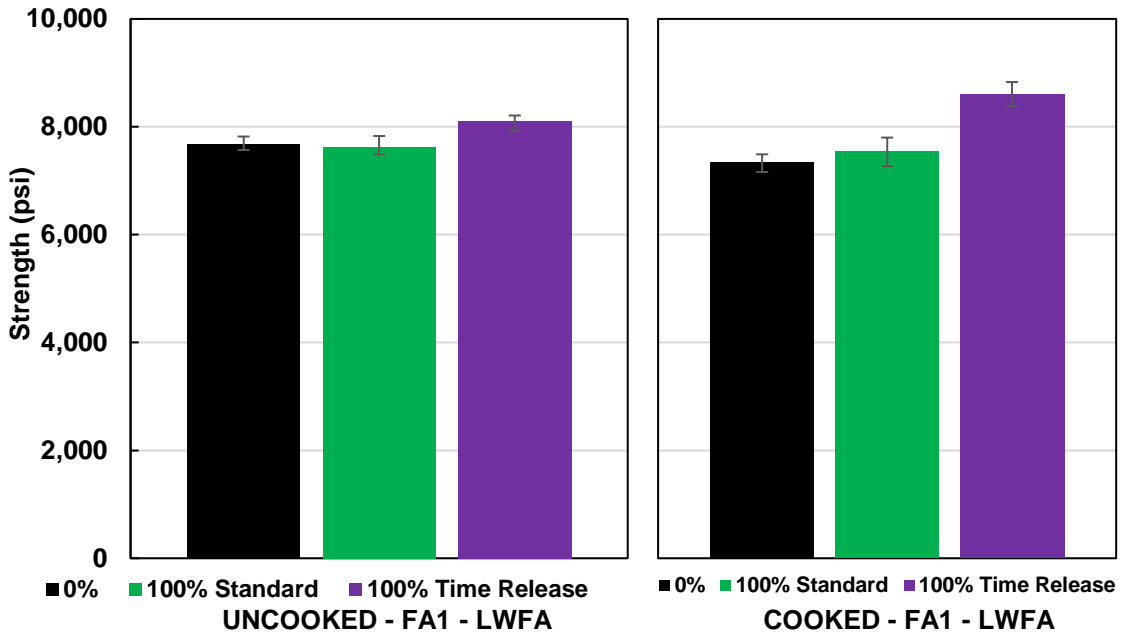


Figure 2.17 28-day compressive strength for LWFA Uncooked (left) and Cooked (right) mixtures with reactive aggregate FA1 as a function of lithium dosage

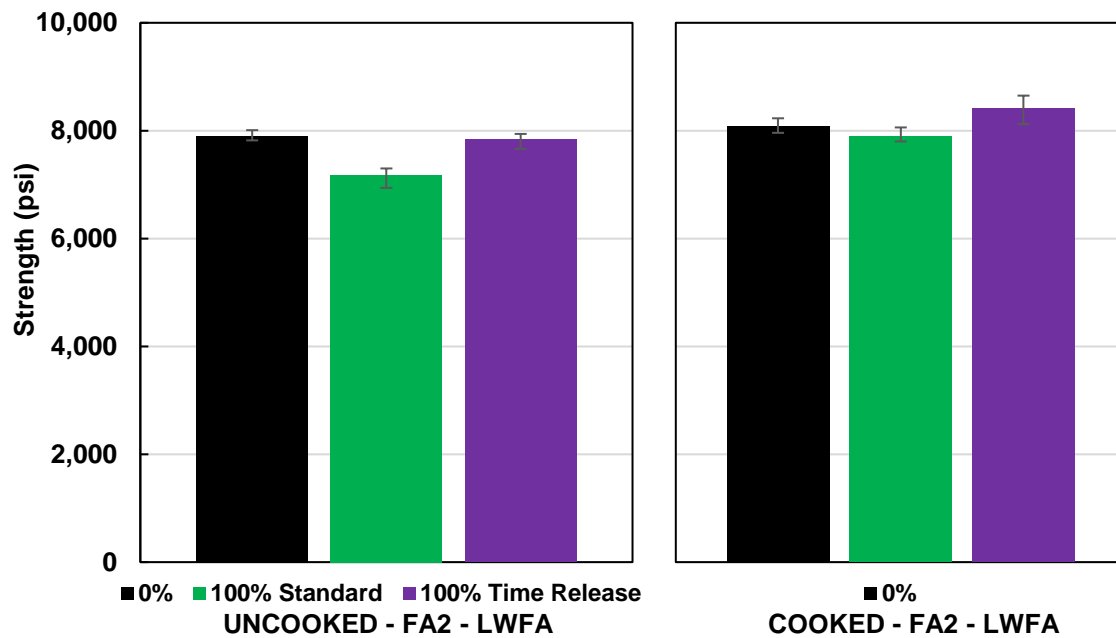


Figure 2.18 28-day compressive strength for LWFA Uncooked (left) and Cooked (right) mixtures with reactive aggregate FA2 as a function of lithium dosage

2.3.4. Lab Specimens—Concrete Prisms

2.3.4.1. Standard Concrete Prism Test ASTM C1293

As expected, FA1 was found to be more aggressive than FA2. The FA1 control mixture reached the failure criteria of 0.04% expansion at approximately 40 days. Conversely, the FA2 control mix took over 100 days to reach this point. For both aggregates, however, the use of lithium at any dosage kept expansions below the failure criteria after two years and consequently passed this accelerated laboratory test. Since no discernible difference could be observed between lithium dosages at that point, the samples continued to be monitored past the specified test timeline of two years and have been measured periodically over four years (Figures 2.19 and 2.20).

Figures 2.21 and 2.22 include replicate versions of the expansion plots without controls. Based on these plots it can be observed that while all lithium mixtures passed the official test at two years, a general upwards trend in expansion exists. This trend appears to be slowly creeping towards the failure criteria but shows little difference between dosages. While the continued monitoring of specimens is technically outside of the scope of the standard, it could provide valuable information regarding dosage effectiveness in lab samples.

As previously mentioned, alkali leaching is a major issue in lab samples. Both control mixtures shown in Figures 2.19 and 2.20 exhibit an S-shaped expansion curve, indicating a plateau has occurred at around one year, likely due to alkali leaching. It remains to be determined what effect alkali leaching will have on the lithium mixtures. If alkali leaching is assumed to affect all samples alike, then lithium itself may be subject to leaching. Examining the pore solution of mixtures with and without lithium is recommended to determine the role of this possible effect.

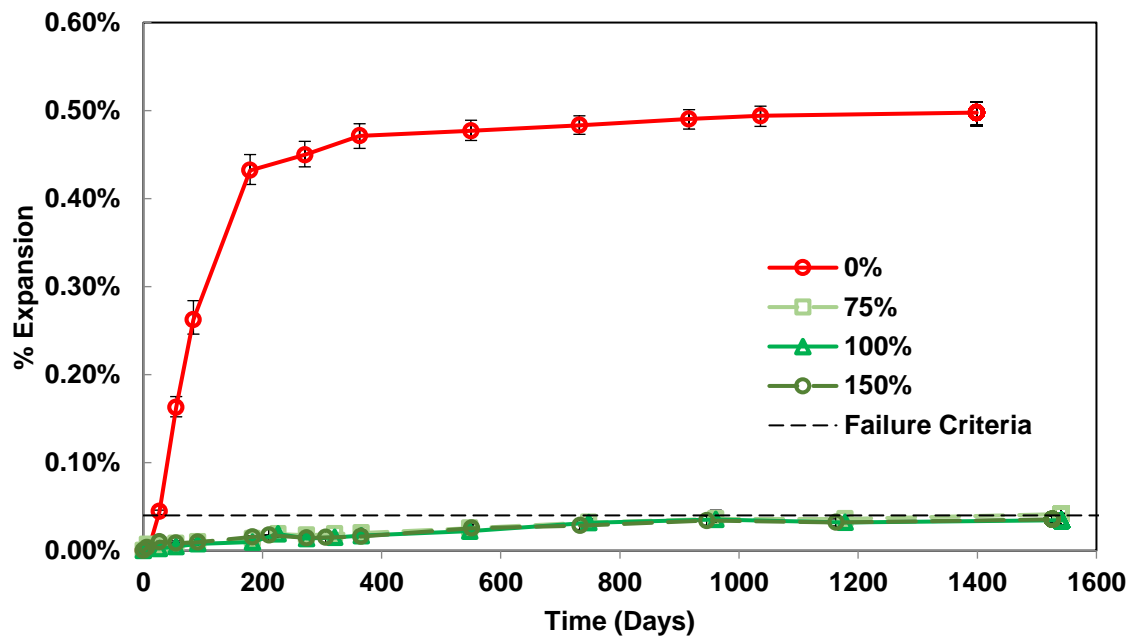


Figure 2.19 ASTM C1293 expansion over time for reactive aggregate FA1 with varying lithium dosages

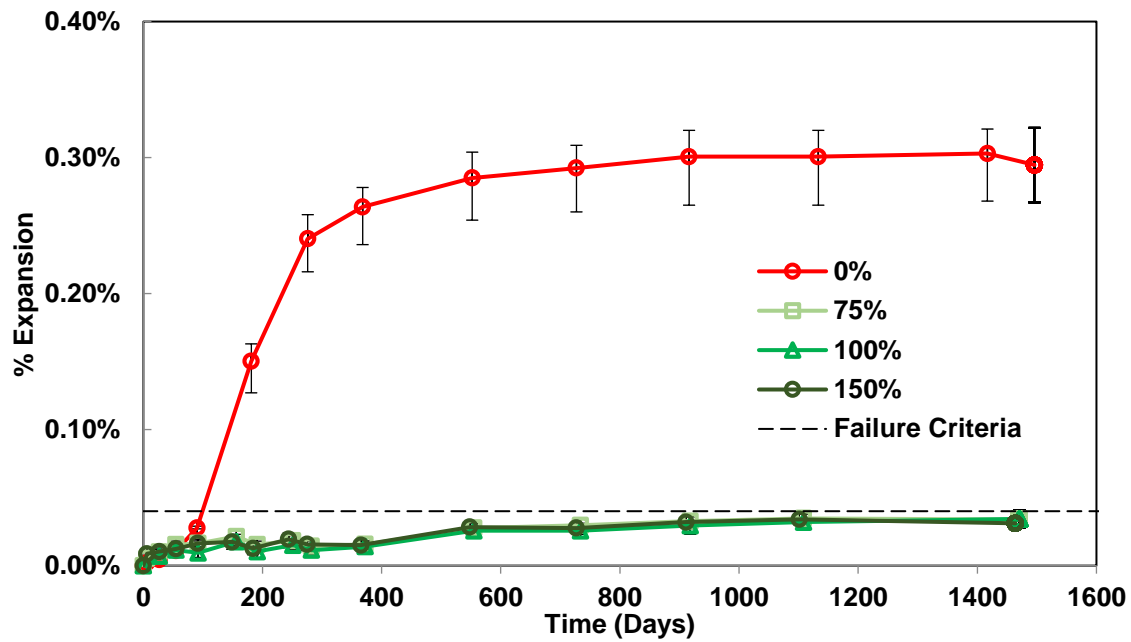


Figure 2.20 ASTM C1293 expansion over time for reactive aggregate FA2 with varying lithium dosages

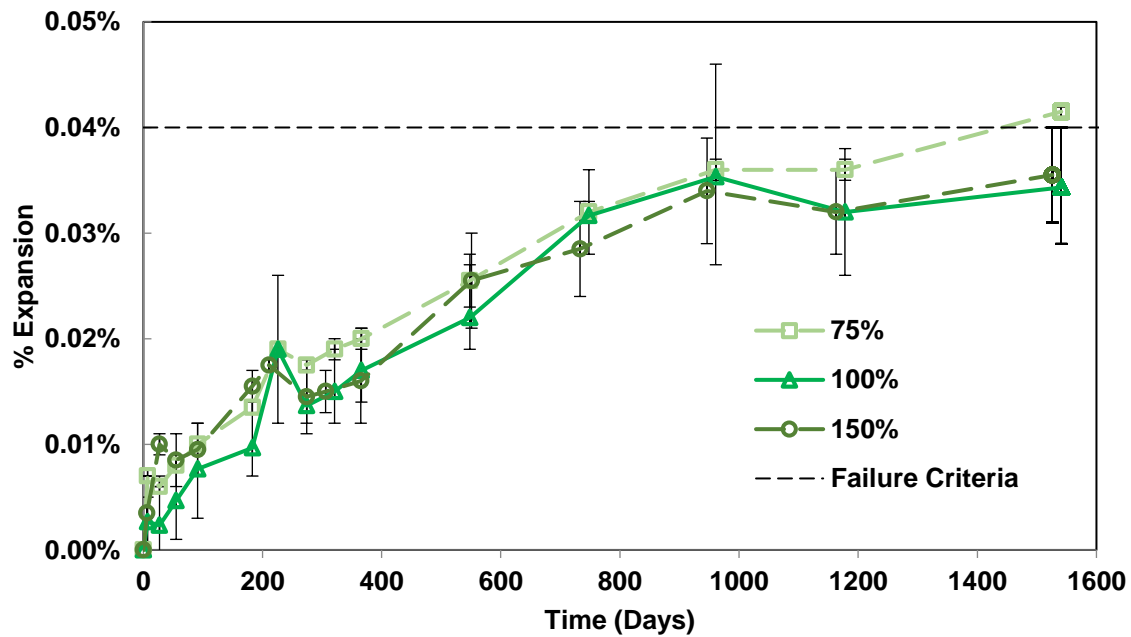


Figure 2.21 ASTM C1293 expansion over time for reactive aggregate FA1 with varying lithium dosages without control

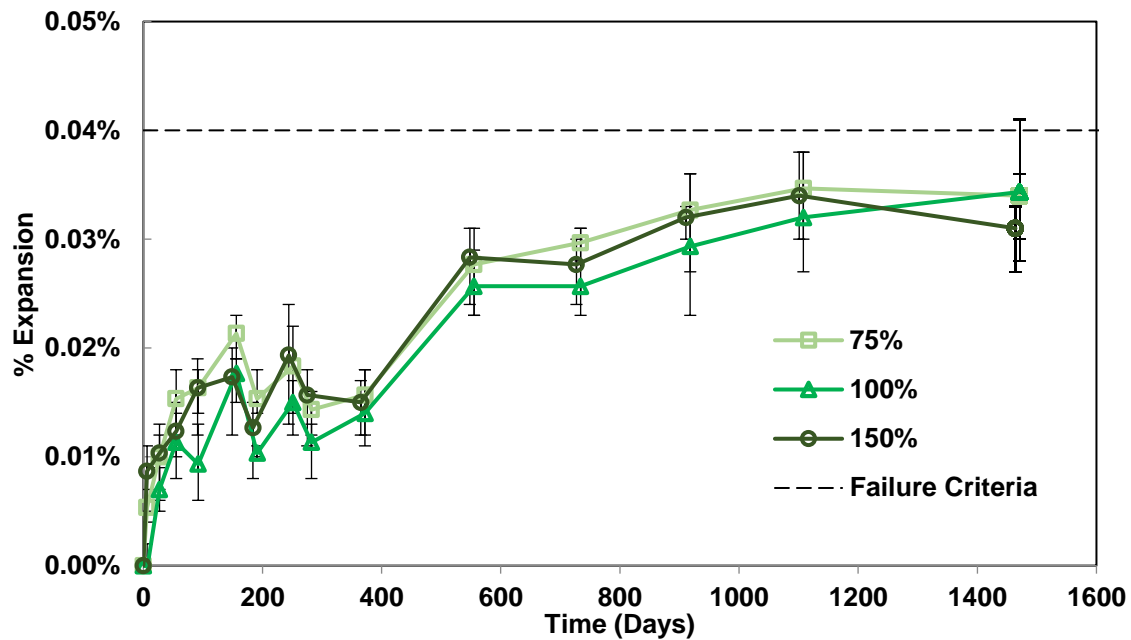


Figure 2.22 ASTM C1293 expansion over time for reactive aggregate FA2 with varying lithium dosages without control

2.3.4.2. LWFA Concrete Prism Test ASTM C1293

All the LWFA concrete mixtures (Mixtures 11–16) effectively mitigated expansion. However, there is no clear difference at this point between introductory methods. Like the standard mixtures previously discussed, the LWFA lithium mixtures passed the test at two years and continue to be monitored after more than four years (Figures 2.23 and 2.24).

It should be noted that the sharp drops seen for the *100% Admixture* mixture in Figure 2.24 were due to a faulty bucket becoming open inside the 38 °C (100 °F) oven and the consequent drying of the sample causing shrinkage. The bucket has since been replaced.

As previously mentioned, the presence of LWFA is known to reduce expansions due to ASR. This is evident when comparing the controls between the LWFA and the standard mixtures as shown in Figures 2.25 and 2.26. This reduction in expansion is independent of lithium and is theorized to be associated with pozzolanic activity, dilution of the pore solution, and increased presence of alumina. However, the magnitude of these reductions vastly differed between aggregates. FA1 exhibited a 20% reduction in expansion with the use of LWFA at two years, while FA2 exhibited a 90% reduction in expansion for the same conditions. Moreover, the significant reduction in expansion allowed the LWFA FA2 control to behave as a non-reactive aggregate and pass the test at two years without the use of lithium. This unexpected behavior is further complicated by the fact that its corresponding exposure block is expanding as expected. To validate the conflicting results,

replicate concrete prisms were cast for the LWFA FA2 control mixture. While the replicate samples are only an age of one and a half years, the preliminary values appear to confirm the original results. This discrepancy effectively yields a false negative result, indicating in a lab setting that ASR is being mitigated, while in the field sample expansion is occurring.

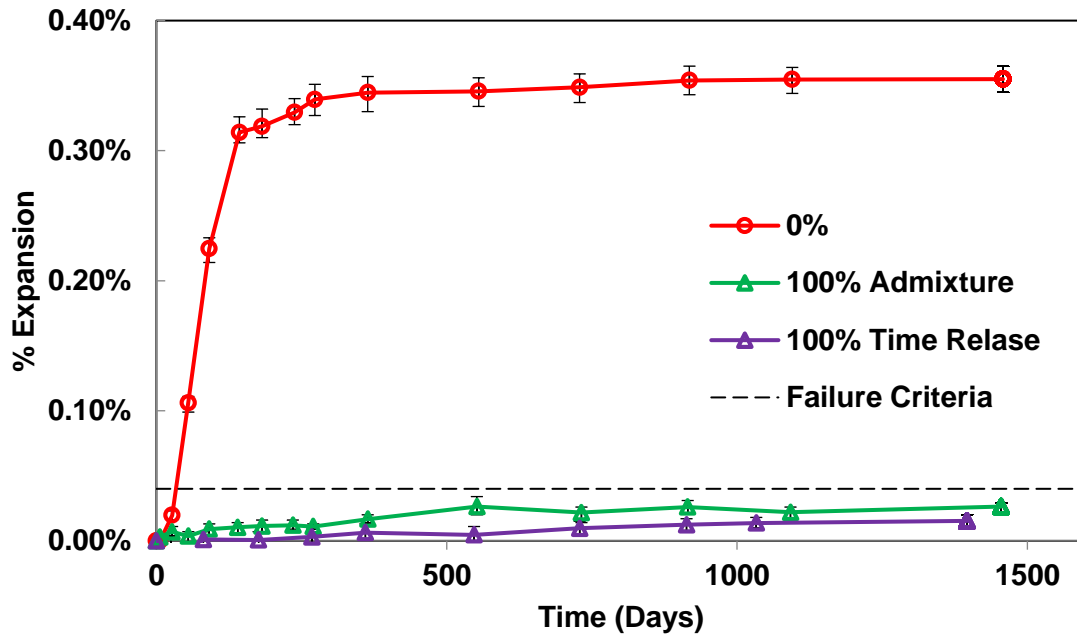


Figure 2.23 ASTM C1293 expansion over time for LWFA FA1 mixtures with varying lithium introductory methods

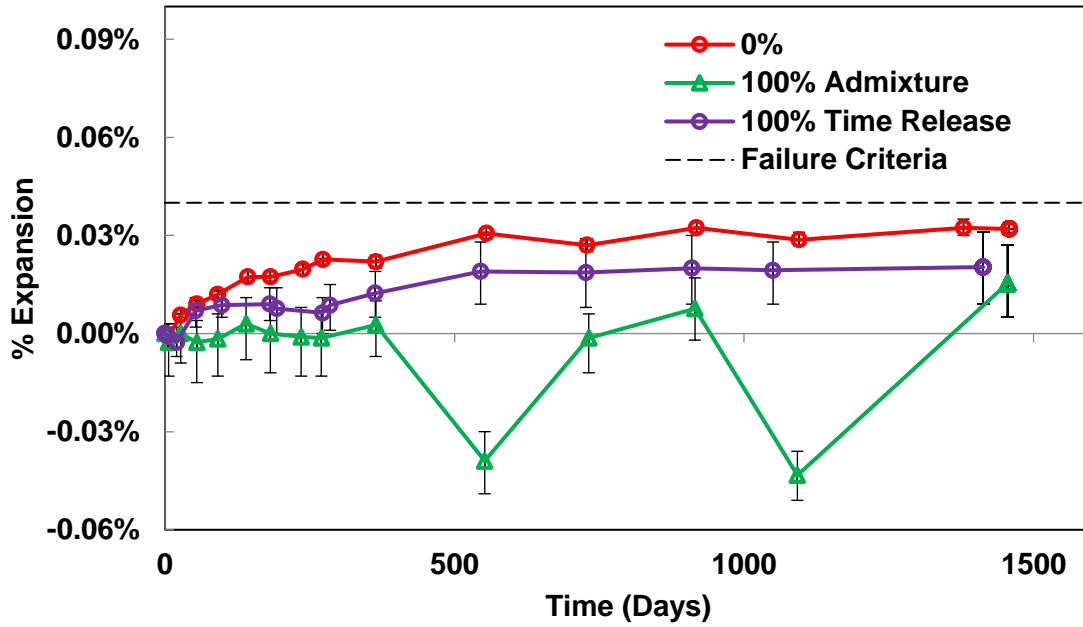


Figure 2.24 ASTM C1293 expansion over time for LWFA FA2 mixtures with varying lithium introductory methods

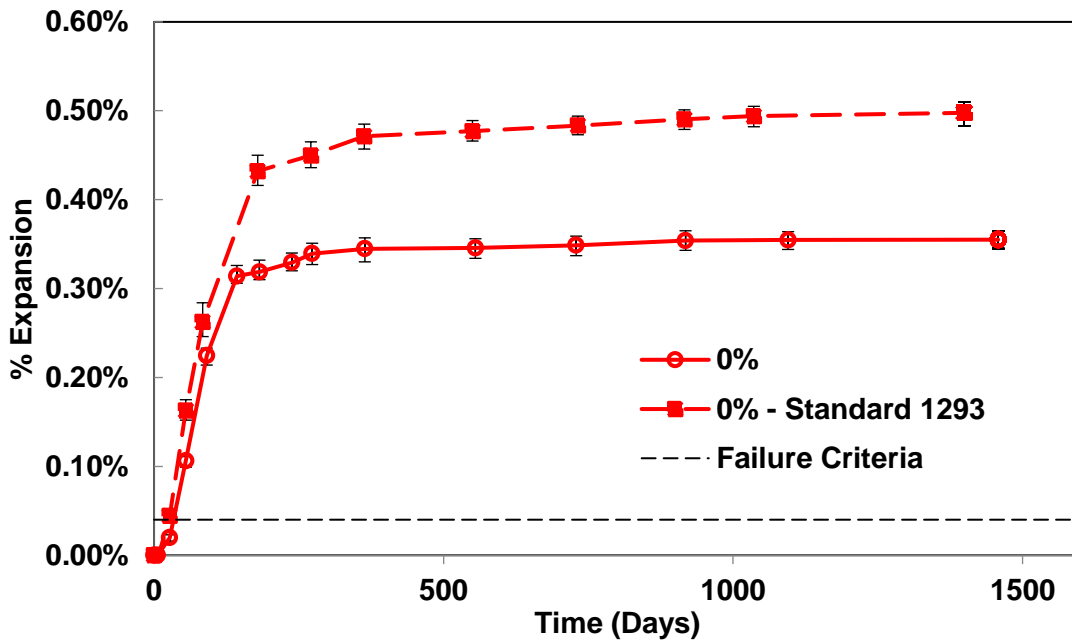


Figure 2.25 Difference in ASTM C1293 expansion over time between LWFA control (solid) and standard control (dashed) for FA1 aggregate

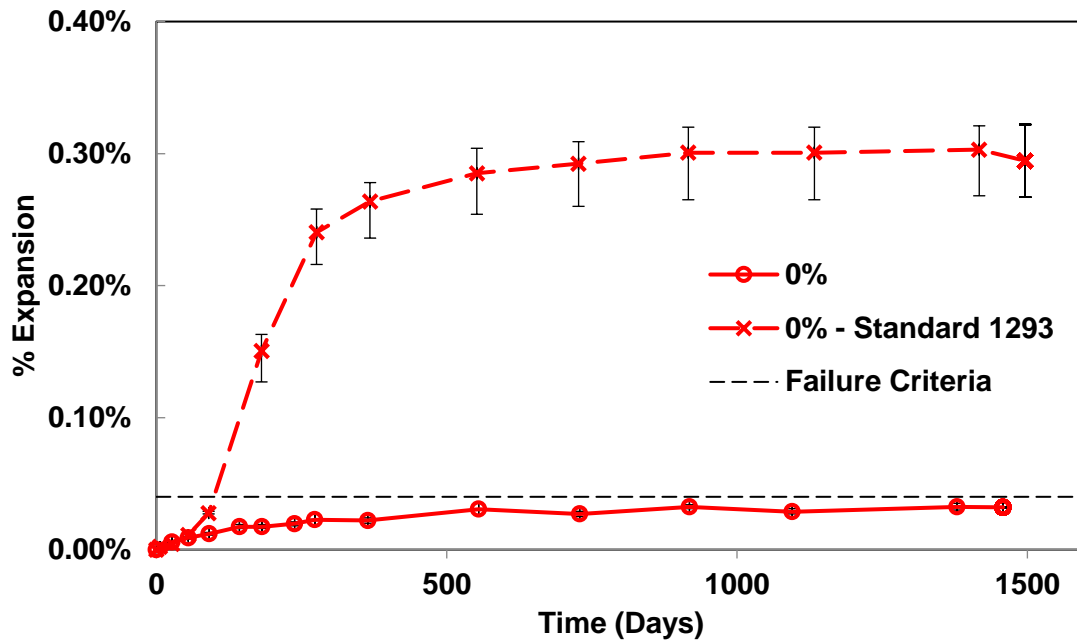


Figure 2.26 Difference in ASTM C1293 expansion over time between LWFA control (solid) and standard control (dashed) for FA2 aggregate

2.3.5. Lab Specimens—Mortar Bars

DEF mortar bars were cast based on the Kelham method. Mortar bars were immersed in limewater to isolate DEF or stored above water at 38 °C (100 °F) to develop a combination of ASR and DEF. Mortar bar mixtures containing LWFA were only cast with the less reactive FA2 aggregate. An additional exposure condition comprised of ponding samples in a combined limewater and lithium solution was used to determine if the leaching of lithium could affect its effectiveness. However, the exposure condition negatively affected the samples, and its data is not presented.

The failure criteria designated for DEF mortar bars is an expansion exceeding 0.10%. This value is comparatively higher than the 0.04% expansion limit used in the concrete prism test (ASTM C1293) because of the initial water uptake in mortar bar specimens. The specified heat curing treatment inherently dries specimens, leading them to absorb a significant amount of water from their storage environment (immersed in water or standing above water) at an early age.

2.3.5.1. Mortar Bars Immersed in Water (DEF Only)

Figures 2.27, 2.28, and 2.29 include the expansion measurements for mortar mixtures immersed in water (DEF only) containing FA1, FA2, and LWFA FA2 aggregates, respectively. These plots indicate that lithium is effectively mitigating expansions due to

DEF up to an age of 1,000 days, which corresponds with results by Ekolu et al. (2017) that show DEF mitigation in concrete prism samples even after six years.

According to Taylor et al. (2001), DEF lab samples expand within a few months and expansion is completed within one or two years. However, preliminary results from DEF control mixtures indicate a rate of reaction that is slower, varies based on aggregate type, and has likely not yet peaked at 1,000 days. Lithium mixtures, while curbing expansion, appear to have a slight upwards trend. It remains to be seen how the lithium mixtures will behave once the controls have reached a plateau.

Figure 2.30 includes the control mixtures for the three varying aggregate conditions. It can be observed that while FA2 was slower to develop DEF, it has managed to catch up to the expansion level of FA1 at 1,000 days and the reaction appears to be developing at a higher rate. Additionally, similar to its effect on ASR, the use of LWFA, independent of lithium, is seen to delay and reduce expansion due to DEF.

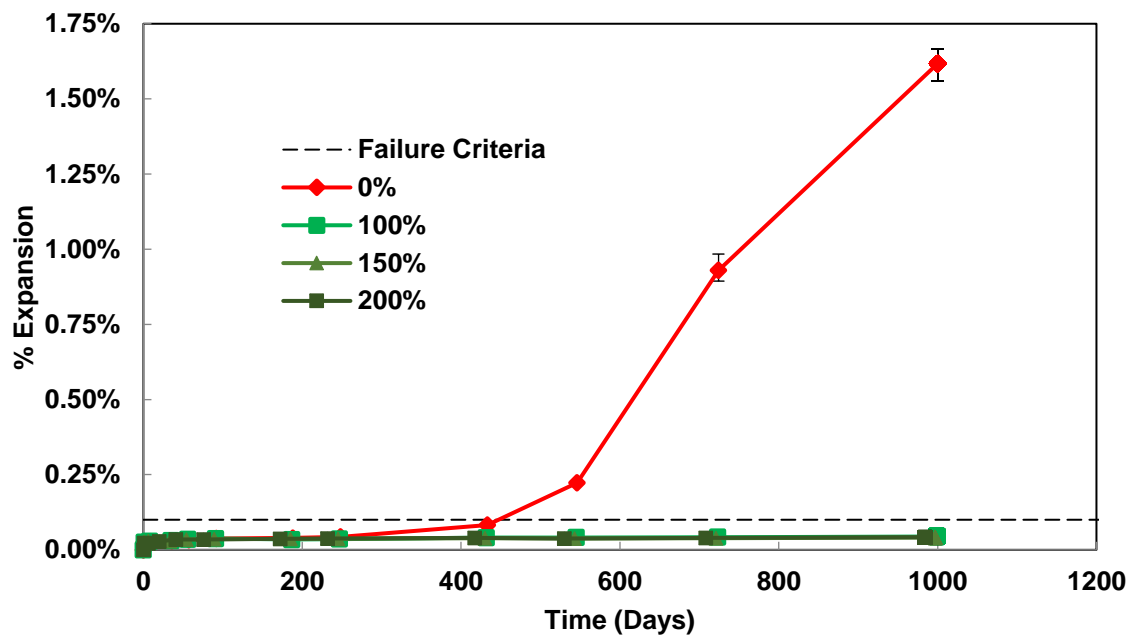


Figure 2.27 Expansion over time for Standard DEF mortar bar immersed in water (DEF only) with reactive aggregate FA1 with varying lithium dosages

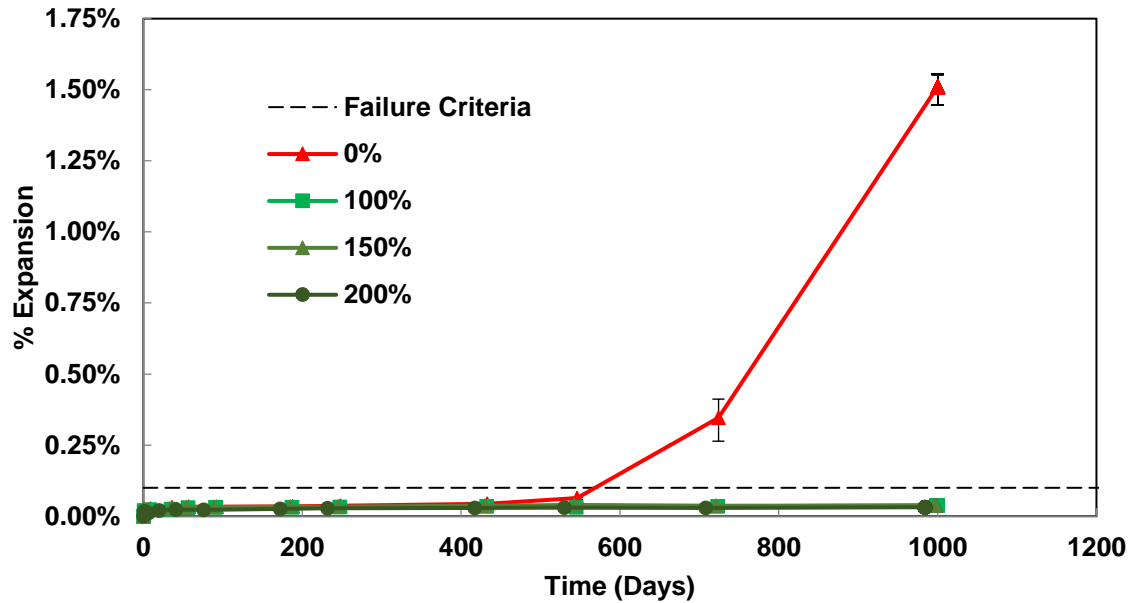


Figure 2.28 Expansion over time for Standard DEF mortar bar immersed in water (DEF only) with reactive aggregate FA2 with varying lithium dosages

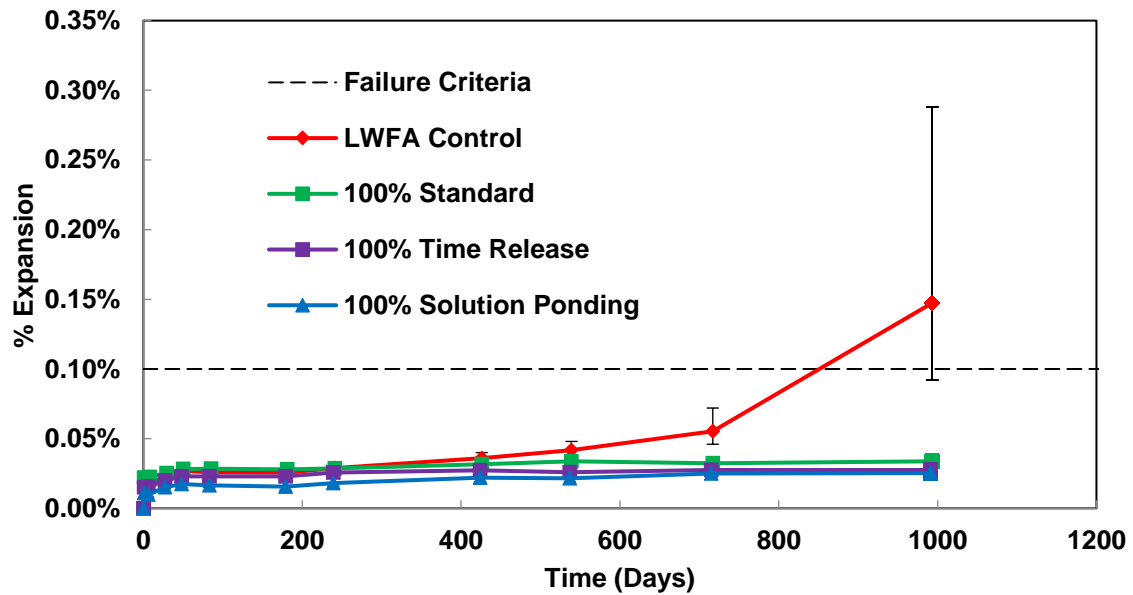


Figure 2.29 Expansion over time for LWFA DEF mortar bars immersed in water (DEF only) with reactive aggregate FA2 and with varying lithium introductory methods

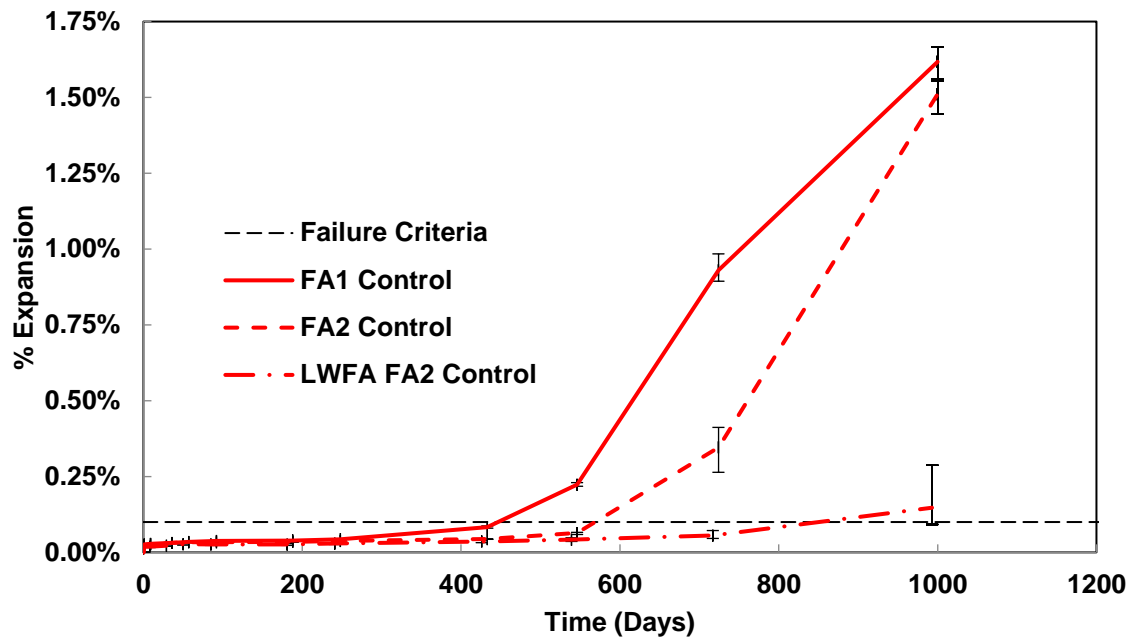


Figure 2.30 Expansion over time for control mortar bars immersed in water (DEF only) with various forms of reactive aggregates

2.3.5.2. Mortar Bars Above Water (ASR and DEF)

Figures 2.31, 2.32, and 2.34 include the expansion measurements for mortar mixtures above water (ASR and DEF) containing FA1, FA2, and LWFA FA2 aggregates, respectively. These plots indicate that lithium is decreasing expansions due to ASR and DEF up to an age of 1,000 days. Opposite to the case of isolated DEF, the combined ASR and DEF controls began expanding early on and now appear to be reaching a plateau. In combined cases of ASR and DEF, it is typically expected for ASR to occur first and to subsequently trigger DEF with a drop in pore solution pH.

Lithium was generally effective in reducing expansions. However, the more reactive aggregate, FA1, is beginning to show signs of expansion (increased slope and error) at the lowest lithium dosage (100%) (Figure 2.33). For these mortar bars, error bars indicate the minimum and maximum expansion values obtained from four samples. From data analyzed, it has been observed that samples with previous minimal error can often see an increase in error with the activation of expansive mechanisms. This may well be the case for the 100% dosage in Figure 2.33 as Ekololu et al. (2007) theorized that dosages higher than 100% may be needed to mitigate combined cases of ASR and DEF. It remains to be seen how the higher lithium dosages will behave with the FA1 aggregate. Nonetheless, this trend has not yet become apparent with the use of the less reactive aggregate, FA2, or with the use of LWFA as those lithium mixtures are currently dormant and maintain low error.

Figure 2.35 includes the control mixtures for the three varying aggregate conditions standing above water. Opposite to the isolated DEF case, in the combined ASR and DEF case both aggregates FA1 and FA2 react at similar rates and reach comparable expansion values. Once again, the use of LWFA, independent of lithium, is seen to delay and reduce expansions, in this case due to both ASR and DEF. It should be noted, however, that the LWFA mortar mixtures contained less reactive aggregate than the standard mortar mixtures as a portion of the reactive aggregate (~18% by volume) was replaced by the LWFA.

Figure 2.36 displays a closeup of Figure 2.35. From this figure, two unique expansion slopes can be observed to occur within the first 100 days. Ekolu et al. (2017) states there is a consensus that when both ASR and DEF coexist, ASR occurs earlier and may trigger DEF by reducing the pH. Based on this, the first slope could indicate ASR expansion, while the second, much steeper slope could be due to the initiation of DEF.

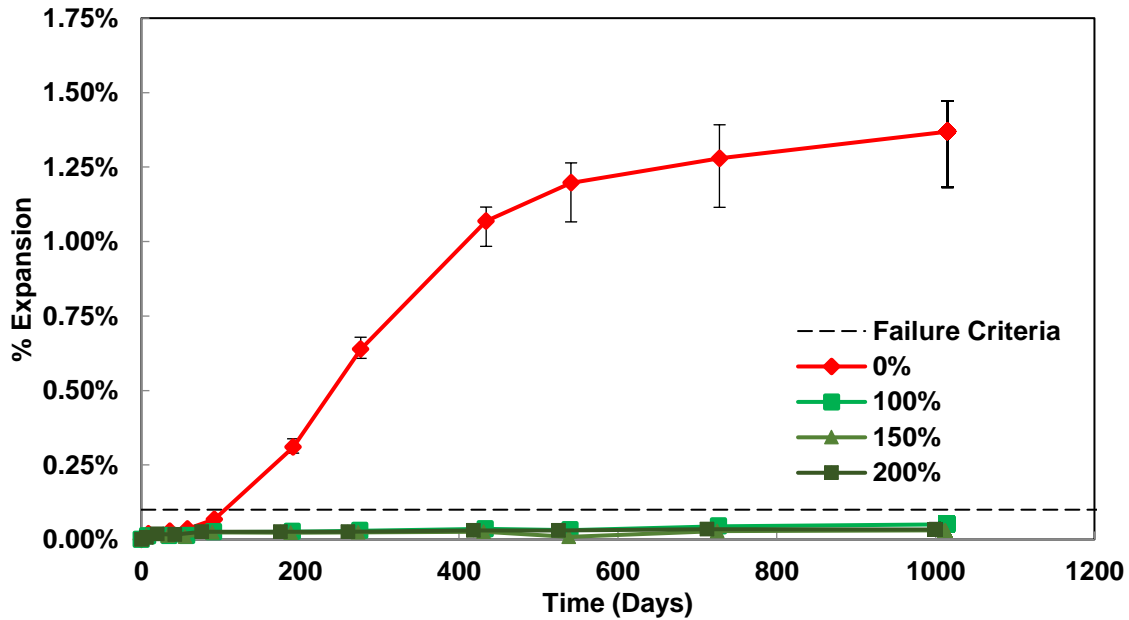


Figure 2.31 Expansion over time for Standard DEF mortar bar above water (ASR and DEF) with reactive aggregate FA1 with varying lithium dosages

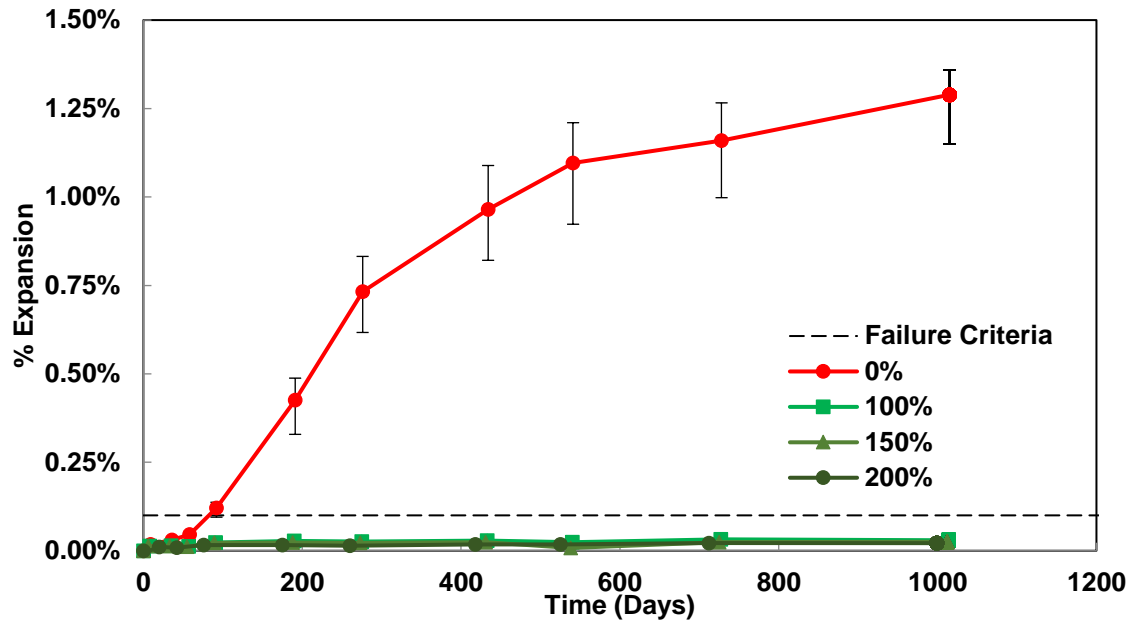


Figure 2.32 Expansion over time for Standard DEF mortar bars above water (ASR and DEF) with reactive aggregate FA2 with varying lithium dosages

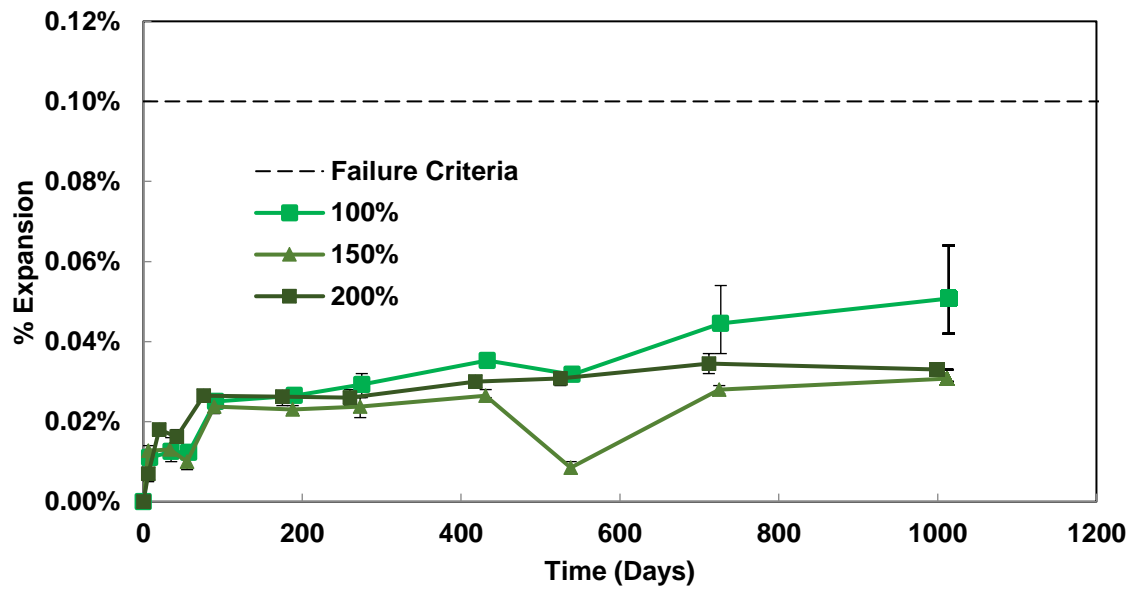


Figure 2.33 Expansion over time for Standard DEF mortar bar above water (ASR and DEF) with reactive aggregate FA1 with varying lithium dosages without control

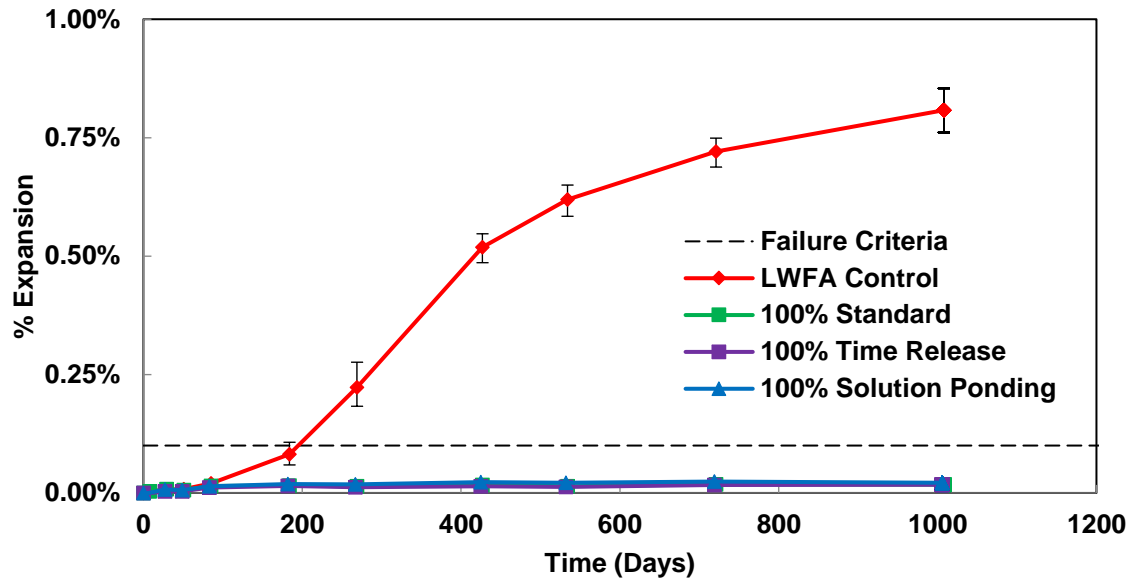


Figure 2.34 Expansion over time for LWFA DEF mortar bars above water (ASR and DEF) with reactive aggregate FA2 and with varying lithium introductory methods

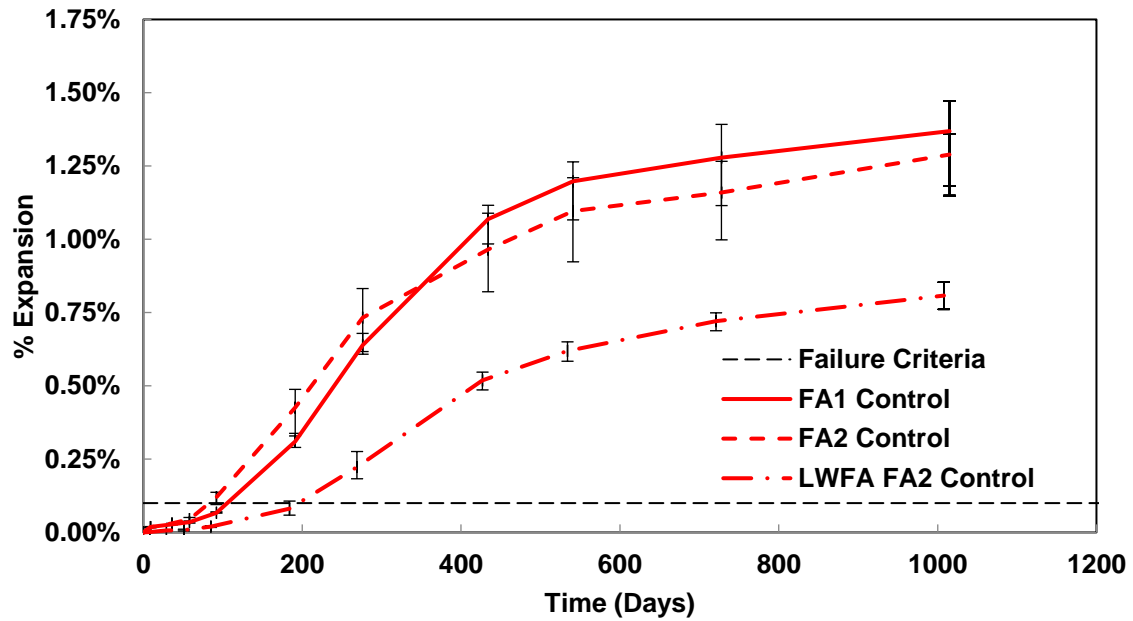


Figure 2.35 Expansion over time for control mortar bars above water (ASR and DEF) with various forms of reactive aggregates

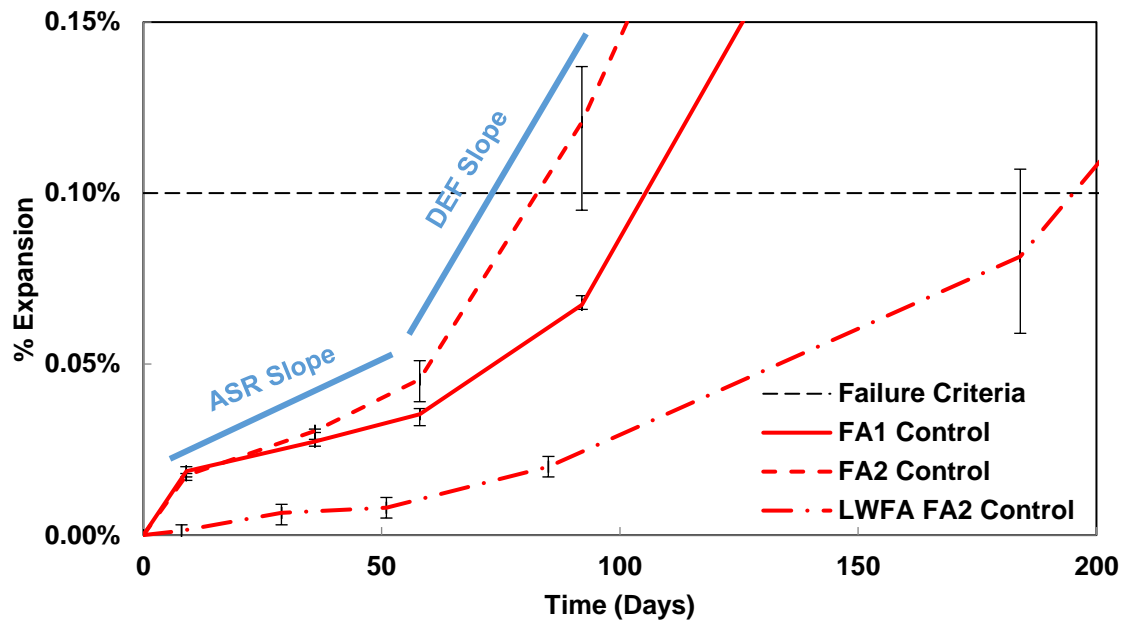


Figure 2.36 Closeup of Figure 2.52

2.3.5.3. Additional Observations

The following additional observations have been made by comparing ASTM C1293 concrete prism test data with mortar bar data as seen in Figures 2.37–2.40:

Figure 2.37

- The isolated DEF case is expected to have higher ultimate expansions than the combined ASR + DEF case for aggregates FA1 and FA2. Ekolu et al. (2017) noticed a similar trend and theorized that higher expansions are observed in isolated DEF cases because the early presence of ASR causes microcracking which provides space for delayed ettringite to form without worsening expansions. It should be noted, however, that reference field data presented in Figure 2.42 appears to indicate the opposite, that combined expansion due to ASR + DEF is ultimately higher than isolated expansions from either mechanism.
- ASR + DEF samples experience expansion at earlier ages than isolated DEF samples. It is presumed that these earlier expansions are due to ASR, with DEF expansion following. ASR is assumed to have been exhausted early on (Figure 2.36) due to alkali leaching and the subsequent expansion is believed to be DEF. However, at an approximate age of 500 days, ASR + DEF expansions appear to plateau, which could indicate the complete dissolution of the sulfate entrapped

within C-S-H layers. Cases of isolated DEF do not appear to have yet reached a plateau.

- It is unclear if one test condition favors DEF development over the other. As observed by Ekolu et al. (2007) in mortar bars immersed in limewater, sodium and potassium ions were found to be highly water-soluble and to leach out of the pore solution within the first few weeks of exposure. This effect would rapidly reduce pH and promote DEF. A similar trend would be expected in ASR + DEF mortar bars standing over water as ASR itself consumes alkalis and the test conditions also result in leaching. However, it is difficult to compare the influence on the rate of leaching as the ASR + DEF test condition is carried at a higher temperature than the DEF only condition and, thus, kinetic effects may also be involved.

Figure 2.38

- The isolated DEF LWFA control mixture has been slower to react than its standard aggregate counterparts. It remains to be seen if isolated DEF expansion in LWFA mixtures will exceed ASR + DEF expansion as observed with the standard aggregates.
- Overall, LWFA was able to lower and delay reactions due to ASR + DEF and isolated DEF when compared to the standard aggregates.
- It should be noted that the LWFA mortar mixtures contained less reactive aggregate than the standard mortar mixtures as a portion of the reactive aggregate (~18% by volume) was replaced by the LWFA.

Figure 2.39

- ASR + DEF mortar bars reached significantly higher expansions than corresponding ASTM C1293 concrete prisms affected by ASR only.
- Concrete prisms reached an expansion plateau around an age of 300 days, likely due to the leaching of alkalis. Under the same test conditions, mortar bars are likely to leach alkalis at a faster rate given their smaller sample size (1/9th the volume of a concrete prism). Based on Figure 2.36, ASR + DEF mortar bars may have primarily been affected by ASR up to an approximate age of 50 days, after which conditions may have promoted DEF.

Figure 2.40

- As previously mentioned, the presence of LWFA was capable of mitigating ASR in concrete prisms without the use of lithium. However, its presence was not able to curb expansions due to combined ASR and DEF cases in mortars.
- It should be noted that the reactive aggregate used, FA2, was graded per ASTM C1260 specifications for the mortar bars (ASR + DEF) but not for the concrete prisms (ASTM C1293 ASR Only). FA2 aggregate for the concrete prisms was used in a stockpile condition. If the interaction between LWFA and FA2 involves a mineralogical or size pessimum effect, a change in gradation would certainly affect it.
- Furthermore, the heat treatment procedure utilized to create the ASR + DEF case may affect the interaction between LWFA and FA2 in a broader way.

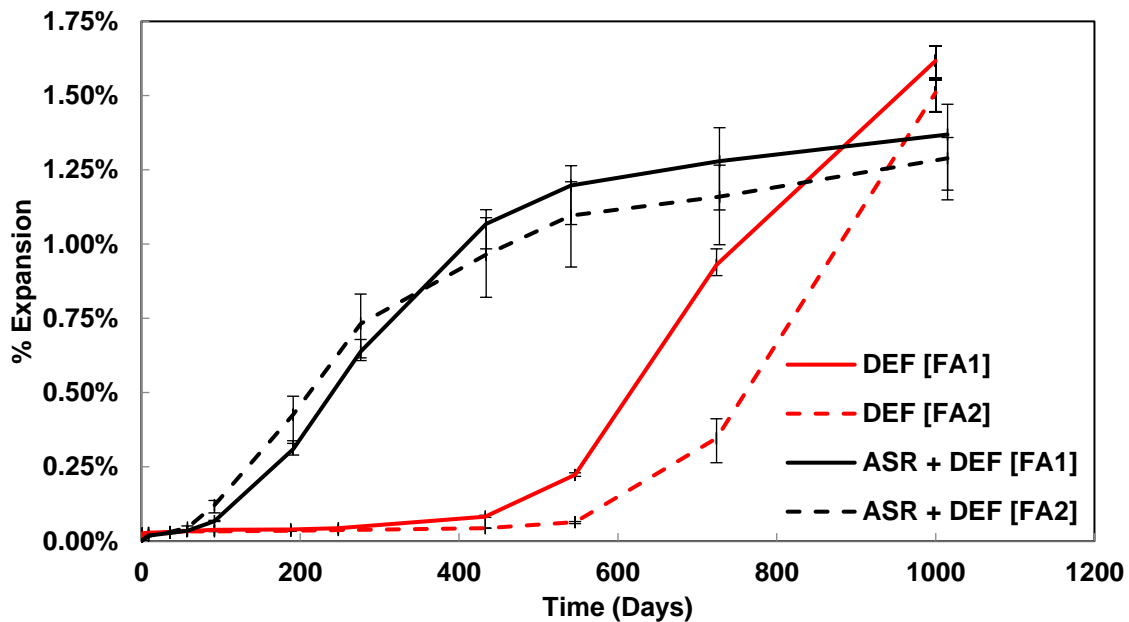


Figure 2.37 Comparison of expansion over time for isolated DEF vs. combined ASR + DEF mortar bars with varying aggregates

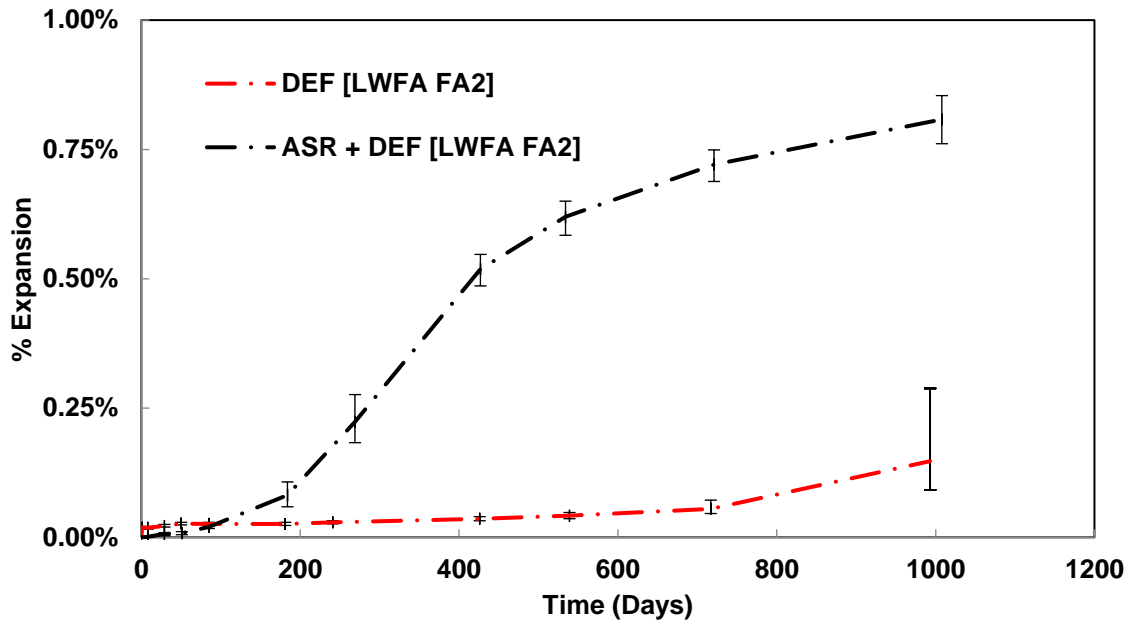


Figure 2.38 Comparison of expansion over time for isolated DEF vs. combined ASR + DEF mortar bars with LWFA FA2 aggregate

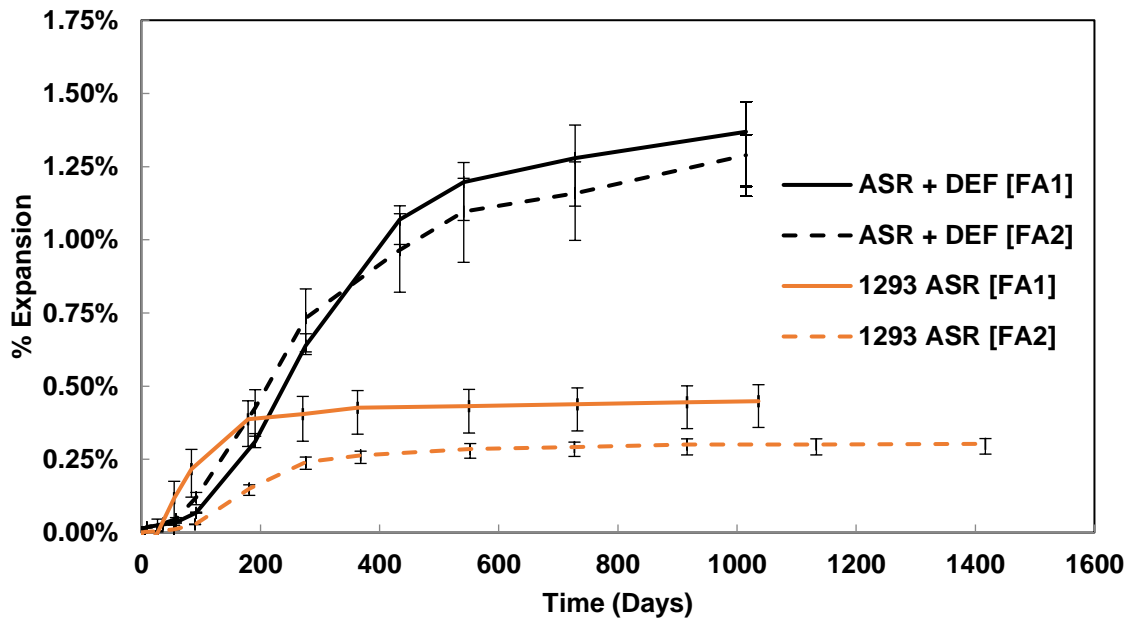


Figure 2.39 Comparison of expansion over time for DEF + ASR mortar bars and 1293 ASR concrete prisms with varying aggregates standing over water

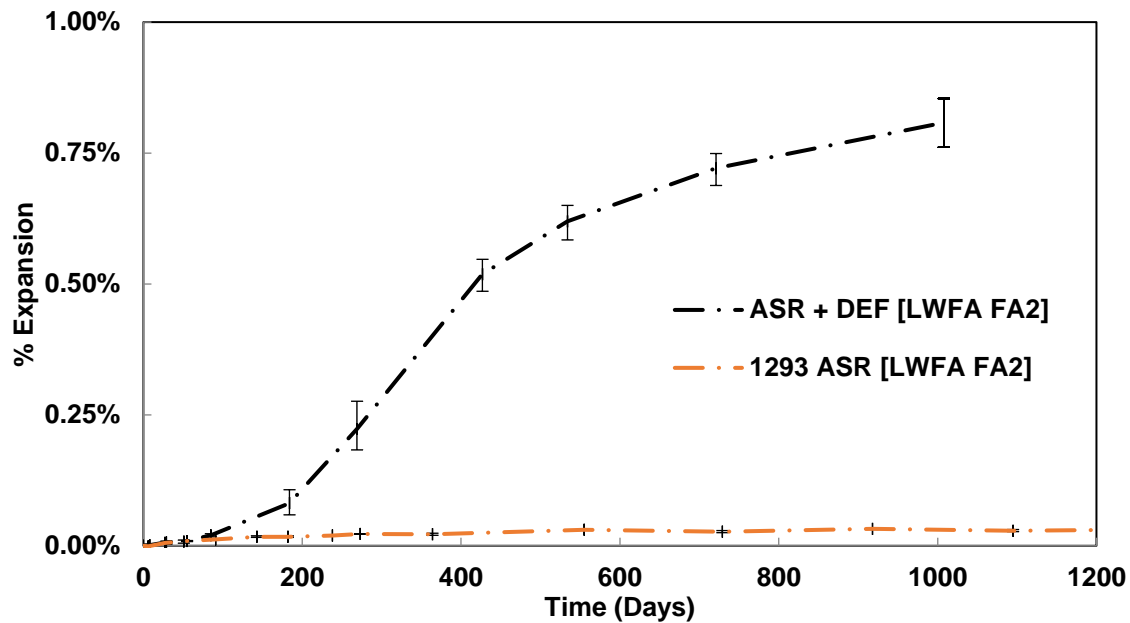


Figure 2.40 Comparison of expansion over time for DEF + ASR mortar bars and 1293 ASR concrete prisms for LWFA mixtures standing over water

2.3.6. Field Specimens—Exposure Blocks

Exposure blocks were made to measure expansion over time and compare results with corresponding lab specimens. The plots included in this section represent the average value of expansion with respect to time across ten different directions in the exposure blocks. Given the different sample and environmental conditions, higher variability is seen in field samples than in lab samples. Moreover, since control mixtures exhibit significant levels of expansion, plots omitting control mixtures are also included to better examine the performance of lithium mixtures.

While the lithium mixtures initially appeared to mitigate expansions, the most recent measurements at sample ages of four years indicate an upwards trend, particularly in the Cooked mixtures. Cracking is now also visible in certain Cooked mixtures even with the use of lithium.

2.3.6.1. Cooked and Uncooked Blocks Comparison [Figures 2.42–2.46]

2.3.6.1.1. Overview

Exposure blocks were cast in either Cooked or Uncooked conditions intended to trigger specific mechanisms (ASR + DEF in Cooked samples and ASR only in Uncooked samples). Current data, however, show that expansions between Cooked and Uncooked

control mixtures have been remarkably similar and severe. At first, this observation was considered to indicate that solely ASR was occurring in both Cooked and Uncooked samples and that DEF had yet to initiate in the Cooked samples. However, after comparing the Uncooked expansion data with the respective reference blocks (Figure 2.44), it appears that the unexpectedly high expansions in Uncooked blocks are a result of them unintentionally becoming Semi-Cooked and developing a combination of ASR + DEF.

Based on previous reference data (Figure 2.41), a clear distinction in expansion between Cooked and Uncooked blocks was anticipated. The presence of ASR in Cooked blocks was expected to accelerate and trigger DEF, while the Uncooked blocks were expected to only undergo expansions due to ASR. Moreover, the combined effect of ASR and DEF in the Cooked blocks was expected to result in expansions far exceeding those of either mechanism on its own. The expansion block data obtained as part of this study, however, did not match the expected trends. Further background information is provided in this section to contextualize the data.

The term Semi-Cooked is being used to describe samples that are theorized not be in either a fully Uncooked or Cooked state. Figure 2.43 compares expansion data from Cooked and Uncooked samples containing lithium. The data show a noticeable difference in expansion between the Uncooked and Cooked samples. Thus, while the Uncooked blocks are believed to be in a Semi-Cooked condition and have the potential to trigger both ASR and DEF, the ‘fully’ Cooked blocks appear to develop a more pronounced case of deterioration that exhausts lithium reserves and leads to expansions at earlier ages.

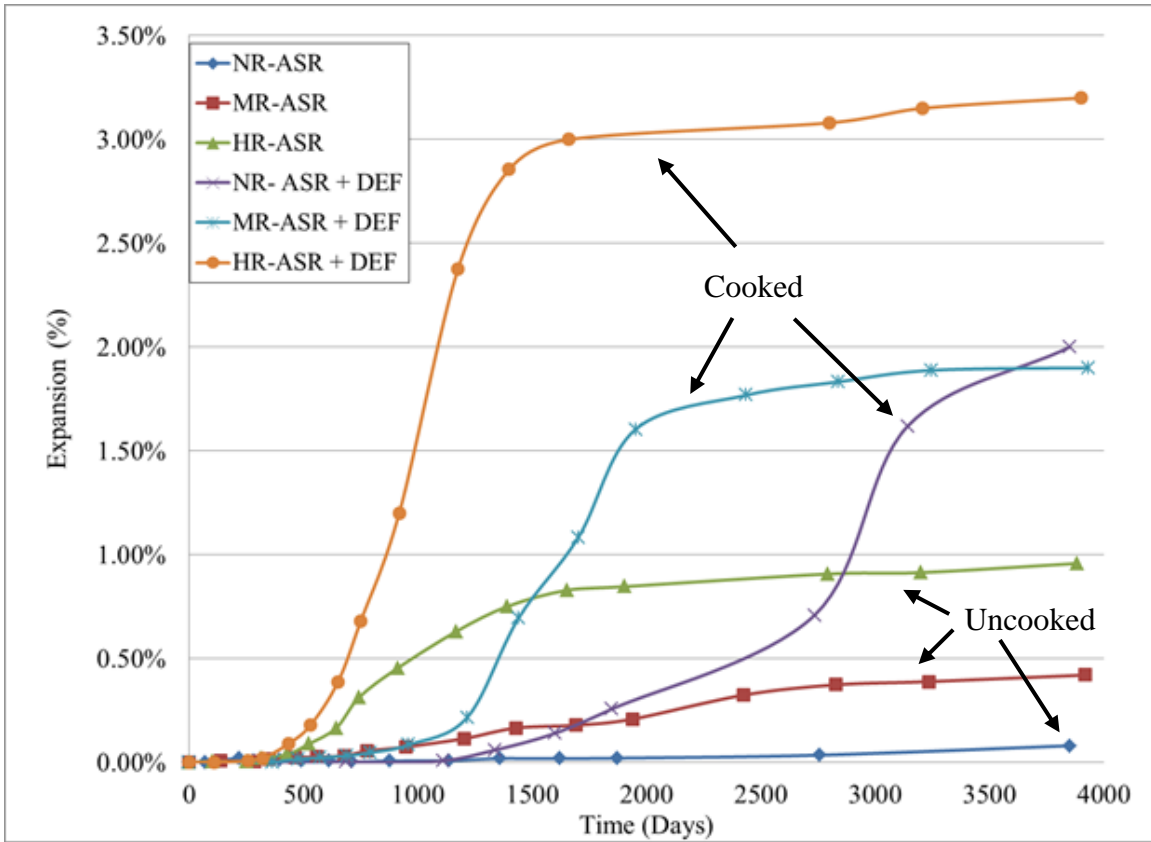


Figure 2.41: Reference data of exposure block expansion over time for three aggregates with varying reactivity (NR – nonreactive; MR – moderately reactive; HR – highly reactive). Blocks are in Uncooked (ASR) and Cooked (ASR + DEF) condition. (Drimalas and Folliard, 2020)

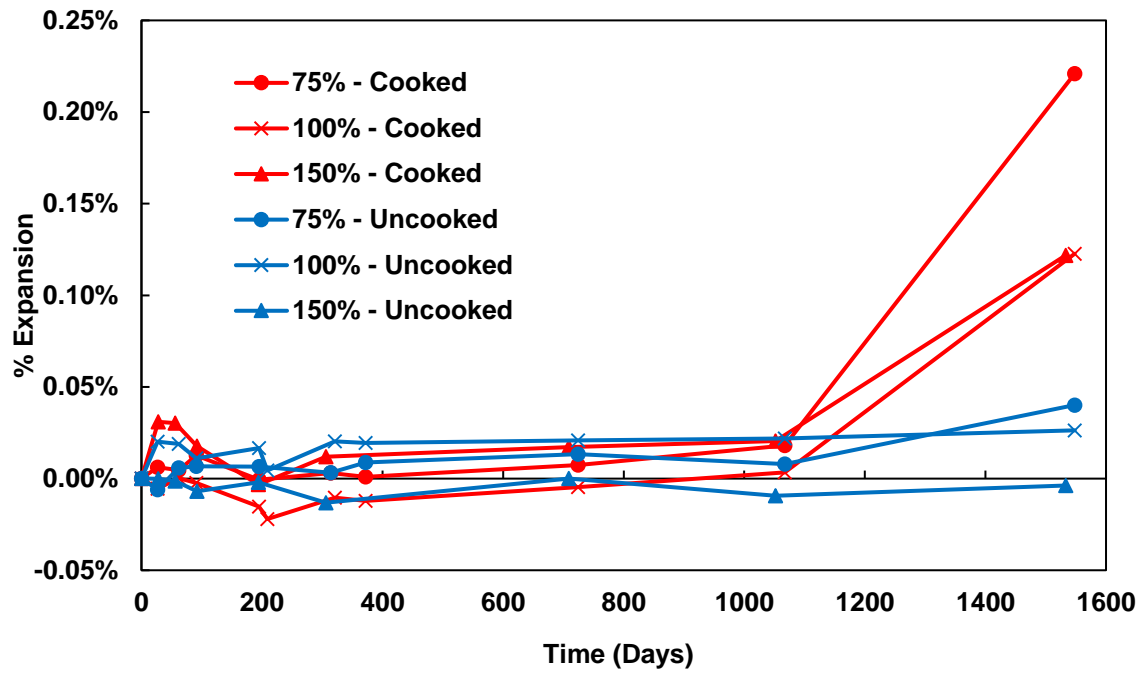


Figure 2.42 Exposure block expansion over time for FA1 aggregate mixtures in Cooked and Uncooked condition with varying lithium dosages

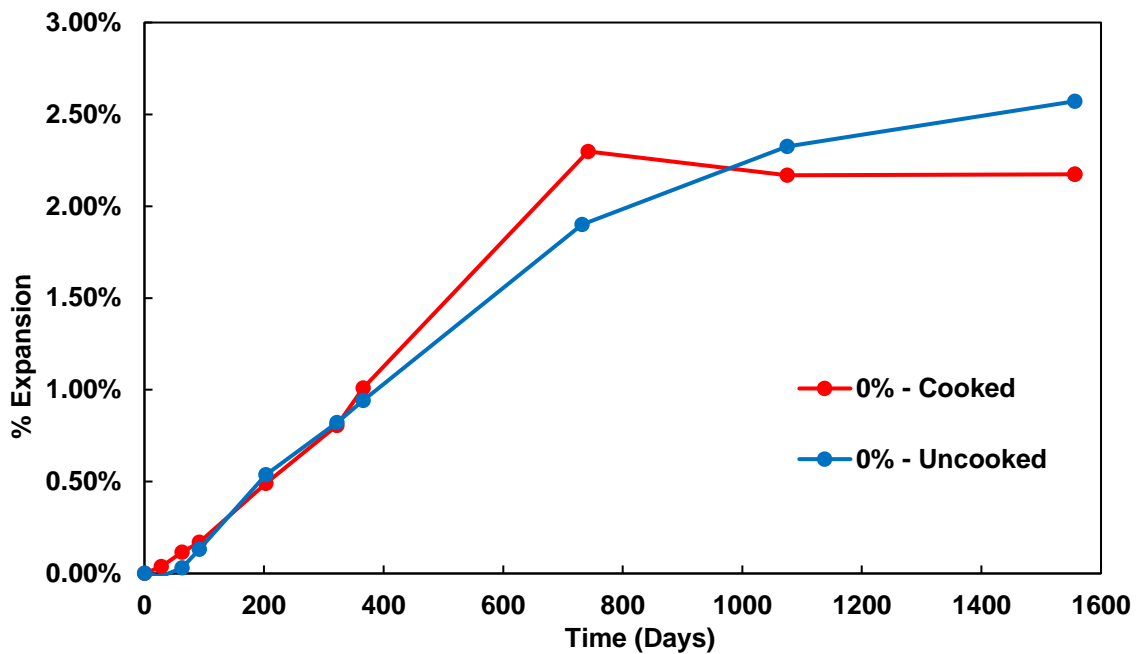


Figure 2.43 Exposure block expansion over time for FA1 aggregate in Cooked and Uncooked condition without lithium

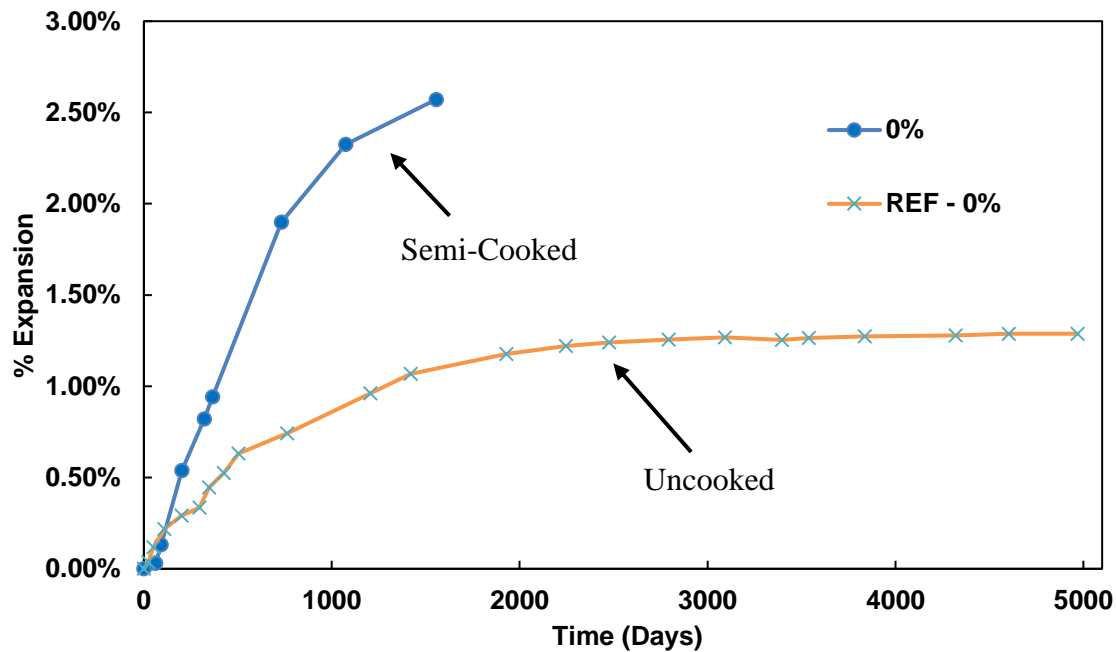


Figure 2.44 Exposure block expansion over time for FA1 aggregate control mixtures in Uncooked condition. Includes reference data from older control specimen cast for previous projects.

2.3.6.1.2. Cement Type

Exposure blocks cast for this study were 38.1 cm (15 in.) cubes made with an ASTM Type III cement. Conversely, most of the blocks being used as references (Figure 2.41) were cast in larger dimensions (38.1 x 38.1 x 71.1 cm) [15 x 15 x 28 in.] and with a different cement (Type I). Nonetheless, data from the reference blocks provides valuable information as measurements have been taken at ages exceeding 13 years.

Given the discrepancy in expansions between Uncooked blocks from this study and reference Uncooked blocks, the use of a different cement appeared as a likely cause. Further investigation, however, has found evidence of previous blocks cast at LIME with a Type III cement and exhibiting the expected behavior, i.e., Uncooked blocks developing ASR only. Data from former LIME researchers (Lute, 2008; Giannini, 2012) describes a noticeable difference in expansion between blocks in the Cooked and Uncooked condition with the use of a Type III cement.

It should be noted that these previous blocks were made using larger dimensions than the cubes cast for this study. Given their larger volume, it would seem more likely for the larger blocks to unintentionally become Cooked than for the cubes, although it is typically the least dimension that governs heat generation and loss. However, the larger reference Uncooked blocks did not exhibit unusual expansions and behaved as an ASR only case.

2.3.6.1.3. Lower Critical Temperature

The established DEF temperature threshold of 70 °C (158 °F) was selected out of convenience and based on previous experience. The actual threshold, however, is unique to each mixture and expansion can occur at temperatures below 70 °C (158 °F). Previous DEF blocks cast at LIME by Lute (2016) showed expansion and microcracking even though temperature data indicated that the blocks had not reached the critical threshold to develop DEF. These blocks included a blend of Type I cement with various rapid-setting materials that could not be preheated and only reached a maximum temperature of 65 °C (149 °F). The rapid-setting materials included components rich in SO₃. Thus, it was theorized that the critical DEF temperature threshold may be lower for mixtures with increased SO₃. It should be noted that the Uncooked blocks cast by Lute (2016) were reported to have much lower expansion levels than their Cooked counterparts as expected. However, the findings are included as a precedent for DEF potentially developing at lower than expected temperatures.

Temperature data for blocks cast for this study is included in Figures 2.9 and 2.10. Cooked blocks were intended to exceed the critical 70 °C (158 °F) threshold for 12 hours. Since the Uncooked blocks were not expected to approach the threshold, temperature data for only one Uncooked block (14U) was recorded as reference. As seen in Figure 2.23, a maximum temperature of 60 °C (140 °F) was reached in the Uncooked block even though the block was cured at ambient temperatures and batch materials were not preheated.

2.3.6.1.4. Additional Exposure Blocks

As part of the work performed for mixtures described in Chapter 4 mixtures, several more exposure blocks were cast with various admixtures. While the particular details regarding these mixtures is not discussed in this chapter, their data are included here for comparison. In Figure 2.18, the Uncooked block pertaining to this chapter is labeled as Type III, while the remaining samples were made with a Type I cement and contain various admixtures. The reference control mixture is also included and labeled as Type I – REF. All samples in Figure 2.18 contain the lesser reactive aggregate (FA2) and were intended to be in an Uncooked condition. Moreover, all mixtures presented had corresponding ASTM C1293 lab samples that failed in similar timelines, indicating that presence of the admixtures did not greatly affect ASR. Thus, the effect of the admixtures can be neglected and a rough comparison between these samples can be made.

Based on Figure 2.45, a clear distinction is observed between the mixtures made with the Type I and Type III cements. Furthermore, the expansions seen in the Type I mixtures fall within expected values from reference block containing ASR only (*Type I - REF*). This data reinforces the notion that the Uncooked blocks pertaining to this chapter may have unintentionally become Semi-Cooked.

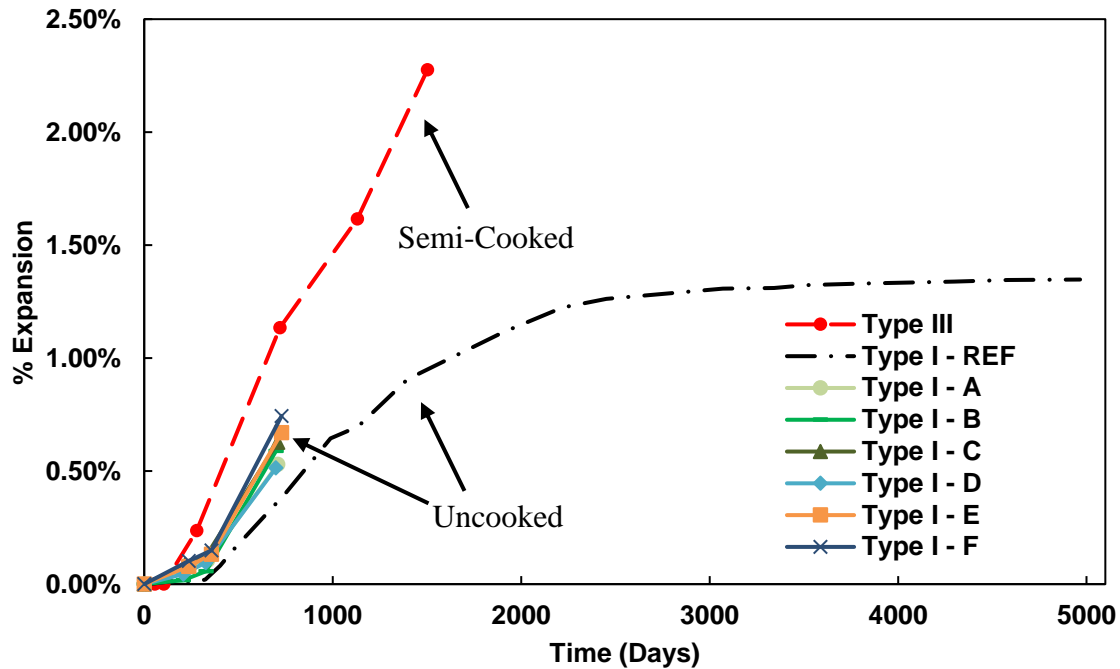


Figure 2.45 Expansion data for Uncooked exposure blocks made with reactive aggregate FA2. Mixture Type III is control (no lithium) for FA2. All other mixtures were made with a Type I cement and contain various admixtures.

2.3.6.1.5. Summary

Expansion in the Uncooked blocks was higher than expected and resembles the expansion level observed in Cooked blocks. It is believed that a combination of factors may have caused the Uncooked blocks to unintentionally become Cooked and develop a combination of ASR and DEF. Evidence presented throughout this section indicates that while this exact issue has previously not been reported, there may still be a possibility for the phenomenon to occur based on several factors. Below is a summary of findings.

- Using a similar Type III cement and larger forms, Lute (2008) and Giannini (2012) did not experience issues with casting Uncooked blocks.
- Lute (2008) found expansion associated with DEF in blocks that did not reach the presumed critical 70° C threshold to develop DEF. This was attributed to an increase in SO₃ potentially lowering the critical DEF temperature. The blocks in this study did not have significant SO₃ contents, but the findings are included as a precedent for DEF potentially developing at lower than expected temperatures.
- As part of the work performed for Chapter 4 mixtures, several more blocks have been cast with various admixtures. The data from these blocks seems to indicate a clear difference in expansion between blocks cast with Type I and Type III cements.

2.3.6.2. Standard Blocks in Central Texas Site [Figures 2.46–2.51]

As expected, control samples rapidly and aggressively expanded due to ASR and/or DEF. While expansions do not appear to have peaked yet, they have become so severe that the distance between measuring points (tapped bolts) has exceeded the limit of the measuring device. In some cases, this has led to fewer points being measured and to an artificial reduction or plateau in expansion (Figure 2.46 and 2.47).

At a sample age of four years, the Uncooked mixtures with lithium are currently matching expansion levels previously reported by Drimalas et al. (2012) and are considered dormant. However, from this previous study, it can be observed that noticeable expansion may occur even in lithium samples at later ages (~ six years). Ultimately, the previous study's long-term data indicate that ASR expansion is indeed a function of dosage as the mixture containing the most lithium (100%) shows the least expansion after 13 years. Nonetheless, the late-age expansion of the 100% lithium sample eventually exceeded the 0.04% failure criteria used for exposure blocks. Thus, exposure blocks cast for this study were made with up to 150% of the standard lithium dosage. It remains to be seen if this higher dosage will be able to mitigate ASR expansion in the long-term.

Lithium effectiveness appears to be diminishing in Cooked samples as a noticeable increase in slope can be observed (Figures 2.48 and 2.49) at around 1,500 days. Ekolu et al. (2017) theorized that lithium may mitigate DEF expansion by creating a modified form of ettringite that is less or non-expansive. Previously, however, Ekolu et al. (2007) found lithium in DEF mortar bars to be slightly water soluble. Thus, the inability for lithium to prevent long-term DEF expansion in field samples could be caused by the eventual release of lithium from the modified ettringite products. Comparable lithium mortar bar samples prone to ASR + DEF appear mostly dormant at an age of 1,000 days (Figures 2.32). It remains to be seen if lithium effectiveness will similarly diminish in mortar bars at later stages.

Cooked samples containing lithium were compared with a DEF only exposure block made with non-reactive coarse and fine aggregates by Drimalas and Folliard (2020), and their expansions were found to be strikingly similar. This could indicate that lithium may be able to transform an ASR + DEF case into a DEF only case. Lithium was observed to effectively mitigate expansions in the first few years of exposure. If this is assumed to be a direct suppression of ASR, then the block could effectively become a DEF only case. Since ASR generally acts as a trigger for DEF, the absence of ASR may prevent the early occurrence of DEF and leads it to occur normally, i.e., based on the rate of sulfate dissolution from within C-S-H layers. The DEF only block data show that DEF can occur on its own around an age of four years. Subsequent measurements and forensic evaluation will be needed to confirm this theory.

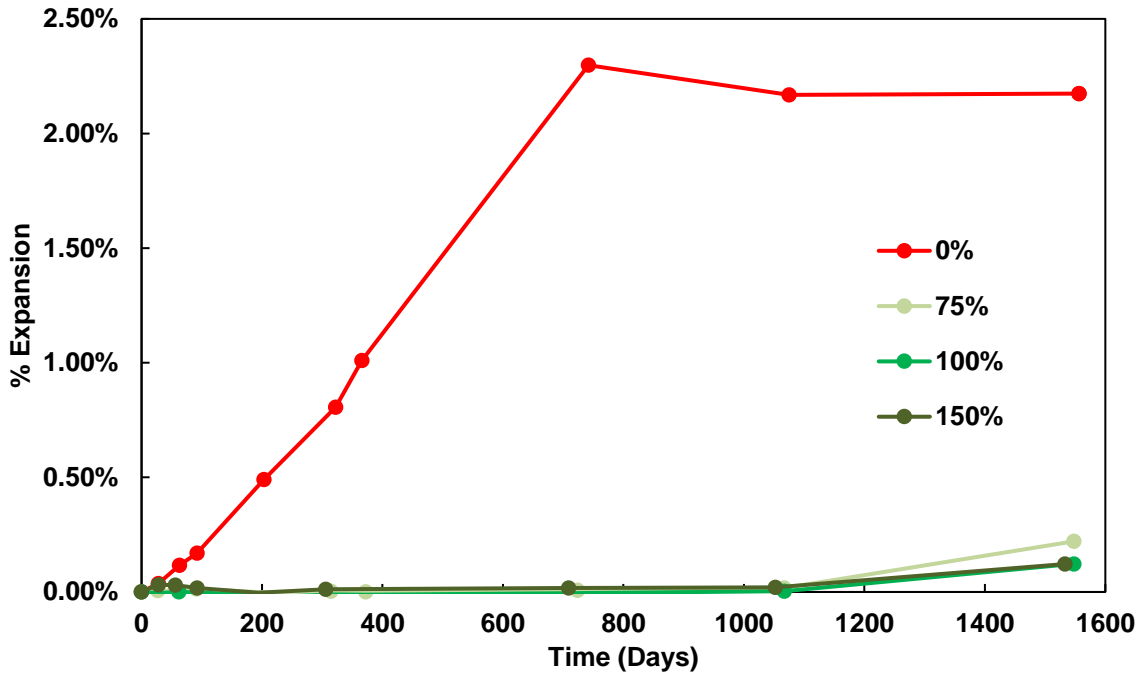


Figure 2.46 Exposure block expansion over time for FA1 aggregate in Cooked condition (ASR + DEF) with varying lithium dosages

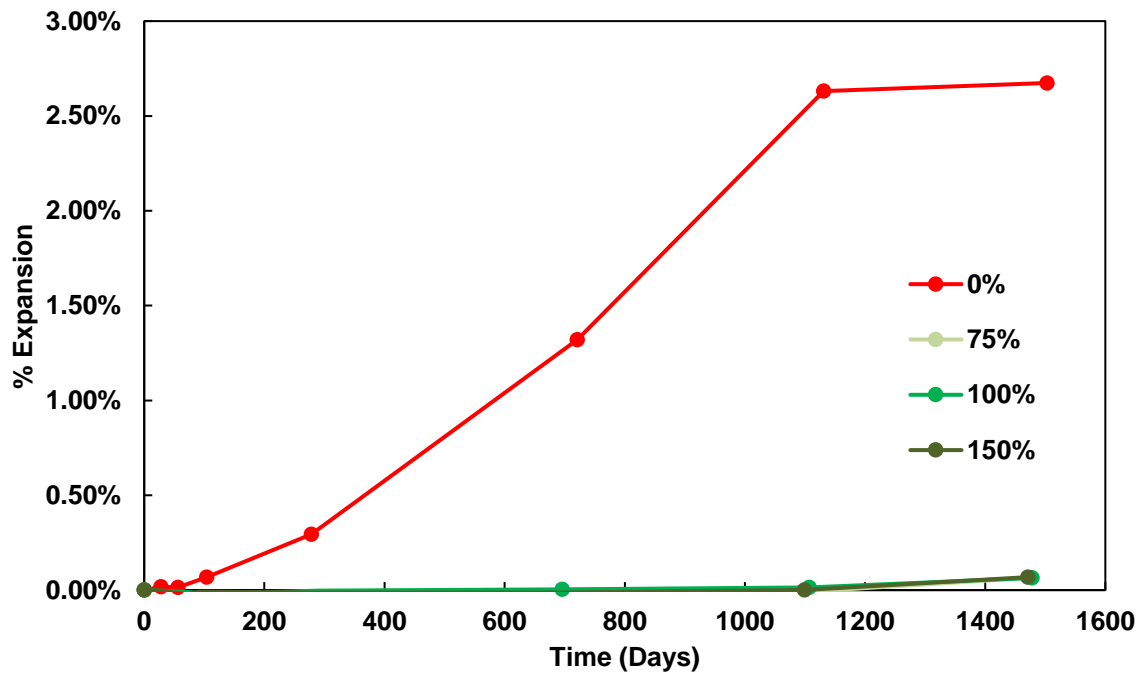


Figure 2.47 Exposure block expansion over time for FA2 aggregate in Cooked condition (ASR + DEF) with varying lithium dosages

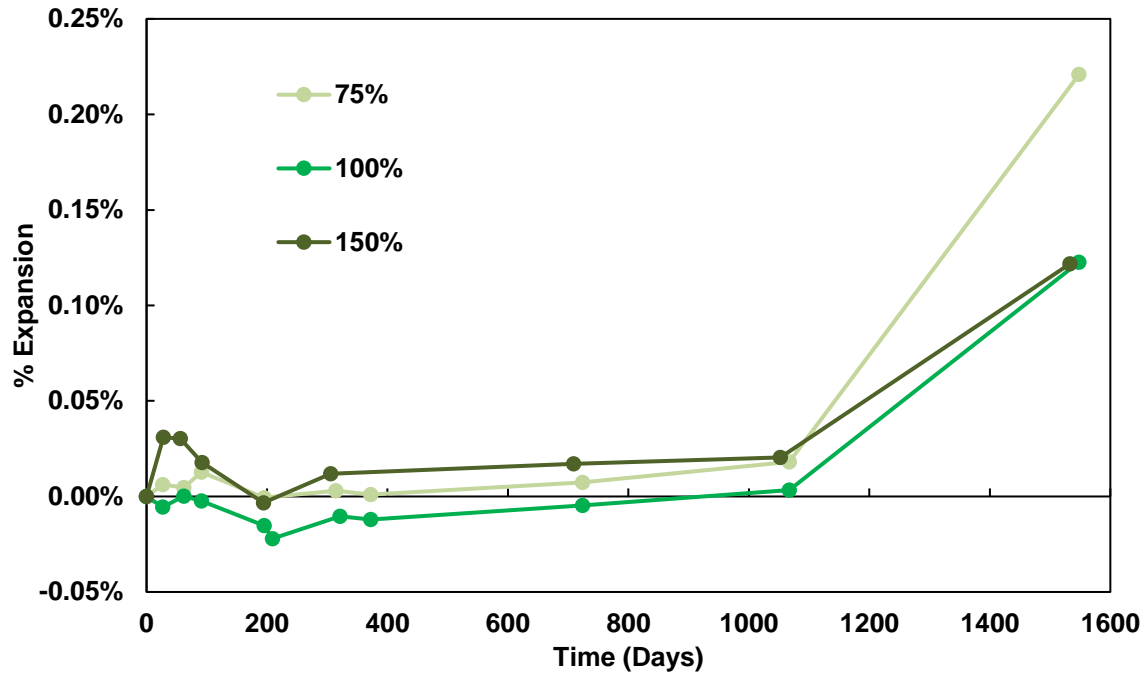


Figure 2.48 Exposure block expansion over time for FA1 aggregate in Cooked condition (ASR + DEF) with varying lithium dosages without control

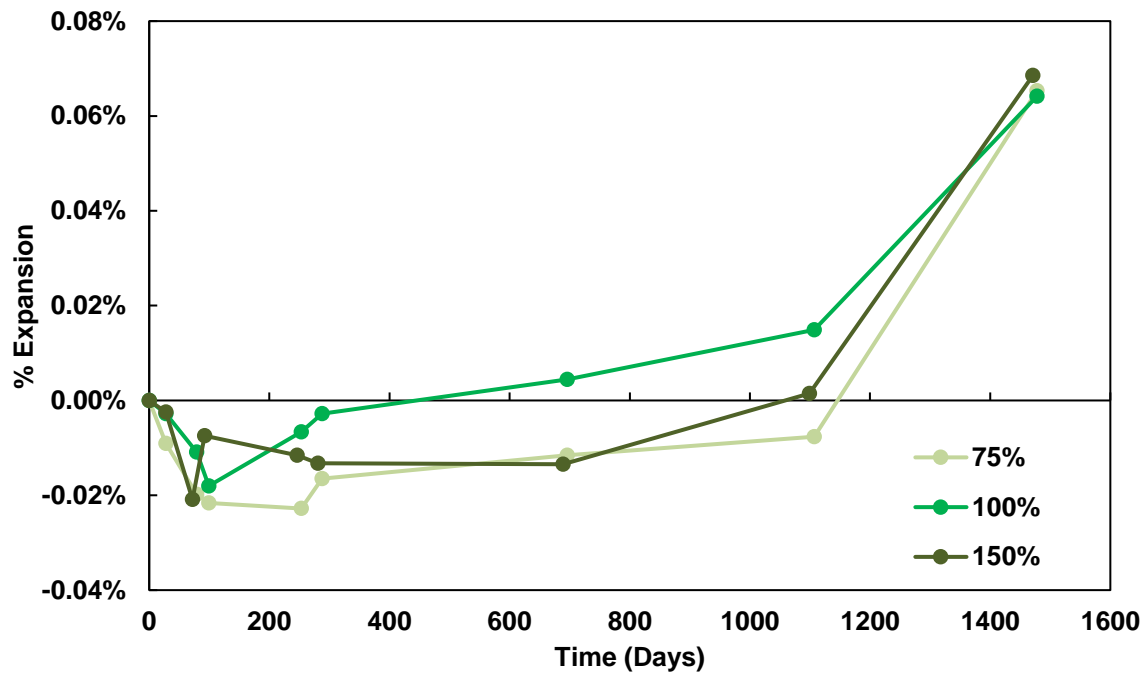


Figure 2.49 Exposure block expansion over time for FA2 aggregate in Cooked condition (ASR + DEF) with varying lithium dosages without control

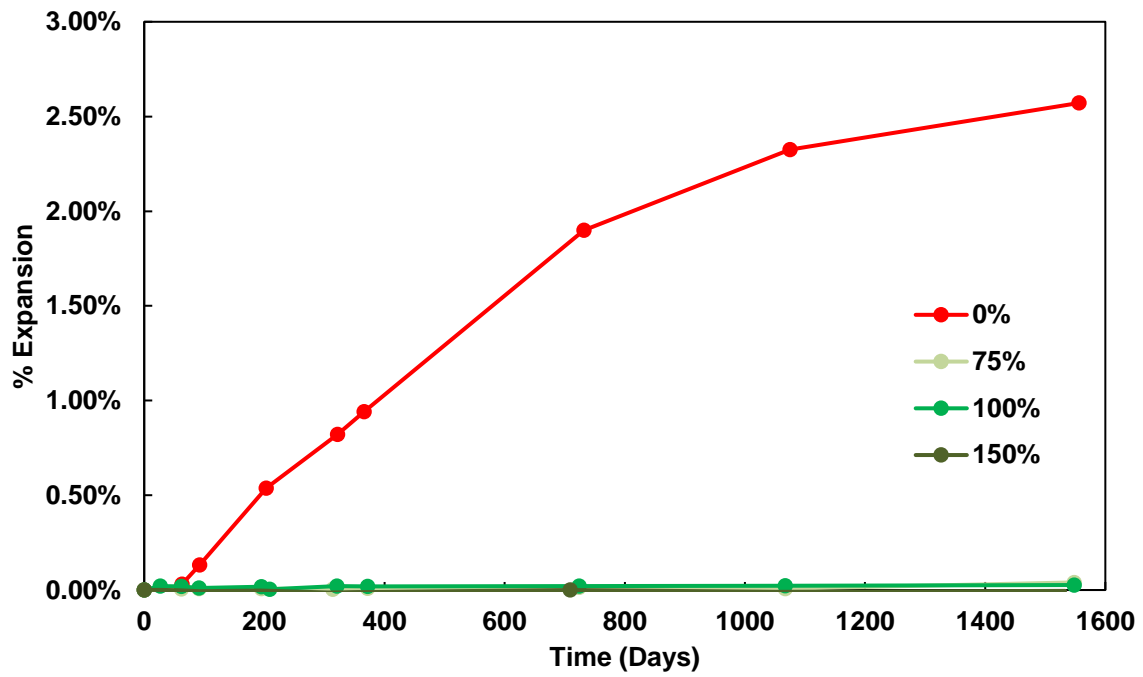


Figure 2.50 Exposure block expansion over time for FA1 aggregate in Uncooked condition with varying lithium dosages

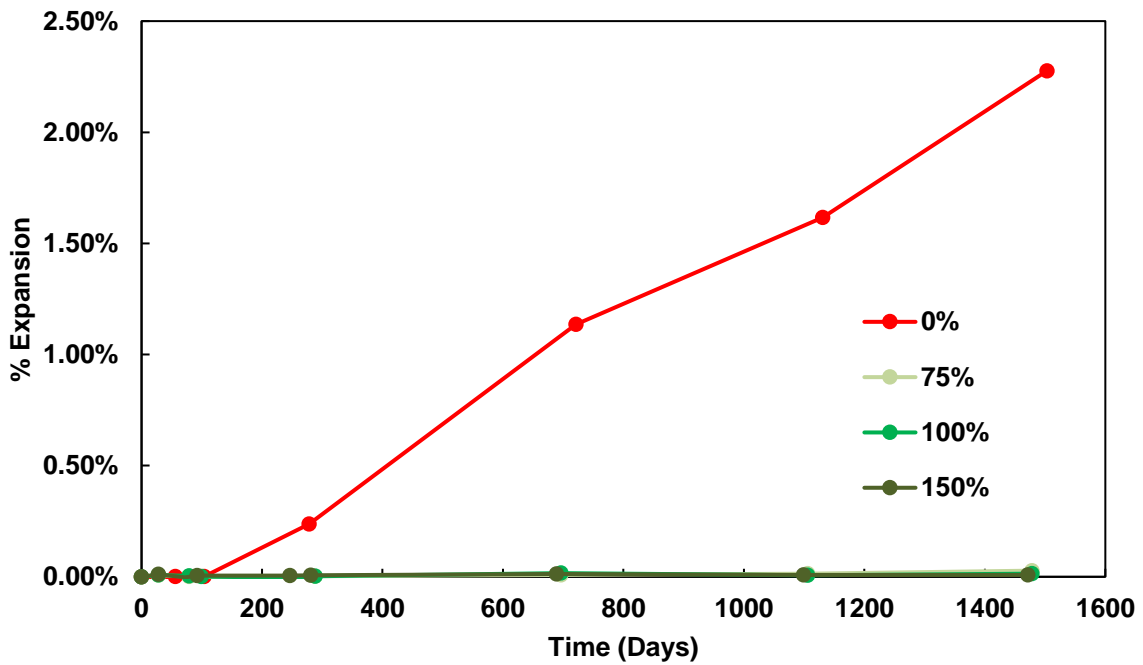


Figure 2.51 Exposure block expansion over time for FA2 aggregate in Uncooked condition with varying lithium dosages

2.3.6.3. Standard Blocks in Texas Marine Exposure Site [Figures 2.52–2.53]

While the Texas Marine Exposure Site is dedicated mostly to corrosion research, exposure blocks were placed there to study the effect of climate on ASR and/or DEF and the potential for alkalis from seawater to exacerbate expansion. A review of the literature found inconsistent claims regarding the effect of sodium chloride ingress on ASR expansion. Certain studies found it to exacerbate damage, while it had no effect in other cases (Rajabipour et al., 2015).

Field samples at the Texas Marine Exposure Site are currently behaving similarly to their counterparts at LIME. That is, control samples are highly expanding, and lithium mixtures show signs of early expansion. The figures include data points for field samples at LIME (labeled as Lab) for reference. The samples have not yet been tested for chloride ingress.

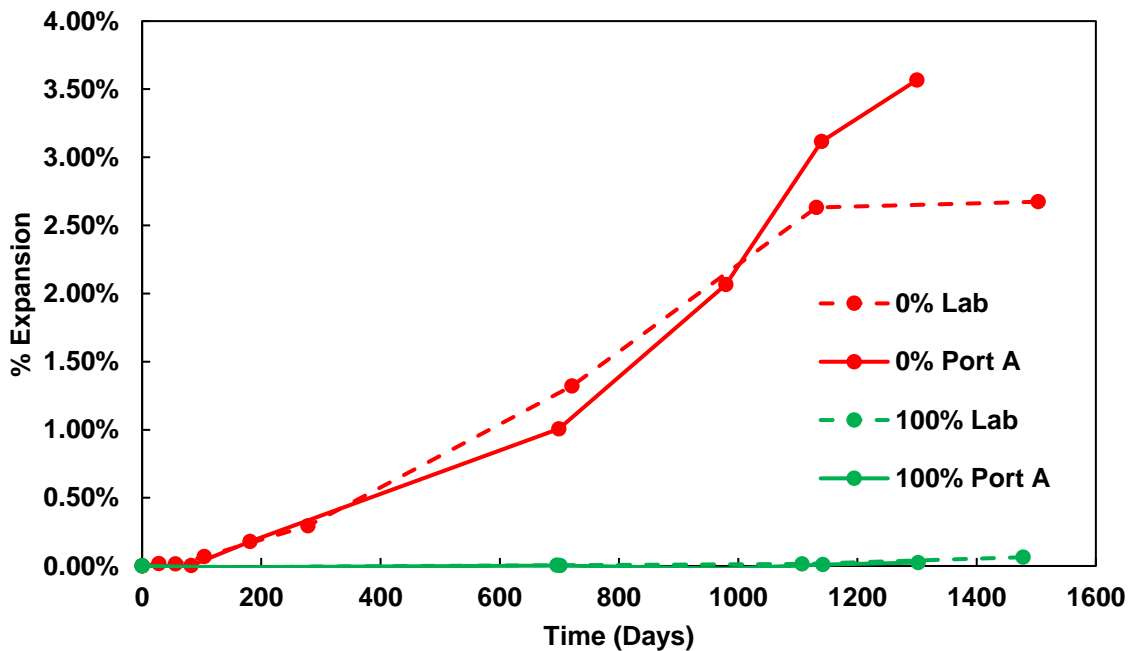


Figure 2.52 Exposure block expansion over time for FA2 aggregate in Cooked condition with and without lithium in Texas Marine Exposure Site

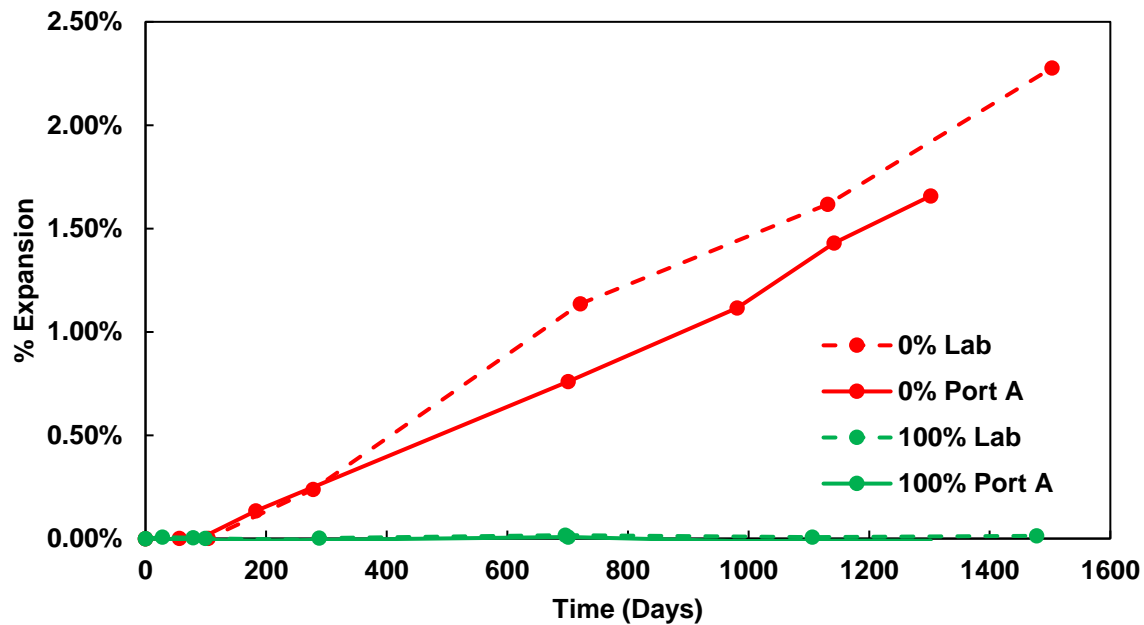


Figure 2.53 Exposure block expansion over time for FA2 aggregate in Uncooked condition with and without lithium in Texas Marine Exposure Site

2.3.6.4. LWFA Blocks in Central Texas Site [Figures 2.54–2.57]

Data points for the standard control mixtures (No LWFA) are included for reference as dashed lines in the figures.

While the expansion for the Cooked LWFA control mixtures shown in Figures 2.54 and 2.55 exceeded that of the mixtures without LWFA, this is likely an artificial effect caused by the loss of measurement points. The results indicate that the presence of LWFA is likely not providing a significant benefit in Cooked control field samples. Contrastingly, corresponding mortar bars with ASR + DEF, show a marked improvement with the use of LWFA (Figure 2.34).

The presence of LWFA, independent of lithium was observed to reduce expansion in control Uncooked samples (Figures 2.56 and 2.57). Similar results were also observed in concrete prism lab samples (Section 2.6.4.2) and by Li et al. (2018).

The Cooked Time Release lithium mixtures appear to exhibit signs of early expansion at 1,500 days like the standard blocks. While it is too early to definitively determine, the current values show higher expansions for the Time Release lithium mixtures when compared to mixtures using the standard introductory method.

The 0% LWFA FA2 control mixture is evidently expanding as seen in Figure 2.57. However, its corresponding ASTM C1293 concrete prism sample passed the test at two years without the use of lithium. This result highlights the potential disconnect between lab and field performance, with lab testing yielding a false negative result but the field specimen expanding in a relatively short period of time (less than one year). The ASTM C1293 test conditions could have provided dual benefits by simultaneously promoting the leaching of alkalis given the humid environment and by accelerating pozzolanic reaction of the LWFA given the elevated temperatures. While both factors are also present to an extent in the corresponding field samples, their effect would inherently take place over a longer time and make their influence less pronounced. Moreover, the discrepant results observed with LWFA lab samples differed based on aggregate reactivity, indicating that the incubation time of each aggregate may play a role in the ability for LWFA to be effective.

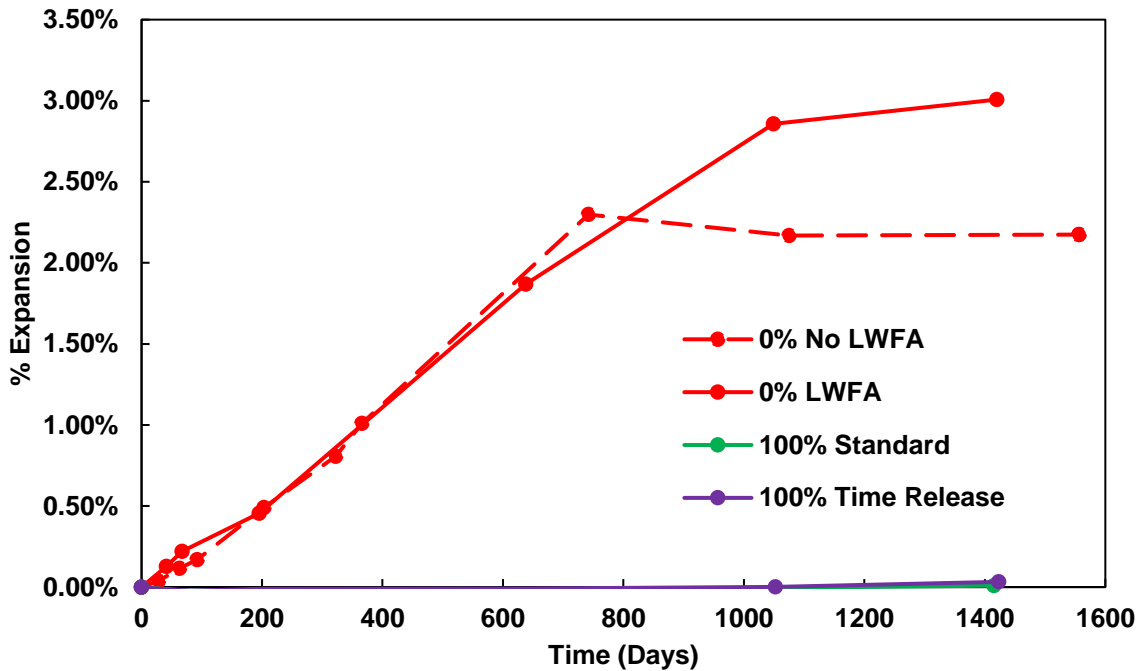


Figure 2.54 Exposure block expansion over time for LWFA FA1 in Cooked condition with varying lithium introductory methods

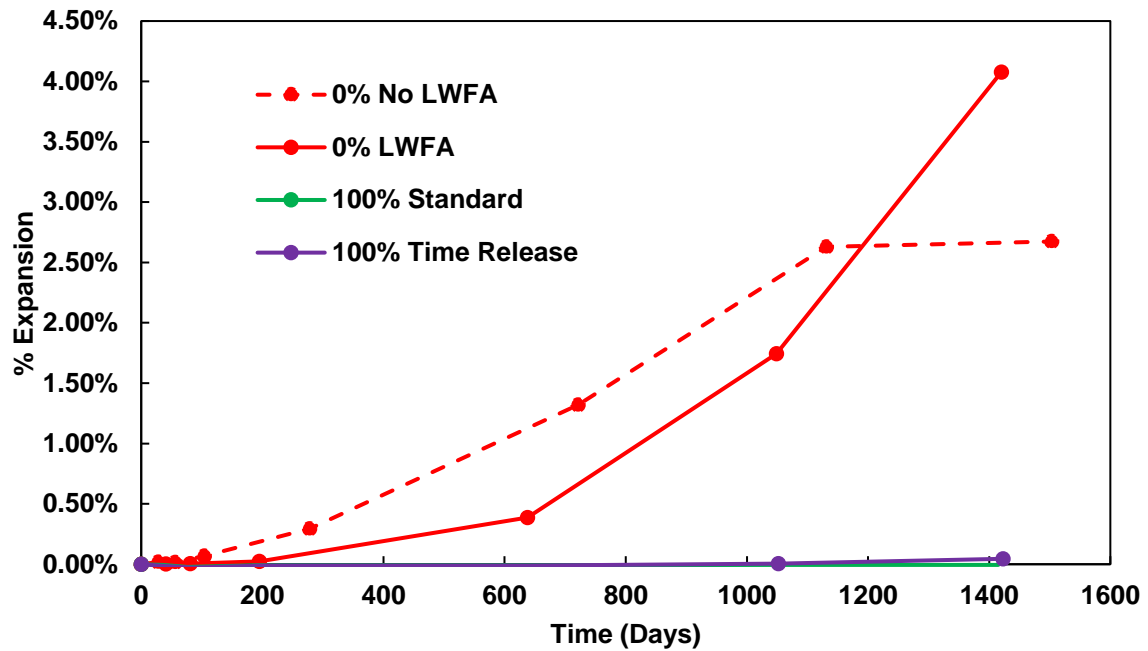


Figure 2.55 Exposure block expansion over time for LWFA FA2 in Cooked condition with varying lithium introductory methods

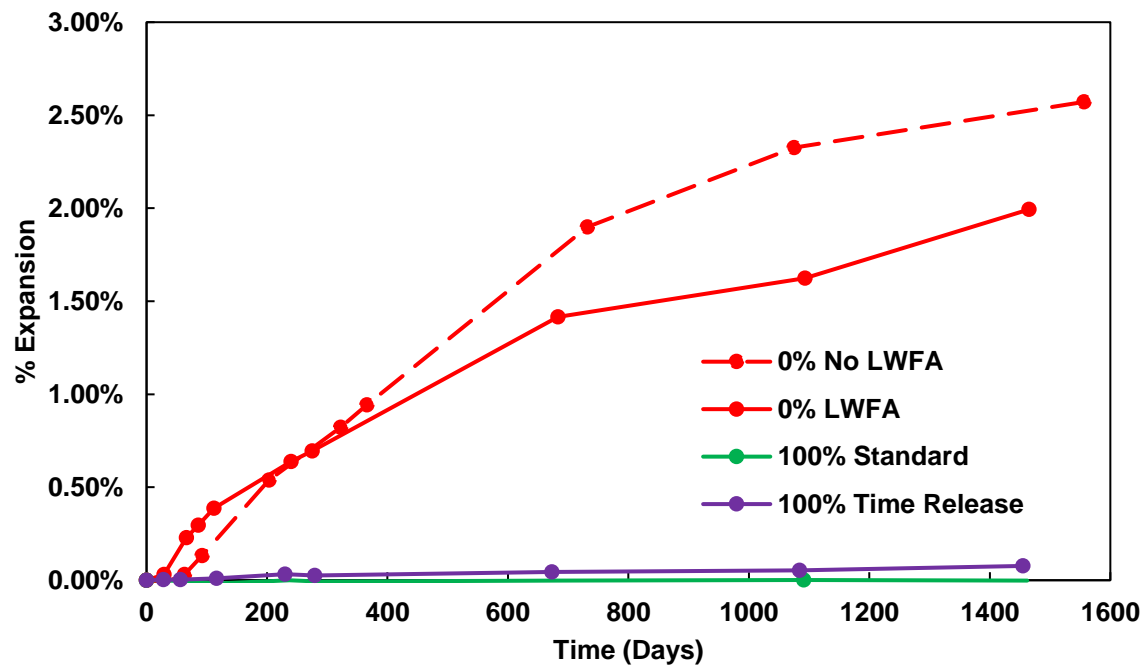


Figure 2.56 Exposure block expansion over time for LWFA FA1 in Uncooked condition with varying lithium introductory methods

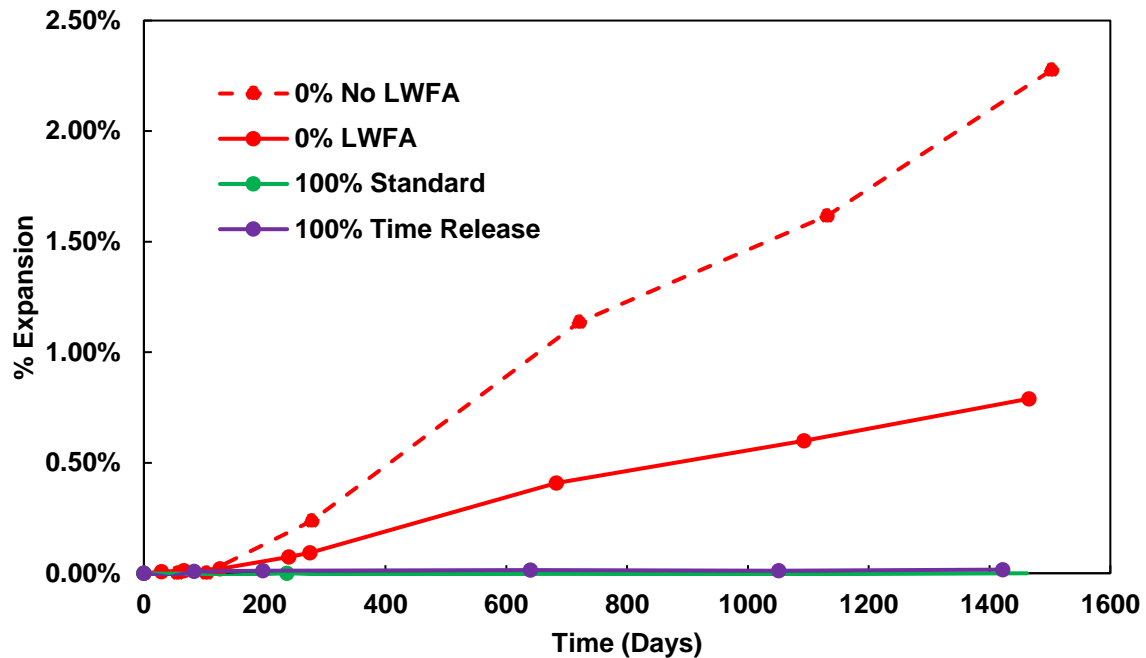


Figure 2.57 Exposure block expansion over time for LWFA FA2 in Uncooked condition with varying lithium introductory methods

2.4. Further Research

Given the slow nature of the ASR and DEF mechanisms in fields samples, many more years of additional exposure may be required before making a final assessment regarding the effectiveness of lithium dosages and introductory methods. Additional research will also be required to fully capture and understand the fundamental mechanisms at play. Special attention should be paid to the LWFA Time Release series since many of the assumptions made for this series have not yet been fully deciphered. Based on the current data and literature review, the following actions are recommended for further research of current and future samples.

2.4.1. Field Samples

- Continue monitoring field samples for expansion.
- Develop new forms for casting of exposure blocks with a more accurate method of measuring expansion. Particular attention should be paid when casting control blocks that are expected to severely expand. Excessive expansion may be beyond the limits of the measuring device and lead to loss of measurement points and expansion data.

- Conduct coring of exposure blocks at the Texas Marine Exposure Site to determine chloride ingress and its effects on ASR and DEF.
- Determine if Uncooked mixtures became Semi-Cooked. This may involve the coring of Cooked and Uncooked control exposure blocks to determine absence or presence of DEF. Core samples could be examined through scanning electron microscopy or by immersing in water and measuring expansion over time. There is precedent in the literature for cores being extracted from field structures and immersed in limewater to test for potential expansion due to DEF (Thomas et al., 2008).
- Consider placing a Cooked block in water storage to isolate and accelerate DEF, like the mortar bars immersed in limewater.
- Determine what is triggering the expansion of Cooked mixtures with lithium at an age of 1,500 days. This may involve the coring of specimens and extraction of pore solution to examine the lithium concentration in Cooked vs Uncooked specimens.

2.4.2. Lab Samples

- Continue monitoring ASTM C1293 concrete prisms, mortar bars over water, and mortar bars immersed in water.
- Examine the pore solution of ASTM C1293 samples to determine if alkali leaching has occurred at similar rates in mixtures with and without lithium.
- Measure extent of alkali leaching in ASTM C1293 test and explore new methods of performing ASR lab testing that minimize leaching.
- Measure mortar bar samples for mass gain as well as expansion.
- Test for leaching or pore solution concentration on samples with combined ASR + DEF to determine when each mechanism is active.

2.4.3. Time Release Method

- Perform early age pore solution testing to determine the molar concentration of lithium at different ages based on introductory method. This will assist in determining if the Time Release method is able to ‘protect’ lithium and allow it to be released at later stages as it is intended.
- Investigate new methods to accurately determine admixture absorption and desorption by LWFA. The use of alternative techniques to the cone test described

in ASTM C128 are recommended and may include the paper towel method (NYDOT, 2008) or the use of cobalt chloride (Kandhal and Lee, 1970) to test for the SD condition.

- Determine if the excess lithium admixture remaining on LWFA surfaces plays a beneficial role in mitigating expansion. Hargis et al. (2013) saw a decrease in ASR expansion when soaking reactive aggregates with LiOH by creating a lithium silicate passivation layer.

2.4.4. Lithium

- Investigate how heat treatment affects the presence of lithium in the pore solution. Ekolu et al. (2017) proposed that lithium is preferentially absorbed within C-S-H layers instead of the released sulfate and alumina from dissolved ettringite.
- Investigate the potentially modified DEF ettringite product formed in the presence of lithium. Ekolu et al. (2017) proposed that a modified ettringite product with lithium instead of calcium may be less or non-expansive and may explain the dual effectiveness of lithium in mitigating DEF expansion.
- Investigate if the absorption of lithium within C-S-H layers during heat treatment is detrimental to lithium's ability to mitigate ASR.

2.4.5. LWFA Effect on ASR

- Pore solution analysis is recommended for the ASTM C1293 concrete prism samples of the FA2 and LWFA FA2 control mixtures to help determine why the LWFA FA2 mixture yielded a false negative result.
- Testing to determine pozzolanic activity and an increase in alumina content is also recommended with the use of LWFA.

2.5. Conclusions

The objective of this study was to assess the performance of a lithium admixture in mitigating deleterious expansion due to ASR and/or DEF and to optimize its use. Current results indicate that lithium may not be effective in mitigating combined ASR and DEF expansion. Previous studies (Ekolu et al., 2007; Ekolu et al., 2017) indicated the potential for lithium to be dually effective in preventing expansion due to ASR and DEF but acknowledged the possibility for lithium to become ineffective in the long-term. This study supplements the previous work by providing long-term field data to validate theories proposed from lab samples.

The use of LWFA was shown to delay and decrease expansion due to ASR and/or DEF independent of lithium. The findings supplement previous results (Li et al., 2018) by providing data from additional lab and field samples cast with various aggregates. Moreover, the use of LWFA in DEF mixtures has not been widely explored and results from this study could provide long-term data on its effects. Field data is particularly valuable for the case of LWFA given that a significant disconnect between lab and field specimens was observed. The effectiveness of the LWFA in reducing expansion was observed to vary based on aggregate mineralogy and reactivity. The mechanism causing variation is not fully understood but may involve temperature and leaching effects.

The novel method for admixture introduction through saturated LWFA did not show an inherent advantage over the standard method. Long-term data from field samples will ultimately determine its potential. Additionally, aggregate absorption was found to profoundly vary when using admixtures as ponding solutions. The procedure also adds several technical and practical complexities such as standardizing batching procedures, determining admixture quantity, and providing the adequate content of LWFA. These factors are bound to increase production cost when compared to the standard method without a guarantee of improved performance.

2.6. References

- AASHTO R80 (2017) *Standard Practice for Determining the Reactivity of Concrete Aggregates and Selecting Appropriate Measures for Preventing Deleterious Expansion in New Concrete Construction*
- ASTM C1260 (2014) *Standard Test Method for Potential Alkali Reactivity of Aggregates (Mortar-Bar Method)*
- ASTM C128 (2015) *Standard Test Method for Relative Density (Specific Gravity) and Absorption of Fine Aggregate*
- ASTM C1293 (2015) *Standard Test Method for Determination of Length Change of Concrete Due to Alkali-Silica Reaction*
- ASTM C150 (2016) *Standard Specification for Portland Cement*
- ASTM C1778 (2016) *Standard Guide for Reducing the Risk of Deleterious Alkali-Aggregate Reaction in Concrete*
- ASTM C192 (2015) *Standard Test Method for Making and Curing Concrete Test Specimens in the Laboratory*
- ASTM C39 (2016) *Standard Test Method for Compressive Strength of Cylindrical Concrete Specimens*
- Bentz, D. P., Lura, P., & Roberts, J. W. (2005). Mixture proportioning for internal curing. *Concrete International*, 35-40.

Bentz, D.P., “Capitalizing on Self-Desiccation for Autogenous Distribution of Chemical Admixtures in Concrete,” Self-Desiccation and Its Importance in Concrete Technology, Proceedings of the 4th International Research Seminar, B. Persson, D.P. Bentz, and L.-O. Nilsson, eds., Gaithersburg, MD, June 2005, pp. 189-196

C.W. Hargis, M.C.G. Juenger, & P.J.M. Monteiro. (2013). Aggregate Passivation: Lithium Hydroxide Aggregate Treatment to Suppress Alkali-Silica Reaction. *ACI Materials Journal*, 110(5), 567–. <https://doi.org/10.14359/51685908>

D.P. Bentz, W.J. Weiss, Internal Curing: A 2010 State-of-the-art Review, US Department of Commerce, National Institute of Standards and Technology, 2011.

Drimalas, T. & Folliard, K. (2020) Unpublished Exposure Block Data. The University of Texas at Austin Laboratory for Infrastructure Materials Engineering (LIME).

Drimalas, T., Ideker, J.H., Bentivegna, A.F., Folliard, K.J., Fournier, B., Thomas, M.D.A. (2012) The long-term monitoring of large-scale concrete specimens containing lithium salts to mitigate alkali–silica reaction, *ACI Spec. Publ. SP289-18.1*–17.

Ekolu, S., Rakgosi, G., & Hooton, D. (2017). Long-term mitigating effect of lithium nitrate on delayed ettringite formation and ASR in concrete – Microscopic analysis. *Materials Characterization*, 133, 165–175. <https://doi.org/10.1016/j.matchar.2017.09.025>

Ekolu, S.O., Thomas, M.D.A., Hooton, R.D. (2007) Dual effectiveness of lithium salt in controlling both delayed ettringite formation and ASR in concretes, *Cement and Concrete Research*, Volume 37, Issue 6, June 2007, Pages 942-947, ISSN 0008-8846

French, W.J. (1995) Avoiding concrete aggregate problems, *Improving Civil Engineering Structures—Old and New*. pp. 65–95.

Giannini, E., Folliard, K., & Zhu, J. (2012). Evaluation of concrete structures affected by alkali-silica reaction and delayed ettringite formation by Eric Richard Giannini. University of Texas, Austin, Tex.

Hansen, W.C. (1944) Studies relating to the mechanism by which the alkali–silica reaction proceeds in concrete, *J. Am. Concr. Inst.* 15, 213–227.

Hobbs, D.W. (1988) *Alkali–Silica Reaction in Concrete*, Thomas Telford, London.

Holm TA, Ooi OS, Bremner TW. Moisture dynamics in lightweight aggregate and concrete. Expanded Shale Clay and Slate Institute, Publication # 9340; 2004, p. 12.

Javier Castro, Lucas Keiser, Michael Golias, Jason Weiss, Absorption and desorption properties of fine lightweight aggregate for application to internally cured concrete mixtures, *Cement and Concrete Composites*, Volume 33, Issue 10, November 2011, Pages 1001-1008, ISSN 0958-9465

Kandhal PS, Lee DY. An evaluation of the bulk specific gravity for granular materials. Highway Research Record 307, HRB, National Research Council: Washington, DC; 1970. p. 44–55.

- Kelham, S., “The Effect of Cement Composition and Fineness on Expansion Associated with Delayed Ettringite Formation,” *Cement and Concrete Composites*, Vol. 18 (1996): 171-179
- Li, C., Thomas, M., & Ideker, J. (2018). A mechanistic study on mitigation of alkali-silica reaction by fine lightweight aggregates. *Cement and Concrete Research*, 104, 13–24. <https://doi.org/10.1016/j.cemconres.2017.10.006>
- Lute, R., & Folliard, K. (2008). Evaluation of coatings and sealers for mitigation of alkali-silica reaction and/or delayed ettringite formation by Racheal Dawn Lute. Thesis (M.S. in Engineering)--University of Texas at Austin, 2008.
- Lute, R., & Folliard, K. (2016). Durability of calcium-aluminate based binders for rapid repair applications / by Racheal Dawn Lute. [University of Texas], Austin, Tex.
- M.D.A. Thomas, B. Fournier, K.J. Folliard, J.H. Ideker, Y. Resendez, The use of lithium to prevent or mitigate alkali-silica reaction in concrete pavements and structures, FHWA Report# FHWA-HRT-06-133, Federal Highway Administration, Washington, D.C., 2007
- McCoy, W.J., Caldwell, A.G. (1951) A new approach to inhibiting alkali-aggregate expansion, *J. Am. Concr. Inst.* 41, 693–706.
- NYDOT. Test method No.: NY 703-19 E: moisture content of lightweight fine aggregate. New York State Department of Transportation, Materials Bureau: Albany, NY; August 2008.
- P. Dahl, H. Justnes, G. Norden, O. Hyrve, Lightweight aggregate fines as pozzolanic additive for high-performance concrete, *ACI Spec. Publ.* 242 (2007) 333–350.
- Pedneault, A. (1996) “Development of testing and analytical procedures for the evaluation of the residual potential of reaction, expansion and deterioration of concrete affected by ASR,” M.Sc. Memoir, Laval University, Québec City, Canada, 133p.
- Rajabipour, F., Giannini, E., Dunant, C., Ideker, J., & Thomas, M. (2015) Alkali-silica reaction: Current understanding of the reaction mechanisms and the knowledge gaps. *Cement and Concrete Research*, 76, 130–146. <https://doi.org/10.1016/j.cemconres.2015.05.024>
- S. Chandra, L. Berntsson, *Lightweight Aggregate Concrete*, Noyes, New York, 2002.
- S. Diamond, S. Ong, Combined effects of alkali-silica reaction and secondary ettringite deposition in steam cured mortars, *Ceram. Trans.* 40 (1994) 79–90.
- Spragg, R., Castro, J., Li, W., Pour-Ghaz, M., Huang, P., & Weiss, J. (2011). Wetting and drying of concrete using aqueous solutions containing deicing salts. *Cement and Concrete Composites*, 33(5), 535–542. <https://doi.org/10.1016/j.cemconcomp.2011.02.009>
- Stanton, T.E. (1940) Expansion of concrete through reaction between cement and aggregate, *Proc. Am. Soc. Civ. Eng.* 66 (10) 1781–1811.
- Stark, D. (1991) The moisture condition of field concrete exhibiting alkali-silica reactivity, *ACI Spec. Publ.*, SP126-52. pp. 973–988.

T.W. Bremner, S.R. Boyd, T.A. Holm, J.P. Ries, The influence of lightweight aggregates additions in concrete mixtures containing alkali-aggregate reactive normal weight aggregate, fly Ash, silica fume, slag, and natural pozzolans in concrete, Proceedings of the Ninth International Conference on Alkali-aggregate Reactions in Concrete, Warsaw, 2007, pp. 497–510.

Taylor, H., Famy, C., & Scrivener, K. (2001). Delayed ettringite formation. *Cement and Concrete Research*, 31(5), 683–693. [https://doi.org/10.1016/S0008-8846\(01\)00466-5](https://doi.org/10.1016/S0008-8846(01)00466-5)

Thomas, M., Folliard, K., Drimalas, T., & Ramlochan, T. (2008). Diagnosing delayed ettringite formation in concrete structures. *Cement and Concrete Research*, 38(6), 841–847. <https://doi.org/10.1016/j.cemconres.2008.01.003>

Thomas, M.D.A. (2001) The role of calcium hydroxide in alkali recycling in concrete, in: J. Skalny, J. Gebauer, I. Odler (Eds.), *Materials Science of Concrete Special Volume on Calcium Hydroxide in Concrete*, American Ceramic Society, Westerville, OH. pp. 269–280.

Tremblay, C., Bérubé, M.A., Fournier, B., Thomas, M.D., Folliard, K.J. (2010) Experimental investigation of the mechanisms by which LiNO₃ is effective against ASR, *Cem. Concr. Res.* 40 (4). 583–597.

Tremblay, C., Bérubé, M.A., Fournier, B., Thomas, M.D.A. (2004) Performance of lithium-based products against ASR: effect of aggregate type and reactivity, and reaction mechanisms, *Proc. 7th CANMET/ACI Int. Conf. on Recent Advances in Concrete Technology 2004 (Suppl. Papers)*, pp. 247–267.

Tremblay, C., Bérubé, Marc-André, Fournier, B., Thomas, M. D. A., & Folliard, K. J. (2007) Effectiveness of lithium-based products in concrete made with Canadian natural aggregates susceptible to alkali-silica reactivity. *ACI Materials Journal*, 104(2), 195-197,199-205.

Chapter 3. Performance of Corrosion Inhibitors in Lab and Field Testing

3.1. Introduction

As part of the corrosion study, three admixture products were used at varying dosages to determine their ability to reduce corrosion potential through either a reduction in permeability, an increase in the chloride threshold, or a combination of both factors. Their performance is being assessed through the evaluation of lab (cylinders, disks, and corrosion beams) and field (marine exposure blocks) specimens. Preliminary testing results show an overall improvement in performance for most products. However, the current ‘early age’ results focus on chloride ingress within the first 25–50 mm (0.5–1.0 in.) cover depths of marine exposure blocks. Since most reinforced concrete structures follow a 50 mm (2.0 in.) cover depth design, more exposure time is required to conclusively determine admixture performance.

3.2. Background

3.2.1. Corrosion Primer

As previously mentioned, corrosion is the leading form of concrete infrastructure deterioration. Consequently, its repair is a source of major economic impact. Costs associated with corrosion are two-fold as they incur direct and indirect costs. Direct costs include maintenance procedures such as materials and labor, while indirect costs in the form of lost productivity time due to traffic delays often exceed direct costs (Broomfield, 2007).

Corrosion refers to the process by which reinforcing steel bars (rebar) oxidize within the concrete, create expansive rust products, and eventually cause cracking and spalling of concrete. Corrosion is an electrochemical process involving the dissolution of iron from the steel and its subsequent reaction with available water and oxygen. Under optimal circumstances, however, steel embedded in concrete is in ideal conditions preventing the initiation of corrosion. That is because concrete is a highly alkaline material due to the high concentration of alkalis in its pore solution. The alkaline conditions (high pH) found within concrete lead to the formation of a protective film around the steel known as the passive layer. This layer, which is itself a form of oxidation, prevents the further ingress of water and oxygen and, hence, protects from corrosion. The passive layer is theorized to be part metal oxide/hydroxide and part mineral from the cement and can repair itself if the proper alkaline conditions are maintained (Broomfield, 2007).

Nonetheless, there are two main mechanisms by which the passive layer can be damaged and corrosion may initiate: carbonation and chloride ingress. Carbonation, which was not part of this study, refers to the process by which CO₂ penetrates concrete, causing a substantial drop in pH that can depassivate the passive layer and lead to corrosion. While both mechanisms induce the same chemical process of corrosion, the ingress of chlorides is generally believed to not affect concrete pH as carbonation does. Chloride induced corrosion will be detailed in the following sections.

Chlorides may be present in concrete either through external ingress or introduced internally within mixing materials containing chlorides. External sources of chlorides include deicing salts used to prevent ice formation on roads and saltwater exposure in marine environments. Internal sources of chlorides can be due to the use of seawater as batch water, the use of chloride-contaminated aggregates, or the use of chemical admixtures such as calcium-chloride based accelerators. In the case of external chloride sources, chlorides will gradually ingress concrete, primarily via diffusion, but also through capillary action and absorption mechanisms. The work done in this study relates to preventing corrosion caused by external sources of chlorides.

In practice, all concrete deficiencies can be traced back to issues in one or more of the following categories: design, construction, or materials. Corrosion is no exception and can occur if omissions or missteps are made in any of those categories. Table 3.1 provides realistic examples of how each category could result in an increased risk of corrosion.

Table 3.1 Deficiency categories

Category	Description	Examples
Design	Environmental conditions have not been properly considered and the structure design is ill equipped to sustain the service requirements.	Improper reinforcement cover depth specified.
Construction	Standard quality control practices and specifications are not followed.	Insufficient concrete curing.
Materials	Use of deleterious material components.	Use of seawater as batch water, admixtures containing chlorides, or chloride-contaminated aggregates.

3.2.1.1. Chloride Induced Corrosion

Specific portions of the passive layer may be at a higher risk of damage due to localized defects at the concrete/steel interface. Chlorides will be preferentially attracted to these areas and will begin to attack the passive layer. While the passive layer can repair itself, if enough chlorides penetrate a specific area, the passive layer in that area will be effectively destroyed or ‘depassivated’. Once chlorides reach the reinforcement and cause

depassivation, corrosion will initiate. The amount of chlorides needed to cause depassivation and induce corrosion is known as the chloride threshold. This parameter, unique to each concrete mixture, is merely an approximation and may vary based on cement and pore solution composition, pH, and temperature (Balonis and Glasser, 2011). A wide range of chloride threshold values have been reported in the literature. In the context of this study, threshold values from 0.1% to 1.96% (by mass of cementitious) have been reported for field structures (Angst et al., 2009).

Once the chloride threshold has been reached and the passive layer has been sufficiently damaged, iron ions from the steel will begin to dissolve in the pore solution. This will initiate the electrochemical oxidation reaction known as corrosion. The area where iron ions begin to dissolve will become the anode in the reaction as electrons are being lost. Nearby sections on the steel will then act as the cathode, which will gain the electrons released from the anode and react with water and oxygen. The reaction at the cathode involves the creation of hydroxyl ions, which increase alkalinity and effectively strengthen the passive layer at the cathode. Conversely, at the anode alkalinity will decrease and chloride content will increase since the negatively charged chloride ions will favor the more positive anodic region (Bertolini et al., 2013). Throughout the reaction, an electrical current will be created by the flow of electrons between the anode and the cathode. Therefore, the conditions required to initiate corrosion in concrete are depassivation of the passive layer either due to carbonation or chloride ingress, creation of a galvanic couple (anode and cathode), electrical connectivity between the anode and cathode (pore solution), and availability of water and oxygen.

Following the initiation of the oxidation process, the dissolved iron will continue to develop through several stages of reactions until it becomes hydrated ferric oxide, a red/brown product commonly known as rust. The reactions are shown in Equations 3.1–3.3 (Broomfield, 2007). While the dissolution of iron can lead to loss of steel strength and cross section, the chief concern is the formation of rust, as it involves a volumetric expansion since rust products effectively occupy three to four times the volume of the original iron (Bertolini et al., 2013). This volumetric expansion creates significant pressures at the steel/concrete interface and creates tensile forces within the concrete that are capable of causing cracking and spalling. Nonetheless, the loss of concrete sections is a significant matter as it may develop beyond being a purely aesthetic issue and become a serious concern for user safety. For example, a significant spalling of concrete due to corrosion may lead to a dangerous risk of falling concrete or to a potential loss in structural capacity in the concrete member.



3.2.1.2. Chloride Binding

As chlorides penetrate concrete, they may become chemically bound by hydration products such as C-S-H or aluminate phases. Thus, a theoretical differentiation can be made between free chlorides present in the pore solution, bound chlorides tied up to hydration products, and total chlorides. It is generally believed that chloride-induced corrosion will only initiate if the amount of free chlorides exceeds the chloride threshold (Bertolini et al., 2013). However, there are opposing claims in the literature indicating that even bound chlorides may be released and contribute to corrosion (Glass and Buenfeld, 1997).

Chlorides bound by aluminate phases create products known as Friedel's salts and are a function of the initial C_3A content in the cement. The use of low C_3A cements (ASTM C150 Type II or Type V) could result in decreased formation of Friedel's salts and may make a concrete mixture more susceptible to corrosion. Similarly, the use of SCMs will affect the amount of bound chlorides. Moreover, certain admixture products containing calcium nitrite and calcium nitrate have been reported to influence chloride binding (Balonis and Glasser, 2011; Mammoliti, 2001).

3.2.1.3. Chloride Diffusion Coefficient

As previously mentioned, diffusion is the primary mechanism through which chlorides will ingress concrete. The diffusion process can be quantified by obtaining the apparent chloride diffusion coefficient. This value is a transport parameter indicating the ease of external chloride penetration into a concrete sample. It is known as D_a and is commonly represented in units of m^2/s . Typical values are in the range of 1×10^{-13} to $1 \times 10^{-11} \text{ m}^2/\text{s}$ (Bertolini et al., 2013). Low permeability mixtures would be expected to have low diffusion coefficients.

3.2.1.4. Corrosion Damage Model

As described by Broomfield (2007), corrosion of steel in concrete can be considered as a three-stage process. Firstly, the initiation stage involves the ingress of enough CO_2 or chlorides to cause steel depassivation. Secondly, the activation stage involves oxidation of the rebar and the formation of rust products. Thirdly, the deterioration stage involves concrete cracking and spalling. The stages will progress until the structure reaches a critical limit state at which repairs must be performed for the structure to remain functional.

ConcreteWorks (2017) estimates significant damage to occur six years after depassivation is reached. After this time, extensive cracking and spalling can be expected as part of the deterioration stage. Once cracking initiates, chlorides have direct access to the reinforcement and the diffusion model is no longer applicable.

3.2.2. Corrosion Prevention Methods

There are several techniques used in the industry to reduce the potential for corrosion to occur in new concrete. Steps can be implemented at the design stage to specify material characteristics that will inhibit corrosion. For example, concrete can be specified to have a low w/c and contain SCMs to achieve low permeability, have adequate cover depth, and contain corrosion inhibitors. Similarly, reinforcement can be specified to be epoxy coated, galvanized, or stainless steel. Additionally, external systems or applications may be employed such as waterproofing membranes or sealers and the use of cathodic protection. These methods will contribute in preventing corrosion by either limiting the availability of chloride, oxygen, and water, increasing the chloride threshold, reinforcing the passive layer, or providing electrochemical treatment. Each of these techniques will have its own benefits and limitations. While it is unreasonable to guarantee that corrosion can be entirely prevented, optimal performance may be most attainable through the synergistic use of multiple methods. The work performed in this study focused on the use of corrosion inhibitors in ordinary portland cement (OPC) mixtures to delay corrosion.

3.2.3. Corrosion Inhibitors

Corrosion inhibitors are chemical admixtures intended to reduce the potential for corrosion to occur and propagate. They are defined by ISO 8044 as a “chemical substance that, when present in the corrosion system at a suitable concentration, decreases the corrosion rate without significantly changing the concentration of any corrosive agent.” As previously mentioned, it is unfeasible to entirely prevent corrosion; therefore, the role of corrosion inhibitors is better described as that of a corrosion retarder. Inhibitors can delay the initiation and propagation of corrosion by decreasing permeability, increasing the chloride threshold, decreasing the corrosion rate after initiation, or a combination of these methods. Inhibitors are considered ‘preventative applications’ aimed at delaying corrosion initiation as well as decreasing corrosion rate. The ASTM C1582 standard outlines performance requirements for corrosion inhibitors.

This study focuses on the use of corrosion inhibiting admixtures that are intermixed with concrete materials as new concrete is cast. Other inhibitors may be applied to hardened concrete surfaces as a repair technique. Given the long-term nature of corrosion, there is limited field data on the use of corrosion inhibitors. Even ten-year studies can yield incomplete results as active corrosion can take decades to initiate (Kessler et al., 2007).

Nonetheless, some manufacturers present claims about their products solely based on short-term lab data. Therefore, the need for field validation on the effectiveness of corrosion inhibitors is much needed.

The following classification of corrosion inhibitors is provided by Broomfield (2007):

A) By their action:

- Anodic inhibitors – suppressing the anodic corrosion reaction.
- Cathodic inhibitors – suppressing the cathodic reaction.
- Ambiodic inhibitors – suppressing both anodes and cathodes.

B) By their chemistry and function:

- Inorganic inhibitors – nitrites, phosphates, and other inorganic chemicals.
- Organic inhibitors – amines and other organic chemicals.
- Vapor phase or volatile inhibitors – a subgroup of the organic inhibitors (generally aminoalcohols) that have a high vapor pressure.

3.2.3.1. Product Background

The study includes the use of two inorganic inhibitors and one organic inhibitor. Background details regarding each product are included below.

3.2.3.1.1. Product D

Product D is an anodic and inorganic inhibitor that is calcium nitrite based. Calcium nitrite inhibitors have been widely used in the industry and have proven to be effective if properly dosed (Virmani and Clemena, 1998). Calcium nitrite can oxidize ferrous ions (Fe^{2+}) to ferric ions (Fe^{3+}), which form poorly soluble iron oxides (Bertolini et al., 2013). This mechanism effectively interrupts corrosion and reinforces the passive layer, requiring more chlorides to depassivate the steel and hence increasing the chloride threshold.

Nitrite is sacrificially consumed as it restores the passive layer; therefore, sufficient nitrites must be present to provide continuous protection (Aitcin and Flatt, 2016). Recommended dosages are a function of expected chloride loadings and can be represented by a chloride-to-nitrite ratio, $[\text{Cl}^-]/[\text{NO}_2^-]$. That is, the higher the admixture dosage, the lower the ratio. It should be noted that only nitrite ions present in the pore solution contribute to this ratio and are effective in preventing corrosion. The ratio may be affected by the leaching of nitrite or by nitrite becoming tied up in hydration products. Beneficial effects of the

admixture have been seen on chloride-to-nitrite ratios as high as 1.8, yet researchers have recommended providing enough admixture as to not exceed a ratio of 1.0 (Virmani and Clemena, 1998). In practical terms, recommended dosages range from 2–6 gal/yd³. Table 3.2 presents the increased chloride threshold values based on calcium nitrite admixture dosage as used by ConcreteWorks (2017). Comparable threshold values are also found in the literature (Berke and Hicks, 2004).

Given that the active ingredient in this admixture, calcium nitrite, is water-soluble, leaching may be a concern when considering long-term performance. Additionally, the use of nitrite admixtures may not be allowed in submerged structures because of environmental and health reasons associated with the leaching of nitrites (Bertolini et al., 2013). Work by Powers et al. (1999) found that relatively permeable slabs ($w/c = 0.53$) containing admixed calcium nitrite were able to maintain significant concentrations of the original nitrite after 17 years. However, it should be noted that these slabs were only ponded with a sodium chloride solution for a matter of weeks and spent most of the 17 years exposed to natural weather conditions, i.e., rain, wind, sunlight, etc. These exposure conditions are vastly different from what could be expected in a marine environment.

Calcium nitrite has been found to preferentially bind with the AFm phase (Balonis and Glasser, 2011). This property creates a ‘smart’ behavior in which nitrites become safely stored within the AFm phase only to be released once chlorides ingress. The process exchanges nitrite for chloride within the AFm phase and effectively ties up chlorides by forming Friedel’s salt while releasing nitrite ions into the pore solution, beneficially reducing the $[Cl^-]/[NO_2^-]$ ratio. Moreover, the storage of the nitrite within the AFm phase protects against leaching. Thus, by virtue of this mechanism, the increase in chloride threshold observed with the use of calcium nitrite could also be a result of enhanced chloride binding.

Calcium nitrite inhibitors have been reported to increase compressive strength and to accelerate setting time (Gaidis, 2004). During early hydration, the presence of the calcium cation requires less C_3S to dissolve before reaching a supersaturated state, effectively accelerating the crystallization and setting process (Hewlett and Liska, 2019). A review by Berke and Rosenberg (1989) found that the admixture has potential to reduce the chloride diffusion coefficient or at least not negatively affect it. Moreover, the presence of calcium nitrite may alter pore solution conductivity, which could influence electrical measurements such as resistivity. It is generally believed that the presence of calcium nitrite artificially increases conductivity in electrical tests (Berke and Rosenberg, 1989).

Table 3.2 Chloride threshold values with calcium nitrite admixture (30% concentration) (ConcreteWorks, 2017)

Dosage (gal/yd ³)	Chloride Threshold (% mass of concrete)
0	0.07
2	0.15
3	0.24
4	0.32
5	0.37
6	0.40

3.2.3.1.2. Product P

Product P is labeled as an accelerator and its active ingredients are a mixture of calcium nitrate, calcium nitrite, and glycols. Similar to the accelerating effect seen with calcium nitrite, the presence of additional calcium cations during early hydration will require less C₃S to dissolve before reaching a supersaturated state, effectively accelerating the crystallization and setting process with the use of calcium nitrate (Hewlett and Liska, 2019).

An increase in strength is reported with the use of calcium nitrate accelerators, theorized to be caused by the formation of nitrate-AFm, C₃A·CA(NO₃)₂·10H₂O, and the stabilization of ettringite (Hewlett and Liska, 2019). Further studies by Balonis et al. (2011) indicate that nitrate and nitrite readily displace sulfate from AFm phases to form nitrate AFm or nitrite AFm. The displaced sulfate is then believed to be able to react and increase the amount of ettringite, which results in a higher volume of solids and consequent densification of the matrix. Nitrate was also found to overwhelmingly be stored in solid phases, while nitrite solubility was much higher. This allowed nitrite to be more readily available in the pore solution, which is beneficial in terms of corrosion protection but disadvantageous in terms of leaching.

Some previous studies have suggested that calcium nitrate products may be used as an inhibitor for chloride-induced corrosion (Holm, 1987; Østnor and Justnes, 2011; Al-Amoudi et al., 2003), with the concept tracing back to work done by Russian researchers in the 1970s (Gaidis, 2004). Contrastingly, calcium nitrate has been reported to be detrimental in the case of carbonation-induced corrosion (Stefanoni et al., 2019) and anodic stress corrosion cracking that may occur in high strength steel members (Bertolini et al., 2013).

While calcium nitrite is the most widely studied and used corrosion inhibitor, there is limited information about calcium nitrate preventing corrosion in the literature. Østnor and

Justnes (2011) suggest that calcium nitrate can be considered as an anodic inhibitor with a similar mechanism to calcium nitrite, i.e., oxidation of ferrous ions (Fe^{2+}) to ferric ions (Fe^{3+}). However, the authors also claim that given its particular chemistry, nitrate can theoretically be three times as effective as nitrite at an equimolar dosage. Nitrate is thus considered to provide a higher corrosion buffer, to be less harmful, and to be available in larger amounts and at a lower cost. A calcium nitrate dosage of 3–4% by mass of cement was found sufficient to retard corrosion (Justnes, 2006). Further work by Østnor et al. (2014) found that the presence of calcium nitrate did not significantly influence the chloride diffusion coefficient of field samples. It should be noted that the previous research was performed with the use of a lab-grade, crystalline form of pure calcium nitrate. Conversely, a commercially available calcium nitrate and calcium nitrite-based product is being used in this study.

3.2.3.1.3. Product R

Product R is an ambiodic and organic inhibitor that contains a water-based combination of amines and esters as its active ingredient. Based on manufacturer claims, the inhibitor provides dual benefits of slowing chloride ingress and forming a protective film on the reinforcing steel. A uniform dosage of 1 gal/yd³ is recommended. When used at the recommended dosage, ConcreteWorks (2017) software reduces the estimated chloride diffusion coefficient, D_{28} , by 10% and the concentration buildup rate, b , by 50%, and increases the default chloride threshold from 0.07% to 0.12%. These changes reflect the potential decrease in permeability and increased reinforcement passivity, as claimed by the manufacturer. These claims, however, have been challenged as a ten-year study by Kessler et al. (2007) showed little beneficial effect of using the admixture.

3.2.4. Alternative Theories on Corrosion Mechanisms

The review of the literature found insightful instances of alternative theories on ‘well-established’ corrosion mechanisms. Selected highlights will be presented here as they may assist in explaining experimental results or may provide useful ideas for further research.

3.2.5. Causes of Long-Term Corrosion

Work by Melchers and Chaves (2019, 2020) proposes that long-term corrosion is caused by a different mechanism than the well-established chloride threshold model for short-term corrosion. It is acknowledged that chloride ingress is capable of initiating corrosion of reinforcement once a certain threshold is reached; however, it is proposed that in low permeability concretes, the initial corrosion reaction will be transient and will stop. The revised model shows a modified version of the original ‘Tuutti’ model with an extended activation period that will delay significant damage. Therefore, it is believed that several

mechanisms are involved in ‘chloride-induced’ corrosion, with chloride ingress being only a part of it. The dissolution of calcium hydroxide (CH) is believed to play a previously undiscovered role in the process. A summary of the experimental process and findings of Melcher and Chaves (2020) is presented below.

- Reinforced concrete specimens were cast with varying cements, w/c ratios, and aggregate contents. Chlorides were introduced internally by using seawater as batch water in certain mixtures. Samples were stored in a fog room for 12 years.
- While samples mixed with seawater contained enough chlorides (0.22–0.30% Cl by mass of concrete) to exceed the chloride threshold, the extent of corrosion was variable based on mixture permeability. Chloride contents also decreased by the end of the test, with the more permeable mixtures having more significant drops. It is presumed that high permeability allowed for the chlorides to leach out of the concrete.
- The dissolution of CH, observed through x-ray diffraction (XRD), was found to be the primary mechanism responsible for long-term corrosion. Compared to concrete alkalis like NaOH and KOH, CH solubility is low in water. However, in the presence of chlorides its solubility increases, and the rate of solubility is directly related to the chloride content.
- In the presence of chlorides, CH in high permeability mixtures is presumed to dissolve and leach out of the concrete. This effectively creates a more permeable outer matrix, which facilitates the ingress of oxygen to the reinforcement and leads to corrosion. Higher permeability is believed to provide greater internal surface area and higher availability of free water for the increased dissolution of CH.
- Analogous to carbonation, the dissolution of CH will decrease the concrete pH. Corrosion is favorable if a pH of 9 or lower is reached at the reinforcement. Low permeability mixtures prevented CH dissolution and maintained a pH above 9, protecting them from corrosion albeit containing internal chlorides.
- The decrease in CH has been ruled to not be related to carbonation given the testing procedures, i.e., fog room curing. Furthermore, the presence of additional calcium carbonate was not observed through energy-dispersive X-ray spectroscopy (EDS) measurements, confirming the absence of carbonation.
- In conclusion, the use of low-permeability concrete is emphasized, not only to mitigate chloride ingress, but also to retain CH and maintain a high level of alkalinity. In this context, the use of SCMs, while effective in creating low

permeability concrete, should also be assessed for its ability to retain high alkalinity levels in the long-term.

3.2.5.1. Mechanism of Corrosion Inhibition by Calcium Nitrite and Calcium Nitrate Admixtures

Previous work has indicated that chloride binding may be influenced by the presence calcium nitrite and calcium nitrate (Balonis and Glasser, 2011; Mammoliti, 2001). Mammoliti (2001) claims that both calcium nitrite and calcium nitrate admixtures enhance the chemical binding of chlorides, reducing the availability of free chlorides to cause corrosion. Additionally, improvements in permeability were noticed with the use of the admixtures. A summary of Mammoliti's findings is presented below.

- Chlorides are bound firstly by formation of Friedel's salt, followed by becoming tied within C-S-H products, and finally as calcium or potassium hydroxychloride (Ca,K-OH-Cl).
- A decrease in free chlorides as measured by pore solution analysis was determined to be related to increased chloride binding.
- Mixtures with nitrite and nitrate had an increased capacity for chloride binding as measured by differential thermogravimetric plots.
- Pore solution analysis found negligible leftover concentrations of nitrite and nitrate, indicating that most of those components are incorporated into hydration products.
- Mixtures containing the admixtures were ineffective in reducing corrosion of steel immersed in synthetic pore solution. There was no evidence for the admixtures' ability to reinforce the passive layer in this case.
- Admixture samples ponded in chloride solution had lower total chloride concentrations than controls. Moreover, the volume of exposure solution absorbed by each sample was measured and the absorbed solution was found to have a lower concentration than the original exposure solution. That is, a diluted composition of the solution was preferentially absorbed.
- Overall, nitrite and nitrate were found to decrease total porosity in OPC pastes as tested by mercury intrusion porosimetry. However, results varied by cement type, exposure condition, and pore type (coarse or fine), and the limitations of the testing procedure were acknowledged. It is speculated that micro-cracks developed in admixture mixtures.

3.3. Experimental Investigation

The corrosion testing series was intended to evaluate the effect of three admixture products in mitigating damage due to corrosion in reinforced concrete in lab and field specimens. While exposure condition and sample size varied between lab and field specimens, a qualitative approach was used to assess performance across testing. Therefore, for select mixtures, large field specimens were cast in conjunction with standard laboratory samples to compare results.

3.3.1. Materials

3.3.1.1. Portland Cement

An ASTM C150 Type I cement was used for all mixtures in the corrosion series. The cement's chemical composition was analyzed by XRF; the results are summarized in Table 3.3. The XRF analysis was performed by TxDOT at the Cedar Park Campus. Based on its chemical composition, Bogue equations estimate the cement to have a C_3A content of 11.5%. A cement SG of 3.15 was used for mixture proportions. The cement chloride content was quantified to estimate baseline measurements when obtaining chloride diffusion coefficients. Based on Blaine testing performed, the cement was found to have a fineness value of 402 m^2/kg .

Table 3.3: Cement chemical composition (% by mass)

	SiO ₂	Al ₂ O ₃	Fe ₂ O ₃	CaO	SO ₃	MgO	K ₂ O	Na ₂ O	Cl
ASTM Type I	19.59	5.75	2.23	64.77	3.73	1.20	1.03	0.16	0.0065

3.3.1.2. Aggregates

Manufactured limestone fine aggregate and limestone coarse aggregate were used for this study. Both aggregates came from the same quarry in San Antonio. Table 3.4 summarizes aggregate properties.

Table 3.4 Aggregate properties

Aggregate Type	Absorption Capacity	Specific Gravity (Saturated Surface Dry)
Fine	2.68%	2.61
Coarse	3.12%	2.54

3.3.1.3. Admixtures

A polycarboxylate-based HRWR admixture with an SG of 1.08 was used to achieve proper workability, typically in a dosage of 3 fl. oz per 100 lbs. of cement (fl. oz./cwt). The three products being assessed for their potential to reduce corrosion potential shall be referred to as Product D, Product P, and Product R. Technical details for each product are included below.

3.3.1.3.1. Product D

- Inorganic inhibitor – calcium nitrite based
- Intended to increase chloride threshold. Also known to accelerate setting time.
- SG – 1.28
- Recommended dosage range of 2–6 gal/yd³
- Water reductions: admixture composition calculated as 34.4% solids content and 65.6% water by mass. Therefore, for every lb. of admixture used, reduce batch water by 0.656 lb.

3.3.1.3.2. Product P

- Inorganic inhibitor – calcium nitrate/calcium nitrite based
- Product labeled as an accelerator with potential to serve as corrosion inhibitor
- SG – 1.35
- Recommended dosage range of 8–60 fl. oz/cwt but may be used up to 100 fl. oz/cwt.
- Water reductions: admixture composition calculated as 42.2% solids content and 57.8% water by mass. Therefore, for every lb. of admixture used, reduce batch water by 0.578 lb.

3.3.1.3.3. Product R

- Organic inhibitor – amines and esters based
- Intended to inhibit corrosion by decreasing permeability
- Potential decrease (5–10%) in compressive strength
- SG – 0.99

- Recommended dosage of 1 gal/yd³
- No mention of water reductions with admixture use

3.3.2. Mixture Proportions

Mixture proportions included 362 kg/m³ (611 lb./yd³) of cement, 163 kg/m³ (275 lb./yd³) of water (w/c = 0.45), 986 kg/m³ (1,662 lb./yd³) of limestone coarse aggregate, and 767 kg/m³ (1293 lb./yd³) of manufactured limestone fine aggregate. Aggregate proportions are based on an oven-dry condition.

Typical batch volumes were around 0.14 m³ (5 ft³) for *Lab and Field* mixtures and 0.02 m³ (0.75 ft³) for *Lab Only* mixtures. Table 3.5 outlines which mixtures were designated as either *Lab and Field* or *Lab Only*. Slumps tended to be low (less than 100 mm [4 in.]) and on several occasions required the addition of superplasticizer (3 fl. oz/cwt) to reach better workability (100–150 mm [4–6 in.] slumps). Factors that could have contributed to the low workability include the high water demand of the fine aggregate and the dusty condition of the coarse aggregate. Air contents were between 2.0–2.5%.

High dosages outside of the manufacturer recommended ranges were used for Product R and Product P. Product R is recommended at a fixed dosage of 1 gal/yd³ independent of exposure condition. Higher dosages of 2 and 3 gal/yd³ were tested as part of this study. Since the manufacturer does not advise to perform water reductions based on admixture addition, no water was removed from the batch water. This omission could have increased the effective w/c, especially for the 3 gal/yd³ mixture.

Product P's dosage is based on environmental conditions as higher amounts of accelerator are required with decreasing temperatures. The recommended dosage range is 8–60 fl. oz/cwt, but it may be used up to 100 fl. oz/cwt. Actual dosages used for this study were 2, 4, and 6 gal/yd³ which are equivalent to 42, 84, and 126 fl. oz/cwt correspondingly. Holm (1987) performed corrosion testing with a calcium nitrate-based accelerator at two dosages (25 and 40 fl. oz/cwt) and found a marked reduction in corrosion activity in the mixture with the higher dosage (40 fl. oz/cwt). Previous research by Østnor and Justnes (2011) claimed that a 3–4% calcium nitrate dosage by mass of cement is sufficient to provide corrosion protection. While the exact chemical composition of Product P is proprietary information, its technical sheet lists calcium nitrate as composing 10–25% of the admixture. If the calcium nitrate concentration is assumed to be 25% by mass, the 2, 4, and 6 gal/yd³ mixtures would be equivalent to a 0.9%, 1.8%, and 2.8% dosage by mass of cement, respectively.

3.3.3. Test Matrix

Each of the three admixture products was tested at three varying dosages. Including the control mixture, a total of ten unique mixtures were cast. Seven mixtures were selected to have corresponding lab and field samples (*Lab and Field*) while the remaining three mixtures only produced lab samples (*Lab Only*). *Lab and Field* mixtures consisted of two G109 corrosion beams, three cylinders, and two marine exposure blocks. *Lab Only* mixtures were composed solely of two G109 corrosion beams and three cylinders. Table 3.5 summarizes the test matrix utilized. The letter corresponding to the Mixture ID refers to the admixture used while the number indicates the admixture dosage in gal/yd³.

Table 3.5 Test matrix

#	Mixture ID	Admixture	Dosage (gal/ yd ³)	Specimens	Date Mixed
1	C0	None	0	Lab and Field	9/7/2016
2	D2	Product D	2	Lab Only	9/26/2016
3	D4		4	Lab and Field	9/14/2016
4	D6		6	Lab and Field	9/14/2016
5	R1	Product R	1	Lab and Field	9/19/2016
6	R2		2	Lab and Field	9/19/2016
7	R3		3	Lab Only	9/26/2016
8	P2	Product P	2	Lab Only	9/26/2016
9	P4		4	Lab and Field	9/21/2016
10	P6		6	Lab and Field	9/21/2016

3.3.4. Specimens

3.3.4.1. Field Specimens – Marine Exposure Blocks

3.3.4.1.1. Overview and Exposure Site

As described in Section 2.2.5.1, LIME has a long tradition of casting concrete blocks. Exposure blocks create a more representative sample that realistically mimics the behavior of an actual field structure. Placing the blocks outdoors in a marine environment provides a much more accurate scenario than the typical salt-solution ponding used in laboratory corrosion testing. The UTMSI exposure site, known as the Texas Marine Exposure Site and shown in Figure 3.1, is located in Port Aransas.

The marine exposure blocks are large concrete samples that are suspended from a sea wall, allowing the blocks to be partly submerged in a marine environment along the Texas coast. The blocks are intended to be immersed halfway in the water, creating the optimal

conditions for corrosion to develop around the splash zone given the abundance of chlorides and the availability of water and oxygen to promote the reaction. Sea water is estimated to contain 35 g/l of dissolved salts, mostly in the form of sodium chloride (NaCl), magnesium chloride (MgCl₂), magnesium sulphate (MgSO₄), calcium sulphate (CaSO₄), potassium chloride (KCl), and potassium sulphate (K₂SO₄) (CEB Design Guide, 1997).

It should be noted that the highest surface chloride concentrations are expected in regions above the splash zone. While chlorides penetrate the deepest at the splash zone, the consistent wave action can effectively ‘wash off’ and lower surface chlorides. Regions above the splash zone, known as spray zones, are not subjected to the same level of ‘wash off’ and can have highly concentrated level of surface chlorides. Nonetheless, spray zones will generally be drier and conditions will not favor corrosion there.



Figure 3.1 Marine Exposure Site in Port Aransas

3.3.4.1.2. Description

The marine exposure block dimensions are 114.3 x 14.0 x 30.5 cm (45.0 x 5.5 x 12.0 in.). Two marine exposure block specimens were cast for each of the seven different *Lab and Field* mixtures, one reinforced and one unreinforced, for a total of 14 blocks. The reinforced specimen is tested through half-cell potential measurement and visual observation while the unreinforced specimen is cast to be cored, evaluated for chloride ingress, and compared to a similar lab specimen that was ponded in a salt solution per ASTM C1556.

The reinforced specimens contain four #4 black rebar at varying depth covers (12.5, 25.0, 37.5, and 50.0 mm) [0.5, 1.0, 1.5, and 2.0 in.]. Stainless steel threaded rods were attached at the ends of the rebar and allowed to protrude out of the concrete. These threaded rods provided electrical conductivity needed to perform half-cell potential measurements and prevented the rebar from being directly exposed. Both, reinforced and unreinforced, blocks contained a stainless-steel smooth rod that was used as a hook to hang the blocks from the seawall. Figure 3.5 displays the cross-section for a reinforced block while Figure 3.6 illustrates the basic set up for the block forms.

The marine exposure blocks were cast in September 2016, wet cured for 7 days, and placed at the exposure site in November 2016 at an average age of 63 days. Figure 3.7 shows the casting and curing process while Figure 3.8 demonstrates the procedure used to hang the blocks and perform half-cell measurements.

3.3.4.1.3. Correlation to Lab Samples

Apparent chloride diffusion coefficients were calculated for marine exposure blocks as described in Section 3.4.1.3. It should be noted, however, that the ASTM C1556 standard states that the chloride diffusion calculation procedure is only applicable to lab specimens subjected to the specific conditions outlined in the standard, and is, therefore, not applicable to specimens such as exposure blocks that are subject to field conditions. The ASTM C1556 procedure is intended to create a pure diffusion environment, whereas field samples are subject to multiple mechanisms such as diffusion, convection, and absorption. Nonetheless, there are examples in the literature indicating that even in the case of field structures the mathematical model from Equation 3.4 can be valid and yield reasonable approximations (Bertolini et al., 2013; Riding et al., 2013).

While the procedure was employed and relevant data was quantified, the obtained diffusion coefficients from the lab and field were not directly compared since the chloride ingress mechanisms and conditions differed greatly in lab and field settings. Rather, samples were assessed based on their performance on either series independently.

3.3.4.1.4. Site Complications

Given the harsh and sometimes unpredictable exposure conditions, several complications and challenges are inherent. Firstly, the process of moving 136 kg (300 lb.) blocks of concrete in and out of the water is anything but simple. While at this point an efficient system for placing and removing blocks has been developed, mishaps have occurred, unfortunately resulting in blocks being dropped as they were moved.

Additionally, within the first few months of exposure, the galvanized chain used to hang the blocks began to exhibit signs of corrosion. This was most apparent at the intersection

of the galvanized chain with the stainless-steel hook (Figure 3.2). The use of dissimilar metals effectively created galvanic corrosion with the chain preferentially corroding. Moreover, the blocks themselves showed signs of abrasion as they rubbed against the seawall with the wave action (Figure 3.2). In an effort to protect the blocks from abrasion, a rubber tire was placed around the block to prevent direct impact with the seawall (Figure 3.2). However, the inclusion of the rubber tires created a variety of problems and the idea was ultimately abandoned. Upon removal of the protective tires and subsequent monitoring, it was concluded that most of the abrasion damage occurred early on and did not significantly affect testing for these specimens.

As time passed, corrosion of the galvanized chain became a bigger concern as loss of chain cross section became apparent along the portion of chain directly swinging and rubbing against the seawall (Figure 3.3). The situation dramatically worsened with the arrival of Hurricane Harvey along the Texas coast in the Fall of 2017. The exposure site and the entire town of Port Aransas were devastated by the storm. Pertaining to the study, the severe conditions led to the loss of a few exposure blocks: by large waves completely lifting blocks off their hooks (Figure 3.4) or by the aggressive wave motion breaking chains that had been weakened by corrosion damage (Figure 3.2).

Learning from that experience, new methods to hang the blocks began to be implemented. Stainless-steel chain as well as the use of marine rope were tested. Stainless-steel chain, while costly, proved to be effective in resisting corrosion. However, the issue of chain-rubbing and abrasion persisted. Based on observations, it appears a minimum stainless-steel chain link diameter of 0.64 cm ($\frac{1}{4}$ in.) is needed to withstand abrasion and survive the environment for several years. Marine rope was chosen as an alternative to chain as it is inherently corrosion-free. A plastic sleeve was included in the marine rope design to counter abrasion damage, which could rapidly and severely affect rope capacity. While the first iteration of rope testing fared positively, the second round of implementation led to the failure of the rope and loss of several specimens (Figure 3.4). The most likely cause of rope failure is a general lack of over-design capacity when compared to steel chain. While the rope was rated to perform well under static loading, a sudden change in wave action could have resulted in dynamic, impact-like loading. Such conditions may have been beyond the rope capacity.

As of July 2020, only five blocks remain out of the initial 14 from this testing series. Fortunately, measurements had previously been performed on all samples, and valuable data were obtained before they were lost. Based on the various schemes employed to suspend the samples into the gulf, it is now recommended to use a 304 stainless-steel chain with minimum 0.64 cm ($\frac{1}{4}$ in.) link diameter in conjunction with a backup system such as marine rope. Future setup tests will also include the use of plastic sleeves to protect the

stainless-steel chain from rubbing against the seawall. Such a robust system is expected to perform well for several years.



Figure 3.2 Galvanized chain corroding & rubber tire (left), visible abrasion on block corners (middle), and galvanized chain failing (right)



Figure 3.3 Galvanic corrosion (left), loss of cross section (middle), and chain/bolt abrasion (right)

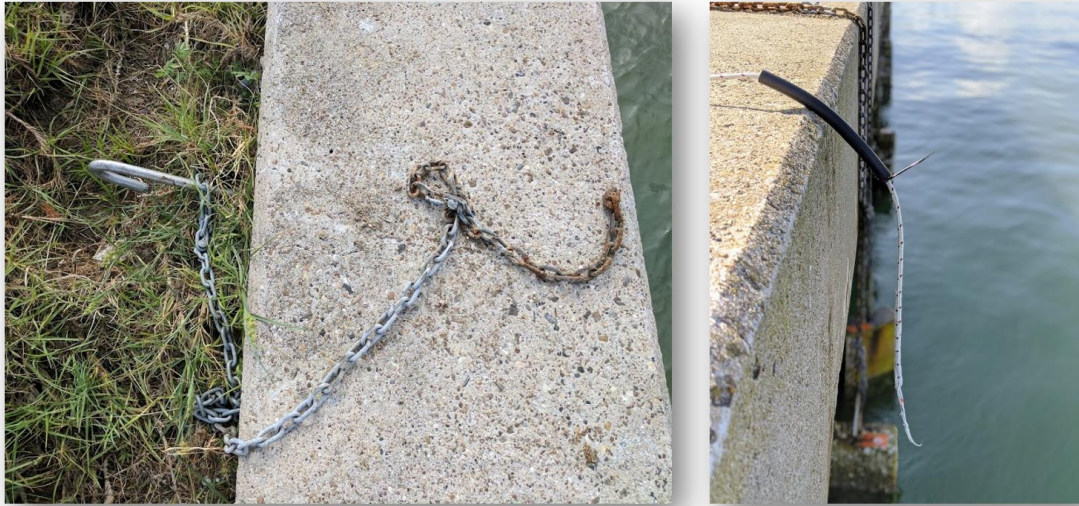


Figure 3.4 Wave lifted block off chain (left) and rope failure (right)

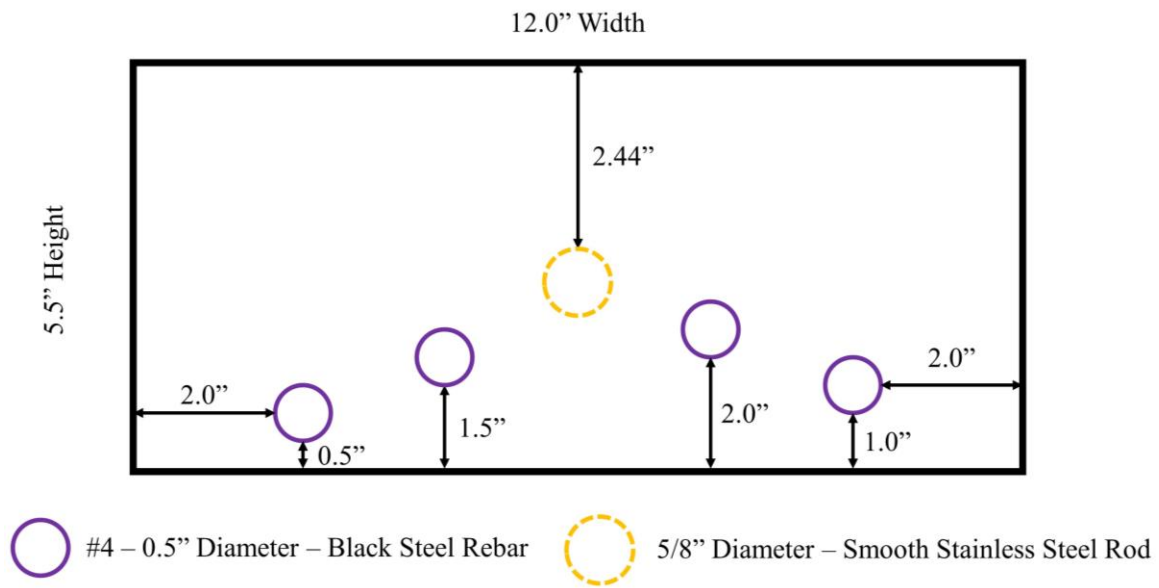


Figure 3.5 Reinforced marine exposure block cross section schematic. Not to scale. (1 in. = 25.4 mm)



Figure 3.6 Marine exposure block materials



Figure 3.7 Marine exposure block casting (left) and curing (right)

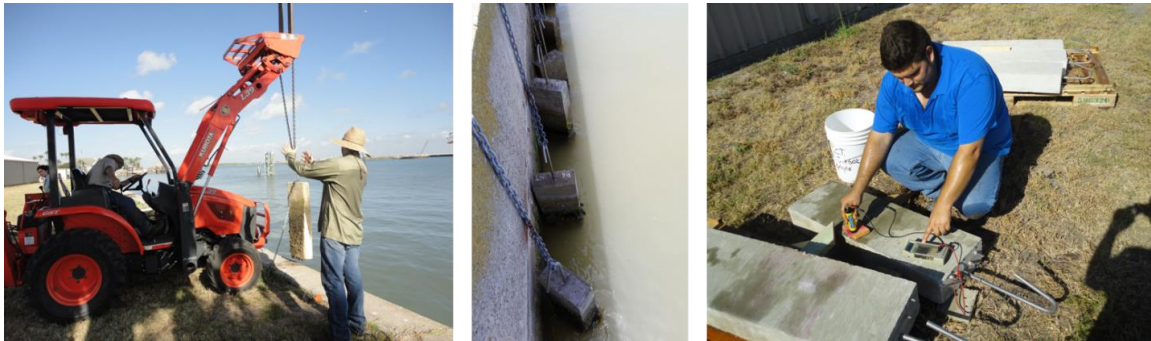


Figure 3.8 Lowering blocks (left), hanging blocks (middle), measuring blocks (right)

3.3.4.2. Lab Specimens – ASTM G109 Concrete Beams

Concrete beams with a 15.2 cm (6.0 in.) height, 11.4 cm (4.5 in.) width, and 27.9 cm (11 in.) length containing two layers of black rebar were cast in accordance with ASTM G109 specifications. Two replicate specimens were cast for each of the ten mixtures for a total of 20 corrosion beams. As directed by the test, a plastic dam was created on top of the beam to allow for cyclical ponding with a sodium chloride solution (3% concentration by mass) and subsequent drying. The test is intended to determine the effect of chemical admixtures on corrosion due to chloride ingress. If performed correctly, the test can provide information regarding time (number of cycles) to corrosion initiation as well as provide an estimate for the chloride content required to initiate corrosion, i.e., the chloride threshold. The chloride threshold is particularly important when evaluating admixtures such as Product D, whose mechanism is primarily reported to increase the chloride threshold. Figure 3.9 shows the specimen schematic provided in ASTM G109 along with an example of an actual beams cast.

While the G109 standard can yield valuable information, the test itself is highly precarious and some difficulty was encountered while performing the test, especially regarding leakage of the salt solution that was ponded atop the beams. Leakage occurred either through microcracks or by the solution itself damaging the sealed joints. Throughout testing, several efforts to reseal the dam with epoxies were made with little success. Salt deposits on the sides and bottom of the specimen were often visibly present (Figure 3.9) as the solution dripped and water evaporated. The messy conditions created by this issue likely contributed to the early corroding of the testing components, i.e., resistor, wiring, threaded rod, and nuts. Furthermore, in one specimen, this defect led to the unintended corrosion of the bottom rebar layer (Figure 3.10) as the trickle of solution allowed chlorides to ingress either through the exposed bottom surface or through imperfections along the epoxied side. For future reference, it is highly recommended to utilize a premade ponding structure, e.g., plastic storage container of approximate dimensions instead of gluing together a makeshift dam.

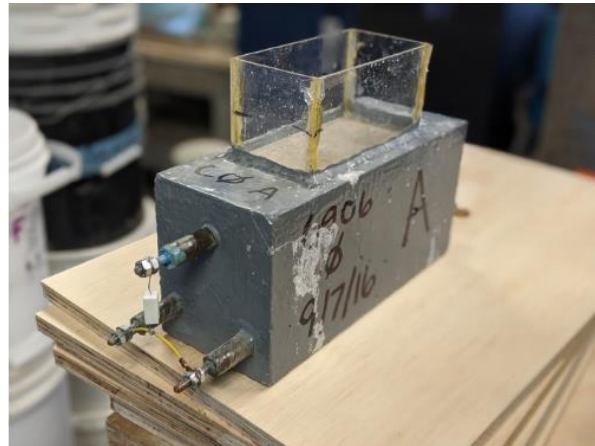
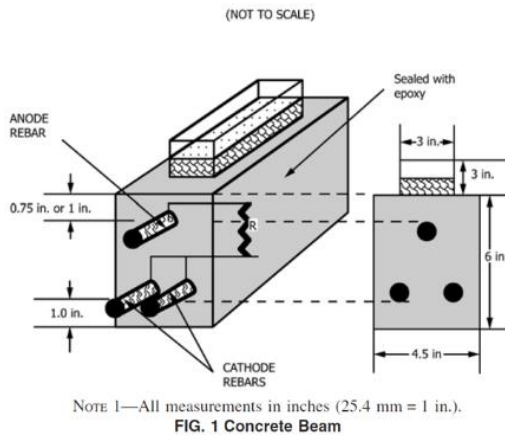


Figure 3.9 ASTM G109 schematic (left), and corrosion concrete beam with visible salt deposits (right)

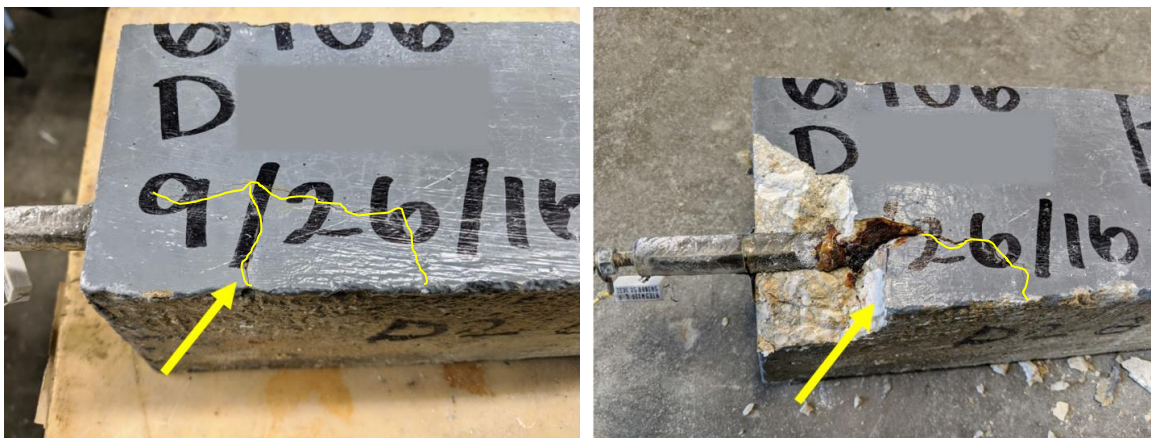


Figure 3.10: Evident cracking on side and bottom of beam specimen (left), and confirmation of unintended corrosion at bottom layer of rebar due to salt solution leaking (right)

3.3.4.3. Lab Specimens – Concrete Cylinders

As part of every mixture, a set of three concrete cylinders of 100 mm (4.0 in.) diameter by 200 mm (8.0 in.) in length was cast for quality control purposes in accordance with ASTM C192. Cylinders were demolded after 24 hours and fog-cured until an age of 28 days. Two of the three samples were tested in compression at 28 days in accordance with ASTM C39. The remaining third cylinder from each mixture was removed from curing at 28 days and stored in an air-conditioned room (23° C [73° F] and 50% RH). These cylinders were later tested for electrical resistivity (ASTM C1876) and subsequently saw-cut to obtain concrete disks for chloride diffusion testing (ASTM C1556). It should be noted that the stored cylinders remained in the air-conditioned room for over two years before resistivity and chloride diffusion testing were implemented. Since the testing reflected some unusual results, it is theorized that the extended, dry environmental conditions could have influenced properties such as internal moisture content.

3.3.4.4. Lab Specimens – Concrete Disks

Concrete disks were saw-cut from the remaining cylinders and used to determine apparent chloride diffusion coefficients per ASTM C1556. Two disk specimens were obtained from each cylinder as described in Figure 3.11: the C_i Specimen was not exposed to chlorides and was used to calculate the baseline initial chloride content, while the test specimen was epoxy-sealed on all sides except the finished surface and ponded on a sodium chloride solution (15% concentration by mass). Figure 3.11 also displays a test specimen undergoing profiling.

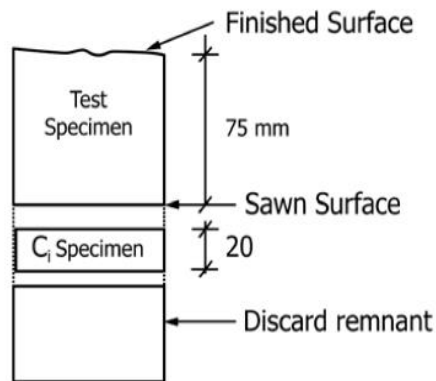


FIG. 3 Sketch of Specimens Obtained from a Typical Sample



Figure 3.11 Sample schematic per ASTM C1556 (left), and test specimen being profiled (right)

3.3.5. Testing Procedures

Several test methods were implemented to comprehensively assess corrosion performance of each admixture. Half-cell potential measurements and resistivity were electrical-based testing techniques utilized. Additionally, extensive chloride profiling and chloride diffusion coefficient data was obtained. Compressive strength was used as a general quality control measurement, and visual examination of samples provided qualitative information. Table 3.6 outlines the testing procedures utilized on lab and field specimens. Descriptions on each procedure are included in this section.

Table 3.6 Testing procedures

Specimen Type	Sample Type	Testing Procedure
Lab Specimens	Cylinders & Disks	Strength
		Resistivity
		Chloride Diffusion Coefficient
	Corrosion Beams	Half-cell Potential
		Chloride Mapping
		Visual Examination
Field Specimens	Marine Exposure Blocks	Half-cell Potential
		Chloride Diffusion Coefficient
		Visual Examination
		Service Life Modeling

3.3.5.1. Strength

Compressive strengths were obtained in accordance with ASTM C39. While compressive strength is not a key factor in corrosion determination, it can be used as a general indicator of concrete quality and consistency. Given that the same w/c and mixture proportions were used across mixtures, similar strengths were expected. Additionally, compressive strength can be used to examine the influence of admixtures on effective w/c.

3.3.5.2. Resistivity

Bulk electrical resistivity measures the impedance of an applied current on a concrete specimen. The resulting value is a function of pore solution composition as well as pore connectivity. The more resistant a concrete is to the movement of ions under the applied current, the less conductive and permeable it is. Resistivity values have been shown to correlate well with other permeability tests such as the rapid chloride permeability test (RCPT) from ASTM C1202 and the chloride diffusion coefficient test from ASTM C1556. For comparison, resistivity values ($k\Omega \cdot \text{cm}$) can be related to RCPT values (Coulombs) and can indicate a degree of resistance to chloride penetration as seen on Table 3.7. Given that one of the products tested (Product R) is reported to reduce the permeability of concrete, this test was implemented to quantify what impact the product has on electrical resistivity, as well as other transport parameters.

The use of chemical admixtures can artificially influence results as they can introduce water-soluble ionic compounds that may alter pore solution conductivity without necessarily reflecting a change in overall transport properties. The ASTM C1876 resistivity

standard lists admixtures containing calcium nitrite and calcium nitrate as potentially interfering with results. Both Product D and Product P contain these components.

Bulk resistivity measurements were performed with a Giatec RCON meter. Following manufacturer recommendations, measurements were performed at a frequency which minimized the phase angle, typically 10, 20, or 30 kHz. The test procedure used was a modified version of ASTM C1876 as the standard had not been released at the time of testing. The main deviation from the standard was that the samples were continually kept in a fog room instead of being conditioned under a simulated pore solution. Both methods intend to provide near full sample saturation, which is critical when measuring electrical conductivity, but standard water curing can lead to the leaching of alkalis within the pore solution. The leaching of potassium and sodium hydroxide is known to influence conductivity and measured resistivity values. Cylinder samples (one cylinder per mixture) that had been stored in an air-conditioned room for over two years were placed in a fog room for a minimum of 28 days to reach a stable saturation level before testing.

Table 3.7: Correlation between bulk electrical resistivity and RCPT (RCON2, Giatec Scientific)

Degree of Chloride Penetration	56-Day Rapid Chloride Permeability Charge Passed (Coulombs)	28-Day Bulk Electrical Resistivity of Saturated Concrete (kΩ.cm)
High	>4,000	<5
Moderate	2,000 to 4,000	5–10
Low	2,000 to 4,000	10–20
Very Low	2,000 to 4,000	20–200
Negligible	<100	>200

3.3.5.3. Chloride Diffusion Coefficient

The standardized testing procedure to measure diffusion coefficients is ASTM C1556. The procedure involves the gradual profile grinding of a concrete sample that has been exposed to chlorides. As outlined in the standard, samples of concrete powder are obtained at given depth intervals. Subsequently, powder samples are analyzed to determine their acid-soluble chloride-ion content. The data can then be plotted, creating a visual representation of the chloride content within the concrete (concrete mass %) as a function of depth (mm). Depth zero indicates the surface directly exposed to external chlorides. Powder samples up to 25–30 mm from the surface are typically obtained to fully capture the curve behavior. Figure 3.12 illustrates a sample plot of chloride content as a function of depth.

The diffusion coefficient is approximated by fitting chloride profile values into Fick's second law of diffusion as outlined in ASTM C1556 Section 10 and seen in Equation 3.4. The calculation creates a mathematical model to predict unknown chloride content values based on actual measurements taken. The model can provide the chloride content for a given depth and exposure time using the chloride diffusion coefficient, D_a , as one of its key parameters. As with any model, a certain level of error is expected between predicted and measured values. Special care was taken to achieve acceptable levels of error given sample and equipment variability. Figure 3.12 displays sample measured Test Values as well as the Model trendline approximation based on the mathematical fitting. The slight gap between some of the Test Values and the Model trendline represents the error in the approximation. The mathematical fitting attempts to find a solution that will minimize the sum of the squared errors. Equation 3.4 represents the Model trendline approximation given the measured Test Values.

The fitting equation solves for the unknown parameters (the chloride content at the surface, C_s , and the apparent chloride diffusion coefficient, D_a) utilizing the measured data. The initial chloride content, C_i , is obtained from a sample that was not exposed to chlorides. The surface chloride content, C_s , is based on the exposure environment. The inclusion of an exposure time parameter, t , in Equation 3.4 is problematic as the diffusion coefficient, D_a , is itself a time-dependent property since the concrete matures with time. More details regarding t and D_a will be discussed in the subsequent sections. In general, chloride diffusion coefficient values can be affected by several factors, such as the age at which specimens were first exposed to chlorides, the length of exposure, the chloride concentration in the exposure solution, and the severity of exposure (static ponding versus wetting and drying cycles).

The procedure specified by ASTM C1556 states that specimens must pond in a sodium chloride solution (15% concentration by mass) for a minimum of 35 days. However, it is also noted that longer ponding times may be needed for more mature, less permeable mixtures. Since the testing series involved straight OPC mixtures, the lab specimens were ponded for 47 days before testing began.

Apparent chloride diffusion coefficients were obtained for both lab and field samples. Lab samples were prepared from the same cylinders used for resistivity and conditioned according to ASTM C1556. It should be noted that the disks were made from cylinder samples that were over two years old. The cylinders were fog-cured for 28 days after casting and then proceeded to be stored in an air-conditioned room until testing began. Field samples consisted of cores removed from unreinforced marine exposure blocks. Given that the blocks had already been exposed to chlorides, the cores were not further conditioned and were profiled as they were.

Once the lab and field samples had been profiled, the acquired concrete powders were analyzed to determine their acid-soluble chloride-ion content as a percentage of total concrete mass. It should be noted that the acid-soluble chloride content refers to the total chloride content of the concrete, which includes both bound and free chlorides. The use of the total chloride parameter in calculations will neglect to account for any potential beneficial effect of chloride binding. The titration procedure used to analyze acid-soluble chloride content from concrete powder samples was a modified version of ASTM C1152 based on guidance from fellow researchers at The University of New Brunswick in Canada. For each mixture, a corresponding sample that had not been exposed to chlorides was profiled and analyzed to obtain the initial chloride content, which is a parameter required for the mathematical approximation described in Equation 3.4. Initial chloride contents, C_i , tended to be between 0.01–0.02% Cl by concrete mass. This small and negligible amount of chlorides is expected as cement, tap water, and aggregates can contain small traces of chlorides. Occasionally, the initial chloride content was so low (<0.01%) that the equipment was not able to quantify it. In these cases, an average value based on similar samples was used as the initial chloride content.

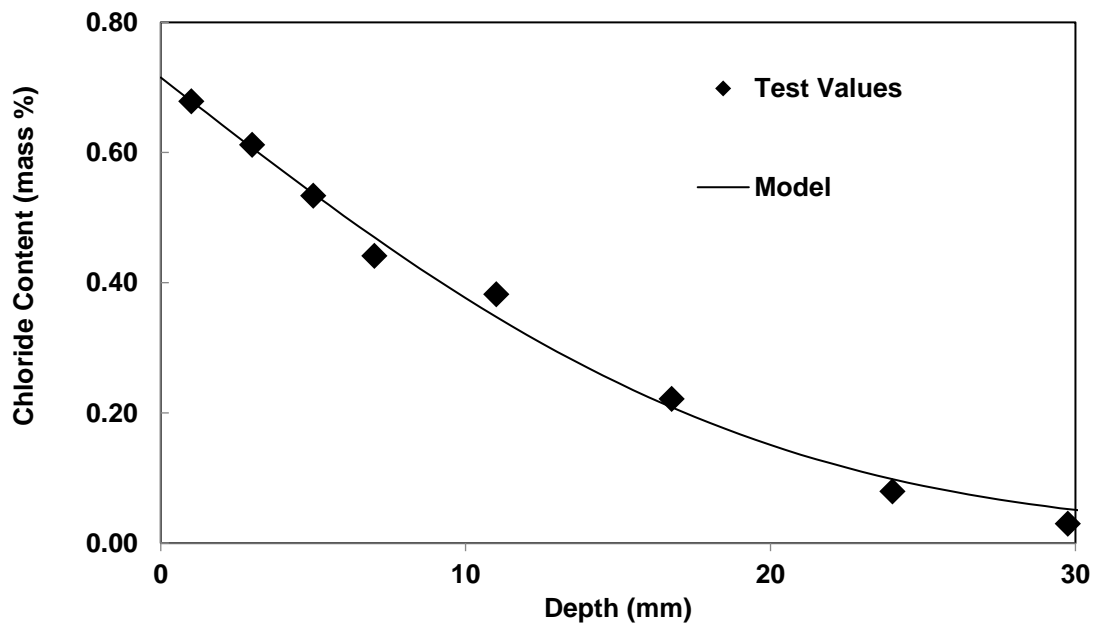


Figure 3.12 Sample plot of chloride profile for a given exposure time

KNOWN UNKNOWN

Equation 3.4: Fitting Equation Based on Fick's Second Law of Diffusion (ASTM C1556)

3.3.5.4. Service Life Modeling

Comparative analysis in this study was performed with the use of the ConcreteWorks (2017) service life modeling software. The predictive model in ConcreteWorks (2017) utilized a 28-day standardized version of the diffusion coefficient, D_{28} . The empirical equation used by the software for OPC mixtures is solely a function of w/c (Equation 3.5). However, since the diffusion coefficient is expected to decrease indefinitely with time as the concrete matures, especially in the presence of SCMs, a decay constant is needed to reflect this effect. The software lists the decay constant for OPC mixtures as $m = 0.26$. Higher decay constants are listed for SCM mixtures, with a maximum value of 0.66 for mixtures with the highest SCM content. The decay constant value can be inputted into Equation 3.7 to estimate the diffusion coefficient as a function of time. The diffusion coefficient reaches a theoretical maximum at an age of 100 years as shown in Equation 3.6. For a 0.45 w/c OPC mixture such as the one used in this study, the D_{28} value is estimated to be $1.1 \times 10^{-11} \text{ m}^2/\text{s}$ and it is expected to decrease to a D_{ult} value of $1.7 \times 10^{-12} \text{ m}^2/\text{s}$.

The standardization of diffusion coefficients such as D_{28} can be problematic as the test itself requires several weeks of ponding, and it can, therefore, be difficult to pinpoint the exact age at which the concrete is being evaluated. Work by Stanish and Thomas (2003) was done to determine an effective age given the concrete age prior to chloride exposure (t_1) and the length of exposure (t_2). For the simple case of an OPC mixture ($m = 0.26$) being tested per ASTM C1556 at the earliest allowed age (63 days: 28 days of curing followed

by 35 days of ponding), the effective age according to Equation 3.8 (Stanish and Thomas, 2003) is 44 days. Thus, the use of D_{28} should not necessarily be considered as a 28-day concrete property, but rather an early age property. Diffusion coefficient values obtained through Equation 3.7 are considered as instantaneous parameters that account for changes over time.

When performing diffusion coefficient testing on lab samples, users must decide an appropriate timeline to better predict actual service performance. For most cases, it would be recommended to wait as long as possible before initiating testing to let the concrete sufficiently mature. Considering this, the use of resistivity testing could be used as a proxy for approximating concrete maturity. Given the fact that resistivity is a non-destructive test, it could be used to monitor samples until measurements plateau, indicating the concrete has sufficiently matured. At this point, the same sample for which resistivity was measured could be saw-cut and conditioned for chloride diffusion testing.

The chloride surface concentration, C_s , is an important parameter used in Equation 3.4 to calculate the diffusion coefficient. The value acts as a boundary condition and is influenced by the proximity to chloride sources, degree of exposure, and environmental factors. For example, rain can effectively wash off surface chlorides and, conversely, evaporation can facilitate the deposit and crystallization of chlorides. While environmental and seasonal factors will cause sudden spikes or drops in surface concentration, on average the surface concentration will increase with time up to a theoretical maximum concentration. The progressive ‘buildup’ of surface chlorides is approximated on ConcreteWorks (2017) by Equation 3.9. $C_{s\ max}$ is the theoretical maximum chloride surface concentration, which is based on exposure condition and is typically 0.6–1.0% Cl by mass of concrete. Time, t , is in years and b is a unitless buildup rate constant also based on exposure condition. This model is valid for structures gradually exposed to chlorides such as parking garages or bridge decks. For marine structures in direct and constant exposure to chlorides, the splash zone can be assumed to reach its maximum surface concentration (0.80% Cl) immediately. The marine exposure blocks included in this study shall be considered as being in this splash zone condition.

$$D_{28} = 2.17 \cdot 10^{-12} \cdot e^{\frac{w/c}{0.279}} \quad \text{Eq. 3.5}$$

$$D_{ult} = D_{28} \cdot \left(\frac{28}{36,500} \right)^m \quad \text{Eq. 3.6}$$

$$D_t(t) = D_{28} \cdot \left(\frac{28}{t} \right)^m + D_{ult} \cdot \left(1 - \left(\frac{28}{t} \right)^m \right) \quad \text{Eq. 3.7}$$

$$t_{\text{eff}} = \begin{cases} \left[\frac{(1-m)(t_2-t_1)}{t_2^{1-m} - t_1^{1-m}} \right]^{1/m} & m \neq 0, 1 \\ \frac{t_2-t_1}{\ln\left(\frac{t_2}{t_1}\right)} & m = 1 \end{cases} \quad \text{Eq. 3.8}$$

$$C_s(t) = C_{s \text{ max}} \cdot \frac{b \cdot t}{1 + b \cdot t} \quad \text{Eq. 3.9}$$

3.3.5.5. Corrosion Beams (ASTM G109)

The ASTM G109 procedure involves the measurement of corrosion current and corrosion potential. The specimen includes top and bottom layers of reinforcement connected by a resistor as shown in Figure 3.9. The corrosion current is created between the connected top bar (anode) and the bottom bars (cathode). The voltage drop across a resistor is measured to calculate the corrosion current at a given time. Specimens undergo cycles of wetting and drying until a specified current value is reached, indicating the presence of sufficient corrosion. Corrosion potential (half-cell) evaluations are performed jointly with corrosion current measurements and are expected to correlate based on the guidelines from Table 3.12.

3.3.5.6. Half-cell Potential

Corrosion involves electrochemical reactions which produce electrical currents. These currents can be monitored through half-cell potential measurements to give a probabilistic determination of the presence of corrosion. The measured values are an indication of the dissolution of iron but are also influenced by temperature and oxygen availability.

The procedure, outlined in ASTM C876, involves measuring the voltage potential difference between the reinforcement and a reference electrode at the concrete surface. The negative voltmeter terminal is commonly connected to the reference electrode, while the positive terminal is directly attached to the reinforcement. If the reinforcement is not exposed, coring may be performed to ensure connectivity. Figure 3.13 illustrates the half-cell measurement procedure. Measurements can be performed along the length of the reinforcement and increasingly negative voltage values will indicate a higher probability of corrosion. As the dissolution of iron is greatest at the anode, the most negative values can be expected there. Half-cell potential measurements were taken with a copper/copper-sulfate reference electrode on marine exposure blocks and G109 corrosion beams. On marine exposure blocks, measurements were concentrated around the approximate splash zone.

Half-cell values only provide a probabilistic likelihood of the presence of corrosion and cannot guarantee neither its presence nor absence. Therefore, the interpretation of such measurements should be done with care and with a qualitative approach. Various guides to interpreting half-cell values exist in the literature. Table 3.8 presents the recommendations outlined by ASTM C876. Generally, as the values become more negative, the likelihood of corrosion increases. Cracking and rust staining were occasionally observed in samples with half-cell potentials approaching -500 mV in this study. However, there is a large range of uncertainty and other factors can also influence results.

The unique conditions of each concrete can lead to artificial half-cell values that do not necessarily reflect corrosive environments. Underwater concrete, considered as fully saturated, will have a lower resistivity and low oxygen availability. Both of those factors can result in seemingly high negative values incorrectly predicting corrosion. However, the lack of oxygen in submerged conditions will generally prevent corrosion (Broomfield, 2007). Measurements can also be influenced by adjacent reinforcement in cover depths exceeding 75 mm (3.0 in.). The highest cover depths included in this study were 50 mm (2.0 in.), which the ASTM C876 standard allows without modification. Additionally, the use of chemical admixtures may affect pore conductivity and influence corrosion potential measurements.

Half-cell measurements should only be interpreted as a qualitative indicator of the probability that active corrosion is occurring at the time of measurement. This indicator can detect corrosion activity but does not necessarily provide the location or rate of corrosion. Furthermore, the ASTM C876 standard acknowledges that half-cell potential measurements should be used in conjunction with other tests to make proper assessments regarding corrosion activity.

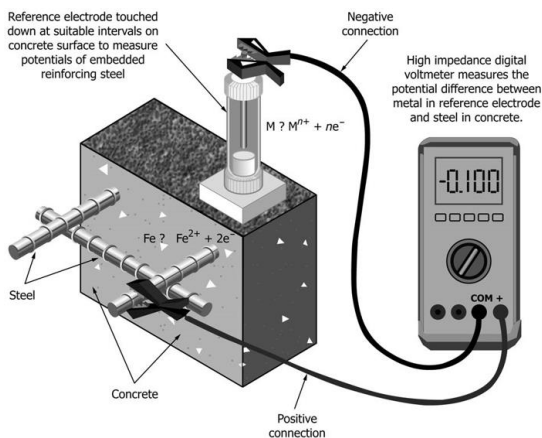


Figure 3.13 Half-cell potential measurement diagram ASTM C876 (left), Measurement on field specimen (right)

Table 3.8: Notes on interpretation of half-cell measurements with copper-copper sulfate reference electrode (ASTM C876, Appendix X1.1)

Measured Potential, E (mV)	Probability of Corrosion
E > -200	10%
-200 > E > -350	Uncertain
E < -350	90%

3.3.5.7. Chloride Mapping

As part of the G109 forensic evaluation, corrosion beam specimens were saw-cut above the top rebar layer and the corresponding surface was profiled and analyzed for chlorides. This procedure was intended to quantify the chloride threshold that would initiate corrosion for each mixture. However, due to technical (and practical) issues encountered during the ASTM G109 test, the forensic evaluation was performed at a later date past the point of corrosion initiation and accurate chloride thresholds were not able to be identified. In the absence of empirically obtained values, a moderate chloride threshold approximation of 0.07% (by mass of concrete), as used by the ConcreteWorks (2017) service life modeling software was employed in this study.

Upon saw-cutting the surface intended for profiling, it was observed that some samples exhibited evident rust staining from corrosion of the top rebar layer (Figure 3.14). The presence of rust stains introduced a new question and variable: would the chloride content vary along the beam surface for a given depth? The ASTM G109 procedure simply states to determine the chloride content at the depth corresponding to the cover of the top layer of rebar, but it has no mention of where along that depth to take the measurement. Theoretically, it would be reasonable to assume that within the ponded area, the ingress of chlorides would occur at similar rates. However, once localized cracking occurs (Figure 3.17), chlorides will have unrestricted access to specific areas and a vicious cycle will ensue. The visible presence of rust staining indicates the formation of expansive corrosion products, which could likely have caused micro and macro cracking.

A preliminary inspection of chloride content in a rust-stained section versus a non-stained section proved that drastic differences in chloride content may occur a mere centimeter away (Figure 3.16). Further testing led to the implementation of the ‘chloride mapping’ method, which evaluates chloride contents at distinct regions along a constant depth (Figure 3.16). Test samples were evaluated as five separate regions which included sectors inside and outside of the ponding area. Regions outside of the ponding area, designated by the rectangular perimeter in Figure 3.16, were analyzed to study the effect of nearby chloride ingress on zones presumed unaffected by cracking. Results were asymmetrical

and did not follow a discernible pattern, indicating that localized cracking was likely the key factor in determining the severity of the chloride ingress.

Moreover, the impact of local chloride ingress initiating localized corrosion followed by cracking, leading to further chloride ingress, often resulted in excessively high levels of chloride loading. These high values, up to 0.98% Cl, indicate a region that is considerably past the assumed chloride threshold of 0.07% Cl. At such high levels, the actual magnitude of the chloride loading is inconsequential as it is likely a reflection of the extent of localized cracking and not related to transport properties. Thus, to better assess the data, three different degrees of chloride loading were characterized as described in Table 3.9.



Figure 3.14 Saw-cutting corrosion beams (left), and rust staining visible after saw-cutting (right)

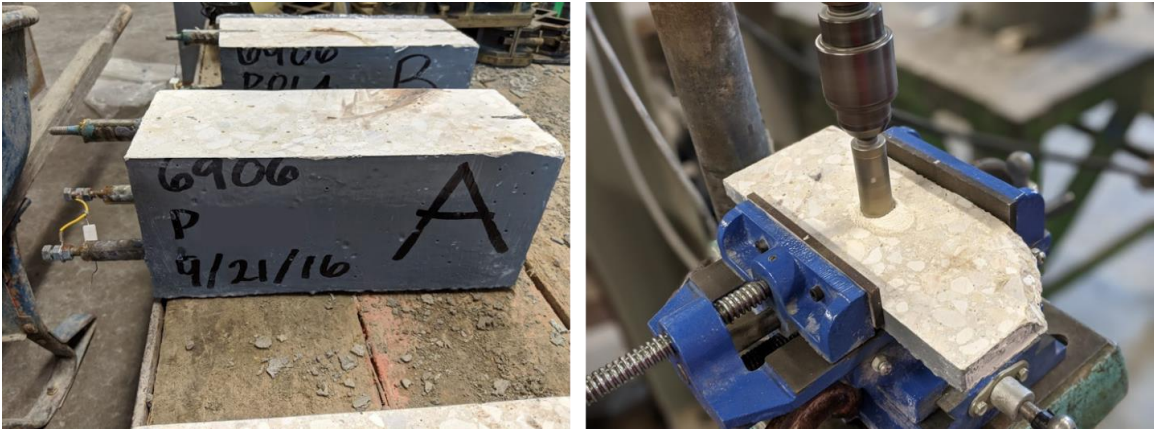


Figure 3.15 Bottom portion of beam after saw-cutting (left), and profile grinding at rebar cover depth (right)

Table 3.9 Chloride loading zone

Zone	Chloride Content (% concrete mass)	Description
Negligible	<0.02	Uncracked zone. Active mitigation of chloride ingress, potentially due to decrease in permeability.
At Risk	0.02-0.15	Likely uncracked zone. Has experienced a significant ingress of chlorides. At risk of corrosion or corrosion already ongoing.
Damaged	>0.15	Likely cracked zone. Allows for ample chloride ingress. Severe corrosion has occurred.

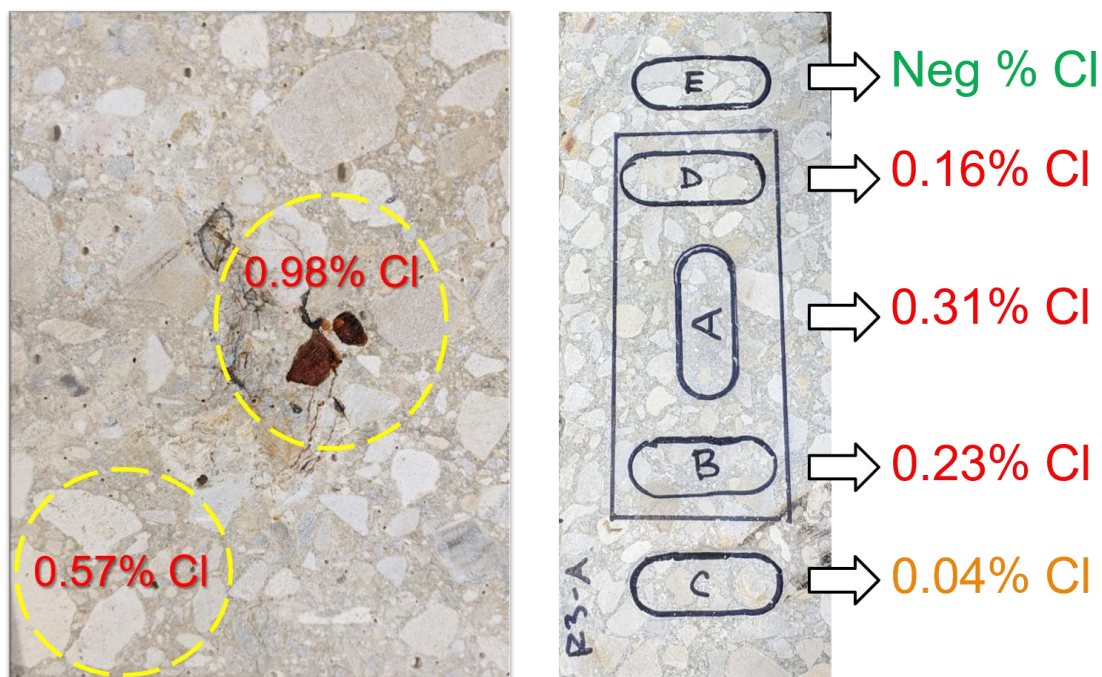


Figure 3.16 Varying chloride loadings across surface (left), and chloride mapping system – rectangle indicates ponding area (right)

3.3.5.8. Visual Examination

Visual examination of marine blocks and corrosion beams provided a qualitative assessment of performance. Inspections on concrete focused on locating signs of cracking, rusting, or abrasion. Forensic evaluation of the corrosion beams involved the removal of the top reinforcement bar, which allowed for its subsequent visual examination (Figure 3.17).

Upon retrieval from the corrosion beams, the top rebars were saw-cut to remove the epoxied ends, leaving an 18 cm (7 in.) section of bar for inspection. The bars were then

ponded for 24 hours in a solution of Lime-A-Way to remove traces of concrete and rust. An example of bar condition before and after ponding is shown in Figure 3.18. An attempt to quantify mass loss was made; however, the mass difference between samples was negligible and did not provide meaningful data. Instead, an approximate visual damage rating scale of Minor, Moderate, and Severe was adapted from Fahim (2018) to evaluate the rebar. The rating methodology is outlined in Table 3.10 and an example of each rating is shown in Figure 3.18.

For future reference, it is not recommended to clean rebar by ponding in a solution of Lime-A-Way. The ASTM G1 standard provides technical guidance on the preparation, cleaning, and evaluation of corrosion specimens. Procedure C.3.5 within G1 was utilized by Fahim (2018) to condition specimens.

Table 3.10 Visual rating methodology adapted from Fahim (2018)

Rating	Rebar Condition
Minor	Minor signs of pitting corrosion
Moderate	Clear signs of pitting corrosion visible over general sample area
Severe	Severe pitting visible over majority of sample area

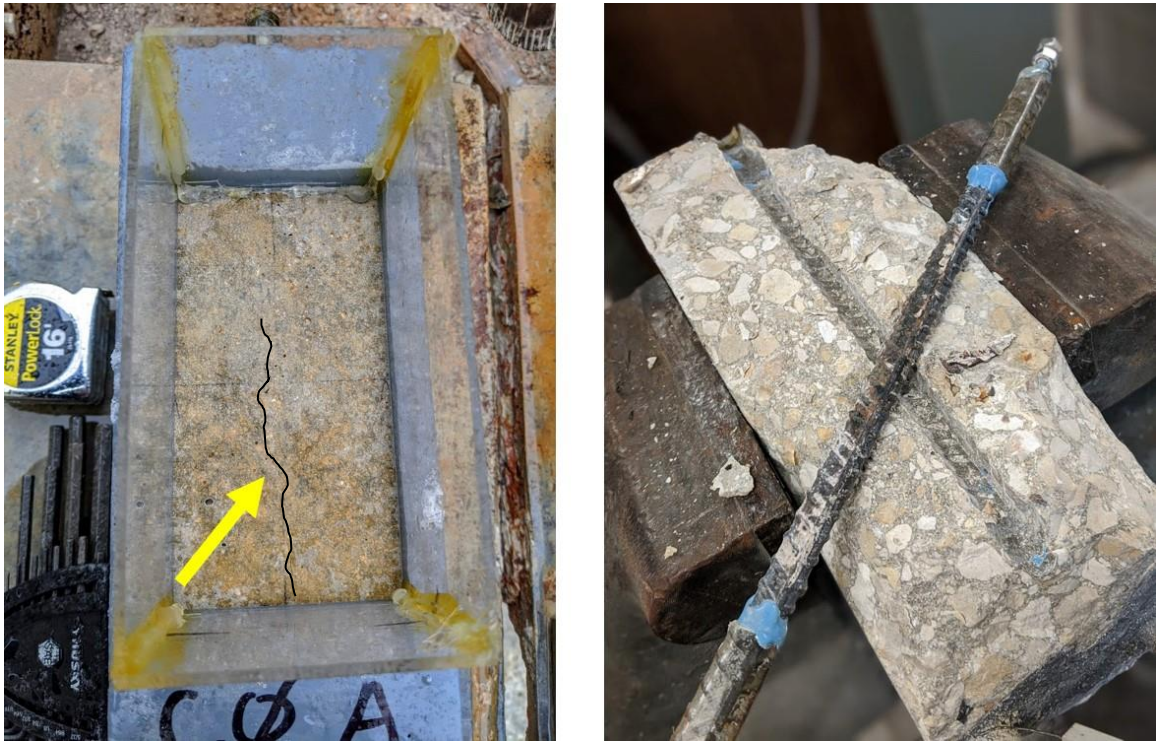


Figure 3.17 Visible crack in corrosion beam ponding area (left), and removal of top reinforcement bar from corrosion beam (right)



Figure 3.18 Rebar visual rating example—after removal from corrosion beam (left sample) and after cleaning procedure (right sample)

3.4. Experimental Results and Discussion

3.4.1. Lab Specimens—Cylinders and Disks

3.4.1.1. Compressive Strength

Compressive strength was nominally affected by admixtures. On average and across dosages, Product D had an 11% increase, Product P had a 7% decrease, and Product R had a 13% decrease in strength when compared to the control. Figure 3.19 presents the strength results for each mixture. Previous work in the literature had reported a slight increase in strength for both calcium nitrite and calcium nitrate admixtures (Gaidis, 2004; Al-Amoudi et al., 2003). Product R's technical sheet warns of a potential 5–10% decrease in strength and is the only admixture that did not require water reductions. This omission may have played a significant role in increasing the water content and lowering strength, especially in mixtures with 2 and 3 gal/yd³ dosages. It should be noted that previous work by Li et al. (1999) found that there is no direct correlation between compressive strength and chloride diffusion of concrete. Compressive strength is not a direct indicator of permeability and, thus, was intended to primarily be used as a quality control tool.

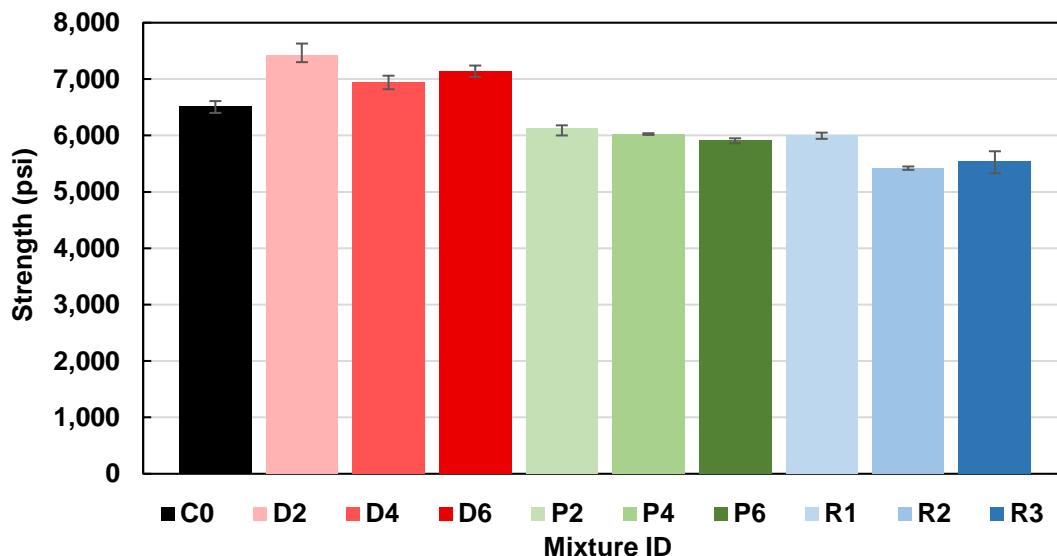


Figure 3.19 Compressive strength at 28 days

3.4.1.2. Resistivity

Bulk resistivity measurements were performed on individual cylinders that had been stored in a dry environment for over two years. While the samples were placed in a fog room for at least 28 days prior to resistivity testing, it is believed that the extended storage conditions

may have influenced some resistivity measurements given the test's sensitivity to sample moisture content. This was particularly evident with Product R mixtures.

As previously mentioned, resistivity measurements can be correlated with RCPT values and provide an expected degree of chloride penetration. Based on previous experience, it is expected for OPC mixtures to barely reach the Moderate chloride penetration region with values slightly above 5 k Ω .cm. The use of SCMs is typically needed to reach the Low chloride penetration region and beyond. Given this, it was quite surprising to see the high resistivity values initially obtained with Product R (Figure 3.20). Duplicate mixtures with Product R were cast to validate the extraordinary results but, unfortunately, they were not matched (Figure 3.21). The duplicate mixtures were immediately placed in a fog room upon demolding to ensure full sample saturation and were tested for resistivity at an age of 28 days and once again at approximately 1 year with minimal changes. It is now believed that the seemingly high resistivity values of Product R seen in Figure 3.20 were influenced by sample conditioning.

Based on the literature (Berke and Rosenberg, 1989; ASTM C1876) a decrease in resistivity had been expected with Product D and Product P given that the admixtures contain ionic compounds that can alter pore solution conductivity. These effects, however, were not observed as all mixtures behaved similarly after accounting for Product R's inconsistencies as previously mentioned. The similarity in resistivity values may indicate that admixture nitrites and nitrates are no longer present in the pore solution at this later age (over two years). This assumption echoes previous findings by Mammoliti (2001), who theorized most of those components had been incorporated into hydration products.

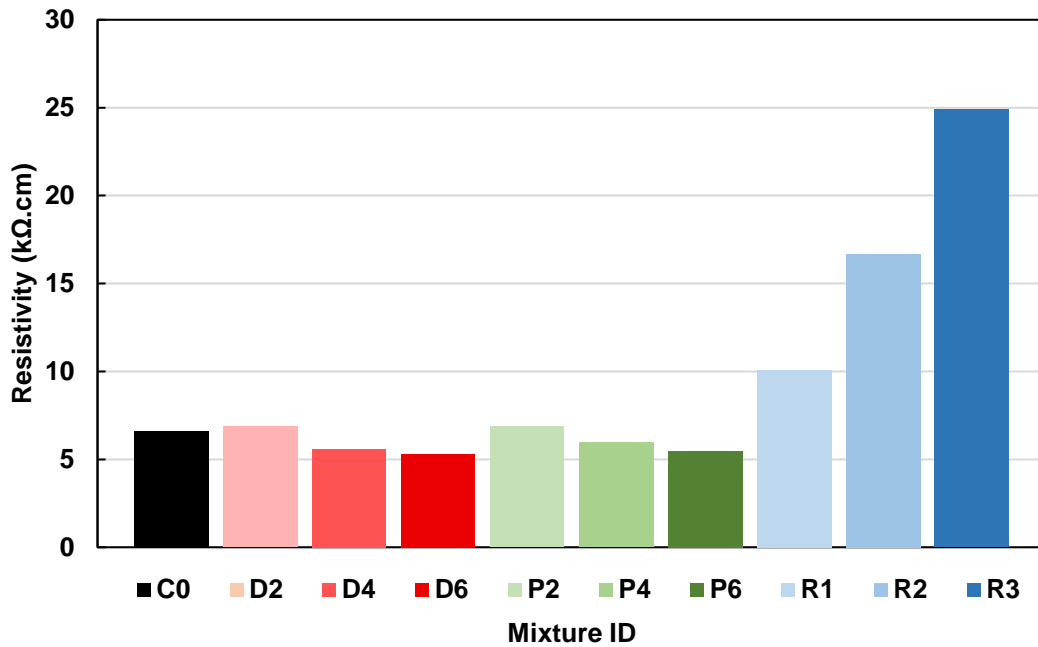


Figure 3.20 Resistivity values after two years of storage

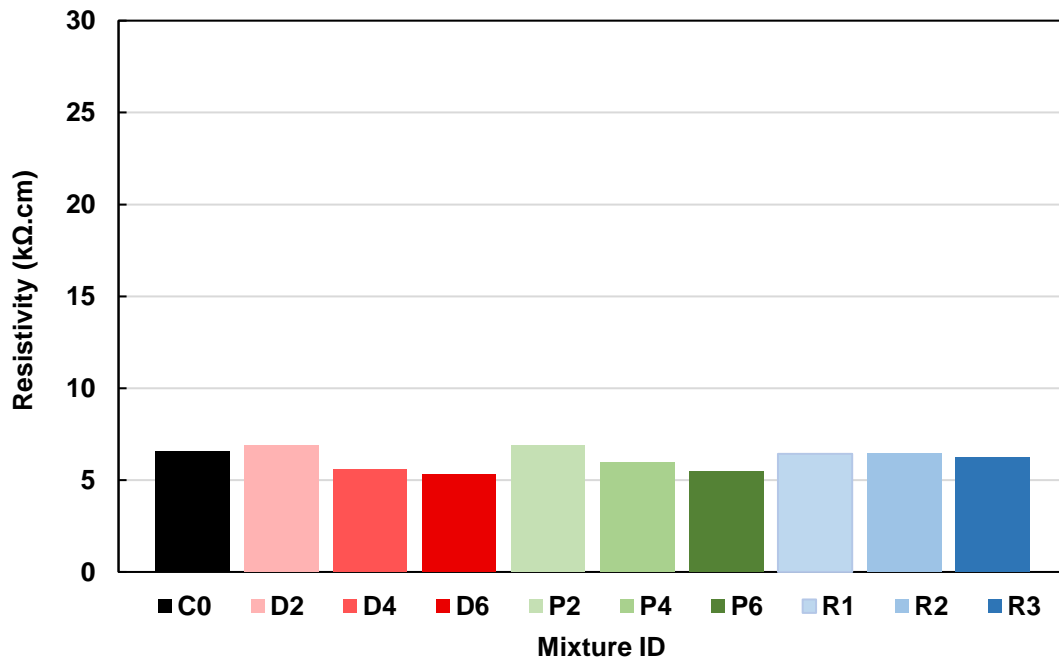


Figure 3.21 Revised resistivity values

3.4.1.3. Chloride Diffusion Coefficient

Apparent chloride diffusion coefficients for lab samples were calculated based on ASTM C1556 and are shown in Figure 3.22. The diffusion coefficient, D_a , is based on a

mathematical model with inherent error. The sum of errors squared associated with each calculated value is shown in Figure 3.23. The measured errors were deemed to be within an acceptable range. The average sum of errors squared for lab samples was 1.5×10^{-2} . The increased error for Mixtures P4 and P6 is attributed to their increased ability to mitigate chloride ingress. The drop in chloride content in both of those mixtures is so sharp that the mathematical model cannot approximate it as a curve, thus leading to increased error. The mean absolute error (MAE) for lab samples as described by Equation 3.10 is presented in Table 3.11. The MAE provides a measure of the average difference between predicted values, y_i , and measured values, x_i . Error values were calculated for two reference cases: the $k = n-1$ case omits the error derived from the first data point obtained while the $k = n$ case includes it. The ASTM C1556 standard uses the $k = n-1$ case and specifically omits the first data point since it inherently increases error based on the mathematical model but does not necessarily reflect actual conditions.

In general, diffusion coefficient values for lab samples were higher than expected, i.e., more susceptible to chlorides. Based on Equation 3.5 (Riding et al., 2013), it was expected that D_a would be around 1.1×10^{-11} m²/s for the given w/c. However, the control mixture had a measured diffusion coefficient of 7.8×10^{-11} m²/s. While the determination of the diffusion coefficient involves several steps, each with significant potential for variability, this trend was exclusively seen in the lab samples. Diffusion coefficients calculated for field samples yielded more expected values. These differences, like with resistivity values, may be associated with the extended sample storage time and subsequent conditioning process. Nonetheless, when assessed independently, the obtained lab data provide valuable information regarding the effect of admixtures on diffusion coefficients.

As observed in Figure 3.22, Product P and Product R showed signs of a beneficial impact via reduced chloride diffusion values when compared to the control. Product D showed irregular lab results as its effect was variable upon dosage. Since this discrepancy was not apparent in field samples, the variability could be related to the unusual sample conditions previously mentioned. Based on the admixture background information, Product D was not expected to influence the diffusion coefficient.

Product P showed a significant ability to rapidly reduce chloride contents to negligible values. This resulted in steadily decreasing diffusion coefficients with increasing admixture dosage. Mixtures P4 and P6 in particular were able to reach baseline chloride contents at considerably shallow depths, 10–15 mm and 5–10 mm respectively. This contrasts most other mixtures where the baseline was either achieved at depths of 25–30 mm or deeper. Figure 3.24 contains the chloride plots for the control and Product P mixtures. Figure 3.25 illustrates the predicted chloride content model based on the measured values from Figure 3.24. It should be noted that the high surface concentrations predicted by the model for the P4 and P6 mixtures, 1.7% and 1.0% respectively, are a

mathematical expression and do not reflect actual conditions. Nonetheless, the lab model clearly illustrates that for the same level and time of chloride exposure, mixtures containing Product P can greatly decrease the ingress of chlorides.

$$MAE = \frac{\sum_{i=1}^k |y_i - x_i|}{k} \quad \text{Eq. 3.10}$$

Table 3.11 Mean absolute error (MAE) for chloride analysis on lab samples

Mixture	Data Points			
	k = n-1		k = n	
	k	MAE (%)	k	MAE (%)
C0	7	0.04	8	0.08
R1	7	0.03	8	0.02
R2	5	0.01	6	0.01
R3	7	0.02	8	0.02
D2	6	0.03	7	0.08
D4	7	0.01	8	0.04
D6	6	0.02	7	0.03
P2	7	0.03	8	0.04
P4	7	0.06	8	0.10
P6	6	0.06	7	0.08

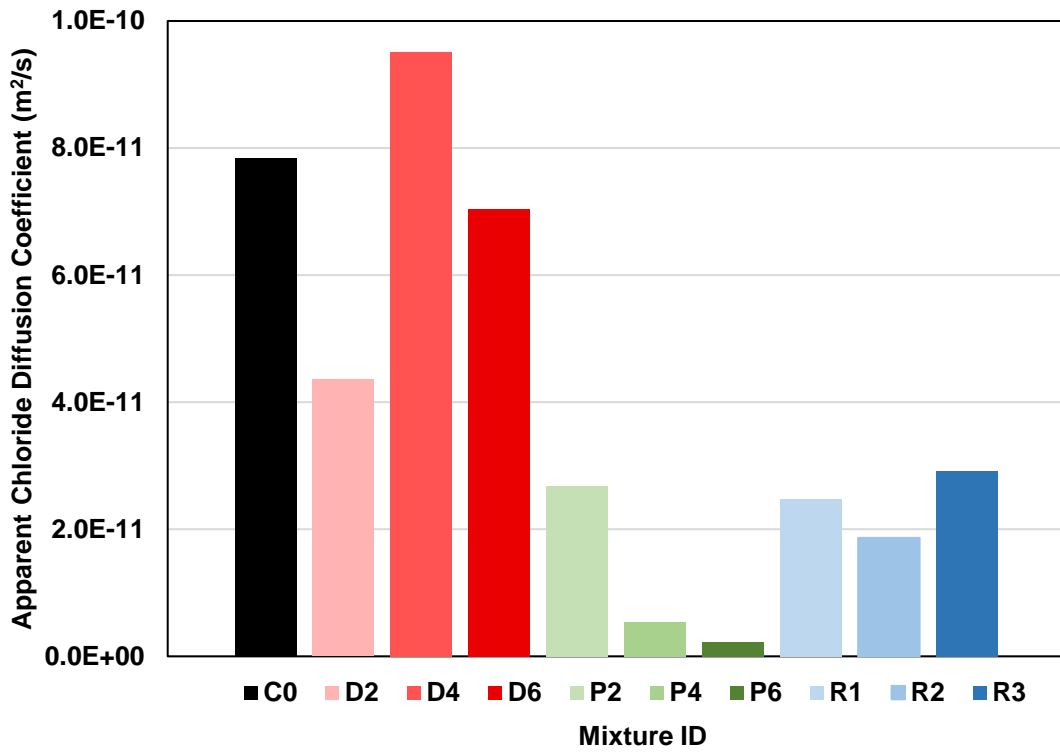


Figure 3.22 Apparent chloride diffusion coefficients of lab samples

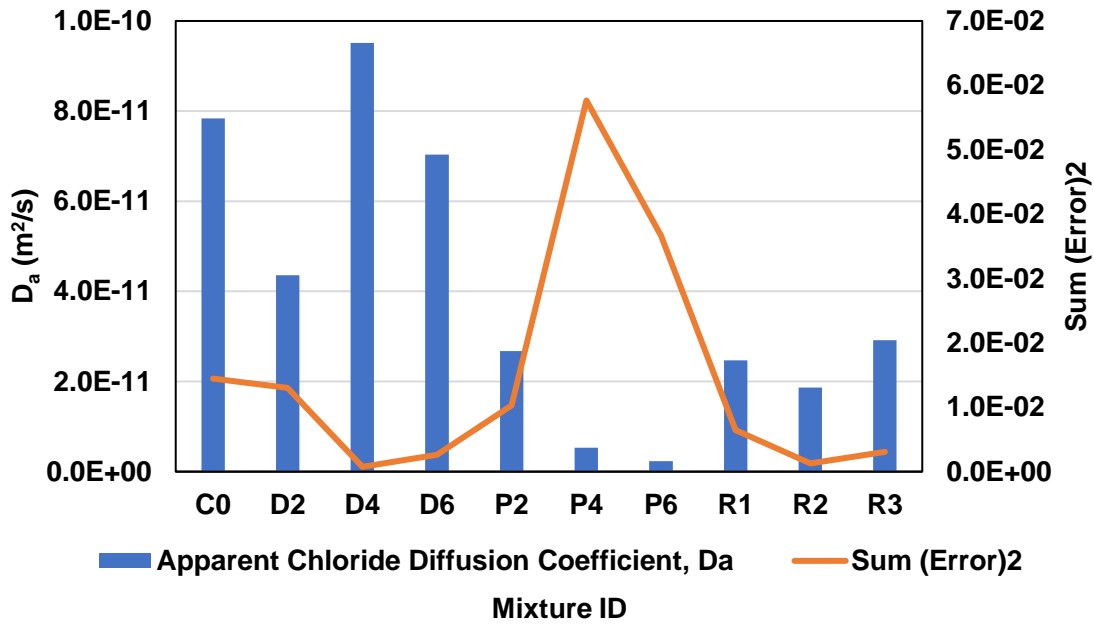


Figure 3.23 ASTM C1556 sum of squared errors for diffusion coefficients of lab samples

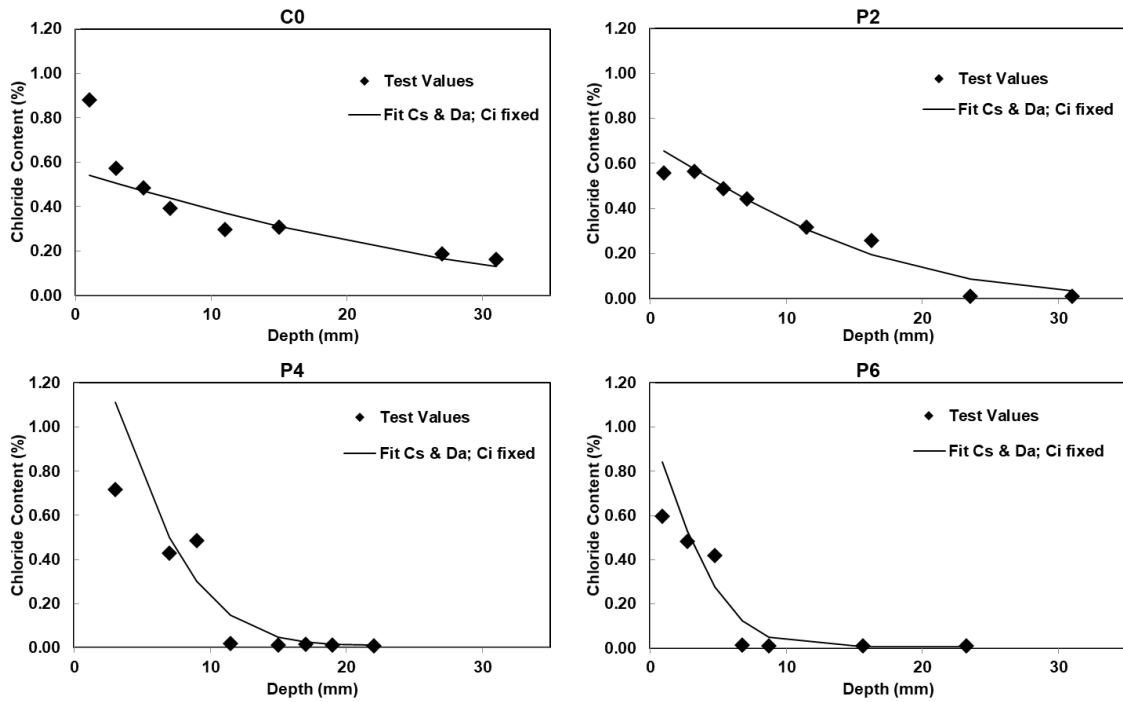


Figure 3.24 Selected chloride profiles for lab samples

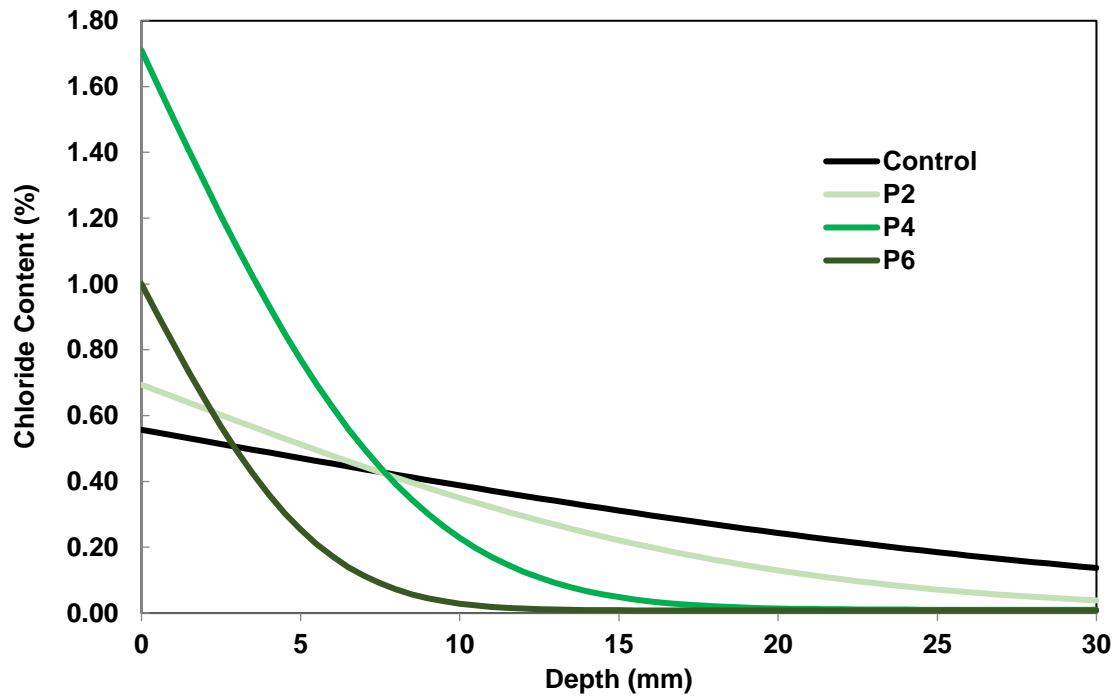


Figure 3.25 Selected chloride content models for lab samples

3.4.2. Lab Specimens—Corrosion Beams

Unfortunately, due to experimental errors and lack of familiarity with the testing equipment and conditions, corrosion current measurements were incorrectly taken for the duration of the test, and it was not possible to accurately assess at which time corrosion initiated. The samples were cycled between wetting and drying as specified for two years before testing was discontinued. At an age of 3+ years, final half-cell potential measurements were made before the samples underwent forensic evaluation. Details regarding these items are included below.

3.4.2.1. Half-cell Potential

Samples were ponded with solution and half-cell potential measurements were made for a final time on January 31st, 2020. The final measurements, shown in Figure 3.26, give a qualitative probability of the presence of corrosion based on the guidelines from Table 3.12. Samples with highly negative values (~ -500 mV) had visible cracks at the surface (Figure 3.17) and were confirmed to have severe corrosion through forensic evaluation. However, it was difficult to interpret intermediate values, and, as it will be later discussed, signs of corrosion were even present in samples with low potentials. Figure 3.26 includes measurements from two samples for each mixture (Sample A and Sample B). A discussion regarding sample variability is included in the following section.

Given the inconsistent testing schedule and scattered data, it is difficult to draw conclusive information from the corrosion beam half-cell measurements alone. Overall, however, the data seems to match trends seen with the chloride diffusion testing. That is, Product D shows irregularities; Product P appears promising; and Product R shows moderate improvements. Except for P4-B, the Product P mixtures exhibit lower voltage differences and the trend is nearly consistent with increased dosage.

Table 3.12 Notes on interpretation of half-cell measurements with copper-copper sulfate reference electrode (ASTM C876, Appendix X1.1)

Measured Potential, E (mV)	Probability of Corrosion
$E > -200$	10%
$-200 > E > -350$	Uncertain
$E < -350$	90%

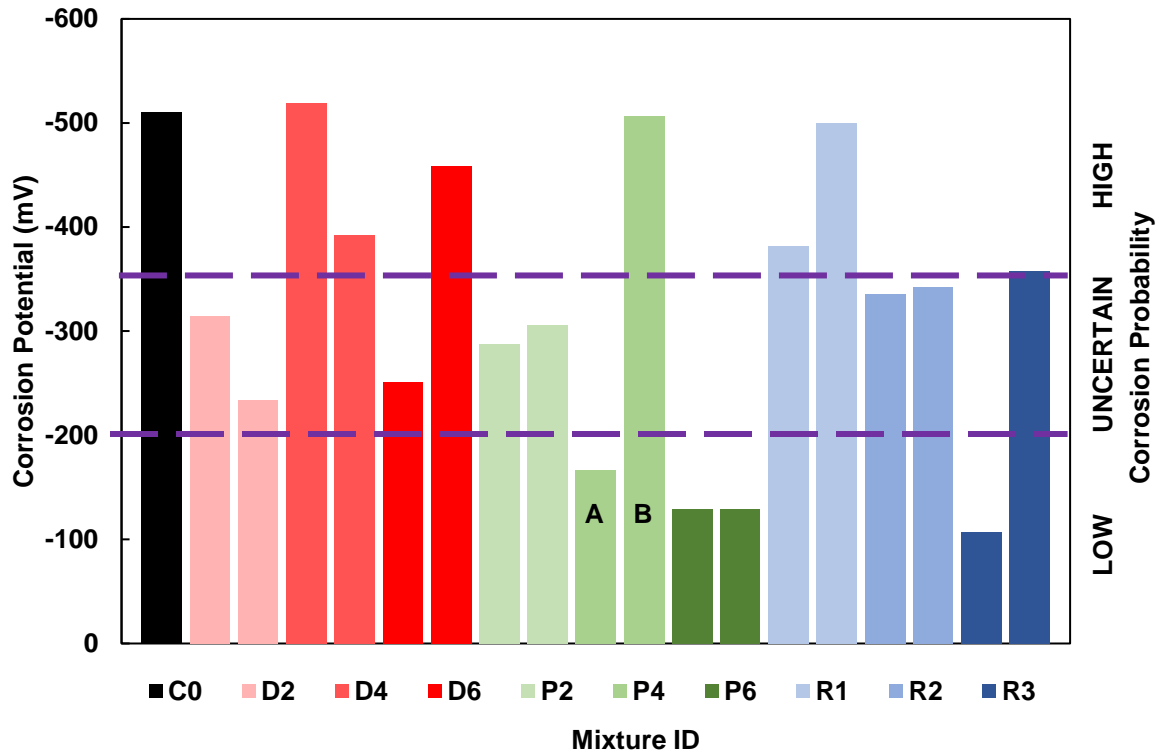


Figure 3.26 G109 final half-cell potential measurements

3.4.2.2. Sample Variability

As shown in Figure 3.26, it is evident that wide discrepancies exist between replicate samples. A theory to address sample variability is presented below using Mixture P4 Sample A (low voltage) and Sample B (high voltage) from Figure 3.26 as examples.

- Due to general sample variability and imperfections, Sample B could have been more susceptible to chloride ingress than Sample A.
- Sample B could have formed corrosion products at a faster rate than Sample A. This could have been monitored and validated through proper corrosion current and half-cell potential measurements.
- If proper measurements had been made, the test could have concluded at an earlier point at which Sample B had reached the designated corrosion current limit. Sample A would have been expected to have relatively close measurement values to Sample B at that point.
- However, given that the corrosion current measurements were not made correctly, testing cycles were continued indefinitely without proper assessment. The continuation of testing could have preferentially affected Sample B as the formation

of corrosion products could have caused cracking and rapidly worsened conditions. It is believed that once localized cracking occurred, chlorides had direct access to the reinforcement and corrosion was exacerbated, leading to the significant differences in half-cell measurements between Sample A and Sample B.

3.4.2.3. Chloride Mapping

Chloride mapping refers to the profiling of chlorides across various sample regions but at a constant depth equal to the reinforcement cover depth (25.0 mm [1.0 in.]). Select mixtures were chosen for chloride mapping examination and are shown in Figure 3.27. Regions examined included sections within the ponding area, marked by the rectangular perimeter, and sections outside of it. It was theorized that chloride levels would be relatively similar within the ponding area and lower on the outside. While some mixtures followed this expected trend, mixtures containing Product P once again produced surprising results. Table 3.13 is used to qualitatively assess chloride mapping values.

Samples P4-A and P6-B show that even mixtures with low and relatively ‘safe’ half-cell measurements (Figure 3.26) can have considerable chlorides at the reinforcement (Figure 3.27). Remarkably, however, the samples also contained regions of negligible chlorides within the ponding area and adjacent to the high chloride zones. These results indicate Product P’s enhanced ability to mitigate the ingress of chlorides, a trend previously observed in chloride diffusion results. The presence of high chloride zones at the given depth is believed to be a result of localized cracking from the formation of corrosion products as diffusion alone would likely require much longer exposure times for chlorides to reach such high levels. Regions not affected by localized cracking are believed to effectively mitigate chloride ingress through decreased permeability. Given that the time of corrosion initiation was undetermined, it is not possible to conclude whether the admixture also provides an increased chloride threshold.

Table 3.13 Chloride loading zone

Zone	Chloride Content (% mass)	Description
Negligible	<0.02	Uncracked zone. Active mitigation of chloride ingress, potentially due to decrease in permeability.
At Risk	0.02-0.15	Likely uncracked zone. Has experienced a significant ingress of chlorides. At risk of corrosion or corrosion already ongoing.
Damaged	>0.15	Likely cracked zone. Allows for ample chloride ingress. Severe corrosion has occurred.

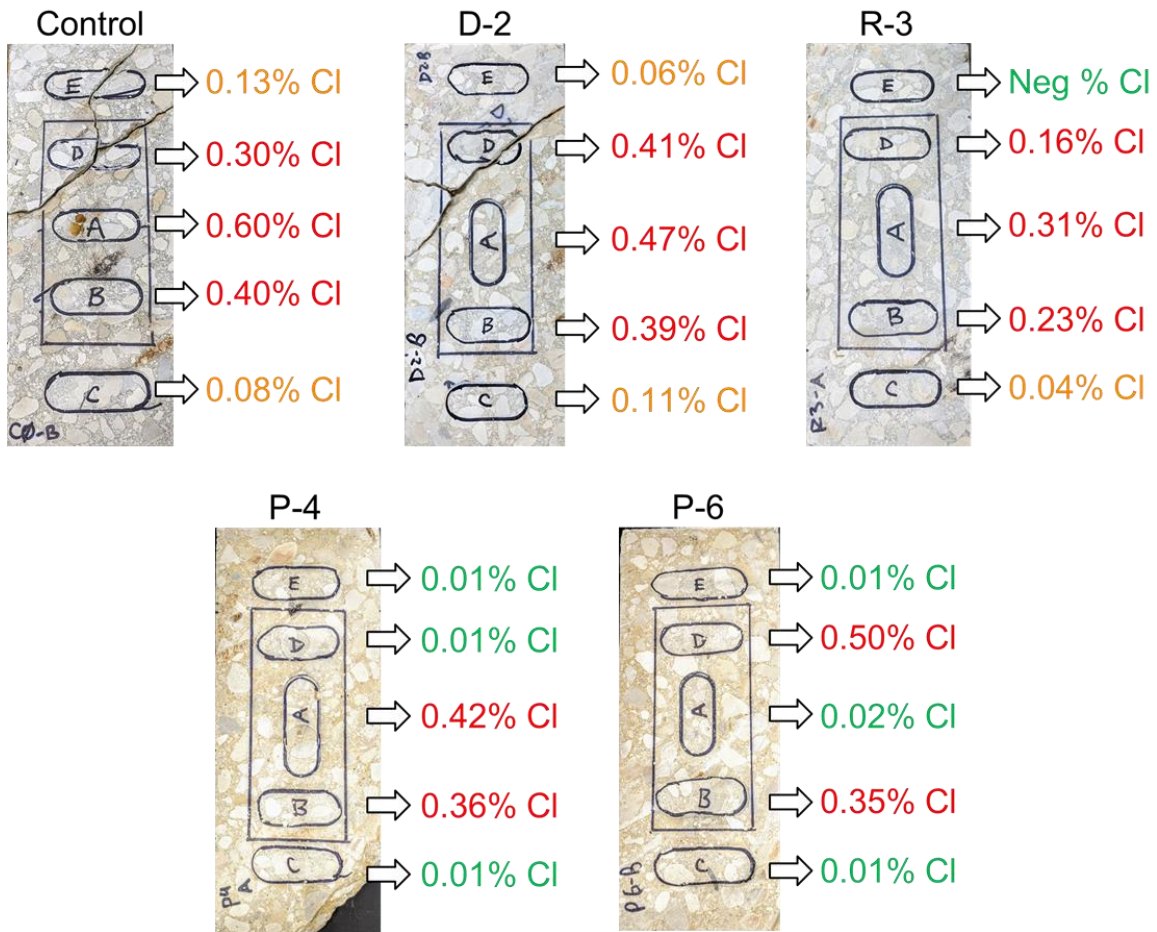


Figure 3.27 Chloride mapping of select G109 samples

3.4.2.4. Visual Examination and Summary

Corrosion beam specimens were visually examined before and after the removal of reinforcement bars. Inspections prior to the removal of reinforcement were intended to identify specimens with visible signs of cracking (Figure 3.17). As seen in Table 3.14, specimens with visible cracks correspondingly had the highest half-cell values. Once the top reinforcement bars were removed and cleaned, each bar was assigned a visual damage rating as established by Table 3.10.

Table 3.14 presents a summary of the corrosion beam testing including half-cell measurements, presence of visible cracks, chloride mapping values, and visual examination ratings. It should be noted that chloride contents listed are from Region A of each chloride mapping surface. As previously mentioned, chloride contents can vary across surfaces and their inclusion is intended only as an overview. As seen in Table 3.14 and Figure 3.28, evaluating corrosion is a complex process with no single test being capable of

confirming its presence. Even the forensic examination of a corroded bar can prove difficult to characterize beyond a qualitative rating. Additionally, test results can seemingly oppose each other: samples with low half-cell measurements can also contain regions of high chlorides and moderate corrosion (P6-B in Figure 3.28).

Considering sample variability and the issues encountered with the G109 procedure, it is not possible to draw conclusive information from the test results as seen in Table 3.14. However, there are signs of improved performance with certain admixtures and valuable information was gathered as part of the corrosion beam investigation. These details will be later used to provide a comprehensive performance assessment of the products.

Table 3.14 Corrosion beam testing summary

Mixture ID	Sample	Half-Cell (mV)	Visible Cracks	Chloride Content (mass %)	Visual Rating
C0	B	-511	Yes	0.25	Extensive
D2	A	-315	No	0.47	Moderate
	B	-234		0.47	Minor
D4	A	-519		0.55	
	B	-392		0.46	N/A
D6	A	-251		0.35	
	B	-459		0.43	
P2	A	-288		0.49	
	B	-306		0.57	
P4	A	-167		0.42	
	B	-507		0.98	
P6	A	-333		0.01	
	B	-129		0.02	
R1	A	-382		0.31	
	B	-500		0.45	
R2	A	-336		0.36	
	B	-343		0.32	
R3	A	-107		0.31	
	B	-358		0.28	

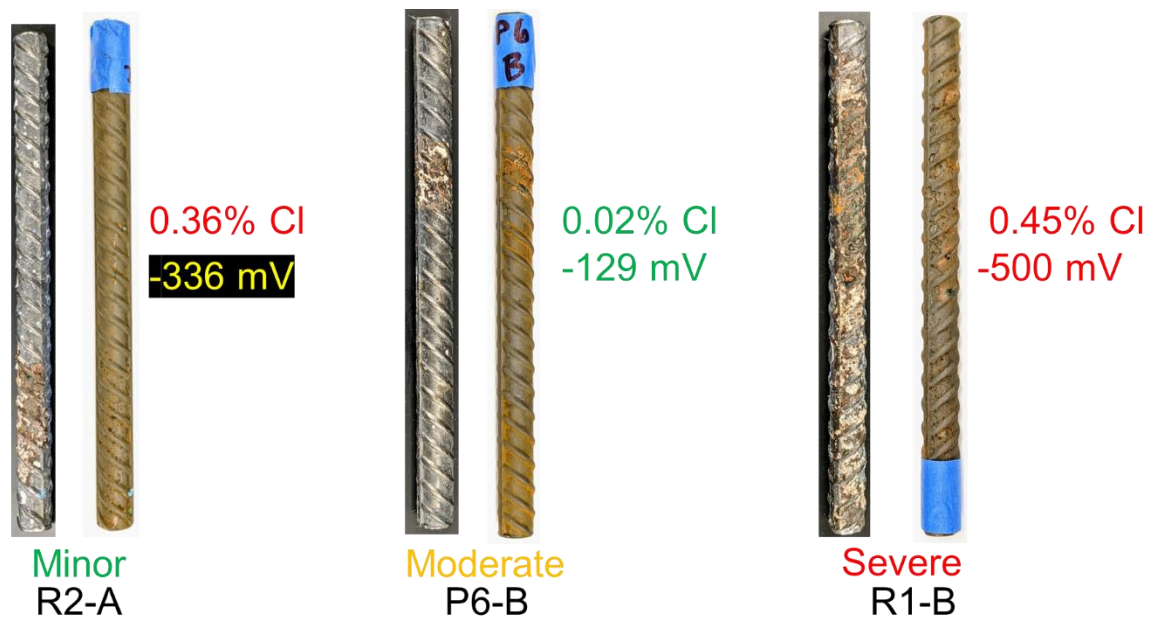


Figure 3.28 Examples of corrosion beam testing including rebar visual examination and rating, chloride content, and half-cell measurements

3.4.3. Field Specimens—Marine Exposure Blocks

Field samples undergo much more variable conditions than their lab counterparts. Fluctuating temperatures and tide levels, cycles of wetting and drying, abrasion, and even biological growth may influence the rate at which chlorides ingress concrete and complicate testing procedures. Nonetheless, as discussed in Section 3.4.3.1, the analysis of field samples has been found to provide realistic and valuable data.

3.4.3.1. Half-cell Potential

Site visits to the Texas Marine Exposure Site in Port Aransas occurred periodically. Half-cell measurements for field samples were approximately taken yearly up to a period of three years of exposure. The half-cell potential data for marine blocks up to an exposure time of 37 months is shown in Figures 3.29–3.32. As previously mentioned, corrosion potential values can be influenced by many factors and should be carefully interpreted in a qualitative manner. It should also be noted that two reinforced blocks were lost: D6 at 25 months and P6 at 37 months.

The data contains a few anomalies such as potential values becoming positive (Figure 3.30), values jumping from high-risk to low-risk zones from one measurement to the next (P4 from 25 to 37 months), and values not strictly decreasing as a function of depth. Nonetheless, when compared with the control, mixtures containing inhibitors demonstrate

overall beneficial trends. The control mixture behaved as expected, with gradually increasing potential values indicating the high probability of corrosion at all cover depths after 3 years of exposure.

While two blocks were lost and their respective data were not gathered, it is likely that all mixtures would have indicated a high probability of corrosion at the first two cover depths (12.5 and 25.0 mm [0.5 and 1.0 in.]) after 3 years of exposure. As it will be later shown with the blocks' chloride profiles, it is reasonable to assume that enough chlorides could have reached the second layer of reinforcement (25.0 mm [1.0 in.] cover) and exceeded the chloride threshold after 3 years of exposure. Data from the third and fourth layers of reinforcement (37.5 and 50.0 mm [1.5 and 2.0 in.] covers) show a significant improvement in performance with the use of admixtures. Product D in particular has consistently predicted low corrosion risk at those depths. Product P and Product R have shown moderate performance improvements but have either been inconsistent or are gradually approaching high-risk zones. These results contrast findings by Østnor and Justnes (2011), who found that the use of anodic inhibitors resulted in highly negative potential values that incorrectly predicted corrosion. This trend, however, was not observed in this study and the anodic inhibitors (Product D and P) behaved relatively as expected.

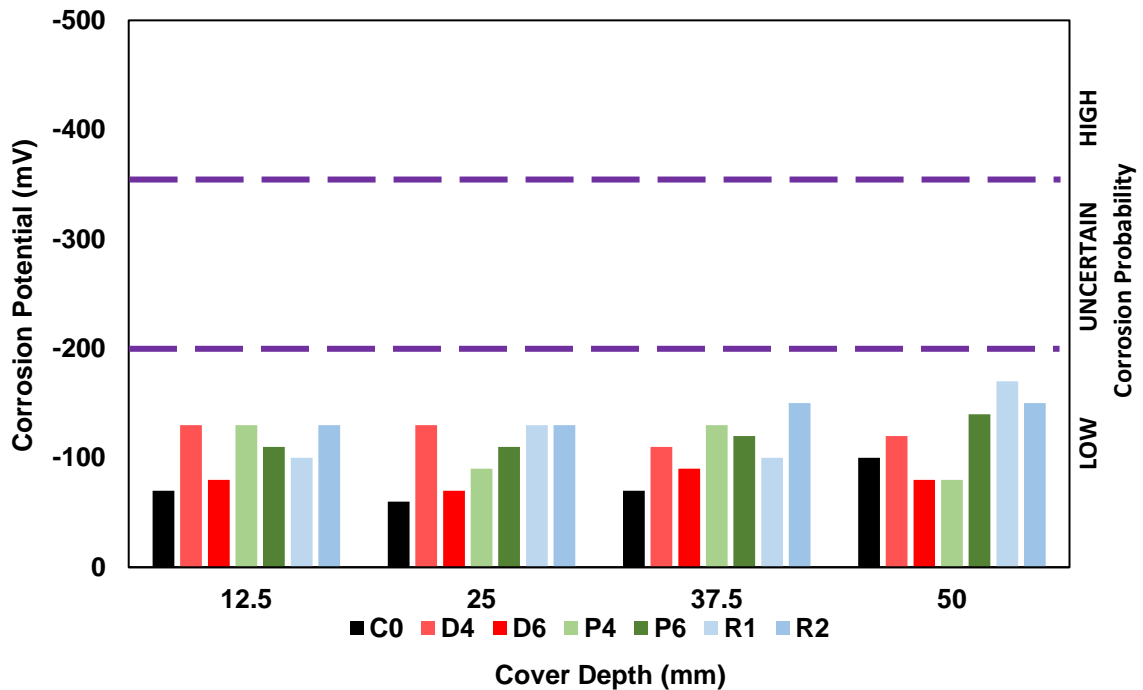


Figure 3.29 Marine exposure block half-cell measurements, initial values

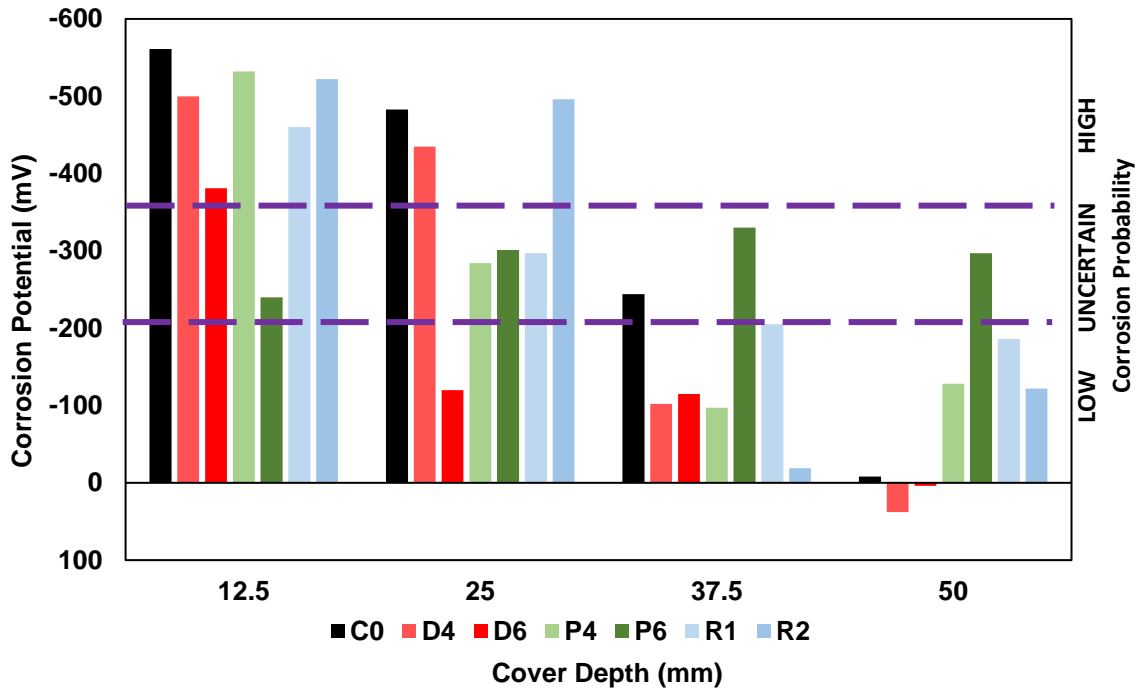


Figure 3.30 Marine exposure block half-cell measurements, 16 months exposure

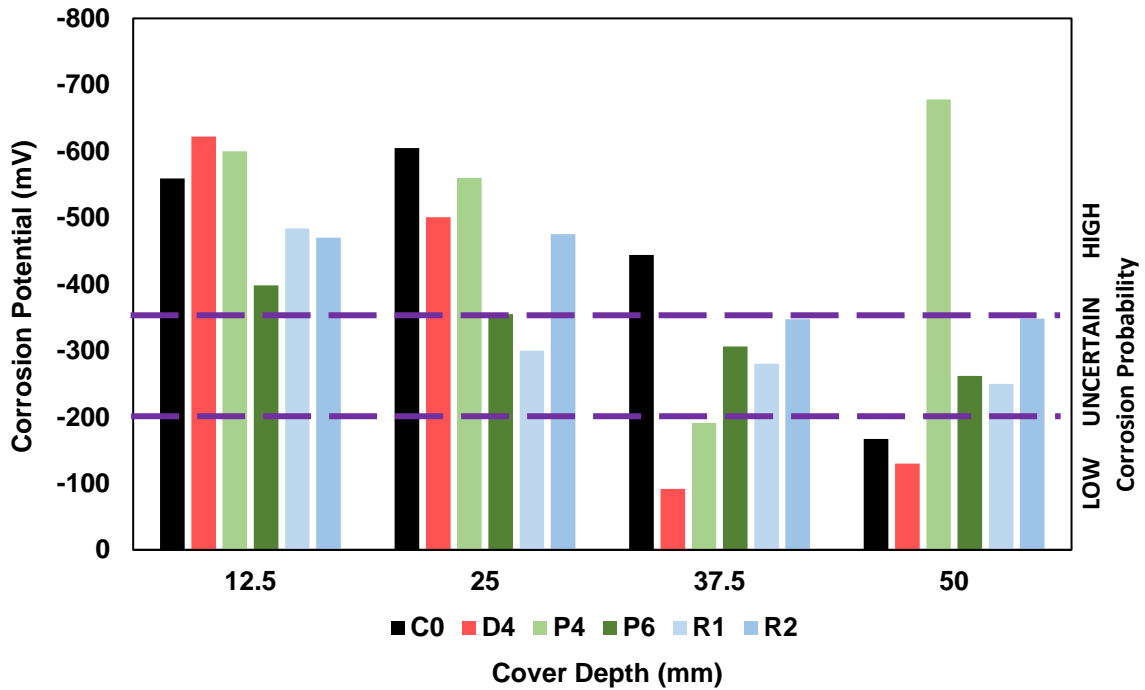


Figure 3.31 Marine exposure block half-cell measurements, 25 months exposure

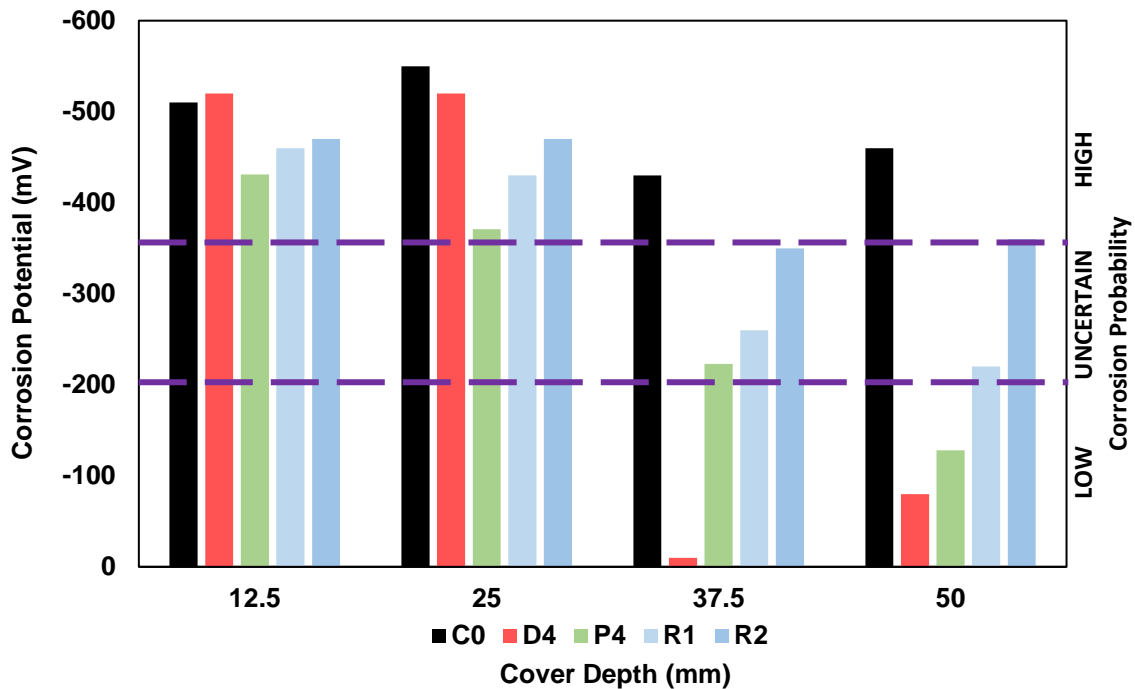


Figure 3.32 Marine exposure block half-cell measurements, 37 months exposure

3.4.3.2. Chloride Diffusion Coefficient

Diffusion coefficients for field samples are shown in Figure 3.33. The sum of errors squared associated with each calculated value is shown in Figure 3.34. The measured errors were deemed to be within an acceptable range. The average sum of errors squared for field samples was 1.9×10^{-2} (compared to 1.5×10^{-2} for lab samples). The MAE for marine exposure blocks as described in Equation 3.10 is presented in Table 3.15. As seen in Table 3.15, for Mixture P6, the inclusion of the first data point greatly increases error; however, this is considered an artificial result based on the mathematical approximation of surface chlorides.

Diffusion coefficients for field samples were closer to expected values than lab samples. Based on Equation 3.5 (Riding et al., 2013), it was expected that D_a would be around 1.1×10^{-11} m²/s for the given w/c. The control field sample had a measured diffusion coefficient of 7.2×10^{-12} m²/s. The decreased value obtained from the control field sample could be attributed to the later age of the specimen (~3 years) when compared to the expected D_a lab value which is considered a 28-day measurement.

The beneficial effects of admixtures were more clearly observed in field samples than in lab samples. All products were able to significantly reduce diffusion coefficients across dosages. Even Product D, which was not expected to significantly influence transport properties, had reduced diffusion coefficients across dosages. These results contrast

inconsistent values obtained in lab testing with Product D, which are believed to be a result of inconsistent lab sample conditioning. Product R showed similar levels of improvement as Product D. Product P, as with lab samples, showed a marked ability to rapidly reduce chloride contents to negligible values. Indeed, the diffusion coefficient for P6 was orders of magnitude lower than that of the control and is barely visible in Figure 3.33.

The literature review found only one previous source (Berke and Rosenberg, 1989) that indicated the potential for calcium nitrite admixtures (Product D) to reduce the diffusion coefficient. By far, the primary mechanism associated with calcium nitrite admixtures is an increase in chloride threshold (Berke and Hicks, 2004). Results from these field samples, however, demonstrate the admixture’s ability to reduce the diffusion coefficient and potentially provide a synergistic effect with an increased chloride threshold.

Figure 3.35 shows the mathematical chloride content model for Product P based on its field samples. The field models echo the trend seen in lab samples (Figure 3.25): the admixture greatly reduces chloride ingress and its beneficial effect is directly related to dosage. It should be noted that the high surface concentration predicted by the model for the P6 mixture, 19.6%, is a mathematical expression and does not reflect actual conditions; therefore, it was omitted from the plot.

Diffusion coefficients are a mathematical expression that can be considered as a rate or slope of chloride ingress. However, a lower diffusion coefficient does not necessarily mean an overall lower chloride content. As seen in Figure 3.36, while the diffusion coefficient for Product D mixtures is lower than the control, their predicted surface chloride contents are relatively similar, or in the case of D6, even more pronounced. Thus, the beneficial effects of a decreased diffusion coefficient may only be apparent at deeper depths and in the long-term.

Table 3.15 Mean absolute error (MAE) for chloride analysis on marine exposure blocks

Mixture	Data Points			
	k = n-1		k = n	
	k	MAE (%)	k	MAE (%)
C0	12	0.03	13	0.04
R1	8	0.02	9	0.02
R2	10	0.02	11	0.03
D4	9	0.03	10	0.03
D6	9	0.06	10	0.08
P4	8	0.07	9	0.07

Mixture	Data Points			
	k = n-1		k = n	
	k	MAE (%)	k	MAE (%)
P6	9	0.01	10	0.51

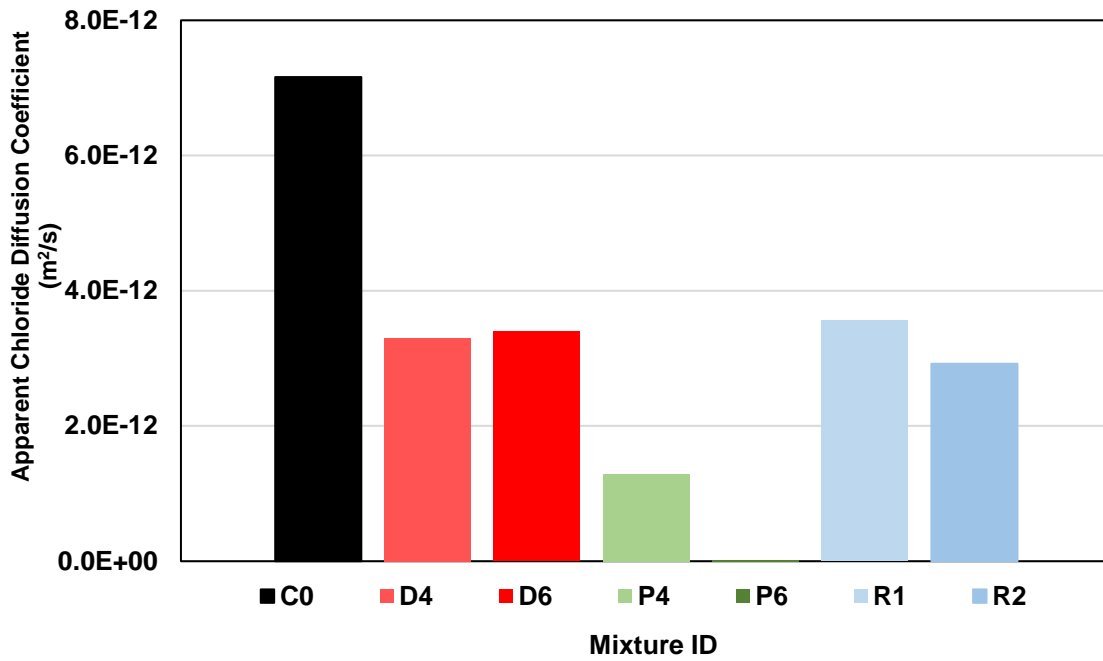


Figure 3.33 Apparent chloride diffusion coefficient of field samples

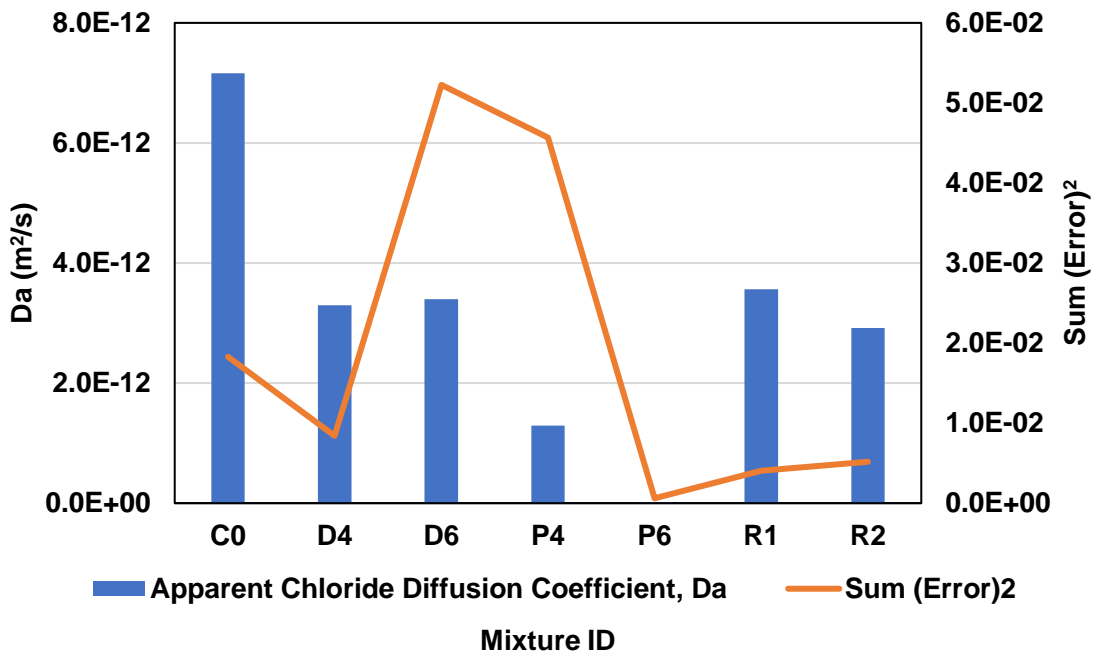


Figure 3.34 ASTM C1556 sum of squared errors for diffusion coefficients of field samples

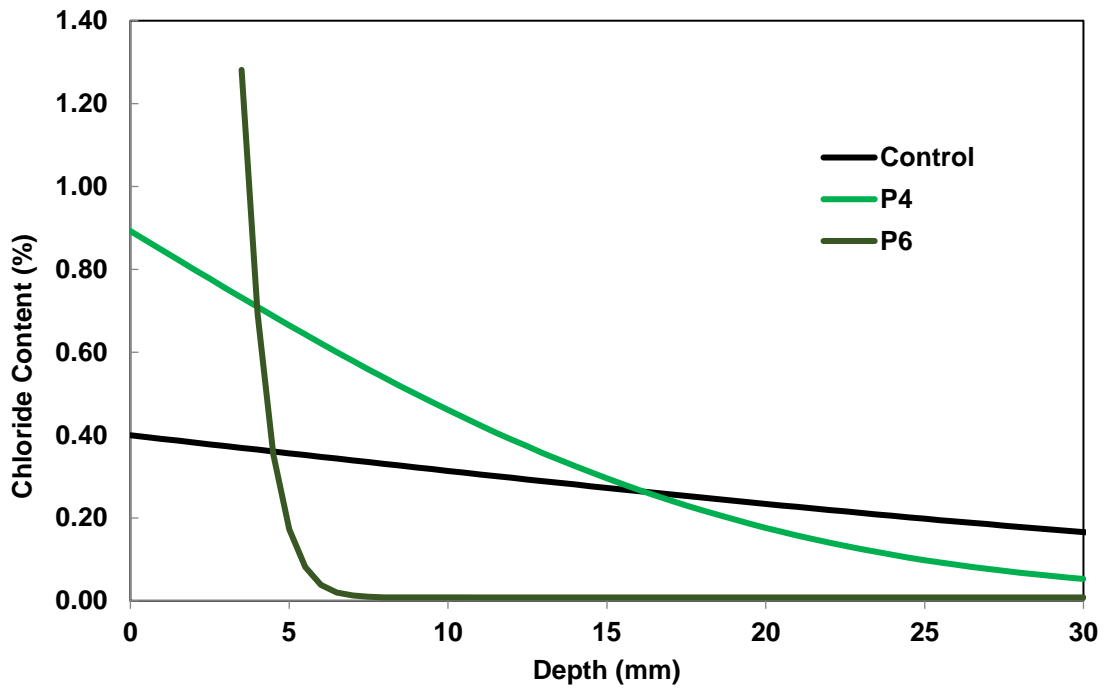


Figure 3.35 Field sample chloride model—Product P (3 years exposure)

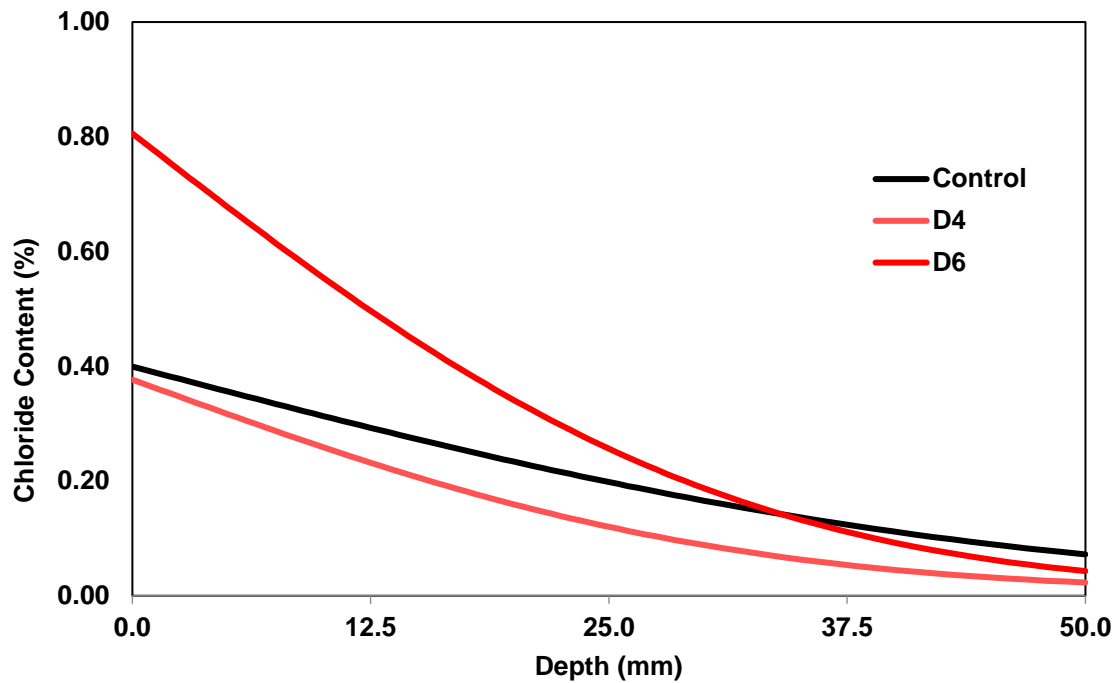


Figure 3.36 Field sample chloride model—Product D (3 years exposure)

3.4.3.3. Comparison of Half-Cell and Chloride Diffusion Coefficient Data

Results from half-cell measurements and chloride diffusion coefficients for Product D and Product P field mixtures will be analyzed in this section.

Half-cell measurements indicate a low probability of corrosion at depths of 37.5 and 50 mm (1.5 and 2.0 in.) for the Product D mixture at a dosage of 4 gal/yd³ (Figure 3.32). Simultaneously, however, the predicted chloride models for the D4 and D6 mixtures (Figure 3.36) project moderate levels of chlorides at a depth of 37.5 mm (1.5 in.) (0.05–0.11% respectively). Similar levels of chlorides (0.12%) appear to be capable of inducing corrosion on the control at that depth. Therefore, the absence of active corrosion in these mixtures could validate Product D’s claims to increase the chloride threshold. A moderate chloride threshold of 0.07% Cl by concrete mass is being assumed for the control mixture. Based on Table 3.2, Mixtures D4 and D6 could have an enhanced chloride threshold of 0.32% and 0.40% respectively. Unfortunately, these values were not able to be confirmed through ASTM G109 testing. Conversely, if active corrosion is assumed to be ongoing in Mixture D4 at a depth of 25.0 mm (1.0 in.) based on the same half-cell data (Figure 3.32), this would indicate that the chloride threshold could be as low as 0.12%. Thus, it is believed that Product D can increase the chloride threshold. However, it was not possible to quantify the increase itself given testing limitations.

The chloride content models for Product P (Figure 3.35) predict the ability to mitigate chlorides within shallow depths. However, half-cell measurements hint at the likelihood of corrosion occurring at the 25.0 mm (1.0 in.) depth for Mixture P4 (Figure 3.32). This disconnect can be related to results seen in the ASTM G109 test. Chloride mapping for Product P mixtures indicated the possibility for high chloride areas to coexist with nearby regions of negligible chlorides due to sample variability and imperfections. Therefore, while Product P demonstrates remarkable abilities to mitigate chloride ingress (capable of suppressing chlorides within the first 25 mm), chlorides are still likely to find imperfections within those shallow depths and lead to localized corrosion. However, most structures are designed with a 50 mm (2.0 in.) minimum cover and test results at those depths will be the concluding factor to determine long-term performance.

3.4.3.4. Visual Examination

Marine exposure blocks are visually examined each time they are measured. Extensive and exotic biological growth is often seen growing on the blocks (Figure 3.37). The submerged block portion appears to be an effective magnet for marine ecosystems. The biological growth is (unfortunately for its inhabitants) removed with a shovel to allow for proper half-cell measurements and visual examination. It remains unclear if the physical presence of marine life affects chloride ingress on specific sections or if certain mixtures are more conducive to its development. Rust staining has been observed on some blocks at the shallowest rebar depth (12.5 mm [0.5 in.]), which validates half-cell data predicting a high possibility of corrosion at this depth for all mixture (Figure 3.32). However, not enough blocks have shown rusting signs to provide quantifiable data.



Figure 3.37 Exposure block visual examination: biological growth (left and middle) and rust staining (right)

3.4.3.5. Service Life Models

Service life models were calculated for each field mixture based on the ConcreteWorks (2017) methodology described in Section 3.5.5.4. The models are intended to provide an estimated structure service life in years based on the time of corrosion initiation and subsequent propagation of corrosion damage. The models can be distinguished as theoretical or empirical. The theoretical model follows the standard instructions outlined by the ConcreteWorks (2017) software. This model uses stock data for most of its inputs. The empirical models use inputs from the chloride diffusion data obtained from field samples. The inputs were then manually entered into the background calculations used by ConcreteWorks (2017) to produce comparable models. Details and assumptions regarding both types of models are discussed below.

3.4.3.5.1. Theoretical Model Details and Assumptions

- Theoretical model will be provided for four mixtures (C0, D4, D6, & R1) since their input information is readily available within the ConcreteWorks software.
- Based on an OPC mixture with a w/c ratio of 0.45. Assumed properties include a decay, m , value of 0.26, diffusion coefficient, D_{28} , of 1.1×10^{-11} m²/s, and chloride threshold of 0.07% Cl by concrete mass.
- Concrete is assumed to have an initial chloride content, C_i , of 0.00% by concrete mass.
- Time to corrosion initiation is defined as the time when the chloride content at a depth of 50.0 mm (2.0 in.) exceeds the chloride threshold.
- Concrete is assumed to be in a splash zone and has a surface chloride concentration, C_s , of 0.80%. This surface concentration is assumed to be reached ‘instantaneously’ given the exposure conditions, and, thus, the buildup rate, b , can be omitted.
- Concrete was exposed to chlorides at an age of 63 days, which is the average age at which the marine exposure blocks were placed at the exposure site.
- Theoretical concrete is located in Corpus Christi, TX, which is expected to have similar weather conditions as the actual exposure site in Port Aransas.
- Local weather conditions are considered by the software, which will adjust the diffusion coefficient accordingly.
- Diffusion coefficient is capped by an ultimate value, D_{ult} , per Equation 3.6.

- Based on Section 3.4.2.2, the use of certain admixtures will change concrete properties as follows: increase in chloride threshold for Mixtures D4 and D6 to 0.32% Cl and 0.40% Cl respectively and a 10% decrease in diffusion coefficient (D_{28}) for Mixture R1 to $9.8 \times 10^{-12} \text{ m}^2/\text{s}$.

3.4.3.5.2. Empirical Model Details and Assumptions

- Empirical models will be provided for all seven exposure block mixtures present at the exposure site.
- Based on an OPC mixture with a w/c ratio of 0.45. Assumed properties include a decay, m , value of 0.26, chloride threshold of 0.07% Cl by concrete mass, and parameters used by the mathematical chloride diffusion coefficient summarized in Table 3.16.
- Concrete has an average measured initial chloride content, C_i , of 0.01% Cl by concrete mass.
- Concrete blocks are in a splash zone, which is assumed by ConcreteWorks to yield a surface chloride concentration, C_s , of 0.80%. Empirical data indicates approximate surface values to be in the range of 0.35–1.00%. However, the mathematical models project a much wider range from 0.33–19.56% (Table 3.16). It should be noted that the models tend to underestimate (or in the case of Mixture P6 grossly overestimate) surface concentrations to minimize mathematical error and do not necessarily reflect actual conditions.
- Concrete was placed at the exposure site in Port Aransas and exposed to chlorides at an average age of 63 days.
- Diffusion coefficients at 28 days, D_{28} , were back calculated from the coefficients obtained by profiling field samples, D_t , based on Equations 3.6, 3.7, and 3.11. The coefficient obtained from field samples are considered as D_t at time $t = 1,034$ days, which is how long the blocks were at the exposure site prior to removal, and m is approximated as 0.26 for OPC mixtures.

$$D_{ult} = D_{28} \cdot \left(\frac{28}{36,500} \right)^m \quad \text{Eq. 3.6}$$

$$D_t(t) = D_{28} \cdot \left(\frac{28}{t} \right)^m + D_{ult} \cdot \left(1 - \left(\frac{28}{t} \right)^m \right) \quad \text{Eq. 3.7}$$

$$D_{28} = \frac{D_t}{\left(\frac{28}{t}\right)^m + \left(\frac{28}{36,500}\right)^m \cdot \left(1 - \left(\frac{28}{t}\right)^m\right)} \quad \text{Eq. 3.11}$$

- D_{28} diffusion coefficients were not adjusted based on temperature effects. Since the values were empirically obtained from samples that were exposed to local weather conditions, it is assumed that all external factors have been inherently accounted in the calculations.
- Since it was not possible to empirically obtain revised chloride thresholds for each mixture, two cases will be modeled. The first case will assume thresholds remain unchanged by admixtures and are fixed at the assumed 0.07% Cl. The second case will adjust thresholds based on the values used in ConcreteWorks (2017). That is, Mixtures D4, D6, and R1 will have increased thresholds of 0.32%, 0.40%, and 0.12% respectively.
- Time to corrosion initiation is defined as the time when the chloride content at a depth of 50 mm exceeds the specific chloride threshold. The calculations are based on Equation 3.4 and use the parameters presented in Table 3.16. The diffusion coefficient, D_a , is $D_i(t)$ as defined by Equation 3.7.

$$C(x, t) = C_s - (C_s - C_i) \cdot \text{erf}\left(\frac{x}{\sqrt{4 \cdot D_a \cdot t}}\right) \quad \text{Eq. 3.4}$$

The theoretical and empirical models were remarkably comparable for the control mixtures and unsurprisingly predict the initiation of corrosion at an early age. This claim is nearly guaranteed as the presence of corrosion throughout the control block has been validated by half-cell and chloride profiling testing after three years of exposure. Empirical models for admixture mixtures, on the other hand, moderately deviated from their theoretical counterparts. Overall, admixture use is seen to extend service life. However, the interpretation of the data can result in a wide range of service life predictions. For example, if Mixture D4 is assumed to have an unchanged chloride threshold, it will relatively match its theoretical model prediction by virtue of a reduction in diffusion coefficient. Nonetheless, that theoretical model itself is based on an adjusted chloride threshold, and if the empirical model uses that same adjusted threshold value combined with the reduced diffusion coefficient, its service life is predicted to be over 650 years. Indeed, the true answer may lie somewhere in between.

Additionally, prediction discrepancies between mixtures with similar diffusion coefficients (D4 and D6) highlight the importance of surface concentrations as part of the chloride mathematical model. As previously mentioned, chloride surface concentration is

influenced by environmental factors and may not necessarily match the diffusion model created for a lab sample in a static environment. While labor intensive, obtaining more than one chloride profile from each field sample could help improve the accuracy of the models.

Product P mixtures were predicted to have increased service lives which were directly related to admixture dosage. The incredibly low diffusion coefficient of Mixture P6 led to an estimated service life of over 450 years without accounting for any increase to the chloride threshold. If the use of Product P is also found to increase the chloride threshold, its estimated service life would be further extended. Given that the admixture is partly calcium nitrite based, it is not unreasonable to consider that the chloride threshold may also increase with its use.

Product R mixtures are also predicted to improve performance; however, increased admixture dosage does not appear to influence results.

Table 3.16 Exposure block chloride parameters based on ASTM C1556 model

Mixture	C _s (mass %)	C _i (mass %)	D _t (m ² /s)	t (year)	D ₂₈ (m ² /s)	D _{ult} (m ² /s)
C0	0.40	0.01	7.16E-12	2.83	1.47E-11	2.28E-12
D4	0.38	0.01	3.30E-12	2.83	6.79E-12	1.05E-12
D6	0.81	0.01	3.40E-12	2.83	7.00E-12	1.08E-12
P4	0.89	0.01	1.29E-12	2.83	2.66E-12	4.12E-13
P6	19.56	0.01	2.02E-14	2.83	4.15E-14	6.43E-15
R1	0.33	0.01	3.56E-12	2.83	7.33E-12	1.14E-12
R2	0.39	0.01	2.92E-12	2.83	6.01E-12	9.32E-13

Table 3.17 Service life models—time to corrosion initiation (years) [chloride threshold, CT, % mass of concrete]

Mixture ID	Theoretical Model	Empirical Model	
	Variable CT (%)	Fixed CT (0.07%)	Variable CT (%)
C0	2.3 (0.07%)	2.7	-
D4	7.5 (0.32%)	7.4	650 (0.32%)
D6	10.3 (0.40%)	3.9	36.7 (0.40%)
P4	-	11.7	-
P6	-	450	-
R1	3.4 (0.12%)	7.5	16.5 (0.12%)
R2	-	7.7	-

3.5. Further Research

Given some of the exceptional test results observed in the study, the need to replicate and expand on those results is key to reaching a more conclusive assessment. Based on the current data and literature review, the following actions are recommended for further research of current and future samples.

- Continual monitoring of marine exposure blocks through half-cell measurement, chloride profiling, and visual examination. Monitoring within the next few years will be particularly critical in determining if chloride threshold has indeed increased for Product D mixtures.
- Consider obtaining multiple core samples when examining chloride ingress in marine exposure blocks. While labor intensive, obtaining more than one chloride profile from each field sample could help improve the accuracy of the models.
- Since all exposure blocks appear to have corrosion at the first rebar layer (12.5 mm [0.5 in.] cover depth) within a relatively short period of time, it may be worth considering removing or adjusting this layer. As observed, even mixtures with low chloride diffusion coefficients are prone to corrosion at such a shallow depth. The early onset of corrosion in this layer could cause cracking that may unintendedly reduce cover depths to other layers.
- Use of additional testing methods, such as linear polarization resistance, on exposure blocks to obtain corrosion rates is recommended.
- Consider the leaching of admixture active ingredients in exposure blocks and determine their potential for long-term effectiveness. May involve pore solution analysis of exposure blocks.
- Consider repeating cylinder lab testing (resistivity and chloride diffusion) since the conditioning employed in this study might have affected results.
- Consider repeating the G109 corrosion beam test or an alternate method to determine chloride threshold. It is also recommended to cast unreinforced corrosion beams subjected to the same ponding condition to analyze chloride ingress independent of possible corrosion cracking. This would help confirm if the high chloride contents observed in this study were in fact due to localized cracking as theorized.
- Considering the unexpected results in chloride profiles of Product P mixtures, it is recommended to have the values be independently corroborated by sending replicate samples to a third-party lab.

- Determine mechanism by which Product P is decreasing chloride ingress. Employ other forms of permeability/transport testing to validate results.
- Determine the chemical composition of Product P. Quantifying the calcium nitrate and calcium nitrite proportions could provide information regarding whether the beneficial effects are a function of calcium nitrate concentration or due to a synergistic effect.
- Examine the chloride binding abilities of the admixtures and the AFm forms developed. Enhanced, ‘smart’ chloride binding was previously reported by (Balonis and Glasser, 2011) with the use of calcium nitrite (Product D) and the use of nitrite and nitrate was found to create distinctive nitrite and nitrate AFm forms which could alter hydration products (Balonis et al., 2011). If Product P has similar abilities, the creation of a nitrate and nitrite AFm phases could be responsible for the decrease in chloride ingress, particularly if it results in a hydration product (potentially increased ettringite) with ‘pore blocking’ properties.
- As mentioned in Section 3.2.3.1.3, Product R appeared to trigger improvements in resistivity values that were directly related to dosage. However, after recasting the mixtures, the results were not replicated. This possibly indicates that the earlier values were influenced by sample moisture content. If this is the case, the admixture may have potential in preventing moisture ingress after samples have been dried for extended periods of time as it was done in this study. This phenomenon may be worth analyzing with further testing.
- Based on the work done by Melchers and Chaves (2020), consider making specimens with internal chlorides and assessing the admixtures’ potential to reduce leaching of calcium hydroxide.
- The resistivity results detailed in Section 3.3.5.2 may indicate that admixture nitrites and nitrates are no longer present in the pore solution. It may be useful to repeat testing and monitor resistivity values from early ages to more accurately determine this. Pore solution analysis can also be performed to track nitrite and nitrate concentrations.

3.6. Conclusions

Overall, the use of admixtures was found to be beneficial in delaying corrosion damage. However, results were varied based on the type of test and the effects were not always directly connected to admixture dosage. The control OPC mixture, while having a

moderate w/c of 0.45, was rapidly susceptible to corrosion damage as anticipated, highlighting the inadequacy of OPC systems in corrosion-prone environments.

The use of the calcium nitrate and calcium nitrite admixture significantly reduced chloride ingress, resulting in a notable decrease in the diffusion coefficient. The observed improvement was directly related to admixture dosage and was consistently observed across lab and field samples. This effect contrasts the limited information available from the literature as Østnor and Justnes (2011) found calcium nitrate to not influence chloride ingress but rather to inhibit corrosion by a similar mechanism to calcium nitrite, i.e., by increasing the chloride threshold. Since the product used in this study was a blend of calcium nitrate, calcium nitrite, and glycols, its alternate mechanism may be due to a synergistic effect between constituents. Possible mechanisms may involve a decrease in permeability, enhanced chloride binding, and the formation of hydration products with potential pore blocking abilities. The use of this product as a corrosion inhibitor appears highly promising as it is an already established accelerator and is considered a more economical alternative than standard inhibitors. Furthermore, the comprehensive testing of this product in a corrosion setting is believed to be a unique contribution from this research as no other study reviewed from the literature was found to include it. Thus, the lab and field data gathered could set a precedent for further exploration.

The calcium nitrite admixture (Product D) was shown to reduce diffusion coefficients. This effect is not commonly attributed to the admixture but may provide a significant benefit when combined with an increase in chloride threshold.

Marine exposure blocks have proven to be the best method to accurately predict long-term field performance as lab testing can produce inconsistent results. Longer exposure times are required before conclusive assessments can be made regarding the state of reinforcement at the deeper 37.5 and 50.0 mm (1.5 and 2.0 in.) cover depths. Moreover, these samples will also provide valuable information regarding the effect of inhibitors on the chloride threshold.

A summary of testing results is presented in Table 3.18, which qualitatively rates each product's performance across the various lab and field tests. The ratings indicate levels of performance, with a slight improvement denoted as (↑), a slight worse performance as (↓), a significant improvement as (↑↑), and a major improvement as (↑↑↑). Observations regarding each product are also detailed in this section.

Table 3.18 Testing summary and product rating

	Test	Product		
		D	P	R
Lab	Strength	↑	↓	↓
	Resistivity	↔	↔	↔
	Diffusion Coefficient	↑	↑↑↑	↑↑
	Corrosion Beams	↑	↑↑↑	↑↑
Field	Half-cell Potential	↑↑↑	↑↑	↑
	Diffusion Coefficient	↑↑	↑↑↑	↑↑
	Service Life Model	↑↑	↑↑↑	↑

3.7. References

Aïtcin, P., & Flatt, R. (2016). *Science and technology of concrete admixtures* / edited by Pierre-Claude Aïtcin and Robert J. Flatt. Elsevier.

Al-Amoudi, O., Maslehuddin, M., Lashari, A., & Almusallam, A. (2003). Effectiveness of corrosion inhibitors in contaminated concrete. *Cement and Concrete Composites*, 25(4-5), 439–449. [https://doi.org/10.1016/S0958-9465\(02\)00084-7](https://doi.org/10.1016/S0958-9465(02)00084-7)

Angst, U., Elsener, B., Larsen, C., & Vennesland, Ø. (2009). Critical chloride content in reinforced concrete — A review. *Cement and Concrete Research*, 39(12), 1122–1138. <https://doi.org/10.1016/j.cemconres.2009.08.006>

ASTM C1152 (2012), *Standard Test Method for Acid-Soluble Chloride in Mortar and Concrete*

ASTM C150 (2016), *Standard Specification for Portland Cement*

ASTM C1556 (2016), *Standard Test Method for Determining the Apparent Chloride Diffusion Coefficient of Cementitious Mixtures by Bulk Diffusion*

ASTM C1582 (2017), *Standard Specification for Admixtures to Inhibit Chloride-Induced Corrosion of Reinforcing Steel in Concrete*

ASTM C1876 (2019), *Standard Test Method for Bulk Electrical Resistivity or Bulk Conductivity of Concrete*

ASTM C192 (2015), *Standard Practice for Making and Curing Concrete Test Specimens in the Laboratory*

ASTM C39 (2015), *Standard Test Method for Compressive Strength of Cylindrical Concrete Specimens*

ASTM C876 (2015), *Standard Test Method for Corrosion Potentials of Uncoated Steel in Concrete*

ASTM G1 (2017), *Standard Practice for Preparing, Cleaning, and Evaluating Corrosion Test Specimens*

ASTM G109 (2013), *Standard Test Method for Determining Effects of Chemical Admixtures on Corrosion of Embedded Steel Reinforcement in Concrete Exposed to Chloride Environments*

Balonis M., Glasser F.P., Medala M. Influence of calcium nitrate and nitrite on the constitution of AFm and AFt cement hydrates. *Adv. Cem. Res.* 2011; 23:129–143. doi: 10.1680/adcr.10.00002.

Balonis, M., & Glasser, F. (2011). Calcium Nitrite Corrosion Inhibitor in Portland Cement: Influence of Nitrite on Chloride Binding and Mineralogy. *Journal of the American Ceramic Society*, 94(7), 2230–2241. <https://doi.org/10.1111/j.1551-2916.2010.04362.x>

Berke, N. S., & Rosenberg, A. (1989). Technical review of calcium nitrite corrosion inhibitor in concrete. *Transportation Research Record*, (1211).

Berke, N., & Hicks, M. (2004). Predicting long-term durability of steel reinforced concrete with calcium nitrite corrosion inhibitor. *Cement and Concrete Composites*, 26(3), 191–198. [https://doi.org/10.1016/S0958-9465\(03\)00038-6](https://doi.org/10.1016/S0958-9465(03)00038-6)

Bertolini, L. (2013). *Corrosion of steel in concrete prevention, diagnosis, repair / Luca Bertolini ... [et al.]. (2nd ed.). Wiley-VCH.*

Broomfield, J. (2007). *Corrosion of steel in concrete : understanding, investigation and repair / John P. Broomfield. (2nd ed.). Taylor & Francis.*

ConcreteWorks V3 Training/User Manual (2017)
<https://library.ctr.utexas.edu/ctr-publications/0-6332-p1p2.pdf>
<https://www.txdot.gov/business/resources/engineering-software.html>

Durable Concrete Structures – Design Guide. Comite Euro-International Du Beton (CEB). (1997)

Fahim, A. (2018). *Corrosion of Reinforcing Steel in Concrete: Monitoring Techniques and Mitigation Strategies.* University of New Brunswick.

Gaidis, J. (2004). Chemistry of corrosion inhibitors. *Cement and Concrete Composites*, 26(3), 181–189. [https://doi.org/10.1016/S0958-9465\(03\)00037-4](https://doi.org/10.1016/S0958-9465(03)00037-4)

Glass, G., & Buenfeld, N. (1997). The presentation of the chloride threshold level for corrosion of steel in concrete. *Corrosion Science*, 39(5), 1001–1013. [https://doi.org/10.1016/S0010-938X\(97\)00009-7](https://doi.org/10.1016/S0010-938X(97)00009-7)

Hewlett, P., & Liska, M. (2019). *Lea’s chemistry of cement and concrete: / edited by Peter C. Hewlett, Martin Liska. (Fifth edition.). Elsevier.*

Holm, J. (1987). Comparison of the Corrosion Potential of Calcium Chloride and a Calcium Nitrate Based on Non-Chloride Accelerator. *ACI Symposium Publication 102-4*

ISO 8044 (2020), *Corrosion of metals and alloys*

- Justnes, H. (2006). Corrosion Inhibitors for Reinforced Concrete. *ACI Symposium Publication 234-4*
- Kessler, R., Powers, R., Paredes, M., Sagiúés, A., & Virmani, Y. (2007). Corrosion Inhibitors in Concrete - Results of a Ten Year Study. *CORROSION 2007*. <https://www.onepetro.org/conference-paper/NACE-07293>
- Li, Z., Peng, J., Ma, B. (1999) Investigation of Chloride Diffusion for High-Performance Concrete Containing Fly Ash, Microsilica, and Chemical Admixtures. *ACI Materials Journal*, 96(3), 391–396. <https://doi.org/10.14359/638>
- Mammoliti, L. (2001). Examination of the mechanism of corrosion inhibition by calcium nitrite and calcium nitrate-based admixtures in concrete. University of Waterloo.
- Melchers, R., & Chaves, I. (2019). Reinforcement Corrosion in Marine Concretes-1: Initiation. *ACI Materials Journal*, 116(5), 57–66. <https://doi.org/10.14359/51716827>
- Melchers, R., & Chaves, I. (2020). Reinforcement Corrosion in Marine Concretes-2. Long-Term Effects. *ACI Materials Journal*, 117(2), 217–228. <https://doi.org/10.14359/51722400>
- Østnor, T., & Justnes, H. (2011). Anodic corrosion inhibitors against chloride induced corrosion of concrete rebars. *Advances in Applied Ceramics: Cement and Concrete Research*, 110(3), 131–136. <https://doi.org/10.1179/1743676110Y.0000000017>
- Østnor, T.A., Justnes, H. and Franke, W.: "A Condition Survey of Concrete Elements with Corrosion Inhibitors Exposed 12 Years for Sea Water in Tidal Zone", Proceedings of the 2nd International Congress on Durability of Concrete (2nd ICDC), 4-6 December 2014, New Delhi, India, Paper 64, 13 pp.
- Powers, R.G., Sagues, A.A., Cerlanek, W.D., Kasper, C.A., Li, L. (1999) Time to Corrosion of Reinforcing Steel in Concrete Containing Calcium Nitrite. Report No. FHWA-RD-99-145, Federal Highway Administration, Washington DC.
- RCON2 Concrete Bulk Electrical Resistivity Test Device – User Manual Version 4.0. Giatec Scientific Inc.
- Riding, K., Thomas, M., & Folliard, K. (2013). Apparent Diffusivity Model for Concrete Containing Supplementary Cementitious Materials. *ACI Materials Journal*, 110(6), 705–713. <https://doi.org/10.14359/51686338>
- Stanish, K., & Thomas, M. (2003). The use of bulk diffusion tests to establish time-dependent concrete chloride diffusion coefficients. *Cement and Concrete Research*, 33(1), 55–62. [https://doi.org/10.1016/S0008-8846\(02\)00925-0](https://doi.org/10.1016/S0008-8846(02)00925-0)
- Stefanoni, M., Angst, U., & Elsener, B. (2019). Influence of Calcium Nitrate and Sodium Hydroxide on Carbonation-Induced Steel Corrosion in Concrete. *Corrosion*, 75(7), 737–744. <https://doi.org/10.5006/3085>
- Virmani, Y.P. and Clemena, G.G. (1998) Corrosion Protection-Concrete Bridges. Report No. FHWA-RD-98-088, Federal Highway Administration, Washington DC.

Chapter 4. Effect of Permeability Reducing Admixtures on Concrete Durability

4.1. Introduction

Transport properties are a key property when considering concrete durability. The ingress of external moisture, chlorides, and sulfates can lead to serious concrete deterioration. Given the need for concrete to resist the ingress of external agents, a range of products has been developed and marketed to address this growing need.

These products claim to act through a variety of unique mechanisms such as being integral water repellants, pore solution viscosity modifiers, or mix water conditioners. Some products will go as far as to liberally claim the misused term *waterproofing* to describe the admixture effect. However, the term *waterproof* is not applicable to concrete, and at best, the products should only claim to lower the permeability of a given mixture to decrease the ingress of harmful external agents. As mentioned in Chapter 3 when referring to corrosion inhibitors, it is unfeasible to entirely prevent damage due to durability mechanisms. Rather, the focus should be on employing preventative applications that will allow a structure to properly perform during its intended service life. Thus, permeability-reducing admixtures could assist in delaying and/or decreasing the rate of deterioration due to ingress of harmful external agents.

4.2. Background

Background information regarding the several admixture products used, the modified testing procedures employed, and the exposure site details are included in this section.

4.2.1. Admixture Products

4.2.1.1. Integral Water Repellants

Integral water repellants (IWR) are intended to reduce permeability through imparting hydrophobic properties within the concrete or through physical pore blocking. These effects may reduce the ingress of external chlorides and sulfates and delay damage. Similarly, a reduction in concrete humidity could prevent ASR and DEF from occurring.

Hydrophobic liquid admixtures contain molecules that chemically bind with hydration products, leaving the hydrophobic portion of the molecule on pore surfaces. This process effectively creates a hydrophobic lining that electrostatically resists the ingress of external agents. The result is a mixture with decreased absorption.

Pore-blocking admixtures create physical products within concrete pores that act as ‘barriers’ and result in decreased permeability. The admixture is reported to create insoluble crystalline products within the pore structure that inhibit the ingress of external agents. Moreover, pore-blocking crystalline products are also described to form within cracks, further preventing the potential for deterioration.

4.2.1.2. Pore Solution Viscosity Modifiers

Pore solution viscosity modifying admixtures (VMAs) function by increasing the pore solution viscosity. This increased viscosity reduces ionic diffusion rates, resulting in a decreased ingress of external agents (Bentz et al., 2009). The approach is also known by the acronym VERDiCT: viscosity enhancers reducing diffusion in concrete technology.

4.2.1.3. Topical Sealer

According to manufacturer literature, the product uses dual crystalline technology that keeps treated concrete reasonably dry, thus reducing the ingress of external agents. Its features include a distinctive water repellent and crystallization process of hygroscopic and hydrophilic technology, providing a triple action moisture blocker system. As Figure 4.1 shows, upon application of the product, water would visibly bead on the sample surface. This effect, however, diminished with repeated cycles of wetting and drying.



Figure 4.1 Water beading on sample with topical sealer product IWR-C (bottom) when compared to sample without sealer (top)

4.2.1.4. Mixture Water Conditioners

According to manufacturer literature, the product allows mixture water to initiate hydration without a loss in cement potency, which produces smaller and more uniform pores, lower voids content, improves workability, and reduces bleed water and permeability. Moreover, the benefits of the mixture water conditioner (MWC) are compared to the extraordinary filler effects of silica fume (SF), which result in denser, stronger, more impermeable concrete with higher integrity and lower susceptibility to durability issues.

4.2.1.5. Gypsum Addition

Although this approach does not constitute a traditional chemical admixture, the use of gypsum as an additive was included in this testing program as a means of improving the sulfate resistance of concrete containing Class C fly ash. Generally speaking, the use of Class C fly ash is not recommended in sulfate-prone environments due to its increased potential for expansion and deterioration. However, studies by Dhole (2008) indicated the possibility of allowing its use when combining small additions of gypsum to the cementitious materials. The addition of gypsum (“super-sulfating”) would provide enough sulfates to counteract the reactive glassy phases provided by the Class C fly ash addition.

This would effectively provide enough sulfates to promote the early formation of ettringite as a stable product and prevent its subsequent and expansive formation at later stages.

Chapter 6 provides the initial testing that explored this approach of optimizing Class C fly ash sulfate resistance through the use of gypsum additions. In Chapter 6, the focus was on short-term expansion, calorimetry, and XRD tests to analyze the effect of gypsum addition on volumetric stability, hydration kinetics, and the formation of early-age hydration products. Based on the work on pastes and mortars, a 6% gypsum addition in mixtures containing 35% Class C fly ash replacement was found to provide an optimal amount of sulfates to minimize the potential for sulfate attack. Thus, the 6% gypsum addition was considered as an admixture and was employed in this study to cast lab and field concrete samples. Because it has been found that the efficacy of gypsum in improving sulfate resistance is specific to the Class C fly ash used, it was decided to use the same Class C fly ash.

4.2.2. Testing Procedures

4.2.2.1. Wetting and Drying Cycles

Based on previous work at the UT Concrete Lab from Lute (2008) on silane coatings, it was found that cycles of wetting and drying were required for silanes to effectively reduce internal humidity in concrete. The cycling process effectively allows for the admixture to precipitate and redissolve (Bentz et al., 2009). This led to a *Modified* version of tests being employed with supplementary wetting and drying cycles. A similar approach was followed in this study as it was believed that IWRs required a drying period to properly function.

Thus, *Modified* versions of ASR and sulfate testing were implemented. Whereas the standard procedure would call for these samples to be in a wet, 100% humidity environment at all times (standing above water for ASR or immersed in solution for sulfate), the *Modified* tests cycled between 28 days in a ‘wet’ environment and 7 days in a ‘dry’ environment, which meant a 50% RH environmental chamber kept at 23 °C (73 °F). This meant that the samples experienced repeated cycles of contraction and expansion due to moisture loss and gain, which is observed in the numerous dips and peaks in expansion plots. Through this supplementary conditioning, *Modified* samples were in their respective exposure environment 80% of the time when compared to samples undergoing the standard test procedure.

4.2.3. Exposure Sites

The UT Concrete Lab features several outdoor exposure sites where field samples undergo realistic exposure conditions and cycle through the seasons. Thus, exposure sites provide

a more accurate scenario than the typical accelerated lab setup. Samples related to this portion of the study were placed at LIME’s Central Texas Exposure Site located at the UT Concrete Lab research facility in Austin (Figures 4.2 and 4.3), the Texas Marine Exposure Site located in Port Aransas (as detailed in Section 3.4.3), and at the West Texas Exposure Site located in Van Horn, TX (Figures 4.4–4.6). Field samples at the Central Texas and West Texas sites included concrete prisms and were intended to study different forms of external sulfate attack. The following sections outline details regarding these sulfate exposure sites. Field samples at the Texas Marine Exposure Site included large exposure blocks intended to study chloride-induced corrosion. Details regarding the site, samples, and pertinent testing are included in Chapter 3.

4.2.3.1. Central Texas Exposure Site

Concrete prism field samples from this study were placed in two outdoor sulfate troughs at the UT Concrete Lab. The troughs contain soil doped with either sodium sulfate or calcium sulfate at a 5% concentration. Damage due to sodium sulfate can manifest itself in the form of a chemical or physical attack. Thus, the sodium sulfate trough included submerged and standing prisms to trigger chemical or physical forms of sulfate attack, respectively. Calcium sulfate does not trigger a physical form of attack and hence no standing prisms were included in its respective exposure environment. It should be noted that calcium sulfate has limited solubility in water (less than 1500 ppm), so most of the sulfates placed in the trough remain undissolved as part of the solid (soil) fraction.



Figure 4.2 Central Texas Exposure Site in Austin



Figure 4.3 Outdoors trough at Central Texas Exposure Site. Contains submerged and standing prisms exposed to soil doped with sodium sulfate.

4.2.3.2. Van Horn Exposure Sites

Two locations near Van Horn were selected as natural soil environments containing calcium sulfate (gypsum), which is the predominant sulfate soil in Texas. Site 1 is in a drier location than Site 2. Samples at Site 1 are adjacent to the highway and are easily accessible (Figure 4.4). Conversely, samples at Site 2 are located inside a lobster cage within a creek beneath a bridge (Figures 4.5 and 4.6). These samples must be lifted to the road level for retrieval, typically via bucket and rope. All samples are rinsed and allowed to reach a uniform temperature before length and mass measurements are taken (Figure 4.7).



Figure 4.4 Site 1 in Van Horn (sodium sulfate environment)



Figure 4.5 Site 2 in Van Horn (calcium sulfate environment)—samples are placed in creek (right) below bridge (left)



Figure 4.6 Site 2 samples are stored inside a lobster cage below bridge (left) and samples are lifted to road level via bucket (right)



Figure 4.7 Samples being rinsed (left) and measured (right)

4.3. Experimental Investigation

The testing series was designed to evaluate the effect of various admixture products on concrete permeability and durability properties. The products were added to both OPC and SCM mixtures to compare effectiveness. Several types of lab samples were cast to assess product performance across compressive strength, permeability, calorimetry, ASR, and sulfate testing. Field specimens were cast and placed in environments prone to developing deterioration due to ASR, corrosion, and external sulfate attack.

4.3.1. Materials

4.3.1.1. Portland Cement and Fly Ash

ASTM C150 Type I cement and a Class C fly ash from Texas were used in the testing series. Chemical composition of the cementitious materials was analyzed by XRF; Table 4.1 summarizes the results. Based on its chemical composition, Bogue equations estimate the cement to have a C_3A content of 11.1% and its Na_2O_{eq} content is 0.77%. Specific gravities used for mixture proportions were 3.15 for cement and 2.70 for fly ash.

Table 4.1 Chemical composition of cementitious materials (% by mass)

Material	SiO ₂	Al ₂ O ₃	Fe ₂ O ₃	CaO	SO ₃	MgO	K ₂ O	Na ₂ O	LOI
ASTM Type I	20.48	5.39	1.90	65.06	3.40	1.17	0.96	0.14	2.57
Class C Fly Ash	35.4	17.7	5.2	26.6	1.5	6.2	0.4	1.5	N/A

4.3.1.2. Aggregates

Two fine aggregates were used throughout testing. A fine aggregate known to be reactive was used for ASR testing, while a non-reactive, manufactured limestone fine aggregate was used in all other mixtures. Non-reactive, limestone coarse aggregate was used in all samples. Table 4.2 summarizes aggregate properties.

Table 4.2 Aggregate properties

Aggregate Type	Absorption Capacity	Specific Gravity (Saturated Surface Dry)
Fine - Reactive	0.70%	2.62
Fine - Non-Reactive	1.49%	2.54
Coarse	2.53%	2.49

4.3.1.3. Admixtures

Given the higher water demand of the limestone fine aggregate, a polycarboxylate-based HRWR admixture was used to achieve proper workability on mixtures containing this type of aggregate. The HRWR had an SG of 1.08 and was used at a dosage of 3 fl. oz per 100 lbs. of cementitious (fl. oz./cwt).

A summary of the several admixture products used is included in Table 4.3. Each admixture will be referred to by its Product ID and will be identifiable by color in data plots.

Table 4.3 Admixture product details

Product Type	Product ID and Color	Description and Recommended Dosage	Notes
IWR	IWR-A	Liquid admixture. Stable dispersion of stearate and other water-repellant compounds. 3–6 fl. oz./cwt.	Used at 4.5 fl. oz./cwt
	IWR-B	Powder admixture. Products create reactions that generate non-soluble crystalline formations throughout pores and capillary tracts. 2–3% by mass of cement.	Used at a 2% dose by mass of cementitious. Cementitious content was not reduced by this addition and water content was not adjusted.
	IWR-C	Topical sealer with water repellent and crystallization properties. Coat at a rate of 150–175 ft ² /gal.	To maximize product penetration, lab specimens were allowed to dry for 7 days before being fully submerged in an excess of the admixture. Field specimens were similarly allowed to dry and then a coating was applied at the recommended dosage rate. For these specimens, excess admixture on the surface tended to cause dripping.
	IWR-D	Powder admixture. Hydrophilic crystalline waterproofing admixture that reacts with unhydrated cement to form needle-like crystals that act as pore-blockers. 2% by mass of cement.	Used at a 2% dose by mass of cementitious. Cementitious content was not reduced by this addition and water content was not adjusted.
	IWR-E	Liquid waterproofing admixture that reduces absorption and forms a protective coating around steel reinforcement. 1.0 gal/ yd ³ .	Used at a rate of 1.0 gal/ yd ³ . Water content was not adjusted based on this addition.
	IWR-F	Liquid admixture targeted at mitigating ASR. The technology behind the product effectively manipulates the molecular kinetics of cementitious hydration to increase the durability to ASR. 5–20 fl. oz./cwt.	Used at 10.0 fl. oz./cwt
VMA	VMA	Liquid admixture. Commercially available shrinkage reducing admixture (SRA). Based on previous studies (Bentz et al., 2009; Snyder et al., 2012), SRAs, when used in high dosages, have potential to act as a pore solution viscosity modifier.	Based on previous studies, the SRA was used to replace 10% of the batch water by mass to act as a VMA. This dosage is much higher than typical ranges used to mitigate shrinkage.
MWC	MWC	Liquid admixture that strengthens, densifies, and decreases permeability. 10 fl. oz./cwt.	Used at 10.0 fl. oz./cwt
Gypsum	GYP	Powder admixture. Commercially available source of calcium sulfate dehydrate. Based on studies from Wheelless (2018), a dosage of 6% gypsum was found to be optimal in mitigating sulfate attack in mixtures with 35% of the specific Class C fly ash used.	Used at a 6% dose by mass of cementitious. Cementitious content was not reduced by this addition and water content was not adjusted.

4.3.2. Mixture Proportions

Two main concrete mixture designs were employed throughout this study, one for ASR procedures and another for all other testing. The ASR mixture contained a reactive fine aggregate and followed the proportions specified by ASTM C1293 (0.42 w/c). The other, non-ASR mixture included 362 kg/m³ (611 lb./yd³) of cement, 163 kg/m³ (275 lb./yd³) of water (w/c = 0.45), 986 kg/m³ (1,662 lb./yd³) of limestone coarse aggregate, and 767 kg/m³ (1293 lb./yd³) of manufactured limestone fine aggregate. Aggregate proportions are based on an oven-dry condition. Select non-ASR mixtures contained Class C fly ash at a 35% replacement level by mass of total cementitious. These mixtures will be referred to as the FA series.

4.3.3. Test Matrix and Testing Procedures

Several mixtures with various products were cast as described in Table 4.4. Testing procedures employed on each mixture are detailed in Table 4.5. OPC mixtures were cast at 0.45 and 0.70 w/c ratios to determine if admixture effect varies by w/c.

Table 4.4 Test matrix

Series	Mechanism	Mixture ID	Product Used
OPC	ASR	VMA-A0	Control
		VMA-A1	VMA
		MISC-A1	IWR-F
		MISC-A2	MWC
		IWR-A1	IWR-A
		IWR-A2	IWR-B
		IWR-A3	IWR-C
		IWR-A4	IWR-D
		IWR-A5	IWR-E
		Sulfate Attack	VMA-S0
	VMA-S1		VMA
	IWR-S1		IWR-A
	Permeability	45-0	Control
		45-2	IWR-B
		45-3	IWR-D
		45-4	IWR-C
		45-5	IWR-E
		70-0	Control
		70-2	IWR-B
		70-3	IWR-D
70-4	IWR-C		

Series	Mechanism	Mixture ID	Product Used
		70-5	IWR-E
FA	Sulfate Attack and Permeability	FA-0	Control
		FA-1	GYP
		FA-2	IWR-B
		FA-3	IWR-C
		FA-4	IWR-D
		FA-5	IWR-E

Table 4.5 Test Procedures Matrix

Series	Mixture ID	Product	Permeability				Sodium Sulfate						Calcium Sulfate			ASR		Corrosion
			Resistivity	Absorption	Chloride Diffusion Coefficient	NCHRP 244 Series II	Standard Solution	Modified Solution	Trough - Submerged	Trough - Standing	West Texas - Submerged	West Texas - Standing	Standard Solution	Trough - Submerged	West Texas - Submerged	Standard 1293	Modified 1293	Exposure Blocks
OPC	VMA-A0	Control													X	X		
	VMA-A1	VMA													X			
	MISC-A1	IWR-F													X		X	
	MISC-A2	MWC													X		X	
	IWR-A1	IWR-A													X	X		
	IWR-A2	IWR-B													X	X	X	
	IWR-A3	IWR-C													X	X	X	
	IWR-A4	IWR-D													X	X	X	
	IWR-A5	IWR-E													X	X	X	
	VMA-S0	Control					X	X	X	X								
	VMA-S1	VMA					X		X	X								
	IWR-S1	IWR-A					X	X	X	X								
	45-0	Control	X	X	X	X												
	45-2	IWR-B	X	X	X	X												
	45-3	IWR-D	X	X	X	X												
	45-4	IWR-C	X	X	X	X												
	45-5	IWR-E	X	X	X	X												
	70-0	Control	X	X		X												
	70-2	IWR-B	X	X		X												
	70-3	IWR-D	X	X		X												
70-4	IWR-C	X	X		X													
70-5	IWR-E	X	X		X													
FA	FA-0	Control	X	X	X		X	X	X	X	X	X	X	X				X
	FA-1	GYP	X	X			X	X	X	X	X	X	X	X				X
	FA-2	IWR-B	X	X			X	X	X	X	X	X	X	X				X
	FA-3	IWR-C	X	X			X	X	X	X	X	X	X	X				X
	FA-4	IWR-D	X	X			X	X	X	X								X
	FA-5	IWR-E	X	X			X	X	X	X								X

4.4. Experimental Results and Discussion

4.4.1. Isothermal Calorimetry

The use of calorimetry at the preliminary testing stages has proved to be an efficient and valuable method of assessing admixture compatibility and early-age properties. Figures 4.8 and 4.9 include a summary of the effect of select admixtures on isothermal calorimetry of cement pastes.

The admixtures used appear to develop similar heat patterns. However, the magnitude of their peaks is smaller when compared to the control, leading to significantly lower cumulative heat at early ages (48 hours). This could indicate a decrease in the development of hydration products, which could result in lower strengths at early ages. Nonetheless, since early-age strength was not a property of interest, the analysis focused on ensuring that proper peaks were being achieved at reasonable times.

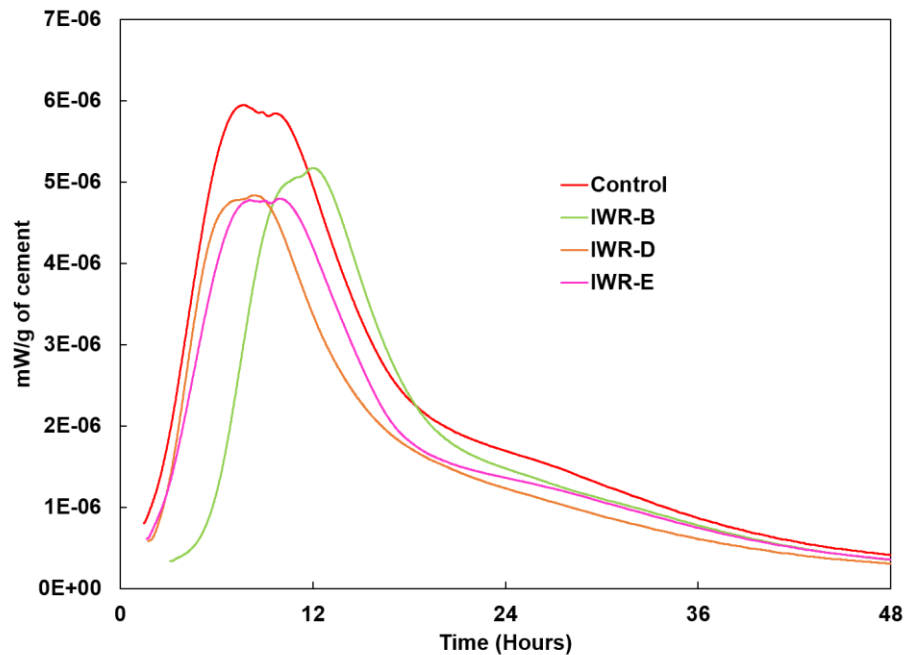


Figure 4.8 Rate of heat evolution from isothermal calorimetry on pastes with various admixtures

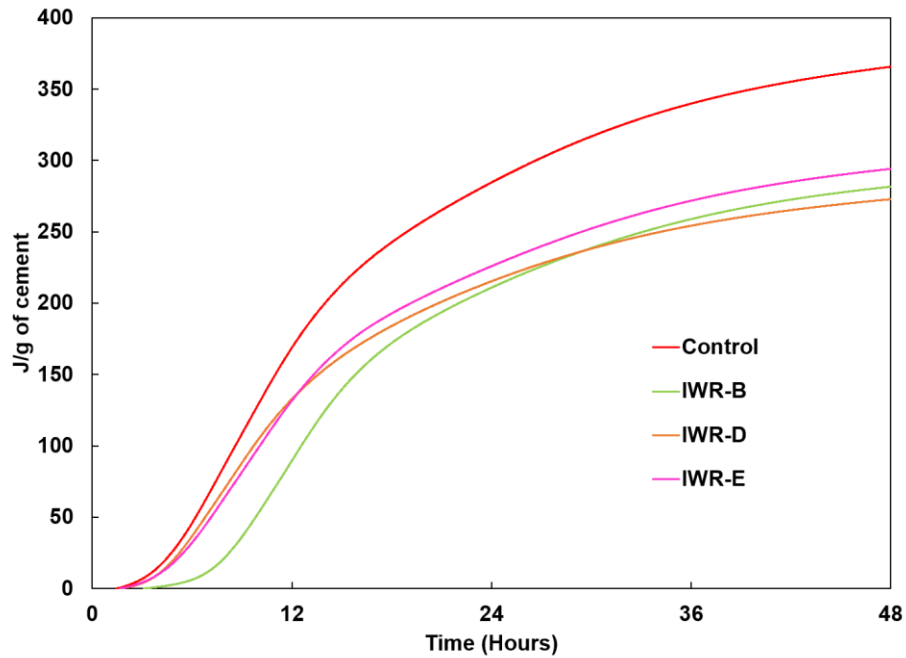


Figure 4.9 Cumulative heat from isothermal calorimetry on pastes with various admixtures

4.4.2. Compressive Strength

Compressive strengths for relevant concrete mixtures are presented in Figures 4.10 and 4.11. Notably, the admixtures were able to increase strengths by approximately 6.9 MPa (1,000 psi) at 28 days for the 0.45 w/c OPC mixtures (Figure 4.10). This increase, however, was not observed in the 0.70 w/c OPC mixture or in the 0.45 FA mixtures. Given the slower reactivity of SCMs, the lower strength values at 28 days for SCM mixtures were expected. However, in the long term, higher strengths would be expected for the SCM mixtures.

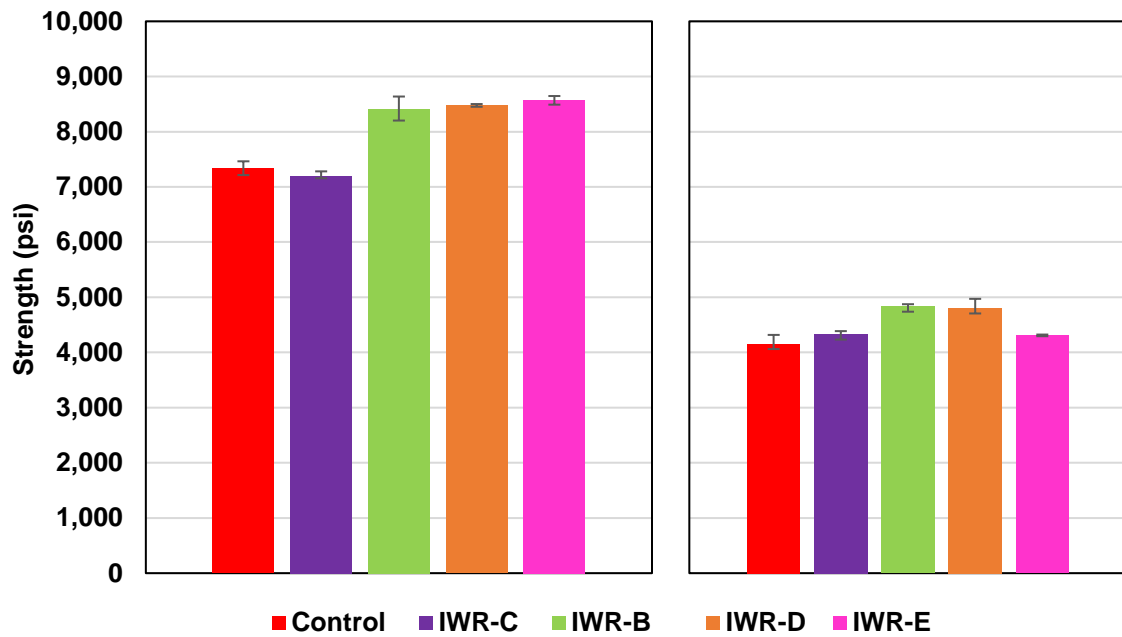


Figure 4.10 Concrete compressive strength at 28 days for OPC mixtures at 0.45 w/c (left) and 0.70 w/c (right)

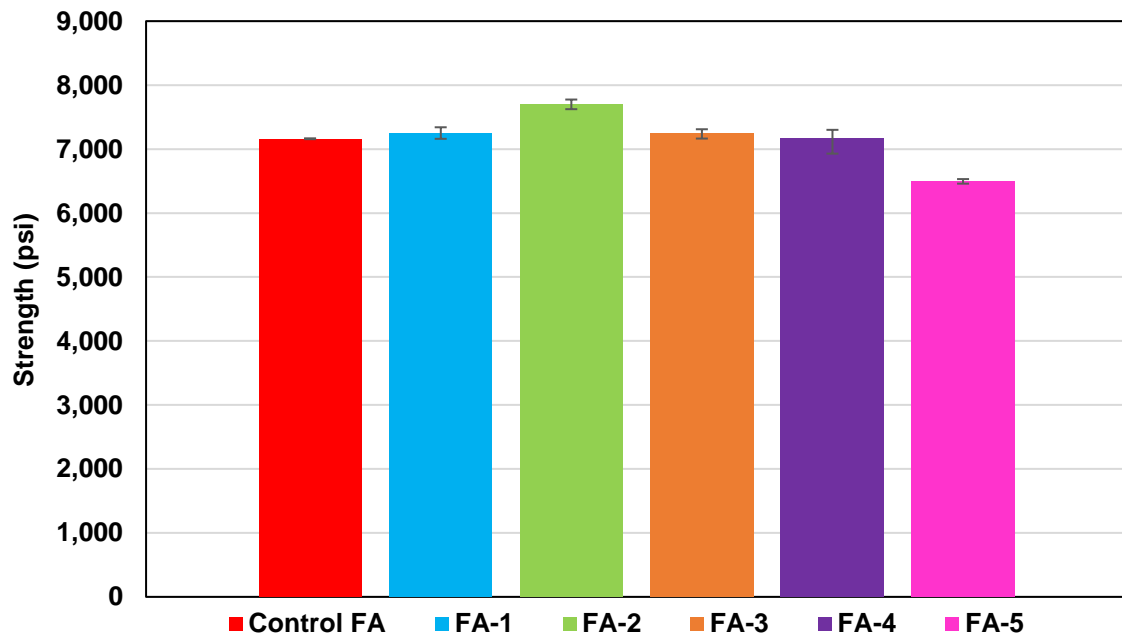


Figure 4.11 Concrete compressive strength at 28 days for FA mixtures at 0.45 w/c

4.4.3. Resistivity

Bulk electrical resistivity measures the impedance of an applied current on a concrete specimen. This value correlates well with permeability as denser, less permeable concrete tends to have higher resistivity values. For qualitative comparison, resistivity values ($\text{k}\Omega\cdot\text{cm}$) can be related to chloride penetration zones as follows:

- 0–5 $\text{k}\Omega\cdot\text{cm}$: High Chloride Penetration
- 5–10 $\text{k}\Omega\cdot\text{cm}$: Moderate Chloride Penetration
- 10–15 $\text{k}\Omega\cdot\text{cm}$: Low Chloride Penetration

Figure 4.12 includes resistivity measurements for OPC mixtures at 28 days. As expected, OPC mixtures plateau around the *Moderate* region. Subsequent measurements were performed at 90 days without significant change, and, hence, that data is not presented. FA mixtures containing SCMs develop much lower permeability (and higher resistivity) in the long term, allowing them to reach the *Low* region and beyond. Their resistivity values as a function of time are shown in Figure 4.13 and appear to reach a plateau around an age of 6 months. Given the qualitative nature of resistivity, the products do not seem to have a significant effect on the long-term results. That is, the FA control mixture was able to achieve low permeability with only the use of fly ash and without admixtures.

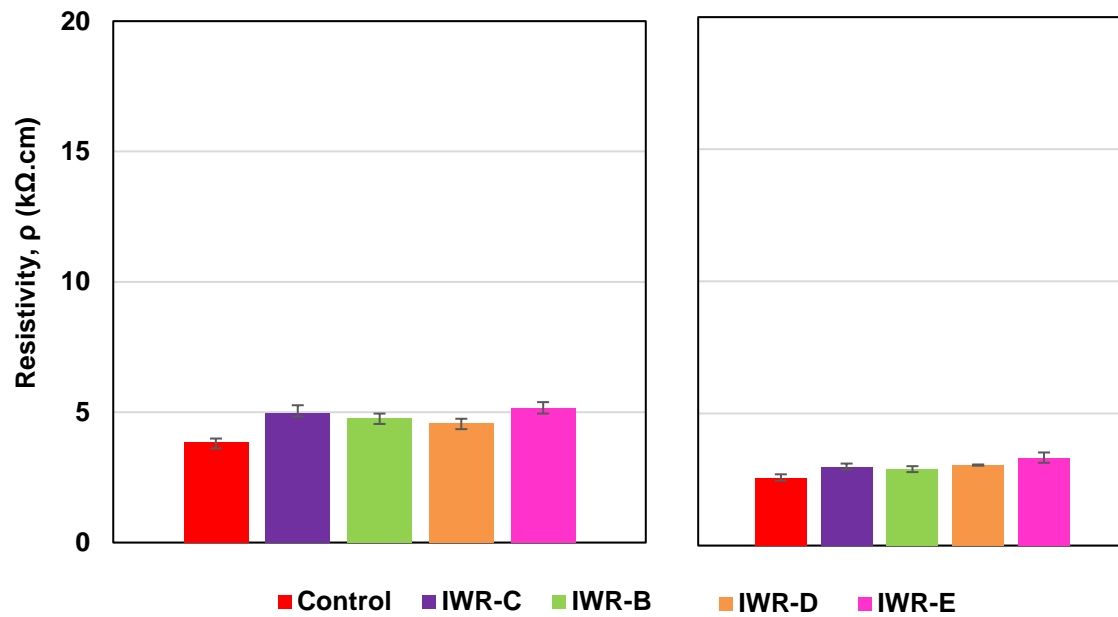


Figure 4.12 Resistivity at 28 days for OPC mixtures with various admixtures at 0.45 w/c (left) and 0.70 w/c (right)

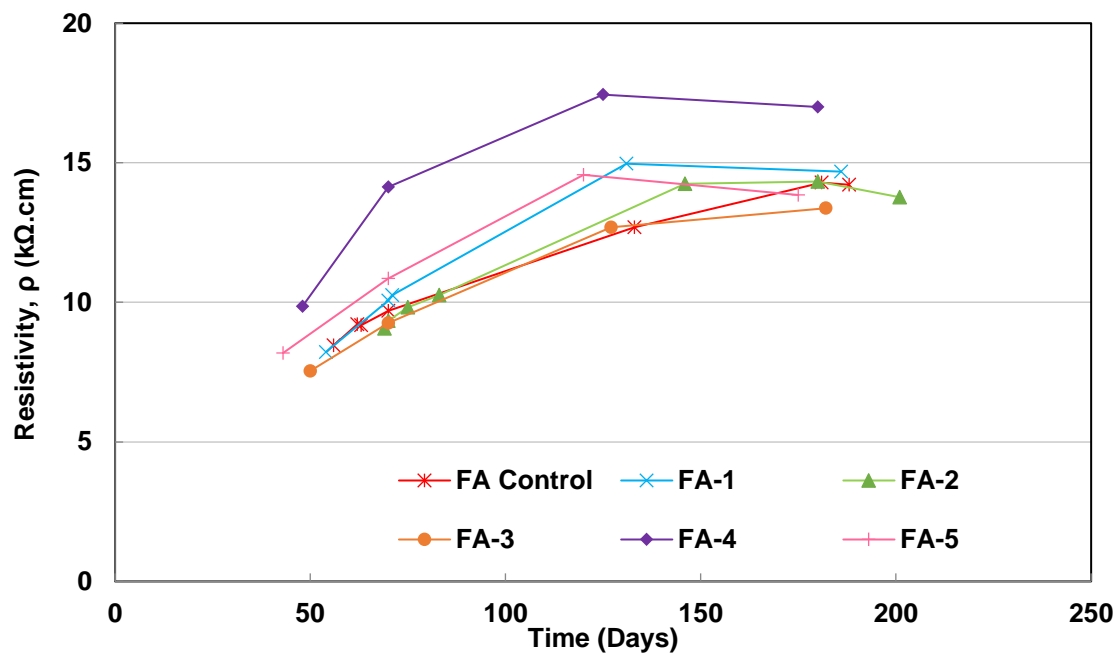


Figure 4.13 Resistivity values at various ages for FA mixtures

4.4.4. Absorption

The ASTM C1585 test is intended to determine the susceptibility of an unsaturated concrete to the penetration of water (ASTM, 2013). A higher absorption rate indicates a mixture is more susceptible to the ingress of water. Initial and secondary absorption rates obtained through this method are included in this section. Initial absorption rate quantifies the mass gain that occurs within the first 6 hours of exposure, while the secondary absorption rate relates to measurements taken at longer intervals between 6 hours and 7 days of exposure.

Absorption tests were performed on disk samples belonging to FA and OPC mixtures (Figure 4.14). Initial rates involved repeated mass measurements within short time intervals. This factor, along with general inexperience with the test procedure, led to significant error in its first test iteration with the FA mixtures (Figure 4.15). Subsequent tests with OPC mixtures had much lower error (Figures 4.16 and 4.17).

Admixture effect was inconsistent in the FA mixtures. Nonetheless, the presence of FA drastically reduced both the initial and secondary absorption rates when compared to OPC mixtures. Moreover, the FA specimens were between an age of 1–2 months at the time of testing, which could be considered an early age for mixtures containing SCMs. Based on resistivity values (Figure 4.13), the FA mixtures likely reached peak maturity around an age of 6 months. If testing had taken place at that time, absorption values would have likely been even lower.

More consistent results were achieved with the OPC mixtures, which saw more significant changes with the use of admixtures. Notably, the IWR-C hydrophobic product was able to greatly reduce initial absorption. However, its effects faded in the longer term and secondary rates were worse than the control. Products IWR-B and IWR-D showed moderate improvements in performance, while Product E was the best performer.



Figure 4.14 ASTM C1585 absorption samples

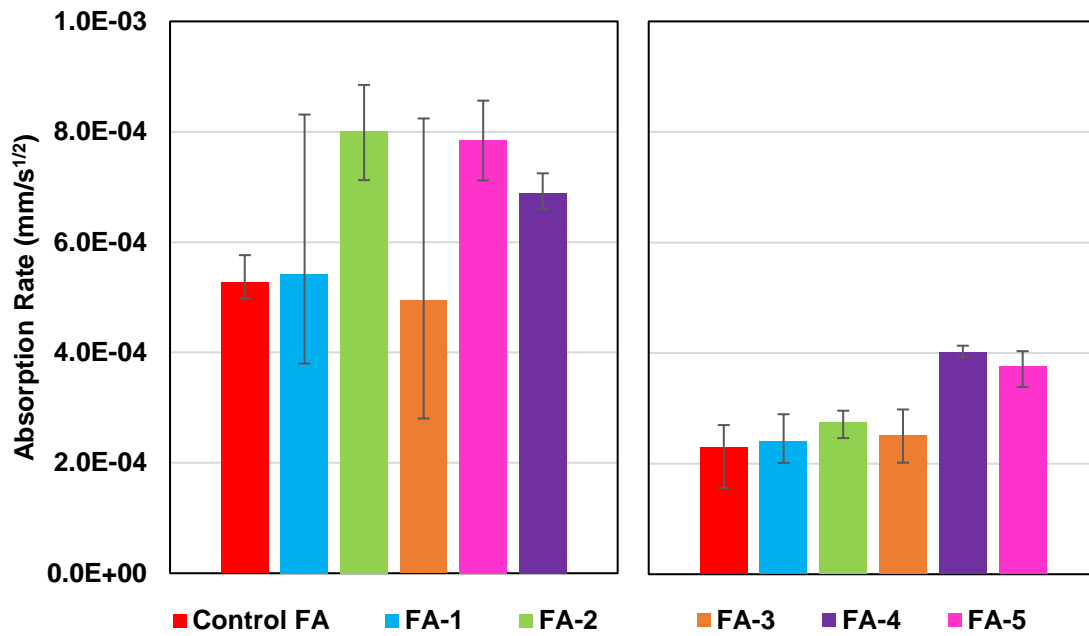


Figure 4.15 Initial (left) and secondary (right) absorption rate per ASTM C1585 for FA mixtures with 0.45 w/

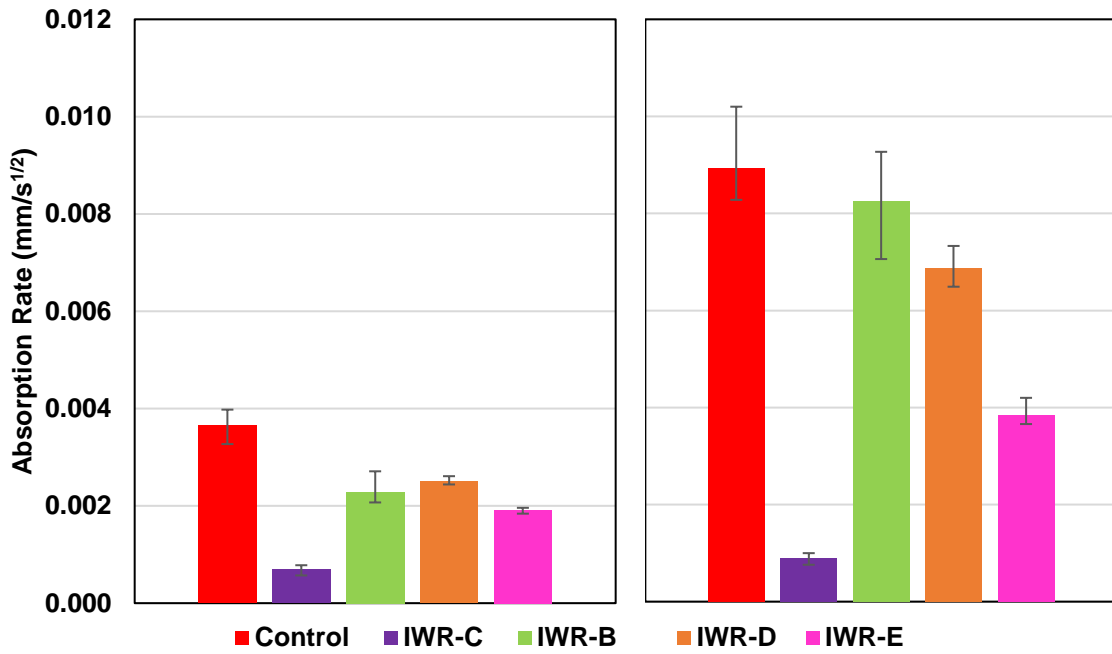


Figure 4.16 Initial absorption rate per ASTM C1585 for OPC mixtures with 0.45 w/c (left) and 0.70 w/c (right)

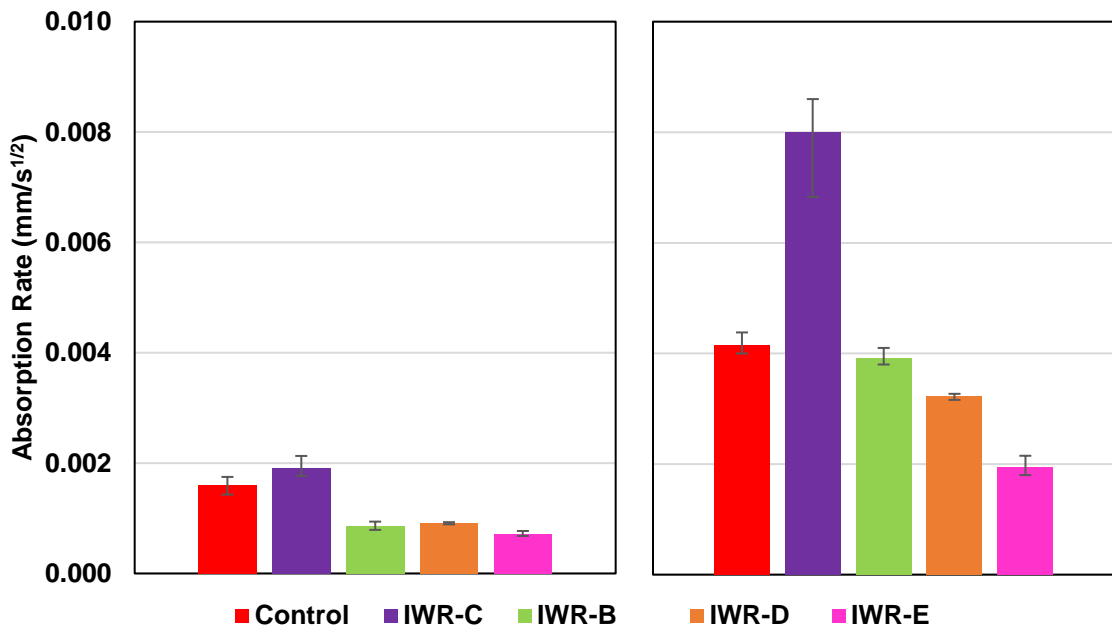


Figure 4.17 Secondary absorption rate per ASTM C1585 for OPC mixtures with 0.45 w/c (left) and 0.70 w/c (right)

4.4.5. Chloride Diffusion Coefficient

The apparent chloride diffusion coefficient is a transport parameter indicating the ease of external chloride penetration into concrete. Mixtures with reduced permeability would be expected to have low diffusion coefficients. Diffusion coefficients per ASTM C1556 for OPC and the FA control mixtures are presented in Figure 4.18.

The diffusion coefficient, D_a , is based on a mathematical model with inherent approximation error. The sum of errors squared associated with each calculated value is shown in Figure 4.19. The measured errors were deemed to be within an acceptable range. The average sum of errors squared for the samples was 2.69×10^{-3} . The MAE for samples as described in Equation 4.1 is presented in Table 4.6. The MAE provides a measure of the average difference between predicted values, y_i , and measured values, x_i . Error values were calculated for two reference cases: the $k = n-1$ case omits the error derived from the first data point obtained while the $k = n$ case includes it. The ASTM C1556 standard uses the $k = n-1$ case and specifically omits the first data point since it inherently increases error based on the mathematical model but does not necessarily reflect actual conditions.

The OPC mixtures had an approximate age of 100 days at the time of the exposure to chlorides. The Control FA mixture was included in this series as a reference; however, this mixture was cast at an earlier date and was an age of 200 days at the time of exposure. All specimens in this testing series remained in the exposure salt solution for a total of 59 days. Given their respective timelines, all mixtures were expected to have relatively peaked in maturity by the time testing occurred. Thus, the Control FA mixture was able to greatly outperform the OPC mixtures. Admixtures had a beneficial effect in reducing diffusion coefficients, and Product IWR-E was once again the best performer.

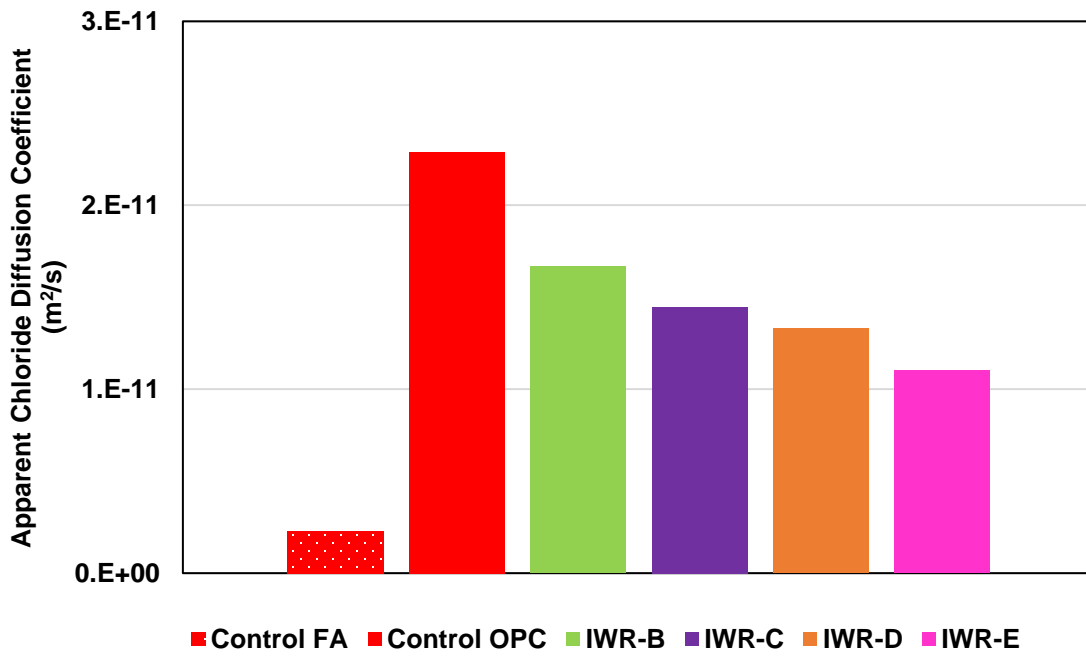


Figure 4.18 Apparent chloride diffusion coefficient for various mixtures

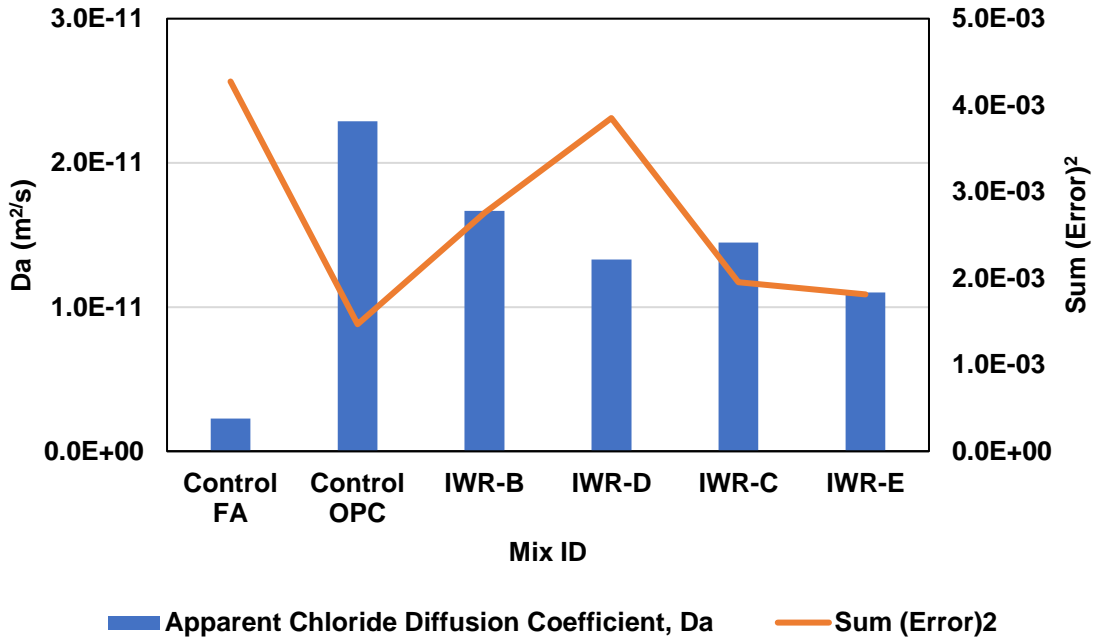


Figure 4.19 Sum of squared errors for diffusion coefficient calculations per ASTM C1556

Table 4.6 Mean absolute error (MAE) from chloride analysis

Mixture	Data Points			
	k = n-1		k = n	
	k	MAE (%)	k	MAE (%)
Control FA	5	0.02	6	0.03
Control OPC	5	0.01	6	0.02
IWR-B	5	0.02	6	0.04
IWR-C	5	0.02	6	0.06
IWR-D	7	0.02	8	0.04
IWR-E	7	0.01	8	0.04

$$MAE = \frac{\sum_{i=1}^k |y_i - x_i|}{k} \quad \text{Eq. 4.1}$$

4.4.6. NCHRP 244 Series II

The NCHRP 244 Series II procedure is intended to rank the performance of concrete sealer products in terms of their ‘waterproofing’ ability (Pfeifer and Scali, 1981). As previously mentioned, the term ‘waterproof’ is a misnomer in the concrete world. In practical terms, the procedure quantifies mass changes as a mixture undergoes cycles of wetting (salt solution) and drying (50% RH). Thus, the test can be used as another method to quantify permeability. The test is particularly applicable since it includes cycles of wetting and drying, which is an influential factor in the performance of the products used. Moreover, the procedure has been extensively used by previous researchers at the UT Concrete Lab to investigate the effect of coatings and sealers on ASR and DEF mechanisms (Lute, 2008; Wehrle, 2010). Based on this work, a recommended practice was devised indicating that products able to reduce mass gain by 85% (compared to the untreated control) per the NCHRP 244 Series II procedure could be effective in mitigating ASR and DEF.

A summary of the test results for OPC mixtures at 0.45 and 0.70 w/c is included in Figure 4.21. Figures 4.22 and 4.23 include the plotted mass change throughout the two drying and wetting cycles across 100 days. The summary data shown in Figure 4.21 pertains to the mass gain incurred during the first wetting cycle (days 35–56). As can be observed, the products had a moderate effect on decreasing mass gain. However, the effects were considerably lower than those recommended for ASR and DEF mitigation. In fact, in order to meet the 85% reduction recommendation, the 0.45 and 0.70 w/c mixtures would need to

achieve mass gains lower than 0.26% and 0.54%, respectively, far lower than any of the admixture effects could provide.



Figure 4.20 Concrete cube samples for NCHRP 244 Series II testing in drying condition

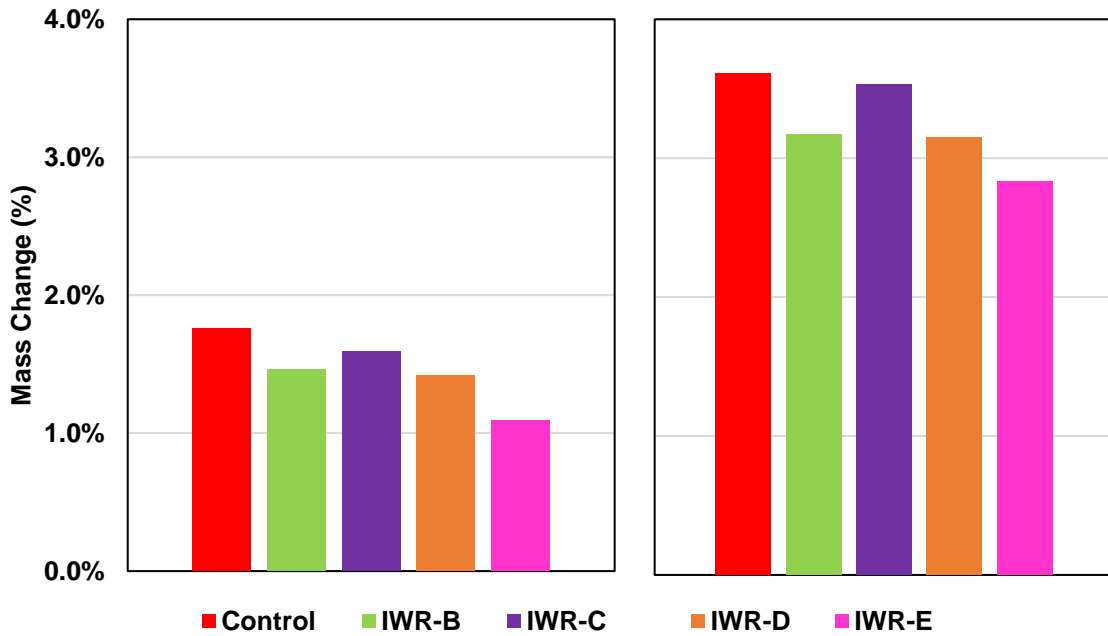


Figure 4.21 Mass gain summary per NCHRP 244 Series II for OPC mixtures with 0.45 w/c (left) and 0.70 w/c (right)

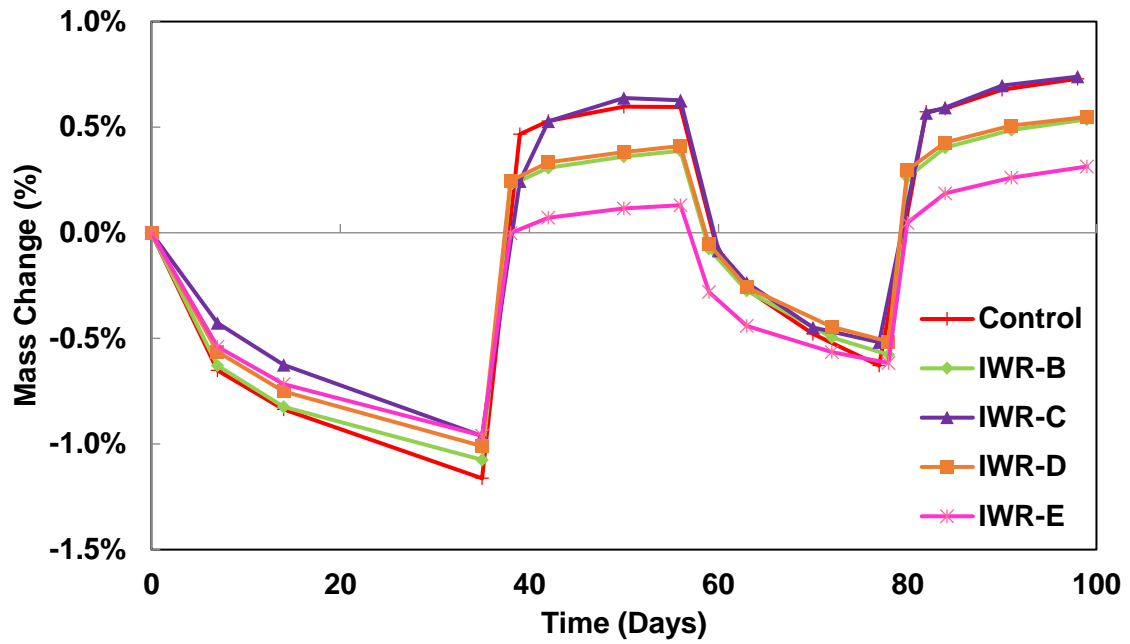


Figure 4.22 Mass change with time based on NCHRP 244 Series II conditioning for OPC mixtures with 0.45 w/c

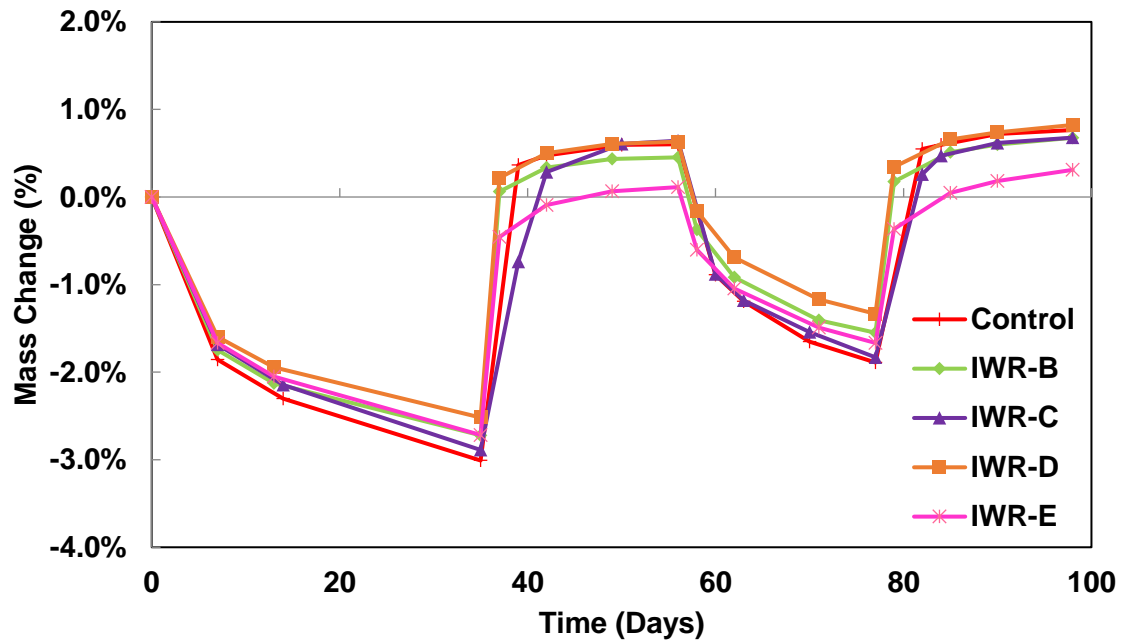


Figure 4.23 Mass change with time based on NCHRP 244 Series II conditioning for OPC mixtures with 0.70 w/c

4.4.7. Sodium Sulfate

Concrete prisms were subjected to sodium sulfate environments through six different exposure conditions. Two of the conditions were for lab samples, while the remaining four were for field samples. Table 4.7 outlines the different exposure conditions and the types of deterioration intended for each condition. All samples were placed in their respective exposure environment after a minimum 28 days of curing.

Table 4.7 Exposure conditions for sodium sulfate samples

Sample Type	Condition	Deterioration Type
Lab	Standard Sodium Solution	Chemical Sulfate Attack
	Modified Sodium Solution	Chemical Sulfate Attack
Field	Outdoors Trough – Submerged	Chemical Sulfate Attack
	Outdoors Trough – Standing	Chemical and Physical Sulfate Attack
	West Texas - Site 1 – Submerged	Chemical Sulfate Attack
	West Texas - Site 1 – Standing	Chemical and Physical Sulfate Attack

4.4.7.1. Sodium Sulfate Solution

A 5% sodium sulfate solution was used throughout this program, which is consistent with the testing outlined in ASTM C1012 for evaluating the sulfate resistance of mortar. Expansion measurements were performed periodically, and each time fresh solution was replenished.

The samples steadily expanded and deteriorated. Loss of cohesion was becoming severe on most samples after an exposure age of 500 days. OPC mixtures were cast at an earlier age; thus, later measurements are available for them. As observed in Figure 4.25, the OPC Control mixture had one specimen fail and continued to expand. The loss of cohesion, as seen in Figure 4.24, was most severe at the prism ends, likely due to the increased exposed surface area. This deterioration directly affects expansion measurements, as the comparator pin required for length measurements is located at the prism end and is prone to removal with loss of cohesion.

Overall, the admixtures did not appear to effectively mitigate expansions due to sulfate attack and in some cases even worsened expansion. However, notable results include the performance of the VMA-OPC mixture when compared to its control and the sturdiness of the gypsum mixture (FA1), which appears to be in a near-intact shape (Figure 4.24). It should also be noted that the Control FA mixture did not appear to expand as much as its OPC counterpart. As previously mentioned, the use of Class C fly ash was theorized to

worsen sulfate attack. As of the time of this report, it remains to be seen which mixture will ultimately develop more damage.



Figure 4.24 Sodium sulfate solution samples exhibiting minimal (left) and significant (right) loss of cohesion

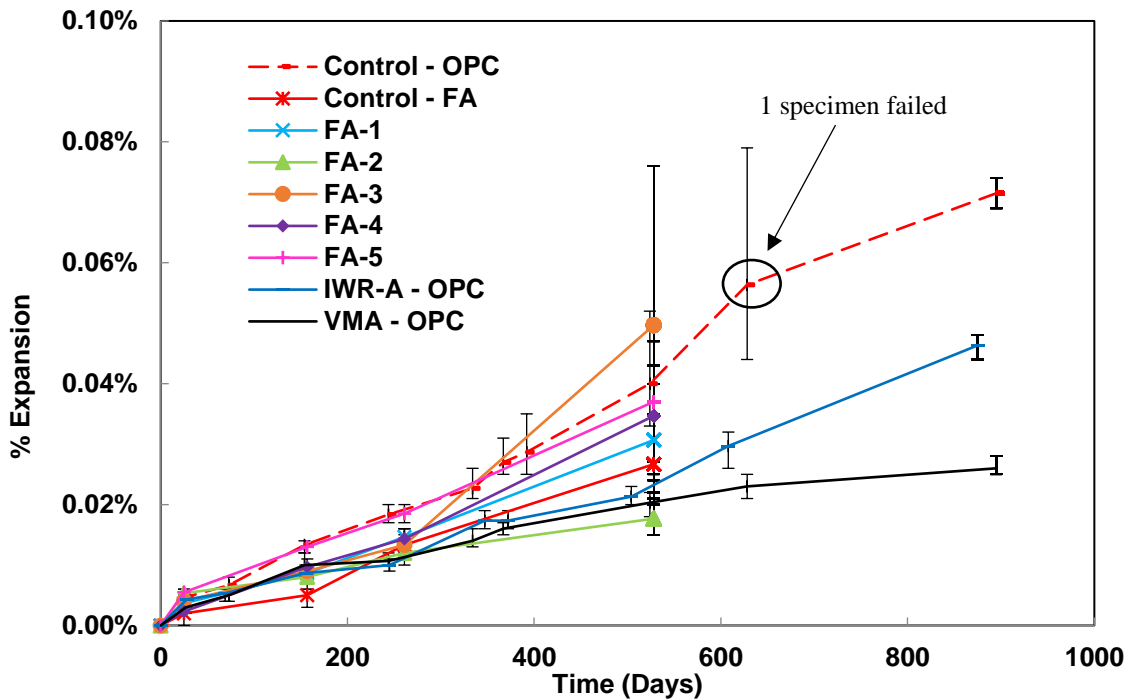


Figure 4.25 Concrete prism expansion over time for mixtures exposed to standard sodium sulfate solution testing

4.4.7.2. Modified Sodium Sulfate Solution

The modified version of the test was intended to allow for the admixtures to properly develop their beneficial effects through repeated cycles of wetting and drying. Expansion measurements were made each time the samples went into either a wetting or drying condition, and at each new wetting cycle the sulfate solution was replenished. Periods of drying induced a loss of moisture and consequent shrinkage, while periods of wetting induced a water-intake expansion unrelated to sulfate attack. The most recent measurements, however, indicated a sharp increase in expansion for all samples (Figure 4.26).

Interestingly, the expansion of the modified samples significantly exceeded that of the standard samples even though they were technically exposed to the sulfate solution for a lesser time given the duration of cycles. Nonetheless, the modified samples were measured more often than the standard samples and thus their sulfate solution was replenished at a higher rate. This factor could have created a more aggressive environment in which the ponding solution could continue to provide harmful sulfates without reaching an equilibrium. Moreover, the drying period could exacerbate the absorption of solution upon the beginning of each new wetting cycle, accelerating deterioration. However, despite their increased expansion, it should be noted that none of the modified mixtures failed due to

lost pins. This could indicate that while expansion is rampant, loss of cohesion is occurring to a lesser extent than in the standard samples.

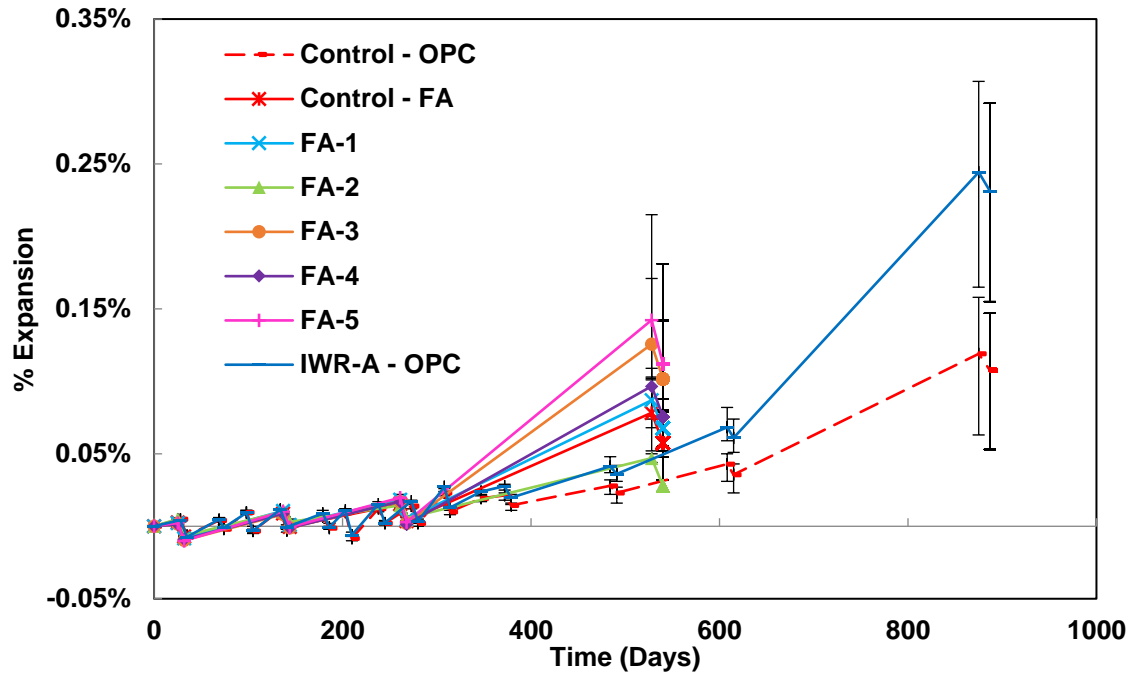


Figure 4.26 Concrete prism expansion over time for mixtures exposed to cyclical sodium sulfate solution testing

4.4.7.3. Sodium Sulfate Trough—Submerged

The submerged field specimens in the outdoors trough were prone to extensive damage. Notably, two OPC mixtures spectacularly failed between exposure ages of 600–900 days (Figure 4.27). The VMA-OPC mixture performed well, just as in the standard solution case; however, its error significantly increased as of the latest measurement, possibly indicating the onset of serious deterioration. The FA mixtures were behaving similarly. Expansion data is shown in Figure 4.28.



Figure 4.27 Failed samples submerged in sodium sulfate trough

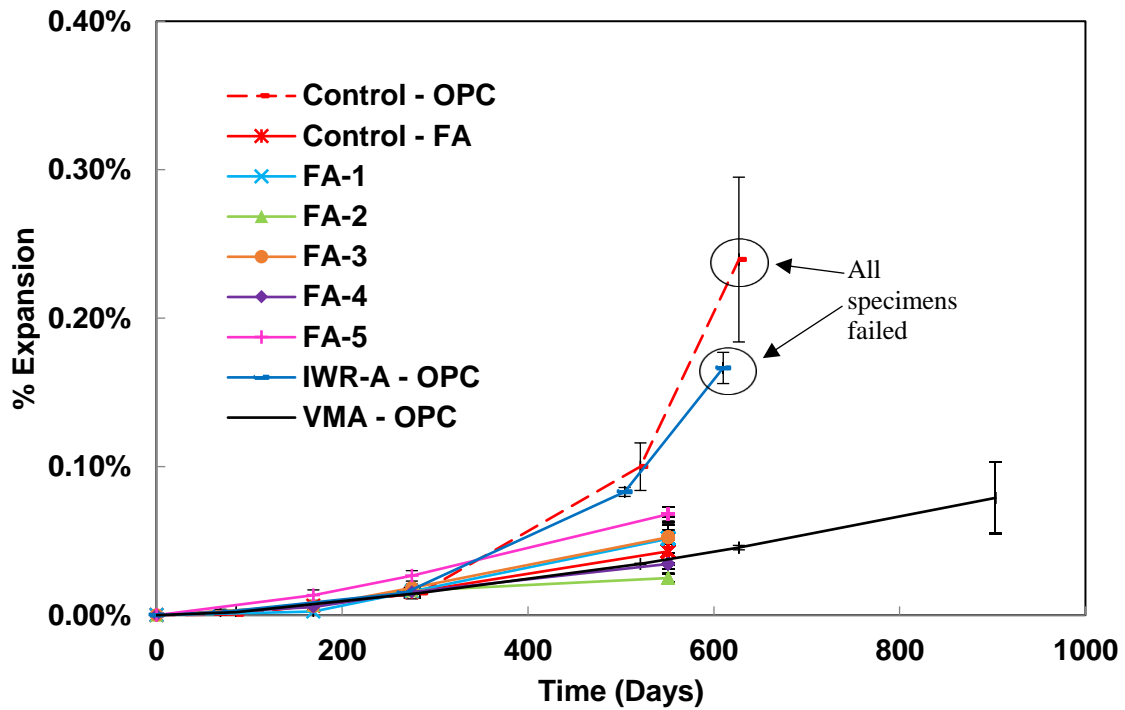


Figure 4.28 Concrete prism expansion over time for mixtures submerged in outdoors sodium sulfate trough

4.4.7.4. Sodium Sulfate Trough—Standing

The standing samples were subjected to a combination of chemical and physical sulfate attack. The portion of the specimen submerged in the sulfated soil was exposed to chemical attack as with the previously discussed samples. However, the interface between the submerged and exposed portions of the specimen were subject to a physical form of attack that causes delamination (Figure 4.29).

At the time of this report, the chemical form of the attack was dominating, leading to the failure of two mixtures due to lost pins (Figure 4.30). The VMA-OPC mixture was once again the only remaining OPC mixture, but increased error was also observed in it. The FA mixtures were behaving similarly and had a lower expansion level than their submerged counterparts.

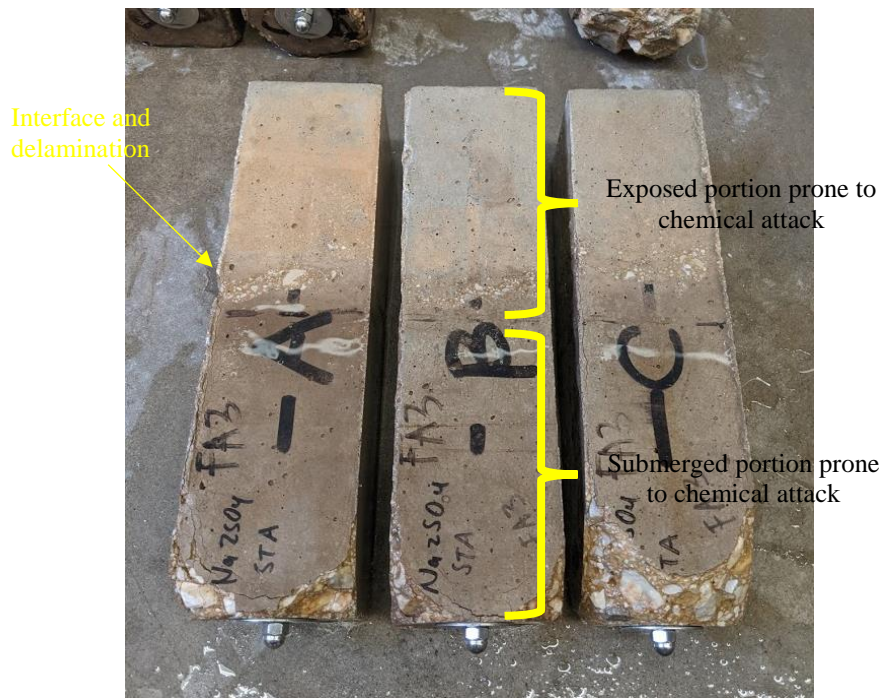


Figure 4.29 Samples standing in sodium sulfate trough

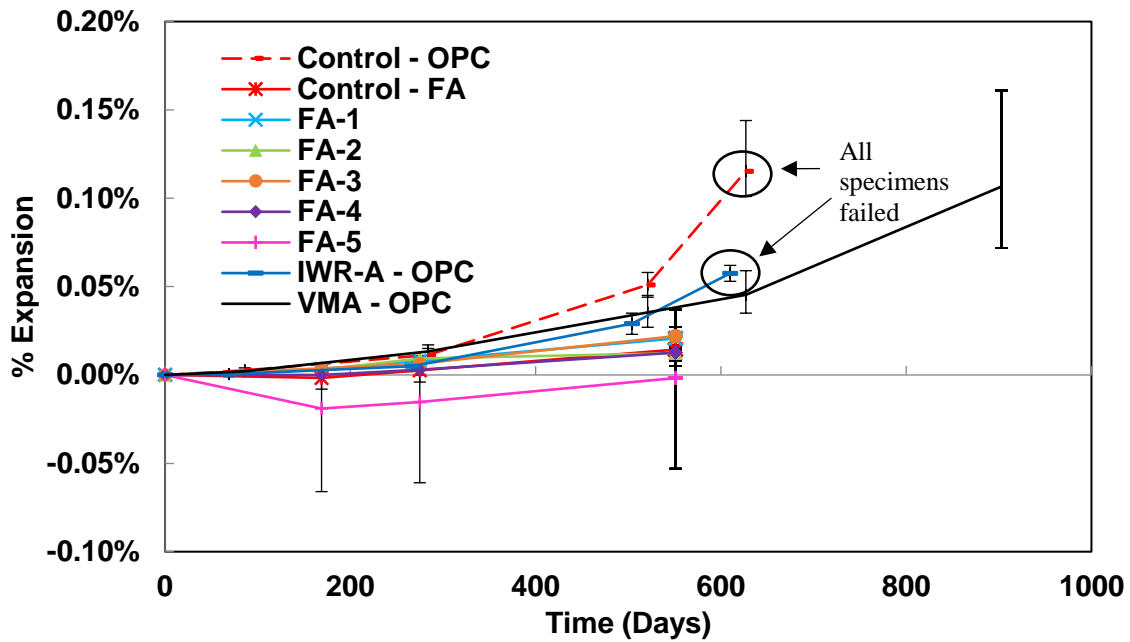


Figure 4.30 Concrete prism expansion over time for mixtures standing in outdoors sodium sulfate trough

4.4.8. Calcium Sulfate

Concrete prisms were subjected to calcium sulfate environments through three different exposure conditions. One of the conditions was for lab samples, while the remaining two were for field samples. Table 4.8 outlines the different exposure conditions and the types of deterioration intended for each condition. All samples were placed in their respective exposure environment after a minimum 28 days of curing.

Table 4.8 Exposure conditions for calcium sulfate samples

Sample Type	Condition	Deterioration Type
Lab	Standard Calcium Solution	Chemical Sulfate Attack
Field	Outdoors Trough – Submerged	Chemical Sulfate Attack
	West Texas - Site 2 – Submerged	Chemical Sulfate Attack

4.4.8.1. Calcium Sulfate Solution

These samples were immersed in a solution composed of 5% concentration calcium sulfate by mass. Calcium sulfate is poorly soluble in water and excess solids were present in the solution. Expansion measurements were performed periodically, and each time fresh

solution was replenished. Samples appeared relatively inactive at an exposure age exceeding 500 days (Figure 4.31).

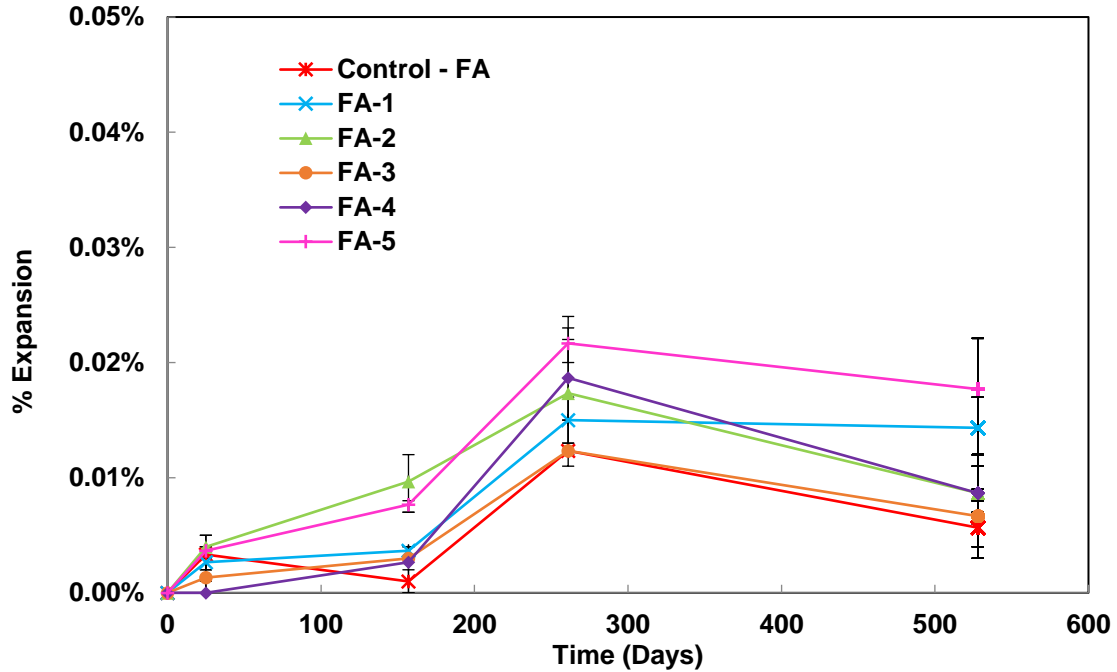


Figure 4.31 Concrete prism expansion over time for mixtures submerged in calcium sulfate solution

4.4.8.2. Calcium Sulfate Trough – Submerged

Similar to their lab counterparts, the field specimens in the outdoors calcium sulfate trough appeared inactive at an exposure age exceeding 500 days (Figure 4.32).

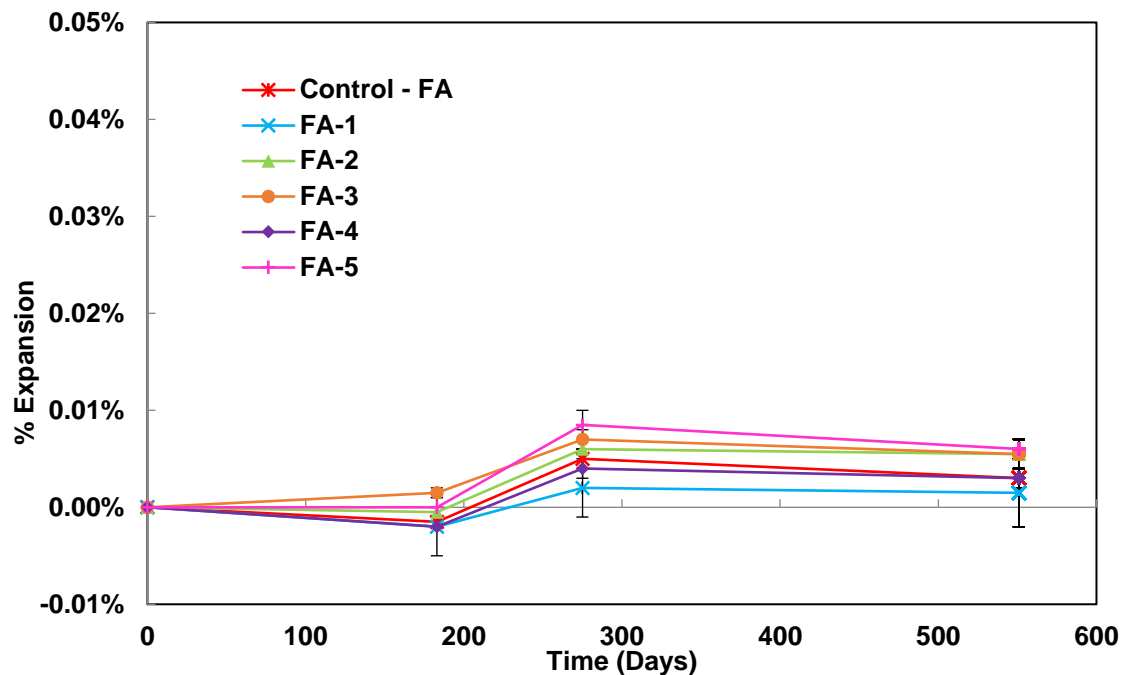


Figure 4.32 Concrete prism expansion over time for mixtures submerged in outdoors calcium sulfate trough

4.4.8.3. West Texas – Site 1 and 2

Concrete prism samples were placed at the West Texas Site 1 and 2 locations in July 2018. At the time of this writing, no subsequent measurements have been performed on these samples.

4.4.9. Alkali-Silica Reaction

4.4.9.1. Concrete Prisms

Concrete prisms per ASTM C1293 were cast using various products in OPC mixtures. Similar to the sodium sulfate testing, a modified wetting and drying cycle condition was implemented for these samples. ASR expansion results are shown in Figures 4.33 and 4.34.

None of the products were able to reduce expansions due to ASR in either the standard or modified test conditions. The modified, cyclical condition did not considerably reduce expansion even though samples spent 20% of time in dry conditions at room temperature. For the most part, mixtures containing products tended to exacerbate expansions. This could indicate that the admixtures may contain additional alkalis that contribute to the reaction. Notably, the VMA-A1 mixture had the highest expansion, far greater than that of the control. The same product showed improved performance throughout sodium sulfate

testing (Section 4.6.7), potentially due to an improvement in permeability. If this is the case, an improvement in permeability could have prevented the leaching of alkalis during testing and driven expansion to higher levels.

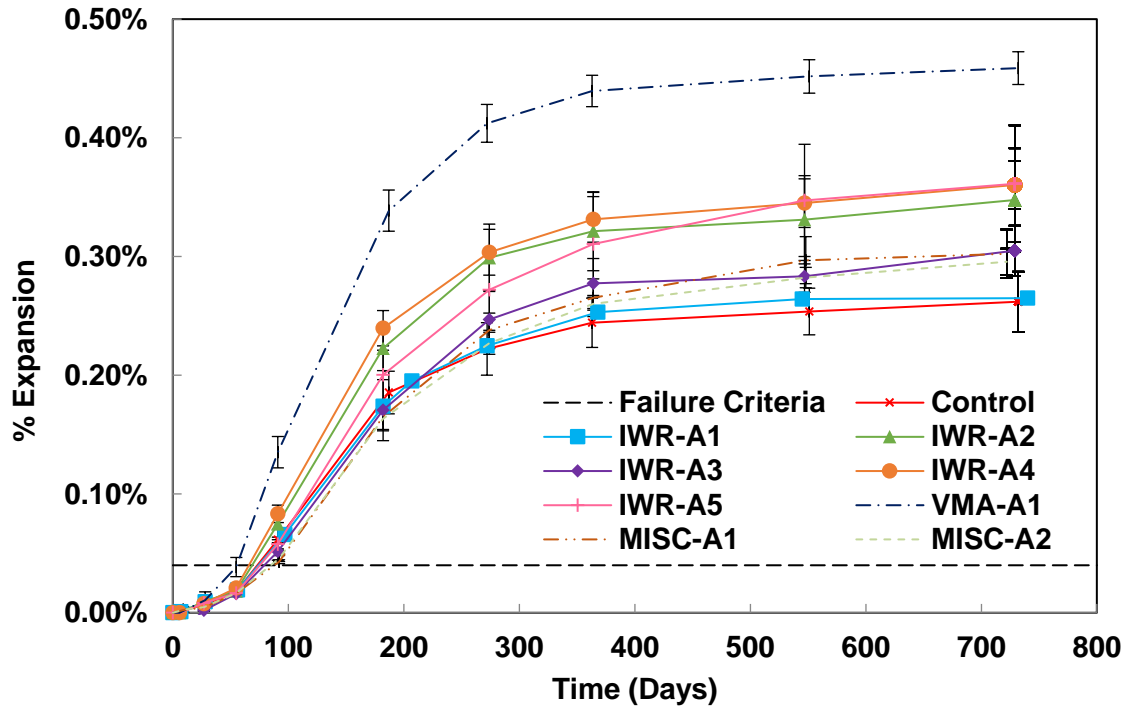


Figure 4.33 Standard ASTM C1293 concrete prism expansion for various admixtures

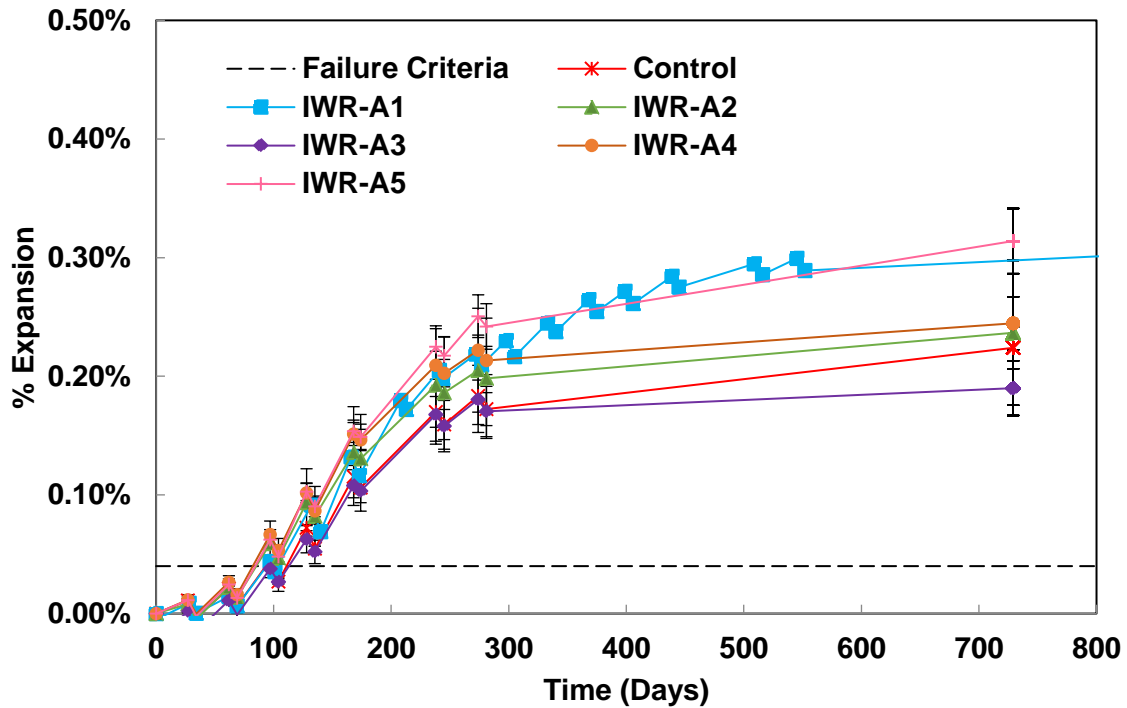


Figure 4.34 Modified ASTM C1293 concrete prism expansion for various admixtures

4.4.9.2. Exposure Blocks

ASR exposure blocks were cast with select products and their expansion data is included in Figure 4.35. A block specimen from Chapter 2 was intended to serve as a control sample for comparison. That sample, however, is believed to have reached a semi-cooked condition and potentially contain a combination of ASR and DEF. Therefore, no control sample is included on Figure 4.35. Nonetheless, all products performed poorly in ASTM C1293 lab testing and have correspondingly expanded as field samples. A true control sample would be expected to behave similarly.

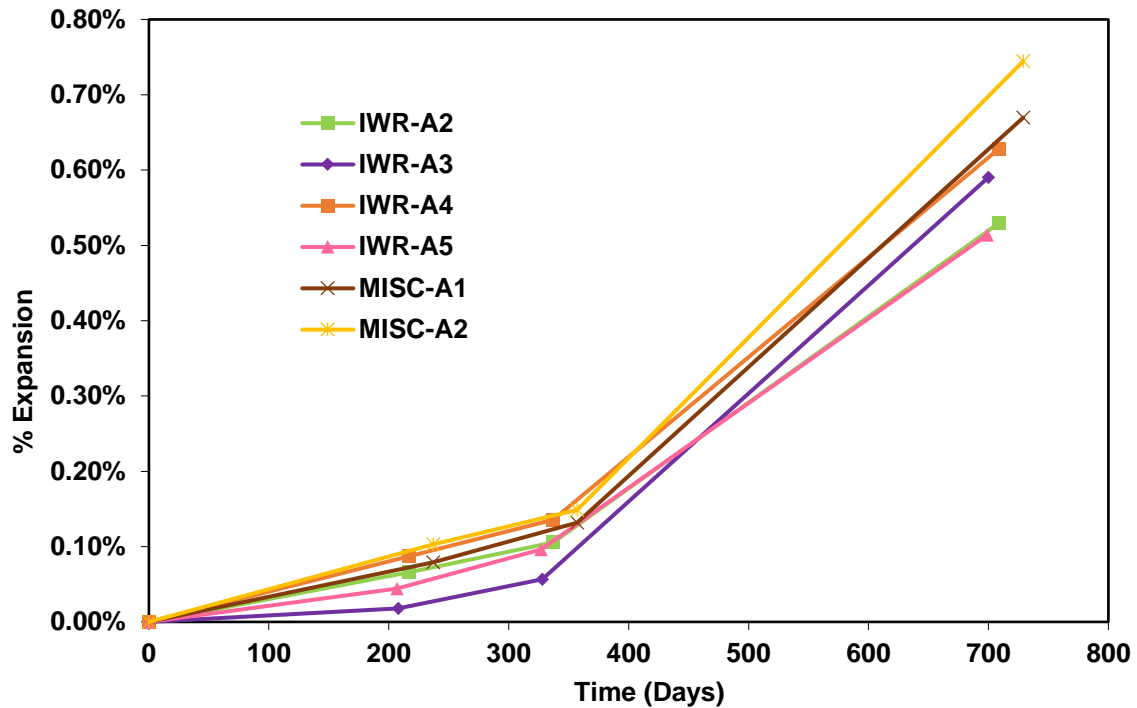


Figure 4.35 ASR exposure block expansion over time for various product

4.4.10. Marine Exposure Blocks

Sets of reinforced and unreinforced marine exposure blocks were cast for the six FA mixtures. At the time of this writing, only two half-cell potential measurements of these specimens had been taken: the first initial value and another after 5 months of exposure (Figures 4.36 and 4.37). As discussed in Chapter 2, field specimens undergo variable conditions and measurements can vastly vary from one time to another. Thus, half-cell potential data from marine exposure blocks is best assessed qualitatively and should be based on steady trends. Given that only two sets of data are currently available, not enough information is available to comment on the effectiveness of each product in reducing corrosion potential.

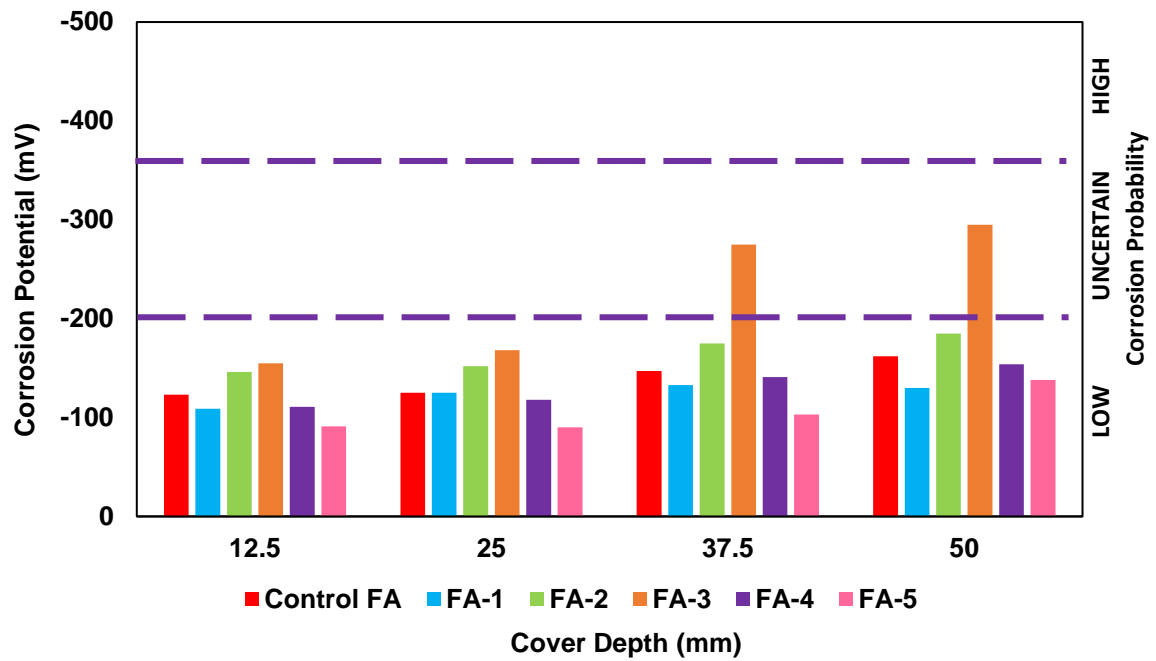


Figure 4.36 Marine exposure block half-cell measurements, initial values

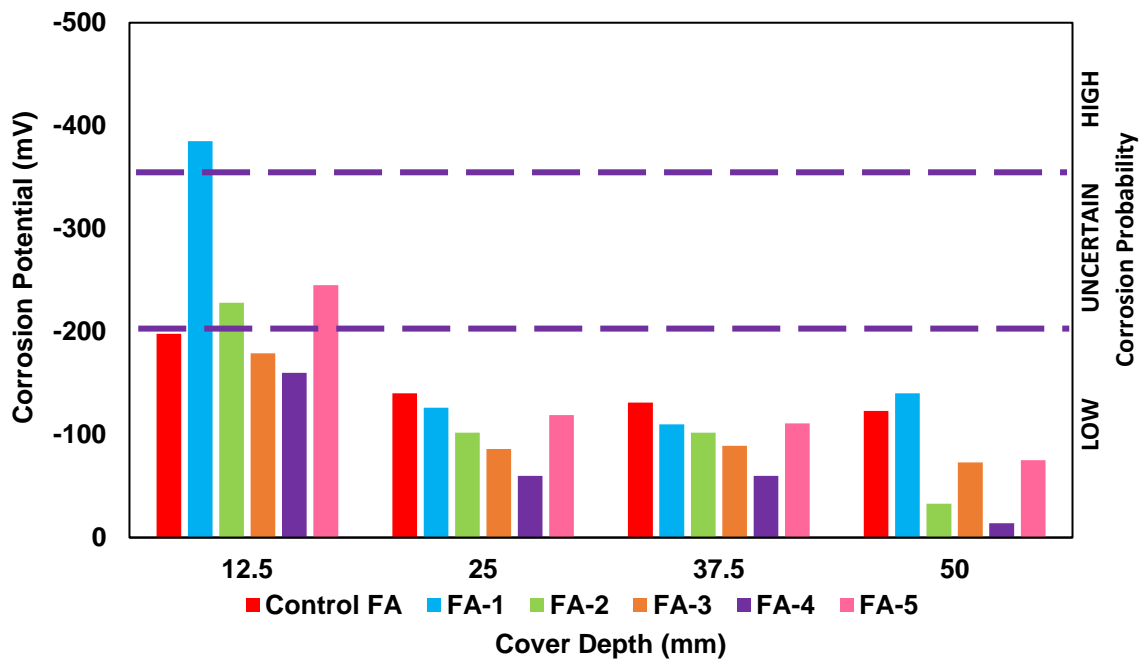


Figure 4.37 Marine exposure block half-cell measurements, 5 months exposure

4.5. Further Research

The following actions are recommended for further research of current and future samples:

- Continue measuring concrete prisms in sulfate environments: sodium sulfate solution and trough, calcium sulfate solution and trough, and specimens in the West Texas Exposure Site.
- Continue measuring ASR blocks at the Central Texas Exposure Site.
- Continue measuring marine exposure blocks at the Texas Marine Exposure Site.
- Perform chemical analysis of select admixtures. Specifically, determine if products are contributing alkalis that could explain the higher expansion in ASTM C1293 samples.
- Core samples out of marine exposure blocks and obtain chloride plots to compare diffusion coefficients from lab and field samples.
- Determine if sulfate attack is occurring differently in the modified samples, which are significantly expanding but do not show the same level of cohesion loss as the standard samples.
- Evaluate the detrimental impact of VMA on ASR-induced expansion. The use of the VMA product has shown promising results in sulfate testing and should be considered for further work. However, its detrimental effect on ASR should also be highlighted and determined.

4.6. Conclusions

Given the number of products utilized and the comprehensive scale of testing performed, the currently preliminary results have been unimpressive. In OPC mixtures, the products have been able to demonstrate slight improvements in performance. However, these effects have not been found to be significant enough to fully prevent deleterious mechanisms from occurring. The FA mixtures benefit from the presence of SCMs, but conclusive results from these samples will require longer time spans. Moreover, the beneficial effect of the SCM may ultimately overshadow the admixture effect.

Based on these results, the products may be better tailored to address specific issues rather than to provide broad improvements in durability. Products showed potential to slightly increase strength and decrease permeability in lab testing. Product IWR-E was the overall best performer in terms of decreasing permeability. However, this improvement did not result in improved performance of field samples. The VMA product showed promising results in sulfate samples, but its ASR performance was substantially worse than the

control. Its practicality is also questionable as it employs a considerably high amount of admixture. Nonetheless, its further study is recommended. The use of gypsum to improve sulfate resistance of concrete containing Class C fly ash shows promise but requires further time to monitor the laboratory and field specimens cast during this project.

4.7. References

ASTM C1012 (2015), *Standard Test Method for Length Change of Hydraulic-Cement Mortars Exposed to a Sulfate Solution*

ASTM C1293 (2015), *Standard Test Method for Determination of Length Change of Concrete Due to Alkali-Silica Reaction*

ASTM C150 (2016), *Standard Specification for Portland Cement*

ASTM C1556 (2016), *Standard Test Method for Determining the Apparent Chloride Diffusion Coefficient of Cementitious Mixtures by Bulk Diffusion*

ASTM C1585 (2013), *Standard Test Method for Measurement of Rate of Absorption of Water by Hydraulic-Cement Concretes*

Bentz, D.P, M.A. Peltz, K.A. Snyder, J.M. Davis, “Verdict: Viscosity Enhancers Reducing Diffusion in Concrete Technology,” *Concrete International.*, pp. 31-36. 2009.

Dhole, R., “Sulfate Resistance of High Calcium Fly Ash Concrete,” *Dissertation.*, University of New Brunswick. 2008

Folliard, K. (2010). Recommended Practice for Application of sealers and coatings to reduce future expansion of concrete structures affected by alkali-silica reaction (ASR) and/or delayed ettringite formation (DEF) [Prepared for Houston TxDOT District]

Lute, R., & Folliard, K. (2008). Evaluation of coatings and sealers for mitigation of alkali-silica reaction and/or delayed ettringite formation by Racheal Dawn Lute. Thesis (M.S. in Engineering)--University of Texas at Austin, 2008.

Pfeifer, D.W. and Scali, M.J., NCHRP Report No. 244: Concrete Sealers for Protection of Bridge Structures, NCHRP No. 244, TRB, Washington, D. C. 1981

Snyder, K., Bentz, D., & Davis, J. (2012). Using Viscosity Modifiers to Reduce Effective Diffusivity in Mortars. *Journal of Materials in Civil Engineering*, 24(8), 1017–1024. [https://doi.org/10.1061/\(ASCE\)MT.1943-5533.0000524](https://doi.org/10.1061/(ASCE)MT.1943-5533.0000524)

Wehrle, E., & Folliard, K. (2010). The effects of coatings and sealers used to mitigate alkali-silica reaction and/or delayed ettringite formation in hardened concrete / by Evan Richard Wehrle. [University of Texas].

Wheless, J., & Folliard, K. (2018). Improving the sulfate resistance of Class C fly ash : a scientific approach to making bad ash concrete / by Jeremy Oran Wheless. [University of Texas].

Chapter 5. Effect of Nano-Admixtures on Concrete Durability

5.1. Introduction

As the concrete industry enters a new decade, there is an ever present need to develop the next generation of concrete that will be able to deliver strength, performance, and durability all while providing sustainability (Singh et al., 2013). As optimization of the standard concrete mixture (cement, water, coarse and fine aggregates) reaches its maximum potential, the use of admixtures and nanomaterials could potentially serve to push the next generation of concrete beyond its current limitations. In practical terms, these additives should be able to enhance concrete properties such as strength and permeability. Once these benefits can be verified and validated, the use of nano-engineered admixtures could allow for quality concrete to be made with a reduced cementitious content and potentially a lower environmental impact. However, given that nano-admixtures are synthetically produced products, their environmental and economic costs must also be assessed.

5.2. Background

The use of nanoparticles in concrete, while a novel concept in the industry at large, has been recently gaining traction. In fact, the recent Spring 2019 ACI Convention featured a session dedicated to it, *Nanoparticle Dispersion and Applications in Concrete* (ACI, 2019). The session aimed to provide information about ongoing research in the field of nanoparticle use in concrete. Nanoparticles such as nano-silica and carbon nanotubes/fibers are increasingly appealing to the concrete industry because of their potential to improve concrete quality. The extremely fine particle size of nanoparticles has the potential to improve cement hydration and create a denser microstructure. However, their small size also leads to particle agglomeration, which reduces its effectiveness (Belkowitz et al., 2015). The following sections detail the current understanding of nano-silica mechanisms, challenges, and effectiveness. Background information on the use of nano-CSH is far more limited and is presented in Section 5.4.5.

5.2.1. Mechanisms

Nano-silica (NS) can be considered as a smaller or ‘nano’ version of SF, which itself can be referred to as micro-silica. NS particles range in size from 10–150 nm, compared to 200–300 nm for SF (Ghafoori et al., 2016). Like SF, NS is a highly pure form of amorphous silica (SiO_2) that is utilized in concrete as an SCM and replaces a given percentage of cement content by mass. However, given its smaller particle size and higher surface area,

the typical dosages of NS (~2%) are lower than those of SF (~8%). As discussed in Section 5.4.2, there is currently no consensus as to what the appropriate dosage of NS should be.

As with SF, the highly pure nature of NS gives it the potential of being an extremely reactive pozzolanic material with many beneficial aspects to concrete. NS manufacturers, however, have reported that NS is a superior product to SF because it is a synthetically made and engineered material as opposed to being a byproduct of the iron industry. Given its synthetic nature, manufacturers report NS products to be free from impurities and to have robust quality control (GCP, 2018).

The mechanisms by which NS can improve concrete performance are directly related to its small particle size and its near pure silica composition. The mechanisms can be broadly separated into three categories: small particle filler effect, increased pozzolanic reaction, and improved cement dissolution and nucleation sites (Belkowitz, 2015).

5.2.1.1. Small Particle Filler Effect

Introducing small particles that are orders of magnitude smaller than cement grains will improve their overall ability to pack and will result in a denser microstructure. This mechanism considers the NS particle as an inert material that by virtue of having a small particle size will be able to create a beneficial nano-filler effect. This improvement will be particularly effective when considering the interfacial transition zone (ITZ) present at the aggregate-paste boundary. The small NS particles will be able to close-pack voids that are unreachable to the coarser cement grains and hence will decrease the negative implications of the wall effect and will improve the ITZ, which is generally considered to be a weak zone (Folliard, 2015). These benefits have been widely studied and validated using SF and are expected to be enhanced with NS. However, it remains to be determined whether the inherently lower dosage of NS (~2%) when compared to SF (~8%) will prevent it from having such a prevalent filler effect. While the lower dosage of NS may effectively be providing a higher available surface area and total number of particles than a standard dosage of SF, the lower presence of it by mass may still play an influential role.

5.2.1.2. Increased Pozzolanic Reaction

As with other SCMs, NS can provide amorphous silica to react with the available calcium hydroxide (CH) and form the more stable C-S-H hydration product, which is essentially the backbone of concrete (Belkowitz et al., 2015). CH is generally considered as an unwanted hydration product with little contribution to strength or matrix densification. Therefore, the transformation of CH into C-S-H has dual benefits in terms of reducing an unwanted product while increasing a product that directly increases strength development. While pozzolanic reaction occurs to some extent with most SCMs, it is theorized that the small particle size and increased surface area of NS will enable it to provide an increased

amount of it at an earlier time when compared to standard SCMs. Pozzolanic reaction may be quantified through XRD, thermogravimetric analysis (TGA), and calorimetry.

5.2.1.3. Improved Cement Dissolution and Increased Nucleation Sites

The presence of NS introduces a large amount by surface area of reactive, amorphous silica that can accelerate cement dissolution. The higher availability of silica accelerates the dissolution of C_2S and C_3S , promotes the formation of C-S-H products, and ultimately leads to a higher degree of hydration of the cement particle (Bjornstrom and Panas, 2000). Additionally, the small NS particles serve as nucleation sites, effectively allowing for C-S-H to develop in more places than just the cement grain boundary. It has been shown that the presence of inert nanomaterials such as titanium dioxide serve as nucleation sites and accelerate the rate of cement reaction as observed in an increased heat of hydration (Jayapalan et al., 2009).

5.2.2. Challenges

While the theoretical benefits of using NS are promising, there are still challenges that limit its widespread use in the industry. While the fact that NS is a synthetically made and engineered material is advantageous to its overall quality control, it is also a detriment to its potential cost when compared to industrial byproducts such as fly ash and SF. Manufacturers claim that the cost savings would be reflected in the lower dosages required with NS when compared to SF, but there is currently no consensus as to what that dosage may be. Cost aside, there are other major challenges that NS faces related to mixing procedures and performance. These challenges can be broadly divided into two categories: agglomeration, and dosage and workability.

5.2.2.1. Agglomeration

The tendency for small particles to agglomerate and cluster is a result of their surface charges and high surface area. At the nanoscale it is incredibly difficult to prevent particles from agglomerating and much of the current research on the topic is based on how to properly disperse the material before, during, and after mixing. The issue of agglomeration can be further dissected by considering physical form, particle size, and mixing procedure.

NS is available in two physical forms for concrete use, as a dry powder and as a colloidal suspension. The current literature tends to agree that the use of NS as a dry powder increases the potential for particles to agglomerate. Ghafoori et al. (2016) encountered this problem while studying the use of NS to mitigate sulfate attack. When their NS mixes did not perform as expected, the researchers suspected agglomeration to be the cause of the discrepancy. After performing laser diffraction particle analysis on dry powder NS samples, they found that significant agglomeration was present even after mixing the

sample ultrasonically. In fact, the results showed the NS particles to be orders of magnitude larger than what the manufacturer specified, closer in size to cement particles and much larger than SF. Therefore, it has been shown that the dispersion of a dry form of NS in water is a challenge even with advanced mechanical mixing and may require the use of additional chemical dispersants.

In its colloidal form, NS is available as an aqueous dispersion consisting of 30–50% solids by mass, having an SG of 1.2 to 1.4, and containing variable particle sizes available (GCP Technical Bulletin). It resembles a white, milky liquid, and given its 30–50% solids content, its remaining water contribution should be subtracted from the batch water. Moreover, manufacturers promote the idea that NS in a colloidal form is much easier to handle as compared to SF which may require additional storage containers and safety measures (GCP Technical Bulletin). A colloidal form of NS was used for this study.

Regarding particle size, it has been found that the average particle size (small → 5 nm, large → 50+ nm) and particle size distribution (wide or narrow) can play a role in the material's potential to agglomerate and its effectiveness. Belkowitz et al. (2015) found that smaller NS particles had a higher tendency to agglomerate even in a colloidal form. When these particles agglomerated, they created clusters which effectively acted as pores or defects and reduced overall performance. In order to disperse these small NS particles an impractical amount of HRWR admixture or other mixing procedures may be needed. Larger NS particles were found to enhance concrete performance as it was theorized. These results hint at the existence of an agglomeration threshold based on particle size, particle size distribution, and dosage. An optimal amount of NS surface area could be achieved either through a low dosage of small NS particles or a higher dosage of larger particles.

As previously mentioned, agglomeration can even be found in cases where samples underwent ultrasonic mixing. Therefore, mixing procedures may have to be adjusted for the material to make its way into full-scale production.

5.2.2.2. Dosage and Workability

Given its small particle size and akin to SF, the use of NS, especially in its dry powder form, tends to decrease workability and increase paste cohesiveness, resulting in 'sticky' mixtures which make it a desirable product for the shotcrete industry. Given this property, the use of NS often requires the use of a superplasticizer in order to have proper dispersion and workability. Previous research has found a unique interaction between specific NS and superplasticizer product dosages leading to variability in strength and workability values (Brace and Garcia-Taengua, 2019). These findings emphasize the challenge of compatibility and dosage when using NS. Widespread use of the material is not likely to develop if sensitivity and compatibility issues are not resolved.

5.2.3. Current Research

Current research efforts focusing on certain fresh and hardened properties are presented in this section. While evidence of positive results from the use of NS exist, there is not yet a consensus on the material's proven benefits within the literature. There also exist instances in which agglomeration issues resulted in a worse performance than a control (Ghafoori et al., 2016), or in which the beneficial effect of NS was insignificant or inconsistent across w/c ratios and dosages (Isfahani et al., 2016). The inconsistency of results found in the literature could be attributed to the many challenges that have been previously mentioned. The limited availability of commercial NS products also likely contributes to the disparity in results since researchers may be acquiring different products with different physical forms, particle sizes, and compatibilities, all of which are factors that can influence NS effectiveness. Moreover, there is no established dosage or mixing procedure for the use of NS in order to ensure proper dispersion and effectiveness. These are all factors that may contribute to the inconsistent set of results found in the literature. Additionally, most of the current nano-admixture research is focused at the paste and mortar scale since its mechanisms mainly improve the quality of the cement paste; however, it could be inferred that given the potential for nano-admixtures to significantly enhance the ITZ, there may be a more drastic improvement in actual concrete containing nano-admixtures. Further investigation is required to properly validate the many potential benefits on the use of NS.

5.2.3.1. Fresh Properties

Regarding fresh properties, there have been observations detailing the acceleration of hydration accompanied by a shortened dormant period (Senff et al., 2009). These observations relate to the accelerated cement dissolution and nucleation site mechanisms previously mentioned and were validated via time of set and hydration temperature tests. Additionally, rheological tests such as the use of a viscometer and standard flow tests indicate the use of NS results in an increase in yield stress and reduction in flow (Senff et al., 2009). These properties (a reduction in bleed water, increased in cohesiveness, and overall reduced workability) are a result of the NS small particle size, whose high surface area requires more lubricating water to provide appropriate flow.

5.2.3.2. Hardened Properties

Regarding hardened properties, an increase in the production of C-S-H and a reduction in CH is theorized to be a result of the accelerated cement dissolution, nucleation sites, and pozzolanic reaction mechanisms. Work done by Mondal et al. (2010) aimed to quantify binder phases and evaluate each of their elastic moduli via nanoindentation. As part of their criteria, the researchers separated and quantified these phases: low stiffness C-S-H, high stiffness C-S-H, calcium hydroxide (CH), and porous phases. Their results indicated an

increase in the volume of high stiffness C-S-H accompanied by a decrease in CH in mixes with NS. This increase was hinted as either being a result of an enhanced pozzolanic reaction (when compared to a SF control) or as a result of close packing which may facilitate the formation of high-density C-S-H. It should be noted, however, that the presence of NS did not itself increase the elastic moduli of the high stiffness C-S-H. Rather, it increased the relative amount of it present while decreasing the amount of CH. Across all the mixtures studied (OPC, SF, and NS) the overall volume fraction of C-S-H remained constant at around 85%. This value was surprising in the sense that it also indicated that the volume fraction of porous phase was basically unchanged from an OPC mix to a SF mix. Nonetheless, the SF mix did contain an increased amount of high stiffness C-S-H along with a decreased amount of CH, clear signs of pozzolanic reactivity. Moreover, in order to study and quantify pozzolanic reactivity with the use of NS researchers have employed the use of XRD, TGA, and calorimetry (Belkowitz, 2015).

The synergistic effect of the different NS mechanisms is essentially theorized to increase compressive strength and decrease permeability. Compressive strength of cylinders or cubes at different ages is the most common way to quantify strength while permeability can be evaluated through an array of tests intended to quantify a mixture's transport properties. Such tests include quantifying sorptivity, chloride diffusion, resistivity, and porosity. Work done by Jalal et al. (2012) on high performance self-compacting concrete (HPSCC) found significant improvement in permeability and strength properties with the use of NS. It should be noted that Jalal's work was performed with the use of a dry powder form of NS, which based on Ghafoori's (2016) work was found to be an inferior form of NS.

5.2.4. Research Objectives

As part of the study, nano-admixtures were evaluated for their ability to improve concrete durability. Given the decreased production of fly ash in the industry, there is an increasing push to deliver high quality concrete without heavily relying on fly ash. Thus, the testing explored the possibility of reducing fly ash content while still providing quality concrete mixtures with an extended service life.

Emphasis was placed on efforts to mitigate ASR damage due to its prevalence. The goal was to match the ASR mitigation performance of a given fly ash content with a lower level of fly ash replacement in conjunction with a nano-admixture. For example, as illustrated in Figure 5.1, the listed fly ashes pass the ASTM C1567 expansion limit when utilized at a 25% replacement level but exceed the expansion limit and fail at a 20% replacement. As part of this project, the 20% fly ash mixtures were combined with nano-admixtures to test their ability to enhance a given mixture.

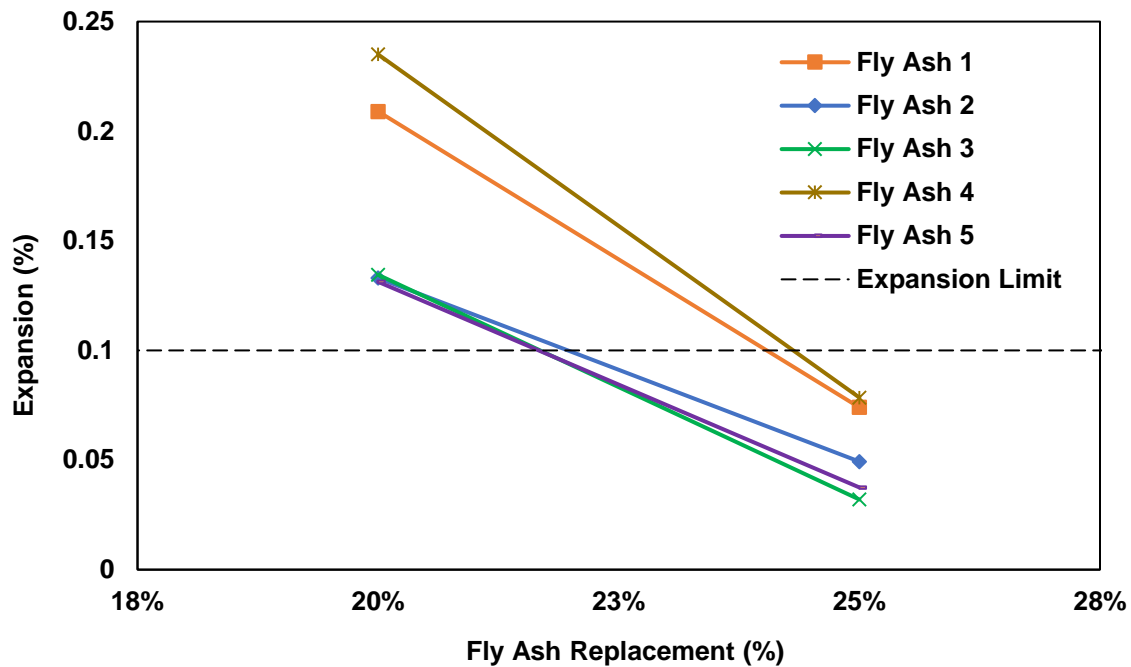


Figure 5.1 Mortar bar 14-day expansion due to ASR per ASTM C1567 for various fly ash types and contents (Drimalas, 2019)

5.2.5. Nano-CSH

Since the nano-CSH admixture is a recent and proprietary innovation, there is limited background information on its mechanisms and effectiveness. The admixture is described to consist of a stable suspension of synthetically produced crystalline C-S-H nanoparticles. The particles behave as active seeds that facilitate the growth of crystals between cement grains during hydration. In this manner, its mechanism is considered to be based around improved cement dissolution and increased nucleation sites. The effect is believed to increase strength development at early ages. This feature makes the product particularly appealing to applications that require considerable material strengths within the first few hours, e.g., precast and rapid repair materials. Additionally, the material could be substituted for cement or used in conjunction with high SCM replacement levels to reduce the mixture’s environmental impact while providing adequate early age strength.

Das et al. (2020) performed extensive testing with the use of synthetically produced nano-CSH from bagasse ash. Bagasse is a byproduct of sugarcane milling. Their testing included setting time, calorimetry, compressive strength, XRD, TGA, and scanning electron microscopy. Their nano-CSH was theorized to reduce the energy required for nucleation and hence promote the formation of early reaction products. In this context, the product served as an accelerator, and set times were observed to be directly related to product dosage. Correspondingly, calorimetry indicated an earlier and shorter induction period with

the use of the product. Compressive strengths were increased at 6–24 hours with the use of the product, while strengths at 3–28 days were unaffected. The products' influence on durability properties has not been extensively studied and is, therefore, the focus of this study.

5.2.6. Testing Procedures

5.2.6.1. Isothermal Calorimetry

Isothermal calorimetry was used to analyze the different stages of hydration in cementitious mixtures. Under this testing procedure, a fresh paste or mortar sample is placed in an insulated chamber and maintained at a uniform temperature (23 °C [73 °F] in this case) for a specified time (24–72 hours in this case). As the sample undergoes hydration and reaction products are formed, heat will be developed. The chamber, however, is maintained at the specified uniform temperature, and the calorimeter measures the power (watts) required to keep the sample at the specified temperature. This measurement is then normalized by the mass of cementitious content in the sample. Thus, heat evolution (mW/g of cementitious) refers to the power required to maintain the chamber at the specified temperature as the sample gains or loses heat. Additionally, the area under the curve of the heat evolution plot can be calculated to provide a measure of the energy (joules) utilized over time. This measurement, known as cumulative heat, is also normalized by cementitious content and is typically presented as J/g of cementitious.

Based on the specific heat peaks identified, the creation of reaction products can be traced across the different hydration stages. Calorimetry data can be related to time-of-set and early-age strength. Higher heat evolution rates and cumulative heat measurements could indicate increased hydration reaction at different stages.

A Calmetrix isothermal calorimeter was used throughout this project to analyze hydration of paste and mortar samples. Samples were mixed in various ways: directly on the sample cup and consolidated with a vibrating surface, with the use of a mortar mixer, or by sieving mortar out of concrete. For all cases, it was important to place the sample inside the calorimeter chamber as soon as possible to allow for temperature stabilization. Since the stabilization process typically took a few hours, the calorimetry plots presented omit values from this initial period and instead begin once a minimum power value has been reached. Time zero is considered as the time when the cementitious materials came in contact with water. The cementitious content of a given sample was estimated based on the mass proportions of the overall paste, mortar, or concrete sample. Based on user experience, optimal results were achieved with samples containing between 20–30 g of cementitious materials.

5.3. Experimental Investigation

The nano-admixtures testing series was designed to evaluate the effect of various nano products on concrete durability properties. The products were added to both OPC and SCM mixtures in order to compare effectiveness. Several types of lab samples were cast to assess product performance across compressive strength, permeability, calorimetry, and ASR testing. There were no field specimens cast with nano-admixtures as part of this study.

Preliminary mixtures involved the use of paste and mortar in order to assess mixture compatibility and establish expected behavior. Subsequent mixtures were made with concrete in order to study the effect of nano-admixtures at full scale.

5.3.1. Materials

5.3.1.1. Cementitious

An ASTM C150 Type I cement was used for all mixtures in the nano-admixtures series. Class F fly ash and SF were used on the SCM mixtures. The chemical composition of the cementitious materials was analyzed by XRF; the results are summarized in Table 5.1. Based on its chemical composition, Bogue equations estimate the cement to have a C₃A content of 11.1% and its Na₂O_{eq} content is 0.77%. Specific gravities used for mixture proportions were 3.15 for cement, 2.70 for fly ash, and 2.20 for SF.

Table 5.1 Chemical composition of cementitious materials (% by mass)

Material	SiO ₂	Al ₂ O ₃	Fe ₂ O ₃	CaO	SO ₃	MgO	K ₂ O	Na ₂ O	LOI
ASTM Type I	20.48	5.39	1.90	65.06	3.40	1.17	0.96	0.14	2.57
Class F Fly Ash	62.86	20.26	2.15	5.65	0.37	0.58	2.21	2.94	N/A
Silica Fume	97.16	0.31	0.12	0.92	0.20	0.28	0.65	0.06	4.42

5.3.1.2. Aggregates

Graded standard sand per ASTM C778 was used for casting mortar cubes. A fine aggregate known to be reactive was used for ASR testing in mortar (ASTM C1567) and concrete (ASTM C1293) samples. Non-reactive, limestone coarse aggregate was used in concrete samples. Table 5.2 summarizes aggregate properties.

Table 5.2 Aggregate properties

Aggregate Type	Absorption Capacity	Specific Gravity (Saturated Surface Dry)
Fine	0.67%	2.59
Coarse	2.53%	2.49

5.3.1.3. Admixtures

A polycarboxylate-based HRWR admixture with an SG of 1.08 was used to achieve proper workability and dispersion of the nano-admixtures. A dosage of 3 fl. oz per 100 lbs. of cementitious (fl. oz./cwt) was used for mixtures with SF and a dosage of 4.5 oz./cwt was used for mixtures containing nano-admixtures.

An NS admixture consisting of an aqueous dispersion of colloidal silica (50% solids by mass) was procured from its manufacturer. The silica dispersion is described to be sodium stabilized and to contain negatively charged amorphous silica particles. The particles are characterized as being discrete, have a smooth, spherical shape, and to be present in a wide particle size distribution. The physical appearance of the product is a white liquid that is slightly more viscous than water (8 cP). Its SG is listed as 1.4.

An additional NS product intended for shotcrete applications was included in preliminary mortar mixtures. However, achieving proper workability with the product was an issue and preliminary test results did not show significant differences from the control. Thus, the use of this product was discontinued, and its data will not be presented.

A nano-CSH admixture was also used in testing. Its use is recommended at a dosage of 4–15 fl. oz./cwt and its SG is listed as 1.12.

5.3.2. Mixture Proportions

Mixture proportions were based on the respective standards: ASTM C109 and ASTM C1567 for mortars, and ASTM C1293 for concrete. In mixtures containing fly ash, 20% of the cementitious content by mass was composed of SCMs. Fly ash, SF, and the nano-admixtures were considered as SCMs in this study, effectively making most of the SCM mixtures ternary blends.

Based on the review of the literature, a single dosage of 2% (cementitious content by mass) was selected for the use of nano-admixtures. The dosage was selected to optimize effectiveness and minimize agglomeration and workability issues. SF (also known as micro-silica) was included at the same 2% dosage and was meant to serve as a control in the study, intended to be compared to its close relative, NS. Thus, fly ash mixtures were

designed with a 20% cementitious content by mass of either purely fly ash (20%) or a combination of fly ash and nano-admixture or SF (18% and 2% correspondingly).

The NS product was replaced in terms of solids content. Since its concentration was known to be 50%, for every pound of the admixture, half a pound of actual NS was provided. The remaining half pound was considered as water and was removed from the design batch water. Enough admixture was utilized to provide 2% of NS solids by mass.

Because the exact components and concentration of the C-S-H product are proprietary information, the admixture was considered to have a 100% solids concentration. This assumption allowed the actual dosage to be closer to the recommended dosage range. Under these conditions, for the ASTM C1293 concrete mixtures, a 2% dosage by mass of cementitious was equivalent to an admixture dosage of approximately 27 fl. oz./cwt. The manufacturer recommended dosage range is 4–15 fl. oz./cwt.

5.3.3. Test Matrix

Mixtures were made with various cementitious materials and contents as described in Table 5.3

Table 5.3 Cementitious mixture proportions

Series	Mixture ID	Distribution of Cementitious Content by Mass %				
		Cement	Fly Ash	Silica Fume	Nano-Silica	Nano-CSH
OPC	OPC Control	100	-	-	-	-
	OPC SF	98	-	2	-	-
	OPC NS	98	-	-	2	-
	OPC CSH	98	-	-	-	2
SCM	SCM Control	80	20	-	-	-
	SCM SF	80	18	2	-	-
	SCM NS	80	18	-	2	-
	SCM CSH	80	18	-	-	2

5.3.4. Samples and Testing Procedures

Testing procedures involved the casting of several paste, mortar, and concrete mixtures. Table 5.4 includes a summary of the samples and testing procedures used.

Table 5.4 Testing procedures

Mixture Type	Sample Type	Testing Procedure				
		Isothermal Calorimetry	Compressive Strength	Resistivity	ASR Performance	Chloride Diffusion
Paste	Cup	✓				
Mortar	Cup	✓				
	Cube		✓	✓		
	Bar				✓	
Concrete	Cylinder		✓	✓		✓
	Prism				✓	

5.4. Experimental Results and Discussion

5.4.1. Isothermal Calorimetry

Figures 5.2 and 5.3 include a summary of admixture effects on isothermal calorimetry of ternary mortar mixtures. SF and NS both resulted in noticeably higher heat measurements, potentially due to increased nucleation sites. However, the nano-CSH admixture displayed abnormally high peaks and retardation effects. The delayed peak could indicate that the nano-CSH mix was plastic for several hours after casting. The unusual behavior observed with the C-S-H product was further explored with paste and mortar samples.

Subsequent calorimetry samples were cast with various nano-CSH dosages to examine its effects on hydration. As previously mentioned, the recommended admixture dosage range is 4–15 fl. oz./cwt. However, the main dosage used as part of this study was as a 2% replacement of cementitious, which is approximately equivalent to a 27 fl. oz./cwt dosage. Thus, paste and mortar mixtures with and without fly ash were examined through calorimetry at 4, 15, and 27 fl. oz./cwt dosages of the nano-CSH admixture. Figure 5.4 includes relevant heat of hydration results for SCM mortar mixtures with various nano-CSH dosages. The results indicate that dosage largely influences early on hydration. Such significant deviations in calorimetry results are noteworthy and are further explored in Section 5.6.1.1.

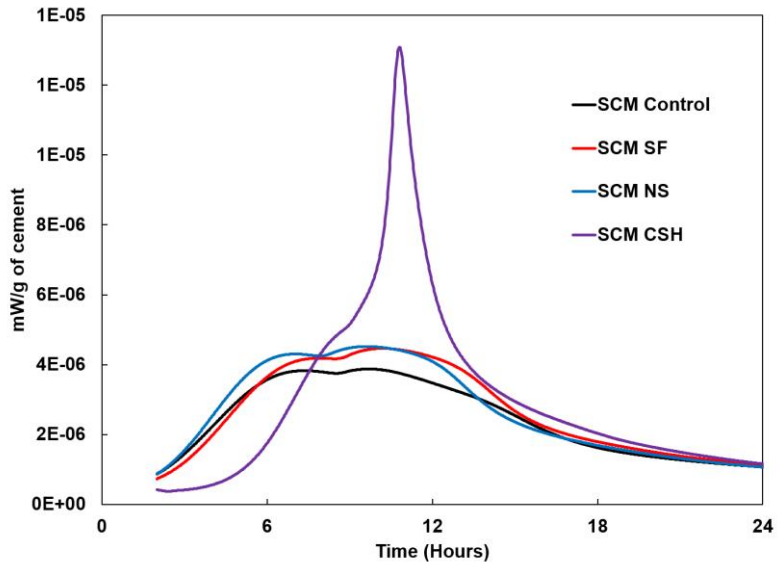


Figure 5.2 Rate of heat evolution from isothermal calorimetry on SCM mortars with various admixtures

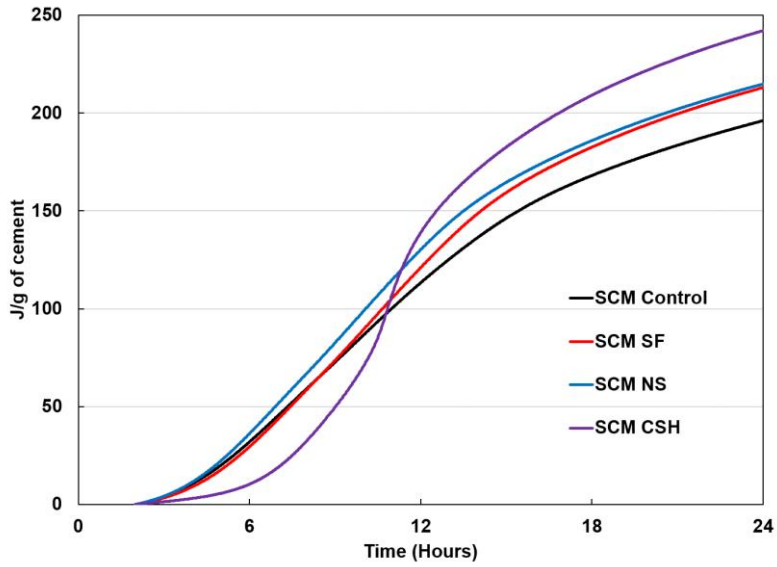


Figure 5.3 Cumulative heat from isothermal calorimetry on SCM mortars with various admixtures

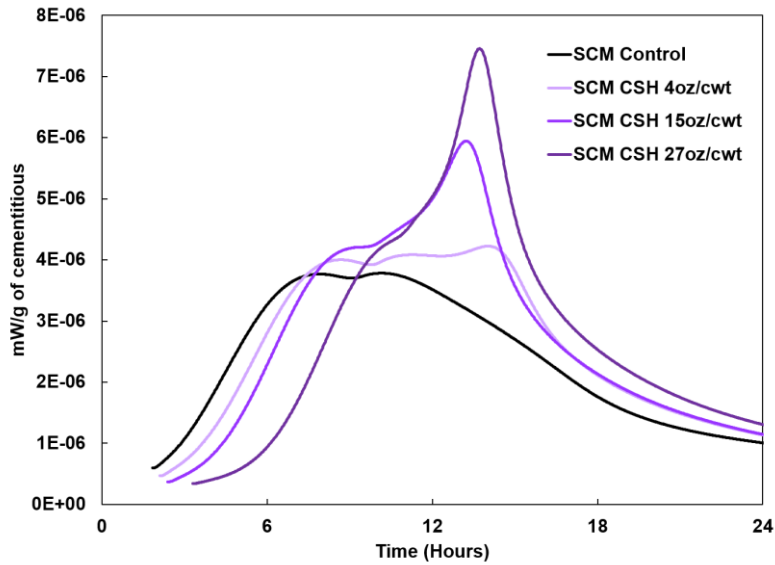


Figure 5.4 Rate of heat evolution from isothermal calorimetry on SCM mortars with various dosages of nano-CSH admixture

5.4.1.1. Sulfate Balance

Zunino and Scrivener (2019) found comparable calorimetry influences while studying pastes with limestone calcined clay cements (LC^3). Their results may provide valuable insights in informing the results observed in this study. In their case, small SCM particles were found to accelerate C-S-H production which tended to adsorb sulfates. In this context, the additional surface area provided by the small SCMs (metakaolin and fine limestone) accelerated the dissolution of C_3S , which increased the precipitation rate of C-S-H. Sulfate ions became adsorbed by the rapidly forming C-S-H and effectively led the mixture to become under-sulfated. The drop in sulfate concentration accelerated the dissolution of C_3A . Simultaneously, the drop in sulfate concentration causes the previously adsorbed sulfate ions to desorb from the C-S-H and become available to react during the aluminate peak. The resultant aluminate peak, which involves the production of ettringite and monosulfate, rapidly produces heat as an increased abundance of sulfates are readily available to react. The result is an acceleration and increase in the alite and aluminate peaks.

In contrast with the LC^3 results, the nano-CSH calorimetry data (Figures 5.2 and 5.4) show a delay in both the alite and aluminate peaks. If the addition of the admixture has an ‘over-sulfating’ effect, this could explain the observed delays. Furthermore, once the induction period is completed, an overabundance of sulfates could also explain the abnormally high aluminate peaks present. The use of in-situ XRD could provide valuable information regarding the creation of hydration products with time.

5.4.2. Compressive Strength

Compressive strengths for concrete mixtures are presented in this section. Mortar samples were also tested in compression. However, since results from mortar samples followed similar trends observed in concrete samples, they are not included.

Figures 5.5 and 5.6 display the 3- and 28-day compressive strengths for the OPC and SCM mixtures. All products seemed to be able to moderately improve early-age strengths. Most notably, the OPC CSH mixture (Figure 5.15, left) was able to achieve a 1,000 psi strength increase when compared to the control at 3 days. This result seems to validate its claims as a strength-enhancing product that can lead to earlier removal of forms or as an aid in optimizing mixture proportions. Compressive strengths at 28 days exhibited similar trends as the 3-day results, but the magnitude of admixture effect was lower. Given the slower reactivity of SCMs, the lower strength values at early ages (3 and 28 days) for SCM mixtures were expected. However, in the long term, higher strengths would be expected for the SCM mixtures.

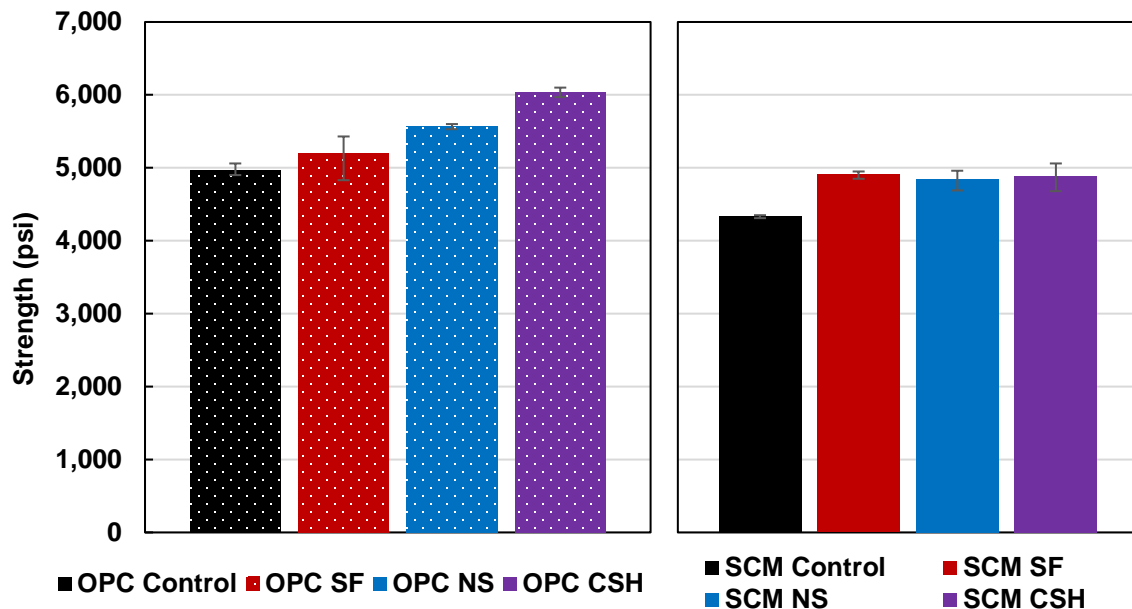


Figure 5.5 Concrete compressive strength at 3 days for OPC (left) and SCM (right) mixtures

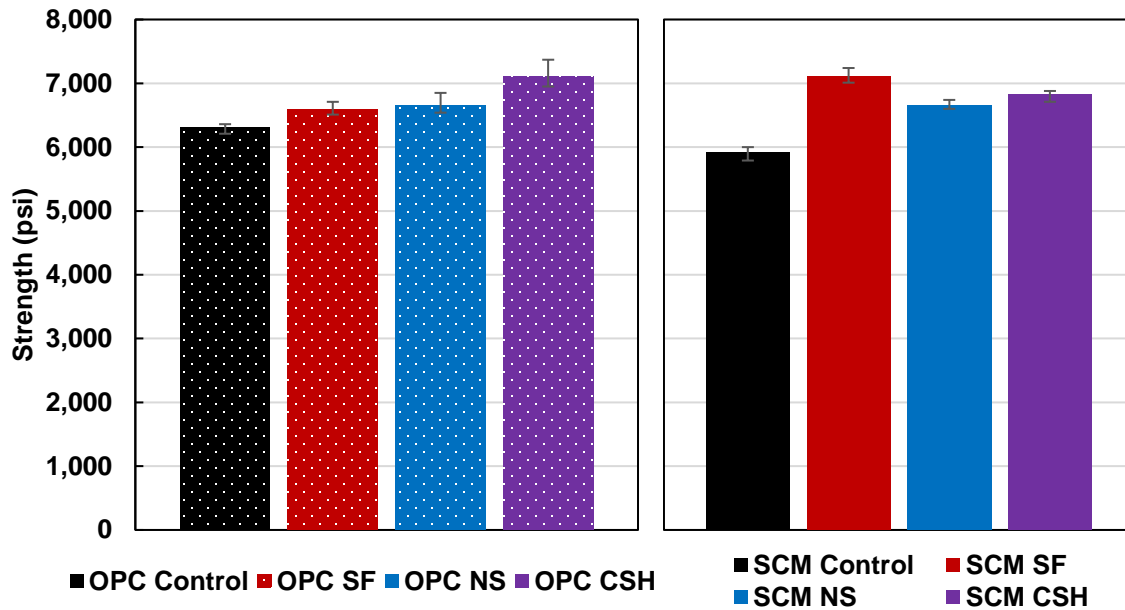


Figure 5.6 Concrete compressive strength at 28 days for OPC (left) and SCM (right) mixtures

5.4.3. Resistivity

Bulk electrical resistivity measures the impedance of an applied current on a concrete specimen. This value correlates well with permeability as denser, less permeable concrete tends to have higher resistivity values. For qualitative comparison, resistivity values (k Ω .cm) can be related to chloride penetration zones as follows:

- 0–5 k Ω .cm: High Chloride Penetration
- 5–10 k Ω .cm: Moderate Chloride Penetration
- 10–15 k Ω .cm: Low Chloride Penetration

Figure 5.7 includes resistivity measurements for concrete mixtures with respect to time. As expected, OPC mixtures plateau around the Moderate region and SCM mixtures develop much lower permeability in the long term, allowing them to reach the Low region and beyond. However, given the qualitative nature of resistivity, the products do not seem to have a significant effect on the long-term results. That is, the SCM control mixture was able to achieve low permeability with only the use of fly ash and without nano-admixtures. Moreover, it is particularly interesting to see the resemblance between the SF and NS mixtures as they are essentially the same material with different particle size.

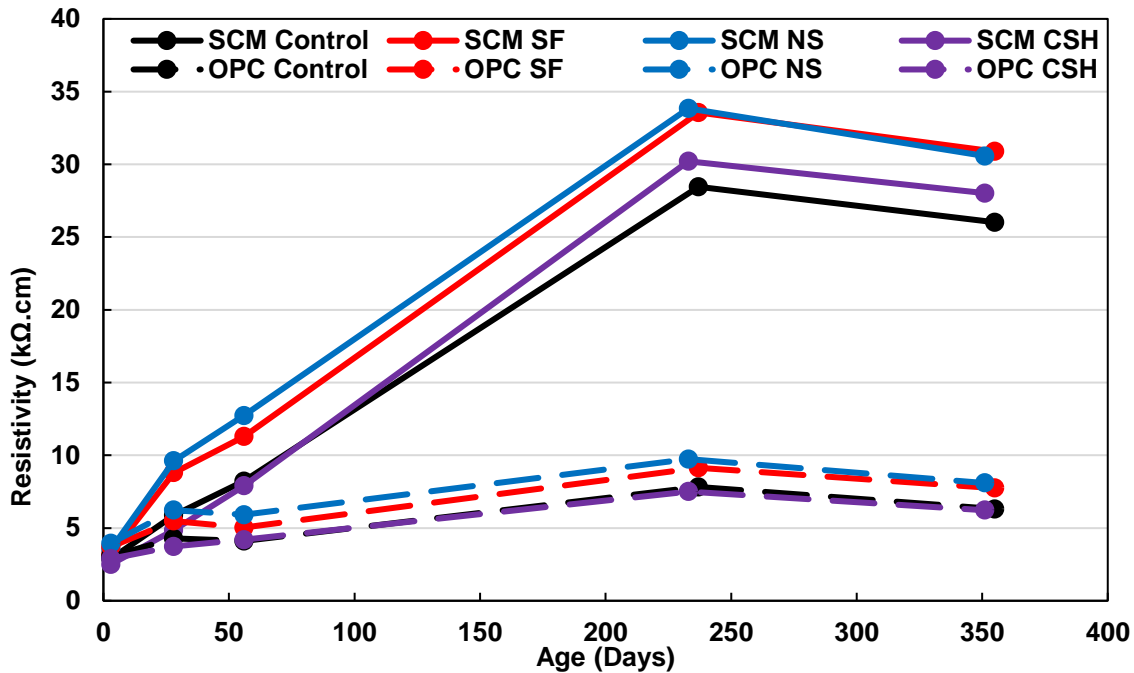


Figure 5.7 Resistivity values at various ages

5.4.4. Chloride Diffusion Coefficient

Apparent chloride diffusion coefficients are transport parameters indicating the ease of external chloride penetration into concrete samples. Mixtures with enhanced hydration products, which tend to have higher strengths and be less permeable, would be expected to have low diffusion coefficients. Diffusion coefficients per ASTM C1556 for OPC and SCM mixtures are presented in Figure 5.8.

The diffusion coefficient, D_a , is based on a mathematical model with inherent approximation error. The sum of errors squared associated with each calculated value is shown in Figure 5.9. The measured errors were deemed to be within an acceptable range. The average sum of errors squared for the samples was 4.30×10^{-3} . The MAE for samples as described in Equation 5.1 is presented in Table 5.5. The MAE provides a measure of the average difference between predicted values, y_i , and measured values, x_i . Error values were calculated for two reference cases: the $k = n-1$ case omits the error derived from the first data point obtained while the $k = n$ case includes it. The ASTM C1556 standard uses the $k = n-1$ case and specifically omits the first data point since it inherently increases error based on the mathematical model but does not necessarily reflect actual conditions.

Testing began after 28 days of curing. Given the relatively early age, the SCM mixtures had likely not yet fully matured (in a permeability sense) and underperformed for the most part. Results of interest include the considerable coefficient reduction seen in the OPC NS

and SCM CSH mixtures. These results contrast resistivity values, which did not indicate drastic differences.

$$MAE = \frac{\sum_{i=1}^k |y_i - x_i|}{k} \quad \text{Eq. 5.1}$$

Table 5.5 Mean absolute error (MAE) from chloride analysis

Mixture	Data Points			
	k = n-1		k = n	
	k	MAE (%)	k	MAE (%)
SCM Control	5	0.04	6	0.15
SCM SF	5	0.01	6	0.11
SCM NS	5	0.02	6	0.1
SCM CSH	5	0.03	6	0.03
OPC Control	5	0.03	6	0.1
OPC SF	4	0.002	5	0.03
OPC NS	5	0.03	6	0.09
OPC CSH	5	0.02	6	0.09

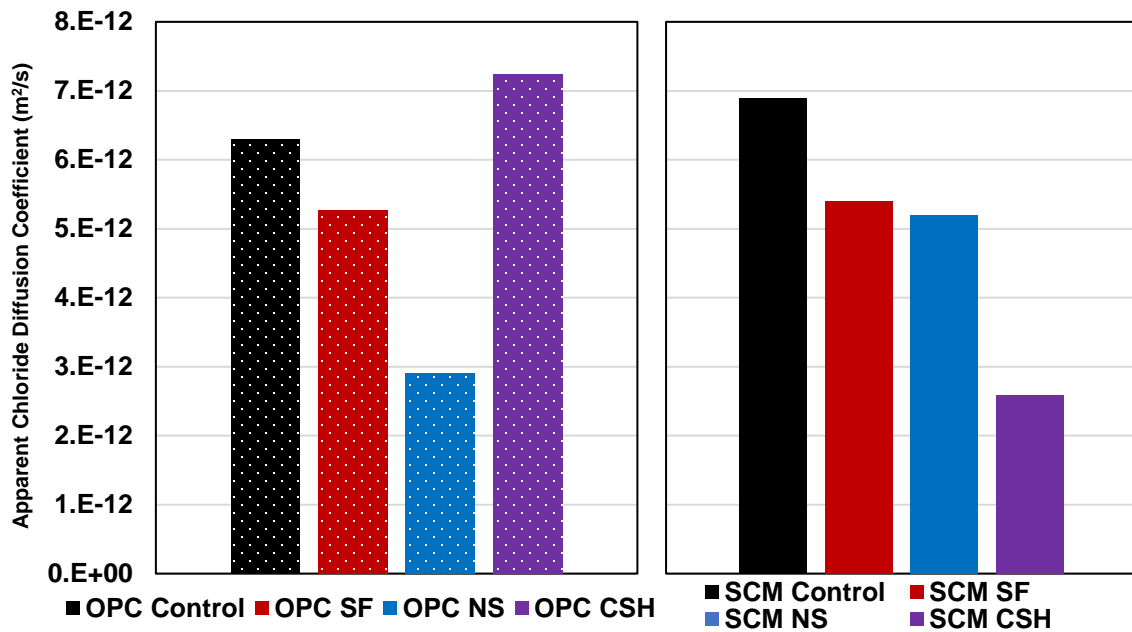


Figure 5.8 Apparent chloride diffusion coefficient for OPC (left) and SCM (right) mixtures

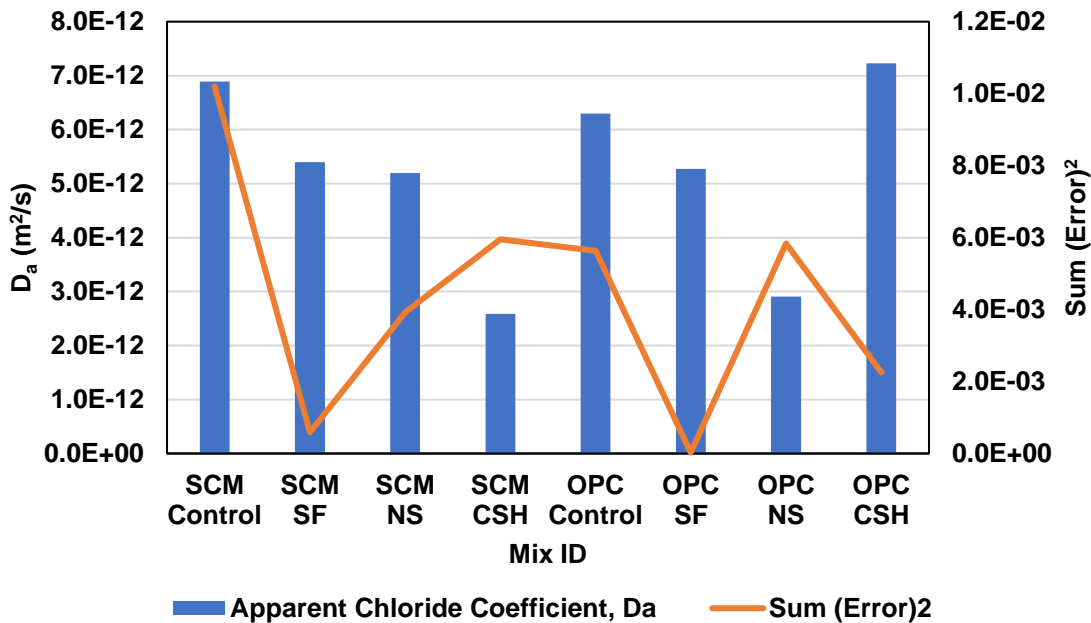


Figure 5.9 Sum of squared errors for diffusion coefficient calculations per ASTM C1556

5.4.5. Alkali-Silica Reaction

5.4.5.1. Mortar

Mortar bar expansions per ASTM C1567 are presented in Figure 5.10. The reactive fine aggregate used was known to fail the test (0.10% expansion at 14 days) at a 20% fly ash replacement but pass at 25% replacement. The goal was to potentially achieve 25% fly ash performance with 18% fly ash and 2% nano-admixture.

The NS mixture slightly lowered expansions and nearly passed the test. While pozzolanic activity can tie up alkalis and reduce ASR, given the wide availability of alkalis in the test, it is more likely that the improved performance was a result of decreased permeability at an early age as seen in the chloride diffusion and resistivity results. The slight worse performance of SF over the control was likely due to mixing procedure errors. SF tends to easily agglomerate in clumps, which effectively turn the SCM into additional reactive aggregate that can worsen expansion. The significantly higher expansion of nano-CSH was unusual and replicate mixtures were cast to further examine this effect.

It was theorized that given the considerable retardation observed with the use of the CSH admixture (Figure 5.2), this delay in hydration could have rendered the mix vulnerable (more permeable) at the start of the ASR test (24 hours) and led to the higher expansions. Thus, replicate mixtures were cast and allowed to cure for a longer time in order to

normalize for the presumed maturity delay. Since concrete compressive strength had indicated increased strengths at 3 days with the use of the CSH admixture (Figures 5.15 and 5.16), mortar bars were allowed to cure in a fog room at room temperature until reaching an age of 3 days. At that point, the standard ASTM C1567 procedure was followed and the bars were immersed in water and placed in an oven at 80°C. Corresponding sets of repeat bars that followed the standard testing procedure were also cast. Thus, the standard bars initiated the testing procedure upon demolding at one day, while the ‘delayed’ bars did so at an age of three days. The data, presented in Figure 5.11, indicates that the delay had a minimal effect on expansion. In fact, the delayed mixture with nano-CSH reached a higher expansion than the corresponding mixture without the delay. The control mixture was expected to be largely unaffected by the delay as hydration products are still largely underdeveloped at three days. Nonetheless, the results indicate that the worse performance with the use of nano-CSH is not due to an early age delay in hydration.

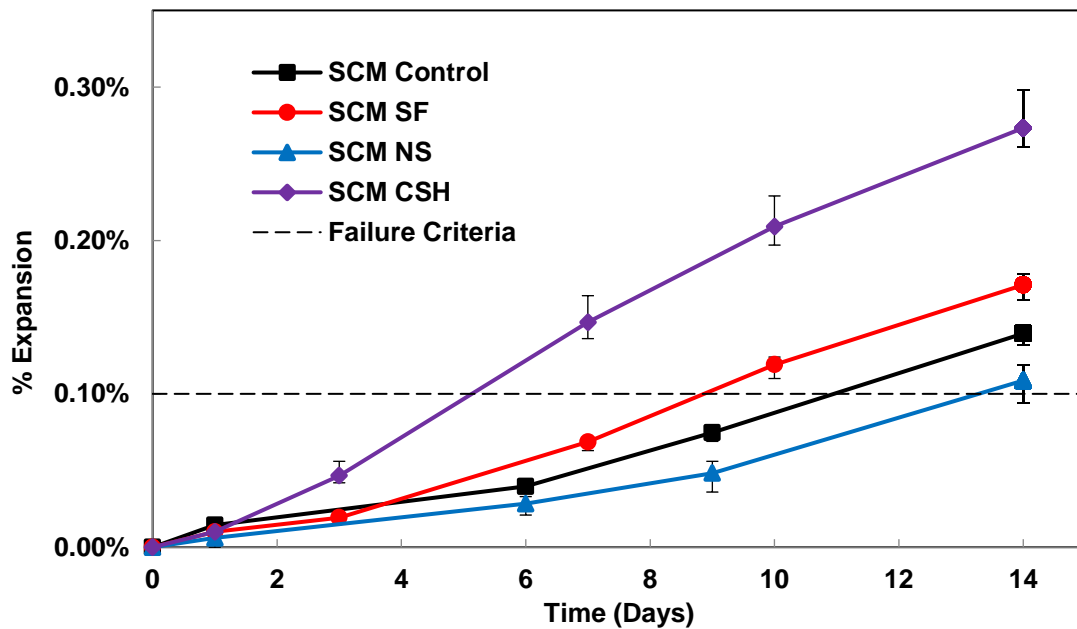


Figure 5.10 ASTM C1567 mortar bar expansion for SCM mixtures

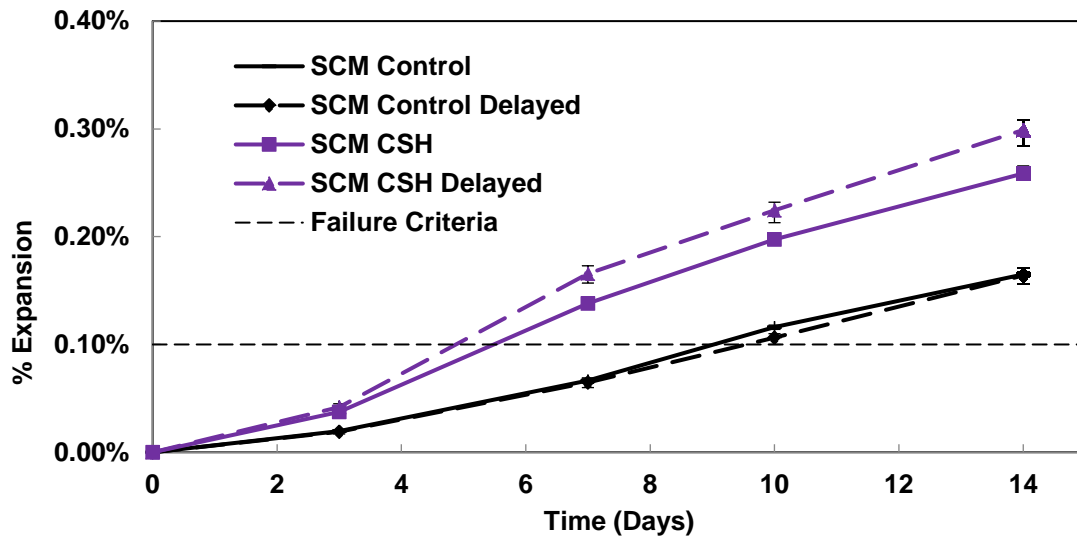


Figure 5.11 ASTM C1567 mortar bar expansion for delayed SCM mixtures with nano-CSH and without

5.4.5.2. Concrete

Concrete prisms per ASTM C1293 were also cast for OPC and SCM mixtures and expansion results are shown in Figures 5.12 and 5.13.

OPC mixtures followed similar trends seen with mortar bars and rapidly expanded and failed the two-year test within 60 days. In this case, however, the nano-CSH mixture did not expand significantly more than the control. This appears to indicate that the nano-CSH product does not contain additional alkalis. Instead, the increased expansion observed in mortar bars may be due to a harmful interaction between the admixture and the excess of alkalis present in the mortar bar ponding solution.

SCM mixtures are currently mitigating expansion below the failure criteria at 1 year (Figure 5.13). However, the control and nano-CSH mixtures exhibit an increased slope, indicating expansion may soon ensue. Moreover, the nano-CSH mixture displays a recent increase in error which is often observed in samples that are beginning to deteriorate. The NS and SF mixtures are currently mitigating expansion at similar rates.

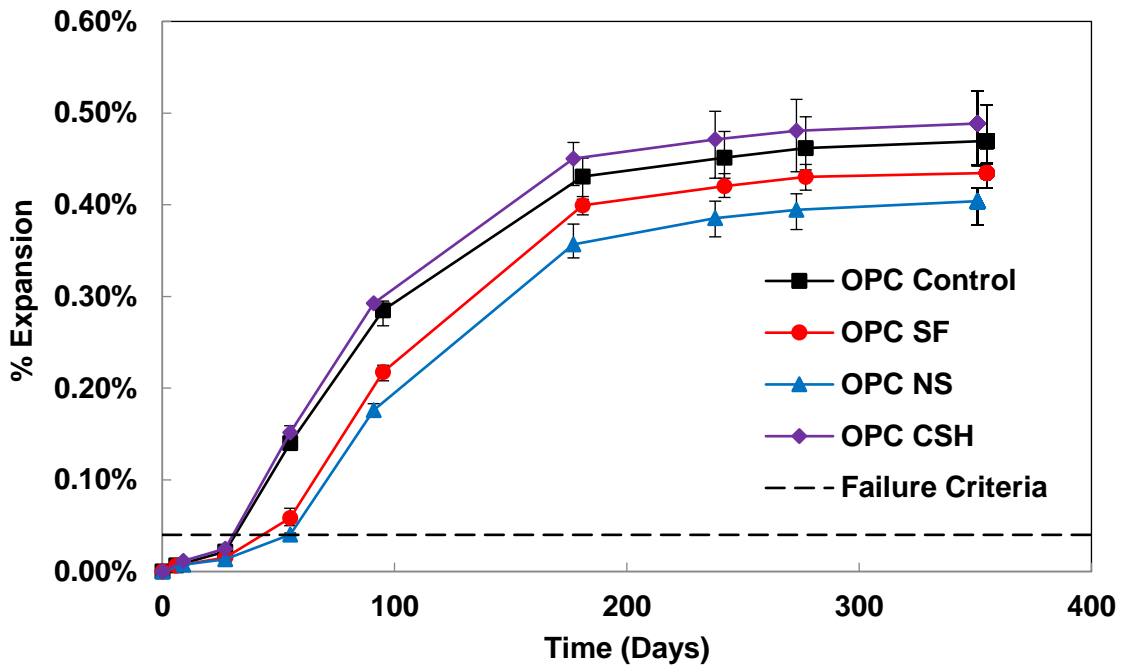


Figure 5.12 ASTM C1293 concrete prism expansion for OPC mixtures

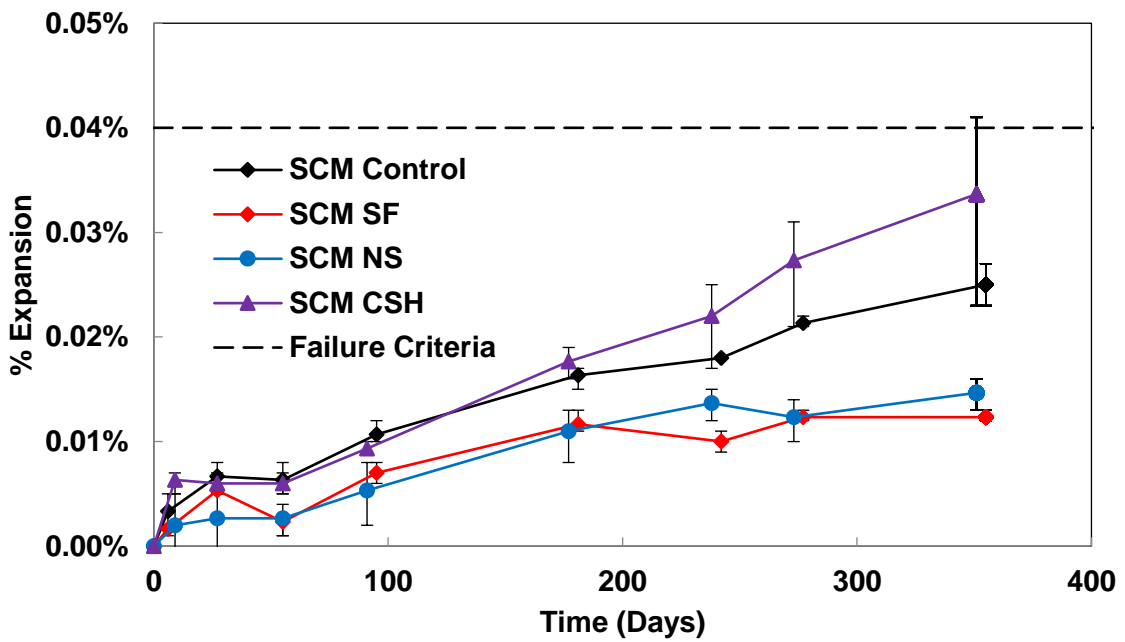


Figure 5.13 ASTM C1293 concrete prism expansion for SCM mixture

5.5. Further Research

The following actions are recommended for further research of current and future samples:

- Continue measuring ASTM C1293 concrete prisms up to an age of 2 years.
- Continue measuring resistivity on concrete cylinders.
- Consider casting field specimens (ASR and corrosion blocks) with select nano-admixtures.
- Consider examining the effect of mixing procedure and superplasticizer dosage on the agglomeration of nano-admixture particles to ensure optimal performance.
- Consider performing chloride diffusion testing on SCM mixtures now that resistivity values appear to indicate a plateau in maturity.
- Determine what led to the decreased diffusion coefficient for mixtures OPC NS and SCM CSH. Other tests do not seem to indicate these particular two mixtures have a significant improvement in permeability.
- Further examine the effect of the nano-CSH admixture on hydration through in-situ XRD, calorimetry, and time of set testing.
- Further examine the effect of the nano-CSH admixture on ASR mortar bar testing. Determine if the observed worse performance is a dosage, material, or test issue. The ASR testing performed thus far has only included the admixture at one dosage (2% replacement) which is significantly higher than its recommended range.
- Based on results, designate promising mixtures to be evaluated via scanning electron microscopy.

5.6. Conclusions

Lab test results show an overall improvement in performance across products. However, the degree of improved performance appears to be slight when compared to controls and may not justify the use of potentially costly additives. Considering SF (micro-silica) as a control, its use at the same replacement level (2%) was able to achieve relatively similar performance to that of the NS product. Based on results, the products may be better tailored to address specific issues (e.g., early age strength with nano-CSH) rather than to provide broad improvements in durability.

5.7. References

- ACI (2019), Spring 2019 Convention – Quebec City, Canada – PDF program: https://www.concrete.org/Portals/0/Files/PDF/ACI_S19_QCProgram.pdf
- ASTM C109 (2016), *Standard Test Method for Compressive Strength of Hydraulic Cement Mortars (Using 2-in. or [50-mm] Cube Specimens)*
- ASTM C1293 (2015), *Standard Test Method for Determination of Length Change of Concrete Due to Alkali-Silica Reaction*
- ASTM C150 (2016), *Standard Specification for Portland Cement*
- ASTM C1556 (2016), *Standard Test Method for Determining the Apparent Chloride Diffusion Coefficient of Cementitious Mixtures by Bulk Diffusion*
- ASTM C1567 (2013), *Standard Test Method for Determining the Potential Alkali-Silica Reactivity of Combinations of Cementitious Materials and Aggregate (Accelerated Mortar-Bar Method)*
- ASTM C778 (2017), *Standard Specification for Standard Sand*
- Belkowitz, J. (2015). An Analysis of the use of Nano Silica to Alkali-Silica Reaction in Concrete. PhD Dissertation. Stevens Institute of Technology.
- Belkowitz, J. S., Belkowitz, W. B., Nawrocki, K., & Fisher, F. T. (2015). Impact of Nanosilica Size and Surface Area on Concrete Properties. *ACI Materials Journal*, 112(3). doi:10.14359/51687397
- Bjornstrom, J., and I. Panas. Effects of Colloidal Nano Silica on the Early Cement Hydration of Belite Cement. *Chemistry of Materials*, 2000. 12: p. 1501-1522.
- Brace, H., & Garcia-Taengua, E. (2019). Superplasticizer-Nanosilica Compatibility: Assessment and Optimization. *ACI Materials Journal*, 116(2). doi:10.14359/51714454
- Drimalas, T. (2019) Unpublished ASTM C1567 Data. The University of Texas at Austin Laboratory for Infrastructure Materials Engineering (LIME).
- Folliard, K. (2015). CE 393- Advanced Concrete Materials Class (Fall 2015). The University of Texas at Austin.
- Franco Zunino, Karen Scrivener. (2019) The influence of the filler effect on the sulfate requirement of blended cements. *Cement and Concrete Research*, Volume 126, 105918, ISSN 0008-8846, <https://doi.org/10.1016/j.cemconres.2019.105918>.
- GCP Applied Technologies (2018), TYTRO Technical Bulletin 1.
- Ghafoori, N., Batilov, I. B., & Najimi, M. (2016). Sulfate Resistance of Nanosilica and Microsilica Contained Mortars. *ACI Materials Journal*, 113(4). doi:10.14359/51688989
- Isfahani, F. T., Redaelli, E., Lollini, F., Li, W., & Bertolini, L. (2016). Effects of Nanosilica on Compressive Strength and Durability Properties of Concrete with Different

Water to Binder Ratios. *Advances in Materials Science and Engineering*, 2016, 1-16.
doi:10.1155/2016/8453567

Jalal, M., Mansouri, E., Sharifipour, M., & Pouladkhan, A. R. (2012). Mechanical, rheological, durability and microstructural properties of high performance self-compacting concrete containing SiO₂ micro and nanoparticles. *Materials & Design*, 34, 389-400. doi:10.1016/j.matdes.2011.08.037

Jayapalan, A., B. Lee, and K. Kurtis. Effect of Nano-sized Titanium Dioxide on Early Age Hydration of Portland Cement. *Nanotechnology in Construction*, 2009. 3: p. 267-272.

Mondal, P., Shah, S. P., Marks, L. D., & Gaitero, J. J. (2010). Comparative Study of the Effects of Microsilica and Nanosilica in Concrete. *Transportation Research Record: Journal of the Transportation Research Board*, 2141(1), 6-9. doi:10.3141/2141-02

Saikat Das, Sonalisa Ray, Sudipta Sarkar. (2020) Early strength development in concrete using preformed CSH nano crystals. *Construction and Building Materials*, Volume 233, 117214, ISSN 0950-0618, <https://doi.org/10.1016/j.conbuildmat.2019.117214>.

Senff, Luciano, et al. (2009) "Effect of Nano-Silica on Rheology and Fresh Properties of Cement Pastes and Mortars." *Construction and Building Materials*, vol. 23, no. 7, 2009, pp. 2487–2491., doi:10.1016/j.conbuildmat.2009.02.005.

Singh, L.P., et al. "Beneficial Role of Nanosilica in Cement Based Materials – A Review." *Construction and Building Materials*, vol. 47, 2013, pp. 1069–1077, doi:10.1016/j.conbuildmat.2013.05.052.

Chapter 6. Use of Gypsum for Sulfate Resistance of Mortars and Concrete

6.1. Background

Historically, fly ash has proven to be a suitable partial replacement in a cement binder. In general, the type of fly ash used (class F or class C per ASTM C618) will produce different effects on the cement binder. Extensive research has shown that low-calcium (class F) fly ash produces a pozzolanic reaction that is beneficial to concrete in many ways. An equally thorough amount of research has shown that high-calcium (class C) fly ash can produce a cement binder that is beneficial to concrete but is susceptible to a form of concrete degradation known as external sulfate attack. Recent changes in the raw material stream at coal-burning power plants have led to an increase in the availability of class C fly ash, presenting a common scenario where engineers, contractors, and ready-mix concrete producers only have access to class C ashes for use in concrete. This scenario has left many in the industry questioning how this material can be used safely in various applications. This research investigates how gypsum, when used as an admixture, affects the hydration kinetics, hydration product formation, volumetric stability, and long-term sulfate exposure resistance of blends of class C fly ash in neat cement paste and mortar. The findings of this study show a correlation between the formation of hydration products, volumetric stability, and heat of hydration, and also confirm theories posed in previous research.

External sulfate attack (“classical” sulfate attack) is a complex process that involves the formation of cement hydration products that depend on many factors, including raw materials in the concrete mixture, time of exposure, and environment. In general, the onset of sulfate attack may occur when a concrete specimen is in direct contact with one of multiple forms of sulfate that exist naturally in the earth’s crust or in ground water [1]. Presently, there is agreement in literature [1, 2], material testing societies [3], and a considerable amount of research that the primary way to produce a sulfate-attack-resistant (sulfate-resistant) cement binder is to limit the amount of tri-calcium aluminate (C_3A) within a given mixture.

A relatively recent compilation of research [4] outlines the typical hydration process of C_3A in portland cement. The compilation indicates that C_3A reacts with sulfates, mainly $CaSO_4 \cdot 2H_2O$ (gypsum), to rapidly form $C_6A\bar{S}_3H_{32}$ (AFt or ettringite). This reaction continues until the C_3A has depleted the sulfates, at which point the C_3A begins to react with the newly formed AFt, thereafter producing $3C_4A\bar{S}H_{12}$ (AFm or monosulfoaluminate). Once hydrated, most portland cements will have some amount of AFm or AFt within the cement paste matrix. If the AFm within the matrix comes in contact with external sulfates (from ground water or soil), the AFm will revert back to

AFt. The reversion from AFm to AFt is external sulfate attack. It is an expansive reaction that may lead to cracking and degradation of the concrete and general loss of cohesion between constituent materials within the cement paste matrix.

Several researchers have shown that using high-calcium fly ash at normal replacement levels (nominally less than 40% by weight) will produce cement binders with inferior sulfate resistance [5, 6, 7, 8, 9, 10, 11, 12]. The decrease in sulfate resistance has been attributed to mineralogical aspects of fly ash, namely calcium aluminate glass and C_3A content within the fly ash [5, 13, 14, 15]. The presence and form of C_3A in fly ash is the result of the type of coal burned and the coal-burning process respectively. Researchers [10, 15] have shown that high-calcium fly ashes containing a combination of calcium aluminate glass and crystalline forms of C_3A will typically lead to reduced sulfate resistance.

Research conducted on a wide variety of United States fly ash [16] showed that common crystalline phases in fly ash are lime, hematite, magnetite, C_3A , periclase, mellite, quartz, mullite, and anhydrite. Researchers [7] have determined that the crystalline phases most responsible for initiating the sulfate attack mechanism in cementitious blends of fly ash and cement are C_3A , ghelenite, periclase, and anhydrite.

The location of the amorphous fraction of a fly ash when plotted on a ternary phase diagram of CaO , SiO_2 , and Al_2O_3 has been used in previous research to indicate a fly ash's tendency to initiate sulfate attack when used in a cement binder. One researcher [5] plotted the amorphous composition of fly ashes (known to produce inferior sulfate resistance) on a ternary phase diagram that indicated the amorphous content will generally fall into one of three regions on the ternary phase diagram: mullite (A_3S_2), anorthoite (CAS_2), or gehlenite (C_2AS), each of which contain alumina (Figure 6.1). When the ash composition falls within the gehlenite region of the diagram, that ash will reduce the sulfate resistance, as it was concluded [5] and has been shown [9, 17]. Research on this topic indicates that ashes falling within the lower anorthoite and the gehlenite regions are believed to contain highly reactive calcium aluminate glass, which will reduce the sulfate resistance when used in a cement binder. In general, when a given fly ash is known to produce inferior sulfate resistance, and its mineralogical composition is plotted on a ternary phase diagram ($CaO - SiO_2 - Al_2O_3$), there will typically be a cluster of points around the gehlenite region.

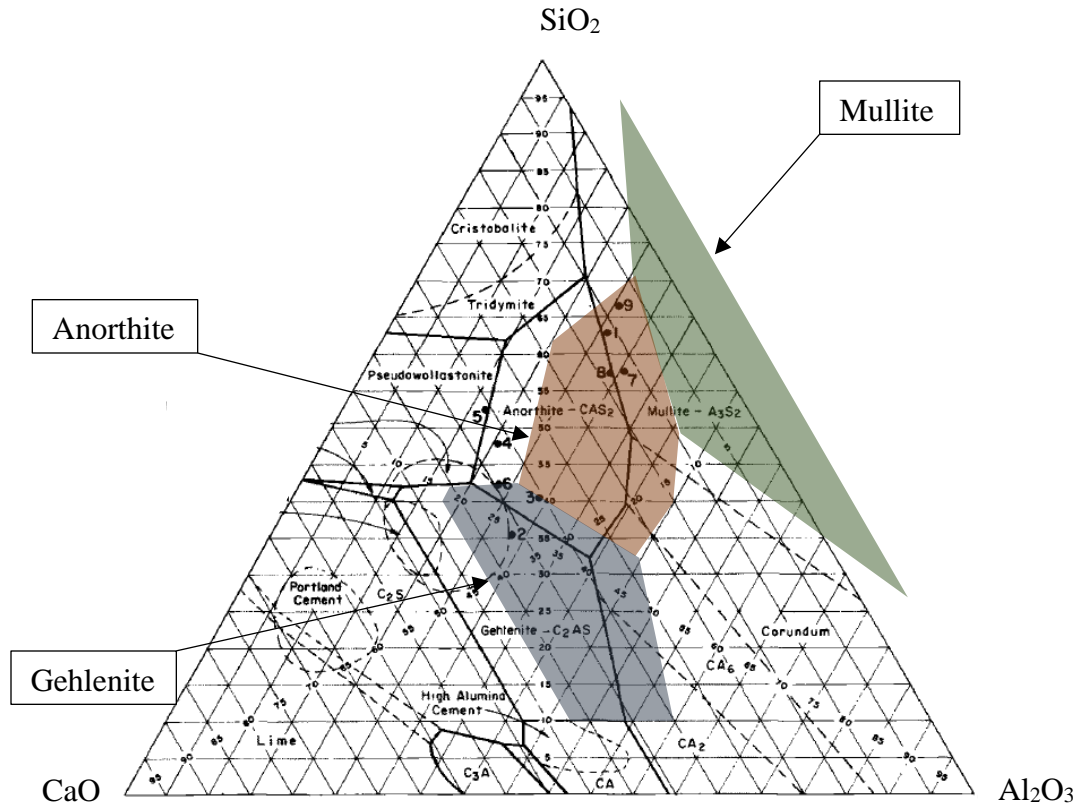


Figure 6.1 $\text{CaO} - \text{SiO}_2 - \text{Al}_2\text{O}_3$ ternary phase diagram [5] with mullite, anorthite, and ghelenite regions annotated by author

Multiple methods for increasing the sulfate resistance of cement binders exist. A common method for producing a sulfate-resistant cement binder is through the use of SCM. Utilizing pozzolanic SCMs such as SF or low-calcium fly ash has shown to be effective at inhibiting or decreasing sulfate attack [5, 6, 18, 14, 17, 9]. Using ultra-fine fly ash as a replacement of cement has produced promising results in promoting sulfate resistance [9, 11]. Research studies [9, 17, 19] have indicated that using high volumes (greater than 60% replacement of cement) of high-calcium fly ash have also proven effective. Another strategy for increasing sulfate resistance was lowering the w/c ratio in an attempt to create a denser cement paste matrix (i.e., less permeable) [9], thereby disallowing the ingress of sulfates into the paste matrix.

Researchers have attempted to mitigate sulfate attack in blends of high-calcium fly ash and portland cement by using gypsum and other sulfates as admixtures [7, 20]. This approach is referred to as “super-sulfating” the mix. The underlying theory in this approach is that the addition of sulfates as an admixture would react with the additional C_3A resulting from the inclusion of high-calcium fly ash to produce and/or stabilize Aft during early ages of the cement or concrete’s lifespan. It is believed that if Aft is stabilized early, and AFm is inhibited from forming, then when the concrete/cement binder comes in contact with

external sulfates, there will be nothing for the external sulfates to react with and the sulfate attack mechanism will be controlled. This theory has been tested by researchers [8, 9, 20] at the UT Concrete Lab and is the primary focus of this research study.

6.2. Naming Convention

A naming convention and mixture identification number (Mix ID) system was established to clearly indicate which materials were used to conduct the research presented in this report. The naming and mixture identification convention consists of the following abbreviations:

C# : cement number

F#(%): fly ash number (% of cement replacement)

G(%): gypsum (% admixture)

Example construction of a Mix ID

Assume the following materials were used:

Cement: C1

Fly Ash: F1 with a 35% replacement of cement

4% gypsum admixture

Solution for the construction of a mixture identification number

Mix ID: C1-F1(35)-G(4)

6.3. Materials

All cements and fly ashes used in this research are commercially available products. Each material was analyzed with XRF to determine the bulk oxide contents, as well as quantitative x-ray diffraction (QXRD) to determine the mineralogical composition of the given material. The XRF testing was performed by the TxDOT Materials Lab in Cedar Park, Texas. The XRD was performed on a Siemens D500 Diffractometer with scanning parameters of 5–70 2 θ degrees, with a step of 0.02, and 6 second dwell time. Rietveld refinement was performed on the XRD scans using TOPAS academic V4.1 software. Sample preparation for XRD included passing the cement or fly ash powders through a number 140 sieve, adding rutile as an internal standard at a constant value of $10.0 \pm 0.01\%$, thoroughly mixing the rutile and the given powder into a slurry using 99.5% pure isopropanol, allowing the slurry to completely dry in a desiccator, followed by scraping

the powder into the sample holder with a razor blade and leveling the sample with a glass plate.

6.3.1. Fly Ash

Three commercially available Texas fly ash sources were utilized in this research study. The bulk oxide content and mineralogical composition for each of the fly ashes is presented in Table 6.1. Fly ash identification numbers shown in Table 6.1 were organized to correlate with low to high CaO contents.

Table 6.1 XRF and QXRD analysis results for fly ashes

	Fly Ashes				Fly Ashes		
XRF	F1	F2	F3	QXRD	F1	F2	F3
Oxides	wt. %	wt. %	wt. %	Phase	wt. %	wt. %	wt. %
CaO	21.7	24.5	26.6	Quartz	6.6	3.9	5.9
SiO ₂	39.1	35.7	35.4	Anhydrite	1.1	2.0	1.5
Al ₂ O ₃	20.6	19.4	17.7	Gehlenite	0.1	0.6	0.6
Fe ₂ O ₃	6.0	6.1	5.3	Periclase	1.7	1.6	3.2
SO ₃	1.0	2.4	1.5	C ₃ A _{cubic}	3.0	3.4	6.4
MgO	4.4	4.5	6.2	C ₃ A _{orthorhombic}	2.3	1.9	4.6
K ₂ O	0.7	0.5	0.4	Merwinite	4.1	2.4	4.5
Na ₂ O	1.3	1.5	1.9	C ₂ S β	3.8	4.3	6.0
Na ₂ O _e	1.8	1.9	2.1	Amorphous	77.3	80.0	67.4
SiO ₂ +Al ₂ O ₃ +Fe ₂ O ₃	65.6	61.1	58.5	Total C ₃ A	5.3	5.3	11.0

6.3.2. Cements

Two commercially available Texas cements were used in this research. The chemical and mineralogical composition for each of the cements is presented in Table 6.2. Also shown are the Bogue values, calculated per ASTM C150-16.

Table 6.2 XRF, QXRD, and Bogue calculations for cements used in this study

	Cements			Cements			Cements	
XRF	C1	C2	QXRD	C1	C2	Bogue	C1	C2
Oxide	wt. %	wt. %	Phase	wt. %	wt. %	Phase	wt. %	wt. %
CaO	64.8	64.5	Alite (C ₃ S)	49.1	46.5	Alite (C ₃ S)	63.2	59.3
SiO ₂	19.8	20.7	Belite (C ₂ S)	19.1	24.2	Belite (C ₂ S)	9.1	14.5
Al ₂ O ₃	5.5	4.9	C ₃ A _{cubic}	6.6	2.4	C ₃ A	10.8	7.1
Fe ₂ O ₃	2.3	3.5	C ₃ A _{orthorhombic}	2.3	2.3	C ₄ AF	6.9	10.8
Na ₂ O	0.2	0.1	C ₄ AF	4.7	8.2			
MgO	1.2	1.2	Periclase	0.0	0.0			
K ₂ O	1.0	0.7	Arcanite	2.7	2.3			
P ₂ O ₅	0.3	0.2	Anhydrite	0.0	0.0			
SO ₃	3.4	2.8	Bassanite	7.3	4.2			
Cl	0.0	0.0	Gypsum	0.1	1.9			
TiO ₂	0.2	0.2	Amorphous	8.2	8.1			
SrO	0.1	0.1	Total C ₃ A	8.9	4.6			
Mn ₂ O ₃	0.0	0.0						
ZnO	0.0	0.0						
Cr ₂ O ₃	0.0	0.0						

6.3.3. Particle Characterization

Extensive work was performed by researchers [9, 10, 15] to characterize physical and chemical characteristics of fly ash. The work cited above was done on fly ashes from the same source as those which are part of this research study, and have nominally the same bulk oxide content, and mineralogical composition. A portion of the research cited above [9, 15] used scanning electron microscopy, in conjunction with energy-dispersive X-ray analysis and XRF, to quantify and delineate the glass and crystalline composition of the fly ashes. That research allowed for the production of the differing fly ashes to be plotted on CaO-SiO₂-Al₂O₃ phase diagrams, presented in Figure 6.2. Additionally, the scanning electron microscopy analysis allowed the researchers to determine an average particle size for the glass, presented in Table 6.3 [15].

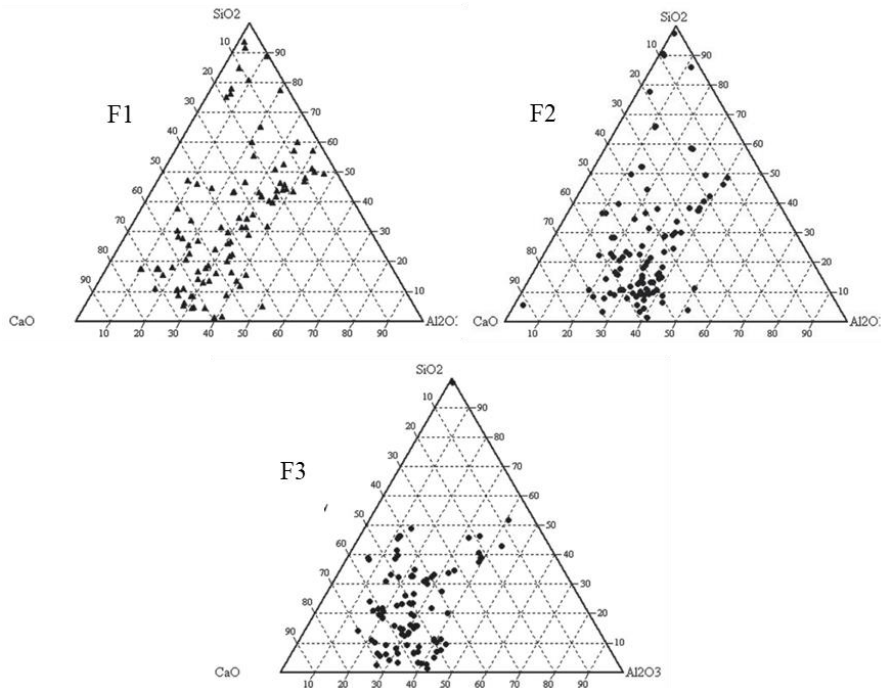


Figure 6.2 Fly ash glass distribution on CaO-SiO₂-Al₂O₃ ternary phase diagram [15]

The second portion of the research cited [10] in this section performed particle distribution analysis on a wide array of commercially available fly ashes. In general, particle size distribution analysis provides insight into the proportion of the volume of a given fly ash that is of a specific size range. Particle size distribution data from the aforementioned study is presented in Table 6.3. One of the notable findings from the referenced study [10] (as it relates to this research) indicated that high-calcium fly ashes containing relatively finer particles (not ultra-fine fly ash) tend to be more susceptible to sulfate attack when used in cement binders.

Table 6.3 Average particle size and particle size distribution for ash used herein

Fly Ash ID	*Average particle size	** Approximate percentage of volume of ash less than or equal to average particle size
	[μm]	[%]
F1	7.1	35
F2	3.7	20
F3	3.1	25

* Research performed by [15]

** Research performed by [10]

6.3.4. Material Characterization

6.3.4.1. Cement

Values shown in Table 6.2 indicate that C1 and C2 meet the standard composition requirements outlined in ASTM C150-16 for a Type I and Type I/II cement respectively [3]. Note the discrepancy between the phase compositions determined by Bogue and those measured using QXRD analysis. The total C_3A content measured by QXRD of C1 and C2 was 8.9% and 4.7% respectively, whereas the Bogue composition showed C1 and C2 having 10.8% and 7.1% C_3A respectively. If the cements were classified using the QXRD analysis, cement C1 would be classified as a type I and cement C2 a type V by ASTM C 150-16.

6.3.4.2. Fly Ash

Information presented in Table 6.1 indicates the fly ashes used in this study meet the chemical requirements in ASTM C618 of a class C fly ash [21]. Additionally, Table 6.1 shows that the C_3A content increases with increasing CaO content.

As indicated in Figure 6.1 the glass (amorphous) content of the fly ashes used in this study form a locust of points in the gehlenite region of the ternary phase diagram (highlighted in Figure 6.1), which indicates that the fly ashes used in this study should produce inferior sulfate resistance when used as a partial replacement for cement.

The research studies cited [9, 15] in Section 6.3.3 provided a delineation between amorphous and crystalline fractions of SiO_2 , Al_2O_3 , CaO, and SO_3 of fly ashes (of nominally equal chemical and mineralogical composition) used in this study. Figure 6.2 indicates the relative percentages of crystalline and amorphous content of the minerals listed above.

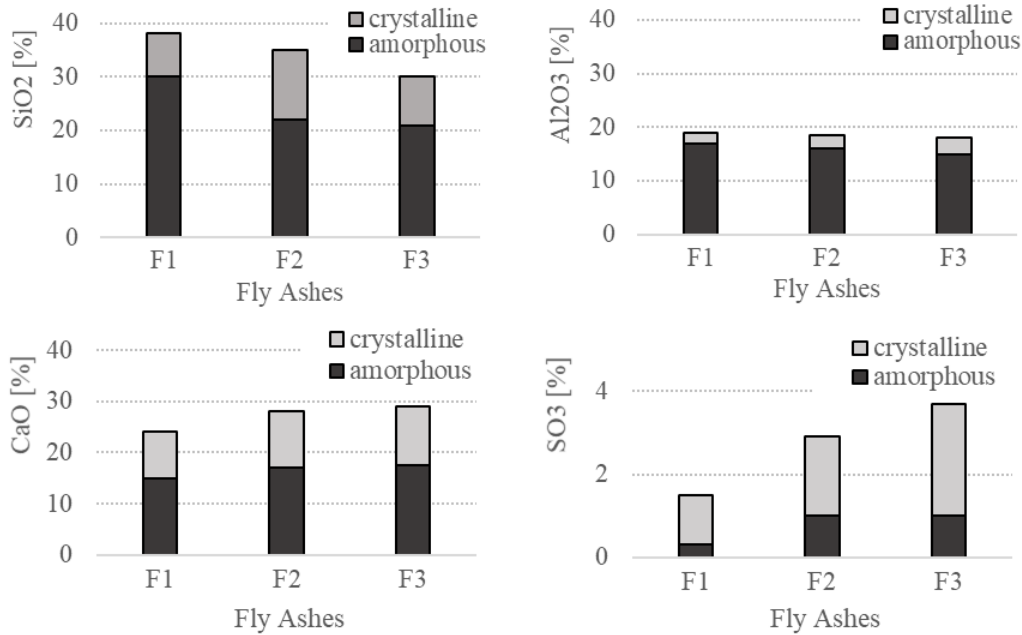


Figure 6.3. Crystalline and amorphous oxide contents of fly ashes [15]

6.3.4.3. Gypsum

A commercially available source of calcium sulfate dehydrate ($\text{CaSO}_4 \cdot \text{H}_2\text{O}$) meeting the requirements of ASTM C452-15 was procured from the U.S. Gypsum Company. The calcium sulfate dehydrate (gypsum) was Terra Alba, Food & Pharmaceuticals grade 100% gypsum by weight [22].

6.4. Testing Methods

6.4.1. ASTM C 1012 Testing

Guidelines and provisions outlined in ASTM C 1012 [23] were followed with the exception that all mixtures were prepared with a constant w/c ratio of 0.485. The mixture proportions for the specimens tested in ASTM C 1012 are presented in Tables 6.4 and 6.5. Two phases of ASTM C 1012 testing were performed, the reason for which will be discussed in Section 6.5.2. To provide a clear distinction between phase one and two of ASTM C 1012 testing, Mix IDs corresponding to testing performed as part of phase 2 have been shaded in Tables 6.4 and 6.5. In total, 40 mixtures were prepared for phase 1, and 16 mixtures were prepared for phase 2.

Table 6.4 Mortar mixture proportions for ASTM C1012 testing of cement C1

MIX ID	Cement Type	Fly Ash			Gypsum (%)
		F1(%)	F2(%)	F3(%)	
C1-F1(20)-G(0)	C1	20			0
C1-F1(20)-G(6)		20			6
C1-F1(20)-G(8.7)		20			8.7
C1-F1(20)-G(11.6)		20			11.6
C1-F1(20)-G(12.2)		20			12.2
C1-F1(20)-G(15.2)		20			15.2
C1-F1(35)-G(0)	C1	35			0
C1-F1(35)-G(8)		35			8
C1-F1(35)-G(10.5)		35			10.5
C1-F1(35)-G(11.8)		35			11.8
C1-F1(35)-G(14)		35			14
C1-F1(35)-G(15)		35			15
C1-F2(20)-G(0)	C1		20		0
C1-F2(20)-G(6)			20		6
C1-F2(20)-G(7.6)			20		7.6
C1-F2(20)-G(10.2)			20		10.2
C1-F2(20)-G(10.7)			20		10.7
C1-F2(20)-G(13.4)			20		13.4
C1-F2(35)-G(0)	C1		35		0
C1-F2(35)-G(8)			35		8
C1-F2(35)-G(8.5)			35		8.5
C1-F2(35)-G(11.4)			35		11.4
C1-F2(35)-G(11.9)			35		11.9
C1-F2(35)-G(14.8)			35		14.8
C1-F3(20)-G(0)	C1			20	0
C1-F3(20)-G(6)				20	6
C1-F3(35)-G(0)	C1			35	0
C1-F3(35)-G(8)				35	8

Table 6.5 Mortar mixture proportions for ASTM C1012 testing of cement C2

MIX ID	Cement Type	Fly Ash			Gypsum (%)
		F1(%)	F2(%)	F3(%)	
C2-F1(20)-G(0)	C2	20			0
C2-F1(20)-G(3.2)		20			3.2
C2-F1(20)-G(4.3)		20			4.3
C2-F1(20)-G(6)		20			6
C2-F1(20)-G(9)		20			9
C2-F1(20)-G(11.2)		20			11.2
C2-F1(35)-G(0)	C2	35			0
C2-F1(35)-G(6)		35			6
C2-F1(35)-G(8)		35			8
C2-F1(35)-G(8)		35			8
C2-F1(35)-G(11.8)		35			11.8
C2-F1(35)-G(14.7)		35			14.7
C2-F2(20)-G(0)	C2		20		0
C2-F2(20)-G(2.1)			20		2.1
C2-F2(20)-G(2.8)			20		2.8
C2-F2(20)-G(6)			20		6
C2-F2(20)-G(7.5)			20		7.5
C2-F2(20)-G(9.4)			20		9.4
C2-F2(35)-G(0)	C2		35		0
C2-F2(35)-G(4.1)			35		4.1
C2-F2(35)-G(5.4)			35		5.4
C2-F2(35)-G(8)			35		8
C2-F2(35)-G(9.23)			35		9.23
C2-F2(35)-G(11.5)			35		11.5
C2-F3(20)-G(0)	C2			20	0
C2-F3(20)-G(6)	C2			20	6
C2-F3(35)-G(0)	C2			35	0
C2-F3(35)-G(8)				35	8

6.4.2. Limewater Submergence Testing

Limewater submergence testing (LST) consisted of submerging mortar bars in a saturated lime water solution and measuring length change over time. The LST of mortar bars used in this study is a modified version of ASTM C 1038. The mortar bars were proportioned, mixed, and cured in accordance with the same specifications outlined in ASTM C 1012 with the exception that the w/c ratio was a constant 0.485 for all mixtures. For each mixture four mortar bars (three for measuring length change and one for XRD measurements) and six to nine mortar cubes (for compressive strength testing) were prepared. After the mortar cured for one day at $35 \pm 3^\circ\text{C}$, the forms were stripped, an initial length measurement was taken, the mortar bars were placed in a saturated lime water solution, and the mortar cubes were tested for their compressive strength. Subsequent length change measurements were taken at 1, 3, 7, 14, 21, 28, 56, 91, and 105 days. Compressive strength was tested until the mortar reached a compressive strength of 20 ± 1.0 MPa. The mixture proportions for LST are presented in Table 6.6.

Table 6.6 Mixture proportions for LST and Isothermal Calorimetry

Mix ID	Gypsum Admixture Dosages (%)							
C1-F1(20)	0	2	4	6	8	10	12	15
C1-F1(35)	0	2	4	6	8	10	12	15
C1-F2(20)	0	2	4	6	8	10	12	15
C1-F2(35)	0	2	4	6	8	10	12	15
C1-F3(20)	0	2	4	6	8	10	12	15
C1-F3(35)	0	2	4	6	8	10	12	15
C2-F1(20)	0	2	4	6	8	10	12	15
C2-F1(35)	0	2	4	6	8	10	12	15
C2-F2(20)	0	2	4	6	8	10	12	15
C2-F2(35)	0	2	4	6	8	10	12	15
C2-F3(20)	0	2	4	6	8	10	12	15
C2-F3(35)	0	2	4	6	8	10	12	15

6.4.3. Isothermal Calorimetry

Mixture proportions for isothermal calorimetry testing are shown in Table 6.6. Neat cement paste (cement, fly ash, de-ionized water, and gypsum) was used for this testing regime. Cement pastes were prepared with a w/c ratio of 0.38. All dry ingredients were kept in a temperature-controlled room allowing for temperature equilibrium (of 23°C) between the constituents to be met prior to mixing. The dry ingredients were placed in an ADIACAL TC isothermal calorimeter container cup, and thoroughly combined using a vibrating table for 90 seconds; thereafter water was added to make a paste. The cement paste was stirred by hand using a glass stir for 60 seconds, then mixed on the vibrating table for an additional 60 seconds. After mixing, the specimens were immediately placed in a Grace ADIACAL

TC isothermal calorimeter where the heat of hydration was measured every 60 seconds for a period of 7 days (168 hours).

6.4.4. X-Ray Diffraction and Rietveld Refinement

XRD techniques were performed on fragments of mortar bars that were extracted from LST at two different ages. Upon an average of two mortar cubes from a respective mixture achieving a compressive strength of 20 MPa (2850 ± 150 psi), a mortar bar was selected from the mix and broken in two equal halves; thereafter an approximate 50 mm (2 inch) portion was removed from one of the halves of the mortar bar for XRD analysis. The remaining pieces of the mortar bar were placed back in the saturated limewater solution. At 28 days after casting, the larger half of the remaining mortar bar was removed from the saturated limewater solution, broken in two more halves, and an approximate 50 mm (2 inch) portion was removed for additional XRD analysis.

The XRD analysis for LST was performed on a Siemens D500 Diffractometer with scanning parameters of 5° to 60° 2θ degrees, with a step of 0.02, and 6 second dwell time. Rietveld refinement was performed on the XRD scans using TOPAS academic V4.1 software. Sample preparation for XRD included grinding a respective 50 mm sample in a mortar and pestle into a fine powder, passing the powder through a number 140 sieve, placing the powder in sealed container and then a desiccator to fully dehydrate the sample of moisture for a period of at least one week, removing the sample from the desiccator and adding rutile as an internal standard at a constant value of approximately $10 \pm 0.01\%$, and finally thoroughly mixing and grinding the rutile and powder into a slurry using 99.5% pure isopropanol, allowing the slurry to completely dry into a powder. Final sample preparation included scraping the powder into the sample holder with a razor blade and leveling the sample with a glass plate.

6.5. Results and Discussion

The tests conducted as part of this research study were carried out to meet two goals, both of which include using high-calcium fly ash as partial replacement of a cement binder. The first goal was to confirm the effectiveness of a method of sulfate attack mitigation developed [7] and tested by previous researchers [8, 9]. The second goal was to develop a short-term testing method by which the proper amount of sulfate (gypsum) dosage could be determined such that the sulfate attack mechanism in cement binders containing high-calcium fly ash would be mitigated.

6.5.1. Exposure Conditions

Deterioration to concrete due to sulfate attack is the result of the type of exposure to which the concrete element is subjected. The American Concrete Institute (ACI) has defined sulfate exposure conditions as shown in Table 6.7.

Table 6.7 Defined exposure conditions per ACI Table 19.3.1.1

Sulfate (S)	Class	Water-soluble sulfate (SO_4^{2-}) in soil, percent by mass ^[1]	Dissolved sulfate (SO_4^{2-}) in water, ppm ^[2]
	S0	$\text{SO}_4^{2-} < 0.10$	$\text{SO}_4^{2-} < 150$
	S1	$0.10 \leq \text{SO}_4^{2-} < 0.20$	$150 \leq \text{SO}_4^{2-} < 1,500$ or seawater
	S2	$0.20 \leq \text{SO}_4^{2-} < 2.00$	$1,500 \leq \text{SO}_4^{2-} < 10,000$
	S3	$\text{SO}_4^{2-} > 2.00$	$\text{SO}_4^{2-} > 10,000$

[1] Percent sulfate by mass in soil shall be determined by ASTM C1580.

[2] Concentration of dissolved sulfates in water, in ppm, shall be determined by ASTM D516 or ASTM D4130.

6.5.2. Limewater Submergence Testing

6.5.2.1. Results

LST was performed to determine the effects that gypsum imposed on the cement binder and/or mortar. Of primary interest was assessing volume stability and identifying hydration products that formed during the early ages (within 28 days). Expansion results from the LST are shown in Tables 6.8–6.11. In the interest of being concise, the tables include expansion data only for 3, 7, 14, 28, and 105 days. Measurements taken at 105 days indicated that the mortar bars were no longer expanding. The data table includes **bolded** values, which indicate when a mortar bar expanded beyond 0.10% (the expansion limit imposed by ASTM C 1012). Additionally, the expansion results are plotted in Figures 6.4–6.7 to provide a graphical representation of the results. Note that the leader lines in the plots indicate the gypsum dosage for the given mix.

Table 6.8 LST expansion results for cement C1 with 35% replacement of ashes F1-F3

Mix ID	Gypsum [%]	Expansion [days]				
		3	7	14	28	105
C1-F1(35)	0	0.013%	-0.001%	-0.015%	0.006%	0.007%
	2	0.011%	0.026%	0.020%	0.010%	0.006%
	4	0.013%	0.014%	0.013%	0.008%	0.004%
	6	0.013%	0.010%	0.012%	0.008%	0.003%
	8	0.047%	0.057%	0.054%	0.047%	0.040%
	10	0.054%	0.092%	0.096%	0.095%	0.087%
	12	0.061%	0.102%	0.134%	0.162%	0.152%
	15	0.050%	0.091%	0.138%	0.234%	0.454%
C1-F2(35)	0	-0.008%	-0.009%	-0.010%	-0.008%	0.009%
	2	-0.009%	-0.013%	-0.017%	-0.008%	-0.010%
	4	-0.002%	-0.002%	-0.002%	-0.003%	-0.005%
	6	0.000%	-0.009%	-0.019%	-0.003%	-0.002%
	8	0.057%	0.059%	0.061%	0.056%	0.054%
	10	0.047%	0.097%	0.146%	0.143%	0.135%
	12	0.042%	0.109%	0.175%	0.265%	0.257%
	15	0.053%	0.123%	0.193%	0.356%	0.783%
C1-F3(35)	0	0.009%	0.002%	0.006%	0.005%	0.010%
	2	0.001%	0.001%	0.005%	0.004%	0.008%
	4	0.006%	0.001%	0.005%	0.004%	0.008%
	6	0.001%	0.001%	0.004%	0.003%	0.006%
	8	0.031%	0.027%	0.030%	0.028%	0.033%
	10	0.055%	0.109%	0.113%	0.110%	0.111%
	12	0.055%	0.119%	0.171%	0.170%	0.171%
	15	0.045%	0.081%	0.132%	0.241%	0.678%

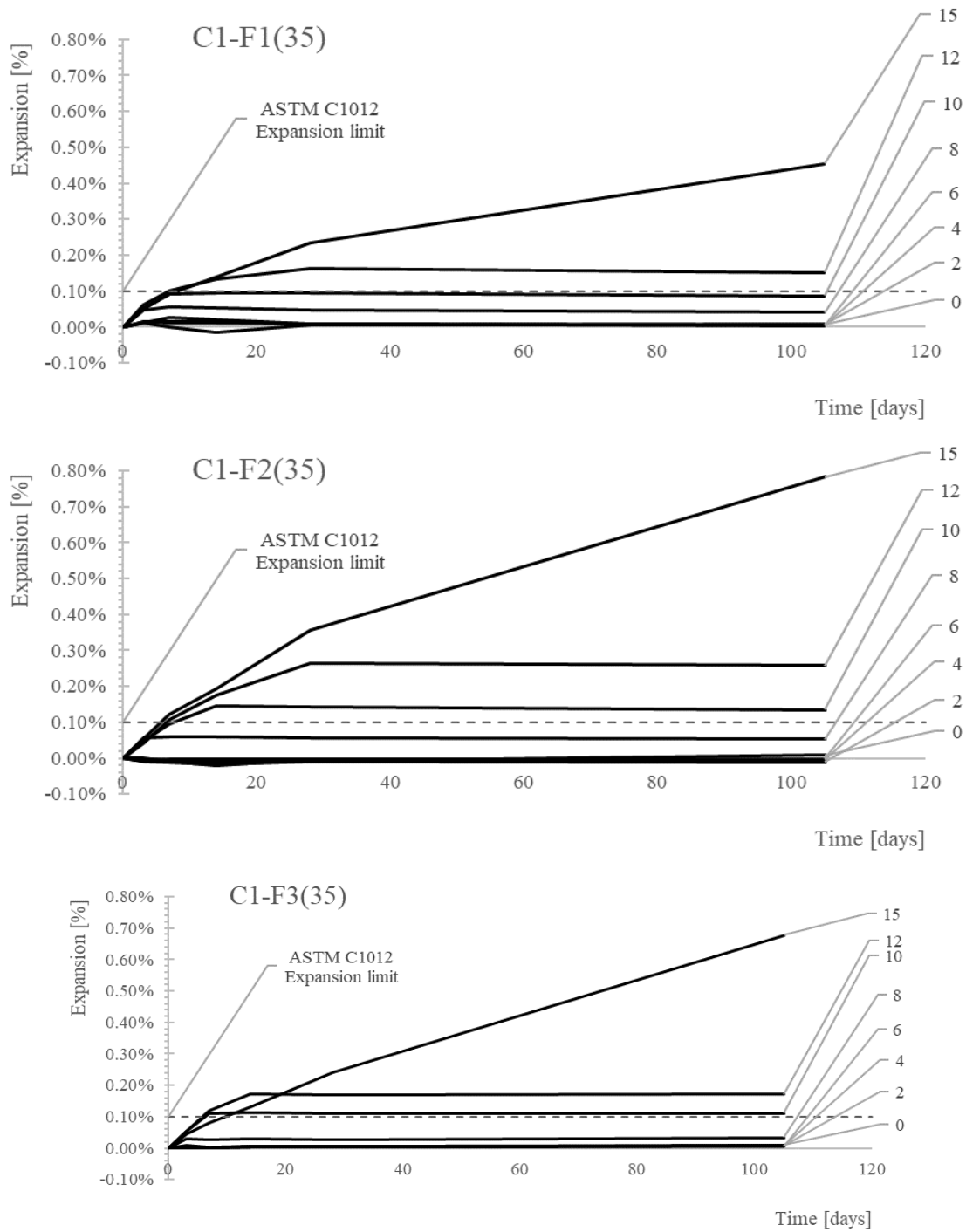


Figure 6.3 LST expansion results for cement C1 with 35% replacement of ashes F1-F3

Table 6.9 LST expansion results for cement C1 with 20% replacement of ashes F1-F3

Mix ID	Gypsum [%]	Expansion [days]				
		3	7	14	28	105
C1-F1(20)	0	-0.010%	-0.007%	-0.009%	-0.012%	-0.005%
	2	-0.009%	-0.012%	-0.012%	-0.015%	-0.007%
	4	0.001%	-0.002%	-0.003%	-0.005%	0.001%
	6	-0.004%	-0.007%	-0.007%	-0.008%	-0.001%
	8	0.028%	0.036%	0.037%	0.035%	0.043%
	10	0.010%	0.028%	0.048%	0.078%	0.092%
	12	0.015%	0.031%	0.056%	0.101%	0.243%
	15	0.012%	0.029%	0.057%	0.108%	0.480%
C1-F2(20)	0	-0.002%	-0.001%	0.001%	0.001%	0.004%
	2	0.007%	-0.004%	0.000%	0.001%	0.002%
	4	0.002%	0.006%	0.007%	0.005%	0.006%
	6	0.016%	0.014%	0.019%	0.014%	0.016%
	8	0.032%	0.067%	0.069%	0.071%	0.074%
	10	0.028%	0.057%	0.096%	0.131%	0.134%
	12	0.032%	0.064%	0.092%	0.159%	0.386%
	15	0.035%	0.069%	0.101%	0.174%	0.632%
C1-F3(20)	0	0.004%	0.002%	0.008%	0.002%	-0.005%
	2	0.009%	0.006%	0.006%	-0.001%	-0.008%
	4	0.005%	0.005%	0.011%	0.006%	0.000%
	6	0.011%	0.012%	0.009%	0.003%	-0.006%
	8	0.023%	0.042%	0.047%	0.046%	0.041%
	10	0.021%	0.038%	0.064%	0.096%	0.096%
	12	0.017%	0.030%	0.050%	0.119%	0.336%
	15	0.019%	0.040%	0.060%	0.112%	0.459%

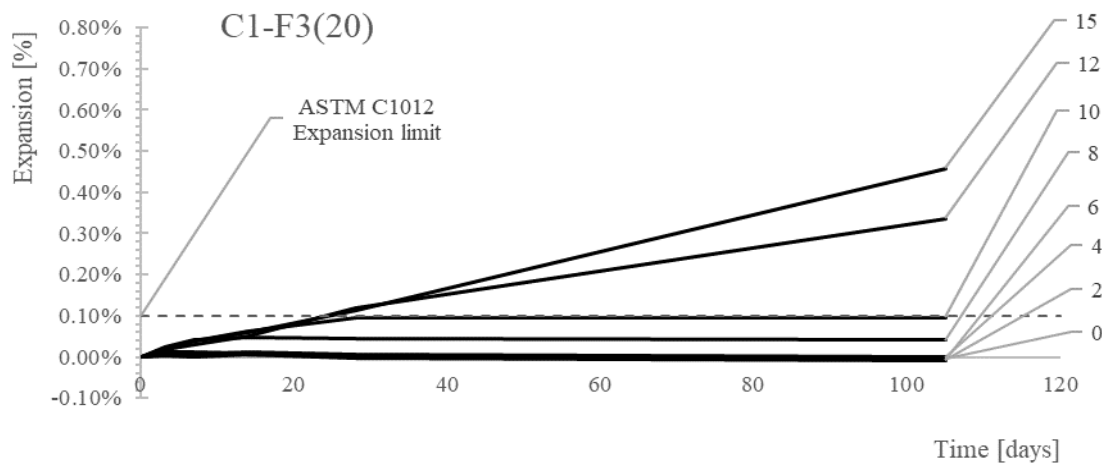
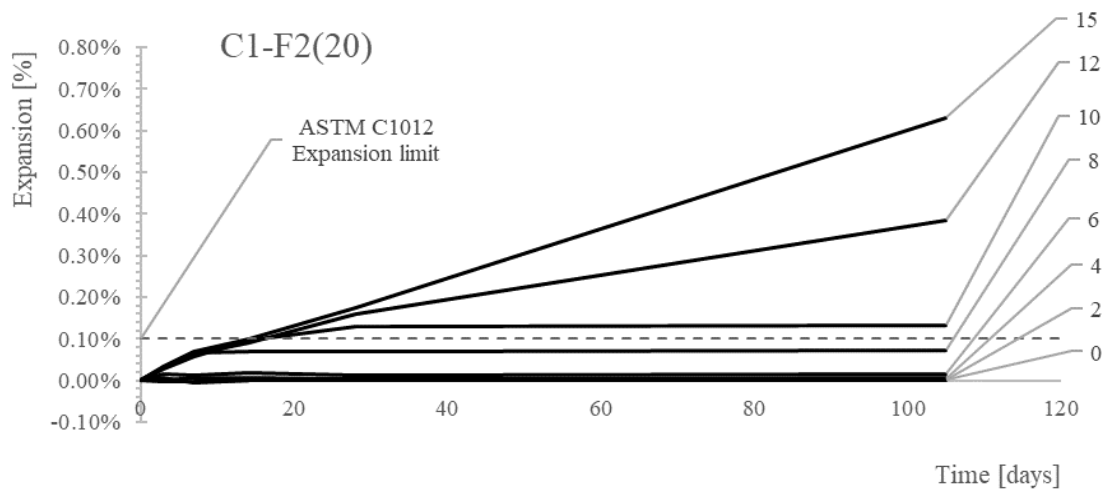
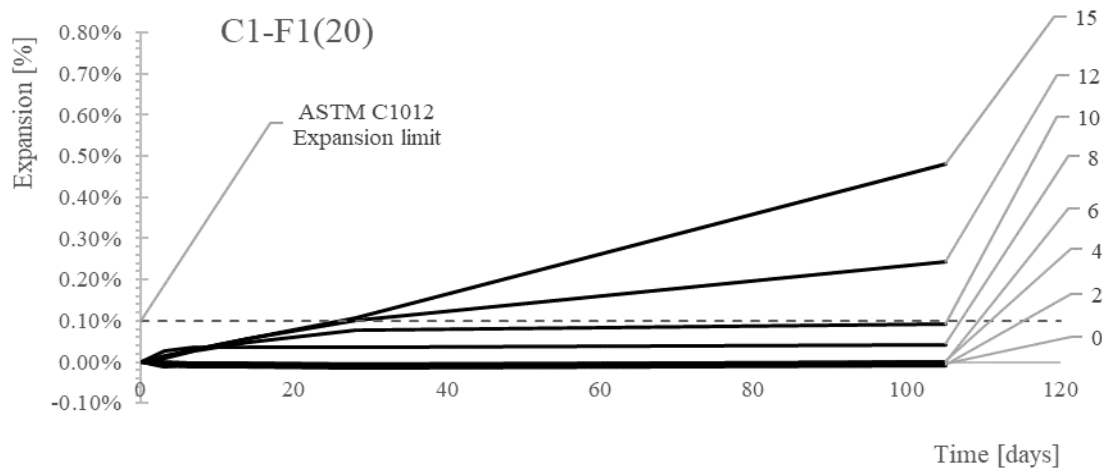


Figure 6.4 LST expansion results for cement C1 with 20% replacement of ashes F1-F3

Table 6.10 LST expansion results for cement C2 with 35% replacement of ashes F1-F3

Mix ID	Gypsum [%]	Expansion [days]				
		3	7	14	28	105
C2-F1(35)	0	-0.008%	-0.010%	-0.011%	0.001%	-0.005%
	2	-0.004%	-0.006%	-0.006%	0.004%	-0.002%
	4	-0.002%	-0.004%	-0.004%	0.010%	-0.002%
	6	-0.003%	-0.005%	-0.002%	0.007%	-0.001%
	8	0.022%	0.019%	0.021%	0.028%	0.021%
	10	0.025%	0.043%	0.052%	0.061%	0.049%
	12	0.028%	0.051%	0.073%	0.098%	0.088%
	15	0.024%	0.045%	0.085%	0.153%	0.261%
C2-F2(35)	0	-0.009%	-0.012%	-0.012%	-0.004%	-0.007%
	2	0.002%	0.000%	-0.001%	0.005%	0.003%
	4	0.004%	0.018%	0.001%	0.005%	0.005%
	6	0.005%	0.016%	0.003%	0.014%	0.008%
	8	0.044%	0.048%	0.044%	0.054%	0.046%
	10	0.055%	0.094%	0.103%	0.104%	0.101%
	12	0.037%	0.069%	0.114%	0.221%	0.494%
	15	0.055%	0.096%	0.147%	0.250%	0.532%
C2-F3(35)	0	-0.005%	-0.004%	-0.002%	0.000%	0.006%
	2	-0.005%	-0.004%	-0.001%	-0.001%	0.005%
	4	-0.004%	-0.002%	0.000%	0.001%	0.005%
	6	-0.001%	0.000%	0.003%	0.003%	0.008%
	8	0.019%	0.020%	0.023%	0.022%	0.028%
	10	0.035%	0.064%	0.068%	0.068%	0.072%
	12	0.037%	0.071%	0.111%	0.118%	0.121%
	15	0.033%	0.062%	0.102%	0.193%	0.398%

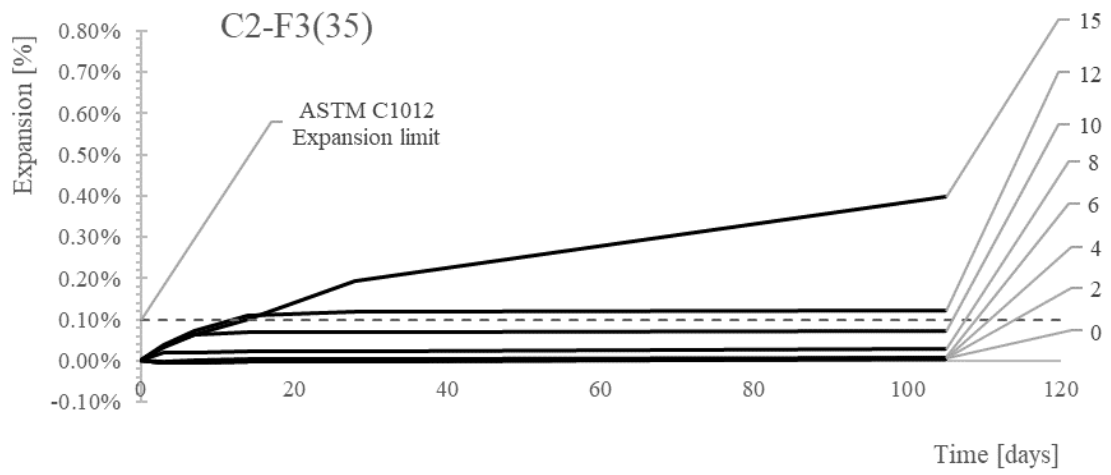
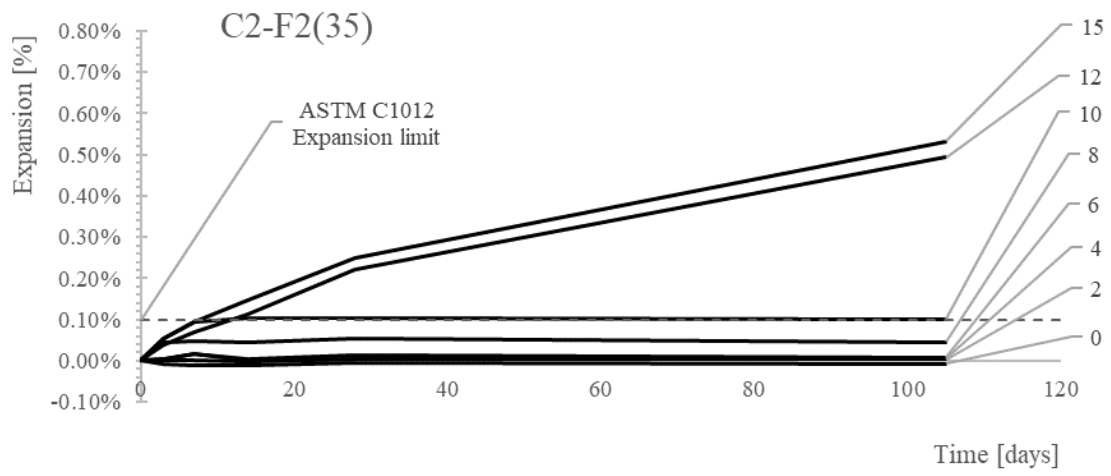
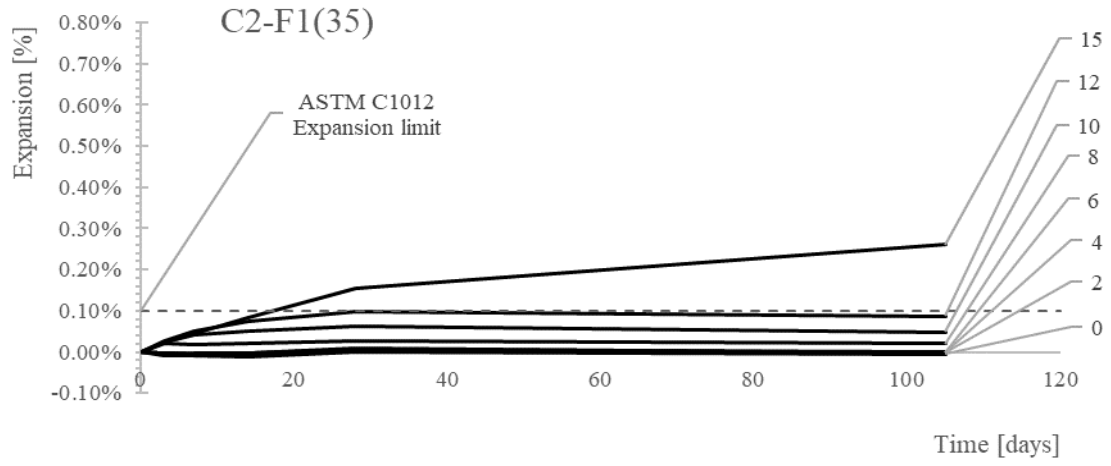


Figure 6.5 LST expansion results for cement C2 with 35% replacement of ashes F1-F3

Table 6.11 LST expansion results for cement C2 with 20% replacement of ashes F1-F3

Mix ID	Gypsum [%]	Expansion [days]				
		3	7	14	28	105
C2-F1(20)	0	-0.002%	-0.002%	-0.004%	-0.002%	-0.001%
	2	-0.002%	-0.005%	0.000%	-0.001%	0.000%
	4	0.002%	0.003%	0.000%	0.002%	0.004%
	6	0.006%	0.005%	0.011%	0.005%	0.009%
	8	0.019%	0.026%	0.027%	0.027%	0.030%
	10	0.015%	0.026%	0.042%	0.056%	0.056%
	12	0.014%	0.028%	0.038%	0.066%	0.139%
	15	0.016%	0.036%	0.049%	0.086%	0.240%
C2-F2(20)	0	-0.004%	-0.006%	-0.008%	-0.005%	-0.008%
	2	-0.005%	-0.004%	-0.003%	-0.017%	-0.007%
	4	-0.006%	-0.006%	-0.007%	-0.007%	-0.006%
	6	0.001%	-0.001%	-0.002%	-0.008%	-0.002%
	8	0.021%	0.026%	0.030%	0.014%	0.025%
	10	0.014%	0.045%	0.077%	0.050%	0.056%
	12	0.016%	0.040%	0.064%	0.081%	0.120%
	15	0.015%	0.037%	0.059%	0.096%	0.329%
C2-F3(20)	0	-0.009%	-0.009%	-0.014%	-0.007%	-0.005%
	2	-0.009%	-0.002%	-0.010%	-0.003%	0.000%
	4	-0.008%	-0.004%	-0.008%	-0.002%	0.001%
	6	-0.009%	-0.003%	-0.007%	0.000%	0.001%
	8	-0.013%	0.000%	-0.007%	0.001%	0.002%
	10	0.001%	0.023%	0.032%	0.061%	0.066%
	12	0.005%	0.025%	0.038%	0.074%	0.119%
	15	0.012%	0.031%	0.044%	0.084%	0.270%

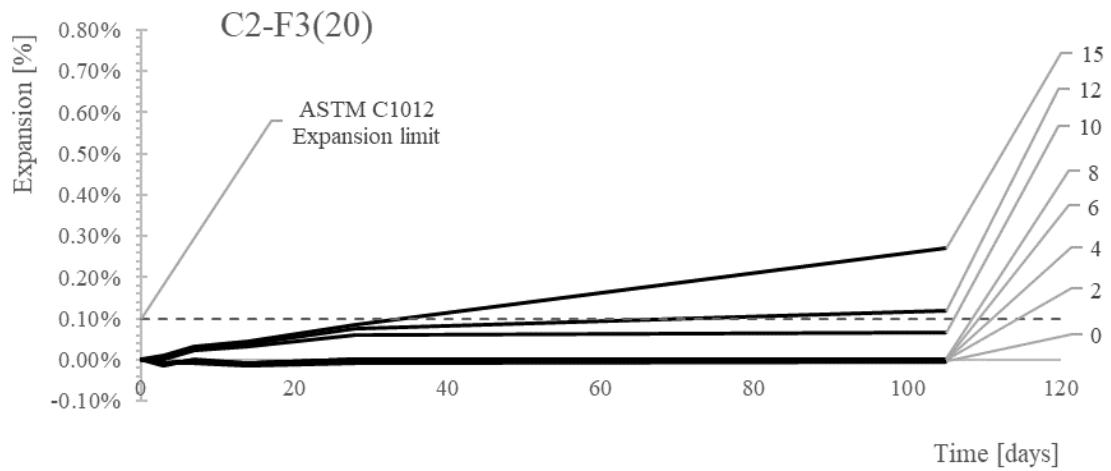
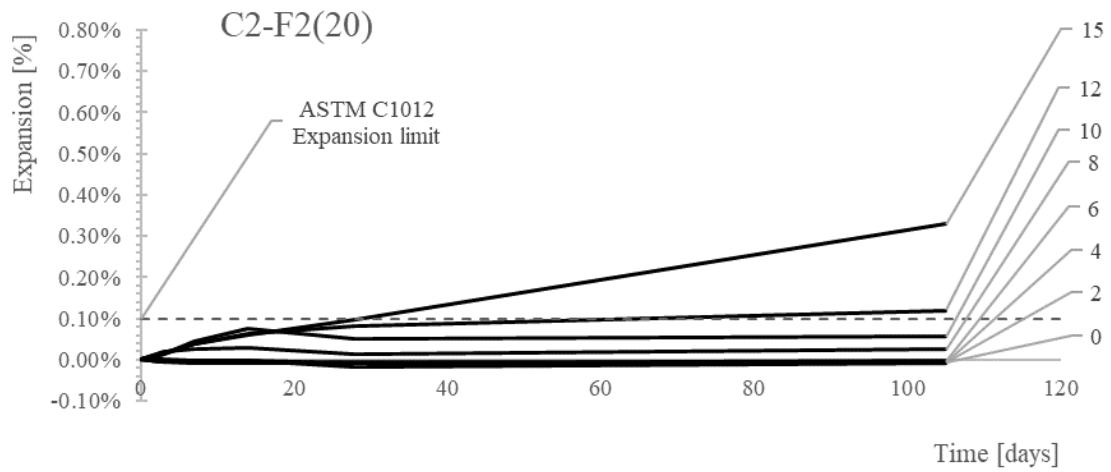
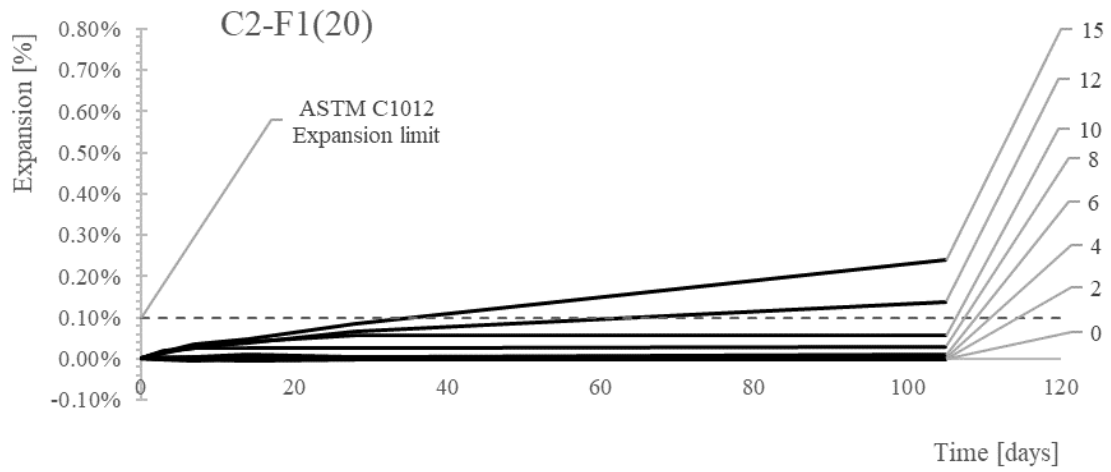


Figure 6.7 LST expansion results for cement C2 with 20% replacement of ashes F1-F3

6.5.2.2. Discussion

The results shown in Tables 6.8–6.11 and plotted in Figures 6.4–6.7 indicate a clear effect of the gypsum admixture on the mortar. As the gypsum quantities are increased, the expansion of the mortar also increases. In general, once the gypsum quantities exceed 6% to 8%, the mortar bars showed an increase in expansion.

The types of cement used in the mixture affected the expansion results; mixtures containing cement C1 expanded more than mixtures containing C2. The increase in expansion may be due to the increase in available sulfates. The XRF results shown in Table 2.2 indicate an approximate 35% difference in SO_3 content between the two cements used in this study.

The type of fly ash and level of replacement affected the expansion results of LST. Mixtures containing fly ash F2 expanded more than mixtures containing ash F3, both of which (generally) expanded more than mixture containing ash F1. In terms of mixture proportions, mixtures containing 35% fly ash replacement (of either C1 or C2) showed a higher likelihood of expanding beyond the 0.1% than those mixtures which contained 20% replacement. As with the cements, the increase in expansion (based on the ash used) is likely due to the sulfate content within the ash. The XRF data shown in Table 6.1 indicates that the SO_3 content in ascending order is $\text{F1} < \text{F3} < \text{F2}$. Additionally, the quantity of amorphous SO_3 of the respective fly ash shown in Figure 6.1 follows a similar trend and may have been a contributing factor.

As stated previously the expansions that occurred are all likely due to the total sulfate content. The sulfates are reacting with C_3A to form AFt and AFm phases. The formation of AFt and AFm as a function of gypsum content will be investigated in the following sections of this report.

6.5.3. Isothermal Calorimetry and Maximum Heat

The heat evolution (heat of hydration) curve of cement binders is often sub-divided into five stages, which are numbered in Figure 6.8 and briefly described here:

- Initial period: dissolution; ettringite (AFt) formation
- Induction period: increase in Ca^{2+} concentration
- Acceleration period: rapid formation of C-S-H and CH
- Retardation period: monosulfoaluminate (AFm) formation and gypsum depletion.
- Steady State period: continuation of hydration product formation

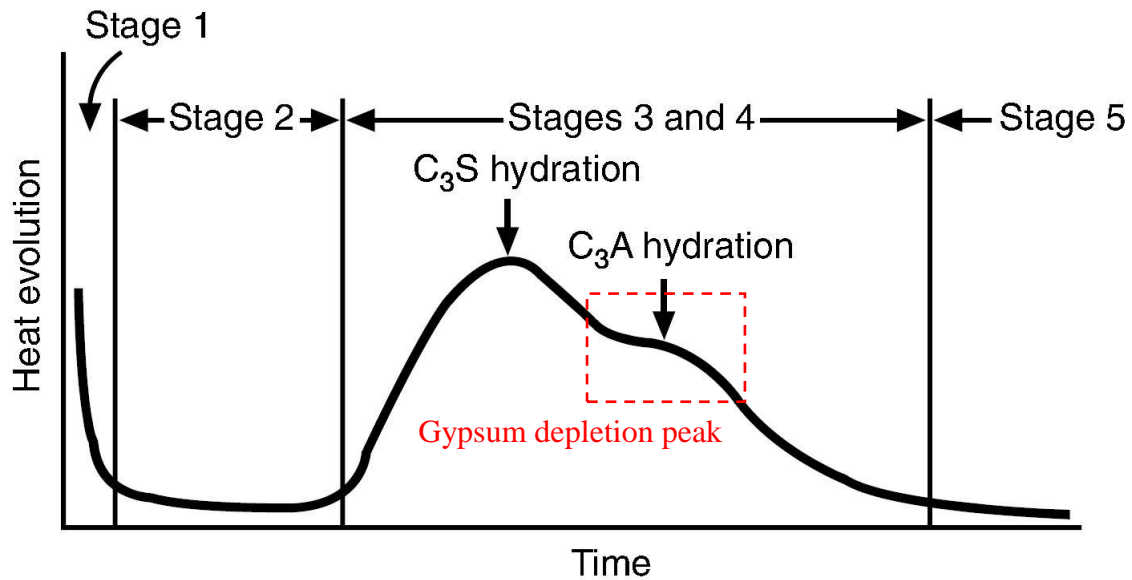


Figure 6.8 Heat evolution as a function of time [2]; additional annotations (in red) by the author of this report

6.5.3.1. Results

Isothermal calorimetry was performed to determine the effects of the gypsum on the heat of hydration, and cumulative heat produced by the neat cement paste. The goal was to examine the point of sulfate depletion (on the heat of hydration curve) and cumulative heat (area under the heat of hydration curve), and thereafter find correlations to the expansion results from LST and hydration product formation using XRD analysis. The heat of hydration and maximum heat produced by each mix are presented in Figures 6.9–6.21. The heat of hydration curves exhibited variable behavior in terms of the location of sulfate depletion peak; therefore, the results that follow include heat of hydration data only for mixtures in which the sulfate depletion peak was observable within 7 days. Additionally, the heat of hydration curves do not show the first three hours of hydration that were recorded by the calorimeter. Typical heat of hydration and cumulative heat curves will be shown and discussed in correlation to the results of this research study in this and following sections.

The maximum heat curves were plotted by recording the value of power (in J/g) at 168 hours (the end of testing) from the cumulative heat curve (Figure 6.9) and plotting the value versus the gypsum content of the respective mix. An example of how the maximum heat curve is constructed follows.

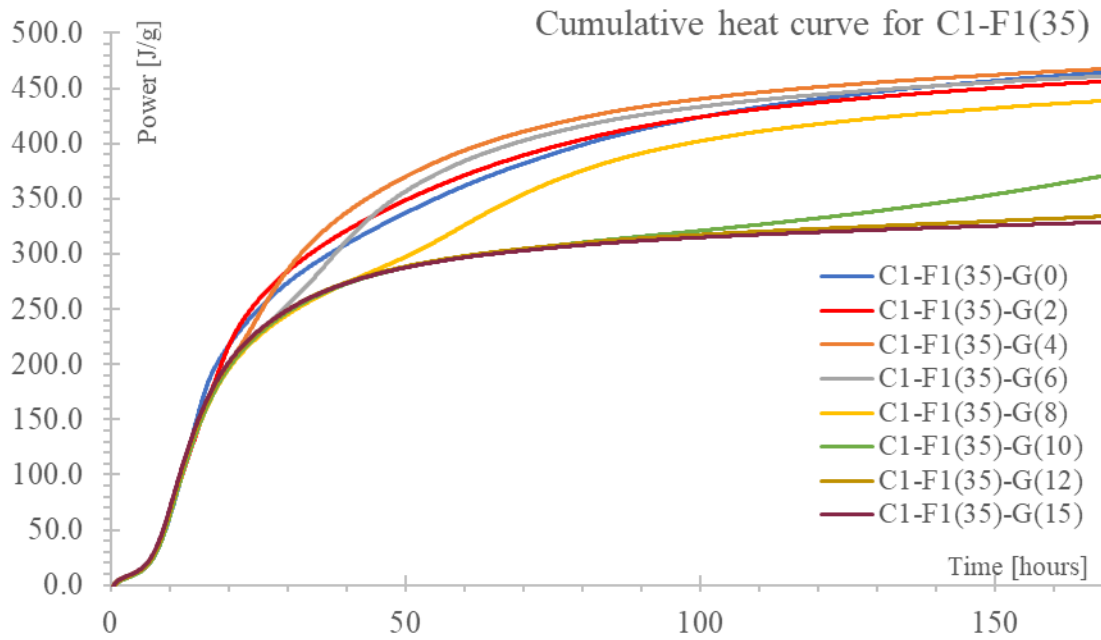


Figure 6.9. Cumulative heat results from isothermal calorimetry of mix C1-F1(35)

From Figure 6.9 a table can be constructed (Table 6.12) that includes the heat output at the end of the test, and the gypsum content that produced the respective amount of heat. When the values are plotted (independent variable gypsum and dependent variable max heat), the maximum heat curve (Figure 6.10) results.

Table 6.12 Maximum heats and corresponding gypsum contents for mix C1-F1(35)

Mix ID: C1-F1(35)								
Gypsum [%]	0	2	4	6	8	10	12	15
Max heat [J/g]	462	454	465	459	436	368	331	327

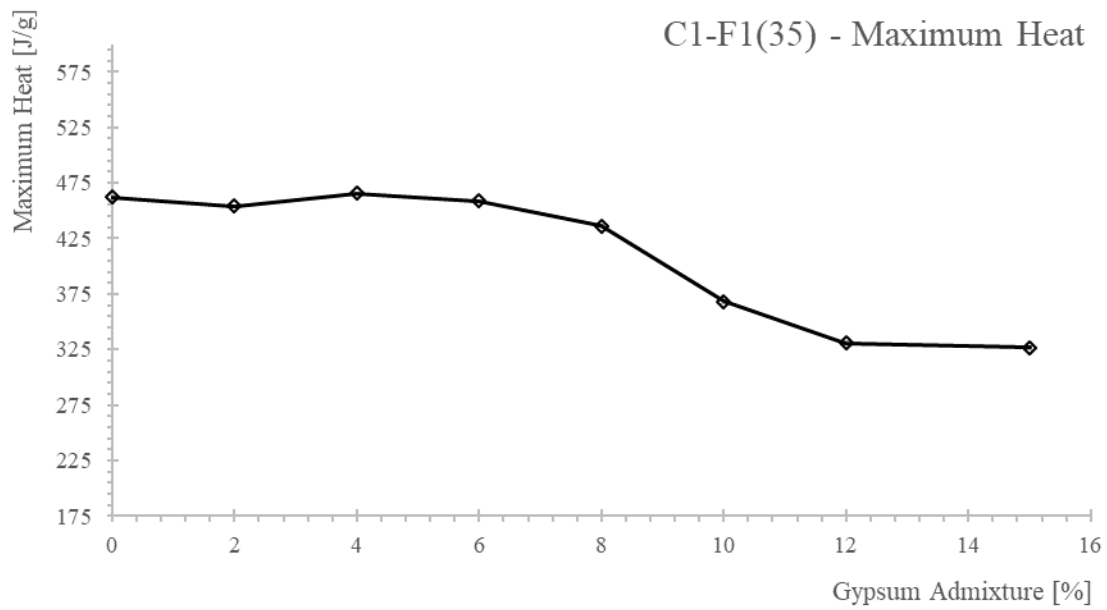
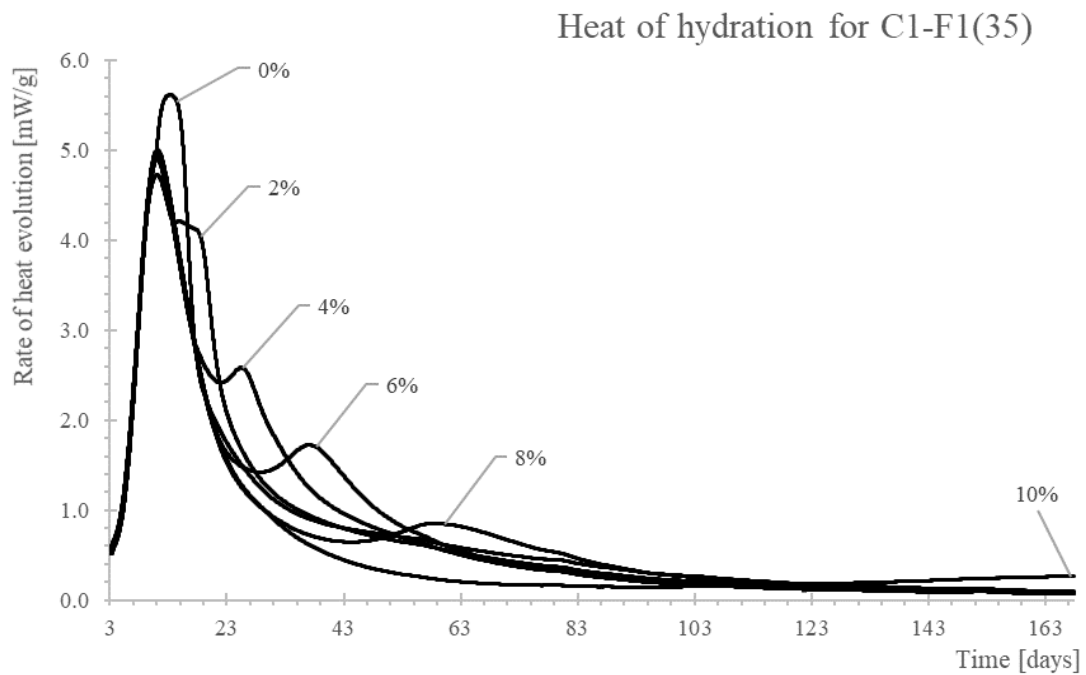


Figure 6.10. Heat of hydration and maximum heat curves for mixture C1-F1(35)

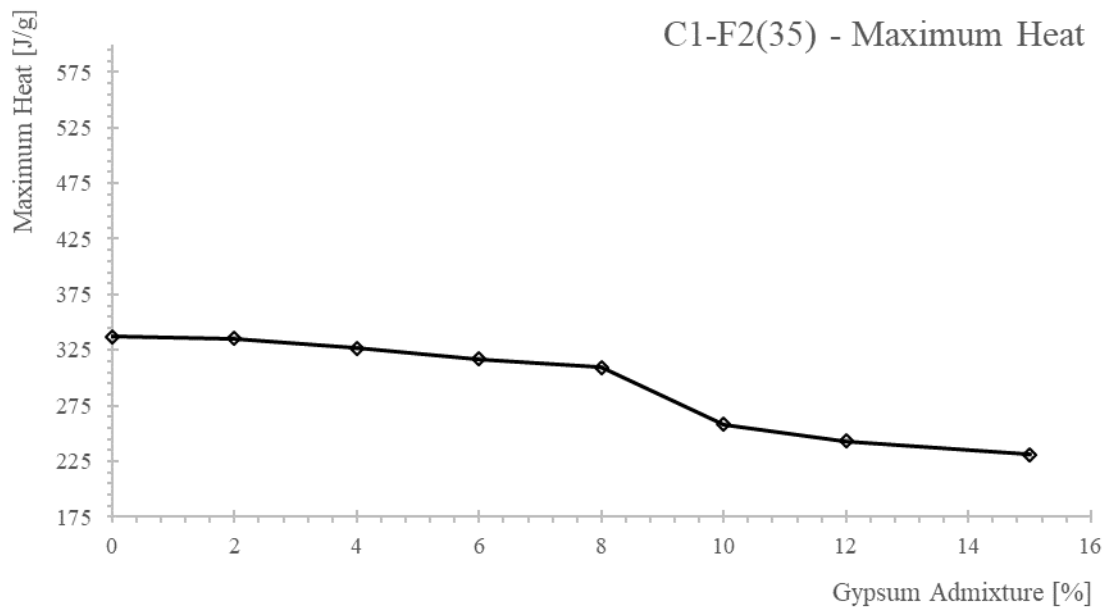
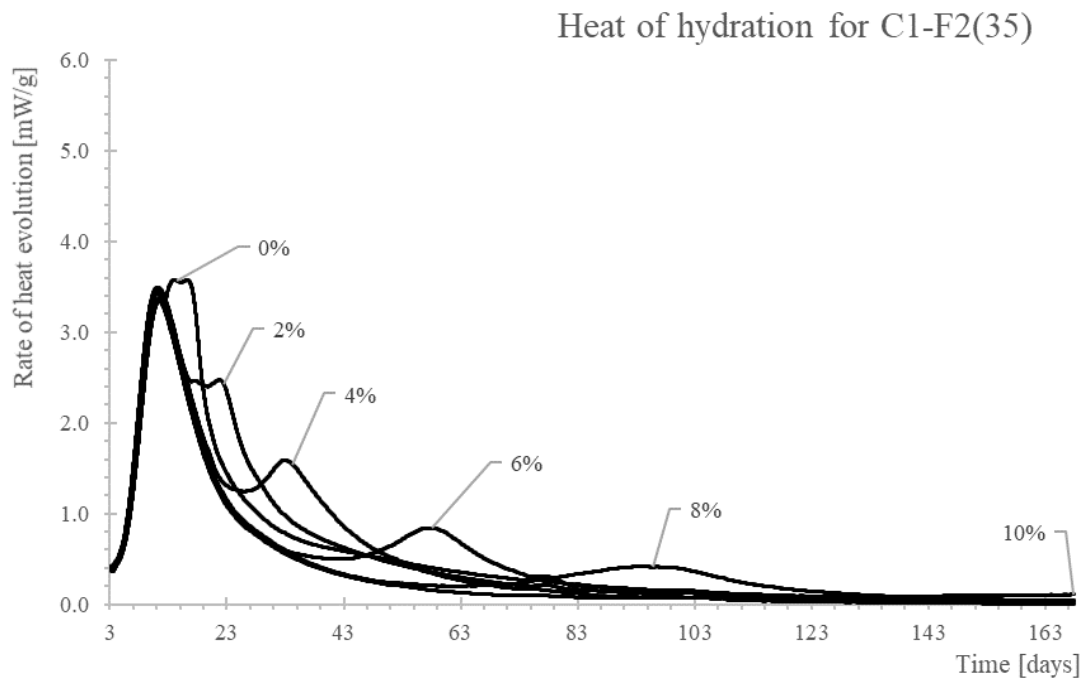
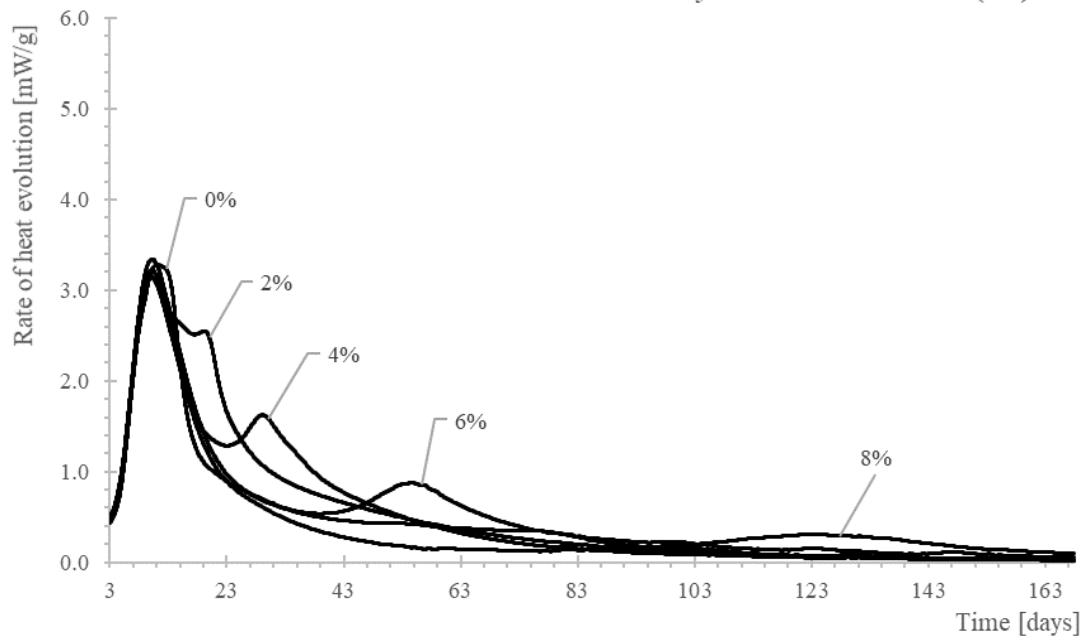


Figure 6.11. Heat of hydration and maximum heat curves for mixture C1-F2(35)

Heat of hydration for C1-F3(35)



C1-F3(35) - Maximum Heat

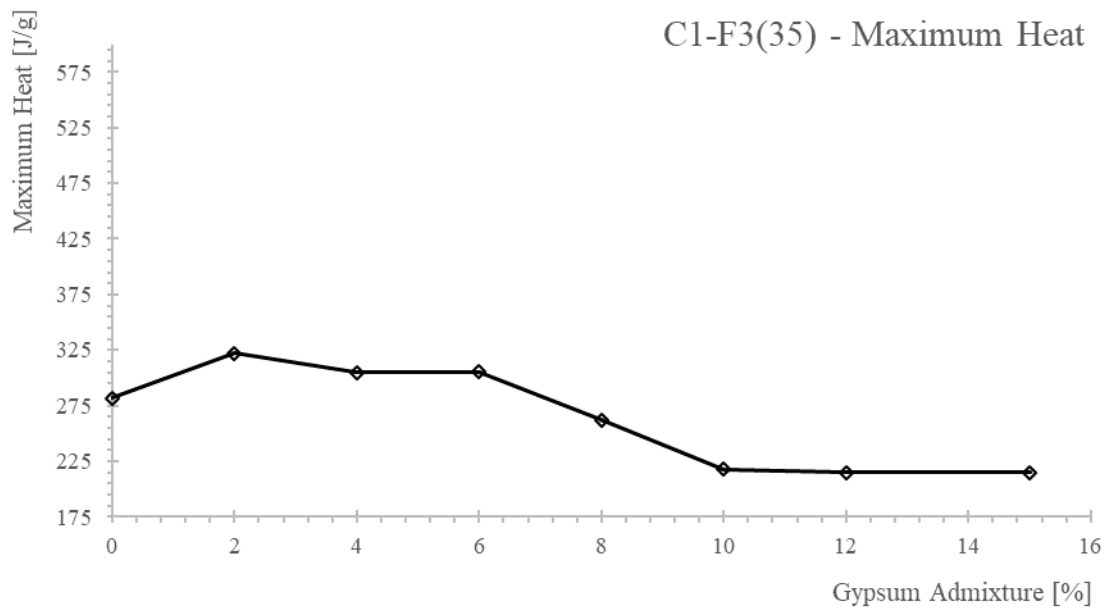


Figure 6.12. Heat of hydration and maximum heat curves for mixture C1-F3(35)

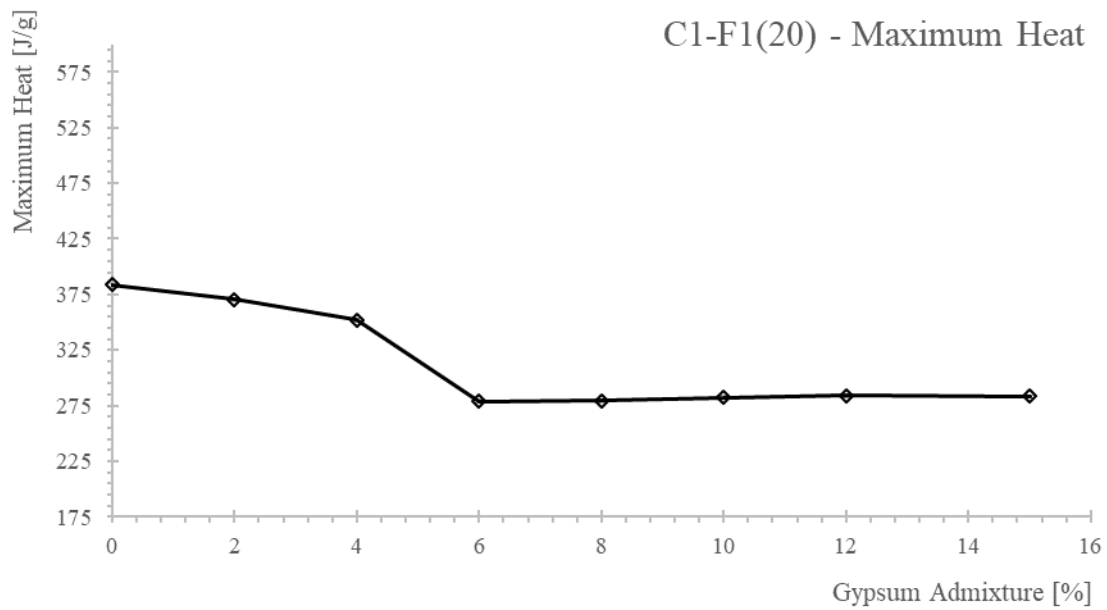
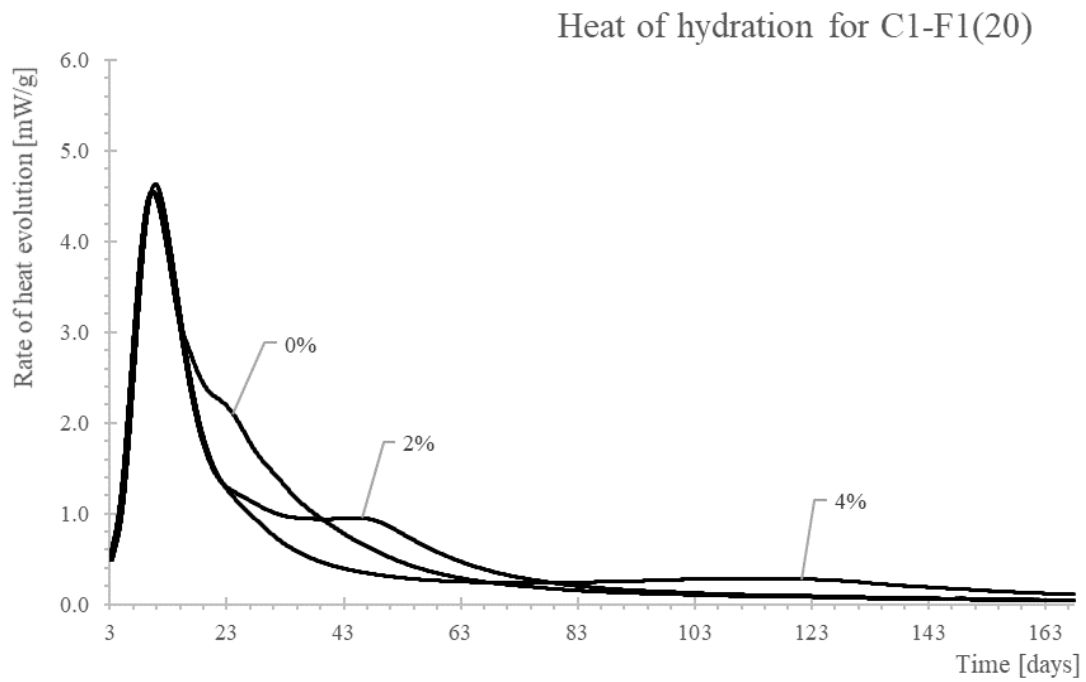


Figure 6.13. Heat of hydration and maximum heat curves for mixture C1-F1(20)

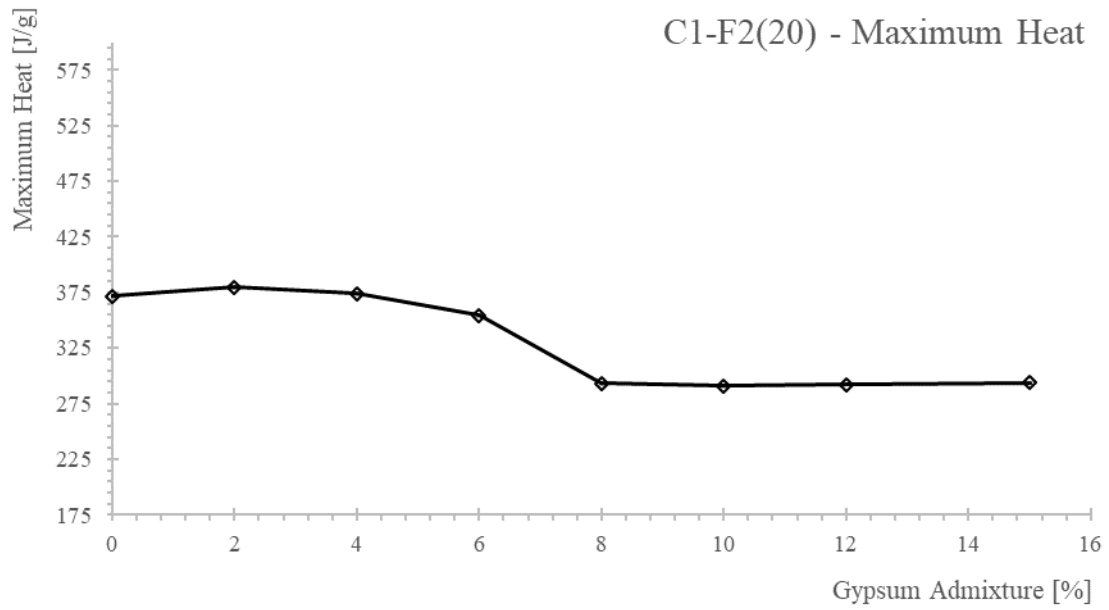
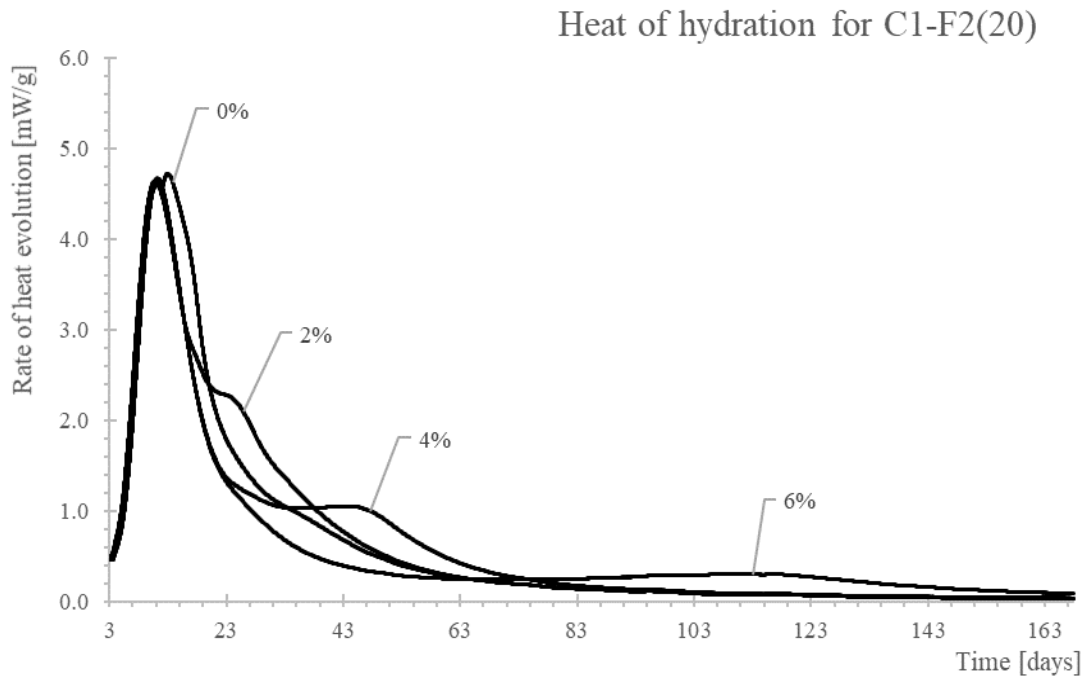


Figure 6.14 Heat of hydration and maximum heat curves for mixture C1-F2(20)

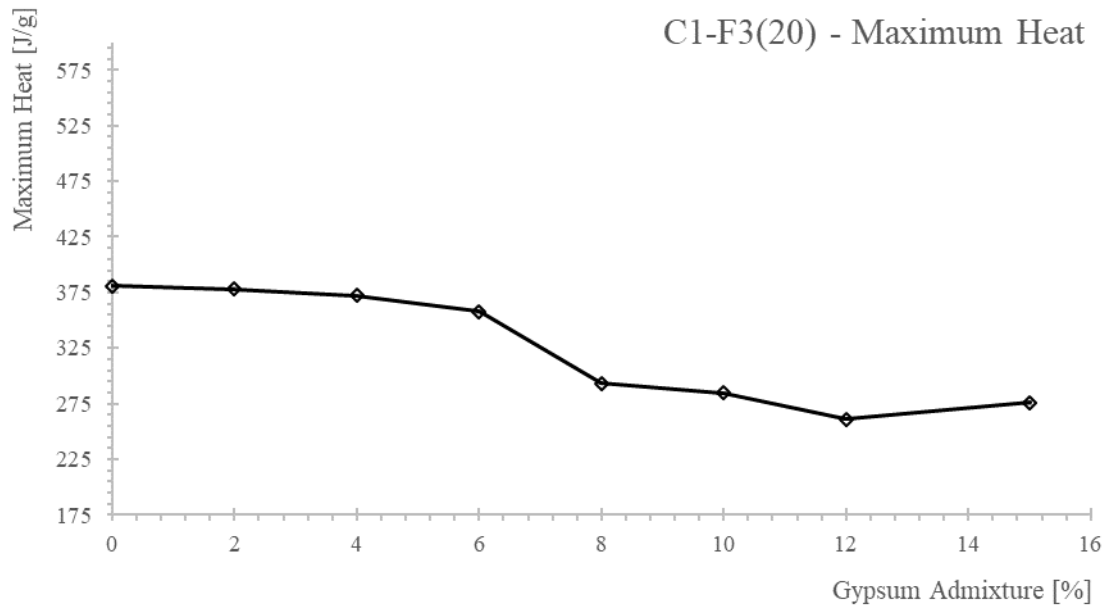
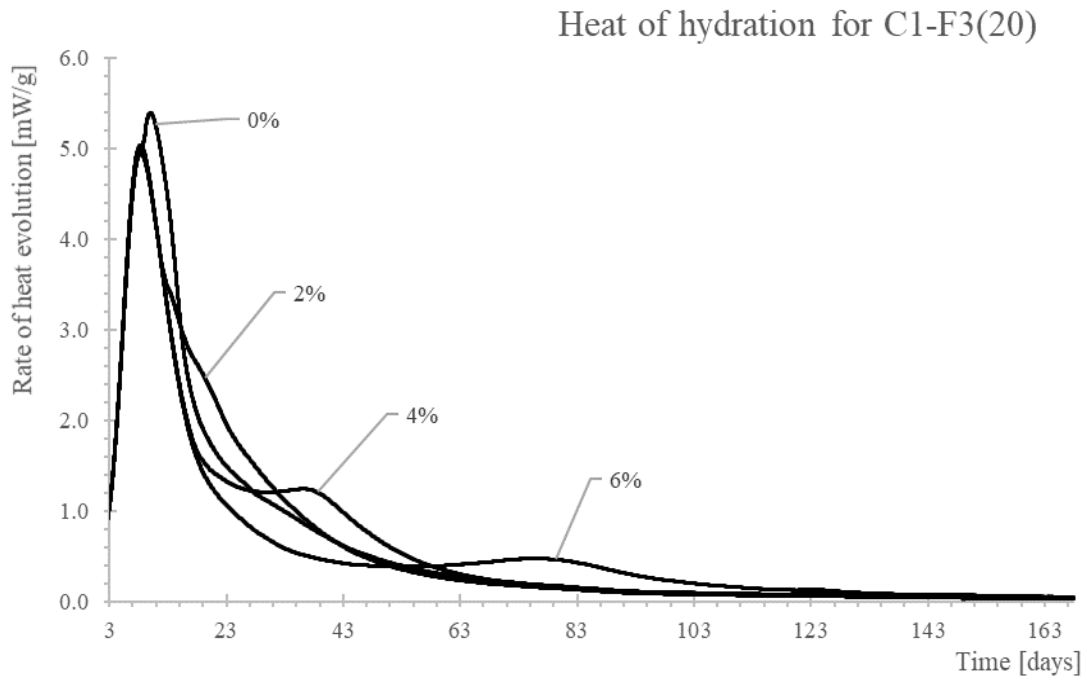
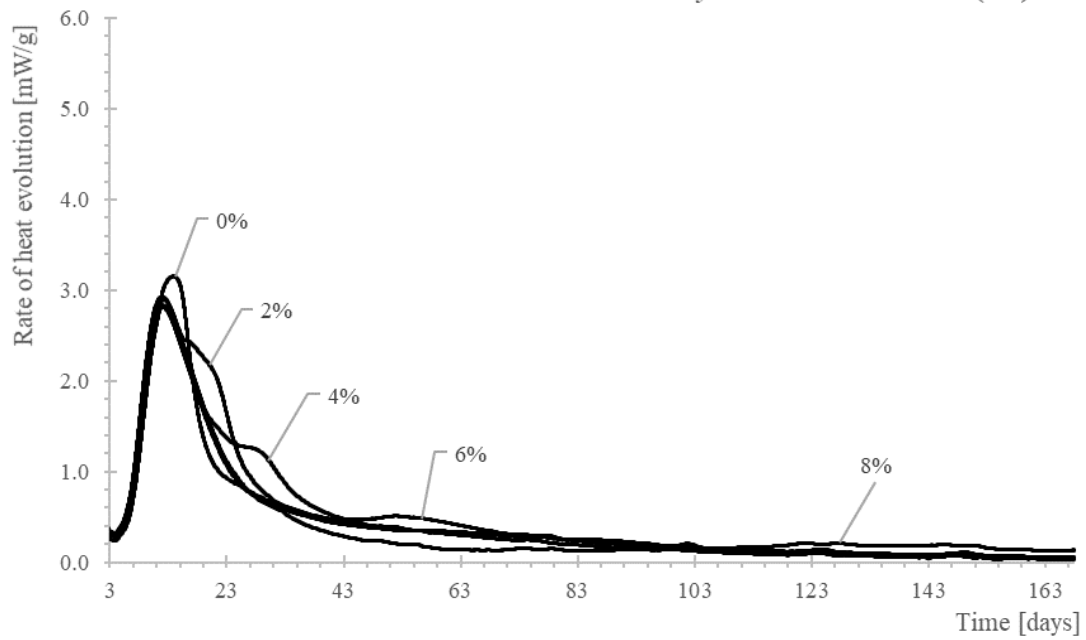


Figure 6.15. Heat of hydration and maximum heat curves for mixture C1-F3(20)

Heat of hydration for C2-F1(35)



C2-F1(35) - Maximum Heat

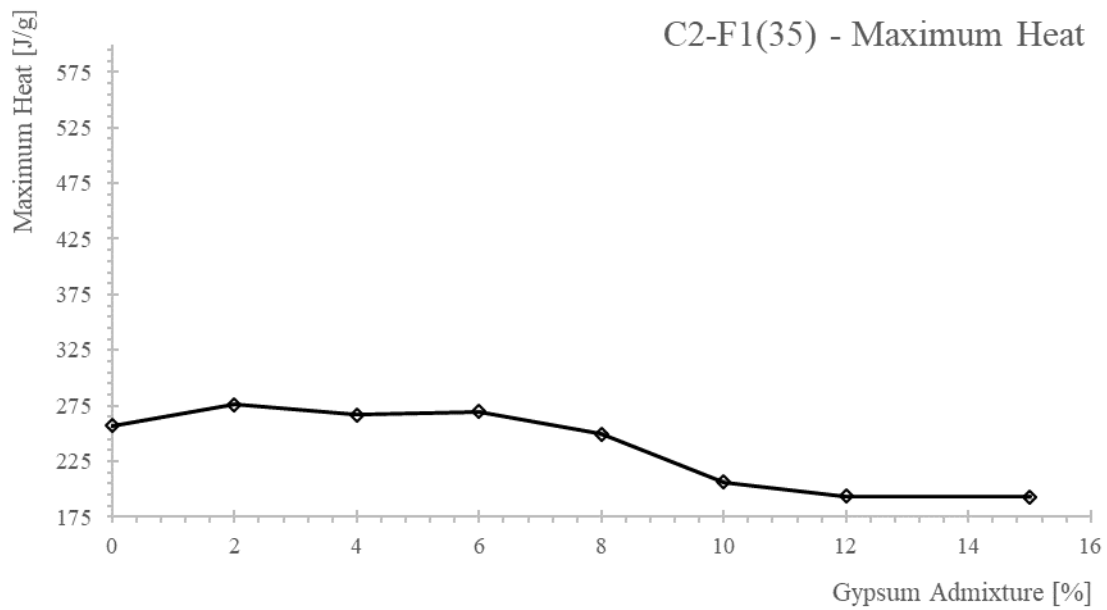


Figure 6.16 Heat of hydration and maximum heat curves for mixture C2-F1(35)

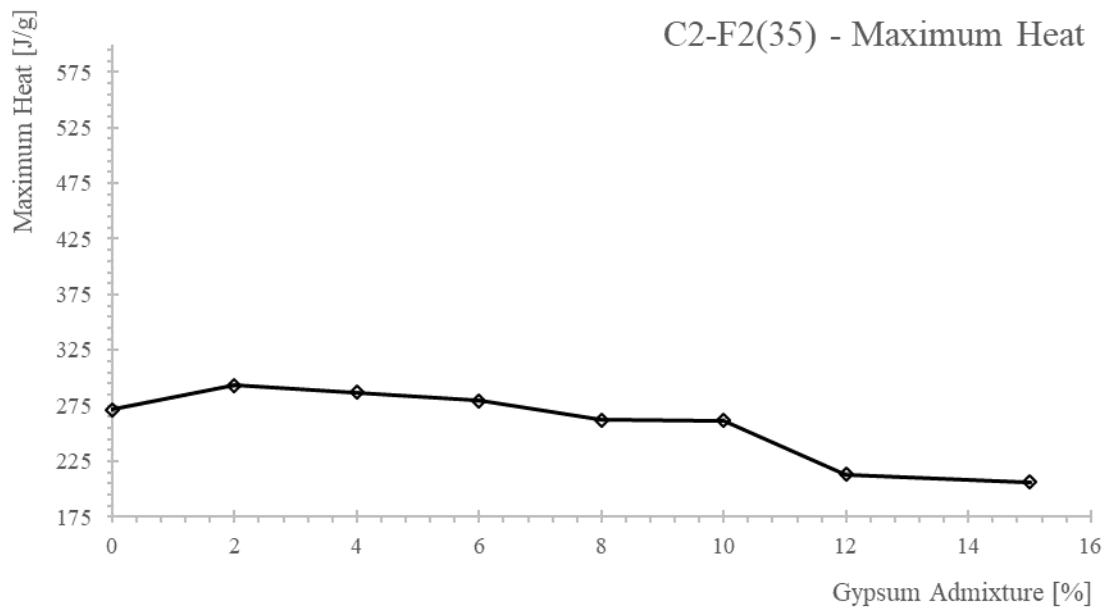
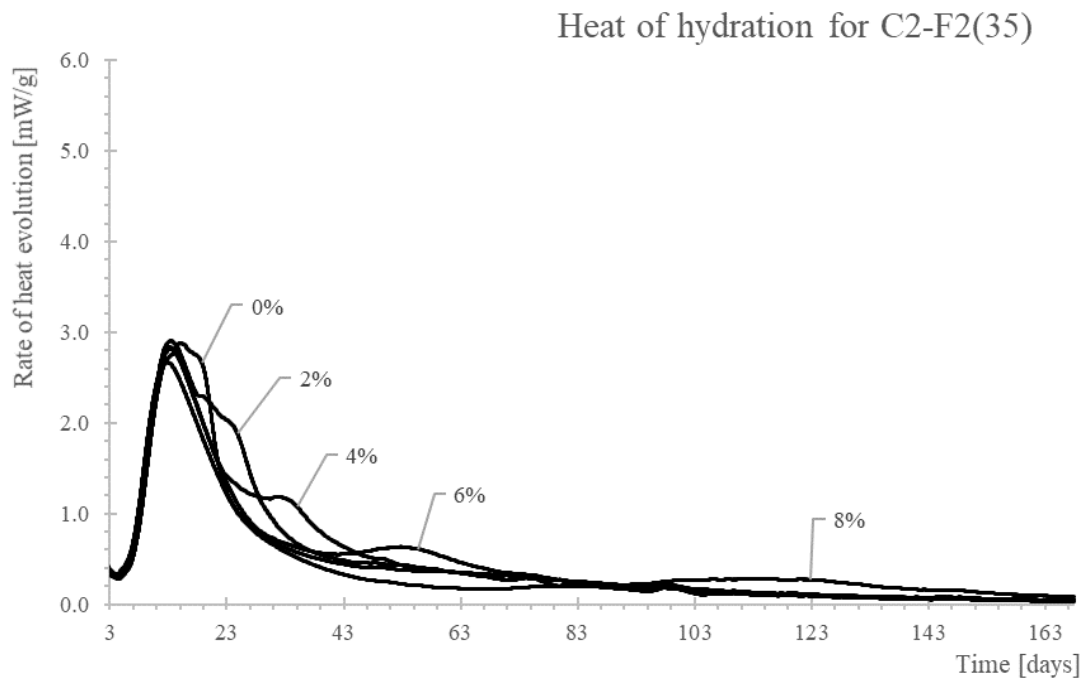
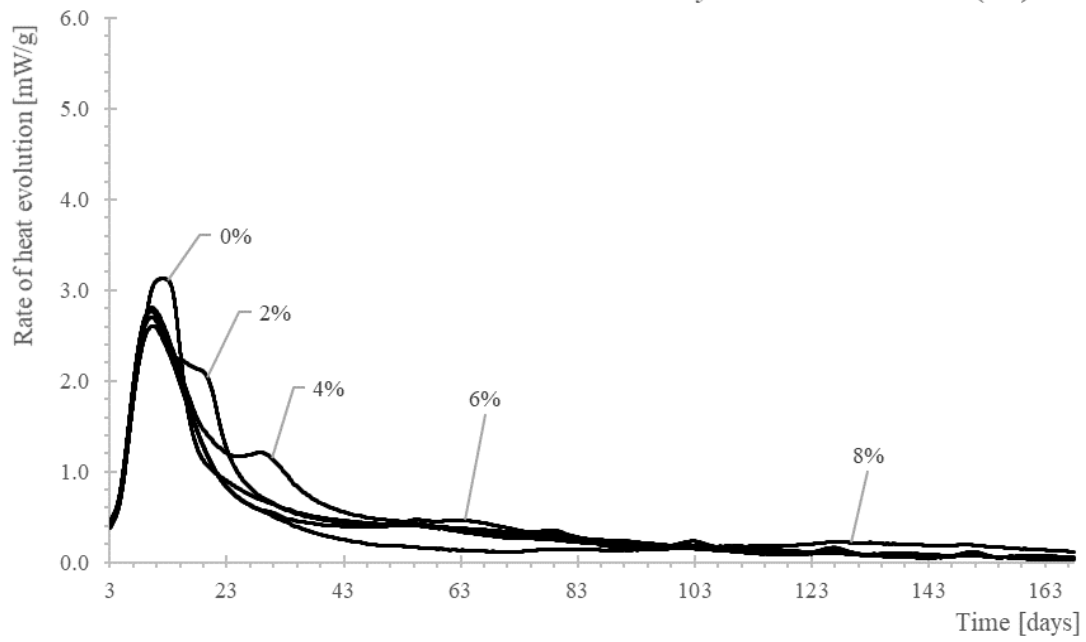


Figure 6.17. Heat of hydration and maximum heat curves for mixture C2-F2(35)

Heat of hydration for C2-F3(35)



C2-F3(35) - Maximum Heat

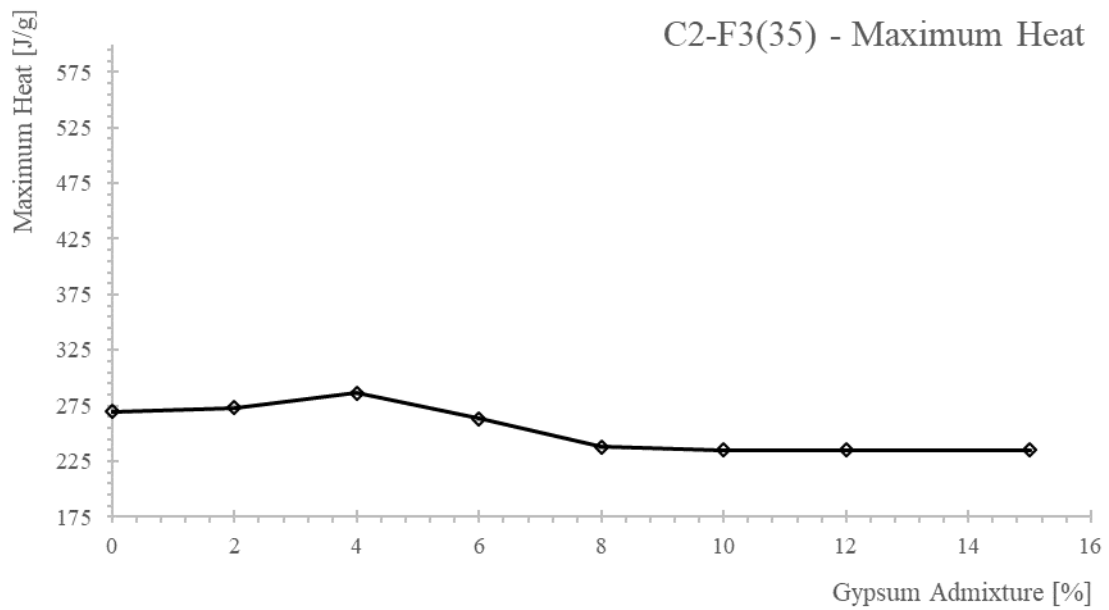


Figure 6.18 Heat of hydration and maximum heat curves for mixture C2-F3(35)

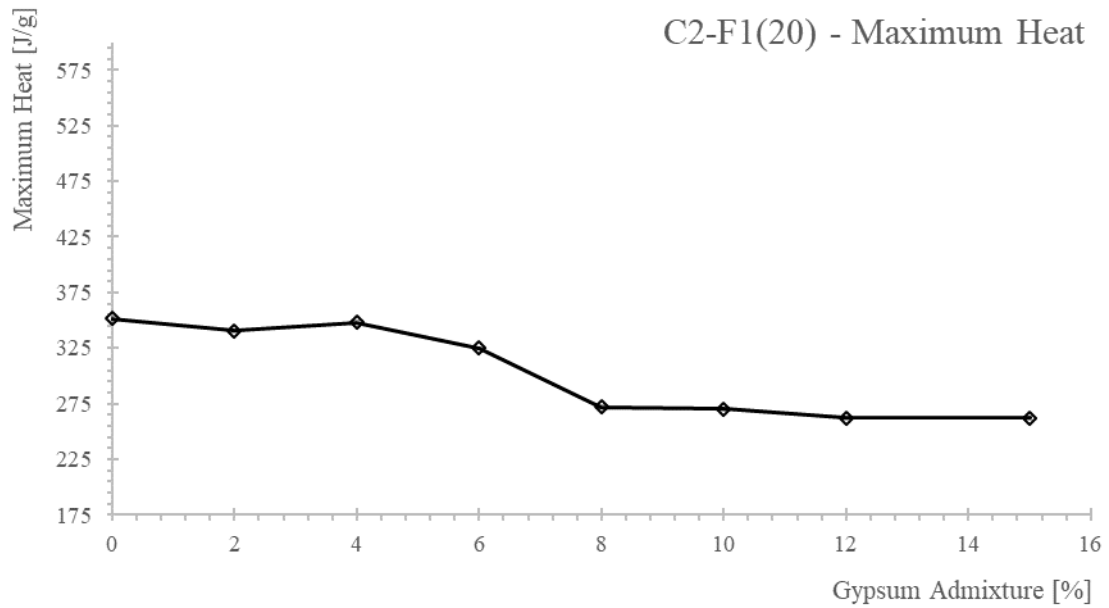
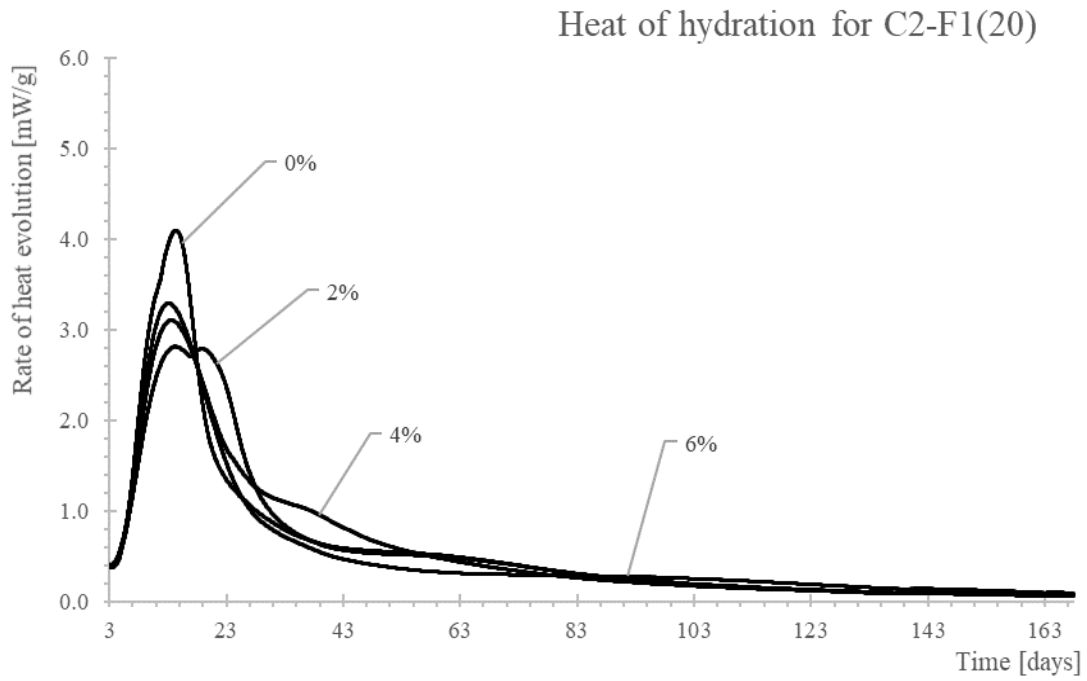


Figure 6.19. Heat of hydration and maximum heat curves for mixture C2-F1(20)

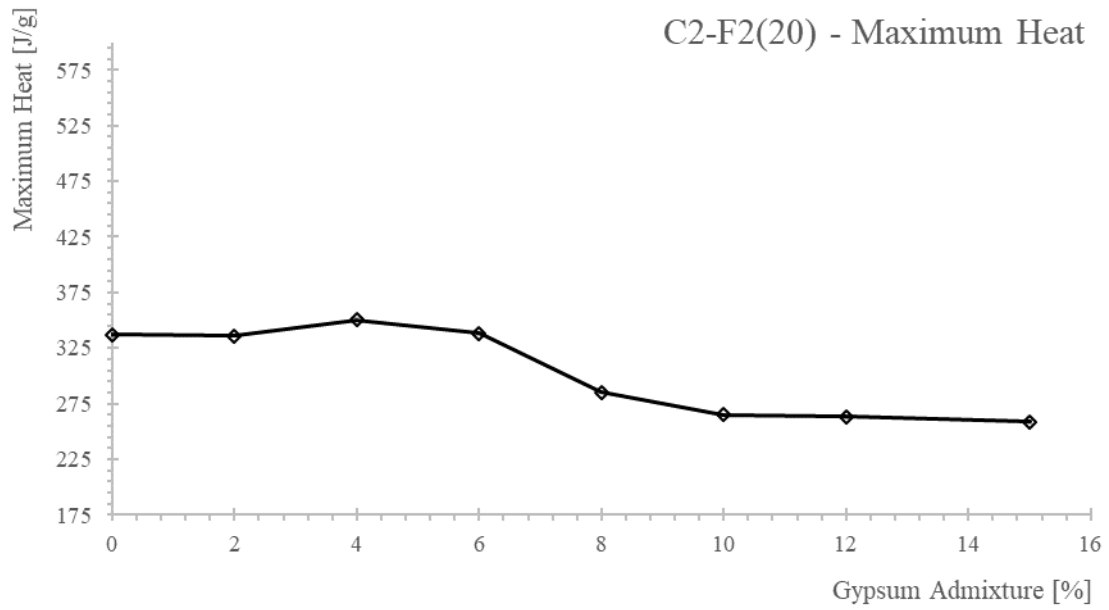
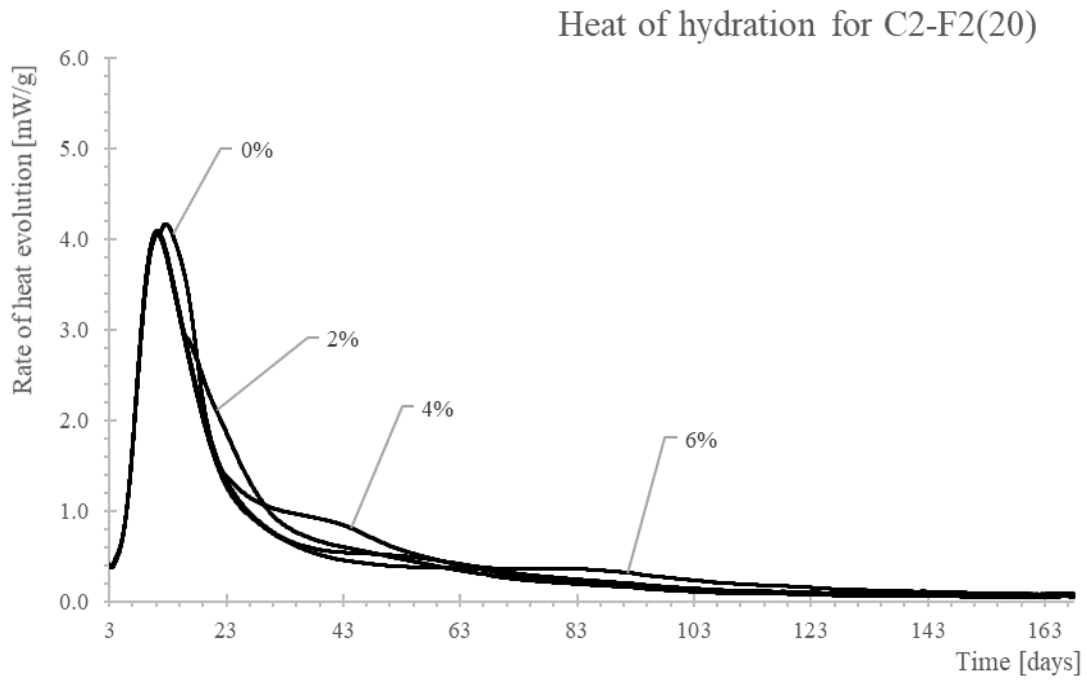


Figure 6.20 Heat of hydration and maximum heat curves for mixture C2-F2(20)

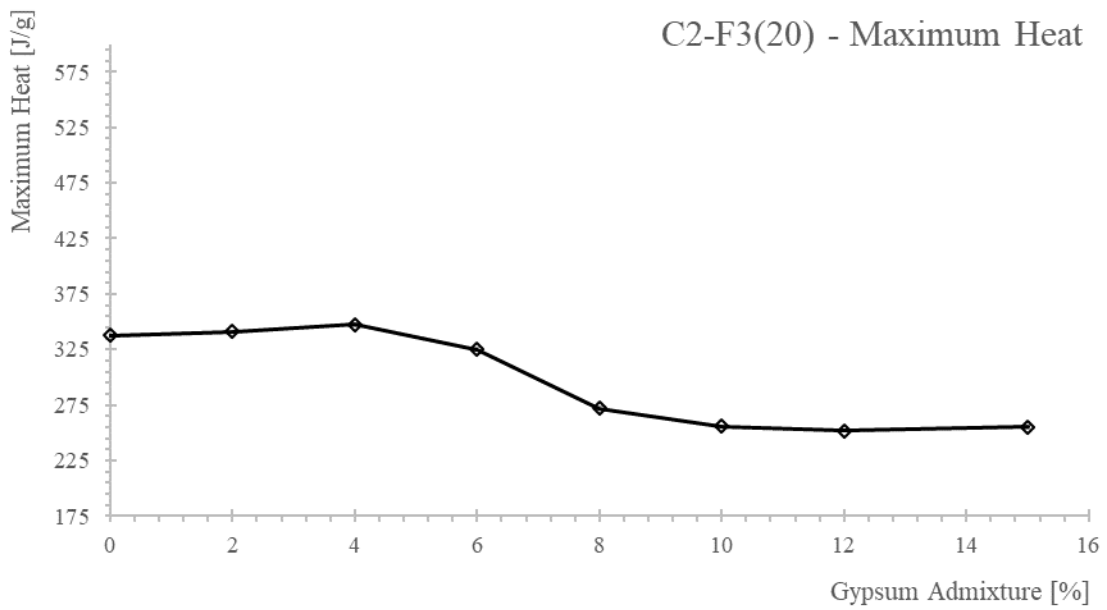
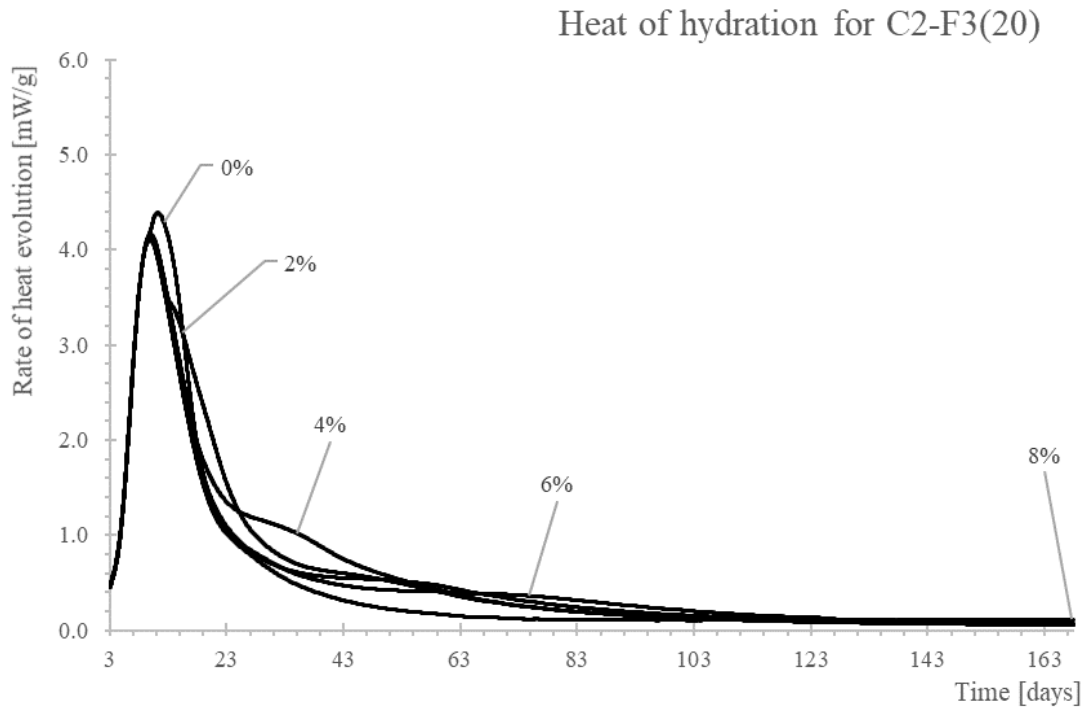


Figure 6.21 Heat of hydration and maximum heat curves for mixture C2-F3(20)

6.5.3.2. Discussion

Researchers have dedicated studies to measuring the effects of SCMs [24] and gypsum [4, 25, 26] on the heat of hydration curve, noting a definitive impact on the characteristic shape of the curve and rate of heat evolution. Thus, the heat of hydration curves shown in Figures 6.10–6.21 indicate multiple points of interest in relation to the aforementioned studies.

When gypsum and C_3A react during the early ages of cement hydration, the reaction produces a change to the shape of the heat of hydration curve (named by Lerch the “gypsum depletion peak”) during stage 4, as shown in Figures 6.22 and 6.23 (as well as in Figure 6.8).

Research [27, 28] has shown through in-situ QXRD in conjunction with heat of hydration testing that the time at which the gypsum depletion peak occurs is coincident with accelerated AFt precipitation and renewed dissolution of C_3A . With this in mind, one can infer from Figures 6.10–6.21 at what time the onset of renewed C_3A dissolution occurred and when the precipitation of AFm begins for the respective mixtures in this research study—the implication being that one can simply analyze the heat of hydration curve, and determine when AFt and AFm phases in the mixture are forming.

Understanding the time at which AFt and AFm may form provides insight into how a mixture will perform in terms of sulfate resistance. If AFt forms at later ages (when the cement binder is completely set), damage in the form of expansive cracking to the paste matrix will likely be incurred, due to the expansive nature of AFt formation. The expansive cracking from the late formation of AFt may allow for the ingress of external sulfates and possibly exacerbate the layering effect researched by [17] that commonly occurs as part of the external sulfate attack mechanism.

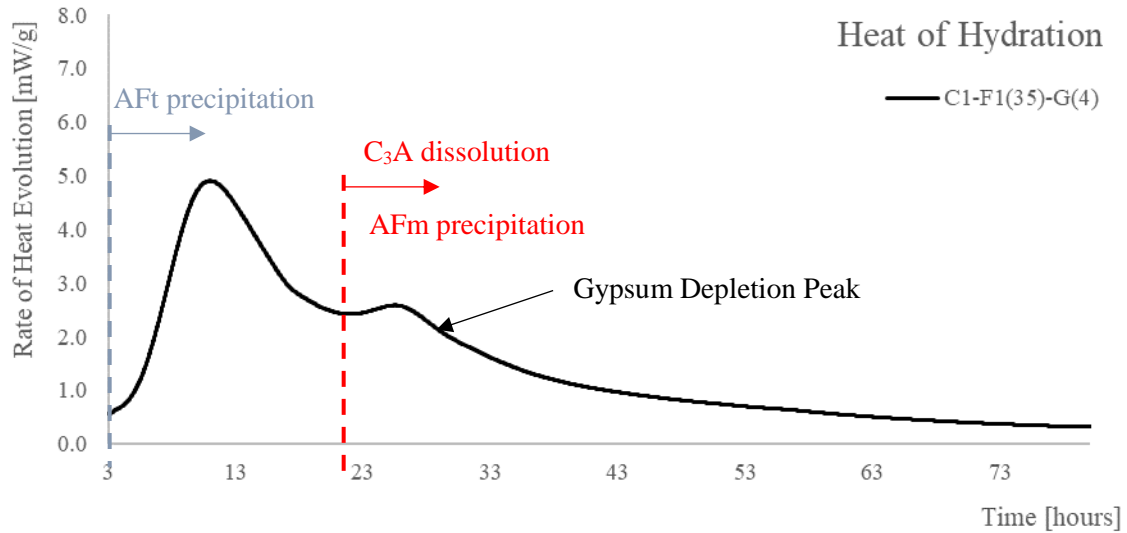


Figure 6.22. Typical heat of hydration curve

Lerch [25] in his early research on the study of the appropriate dosage of gypsum for a given cement/clinker stated the following:

A properly retarded cement can be considered as one which contains the minimum quantity of gypsum required to give a curve that shows two cycles of ascending and descending rates of heat liberation and that shows no appreciable change with larger additions of gypsum during the first 30 hours of hydration.

A plot showing a mixture that meets Lerch's guidelines is shown in Figure 6.23.

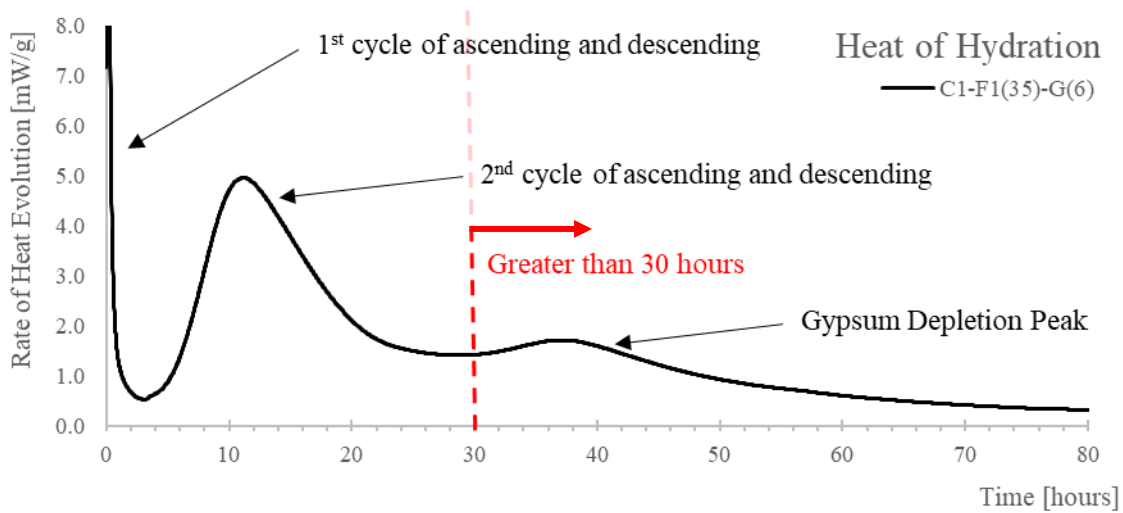


Figure 6.23. Heat of hydration curve meeting Lerch's guidelines

Given Lerch's guidelines, Table 6.13 has been prepared to show which mixtures in this study were under-sulfated (u), properly sulfated (X), or were over-sulfated (o). Given that mixtures used in this study were prepared in approximately even intervals of 2% gypsum admixture, some of the properly sulfated mixtures may have fallen within a range; this is reflected in the provided values shown in Table 6.13.

It has been stated by researchers [4] that modern cements differ from those Lerch was studying in terms of Blaine fineness (amongst other parameters). That is, most modern cements have a finer particle size than those that Lerch studied. Hydration kinetics are affected by the fineness of the cement (also shown by Lerch), thereby altering the shape of the heat of hydration curve. The authors of this report note this distinction and have nonetheless elected to analyze the data with Lerch's guidance in mind.

Table 6.13 Comparison of heat of hydration performance to Lerch's guidelines

		Gypsum [%]								
		0	2	4	6	8	10	12	15	
Mix ID	C1-F1(35)	u	u	u	X	X	o	o	o	
	C1-F2(35)	u	u	u	X	o	o	o	o	
	C1-F3(35)	u	u	u	X	o	o	o	o	
	C1-F1(20)	u	X	X	o	o	o	o	o	
	C1-F2(20)	u	u	X	X	o	o	o	o	
	C1-F3(20)	u	u	X	X	o	o	o	o	
	C2-F1(35)	u	u	X	X	o	o	o	o	
	C2-F2(35)	u	u	X	X	o	o	o	o	
	C2-F3(35)	u	u	X	X	o	o	o	o	
	C2-F1(20)	u	u	X	X	o	o	o	o	
	C2-F2(20)	u	u	X	X	o	o	o	o	
	C2-F3(20)	u	u	X	X	o	o	o	o	

Note: u = under-sulfated, **X** = properly sulfated, o = over-sulfated

Table 6.13 indicates that according to Lerch the proper amount of gypsum addition for most mixtures would be in the range of 4% to 6% for the materials and replacement values used in this study. Mixtures deemed properly sulfated here will be analyzed in comparison with other data collected in this study to be discussed in later portions of this report.

An ascending (1), primary plateauing (2), descending (3), and secondary plateauing (4) pattern (see example shown in Figure 6.24) emerges when examining the maximum heat curves shown in Figures 6.10–6.21. Researchers [26] have found that higher amounts of heat produced during hydration (from the cumulative heat curve) tend to correlate with higher strength gain at earlier ages. Thus, when observing the maximum heat curves shown in Figures 6.10–6.21, one can assume mixtures with the highest relative heat for the given mixture are more likely to achieve higher early strength. Unfortunately, strength gain data was not properly collected and tracked during this research and cannot be presented here. However, it is noted here that mixtures containing nominally greater than 10% gypsum content generally took between 7 and 9 days to achieve a compressive strength of 20 ± 1.0 MPa.

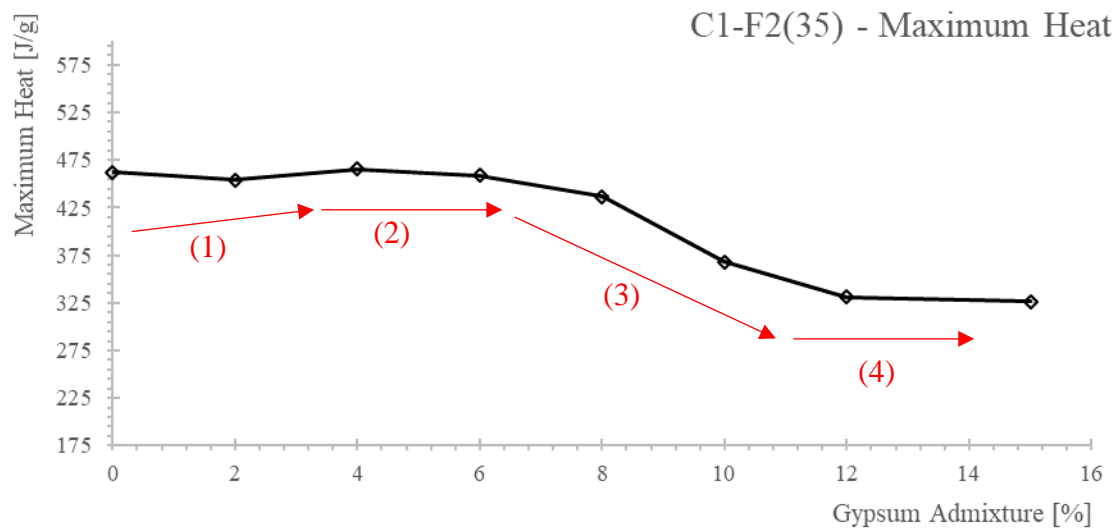


Figure 6.24. Typical behavior observed in the maximum heat curves

An additional pattern emerged when correlating the maximum heat curve to the QXRD analysis; those LST results will be discussed in Section 6.5.6 of this report.

6.5.4. Qualitative and Quantitative X-Ray Diffraction

This testing was performed to provide insight into the hydration product formation as a function of gypsum admixture, and to possibly draw correlations between results from other testing performed as part of this research study.

Both qualitative and quantitative x-ray diffraction (QXRD) were performed on mortar bars of two different ages from LST. The first round of analysis was conducted on mortar samples after the given mortar mixture had achieved a compressive strength of 20 ± 1.0 MPa (hereafter referred to in figures as 20 MPa). The rate of strength gain of the mixtures was variable, where it took mortars anywhere from 1 to 9 days to achieve the compressive strength of 20 ± 1.0 MPa. The second round of testing was conducted when the mortar was 28 days old (hereafter referred to in figures as 28 day) relative to the date of casting the given mixture.

The results of this testing regime are divided into two groups—mixtures with and without gypsum—to fully understand the implications of using gypsum as an admixture for the testing herein.

6.5.4.1. Mortar Mixtures Containing No Gypsum

6.5.4.1.1. Results

To establish a baseline understanding of the hydration products formed in the absence of gypsum admixture, QXRD analysis was performed on straight cement mortar mixtures to compare against mortar mixtures containing fly ash. Figures 6.25–6.28 show the differences in AFt and AFm for the aforementioned mixtures. The maximum standard deviation between any one measurement was $\pm 1.5\%$; thus, error bars of $\pm 1.5\%$ have been broadly applied to all the data. Table 6.14 provides the summary of monosulfate and ettringite for samples without gypsum.

Table 6.14 Summary of AFt and AFm formation of two ages of mortar mixtures containing no gypsum for all mixtures with cement C1 and fly ash replacement amounts of 35%

Mix ID	Analysis at 20 MPa		Analysis at 28 days	
	AFt (%)	AFm (%)	AFt (%)	AFm (%)
C1	7.5	4.7	10.3	3.7
C1-F1(35)	2.6	2.4	1.4	10.7
C1-F2(35)	6.8	0.3	6.5	1.1
C1-F3(35)	5.7	2.8	2.9	3.2

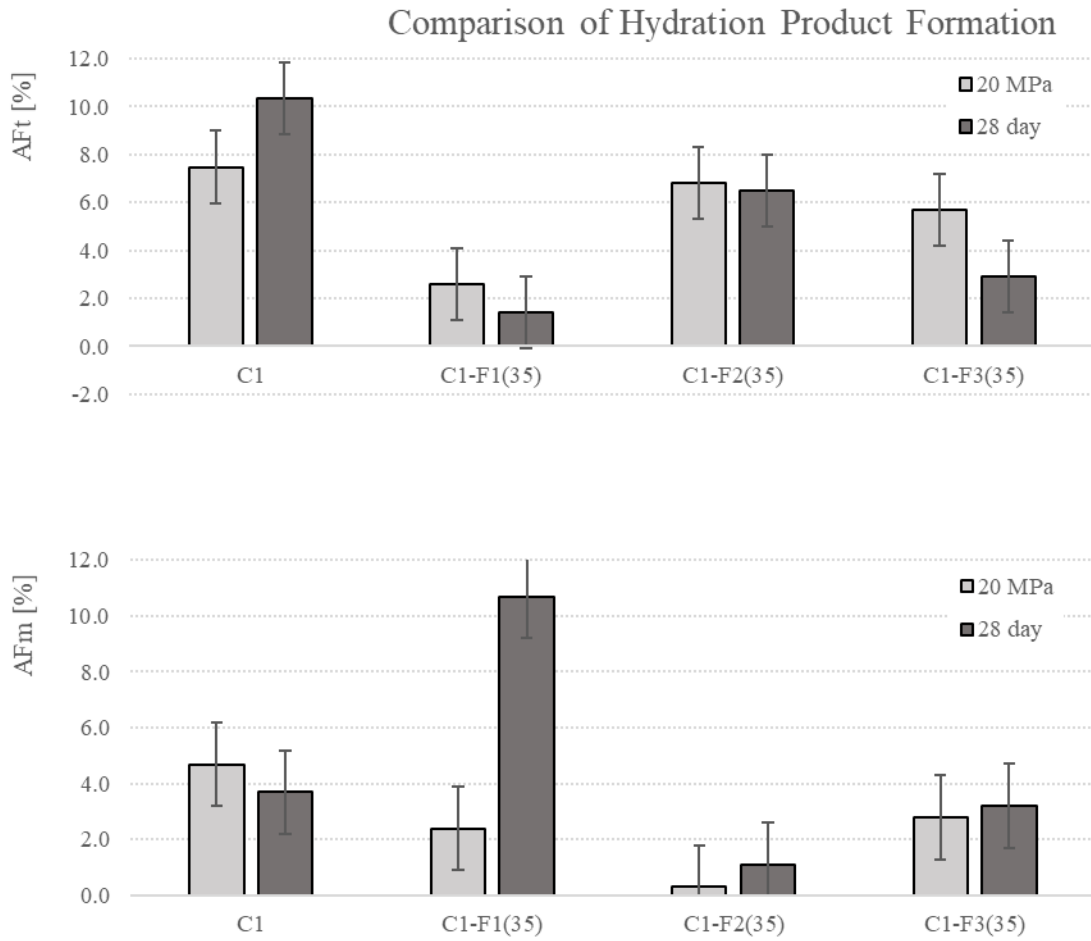


Figure 6.25 Comparison of AFt and AFm formation of two ages of mortar mixtures containing no gypsum for all mixtures with cement C1 and fly ash replacement amounts of 35%

Table 6.15 Summary of AFt and AFm formation of two ages of mortar mixtures containing no gypsum for all mixtures with cement C1 and fly ash replacement amounts of 20%

Mix ID	Analysis at 20 MPa		Analysis at 28 days	
	AFt (%)	AFm (%)	AFt (%)	AFm (%)
C1	7.5	4.7	10.3	3.7
C1-F1(20)	3.8	2.1	3.5	5.3
C1-F2(20)	3.6	2.7	5.1	4.1
C1-F3(20)	3.6	2.8	3.2	5.7

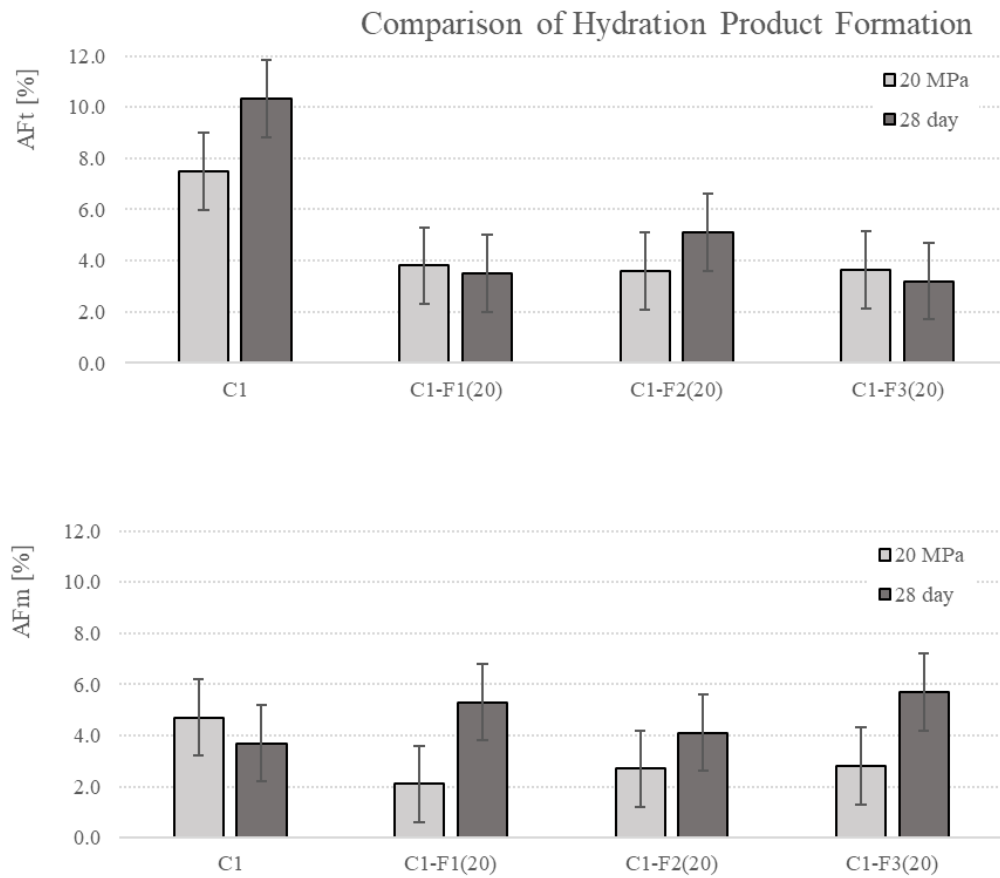


Figure 6.26. Comparison of AFt and AFm formation of two ages of mortar mixtures containing no gypsum for all mixtures with cement C1 and fly ash replacement amounts of 20%

Table 6.16 Summary of AFt and AFm formation of two ages of mortar mixtures containing no gypsum for all mixtures with cement C2 and fly ash replacement amounts of 35%

Mix ID	Analysis at 20 MPa		Analysis at 28 days	
	AFt (%)	AFm (%)	AFt (%)	AFm (%)
C2	3.9	2.5	9.8	4.8
C2-F1(35)	6.2	2.1	4.8	4.9
C2-F2(35)	9.0	0.9	4.0	2.8
C2-F3(35)	5.5	1.9	3.6	3.5

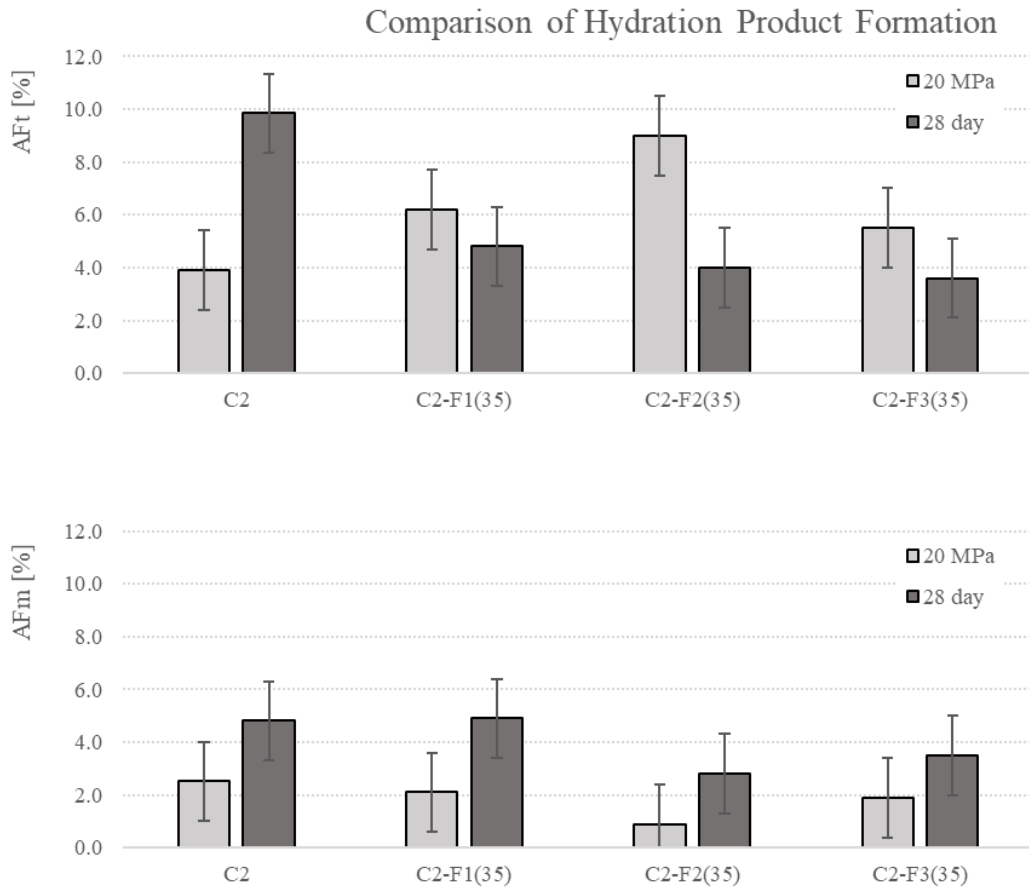


Figure 6.27 Comparison of AFt and AFm formation of two ages of mortar mixtures containing no gypsum for all mixtures with cement C2 and fly ash replacement amounts of 35%

Table 6.17 Summary of AFt and AFm formation of two ages of mortar mixtures containing no gypsum for all mixtures with cement C2 and fly ash replacement amounts of 20%

Mix ID	Analysis at 20 MPa		Analysis at 28 days	
	AFt (%)	AFm (%)	AFt (%)	AFm (%)
C2	3.9	2.5	9.8	4.8
C2-F1(20)	7.0	3.7	7.5	7.9
C2-F2(20)	7.1	1.0	5.7	5.2
C2-F3(20)	4.8	3.3	5.1	10.4

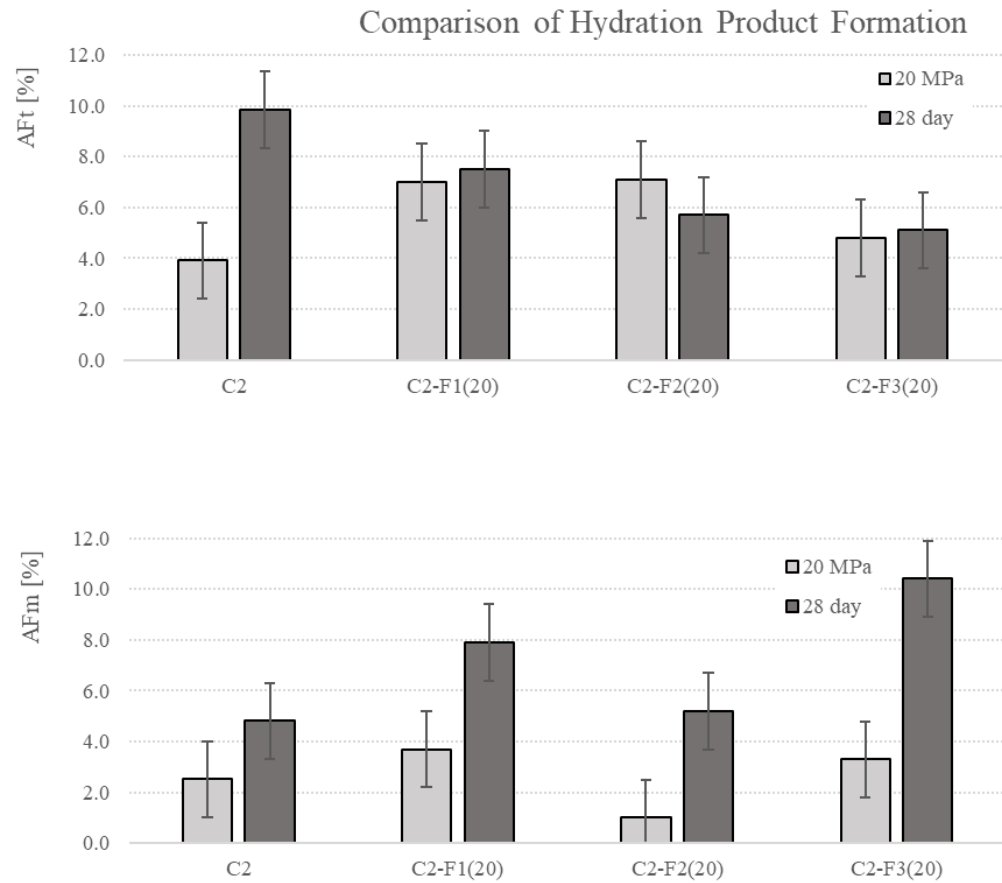


Figure 6.28. Comparison of AFt and AFm formation of two ages of mortar mixtures containing no gypsum for all mixtures with cement C2 and fly ash replacement amounts of 20%

6.5.4.1.2. Discussion

The results from this testing show that the inclusion of fly ash affects the formation of AFt and AFm in early ages of the mortars in this study. The results indicate a difference between the hydration product formation between the two ages. The QXRD analysis shows that measurements taken of 20-MPa and 28-day samples show AFt decreases and AFm increases. This is due to the formation of AFm at the expense of AFt.

It was expected that the C₃A content of the differing fly ashes would affect the outcome of the hydration products measured in QXRD analysis. Specifically, it was assumed that as the C₃A content of the ash increased, an increase in AFm would be observable between the mixtures. This assumption held true for mixtures containing 20% replacement (regardless of the cement type) but was not the case with mixtures containing 35% replacement (regardless of the cement type). It is noted here and in other portions of this report that the AFm phase was difficult to analyze with QXRD due to the solid solution nature of the substance.

A correlation appeared between the SO₃ content of the fly ashes and the amount of AFt formed. The fly ash containing the highest amount of SO₃ (from Table 6.4) content (F2 with 2.5% SO₃) generated more AFt three out of four times in this study, in contrast to the mixtures containing ashes F1 (SO₃ content of 1%) and F3 (SO₃ content of 1.5%). A similar trend between AFt formation and SO₃ content has been observed by other researchers [8].

6.5.4.2. Mortar Mixtures Containing Gypsum

6.5.4.2.1. Results

Both quantitative and qualitative XRD analysis is shown here to provide supporting evidence that Rietveld refinement conducted on the XRD scans was valid. The QXRD data consists of the average of two separate scans. The maximum standard deviation between any one measurement was $\pm 1.5\%$; thus, error bars of $\pm 1.5\%$ have been broadly applied to all the data. Figures 6.29–6.32 show the side by side results for both forms of analysis. In order to capture and clearly delineate the presence of AFt, AFm, and gypsum that occurs at the varying levels of gypsum admixture dosage, the quantitative results shown in the following figures include the XRD 2 θ phase spectrum between the angles of 8.5 and 12.5. Additionally, a summary of the results for each cement and fly ash replacement level is provided in Tables 6.18–6.21.

Table 6.18 Summary of QXR results for mixtures C1-F1(35), C1-F2(35), and C1-F3(35)

MIX ID	Gypsum	AFt	AFt	AFm	AFm
	Admixture	[20 Mpa]	[28 days]	[20 Mpa]	[28 days]
	[%]	[%]	[%]	[%]	[%]
C1-F1(35)	0	2.6	1.4	2.4	10.7
	2	3.5	5.7	1.6	5.7
	4	5.4	7.0	2.0	7.5
	6	9.7	10.5	1.9	9.0
	8	14.6	15.7	2.1	2.8
	10	14.2	18.5	1.9	1.7
	12	14.3	21.9	1.8	1.5
	15	12.3	17.4	1.5	1.5
C1-F2(35)	0	6.8	6.5	0.3	1.1
	2	8.2	9.7	0.7	1.6
	4	12.4	14.1	0.3	2.8
	6	12.3	15.0	0.2	3.0
	8	14.6	18.1	0.4	1.0
	10	15.2	19.1	1.2	1.6
	12	16.9	24.3	0.5	1.7
	15	15.2	24.3	0.4	1.1
C1-F3(35)	0	5.7	2.9	2.8	3.2
	2	6.3	4.5	1.9	8.0
	4	9.3	7.4	3.2	4.8
	6	13.6	13.1	1.8	4.5
	8	16.2	13.5	2.4	2.6
	10	17.6	17.0	2.0	2.7
	12	15.1	21.9	2.7	2.1
	15	13.9	17.5	1.5	2.0

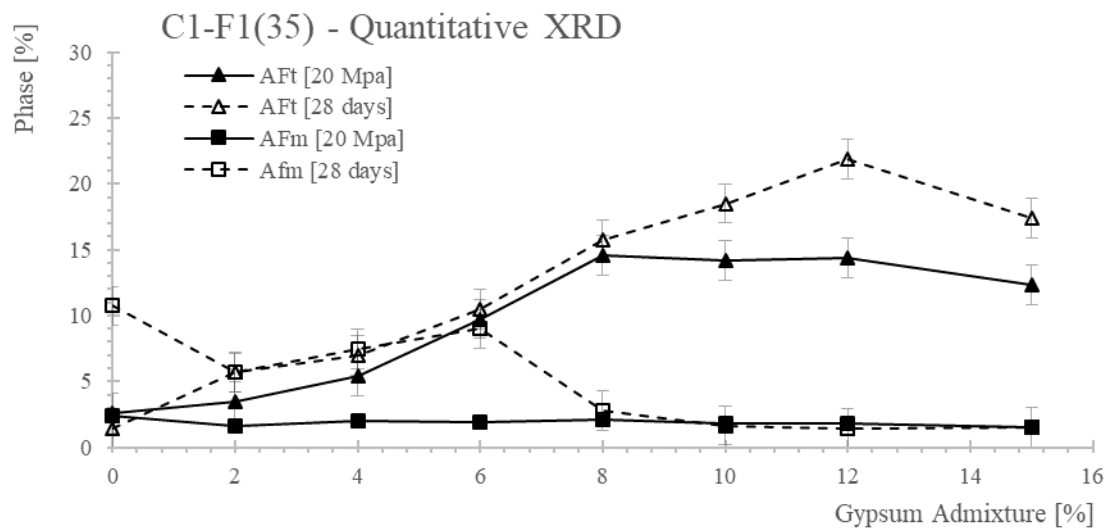
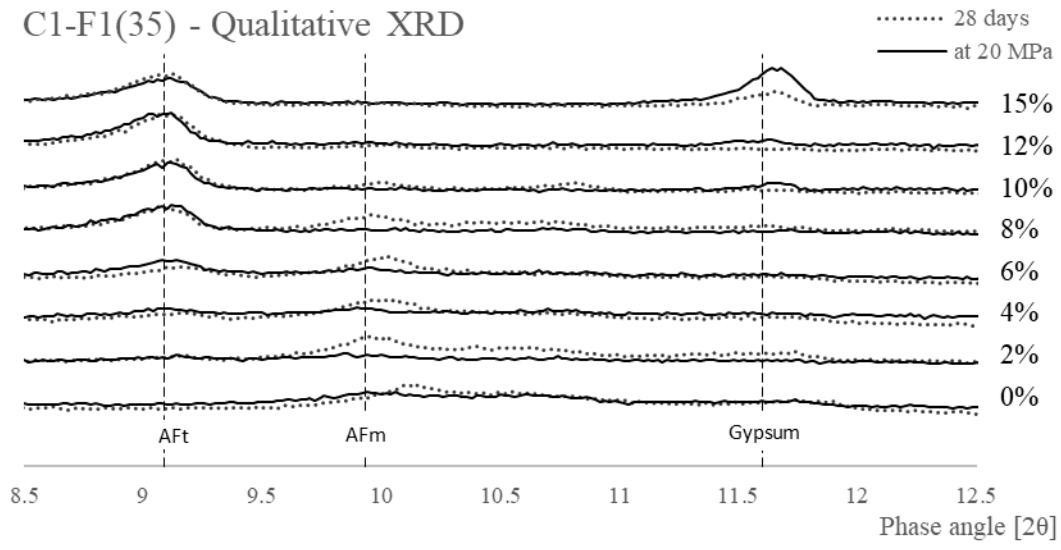


Figure 6.29. Qualitative and Quantitative XRD analysis for mixture C1-F1(35)

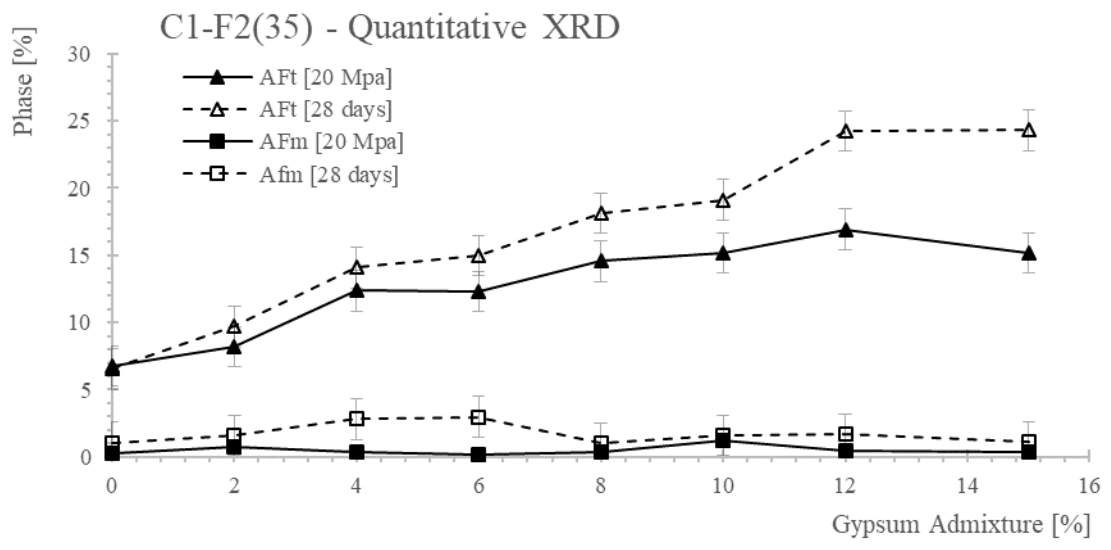
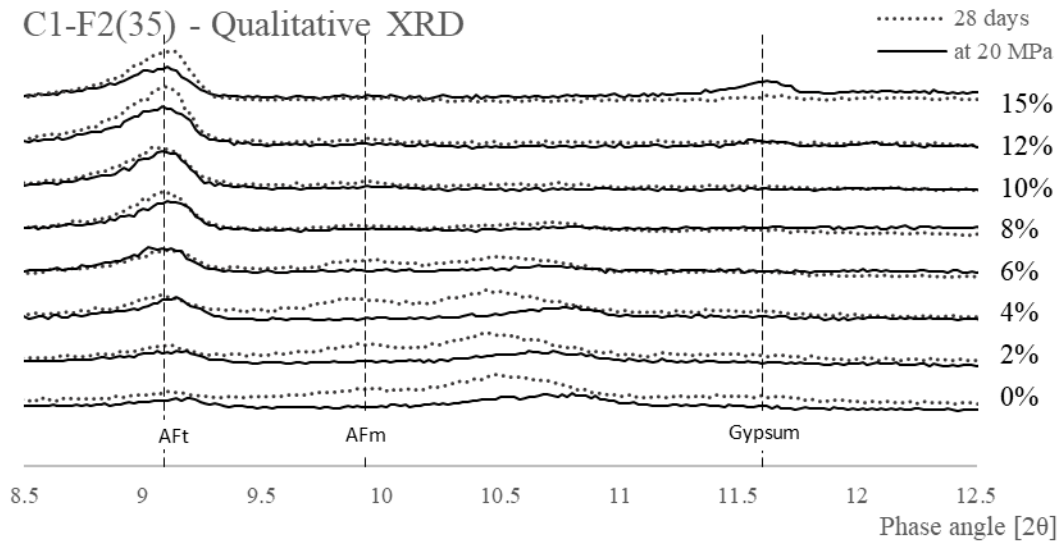


Figure 6.30. Qualitative and Quantitative XRD analysis for mixture C1-F2(35)

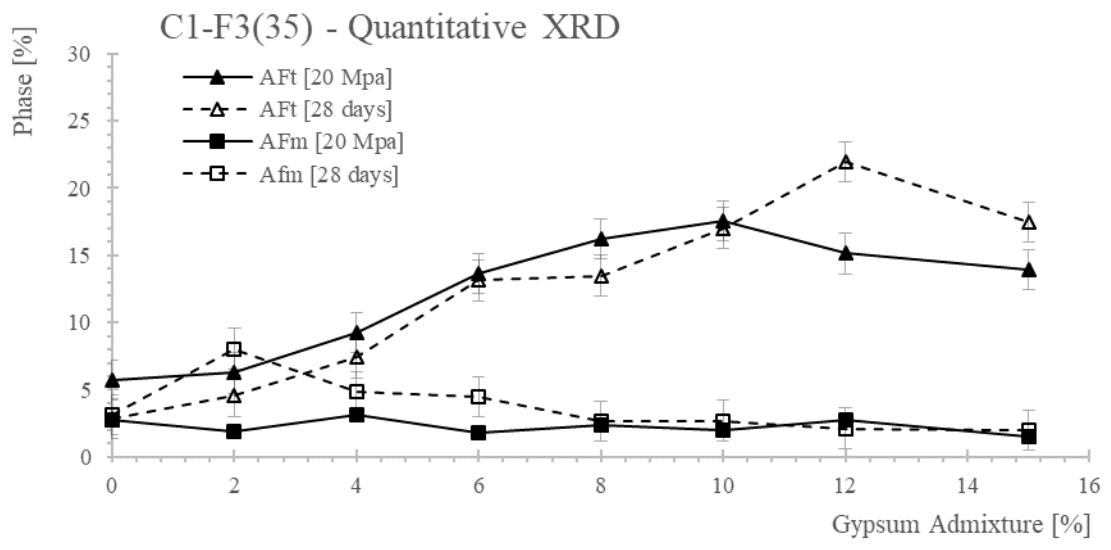
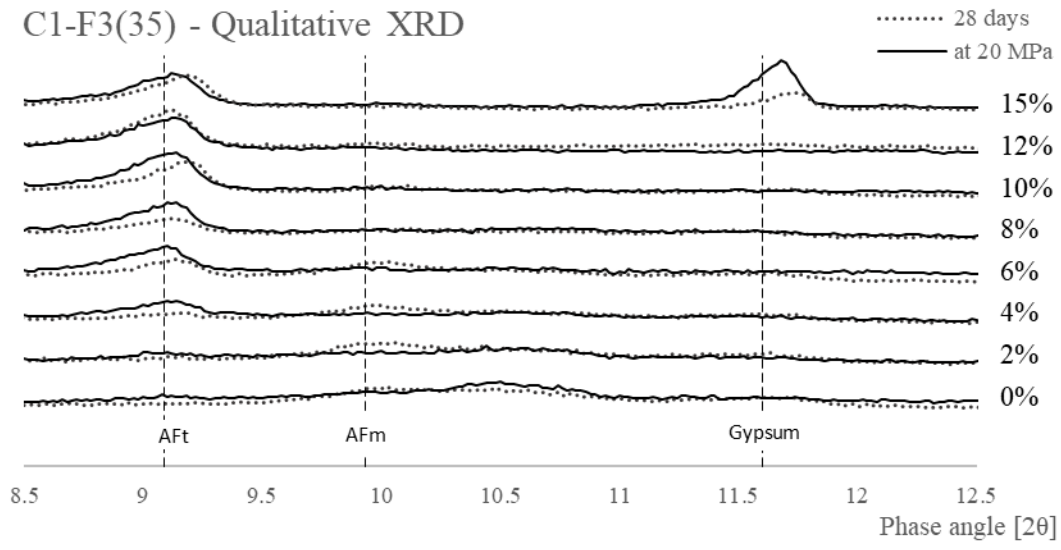


Figure 6.31 Qualitative and Quantitative XRD analysis for mixture C1-F3(35)

Table 6.19 Summary of QXRd results for mixtures C1-F1(20), C1-F2(20), and C1-F3(20)

MIX ID	Gypsum	AFt	AFt	AFm	AFm
	Admixture	[20 Mpa]	[28 days]	[20 Mpa]	[28 days]
	[%]	[%]	[%]	[%]	[%]
C1-F1(20)	0	3.8	3.5	2.1	5.3
	2	5.2	6.9	3.1	5.3
	4	6.5	11.7	2.4	5.3
	6	13.1	17.5	2.6	6.0
	8	14.4	17.8	2.3	2.1
	10	11.6	18.8	2.3	2.8
	12	11.7	16.1	2.1	4.7
	15	10.9	16.6	2.6	5.8

C1-F2(20)	0	3.6	5.1	2.7	4.1
	2	8.6	5.6	3.3	5.3
	4	10.8	12.7	2.2	4.8
	6	11.2	16.0	1.9	4.1
	8	13.2	15.6	1.5	3.0
	10	15.6	19.3	2.3	2.0
	12	13.0	17.1	2.0	1.6
	15	13.1	15.7	1.4	3.3

C1-F2(20)	0	3.6	3.2	2.8	5.7
	2	5.5	4.4	2.8	2.0
	4	7.1	8.1	2.4	2.0
	6	10.7	12.7	2.6	2.4
	8	12.2	13.5	2.5	2.8
	10	13.0	9.6	2.1	1.7
	12	11.2	11.1	2.8	3.2
	15	12.8	10.5	2.6	2.7

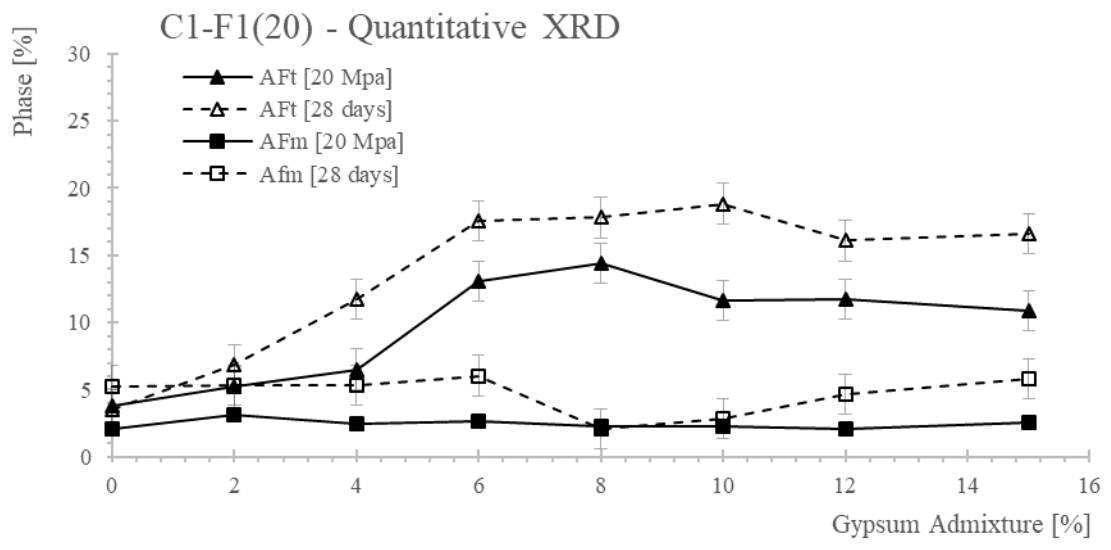
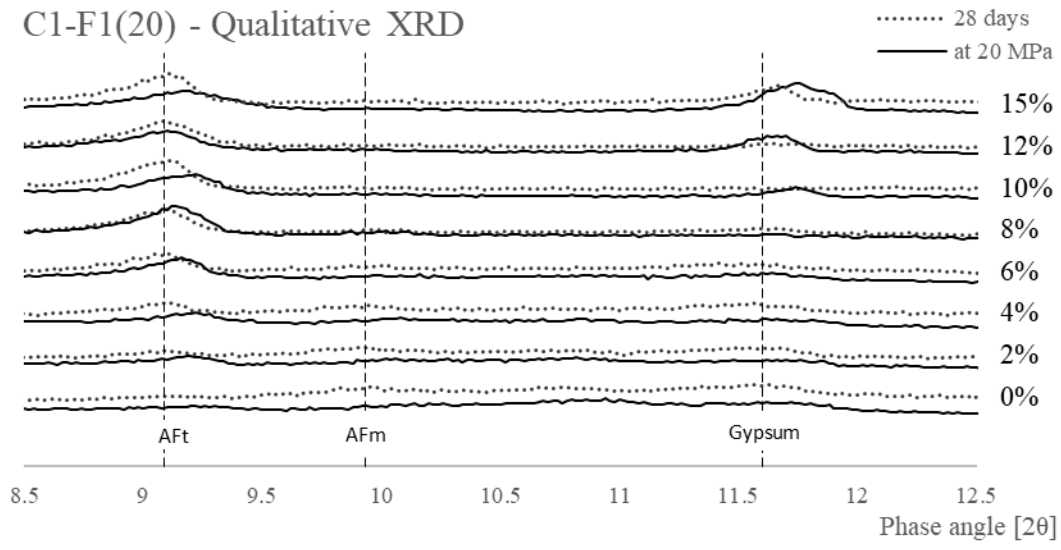


Figure 6.32. Qualitative and Quantitative XRD analysis for mixture C1-F1(20)

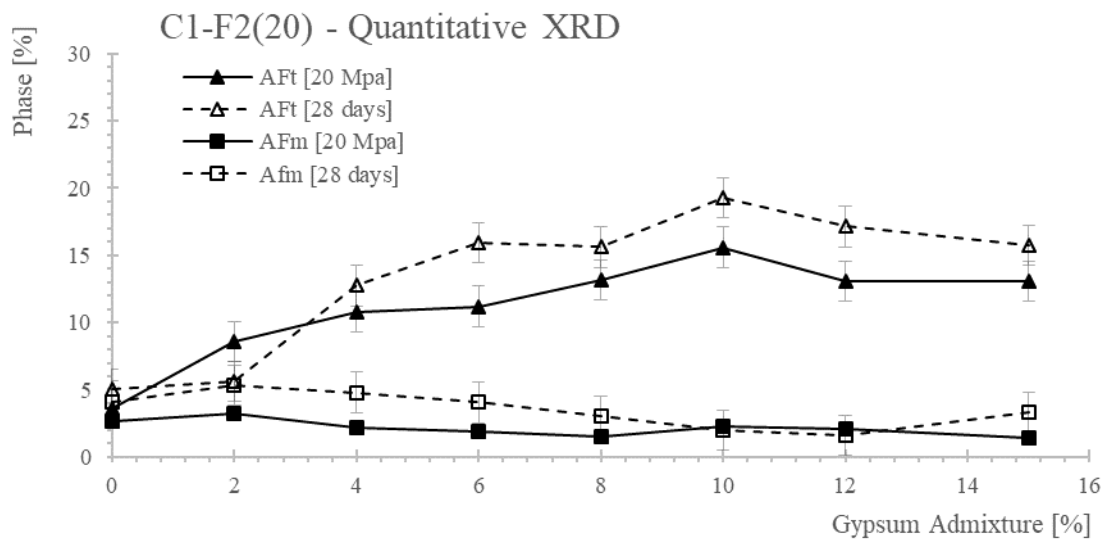
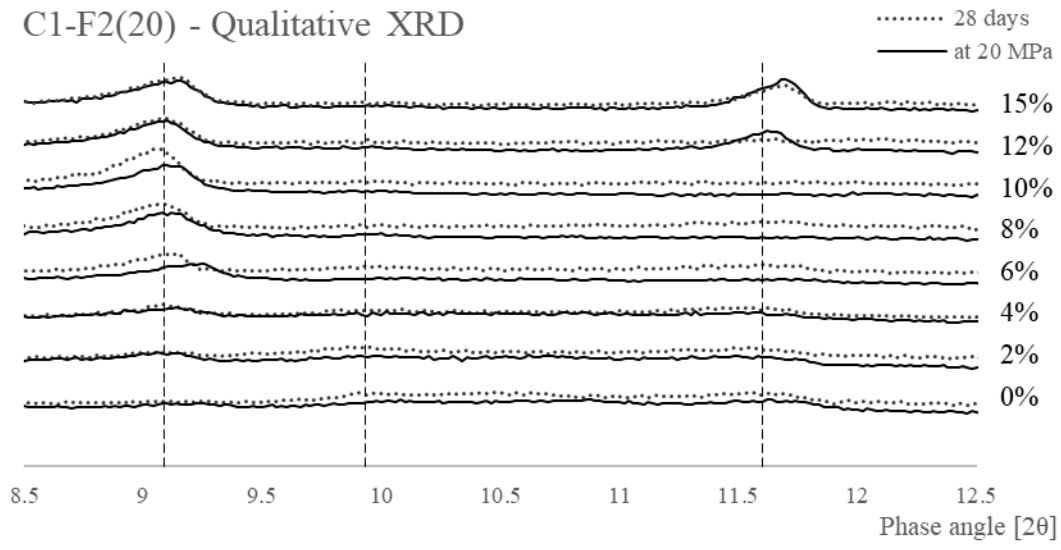


Figure 6.33. Qualitative and Quantitative XRD analysis for mixture C1-F2(20)

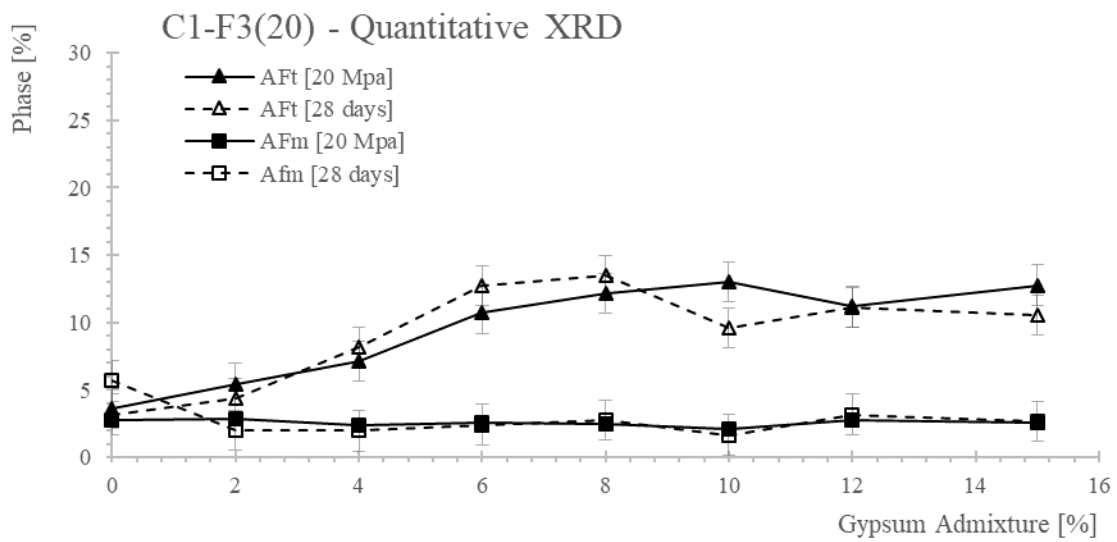
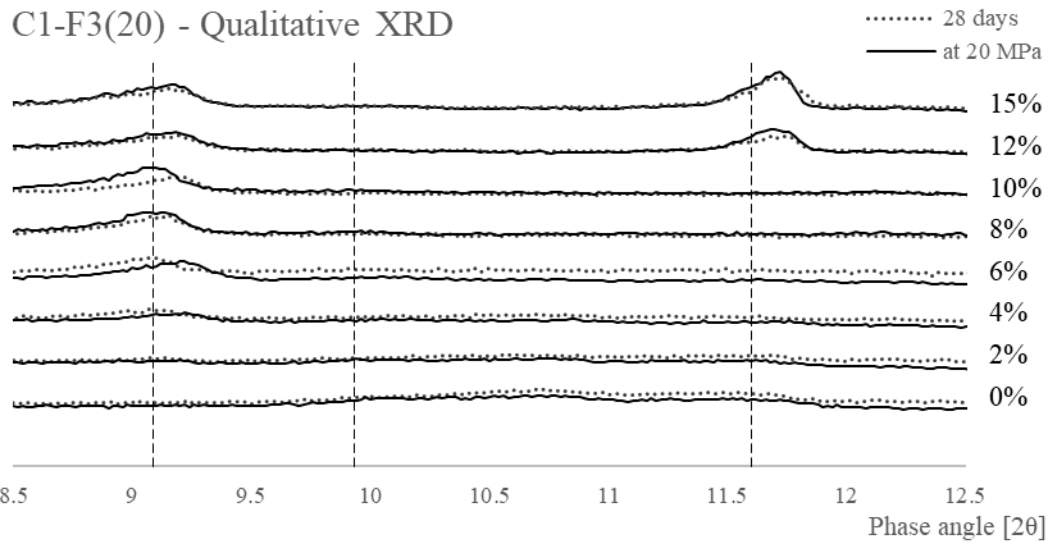


Figure 6.34 Qualitative and Quantitative XRD analysis for mixture C1-F3(20)

Table 6.20 Summary of QXRD results for mixtures C2-F1(35), C2-F2(35), and C2-F3(35)

MIX ID	Gypsum	AFt	AFt	AFm	AFm
	Admixture	[20 Mpa]	[28 days]	[20 Mpa]	[28 days]
	[%]	[%]	[%]	[%]	[%]
C2-F1(35)	0	6.2	4.8	2.1	4.9
	2	7.7	7.6	2.9	4.5
	4	10.6	12.5	2.2	3.6
	6	12.8	16.0	2.7	3.7
	8	16.9	16.0	2.3	3.8
	10	16.4	19.1	2.2	1.8
	12	18.9	19.7	1.8	2.2
	15	18.3	19.8	1.4	2.1
C2-F2(35)	0	9.0	4.0	0.9	2.8
	2	9.6	11.0	1.6	3.2
	4	11.3	14.3	1.1	2.7
	6	14.5	13.1	0.8	1.7
	8	15.7	15.9	0.7	1.7
	10	18.6	18.0	0.8	1.3
	12	15.4	17.4	2.4	1.2
	15	11.9	20.1	1.1	1.7
C2-F3(35)	0	5.5	3.6	1.9	3.5
	2	6.8	5.1	1.9	4.0
	4	7.3	10.7	2.2	4.5
	6	12.7	14.5	5.6	4.1
	8	14.1	14.1	1.4	3.1
	10	15.5	15.3	1.3	2.7
	12	13.4	17.9	2.0	2.0
	15	13.5	17.5	1.6	1.5

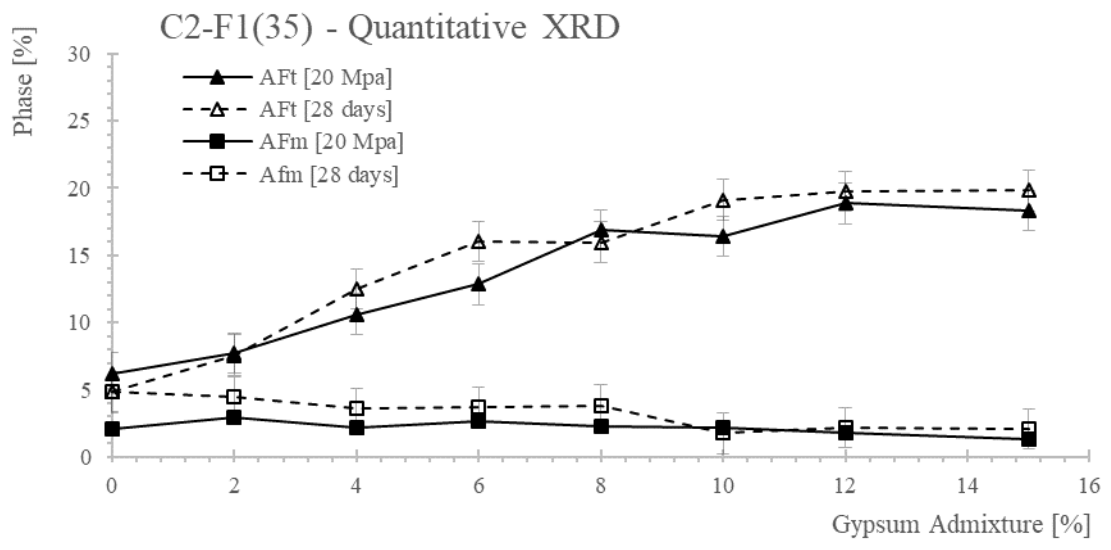
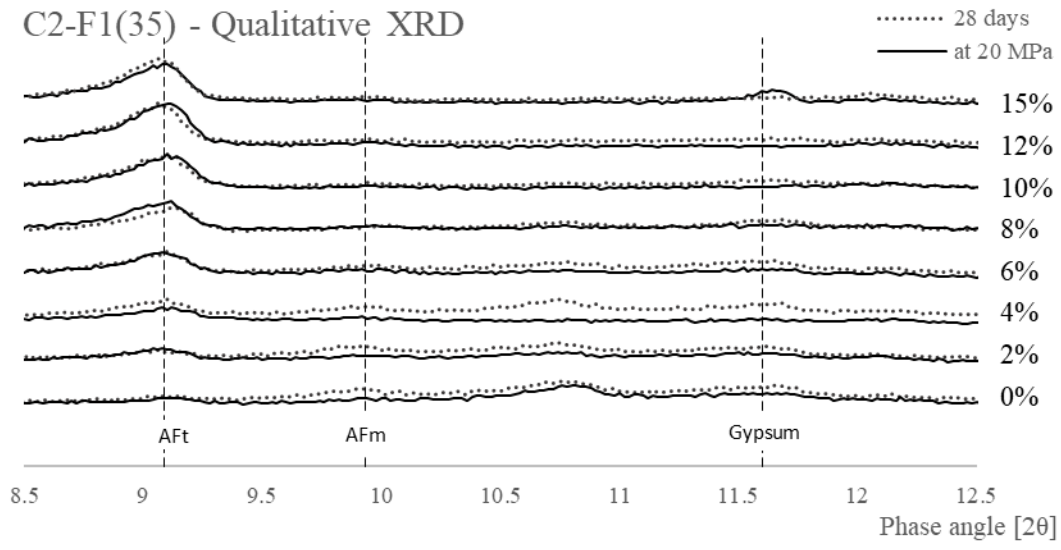


Figure 6.35. Qualitative and Quantitative XRD analysis for mixture C2-F1(35)

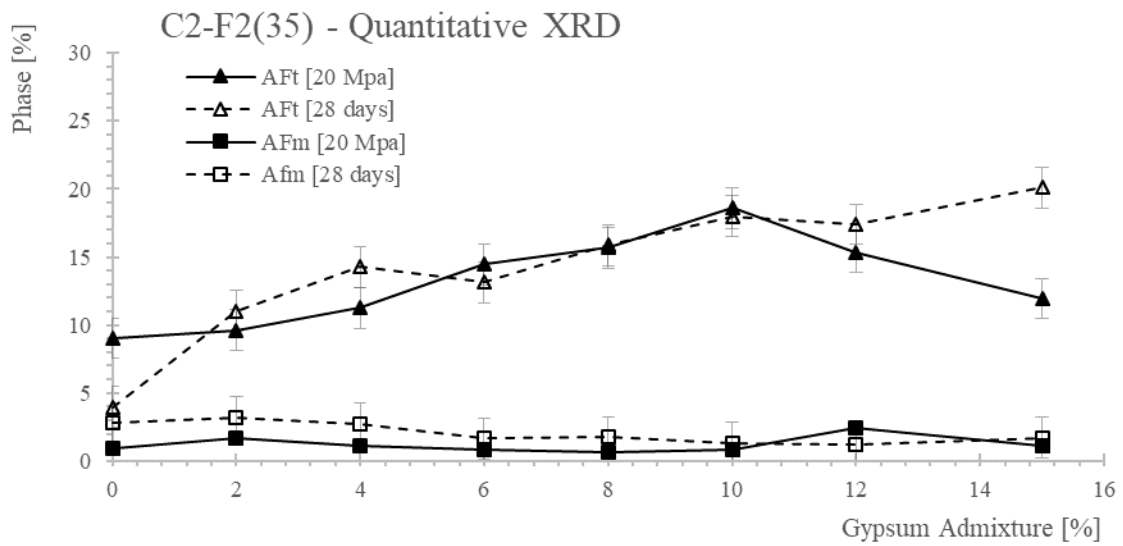
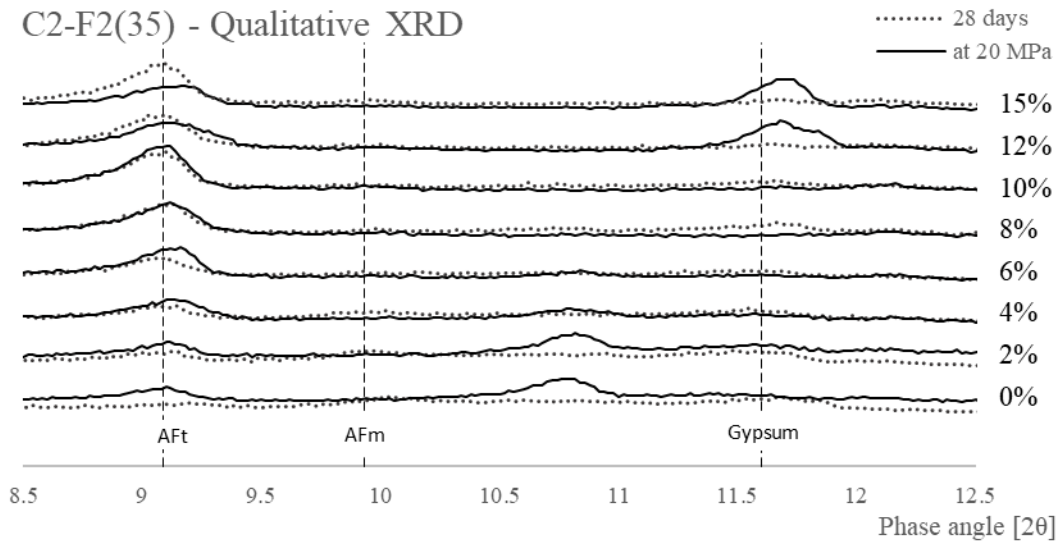


Figure 6.36. Qualitative and Quantitative XRD analysis for mixture C2-F2(35)

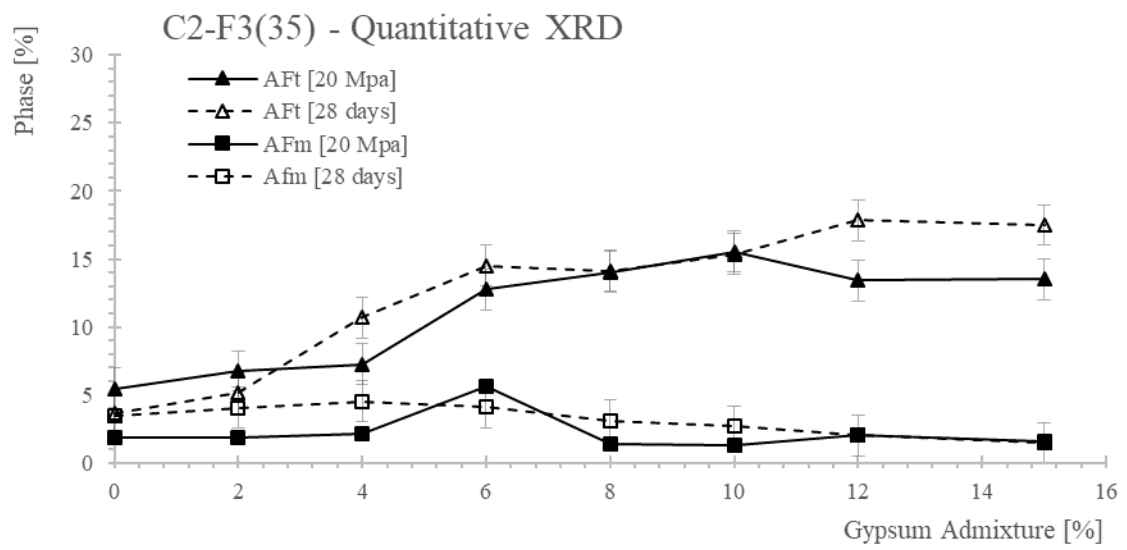
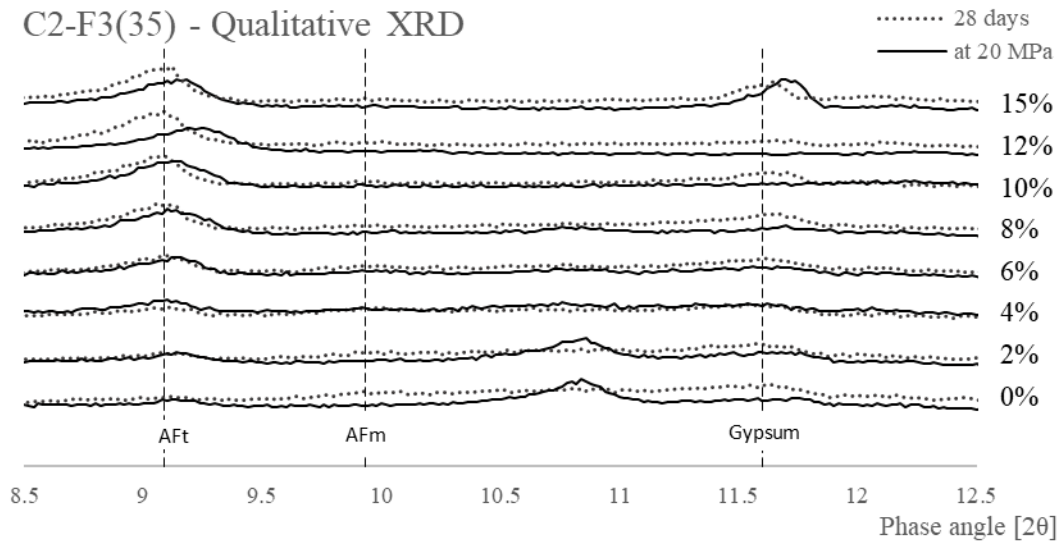


Figure 6.37 Qualitative and Quantitative XRD analysis for mixture C2-F3(35)

Table 6.21 Summary of QXR results for mixtures C2-F1(20), C2-F2(20), and C2-F3(20)

MIX ID	Gypsum	AFt	AFt	AFm	AFm
	Admixture	[20 Mpa]	[28 days]	[20 Mpa]	[28 days]
	[%]	[%]	[%]	[%]	[%]
C2-F1(20)	0	7.0	7.5	3.7	7.9
	2	9.6	8.3	4.3	10.5
	4	12.5	10.8	3.3	9.1
	6	13.3	13.5	2.4	5.8
	8	14.2	16.5	2.5	5.0
	10	12.3	16.5	1.7	3.5
	12	11.3	14.7	1.4	2.7
	15	13.9	15.5	2.3	2.0

C2-F2(20)	0	7.1	5.7	1.0	5.2
	2	9.3	8.6	5.3	13.6
	4	9.6	11.1	3.7	3.5
	6	17.1	16.7	2.3	2.8
	8	14.5	17.1	1.6	7.3
	10	14.4	18.3	0.7	3.9
	12	15.1	19.3	2.4	2.4
	15	13.0	15.0	1.8	2.2

C2-F3(20)	0	4.8	5.1	3.3	10.4
	2	6.4	8.3	3.9	7.9
	4	8.4	11.7	3.7	5.1
	6	9.7	13.3	4.1	7.3
	8	12.9	14.6	1.9	2.7
	10	12.0	14.6	1.8	1.4
	12	13.8	14.4	2.4	2.0
	15	12.0	14.9	2.4	2.9

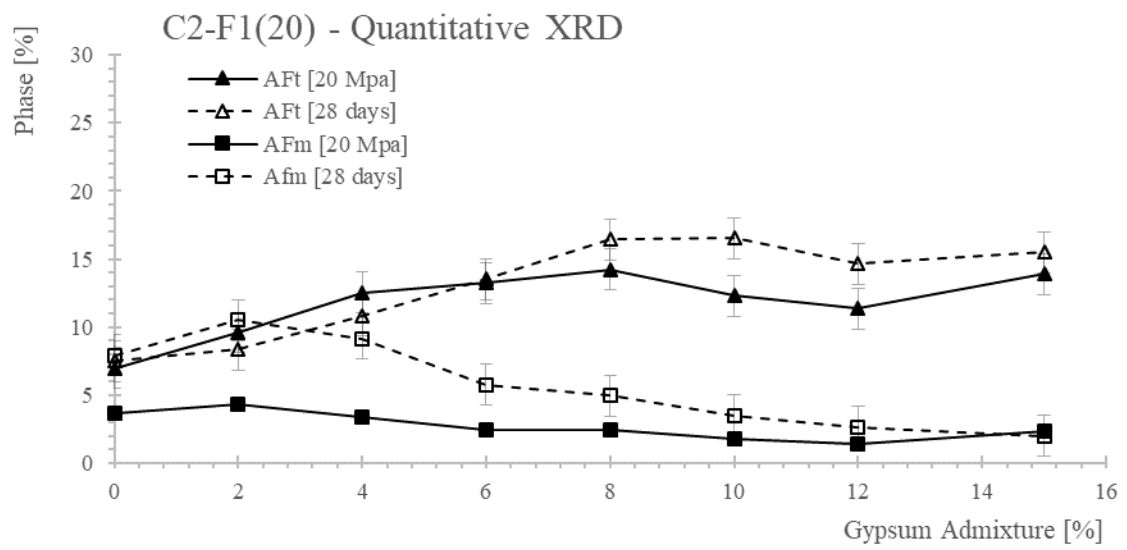
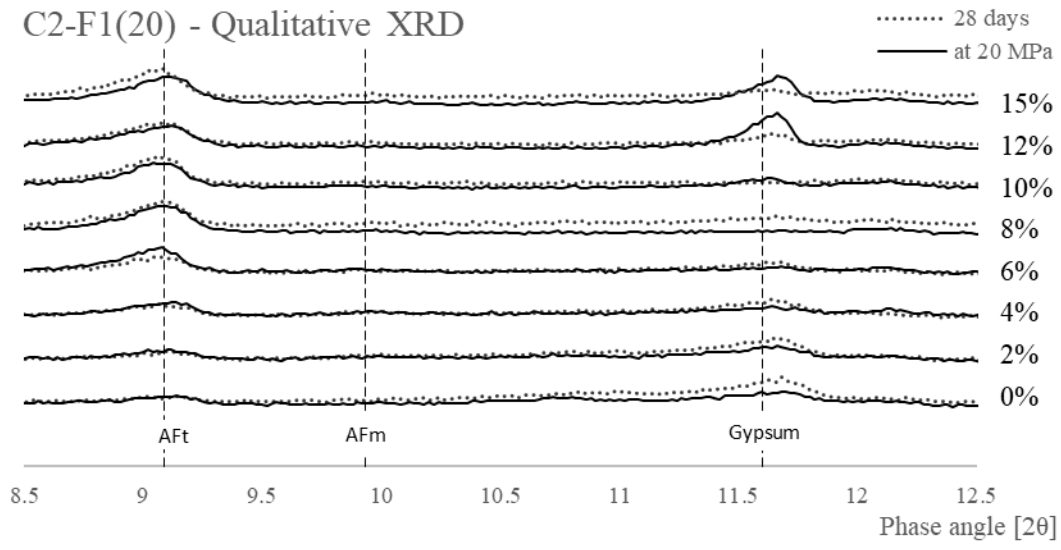


Figure 6.38. Qualitative and Quantitative XRD analysis for mixture C2-F1(20)

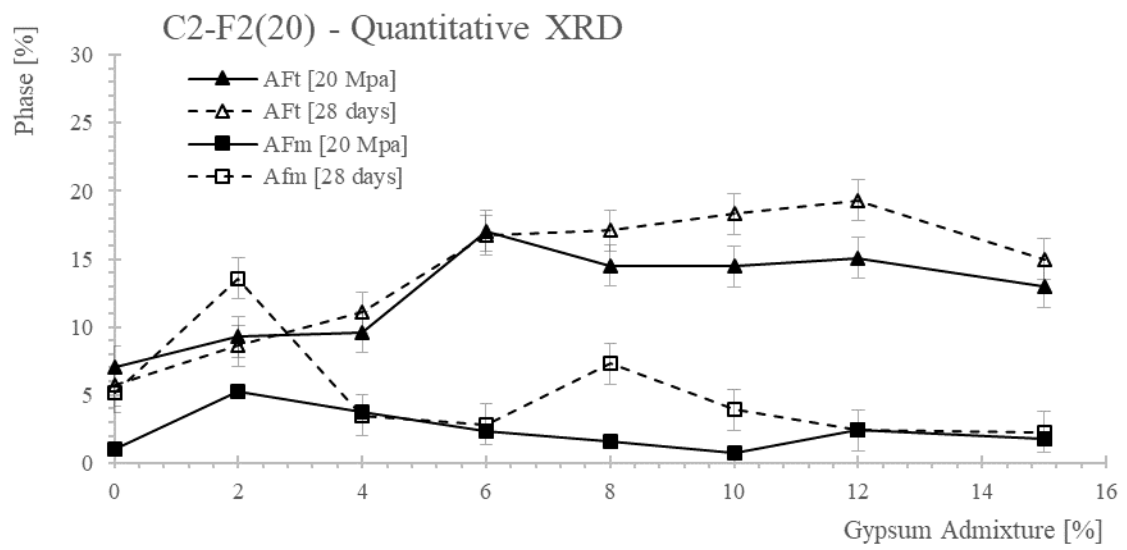
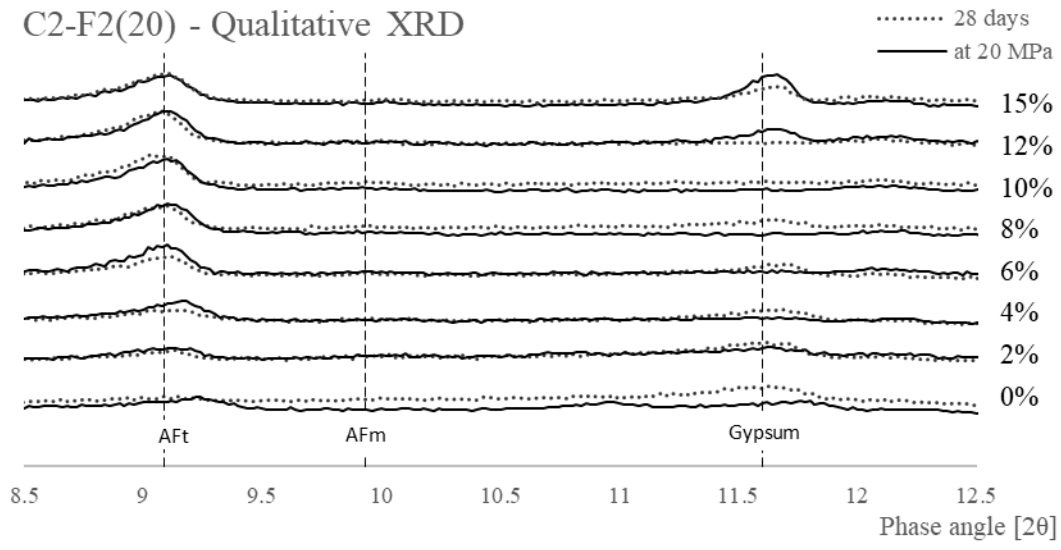


Figure 6.39 Qualitative and Quantitative XRD analysis for mixture C2-F2(20)

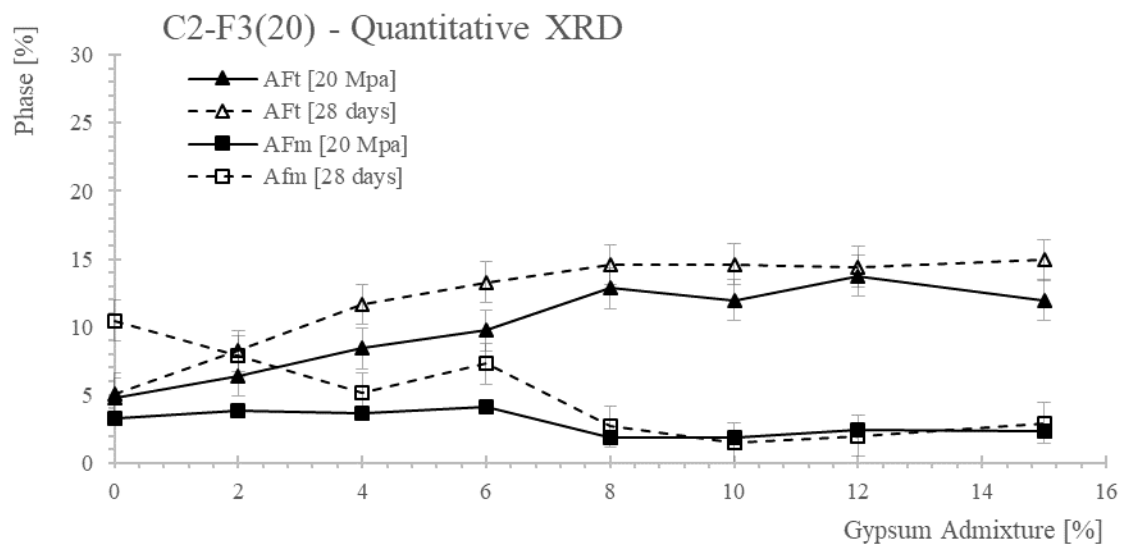
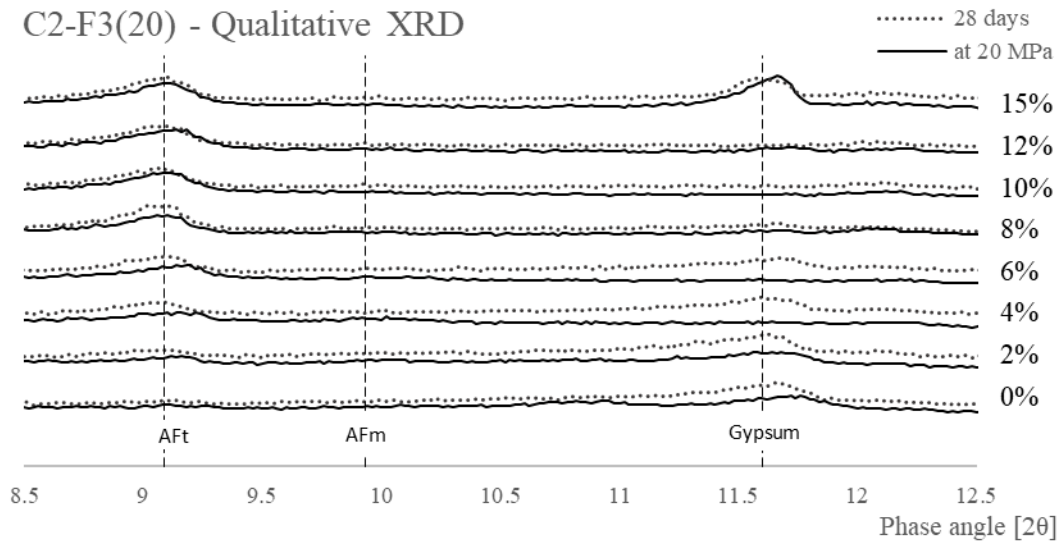


Figure 6.40. Qualitative and Quantitative XRD analysis for mixture C2-F3(20)

6.5.4.2.2. Discussion

The results shown in Figures 6.29–6.40 provide insight into multiple points of interest. The following is a numbered list of observations and corresponding descriptions of common characteristics noted while analyzing the data. The numbered list corresponds to annotations shown in Figure 6.41, which was chosen as a good example to provide graphical representation of the observations.

- The 20-MPa curve in every mixture, regardless of cement type or fly ash replacement level exhibits a point of peak AFt formation.
- There is a general increase in AFt formation between the 20-MPa and 28-day curves, especially at higher gypsum dosages.
- There is an increase in the formation of AFt, followed by a slight decrease, accompanied by a plateau in the 20-MPa curve.
- The AFm phase in both the 20-MPa and 28-day curves are approximately equal after peak AFt has occurred.
- Mixtures containing gypsum produced 2 to 5 times more AFt than mixtures without.

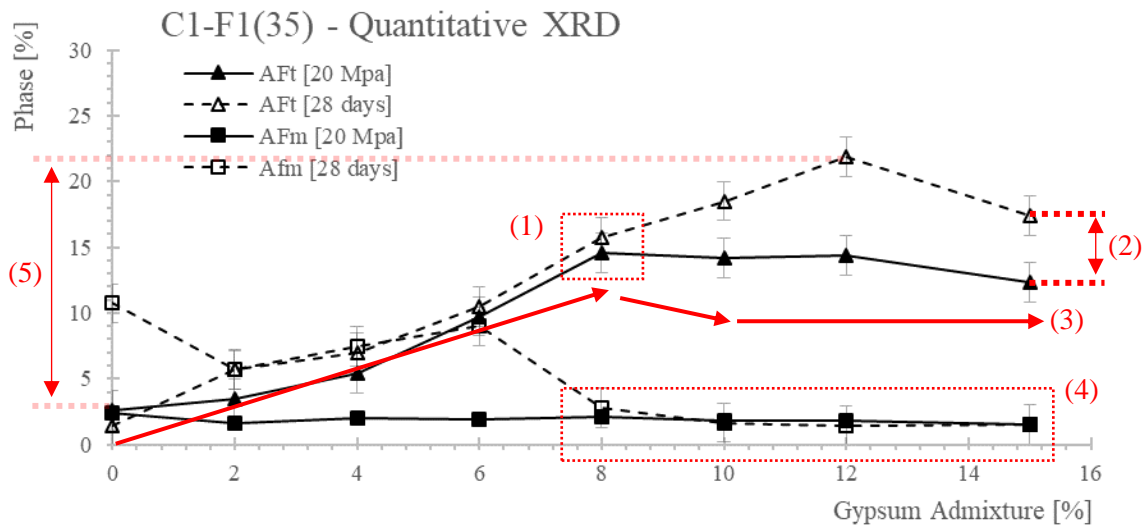


Figure 6.41 Annotated typical characteristics corresponding to numbered list of observations

Peak AFt formation on the 20-MPa curve always occurred at gypsum dosages less than peak AFt on the 28-day curve. The difference between the peak AFt on the 20-MPa curve and peak AFt on the 28-day curve indicates that gypsum is limited in its effectiveness at

producing AFt at early ages. This is a critical point to note because the formation of AFt at later ages is expansive and may result in degradation of the binder.

No analysis has been performed to understand why there is a decrease in AFt after peak AFt formation, and this question is left unanswered here.

The increase in AFm that occurs between the 20-MPa curve and 28-day curve is due to the mixture being under-sulfated. There is ample C₃A available for hydration, and not enough sulfate to stabilize the AFt phase. It is noted here that AFm was difficult to quantify using Rietveld refinement methods. The solid solution nature of AFm as documented by researchers [29] makes quantifying AFm difficult. When visually assessing the Rietveld curve, with respect to the AFm phase of the spectrum, the fit was at times poor. All QXRD data are included in the appendix of the 2018 Wheelless thesis (available at this URL: <http://hdl.handle.net/2152/68158>).

By far the most interesting observation of note is the benefit the gypsum admixture is providing in the precipitation of AFt. With every mixture, regardless of cement type or fly ash replacement levels, an observable increase in AFt corresponds to increasing dosages of gypsum admixture.

In the following sections of this chapter, a comparative analysis will be performed to show correlations between the formation of hydration products with the other testing methods performed as part of this research study.

6.5.5. ASTM C 1012 Testing

The ASTM C 1012 test is an industry standard benchmark test for sulfate resistance. A passing result is required within the cement and concrete industry to prove that a cement or mortar mixture is sulfate resistant. The test is very aggressive (>33,000 ppm SO₃) and is meant to serve as a quasi-short-term test by creating conditions that are considerably harsher than any sulfate exposure condition encountered in practice. The testing conditions are well in excess of the S3 exposure conditions per ACI-318. The test can run for a duration of 18 months, and results are accepted as passing if they meet expansion limit requirements in ASTM C 1157 performance specification for hydraulic cements as well as ASTM C 595 specification for blended cements. The expansion limit criteria in the aforementioned standards are shown in Table 6.22.

Table 6.22 Summary of expansion limits imposed by ASTM C 1157 and C 595

Classification	Maximum Expansion (%)	
	At 6 months	At 12 Months
Moderate sulfate-resistance, Type MS	0.1	-
High sulfate-resistance, Type HS	0.05	0.1

The ASTM C 1012 testing was conducted in two phases. The first phase was to assess the validity of a sulfate attack mitigation strategy proposed by Tikalsky and Carrasquillo [7], which was later tested by Dhole [9] and Aguayo [8]. This strategy entailed making an assumption about the reactive phases of the fly ash based on chemical composition, followed by stoichiometrically solving for the amount of gypsum required to meet the assumed reactivity. The second phase of ASTM C 1012 testing had two goals: to prepare mixtures that correlated to passing results observed in the first phase of testing, and to make mixtures that correlated to mixture tested in LST, isothermal calorimetry, and XRD analysis. The second phase of testing is highlighted green in Tables 6.23–6.34 to clearly delineate the two phases.

6.5.5.1. Results

The plotted expansion results (Figures 6.42–6.53) are truncated at 0.8% expansion in the figures for visual clarity. Additionally, the tabulated form of the expansion results (Tables 6.23–5.34) includes bolded values for expansion measurements in excess of 0.1% (fail), and **highlighted** values to clearly indicate the results that met (pass) the requirements of sulfate-resistance categories indicated in Table 6.23.

Table 6.23 Summary of ASTM C1012 mortar bar expansion results for mixture C1-F1(35)

MIX ID	Exp % 7d	Exp % 14d	Exp % 28d	Exp % 105d	Exp % 6m	Exp % 12m
C1	0.006	0.006	0.017	0.091	0.266	-
C1-F1(35)-G(0)	0.013	0.021	0.032	-	-	-
C1-F1(35)-G(8)	0.019	0.038	0.042	0.062	0.092	
C1-F1(35)-G(10.5)	0.054	0.065	0.096	0.245	0.462	0.875
C1-F1(35)-G(11.8)	0.076	0.095	0.148	0.418	0.829	1.484
C1-F1(35)-G(14.0)	0.119	0.195	0.297	0.663	0.988	1.897
C1-F1(35)-G(14.7)	0.087	0.207	0.399	0.834	1.178	2.194

Note: "-" indicates mortar bar was not measurable

Note: empty portions of the table indicate no measurement taken

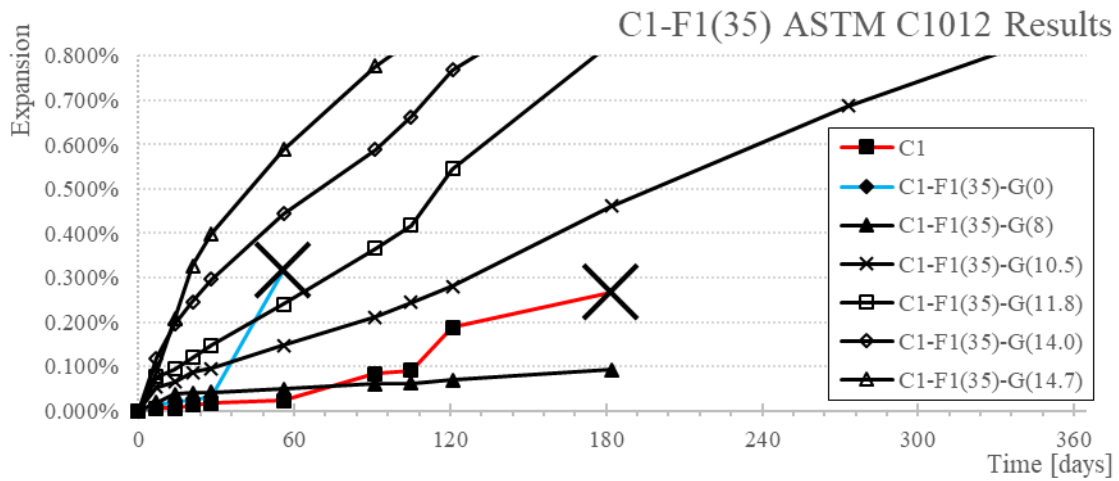


Figure 6.42. ASTM C1012 mortar bar expansion results for mixture C1-F1(35)

Table 6.24 Summary of ASTM C1012 mortar bar expansion results for mixture C1-F2(35)

MIX ID	Exp % 7d	Exp % 14d	Exp % 28d	Exp % 105d	Exp % 6m	Exp % 12m
C1	0.006	0.006	0.017	0.091	0.266	-
C1-F2(35)-G(0)	0.018	0.024	0.034	-	-	-
C1-F2(35)-G(8)	0.038	0.063	0.078	0.143	0.217	
C1-F2(35)-G(8.6)	0.008	0.010	0.012	0.023	0.026	0.051
C1-F2(35)-G(11.4)	0.083	0.107	0.186	0.580	1.080	1.839
C1-F2(35)-G(11.9)	0.098	0.121	0.172	0.516	1.017	1.762
C1-F2(35)-G(14.8)	0.171	0.279	0.575	1.462	1.874	3.511

Note: "-" indicates mortar bar was not measurable

Note: empty portions of the table indicate no measurement taken

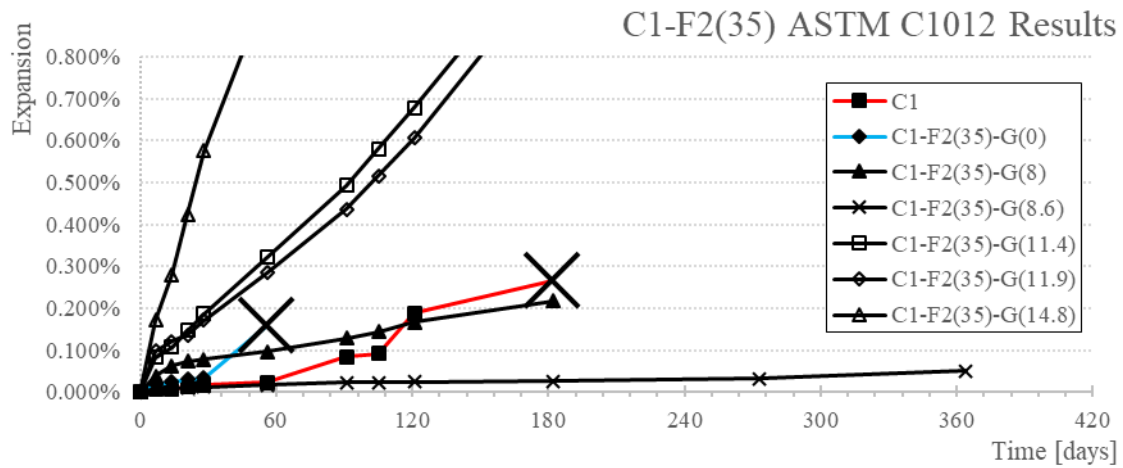


Figure 6.43. ASTM C1012 mortar bar expansion results for mixture C1-F2(35)

Table 6.25 Summary of ASTM C1012 mortar bar expansion results for mixture C1-F3(35)

MIX ID	Exp % 7d	Exp % 14d	Exp % 28d	Exp % 105d	Exp % 6m	Exp % 12m
C1	0.006	0.006	0.017	0.091	0.266	-
C1-F3(35)-G(0)	0.001	0.003	0.014	0.120	-	-
C1-F3(35)-G(8)	0.035	0.049	0.060	0.143	0.249	

Note: "-" indicates mortar bar was not measurable

Note: empty portions of the table indicate no measurement taken

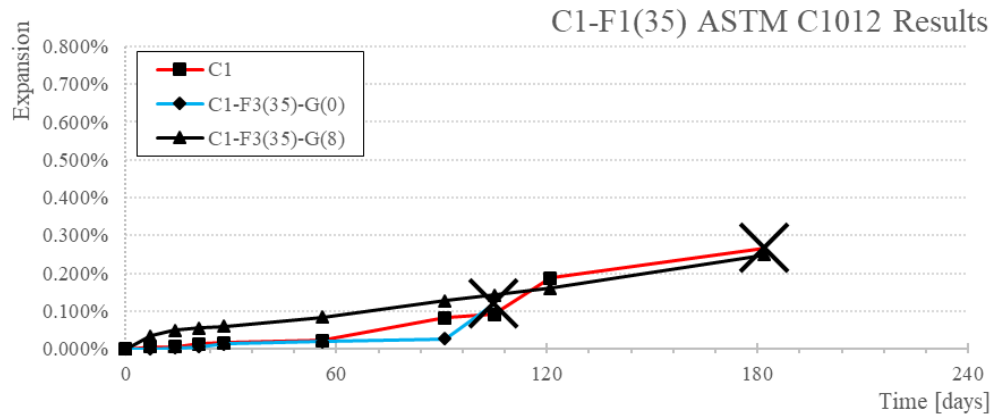


Figure 6.44. ASTM C1012 mortar bar expansion results for mixture C1-F3(35)

Table 6.26 Summary of ASTM C1012 mortar bar expansion results for mixture C1-F1(20)

MIX ID	Exp % 7d	Exp % 14d	Exp % 28d	Exp % 105d	Exp % 6m	Exp % 12m
C1	0.006	0.006	0.017	0.091	0.266	-
C1-F1(20)-G(0)	0.014	0.020	0.027	-	-	-
C1-F1(20)-G(6)	0.055	0.063	0.084	0.158	0.253	
C1-F1(20)-G(8.7)	0.042	0.050	0.071	0.334	0.769	1.588
C1-F1(20)-G(11.6)	0.044	0.106	0.247	0.735	1.265	2.190
C1-F1(20)-G(12.2)	0.085	0.150	0.419	0.883	1.592	2.204
C1-F1(20)-G(15.2)	0.043	0.118	0.278	0.871	1.421	2.302

Note: "-" indicates mortar bar was not measurable

Note: empty portions of the table indicate no measurement taken

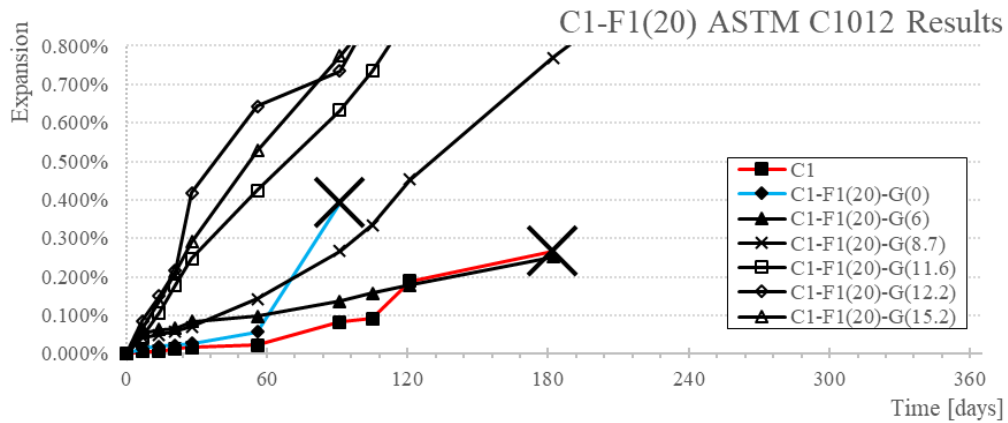


Figure 6.45 ASTM C1012 mortar bar expansion results for mixture C1-F1(20)

Table 6.27 Summary of ASTM C1012 mortar bar expansion results for mixture C1-F2(20)

MIX ID	Exp % 7d	Exp % 14d	Exp % 28d	Exp % 105d	Exp % 6m	Exp % 12m
C1	0.006	0.006	0.017	0.091	0.266	-
C1-F2(20)-G(0)	0.036	0.041	0.039	-	-	-
C1-F2(20)-G(6)	0.050	0.065	0.078	0.177	0.307	
C1-F2(20)-G(7.6)	0.019	0.039	0.060	0.260	0.578	1.662
C1-F2(20)-G(10.2)	0.052	0.121	0.221	0.758	1.184	1.923
C1-F2(20)-G(10.7)	0.056	0.123	0.233	0.682	1.105	1.751
C1-F2(20)-G(13.4)	0.065	0.137	0.291	0.874	1.307	2.484

Note: "-" indicates mortar bar was not measurable

Note: empty portions of the table indicate no measurement taken

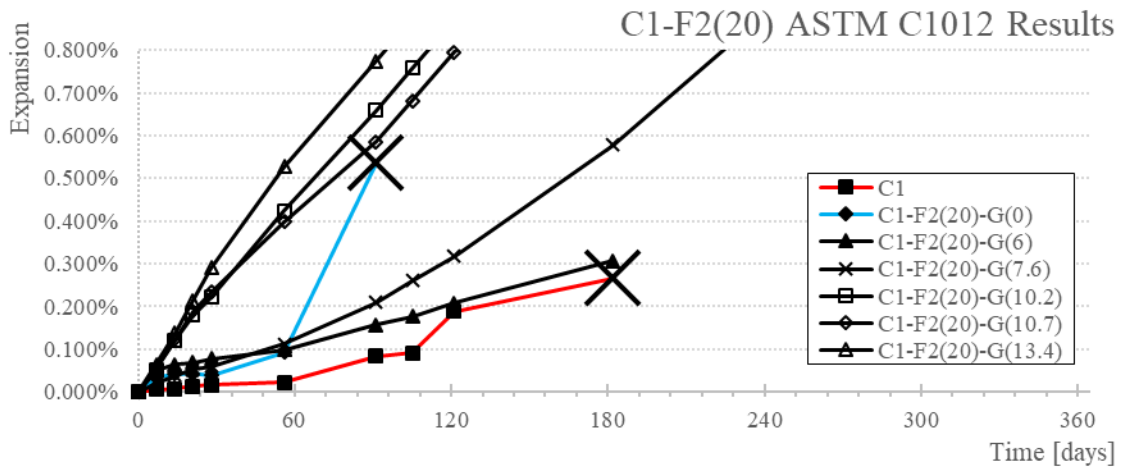


Figure 6.46. ASTM C1012 mortar bar expansion results for mixture C1-F2(20)

Table 6.28 Summary of ASTM C1012 mortar bar expansion results for mixture C1-F3(20)

MIX ID	Exp % 7d	Exp % 14d	Exp % 28d	Exp % 105d	Exp % 6m	Exp % 12m
C1	0.006	0.006	0.017	0.091	0.266	-
C1-F3(20)-G(0)	-0.003	0.009	0.013	0.396	-	-
C1-F3(20)-G(6)	0.014	0.022	0.050	0.122	0.240	

Note: "-" indicates mortar bar was not measurable

Note: empty portions of the table indicate no measurement taken

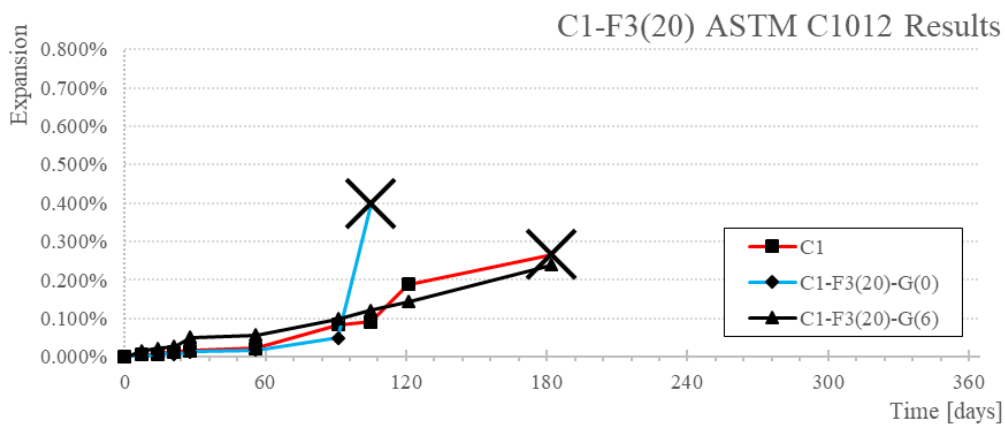


Figure 6.47. ASTM C1012 mortar bar expansion results for mixture C1-F3(20)

Table 6.29 Summary of ASTM C1012 mortar bar expansion results for mixture C2-F1(35)

MIX ID	Exp % 7d	Exp % 14d	Exp % 28d	Exp % 105d	Exp % 6m	Exp % 12m
C2	0.005	0.005	0.013	0.031	0.085	0.768
C2-F1(35)-G(0)	0.023	0.030	0.037	0.133	-	-
C2-F1(35)-G(6.0)	0.019	0.024	0.028	0.040	0.031	0.039
C2-F1(35)-G(8.0)	0.031	0.038	0.043	0.056	0.056	0.073
C2-F1(35)-G(8)	0.008	0.016	0.031	0.036	0.053	
C2-F1(35)-G(11.8)	0.075	0.079	0.095	0.126	0.234	0.306
C2-F1(35)-G(14.7)	0.061	0.099	0.123	0.348	0.690	1.433

Note: "-" indicates mortar bar was not measurable

Note: empty portions of the table indicate no measurement taken

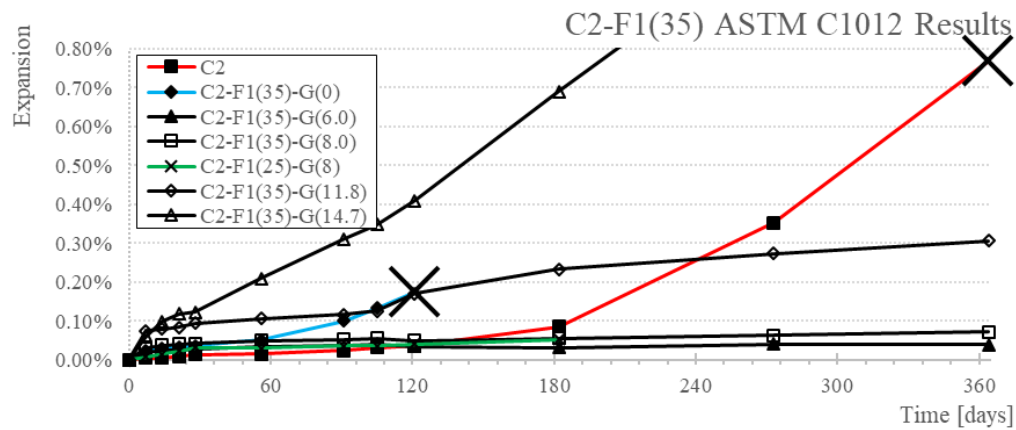


Figure 6.48. ASTM C1012 mortar bar expansion results for mixture C2-F1(35)

Table 6.30 Summary of ASTM C1012 mortar bar expansion results for mixture C2-F2(35)

MIX ID	Exp % 7d	Exp % 14d	Exp % 28d	Exp % 105d	Exp % 6m	Exp % 12m
C2	0.005	0.005	0.013	0.031	0.085	0.768
C2-F2(35)-G(0)	0.008	0.013	0.029	0.271	-	-
C2-F2(35)-G(4.1)	0.050	0.057	0.062	0.074	0.083	0.117
C2-F2(35)-G(5.4)	0.044	0.051	0.071	0.068	0.075	0.090
C2-F2(35)-G(8)	0.039	0.063	0.074	0.089	0.109	
C2-F2(35)-G(9.2)	0.022	0.032	0.041	0.084	0.137	0.233
C2-F2(35)-G(11.5)	0.033	0.045	0.062	0.229	0.443	0.786

Note: "-" indicates mortar bar was not measurable

Note: empty portions of the table indicate no measurement taken

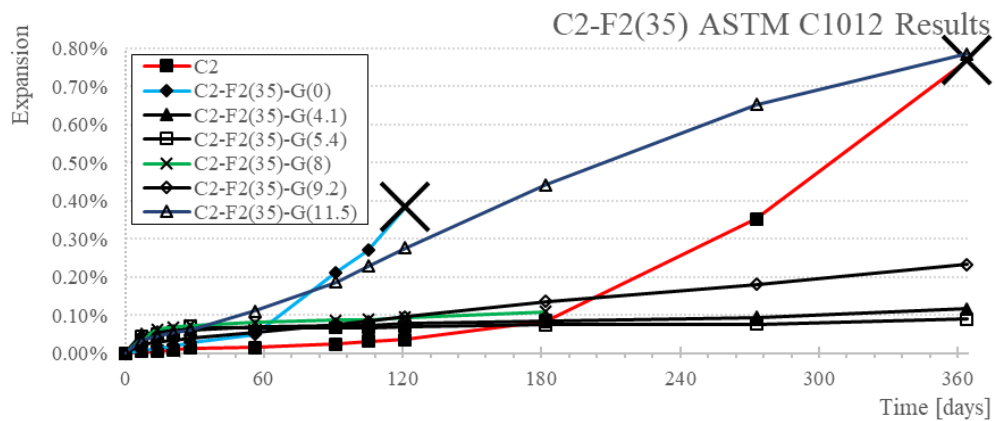


Figure 6.49. ASTM C1012 mortar bar expansion results for mixture C2-F2(35)

Table 6.31 Summary of ASTM C1012 mortar bar expansion results for mixture C2-F3(35)

MIX ID	Exp % 7d	Exp % 14d	Exp % 28d	Exp % 105d	Exp % 6m	Exp % 12m
C2	0.005	0.005	0.013	0.031	0.085	0.768
C2-F3(35)-G(0)	-0.002	0.001	0.014	0.046	0.077	-
C2-F3(35)-G(8)	0.012	0.024	0.029	0.050	0.093	

Note: "-" indicates mortar bar was not measurable

Note: empty portions of the table indicate no measurement taken

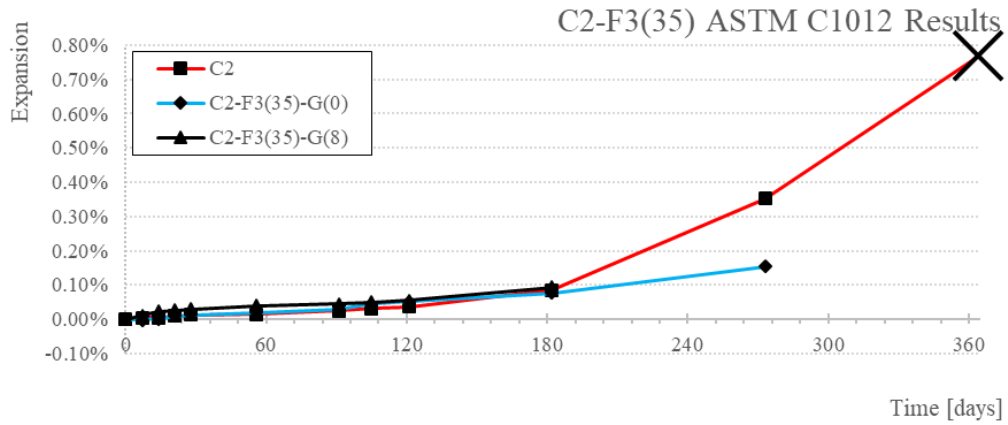


Figure 6.50. ASTM C1012 mortar bar expansion results for mixture C2-F3(35)

Table 6.32 Summary of ASTM C1012 mortar bar expansion results for mixture C2-F1(20)

MIX ID	Exp % 7d	Exp % 14d	Exp % 28d	Exp % 105d	Exp % 6m	Exp % 12m
C2	0.005	0.005	0.013	0.031	0.085	0.768
C2-F1(20)-G(0)	0.014	0.018	0.016	0.076	0.247	-
C2-F1(20)-G(3.2)	0.019	0.023	0.025	0.042	0.062	0.160
C2-F1(20)-G(4.3)	0.020	0.026	0.031	0.052	0.092	0.185
C2-F1(20)-G(6)	0.010	0.040	0.078	0.088	0.125	
C2-F1(20)-G(9.0)	0.015	0.022	0.039	0.136	0.353	0.759
C2-F1(20)-G(11.2)	0.029	0.048	0.071	0.274	0.533	1.281

Note: "-" indicates mortar bar was not measurable

Note: empty portions of the table indicate no measurement taken

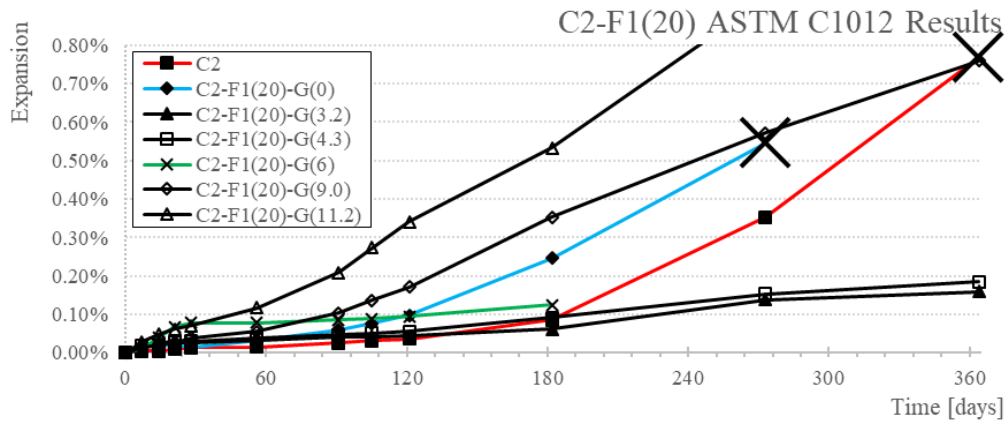


Figure 6.51. ASTM C1012 mortar bar expansion results for mixture C2-F1(20)

Table 6.33 Summary of ASTM C1012 mortar bar expansion results for mixture C2-F2(20)

MIX ID	Exp % 7d	Exp % 14d	Exp % 28d	Exp % 105d	Exp % 6m	Exp % 12m
C2	0.005	0.005	0.013	0.031	0.085	0.768
C2-F2(20)-G(0)	0.004	0.017	0.022	0.080	0.315	-
C2-F2(20)-G(2.1)	0.012	0.019	0.024	0.046	0.076	0.297
C2-F2(20)-G(2.8)	0.010	0.017	0.022	0.039	0.067	0.204
C2-F2(20)-G(6)	0.008	0.021	0.023	0.040	0.060	
C2-F2(20)-G(7.5)	0.023	0.028	0.040	0.122	0.228	0.491
C2-F2(20)-G(9.4)	0.035	0.047	0.061	0.240	0.562	1.097

Note: "-" indicates mortar bar was not measurable

Note: empty portions of the table indicate no measurement taken

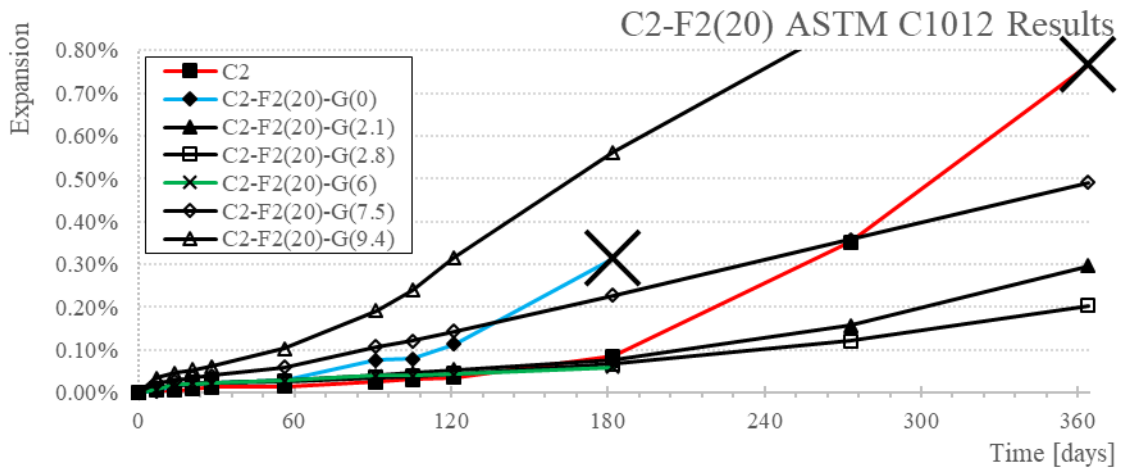


Figure 6.52. ASTM C1012 mortar bar expansion results for mixture C2-F2(20)

Table 6.34 Summary of ASTM C1012 mortar bar expansion results for mixture C2-F3(20)

MIX ID	Exp % 7d	Exp % 14d	Exp % 28d	Exp % 105d	Exp % 6m	Exp % 12m
C2	0.005	0.005	0.013	0.031	0.085	0.768
C2-F3(20)-G(0)	0.000	0.007	0.015	0.028	0.039	
C2-F3(20)-G(6)	0.012	0.017	0.021	0.046	0.083	

Note: "-" indicates mortar bar was not measurable

Note: empty portions of the table indicate no measurement taken

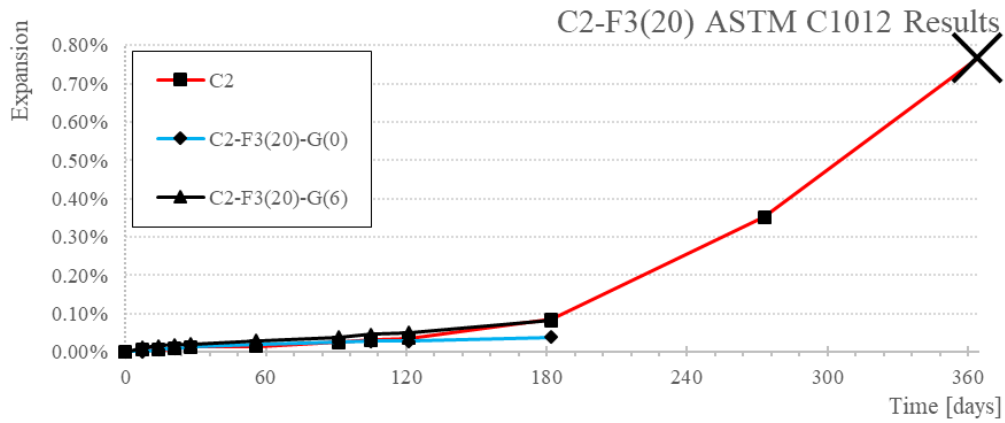


Table 6.35 Complete summary of ASTM C 1012 mortar bar expansion results for all 56 mixtures tested in this research study

MIX ID	Exp % 6m	Exp % 12m	MIX ID	Exp % 6m	Exp % 12m
C1	0.266	-	C2	0.085	0.768
C1-F1(35)-G(0)	-	-	C2-F1(35)-G(0)	-	-
C1-F1(35)-G(8)	0.092		C2-F1(35)-G(6.0)	0.031	0.039
C1-F1(35)-G(10.5)	0.462	0.875	C2-F1(35)-G(8.0)	0.056	0.073
C1-F1(35)-G(11.8)	0.829	1.484	C2-F1(25)-G(8)	0.053	
C1-F1(35)-G(14.0)	0.988	1.897	C2-F1(35)-G(11.8)	0.234	0.306
C1-F1(35)-G(14.7)	1.178	2.194	C2-F1(35)-G(14.7)	0.690	1.433
C1-F2(35)-G(0)	-	-	C2-F2(35)-G(0)	-	-
C1-F2(35)-G(8)	0.217		C2-F2(35)-G(4.1)	0.083	0.117
C1-F2(35)-G(8.6)	0.026	0.051	C2-F2(35)-G(5.4)	0.075	0.090
C1-F2(35)-G(11.4)	1.080	1.839	C2-F2(35)-G(8)	0.109	
C1-F2(35)-G(11.9)	1.017	1.762	C2-F2(35)-G(9.2)	0.137	0.233
C1-F2(35)-G(14.8)	1.874	3.511	C2-F2(35)-G(11.5)	0.443	0.786
C1-F3(35)-G(0)	-	-	C2-F3(35)-G(0)	0.077	-
C1-F3(35)-G(8)	0.249		C2-F3(35)-G(8)	0.093	
C1-F1(20)-G(0)	-	-	C2-F1(20)-G(0)	0.247	
C1-F1(20)-G(6)	0.253		C2-F1(20)-G(3.2)	0.062	0.160
C1-F1(20)-G(8.7)	0.769	1.588	C2-F1(20)-G(4.3)	0.092	0.185
C1-F1(20)-G(11.6)	1.265	2.190	C2-F1(20)-G(6)	0.125	
C1-F1(20)-G(12.2)	1.592	2.204	C2-F1(20)-G(9.0)	0.353	0.759
C1-F1(20)-G(15.2)	1.421	2.302	C2-F1(20)-G(11.2)	0.533	1.281
C1-F2(20)-G(0)	-	-	C2-F2(20)-G(0)	0.315	
C1-F2(20)-G(6)	0.307		C2-F2(20)-G(2.1)	0.076	0.297
C1-F2(20)-G(7.6)	0.578	1.662	C2-F2(20)-G(2.8)	0.067	0.204
C1-F2(20)-G(10.2)	1.184	1.923	C2-F2(20)-G(6)	0.060	
C1-F2(20)-G(10.7)	1.105	1.751	C2-F2(20)-G(7.5)	0.228	0.491
C1-F2(20)-G(13.4)	1.307	2.484	C2-F2(20)-G(9.4)	0.562	1.097
C1-F3(20)-G(0)	-	-	C2-F3(20)-G(0)	0.039	
C1-F3(20)-G(6)	0.240		C2-F3(20)-G(6)	0.083	

Note: "-" indicates mortar bar was not measurable.

Note: empty portions of the table indicate no measurement taken.

6.5.5.2. Discussion

In total, 16 of the 56 mixtures passed ASTM C 1012 by meeting the expansion limits of ASTM C 1157 and C 595, not including the straight cement mixture containing C2 (a type I/II sulfate-resistant cement). Mixtures that did not contain gypsum, straight cement and cement with fly ash, degraded rapidly with a complete loss of cohesion.

Those mortar bars that failed ASTM C 1012 and contained less than nominally 10% gypsum admixture degraded in the same way as the straight cement mixtures, but always took a longer time to fail. When the mortar bars began to fail, cracking and degradation would start at the corners, which would be followed by cracking of the cross-section, then complete loss of cohesion and crumbling.

Two mixtures containing cement C1 passed. Mixtures C1-F1(35)-G(8) and C1-F2(35)-G(8.6) can be classified as exhibiting a moderate sulfate resistance. One of the passing mixtures, C1-F2(35)-G(8.6), was from phase 1. As part of phase 2, a replicate mixture was prepared, C1-F2(35)-G(8), to show repeatable results. Unfortunately, the results from phase 1 could not be repeated. The discrepancy in behavior between the two mixtures is potentially due to a prolonged curing period for mixture C1-F2(35)-G(8.6), which cured for 1 day too many (having achieved strength on a Sunday during a holiday weekend) and was placed in Na₂SO₄ 1 day later than the replicate mixture C1-F2(35)-G(8). The occurrence of C1-F1(35)-G(8.6) having cured too long was a mistake made early on this research project that was not repeated.

Mixtures containing cement C2 performed better relative to mixtures containing cement C1. In total, 14 mixtures passed at 6 months. Cement C2 is a sulfate-resisting cement, which increased the likelihood that mixtures in which it was used would perform better. In general, the mixtures containing C2 that passed also contained less gypsum (nominally less than 6–8%).

In analyzing the ASTM C 1012 data, a pattern emerged with respect to gypsum dosages. Mixtures using either cement C1 or C2 having contained gypsum quantities greater than or equal 10% typically showed:

- Slow strength gain, often taking nominally 5 to 9 days for the mortar cubes to achieve a compressive strength of 20 MPa. These results imply the mixtures will not be feasible for practical use in construction.
- High (nominally greater than 0.5%) expansion levels at 6 months.
- Mortar bars that remained intact despite excessive expansion levels.

- Degradation of the mortar bars that differed in appearance from mixtures containing lower amounts of gypsum. Mortar bars containing greater than 10% gypsum showed very high levels of expansion, with no cracking at one year. However, the mortar bars were often warped with a noticeable curvature, taking on a banana-shaped appearance.

The results of this study indicate that mortars containing the amount of gypsum required by the guidance of Tikalsky and Carrasquillo [7] will expand well beyond limits imposed by ASTM. Other research studies [8, 9] have come to the same conclusion. The mortars in this study that contain the gypsum required to meet the guidance outlined by Tikalsky and Carrasquillo did not fail, in terms of a complete lack of cohesion, but showed excessive levels of expansion (nominally greater than 0.5% at 6 months). Given previous research, in conjunction with the results of this study, we conclude here that the underlying assumptions presented by Tikalsky and Carrasquillo in proportioning the correct dosages of gypsum as an admixture in binary blends of high-calcium fly ash as a replacement for cements will not yield mortars that will meet ASTM standards.

6.5.6. Comparative Analysis of All Testing

Following is a comparison of the data collected from all the testing methods performed in this research study. A pattern emerges when the data from each of the tests is overlaid; thus Figures 6.54–6.65 have been prepared to show this pattern. The independent variable for all the figures shown is gypsum. The comparison of the data will be used to provide analysis pertaining to the passing or failing results obtained in ASTM C 1012 testing. The findings of this study appear to indicate that a comparison like the ones shown in the next section can be used in future research as a means for developing a method for predicting the sulfate resistance of a given mixture. The comparative analysis results will also be examined against Lerch's criteria.

6.5.6.1. Results

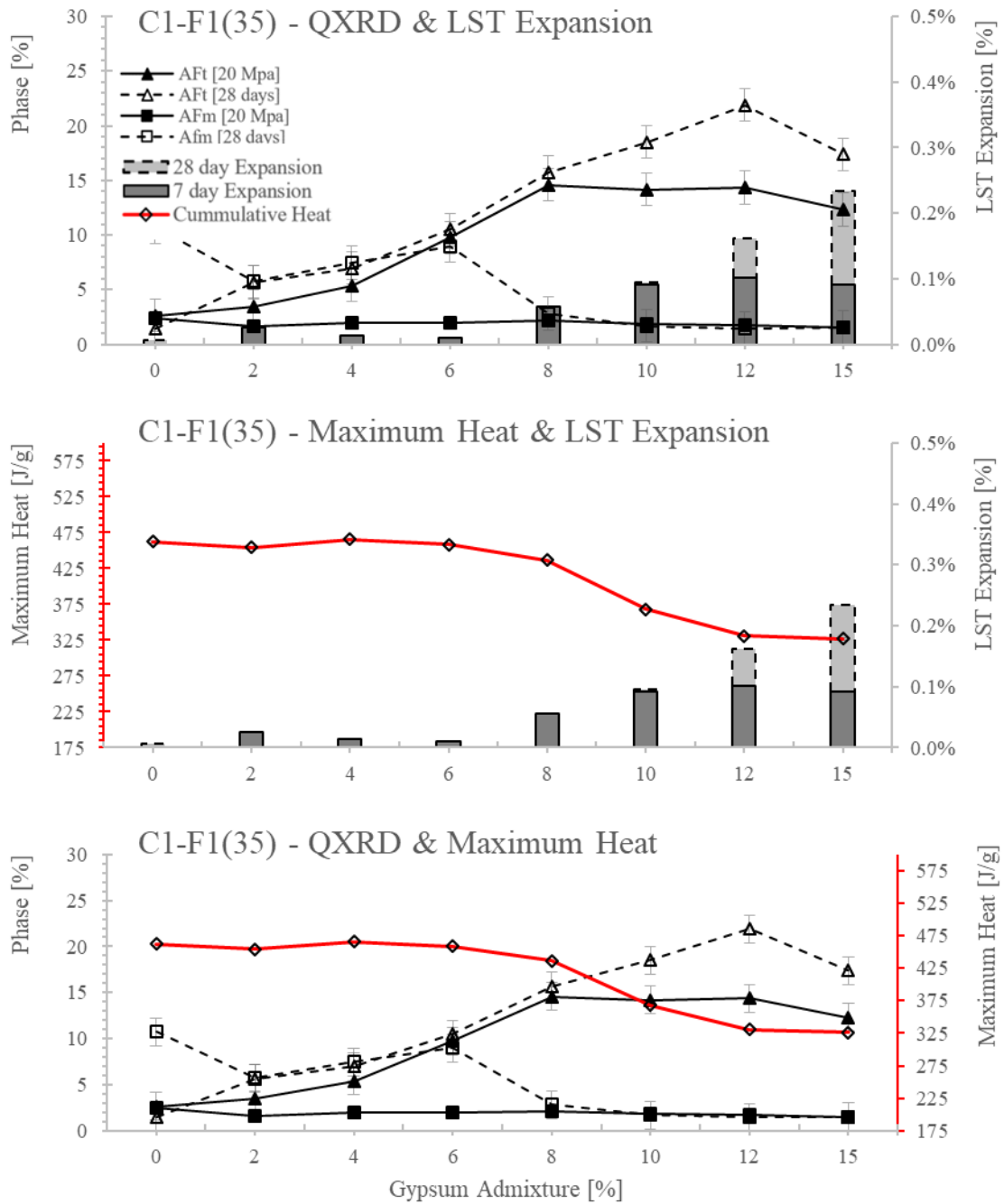


Figure 6.54 Comparison of expansion data from LST, QXRD analysis, and maximum heat curves for mixture C1-F1(35)

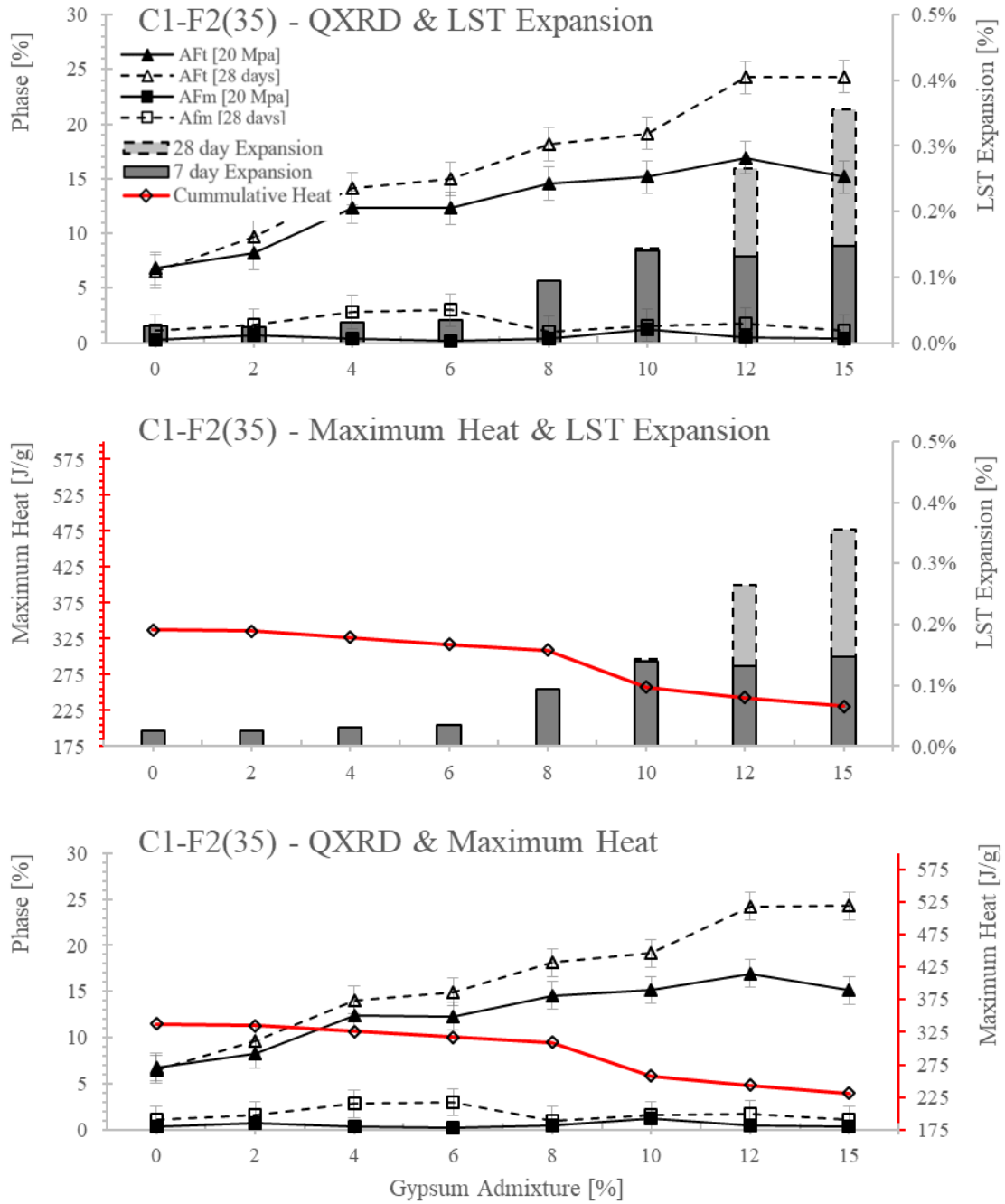


Figure 6.55. Comparison of expansion data from LST, QXRD analysis, and maximum heat curves for mixture C1-F2(35)

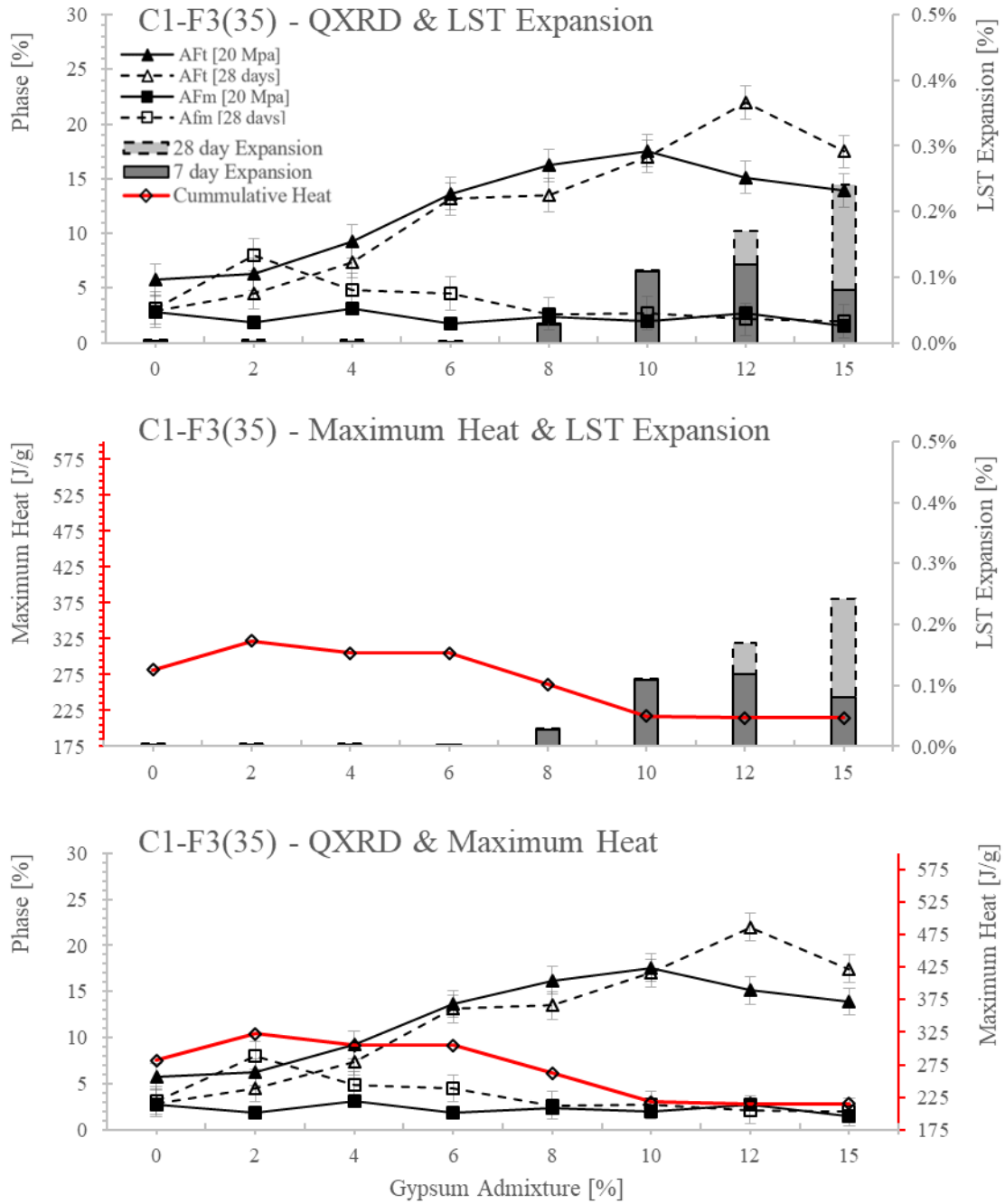


Figure 6.56. Comparison of expansion data from LST, QXRD analysis, and maximum heat curves for mixture C1-F3(35)

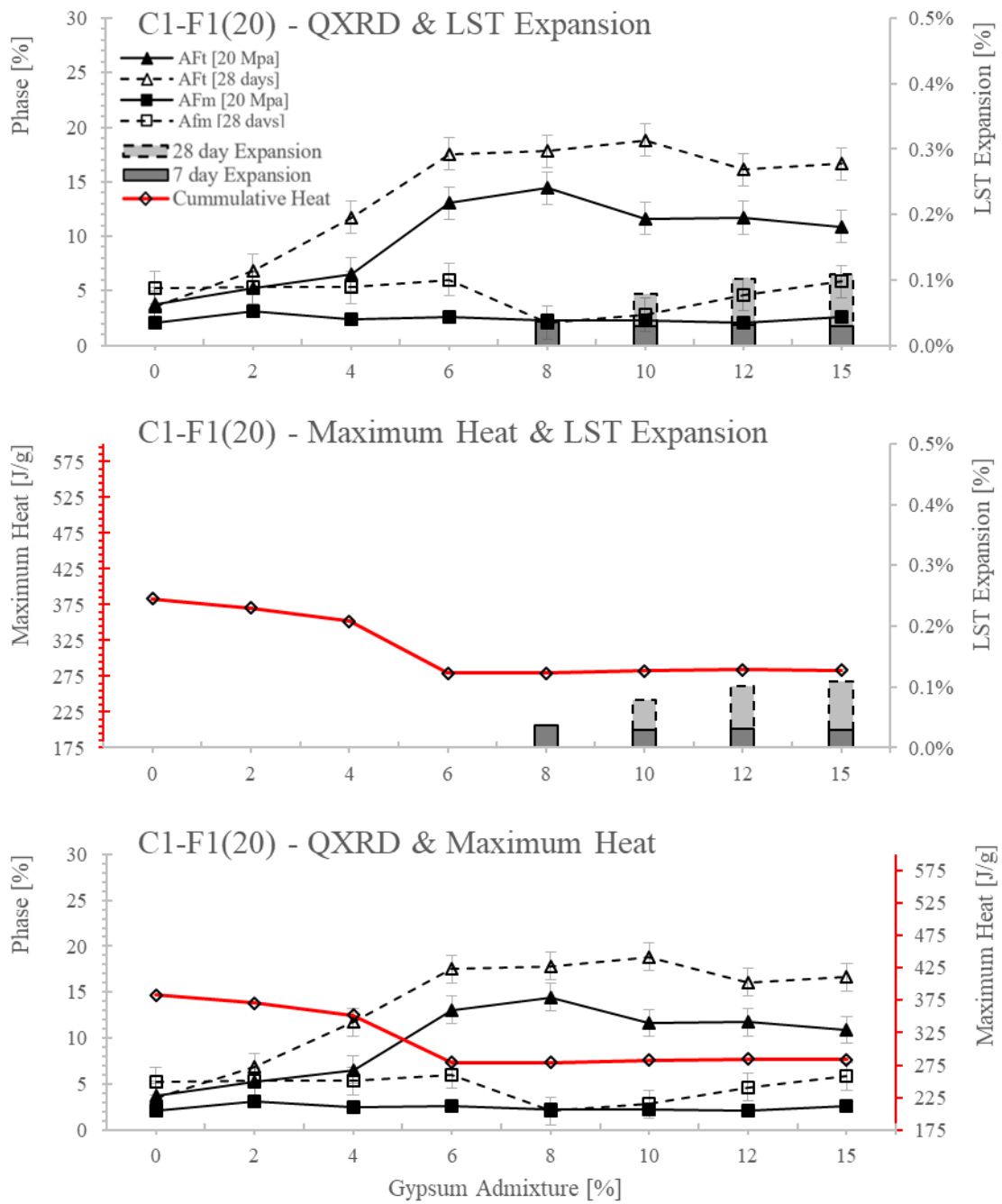


Figure 6.57 Comparison of expansion data from LST, QXRD analysis, and maximum heat curves for mixture C1-F1(20)

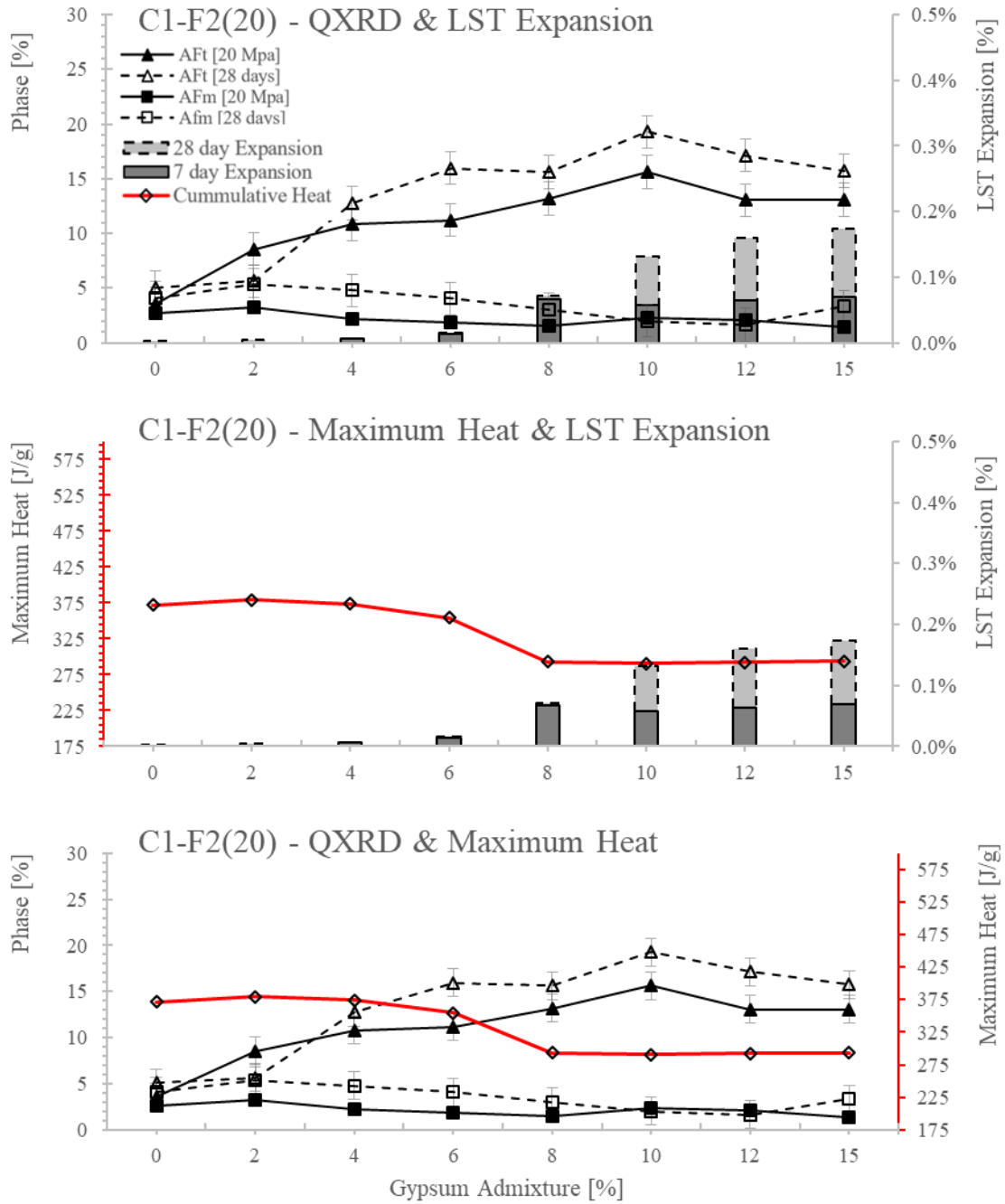


Figure 6.58 Comparison of expansion data from LST, QXRD analysis, and maximum heat curves for mixture C1-F2(20)

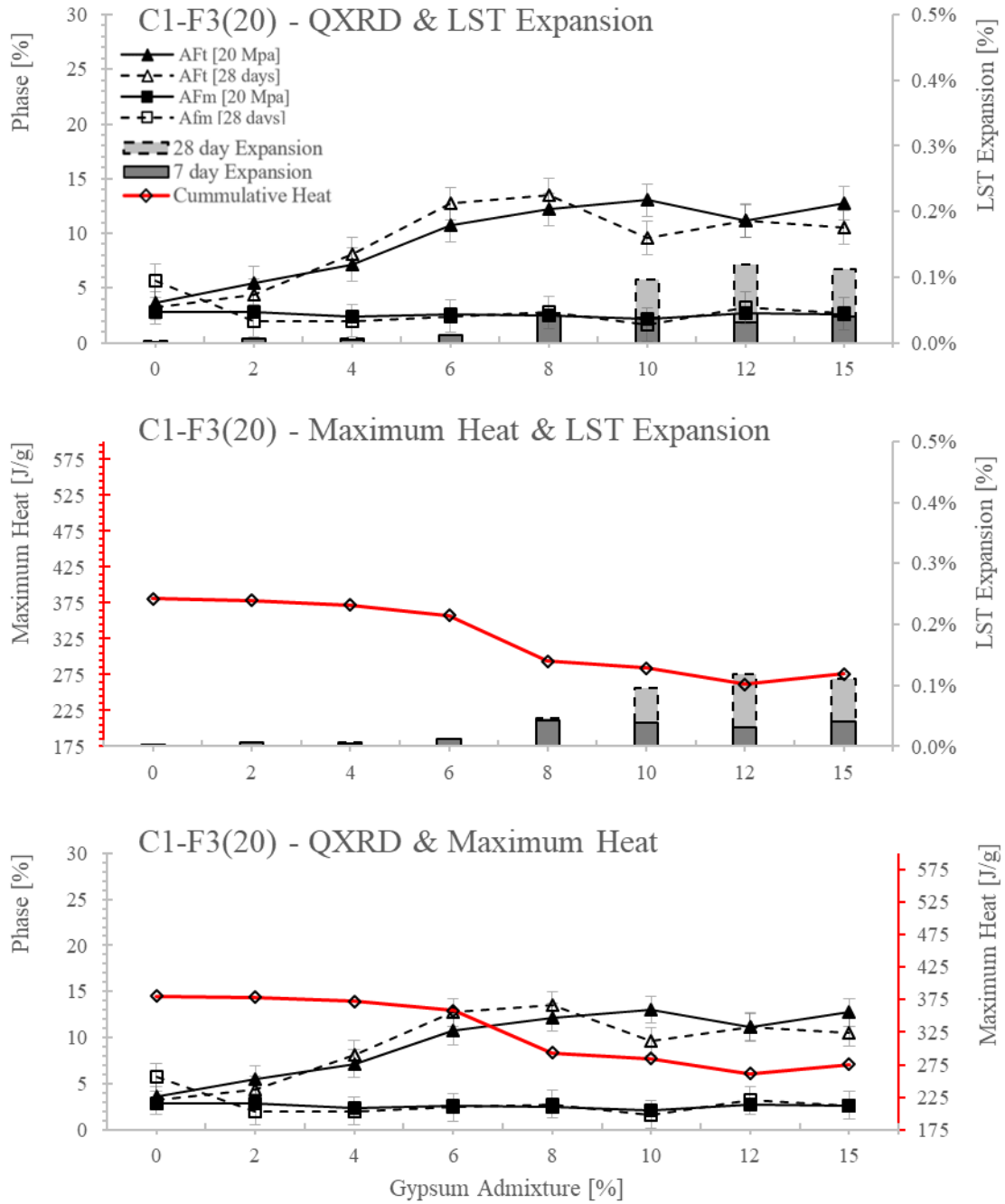


Figure 6.59. Comparison of expansion data from LST, QXRD analysis, and maximum heat curves for mixture C1-F3(20)

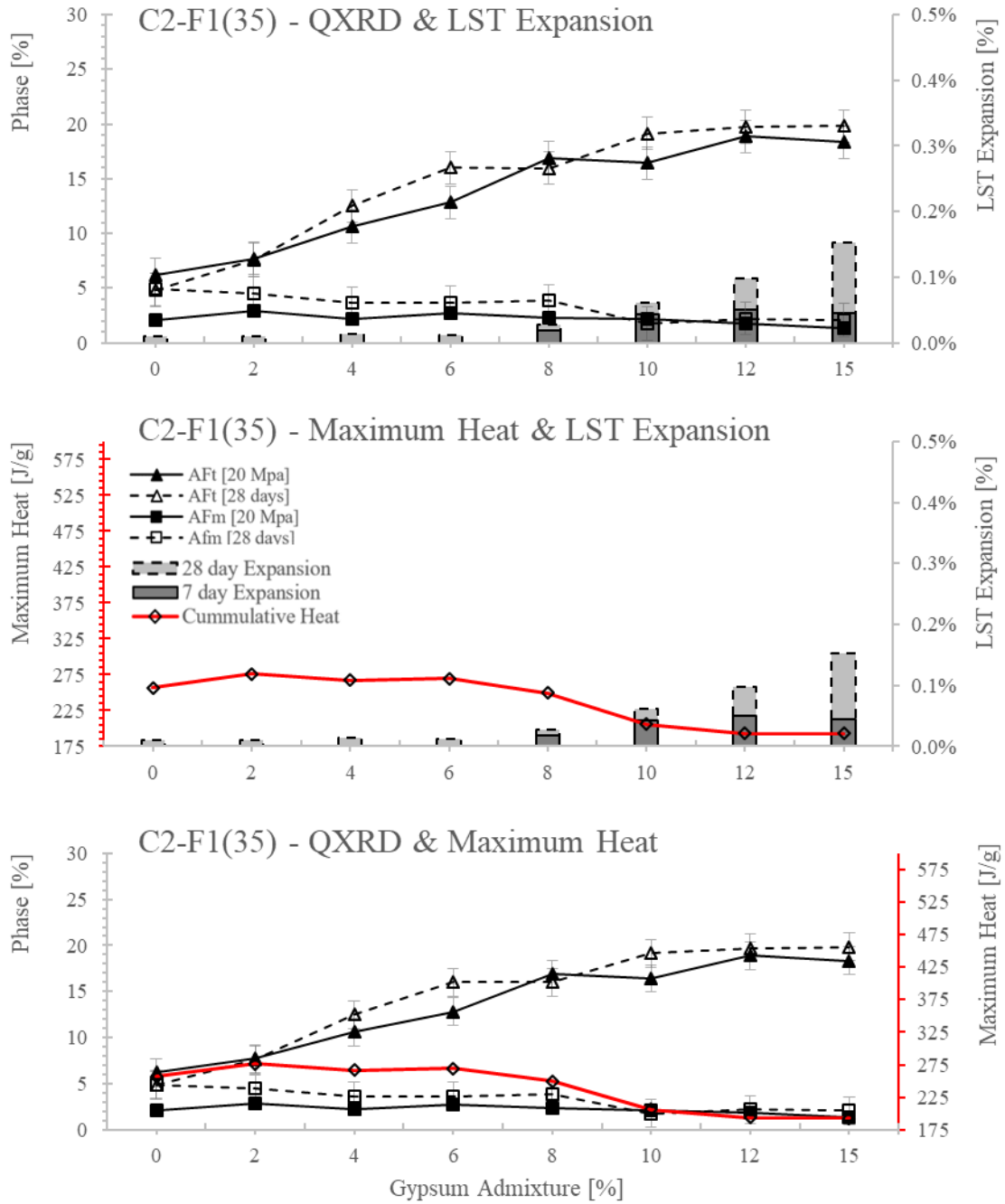


Figure 6.60. Comparison of expansion data from LST, QXRD analysis, and maximum heat curves for mixture C2-F1(35)

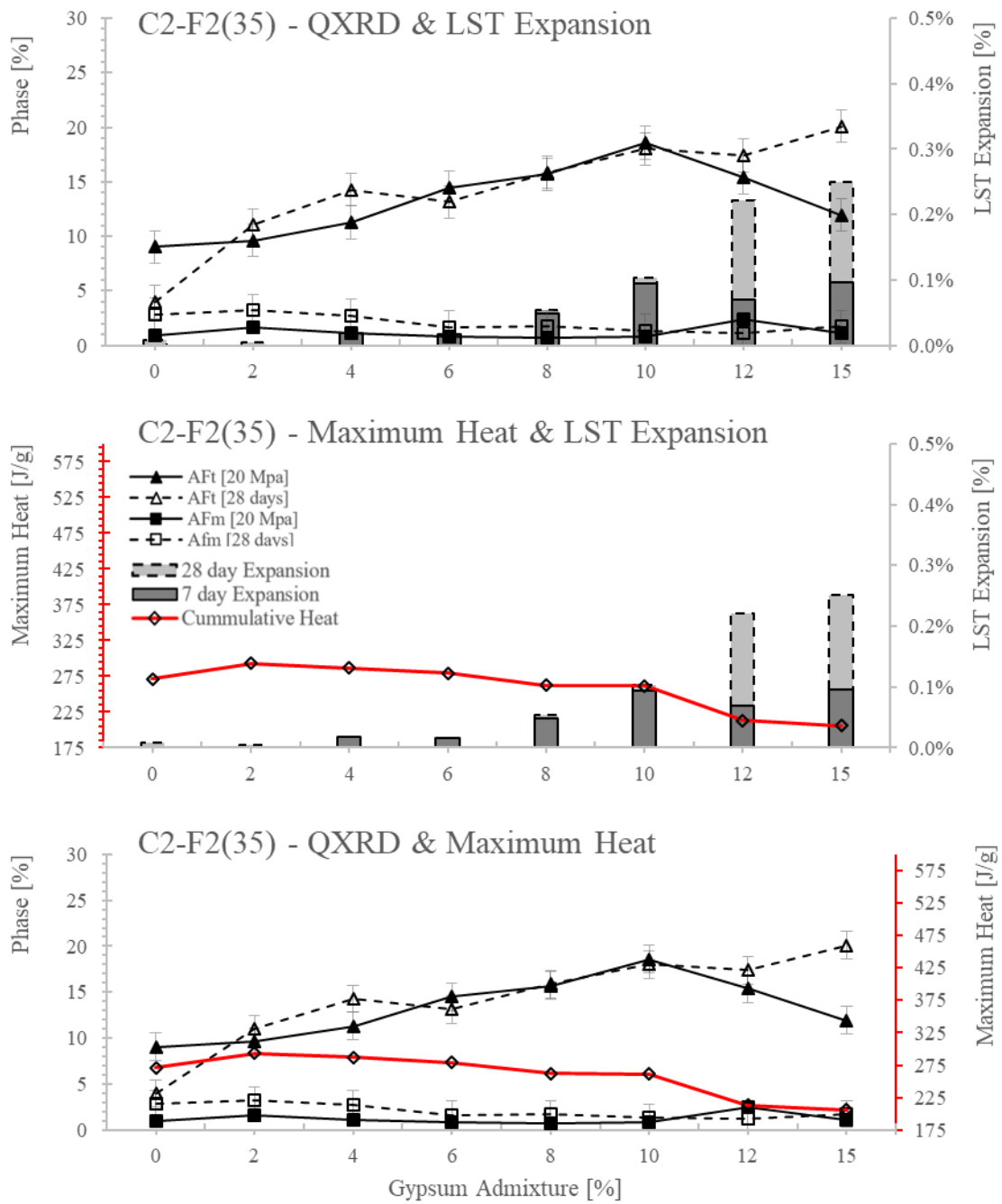


Figure 6.61 Comparison of expansion data from LST, QXRD analysis, and maximum heat curves for mixture C2-F2(35)

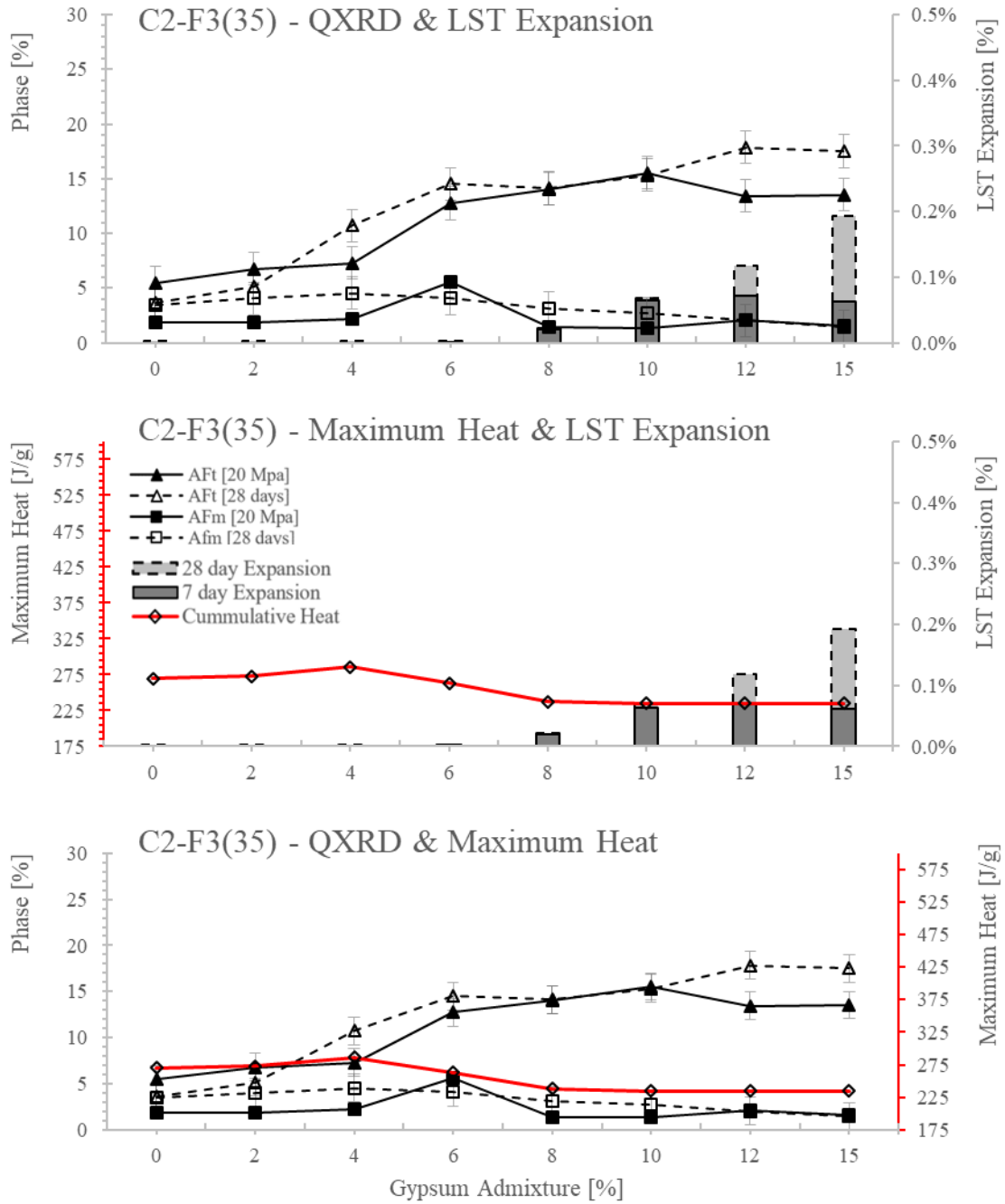


Figure 6.62 Comparison of expansion data from LST, QXRD analysis, and maximum heat curves for mixture C2-F3(35)

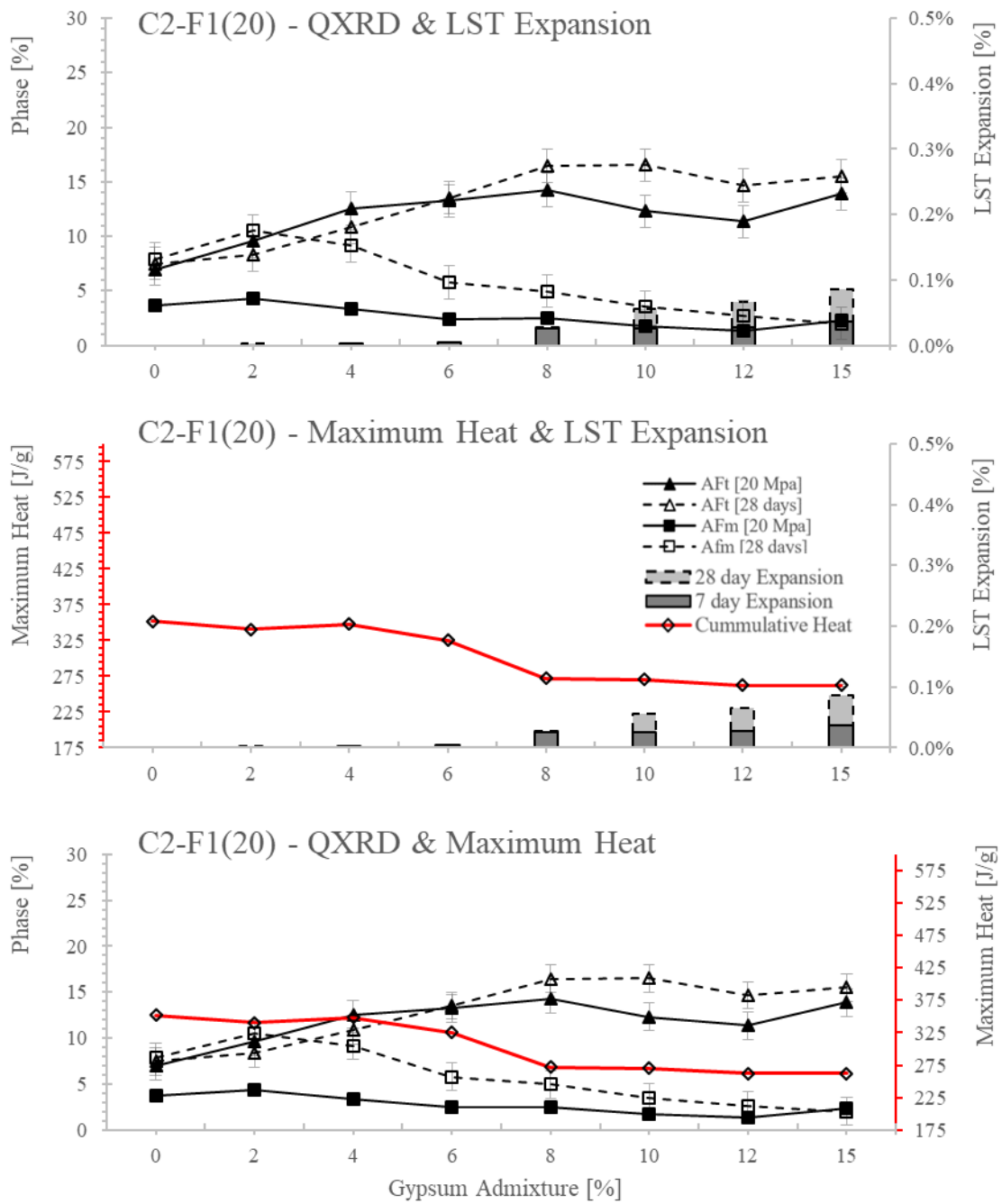


Figure 6.63 Comparison of expansion data from LST, QXRD analysis, and maximum heat curves for mixture C2-F1(20)

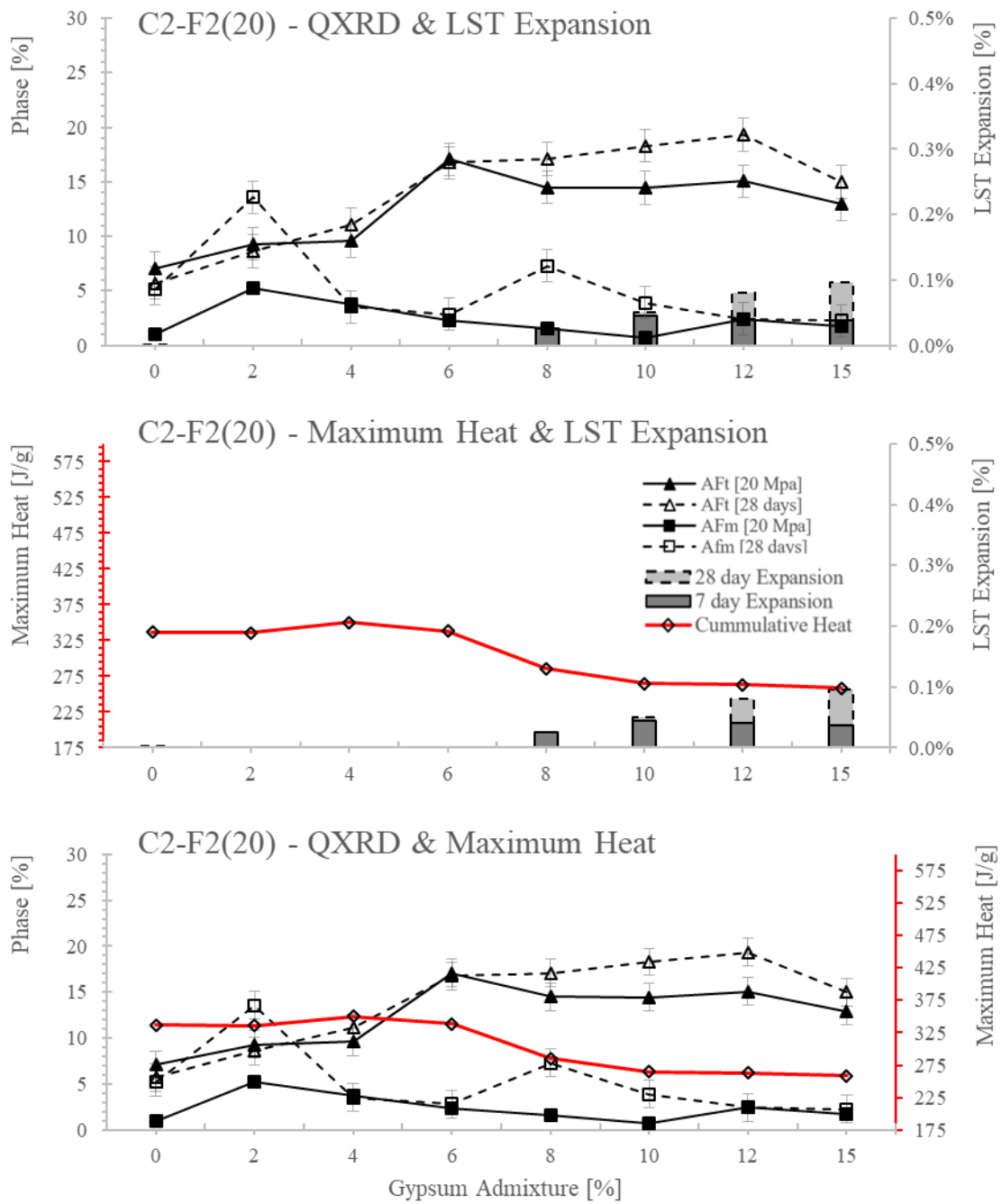


Figure 6.64 Comparison of expansion data from LST, QXRD analysis, and maximum heat curves for mixture C2-F2(20)

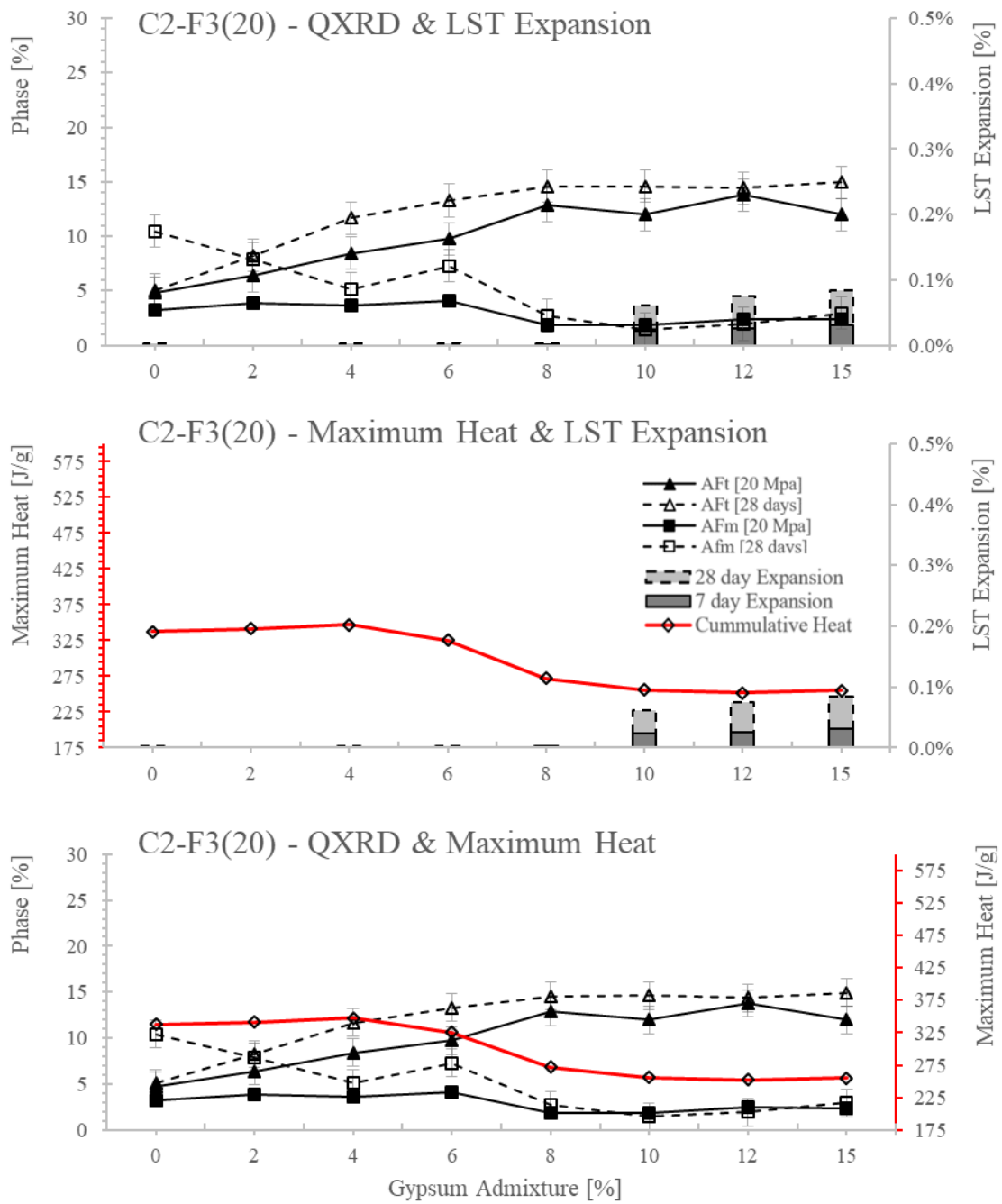


Figure 6.65 Comparison of expansion data from LST, QXRD analysis, and maximum heat curves for mixture C2-F3(20)

6.5.6.2. Discussion

The comparative analysis results shown in Figures 6.54–6.65 indicate two important points of interest which include:

- A drop in maximum heat is coincident with an increase in expansion at 7 days, and peak AFt formation on the 20-MPa curve.
- The second plateau of the maximum heat curve is coincident with peak AFt formation on the 28-day curve and another increase in early age expansion.

These results demonstrate a correlation between the heat of hydration, early age expansion, and hydration product formation. One can infer from the results that when a large drop in maximum heat is recorded in isothermal calorimetry testing, early age expansion (not due to external sulfate attack) will occur. Additionally, the drop in maximum heat indicates that the most benefit from gypsum addition with respect to C_3A dissolution has been achieved, thus forming the maximum amount of AFt possible at early ages of the binder's life (while it is still relatively plastic).

A comparison of mixtures that passed ASTM C 1012 to those that meet Lerch's guidance provides insight into a possible short-term method for determining the sulfate resistance of a cement binder. Mixtures that passed ASTM C 1012 testing and meet Lerch's guidance for a properly retarded cement are presented in Table 6.36.

Table 6.36 Summary of passing results of ASTM C 1012 testing that meet Lerch's recommendations for a properly retarded cement

MIX ID	Exp % 6m	Exp % 12m
C1-F1(35)-G(8)	0.092	
C2-F1(35)-G(6.0)	0.031	0.039
C2-F2(35)-G(4.1)	0.083	0.117
C2-F2(35)-G(5.4)	0.075	0.090
C2-F1(20)-G(4.3)	0.092	0.185
C2-F2(20)-G(6)	0.060	
C2-F3(20)-G(6)	0.083	

When comparing the mixtures that passed ASTM C 1012 testing and those that meet Lerch's guidance, it becomes clear that mixtures containing nominally less than 6% gypsum yield the best results. In total, 7 of the 16 passing results from ASTM C 1012 meet Lerch's criteria, while the remaining 9 mixtures that passed ASTM C 1012 include mixture proportion that include gypsum dosages within nominally $\pm 2\%$ of Lerch's guidance. Interestingly, research conducted at the University of Texas at Austin [9] using fly ashes F2 and F3, with similar replacement quantities as those used in this research, as also achieved passing results with gypsum quantities that also appear to agree with Lerch's guidance.

While it would be seemingly advantageous to try and utilize gypsum additions that achieve the most amount of AFt possible, thereby mitigating the likelihood of sulfate attack, doing so generates excessive early age expansion and low maximum heat. This is a two-fold practical problem: the excessive early age expansion generated by high levels of gypsum would yield concrete and/or mortar elements that do not exhibit the volume stability required by the construction industry, and the low maximum heat does not produce concrete and/or mortar with adequate levels of strength gain that meet the time-sensitive demands of construction.

6.6. Conclusions

Based on a review of literature, testing performed by other researchers, results from testing conducted in this project, the characteristics and chemical composition of the materials used this project's series of tests, and an analysis of the results, conclusions of this research indicate:

- The use of gypsum is an effective method to mitigate external sulfate attack in binary blends of Type I or Type I/II cements with high-calcium fly ash as a replacement for cement.
- The method developed by researchers [7] for determining adequate gypsum content to mitigate sulfate attack in binary blends of type I or type I/II cements with high-calcium fly ash as a replacement for cement will yield a material that does not meet ASTM requirements.
- Mixtures containing C2 (a type I/II cement) generated better sulfate-resistant blends in this study than did mixtures containing C1 (a type I cement).
- It appears possible to run a series of short-term tests as indices for predicting the sulfate resistance of binary blends of type I or type I/II cements with high-calcium fly ash as a replacement for cement. These tests include isothermal calorimetry, early expansion testing (likely ASTM C 1038), and QXRD.

6.7. References

- [1] P. & M. P. Mehta, *Concrete - Microstructure, Properties, and Materials*, Fourth ed., New York: McGraw Hill, 2014.
- [2] S. H. Kosmatka,, B. Kerkhoff and W. C. Panarese, *Design and Control of Concrete Mixtures*, 14th ed., Skokie, Illinois: Portland Cement Association, 2002.
- [3] American Society for Testing and Materials, *ASTM C150/C150M - 16, Standard Specification for Portland Cement*, West Conshohocken, PA: ASTM International, 2016.
- [4] J. W. Bullard, H. M. Jennings, R. A. Livingston, A. Nonat, G. W. Scherer, J. S. Schweitzer, K. L. Scrivener and J. J. Thomas, "Mechanisms of cement hydration," *Cement and Concrete Research*, vol. 41, no. 1, pp. 1208-1223, 2011.
- [5] E. R. Dunstan, "A Possible Method for Identifying Fly Ashes That Will Improve the Sulfate Resistance of Concretes," *Cement, Concrete, and Aggregates, CCAGDP*, vol. Vol. 2, no. No. 1, pp. 20-30, 1980.
- [6] P. K. Mehta, "Effect of Fly Ash Composition on Sulfate Resistance of Cement," *ACI Journal, Technical Paper*, Vols. November-December, no. Title No. 83-39, pp. 83-89, 1986.
- [7] P. J. Tikalsky and R. L. Carrasquillo, "The Effect of Fly Ash on the Sulfate Resistance of Concrete," Center for Transportation Research, The University of Texas at Austin, Austin, Texas, 1989.
- [8] F. M. Aguayo, K. Folliard, M. D. Thomas, D. W. Fowler, J. C. Maria and H. Wheat, "External Sulfate Attack of Concrete: An Accelerated Test Method, Mechanisms,

- and Mitigation Techniques," The University of Texas at Austin, Austin, Texas, 2016.
- [9] R. Dhole, "Sulfate Resistance of High Calcium Fly Ash Concrete," The University of New Brunswick, New Brunswick, 2008.
- [10] K. Kruse, A. Jasso, K. J. Folliard, R. Ferron, M. Juenger and T. Drimalas, "Characterizing Fly Ash," The Center for Transportation Research at The University of Texas at Austin, Austin, 2012.
- [11] S. G. Shashiprakash and M. D. A. Thomas, "Sulfate Resistance of Mortars Containing High-Calcium Fly Ashes and Combinations of Highly Reactive Pozzolans and Fly Ash," American Concrete Institute, SP199, Vol. 1, Farmington Hills, Michigan, 2001.
- [12] M. D. A. Thomas, M. H. Shehata and S. G. Shashiprakash, "The Use of Fly Ash in Concrete: Classification by Composition," *Cement, Concrete, and Aggregates, CCAGDP*, vol. 21, no. No. 2, pp. 105-110, Dec. 1999.
- [13] K. F. von Fay and J. S. Pierce, "Sulfate Resistance of Concretes with Various Fly Ashes," *ASTM Standardization News*, pp. 32-37, 1989.
- [14] P. J. Tikalsky and R. L. Carrasquillo, "Influence of Fly Ash on the Sulfate Resistance of Concrete," American Concrete Institution, Materials Journal, Farmington Hills, Michigan, 1992.
- [15] R. Dhole, M. D. A. Thomas, K. J. Folliard and T. Drimalas, "Characterization of Fly Ashes for Sulfate Resistance," *ACI Materials Journal*, vol. 110, no. No. 2, pp. 159-168, 2013.
- [16] G. J. McCarthy, J. K. Solem, O. Manz and D. J. Hassett, "Use of a Database of chemical, mineralogical and physical properties of north American fly ash to study the nature of fly ash and its utilization as a mineral admixture in concrete," *Materials Research Society*, vol. 178, pp. 3-33, 1990.
- [17] T. Drimalas, J. C. Clement, K. J. Folliard, R. Dhole and M. D. A. Thomas, "Laboratory and Field Evaluations of External Sulfate Attack in Concrete," Center for Transportation Research at The University of Texas at Austin, Austin, Texas, 2010.
- [18] Von Fay, Kurt F.; Bureau of Reclamation, "Effects of Various Fly Ashes on Compressive Strength, Resistance to Freezing and Thawing, Resistance to Sulfate Attack, and Adiabatic Temperature Rise of Concrete," U.S. Department of the Interior, Denver, Colorado, 1995.
- [19] J. R. Prusinski and R. L. Carrasquillo, "Using Medium - to High-Volume Fly Ash Blended Cements to Improve the Sulfate Resistance of High-Lime Fly Ash Concrete," *ACI Materials Journal*, no. SP 153-3, pp. 43-65, 1995.

- [20] R. L. Carrasquillo, "Methods of Producing Concretes Containing Class C Fly Ash That Are Stable in Sulphate Environments". United States of America Patent 5,578,122, 14 February 1994.
- [21] American Society for Testing and Materials, *ASTM C618A -17a, Standard Specification for Coal Fly Ash and Raw or Calcined Natural Pozzolan for Use in Concrete*, Conshohocken, PA: ASTM International, 2017.
- [22] American Society for Testing and Materials, *ASTM C452-15, Standard Test Method for Potential Expansion of Portland-Cement Mortars Exposed to Sulfate*, Conshohocken, PA: ASTM International, 2015.
- [23] American Society for Testing and Materials, *ASTM C1012/C1012M -15, Standard Test Method for length Change of Hydraulic-Cement Mortars Exposed to a Sulfate Solution*, Conshohocken, PA: ASTM International, 2015.
- [24] P. J. Sandberg and L. R. Roberts, "Cement-Admixture Interactions Related to Aluminate Control," *Journal of ASTM International*, vol. 2, no. 6, pp. 1-14, June 2005.
- [25] W. Lerch, "The Influence of Gypsum on the Hydration and Properties of Portland Cement Pastes," American Society for Testing Materials, Philadelphia, PA, 1946.
- [26] S. Bishnoi and P. Sandberg, "Sulfate Optimization of Hydraulic Cementitious Materials Using Isothermal Calorimetry," unknown, Delhi, India, unknown.
- [27] C. Hesse, F. Goetz-Neunhoeffler and J. Neubauer, "A new approach in quantitative in-situ XRD of cement pastes: Correlation of heat flow curves with early hydration reactions," *Cement and Concrete Research*, vol. 41, no. 1, pp. 123-128, January 2011.
- [28] D. Jansen, F. Goetz-Neunhoeffler, B. Lothenbach and J. Neubauer, "The early hydration of Ordinary Portland Cement (OPC): An approach comparing measured heat flow with calculated heat flow from QXRD," *Cement and Concrete Research*, vol. 42, pp. 134-138, 2012.
- [29] L. G. Baquerizo, T. Matschei, K. L. Scrivener, M. Saeidpour and L. Wadso, "Hydration states of AFm cement phases," *Cement and Concrete Research*, vol. 73, pp. 143-157, 2015.
- [30] Stark, David C.; Portland Cement Association, "Performance of Concrete in Sulfate Environments, RD 129," Portland Cement Association, Skokie, Illinois, 2002.
- [31] Mehta, "MECHANISM OF SULFATE ATTACK ON PORTLAND CEMENT - Another Look," Department of Civil Engineering University of California Berkeley, Berkeley, 1982.
- [32] American Society for Testing and Materials, *Standard Specification for Coal Fly Ash and Raw or Calcined Natrual Pozzolan for Use in Concrete*, West Conshohocken, PA: ASTM International, 2017.

- [33] American Concrete Institute, ACI, Building Code Requirements for Structural Concrete (ACI 318-14), Farmington Hills, Michigan: American Concrete Institute, 2014.
- [34] Hemmings, R. T.; Berry, E. E.; Ontario Research Foundation, "On The Glass in Coal Fly Ash: Recent Advances," *Materials Research Society*, vol. 113, pp. 3-38, 1988.
- [35] American Society for Testing and Materials, *ASTM C1157/C1157M -17 Standard Performance Specification for Hydraulic Cement*, West Conshohocken, PA: ASTM International, 2017.
- [36] American Society for Testing and Materials, *ASTM C595/C595M - 18 Standard Specification for Blended Hydraulic Cements*, West Conshohocken, PA: ASTM International, 2018.

Chapter 7. Amarillo Bridge Deck Investigation Report

7.1. Introduction

Extensive bridge deck cracking observed in Amarillo was inspected by the research team. Subsequent testing was performed to determine the cause of the deterioration as well as to prevent it from further occurring. The likely causes of cracking were determined to be a combination of design, material, and construction deficiencies. The unique interaction between chemical admixtures and cementitious materials was noteworthy as it triggered a severe retardation effect. This chapter contains a comprehensive report describing construction details and findings from the field visit as well as an investigation on admixture compatibility.

7.1.1. Background

7.1.1.1. General Information

The research team was tasked with investigating extensive bridge deck cracking observed in Amarillo. The team traveled to Amarillo in September 2017 and inspected two bridge deck sites with the reported deterioration. The sites inspected were Loop 335 at BNSF RR and I-40 at Soncy. The bridge decks of interest were cast in late November 2016, and cracking was reported to appear three to six weeks after placement.

The bridge decks are composed of two parts: precast panel sections and full-depth sections over metal decking. Full-depth sections have an 8.5 in. slab thickness without accounting for metal decking depth. Precast panels have a thickness of 4 in. On top of the precast panels, a 4.5 in. slab of cast-in-place concrete is placed to match the full-depth sections. See Figures 7.1 and 7.2 for more details.

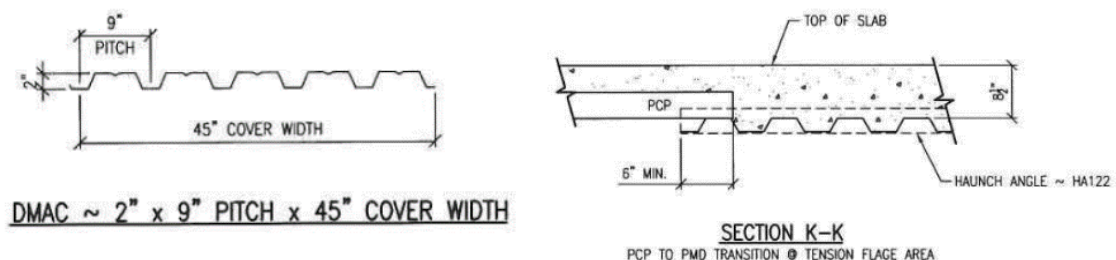


Figure 7.1 Metal deck specifications

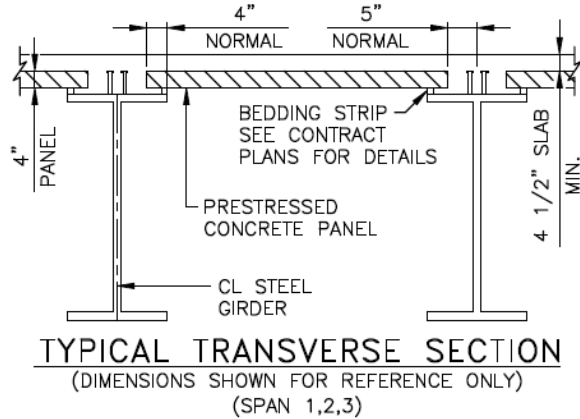


Figure 7.2 Precast concrete panel specifications

7.1.1.2. Mixture Design

Table 7.1 summarizes the mixture design utilized for cast-in-place concrete, which includes full-depth sections and the 4.5 in. slab on top of the precast panel sections. The information presented on Table 7.1 was deduced by combining information from batch tickets (Figure 7.3) and the TxDOT 811 Mix Design guide. The TxDOT 811 guide includes the following requirements and constraints:

- Design strength at 28 days, $f'c$: 4,000 psi
- Maximum w/c: 0.45
- Maximum cementitious content: 541 lb./yd³
- Air Content: 5.5%
- Slump: 5

442043
 11/23/2016
 M100DE 10.00 yd JOHN HIATT 21
 RATE CLASS S W/UFA & CNI M100 FIBER

WWW01 11/23/2016
 21

State Use Only:
 At Plant:
 Drm Coat: Sand _____ Cem _____ cm
 Max Time _____ Mxr Chgd _____ am/pm
 Rev Cnt: Beg _____ End _____ Rev _____
 Water-Max Al'd _____ gal-Batch Wat _____ gal
 -Wat Agg _____ gal-Ice _____ #
 +Drum _____ gal Gal Withd _____
 Plant Insp. _____
 Remarks _____

Material	Required	Batched	% Var	% Moisture	Actual Wat
SAND	12161 lb	12140 lb	-0.17%	3.50% M	49 gl
57 ROCK	19500 lb	19500 lb	0.00%		
POZZ BO	254.50 oz	256.00 oz	0.59%		
FLY ASH	1570.0 lb	1590.0 lb	1.27%		
LDNESTAR	3520.0 lb	3520.0 lb	0.00%		
AIR	30.54 oz	30.00 oz	-1.77%		
CNI	2560.0 oz	2550.0 oz	-0.39%		
WATER	175.72 gl	176.00 gl	0.16%		
159	407.20 oz	408.00 oz	0.20%		176.00 gl
UFA	.0 lb	.0 lb			
DELVO	458.10 oz	458.00 oz	-0.02%		

Num Batches: 1 Manual 6:07:43 gl To Add: 19.8 gl Actual 225.2
 Load Total: 38550 lb Design 0.402 Water/Cement 0.368 A Design 24gl

325 Silica 1100 Fiber

On Jobsite: Water added _____ gal
 Rev Cnt: Beg _____ End _____ Rev _____
 Slump _____ in. Air _____ %
 Conc Temp _____ o Bm/Cy# _____
 Loc/Struct _____
 Mixer Unloaded _____ am/pm
 Job Inspector _____
 Remarks _____

Figure 7.3 Batch ticket

Table 7.1 Cast-in-place concrete mixture proportions (per cubic yard)

Category	Material	Quantity	Unit	Notes
Aggregates	Fine Aggregate	1216.1	lb.	
	Coarse Aggregate	1952.0	lb.	57 Rock
Cementitious	Cement	352.0	lb.	ASTM TI - Lonestar
	Fly Ash	157.0	lb.	Class C - Harrington - 31% replacement
	Ultra-Fine Fly Ash	0.0	lb.	Listed on batch ticket but at 0 quantity. Not listed on TXDOT 811 Mix Design.
	Silica Fume	0.0	lb.	Material listed as 325 Silica is handwritten on batch ticket. No quantity listed. TxDOT 811 Mix Design calls for 6% SF content.
	Total Cementitious		509.0	lb.
		5.09	cwt	
Water	Batch Water	146.6	lb.	
	Aggregate Water	40.9	lb.	
	Total Water	187.4	lb.	
	Held Water	16.5	lb.	
	Actual w/c	0.37		
	Design w/c	0.40		

Category	Material	Quantity	Unit	Notes
	Admixture Water	N/A	lb	Batch sheet does not appear to account for water contribution from admixtures. Based on data sheet information, the corrosion inhibitor alone contains 88% water by weight which should be accounted for in w/c calculations.
Admixtures	Normal-range water reducer	5.0	fl oz/cwt	MasterPozzolith 80 - Recommended dosage 3-10 fl oz/cwt
	High-range water reducer	8.0	fl oz/cwt	Chryso Enviromix 159 - Recommended dosage 3-14 fl oz/cwt for Type A water reductions and 12-20 fl oz/cwt for Type F water reductions.
	Air Entrainer	3.1	oz	No specific product listed. No air entraining mixture listed on TxDOT 811 either.
	Corrosion Inhibitor	2.0	gal	MasterLife CI 30
	Retarder	45.8	oz	MasterSet Delvo - Not listed in TXDOT 811 Mix Design. Was used by contractor to counteract acceleration caused by corrosion inhibitor. Contractor also aimed to place multiple sections at once and hence needed to extend set times.
Fibers	Microfiber	0	lb.	MasterFiber M 100 - Fiber is handwritten on batch ticket. However, no quantity is listed. TxDOT 811 Mix Design calls for 0.5 lb./yd ³ .

7.1.1.3. Bridge Deck Layout

The details presented below pertain to the Loop 335 section at the BNSF RR site. Based on construction documents, the bridge deck was divided into five sections, as illustrated in Figure 7.4, to facilitate the construction process. A given section may contain portions of both precast panel and full-depth concrete. The total bridge deck span is 545 feet.

Bridge Deck Sections 3, 4, and 5 were cast during one continuous pour. The use of the retarding admixture was likely used to extend set times in order to pour multiple sections

at once and perhaps also to reduce cracking above the columns. Bridge Deck Sections 1 and 2 were cast separately.

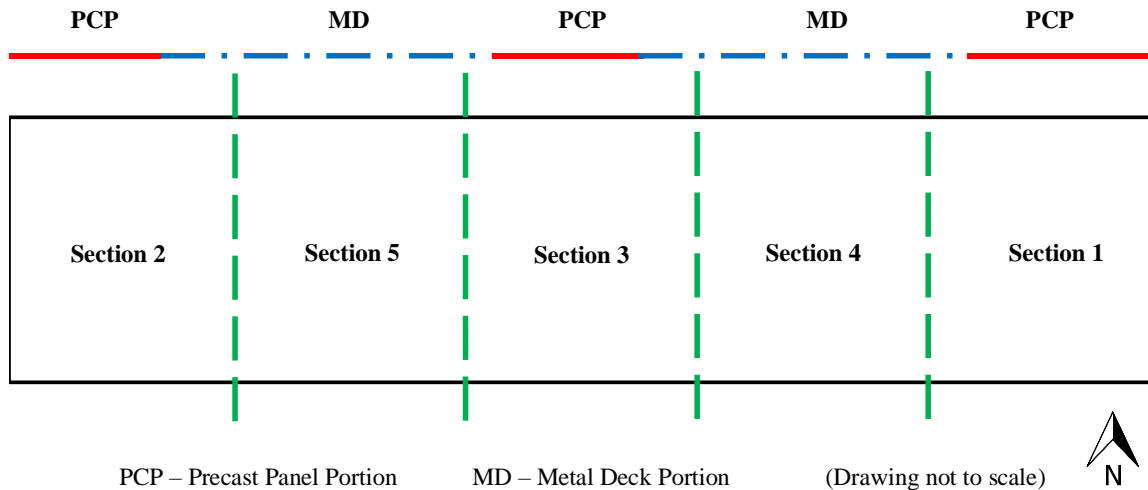


Figure 7.4 Bridge deck layout

7.1.1.4. Construction Practices

According to comments from TxDOT engineers, on some occasions the contractor had issues with setting curing equipment at the appropriate time. It was indicated that cracks were particularly notable in the span where curing was delayed. Moreover, there were general concerns about using low w/c mixtures that are prone to rapid moisture loss in the harsh Amarillo climate.

An overview of the local weather conditions on the day the bridge deck was poured (Wednesday, November 23, 2016) is included in Table 7.2. Figure 7.5 displays the temperature and wind data throughout that day. Since the batch ticket shown in Figure 7.3 was stamped at 6:55 a.m., it can be inferred that the pour took place at temperatures between 2–4 °C (35–40 °F).

Moreover, since the pour took place the day before Thanksgiving Day, it is likely that the concrete was left exposed without proper curing until after the holiday break. During this time, rapid moisture evaporation could have occurred even at low temperatures due to the low humidity and wind conditions. Furthermore, the combination of low temperatures with the admixtures used (especially the use of the retarder Delvo in cold weather) could have severely retarded the mixture and delayed strength gain. The loss of moisture could then have created tensile stresses that exceeded the capacity of the potentially still-plastic concrete, leading to plastic shrinkage cracking.

Table 7.2 Amarillo weather conditions for 11/23/16

Condition	Measurement	Unit
Temperature	Low	34 °F
	High	59 °F
Moisture	Average Humidity	56 %
	Minimum Humidity	30 %
	Maximum Humidity	82 %
Precipitation	None	-
Wind	Average	10 mph

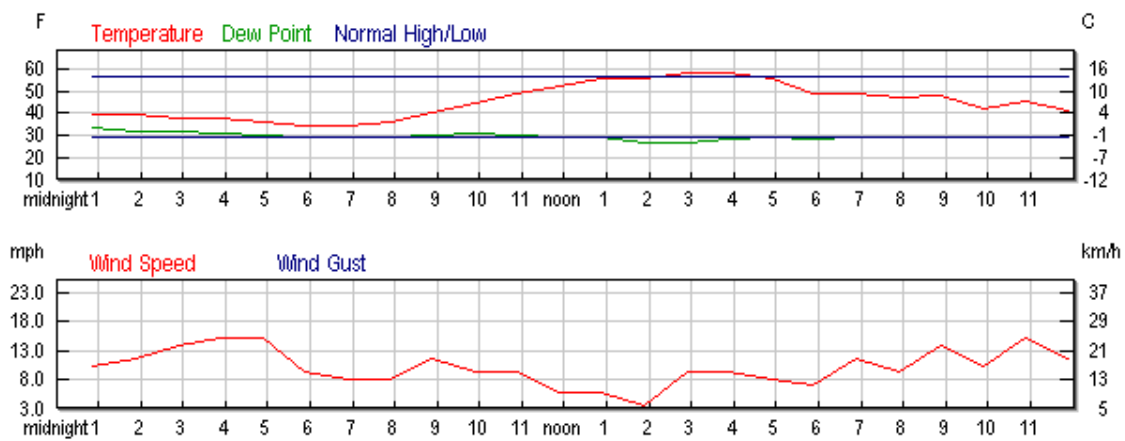


Figure 7.5 Amarillo weather data for 11/23/16 from WeatherUnderground website

7.2. Field Visit

7.2.1. General Information

The research team visited the Amarillo sites on Wednesday, September 13, 2017. Two sites with reported cracking were investigated, Loop 335 at BNSF RR and I-40 at Soncy (Figure 7.6 and 7.7).

The Loop 335 site suffered from extensive cracking and was the focus of this investigation. On the Loop 335 site, the portion examined was the south portion of the west-bound lane. The I-40 site contained moderately low levels of cracking.



Figure 7.6 Loop 335 at BNSF RR inspection

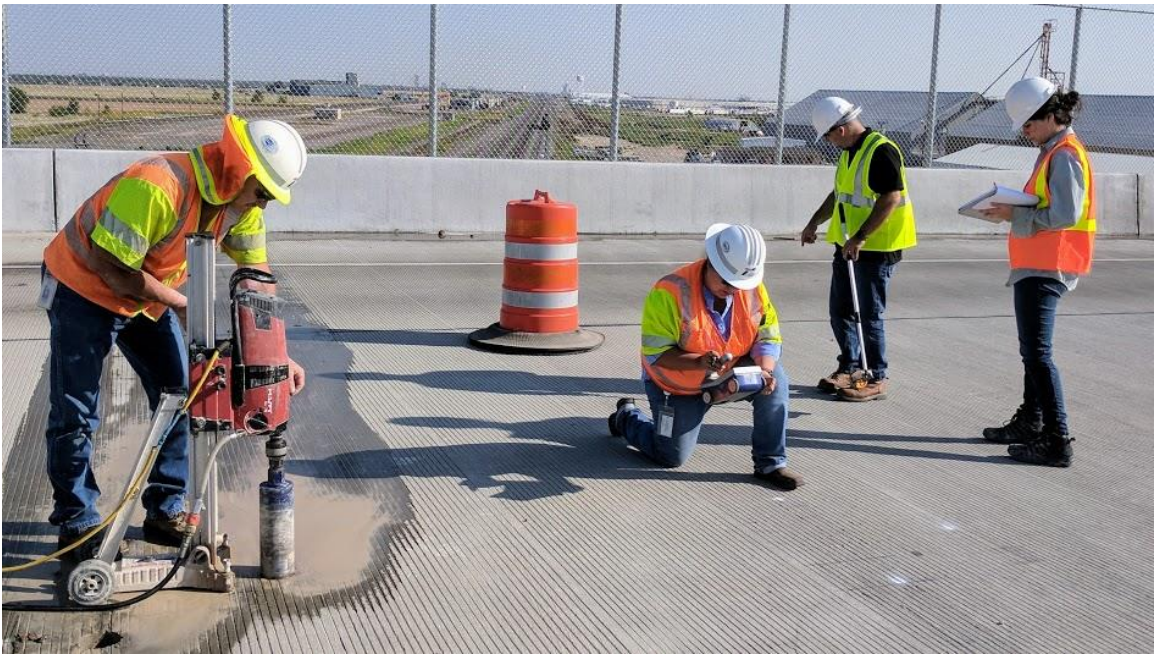


Figure 7.7 Crack documentation and coring procedure

7.2.1.1. Crack Documentation

Extensive cracking was documented on the Loop 335 bridge deck (Figure 7.8). Cracks ranged from hairline width up to 0.3 mm. The crack map presented in Figure 7.9 highlights

the increased presence of cracks over the precast panel portion when compared to the full-depth metal deck segments.



Figure 7.8 Typical cracks observed on Loop 335 bridge deck

PCP – Precast Panel Portion MD – Metal Decking Portion (Drawing not to scale)

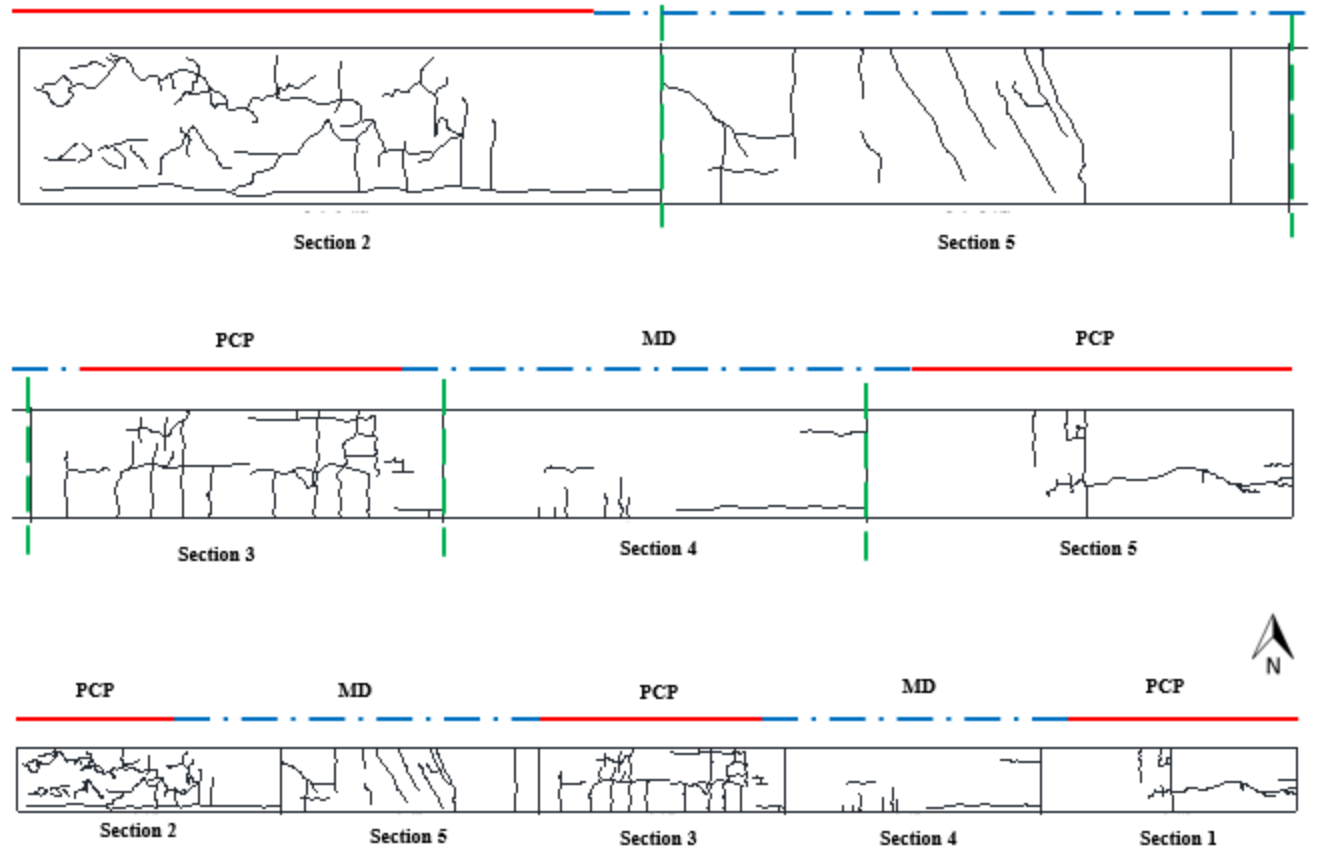


Figure 7.9 Crack map—Loop 335 site

7.2.1.2. Cores

A total of nine cores were obtained for examination. Seven cores were taken from the Loop 335 bridge deck and two from the I-40 bridge deck. Cores from the Loop 335 bridge deck were obtained from specific areas as follows: three cores from Bridge Deck Section 2, three cores from Section 3, and two cores from Section 1. Within a specific area, cores from a portion with extensive cracking were obtained as well as cores with no cracking nearby.

Cracking throughout the core and around the aggregate was observed in cores obtained from a cracked area (Figure 7.10). On several occasions, rebar was struck while coring. Upon inspection of these cores, rebar was observed to be placed at a clear cover depth of 75–87.5 mm (3.0–3.5 in.), indicating it was essentially resting on top of the precast panels (Figures 7.11, 7.12, 7.13, and 7.14). The increased cover for this top mat of reinforcement (Figure 7.15) could have reduced the efficacy in controlling thermal and drying shrinkage cracking.

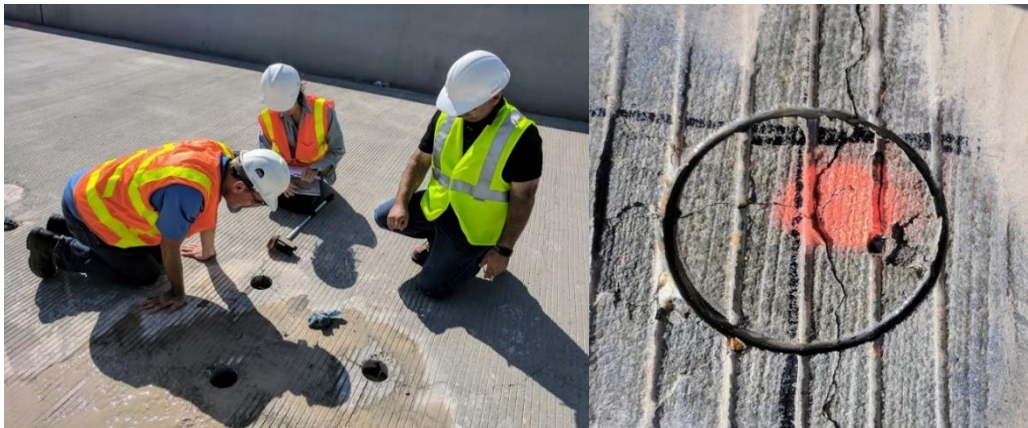


Figure 7.10 Coring area

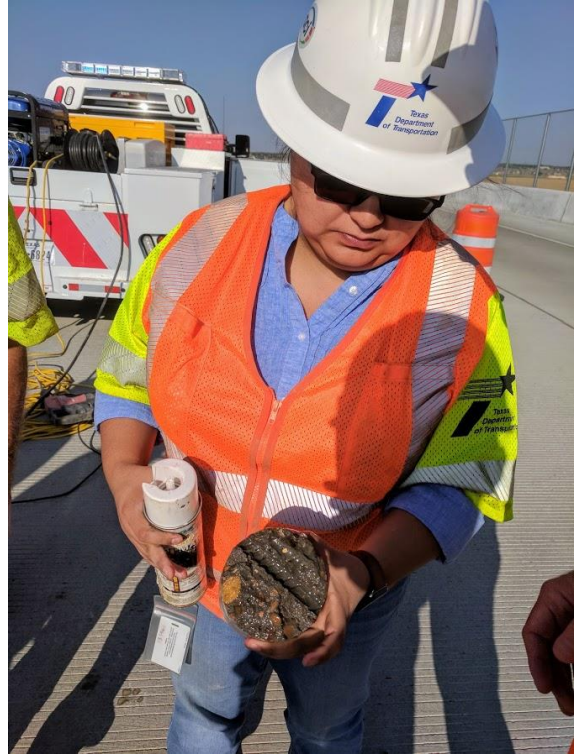


Figure 7.11 Rebar struck while coring

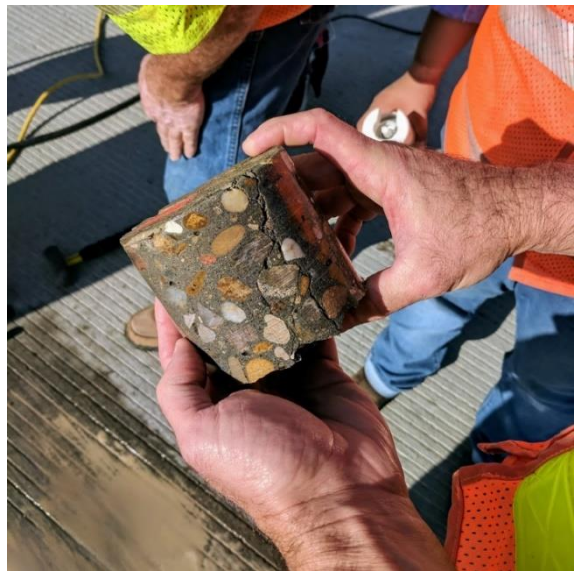


Figure 7.12 Intersection of two precast panels below cast-in-place slab (left), and cracking visible throughout core and around aggregate (right)



Figure 7.13 Core from section with extensive cracking (left), and core from section with no cracking (right)

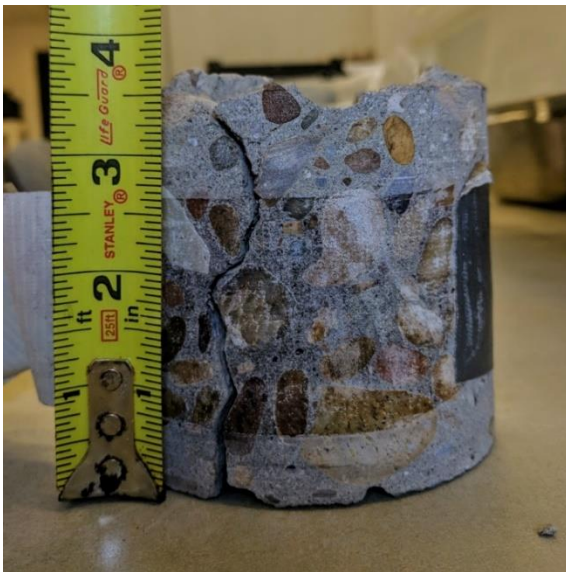


Figure 7.14 Rebar placed at a depth of 3.5 in. from the top of slab (left), and rebar imprint at the bottom of core (right)

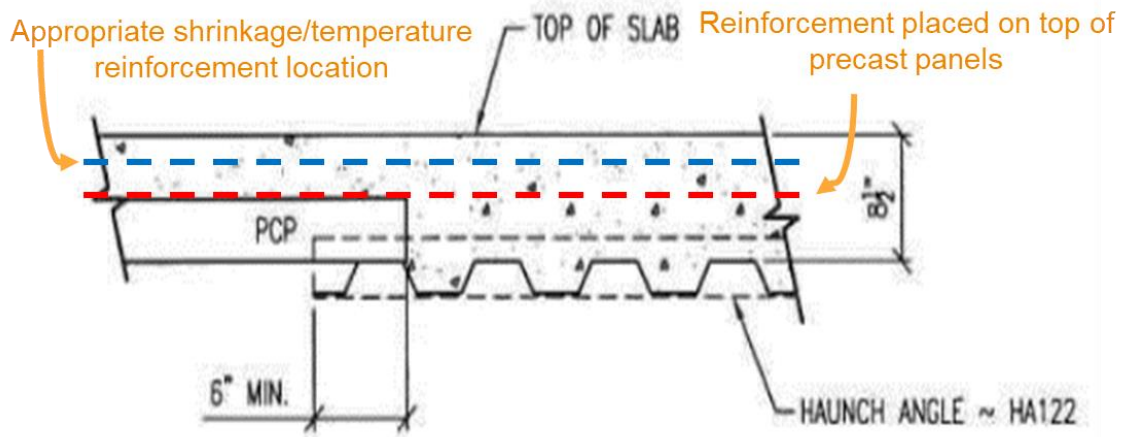


Figure 7.15 Reinforcement placement

7.2.2. Preliminary Determinations

The following determinations were made based on information gathered during the site visit:

- Cracking in cores was present throughout the slab depth and skirted around coarse aggregate particles, indicating that the crack originated while the concrete was still fresh.
- The presence of microfibers was not directly apparent upon core examination and shall be verified through forensic analysis.
- The combination of five different admixtures could have excessively retarded set time, leaving the fresh concrete vulnerable for an extended period of time.
- Improper construction practices could have aggravated the situation by delaying the placement of curing equipment. In the harsh Amarillo weather conditions, the rapid loss of moisture from the exposed top surface could have developed tensile stresses.
- Higher than usual rebar covers (75–87.5 mm [3.0–3.5 in.]) for decks cast over precast panels could have limited the top mat of reinforcement from resisting early tensile stresses.
- The cold temperatures during the pour, and given the use of a high retarder dosage, it is expected that the full-depth sections (8.5 in. thickness) generated substantially more heat than the 4 in. sections cast over precast panels. This increased heat of hydration would have allowed the thicker

sections to gain strength faster than the thinner sections, hence improving the resistance to early tensile stresses and reducing cracking.

7.3. Proposed Experimental Investigation

Based on the information gathered during the site investigation, analysis and testing were proposed to determine the cause of cracking and to provide general guidance to prevent further issues. The proposed lab testing was intended to recreate the bridge deck concrete mixture to assess the role of material interactions. However, most of the proposed testing described in this section was not performed due to major material incompatibilities encountered during preliminary mixtures. The incompatibility issues are discussed further in a later section. The proposed testing that was ultimately not performed is included in this section for reference.

7.3.1. Materials

The following materials were procured from the Amarillo batch plant for lab testing: fine aggregate (475 kg [800 lb.]), coarse aggregate (475 kg [800 lb.]), cement (237 kg [400 lb.]), and fly ash (237 kg [400 lb.]). A reference Type I cement and SF available at the lab were also used. The chemical composition of cementitious materials was analyzed by XRF; Table 7.3 summarizes the results. Aggregate properties are shown in Table 7.4. The specific admixtures listed on Table 7.1 were procured directly from their manufacturer. Since no specific air entraining admixture was listed, MasterAir AE 90 was selected. MasterLife SRA 035, MasterFiber M 100 microfibers, and MasterFiber MAC 100 macrofibers were also procured.

Table 7.3: Chemical composition of cementitious materials (% by mass)

Material	SiO ₂	Al ₂ O ₃	Fe ₂ O ₃	CaO	SO ₃	MgO	K ₂ O	Na ₂ O	LOI
Amarillo Type I/II Cement	21.78	4.08	3.99	64.24	2.25	1.89	0.59	0.10	1.81
UT Lab Type I Cement	20.48	5.39	1.90	65.06	3.40	1.17	0.96	0.14	2.57
Amarillo Class C Fly Ash	35.36	18.32	5.70	27.98	1.36	4.92	0.54	1.48	0.85
UT Lab Silica Fume	97.16	0.31	0.12	0.92	0.20	0.28	0.65	0.06	4.42

Table 7.4: Aggregate properties

Aggregate Type	Absorption Capacity	Specific Gravity (Saturated Surface Dry)
Fine	0.86%	2.63
Coarse	0.71%	2.63

7.3.2. Mixture Proportions

Given the widespread use of the original mixture design, an effort was made to minimize adjustments for the proposed new mixtures. Thus, the aggregate, cementitious, and water content were to remain constant across mixtures per Table 7.1. Moreover, the use of water reducers (Pozzolith 80 and Enviromix 159), air entrainer, and a corrosion inhibitor (CI 30) were intended to be present across mixtures. The proposed new mixtures were meant to analyze the individual effect of retarding, shrinkage reducing, and fiber admixtures.

7.3.3. Test Matrix

Five different mixtures, as listed below, were proposed to evaluate and isolate different variables that could affect shrinkage cracking. Mixture 1 was intended to be a control and reflect the actual mixture design used in the bridge decks, assuming fibers were absent. Mixture 2 was intended to evaluate the effect of removing the retarding admixture from Mixture 1. Mixture 3 was intended to employ an SRA to curb cracking. SRAs are known to retard mixtures; thus, its effect was meant to be compared to that of the Delvo retarder in Mixture 1. Mixture 4 was intended to test the effectiveness of using a combination of micro and macro fibers to prevent shrinkage cracking. Mixture 5 was intended to evaluate the benefit of combining the SRA and fibers from Mixtures 3 and 4.

1. WATER REDUCERS, AIR, CI + DELVO
2. WATER REDUCERS, AIR, CI
3. WATER REDUCERS, AIR, CI + SRA
4. WATER REDUCERS, AIR, CI + MICRO and MACRO FIBERS
5. WATER REDUCERS, AIR, CI + SRA + MICRO and MACRO FIBERS

7.3.4. Samples and Testing Procedures

The proposed testing procedures were intended to evaluate each mixture's fresh, mechanical, and durability properties. Table 7.5 includes a summary of the proposed tests.

Table 7.5: Proposed testing procedures

Category	Test	Sample
Fresh Properties	Slump (ASTM C143)	Slump Cone
	Unit Weight (ASTM C138)	Air Pot
	Time of Set (ASTM C403)	Container
	Air (ASTM C231)	Air Pot
Mechanical Properties	Compressive Strength (ASTM C39)	4x8 Cylinder
	Elastic Modulus (ASTM C469)	4x8 Cylinder
	Split Tensile Strength (ASTM C496)	4x8 Cylinder
Durability Properties	Resistivity (ASTM C1876)	4x8 Cylinder
	Length Change (ASTM C157)	3" Concrete Prism
	Semi-Adiabatic Calorimetry (Q-Drum)	6x12 Cylinder
	Isothermal Calorimetry	Cups
	Shrinkage Ring Test (ASTM C1581)	Ring
	Maturity (ASTM C1074)	4x8 Cylinder

7.3.5. Forensic Investigation

The cores retrieved were intended to be forensically analyzed to provide additional information. The use of optical microscopy on the cores was proposed to verify the presence of fibers, which were not visibly evident. Additionally, carbonation analysis was considered as a possible indicator of crack age.

7.4. Actual Experimental Investigation

Test results from preliminary concrete mixtures were concerning as they indicated a pronounced retardation of the mixture independent from the use of a retarder. Given the surprising results, further concrete testing was halted. Subsequent testing focused on investigating admixture interactions on paste and mortar mixtures. Calorimetry results indicated a gross incompatibility between admixtures and cementitious materials. Thus, a simplified mixture design was sought. Moreover, ASR testing was performed to determine if SF could be removed from the mixture without impairing durability.

7.4.1. Preliminary Concrete Test Results

Time of set testing on mortar sieved from concrete (Figure 7.16), semi-adiabatic calorimetry from a 150x300 cm (6x12 in.) concrete cylinder (Figure 7.17), and isothermal calorimetry from sieved mortar (Figure 7.18) all showed a substantial delay in hydration even in mixtures without a retarder. For the time of set test, mixtures were in fact delayed for so long that it was not possible to determine a

final set time (4,000 psi [27.6 MPa] penetration resistance) even after ~24 hours. Additionally, cylinders demolded at 24 hours were evidently fragile. One cylinder was tested in compression upon demolding and crumbled under negligible loading. Calorimetry testing for the mixture without a retarder (Figure 7.18) indicated two heat peaks: one early peak within the first few hours and a second peak after 36 hours. It is likely that the mixture did not achieve final set until the second peak was achieved.

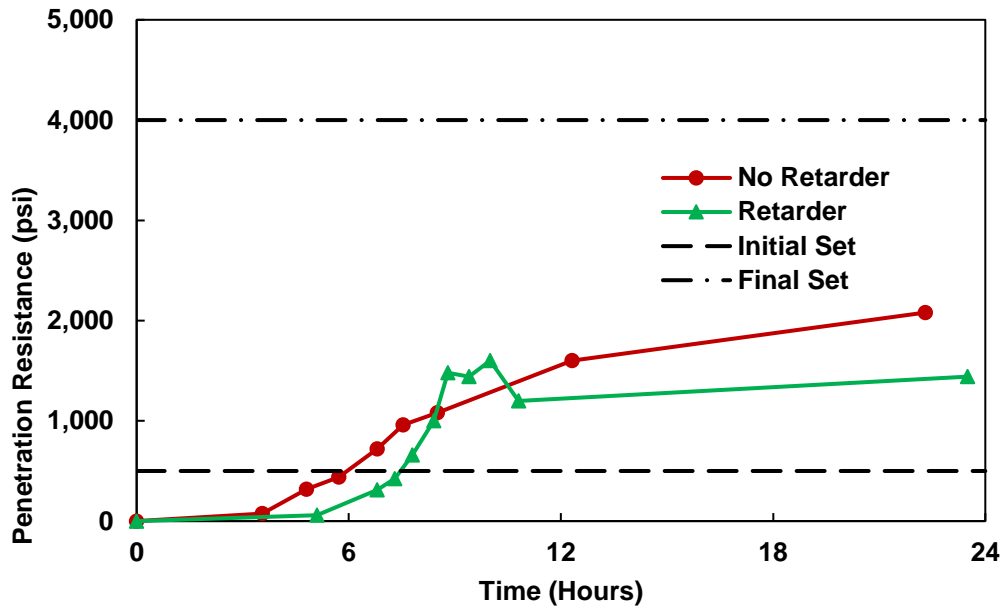


Figure 7.16 Time of set testing [1,000 psi = 6.9 MPa]

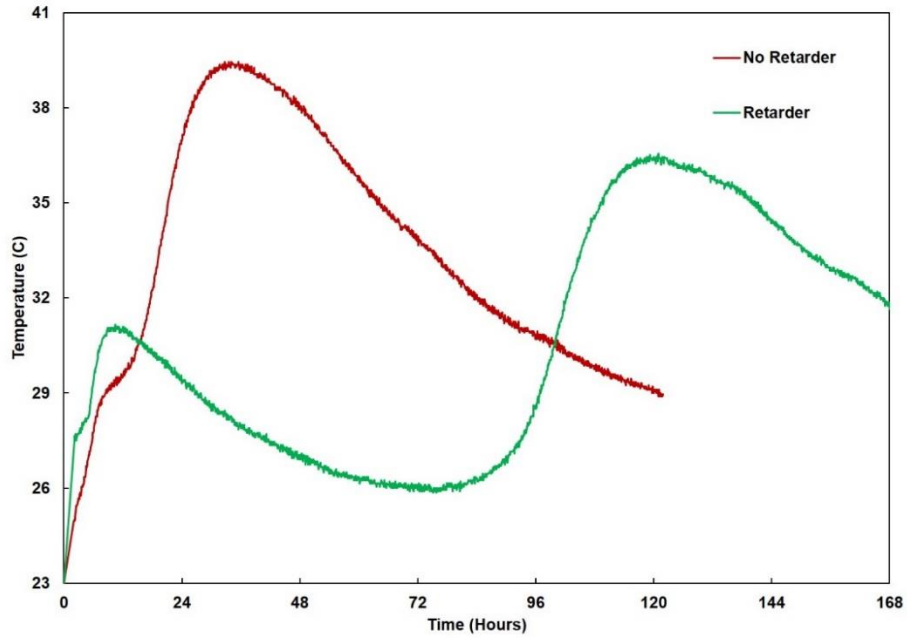


Figure 7.17 Semi-adiabatic calorimetry (Q-Drum) on concrete cylinders [$T(^{\circ}F) = T(^{\circ}C) \cdot 1.8 + 32$]

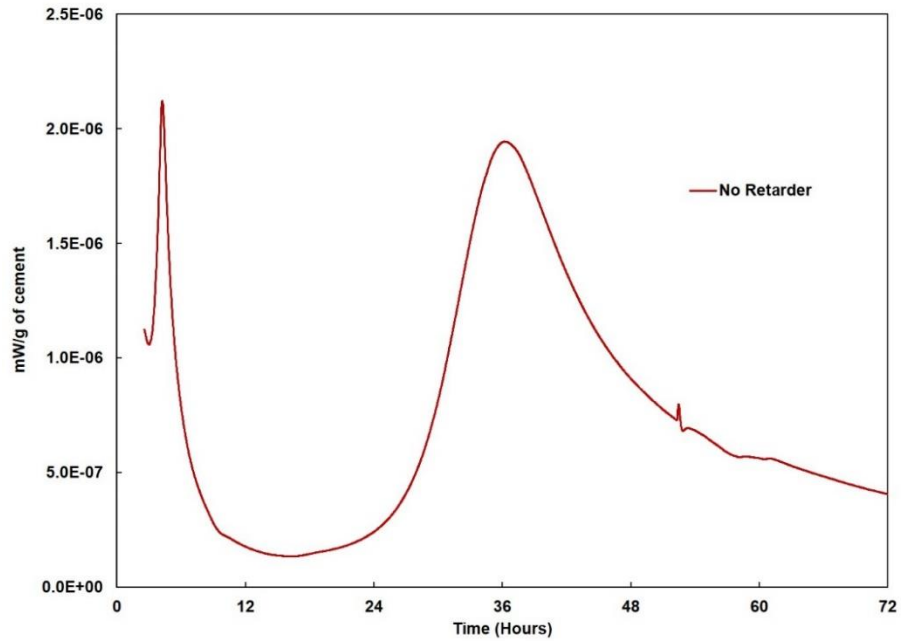


Figure 7.18 Rate of heat evolution from isothermal calorimetry on sieved mortar

7.4.2. Admixture Interaction on Paste Samples

The effect on hydration of each individual admixture and cementitious material was analyzed through isothermal calorimetry on paste samples. Admixtures were tested at varying dosages and in different combinations with other admixtures and

cementitious materials. Paste samples utilized had a w/c ratio of 0.27 and were composed of 30 g of cementitious. A second reference ASTM C150 Type I cement was included in testing as a comparison to the Amarillo Type I/II cement. Mixtures composed of a ternary blend of cementitious materials were composed of 65% cement, 29% fly ash, and 6% SF by mass.

Admixtures and cementitious materials behaved as expected when examined independently. However, synergistic effects were observed on ternary blends including admixtures. After various testing iterations, results indicated that the unique combination of Amarillo cementitious materials with admixtures (two water reducers and a corrosion inhibitor) yielded a grossly incompatible mixture with delayed hydration. This effect was present without the use of a retarding admixture and with only the use of the two water reducers and the corrosion inhibitor. Figures 7.19–7.23 include relevant data that was used to form the following observations:

- Figure 7.19: Cementitious materials without admixtures behave as expected as either OPC mixtures (not shown) or as ternary blends.
- Figure 7.20: The introduction of admixtures severely altered behavior in ternary blends. The reference ternary blend experiences a moderate delay in hydration with the use of admixtures, but its overall response is as expected. Conversely, the use of admixtures on the Amarillo ternary blend causes an unusual first peak followed by a dormant period before restarting hydration for a second peak. This behavior resembles results seen in calorimetry from sieved concrete mortar (Figure 7.18). Based on time of set results (Figure 7.16), it is likely that final set would have occurred around the time of the second hydration peak.
- Figure 7.21: The use of admixtures did not severely affect OPC mixtures with either cement.
- Figures 7.22 and 7.23: The synergistic effects of a ternary blend combined with admixtures did not greatly alter hydration in the reference cement. However, the Amarillo cement, when used as a ternary blend with admixtures, displayed a major delay and reduction in hydration.

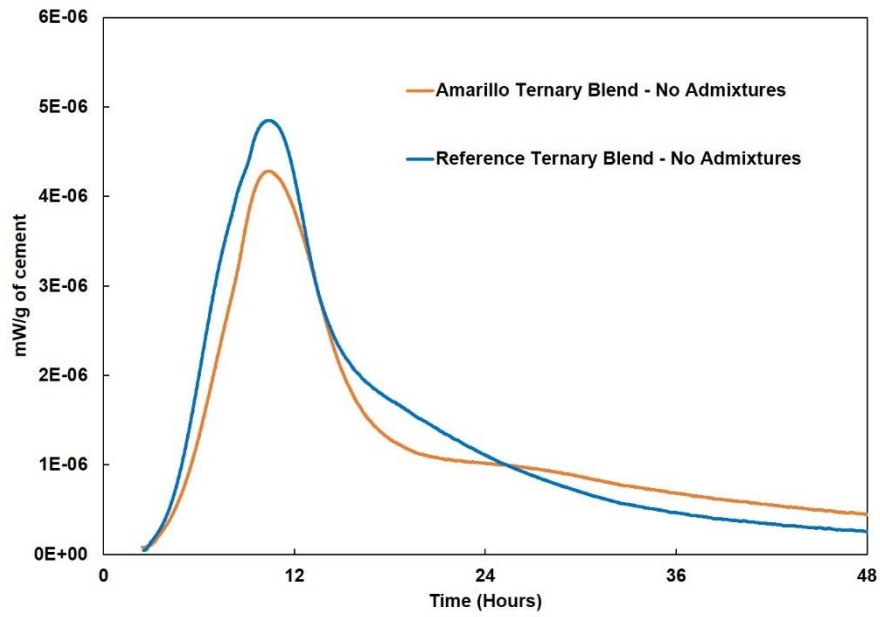


Figure 7.19 Rate of heat evolution from isothermal calorimetry on ternary blend paste samples without admixtures

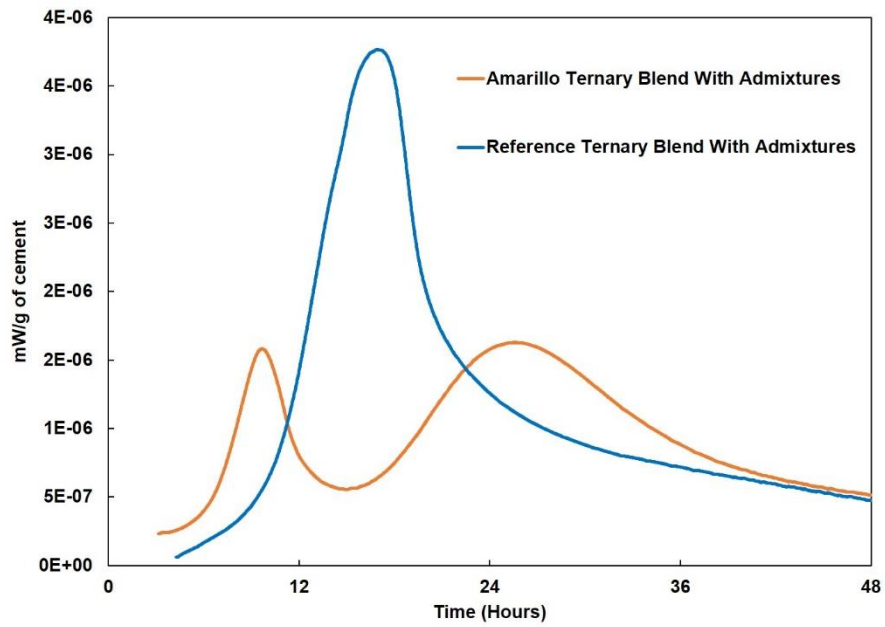


Figure 7.20 Rate of heat evolution from isothermal calorimetry on ternary blend paste samples with admixtures

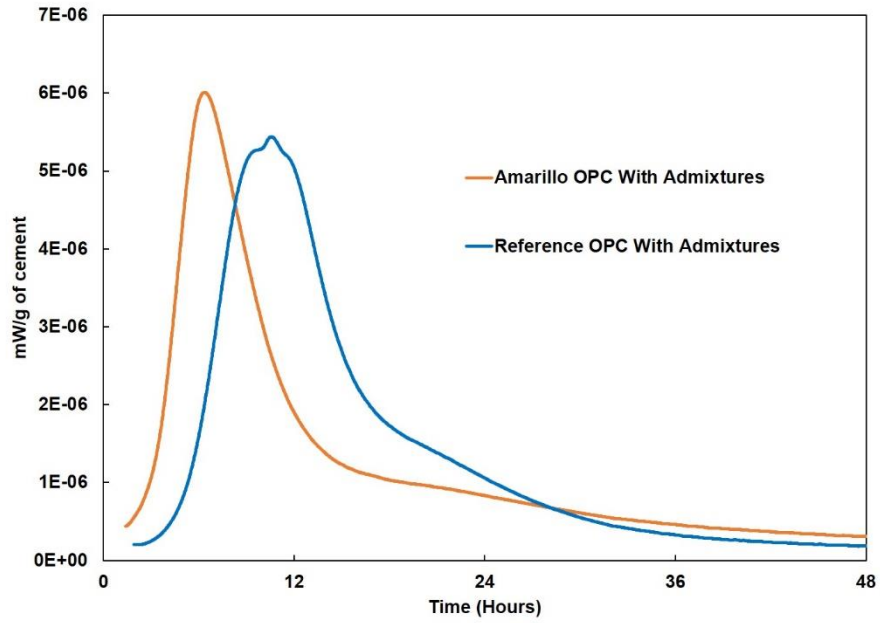


Figure 7.21 Rate of heat evolution from isothermal calorimetry on OPC paste samples with admixtures

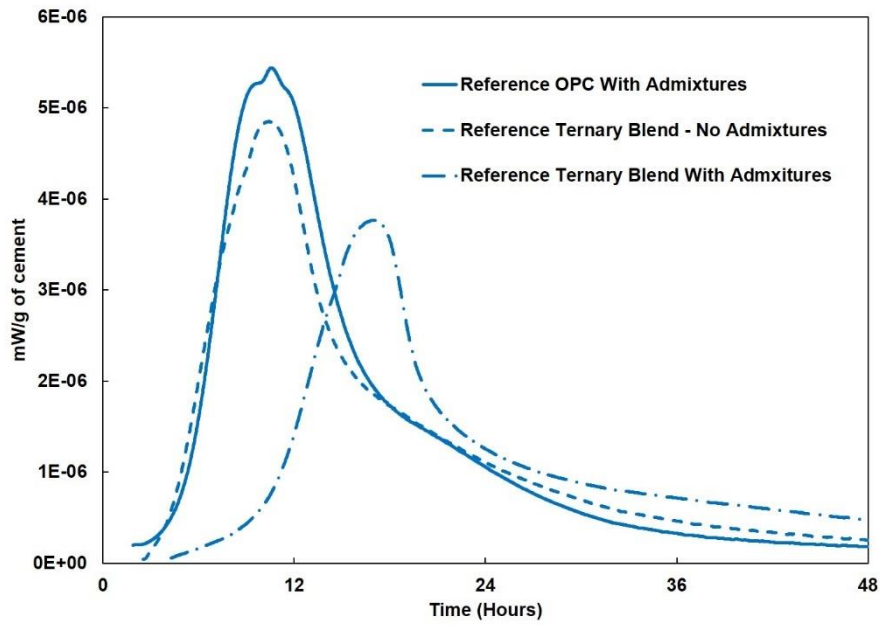


Figure 7.22 Rate of heat evolution from isothermal calorimetry on paste samples with reference cement

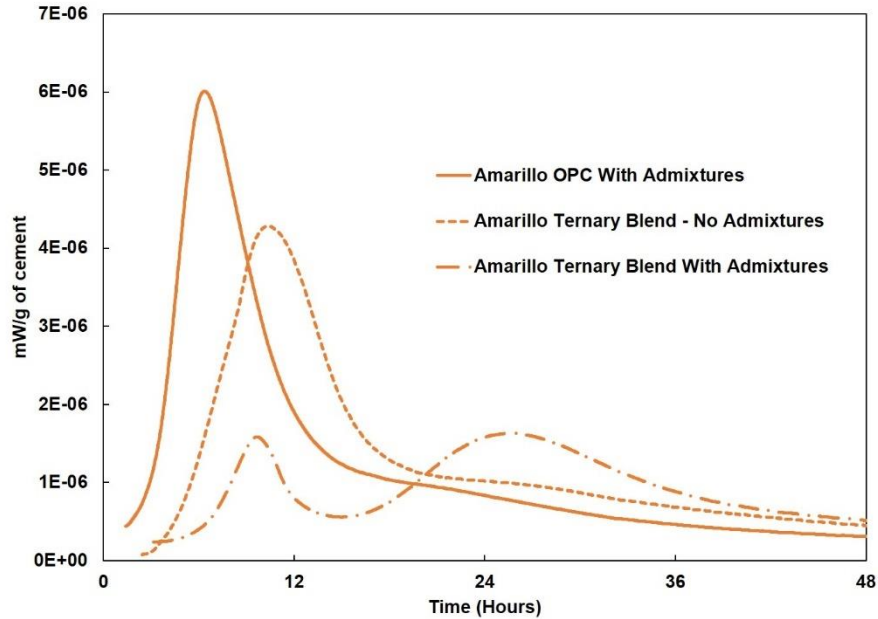


Figure 7.23 Rate of heat evolution from isothermal calorimetry on paste samples with Amarillo cement

7.4.3. Alkali-Silica Reaction Testing

In an effort to provide a simplified mixture design, ASR testing was performed to determine if SF could be removed from the mixture. Fine aggregate and crushed coarse aggregate were tested in accordance with ASTM C1567 with various contents of fly ash and SF to mitigate expansion due to ASR.

According to the results shown in Figures 7.24 and 7.25 (in which “FA” refers to “fly ash”), both aggregates are reactive and SCMs are needed to mitigate expansion. A ternary blend of fly ash and SF performed best with the coarse aggregate. However, a corresponding mixture with fine aggregate exceeded the failure criteria. Nonetheless, this effect is believed to be due to mixing issues as SF is notoriously difficult to disperse in small samples. Thus, it was concluded that SF (6%) in conjunction with fly ash (30%) was indeed required to mitigate potential expansion due to ASR.

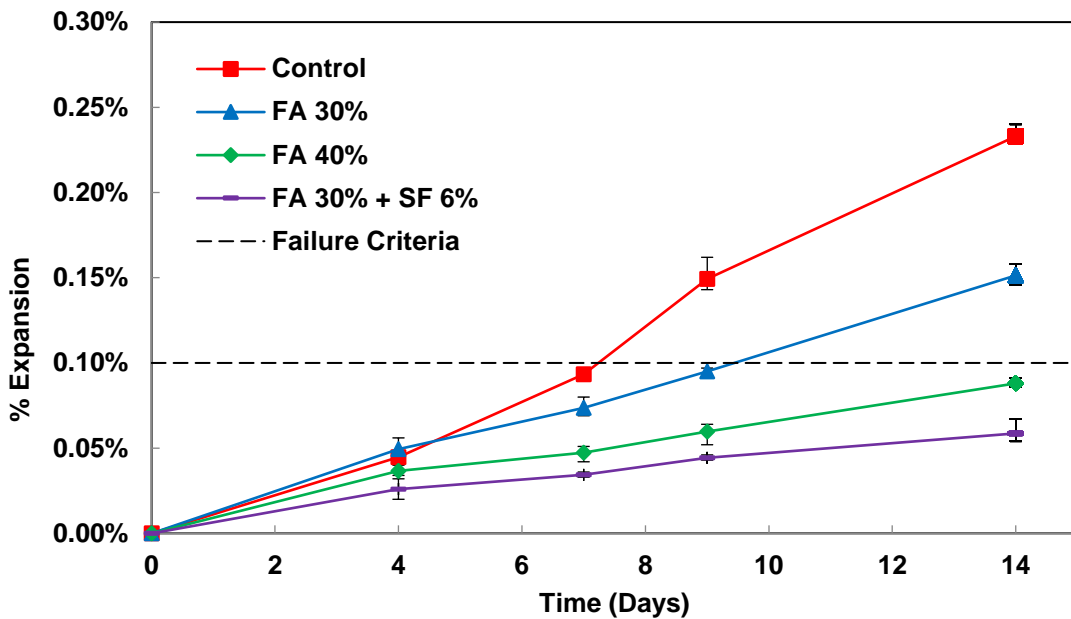


Figure 7.24 Mortar bar expansion with time per ASTM C1567 for Amarillo Coarse Aggregate with varying SCM contents

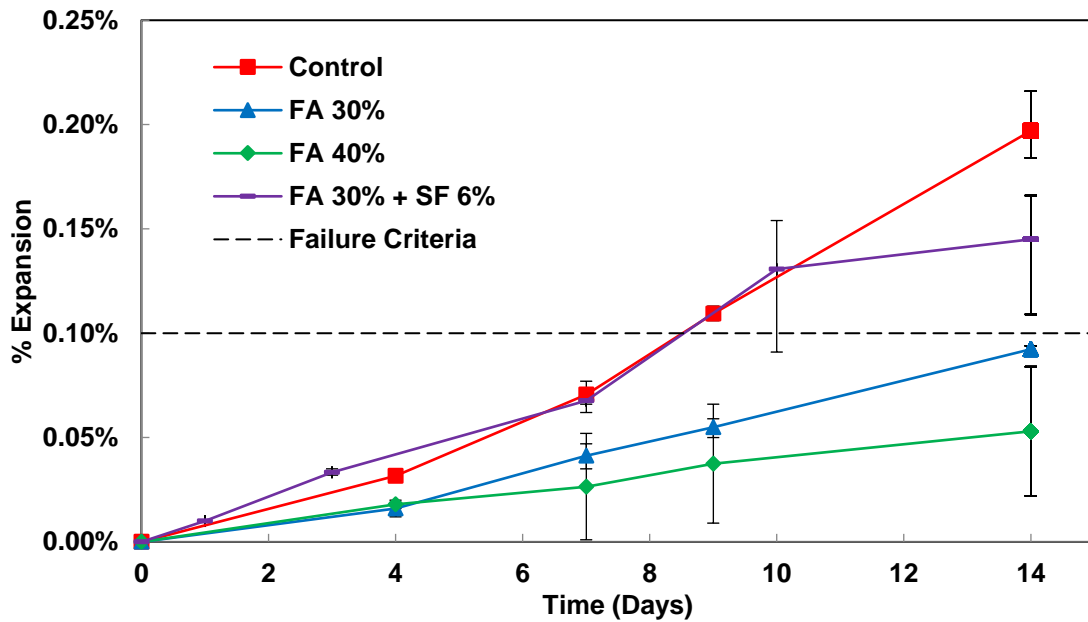


Figure 7.25 Mortar bar expansion with time per ASTM C1567 for Amarillo Fine Aggregate with varying SCM contents

7.5. Further Research

The unique compatibility issues encountered between admixture and cementitious materials are noteworthy and may warrant a separate investigation focusing on this topic. In practical terms, however, test results indicate that changing admixtures or

cementitious materials and providing proper construction practices may be enough to prevent further plastic shrinkage cracking issues. Thus, the following actions are recommended for further research of current and future samples:

- Perform a detailed chemical analysis of cementitious materials and admixtures to determine the source of incompatibility. A key aspect would be to establish if the unusual hydration is caused by over/under sulfation triggered by cementitious and admixture interaction. Based on Bogue equations, the Amarillo cement was estimated to have a C_3A content of 4.1%, while the reference cement had an 11.1% C_3A content.
- Analyze extracted cores to verify presence of microfibers through scanning electron microscopy.
- Chloride diffusion testing (ASTM C1556) could help determine if the use of a corrosion inhibitor is needed given the bridge deck exposure conditions. Since the standard mixture design employs a ternary SCM blend, that factor alone may lower the diffusion coefficient to such an extent that the additional use of a corrosion inhibitor would be redundant.
- Design a simplified mixture with compatible materials that meets the specified requirements. Batch proposed mixture to test for fresh properties and analyze in ConcreteWorks modeling software to determine expected lifetime.
- Potentially revisit sites to updated crack survey and determine crack growth over time. The effect of plastic shrinkage cracking on long term drying shrinkage cracking could be analyzed. New cores could also be obtained for chloride profiling.

7.6. Conclusions

Several factors could have caused cracking on the bridge deck either on their own or in combination with each other. Based on the information gathered during the site investigation and subsequent testing, deficiencies likely occurred in the mixture design, material selection, and construction stages. The deficiencies are summarized in Table 7.6.

This case study highlights the need for compatibility and consistency across all stages of the construction process. Sound engineering design is meaningless if field practices are imprudent and vice-versa.

Focusing on the design and material aspects, simplifying the mixture design, and evaluating hydration through calorimetry or even time-of-set testing are key in ensuring proper mixture performance in the field.

Table 7.6: Deficiencies

Category	Deficiency
Design/Material	Incompatibility between admixtures and cementitious materials
	Potential absence of microfibers
	Differential strength gains between precast and full-depth sections
Construction	Harsh weather conditions: dry, cold, and windy (Wednesday before Thanksgiving 2016)
	High rebar cover (3.0–3.5")
	Delayed curing

7.7. References

- ASTM C39 (2015), *Standard Test Method for Compressive Strength of Cylindrical Concrete Specimens*
- ASTM C138 (2017), *Standard Test Method for Density (Unit Weight), Yield, and Air Content (Gravimetric) of Concrete*
- ASTM C143 (2015), *Standard Test Method for Slump of Hydraulic-Cement Concrete*
- ASTM C150 (2016), *Standard Specification for Portland Cement*
- ASTM C157 (2014), *Standard Test Method for Length Change of Hardened Hydraulic-Cement Mortar and Concrete*
- ASTM C231 (2017), *Standard Test Method for Air Content of Freshly Mixed Concrete by the Pressure Method*
- ASTM C403 (2016), *Standard Test Method for Time of Setting of Concrete Mixtures by Penetration Resistance*
- ASTM C469 (2014), *Standard Test Method for Static Modulus of Elasticity and Poisson's Ratio of Concrete in Compression*
- ASTM C496 (2011), *Standard Test Method for Splitting Tensile Strength of Cylindrical Concrete Specimens*
- ASTM C1074 (2019), *Standard Practice for Estimating Concrete Strength by the Maturity Method*
- ASTM C1556 (2016), *Standard Test Method for Determining the Apparent Chloride Diffusion Coefficient of Cementitious Mixtures by Bulk Diffusion*
- ASTM C1581 (2016), *Standard Test Method for Determining Age at Cracking and Induced Tensile Stress Characteristics of Mortar and Concrete under Restrained Shrinkage*
- ASTM C1876 (2019), *Standard Test Method for Bulk Electrical Resistivity or Bulk Conductivity of Concrete*

Chapter 8. Conclusion

8.1. Conclusions

Significant laboratory and field data were generated during the course of this project. Although some of the tests are ongoing and may require additional time to determine whether a given material improves the long-term durability of concrete, some general observations can be made at this time:

- Lithium nitrate was found to delay the time to ASR- and/or DEF-induced expansion, but the performance in field exposure blocks was not as promising as accelerated laboratory tests.
- Saturating LWFA with lithium nitrate as an attempt to time release lithium nitrate was found to show little benefit over just using lithium nitrate as a chemical admixture added to the mix water.
- The use of LWFA (saturated with water) was shown to delay and decrease expansion due to ASR and/or DEF. The specific benefits of using a given LWFA to avoid ASR and/or DEF requires additional emphasis and future testing.
- Overall, the use of corrosion inhibitors was found to be beneficial in delaying the corrosion of reinforcing steel. The use of the calcium nitrate and calcium nitrite admixture significantly reduced chloride ingress, resulting in a notable decrease in the diffusion coefficient. The observed improvement was directly related to admixture dosage and was consistently observed across lab and field samples.
- The use of IWRs was not found to be effective in improving the transport properties most relevant to concrete durability. Although there were some marginal improvements for some products in some tests, in general, it was not found to be significant enough to fully prevent deleterious mechanisms from occurring.
- Nano products were found to slightly improve the transport and durability properties of concrete, but degree of improved performance appears to be slight when compared to controls and may not justify the use of the products tested. Based on results, the products may be better tailored to address specific issues (e.g., early age strength with nano-CSH) rather than to provide broad improvements in durability.

- The use of gypsum to improve sulfate resistance of concrete containing Class C fly ash shows promise but requires further time to monitor the laboratory and field specimens cast during this project.
- A forensic evaluation of a bridge deck in the Amarillo district identified the potential causes of excessive cracking observed in decks cast over precast panels. Potential admixture compatibility and dosage issues, excessive rebar cover depth, and delayed curing were identified as factors likely contributing to the observed cracking.

8.2. Recommendations for Future Research

Based on the findings to date from this project, the following recommendations are made for future research that is needed to advance the implementation of chemical solutions to minimize or prevent concrete durability problems:

- Continue to monitor laboratory and outdoor exposure site specimens cast and evaluated under this project. This is especially critical for field samples that have not yet exhibited expansion or deterioration, especially those cast at lower w/cm ratios and that contained SCMs.
- Evaluate more thoroughly the benefits of using LWFA, with or without lithium nitrate, to reduce the potential for expansion and cracking due to ASR and/or DEF. The impact of aggregate mineralogy and reactivity on the efficacy of LWFA in reducing expansion should be studied more robustly.
- The potential for using gypsum in combination with Class C fly ash to improve external sulfate resistance should be explored in more depth, especially given the increased relative amount of Class C fly ash (compared to Class F fly ash).